

# DAMES & MOORE

*Consultants in the Environmental and Applied Earth Sciences*

March 28, 1977

Consolidated Edison Company  
of New York, Inc.  
4 Irving Place  
New York, New York 10004

Gentlemen:

We are pleased to submit herewith copies of our report entitled, "Geotechnical Investigation of the Ramapo Fault System in the Region of the Indian Point Generating Station", Volumes I & II, prepared for Consolidated Edison Company of New York, Inc.

The results of this investigation support those of the on-site investigation entitled "Supplemental Geological Investigation of the Indian Point Generating Station", dated November 1975. We conclude that a total evaluation of these investigations consistently indicates that the Ramapo Fault System is not capable within the meaning of Appendix A to 10 CFR Part 100.

On behalf of Messrs. Fischer, Archer and the Dames & Moore professional staff, I would like to convey our appreciation for the cooperation and confidence demonstrated by the Consolidated Edison professional staff and management. Should you have any questions concerning this report, please do not hesitate to contact us, as we would be pleased to provide you with additional assistance if necessary.

Docket # 50-286  
Control # 770910319  
Date 3/29/77 of Document  
REGULATORY DOCKET FILE

Very truly yours,

DAMES & MOORE

*Todd M. Gates*

Todd M. Gates  
Project Manager

TMG/dj  
Enclosure

8110240493 770328  
PDR ADOCK 05000003  
PDR

*Offices in principal cities*

ANCHORAGE • ATLANTA • BETHESDA • CHICAGO • CINCINNATI • CRANFORD, N.J. • DENVER • FAIRBANKS • HONOLULU • HOUSTON • LOS ANGELES • NEW YORK  
PHOENIX • PORTLAND, ORE. • SALT LAKE CITY • SAN FRANCISCO • SANTA BARBARA • SEATTLE • WASHINGTON, D.C.  
CALGARY • JAKARTA • GUAM • JOHANNESBURG • LAGOS • LONDON • MADRID • PERTH • SINGAPORE • SEOUL • SYDNEY • TEHRAN • TOKYO • TORONTO • VANCOUVER

# TABLE OF CONTENTS

## VOLUME I

<u>Section</u>	<u>Page</u>
1.0 INTRODUCTION.....	1-1
2.0 SUMMARY.....	2-1
2.1 GENERAL.....	2-1
2.2 REGIONAL GEOLOGIC SETTING.....	2-1
2.3 PRECAMBRIAN FAULTS.....	2-2
2.4 PALEOZOIC FAULTS.....	2-3
2.5 MESOZOIC REACTIVATION.....	2-5
2.6 WANING OF OROGENIC FAULT MOVEMENTS.....	2-5
2.7 GEOPHYSICAL INVESTIGATIONS.....	2-7
2.8 AGE DATING.....	2-8
2.9 PLEISTOCENE AND HOLOCENE RECORDS.....	2-10
2.10 CONTEMPORARY SEISMICITY.....	2-11
2.11 IN SITU STRESS MEASUREMENTS.....	2-12
2.12 CONCLUSIONS.....	2-13

## APPENDICES

A	THE RAMAPO SYSTEM IN ROCKLAND, WESTCHESTER, AND PUTNAM COUNTIES, NEW YORK	
A1.0	INTRODUCTION AND GENERAL GEOLOGIC SETTING.....	A-1
A2.0	LITHOLOGIES AND STRATIGRAPHY.....	A-3
A2.1	HUDSON HIGHLANDS.....	A-3
A2.1.1	Felsic Gneisses and Associated Intrusives.....	A-3
A2.1.2	Canopus Hollow Marble, Quartzite and Paragneiss.....	A-5
A2.1.2.1	Description.....	A-5
A2.1.2.2	The Age Problem.....	A-7
A2.1.3	Canopus Pluton.....	A-11
A2.2	MANHATTAN PRONG.....	A-12
A2.2.1	Fordham Gneiss.....	A-12
A2.2.2	Poughquag-Lowerre Quartzite.....	A-14
A2.2.3	Wappinger-Inwood Formation.....	A-15
A2.2.4	Annsville Phyllite-Manhattan Formation.....	A-16
A2.3	PALEOZOIC INTRUSIVE ROCKS.....	A-17
A2.3.1	Cortlandt-Type Intrusives.....	A-17
A2.3.2	The Rosetown Pluton.....	A-18
A2.3.3	Peekskill Granite.....	A-20
A3.0	STRUCTURAL GEOLOGY.....	A-22
A3.1	INTRODUCTION AND SUMMARY.....	A-22
A3.1.1	Ductile Deformation.....	A-23
A3.1.2	Brittle Deformation.....	A-25

A3.2	DISTRIBUTION AND OCCURRENCE OF FAULTS.....	A-26
A3.2.1	The Ramapo Fault System.....	A-27
A3.2.1.1	Northeast Trending Faults..	A-27
A3.2.1.1.1	Ramapo Fault...	A-27
A3.2.1.1.2	Thiells Fault..	A-29
A3.2.1.1.3	Cedar Flats Fault.....	A-33
A3.2.1.1.4	Ambreys Pond Fault.....	A-34
A3.2.1.2	North-Northeast Trending Faults.....	A-35
A3.2.1.2.1	Timp Pass Fault.....	A-35
A3.2.1.2.2	Blanchard Road Fault.....	A-35
A3.2.1.2.3	Willow Grove Fault.....	A-36
A3.2.1.3	North Trending Faults.....	A-37
A3.2.1.3.1	Bald Mountain and Buckberg Mountain Faults.....	A-37
A3.2.1.4	East-Northeast Trending Faults.....	A-38
A3.2.1.4.1	Letchworth Fault.....	A-38
A3.2.1.4.2	Mott Farm Road Fault.....	A-39
A3.2.1.5	Dunderberg Fault.....	A-41
A3.2.2	The Canopus Fault System.....	A-42
A3.2.2.1	Northeast Trending Faults..	A-42
A3.2.2.1.1	Canopus Hollow Fault.....	A-42
A3.2.2.1.2	Dennytown Fault.....	A-43
A3.2.2.1.3	Annsville- Oscawana Fault.	A-45
A3.2.2.1.4	Peekskill Hol- low Fault.....	A-50
A3.2.2.2	North-Northeast Trending Faults.....	A-52
A3.2.2.2.1	Manitou Moun- tain Fault.....	A-52
A3.2.2.2.2	The Roa Hook Fault.....	A-54
A3.2.2.2.3	The Dickiebush Lake Fault.....	A-55
A3.2.2.3	Peekskill Fault.....	A-56

A3.2.3	The Croton Falls Fault System.....	A-59
A3.2.3.1	Northeast Trending Faults..	A-60
A3.2.3.1.1	The Croton Falls Fault....	A-60
A3.2.3.1.2	The Prickly Pear Shear Zone.....	A-61
A3.2.3.1.3	Croton-Teatown Shear Zones....	A-63
A3.2.4	Popolopen Brook Structure.....	A-65
A3.2.5	Topographic Expression of Some Faults.....	A-68
A4.0	CONCLUSIONS AND INTERPRETED HISTORY OF FAULT MOVEMENTS.....	A-71
A4.1	PRECAMBRIAN FAULTS.....	A-71
A4.1.1	Grenvillian Faults.....	A-71
A4.1.2	Post-Grenville Precambrian Faults....	A-73
A4.2	PALEOZOIC FAULTS.....	A-74
A4.2.1	Dennytown-Canopus Hollow Faults.....	A-75
A4.2.2	The Annsville-Oscawana Fault.....	A-76
A4.2.3	Peekskill Hollow Fault.....	A-77
A4.2.4	Peekskill Fault.....	A-77
A4.2.5	Croton Falls Fault.....	A-78
A4.3	Mesozoic Faults.....	A-79
A4.3.1	Dennytown Fault Zone.....	A-80
A4.3.2	Annsville-Oscawana Fault.....	A-81
A4.3.3	Peekskill Fault.....	A-81
A4.3.4	Croton Falls Fault System.....	A-82
A4.4	CONCLUSIONS.....	A-83
B	ASSESSMENT OF THE DEFORMATION OF THE NORTHERN END OF THE NEWARK-GETTYSBURG BASIN	
B1.0	INTRODUCTION.....	B-1
B1.1	PURPOSE.....	B-1
B1.2	GEOLOGIC SETTING.....	B-1
B2.0	LITHOLOGIES OF THE NEWARK BASIN IN ROCKLAND COUNTY.....	B-5
B2.1	TRIO-JURASSIC SEDIMENTARY ROCKS.....	B-5
B2.2	DIABASE.....	B-6
B2.3	HORNFELS.....	B-9
B3.0	CONFIGURATION OF THE DIABASE BODIES.....	B-10
B3.1	GENERAL.....	B-10
B3.2	PALISADES DIABASE.....	B-11
B3.2.1	Lower Contact.....	B-11
B3.2.2	Upper Contact.....	B-14
B3.2.3	New City Park Dike.....	B-15
B3.3	LADENTOWN AND UNION HILL BODIES.....	B-16
B3.4	INTERPRETATION.....	B-16

B4.0	NEWARK BASIN FORM AND RATES OF SEDIMENTATION.....	B-18
B4.1	BEDDING ATTITUDES.....	B-18
B4.2	BASIN SUBSIDENCE.....	B-19
B5.0	FAULTING AND FRACTURING.....	B-23
B5.1	THE RAMAPO FAULT.....	B-23
B5.2	FAULTS IN THE AREA OF ROCKLAND AND DEFOREST LAKES.....	B-25
B5.2.1	Rockland Lake Fault.....	B-26
B5.2.2	Trough Hollow Fault.....	B-27
B5.2.3	Hook Mountain Fault.....	B-28
B5.2.4	Long Clove Fault.....	B-29
B5.3	FAULTS PARALLELING THE SOUTH MOUNTAIN DIKE....	B-30
B5.3.1	South Portal Fault.....	B-30
B5.3.2	Lake Lucille Fault.....	B-31
B5.4	FAULTS AT STONY POINT, MT. IVY, AND LITTLE TOR.....	B-32
B5.4.1	Shearing Near the Thiells Fault.....	B-32
B5.4.2	Faulting in the Little Tor Area.....	B-33
B5.5	FRACTURING.....	B-33
B5.6	INTERPRETATION.....	B-34
B6.0	WATER WELL DATA.....	B-41
B6.1	DATA BASE.....	B-41
B6.2	INTERPRETATIONS.....	B-42
B7.0	SEISMIC REFLECTION PROFILING.....	B-46
B7.1	LINE 1 PART 1.....	B-46
B7.2	LINE 5.....	B-47
B8.0	FAULT AND SHEAR FILLING MINERALIZATION.....	B-49
B8.1	DISTRIBUTION OF MINERAL PHASES AND DEFORMATION.....	B-49
B8.2	INTERPRETED REGIONAL PARAGENESIS.....	B-51
B8.3	RADIOMETRIC DATING AND ANALYSES OF FLUID INCLUSION FILLING TEMPERATURES.....	B-52
B8.4	DISCUSSION AND CONCLUSIONS.....	B-54
B9.0	CONCLUSIONS.....	B-63
C	DEFORMATION ALONG THE RAMAPO FAULT IN THE VICINITY OF POMPTON LAKES, NEW JERSEY	
C1.0	INTRODUCTION AND OBJECTIVES.....	C-1
C2.0	STRUCTURAL GEOLOGY.....	C-2
C2.1	REGIONAL GEOLOGIC SETTING.....	C-2
C2.2	READING PRONG.....	C-2
C2.3	NEWARK BASIN.....	C-7
C2.4	RAMAPO FAULT.....	C-9
C2.5	QUATERNARY DEPOSITS.....	C-11
C3.0	SEQUENCE OF DEFORMATION.....	C-15
C3.1	GENERAL STATEMENT.....	C-15
C3.2	PALEOZOIC DEXTRAL TRANSCURRENT FAULTING.....	C-16
C3.3	MESOZOIC WRENCH TECTONICS.....	C-17
C3.4	REGIONAL ROTATION OF BEDDING.....	C-20

C4.0 CONCLUSIONS.....	C-24
D GEOPHYSICAL INVESTIGATIONS	
D1.0 INTRODUCTION.....	D-1
D2.0 GROUND MAGNETIC AND AEROMAGNETIC INVESTIGATION - GENERAL.....	D-3
D2.1 INTRODUCTION.....	D-3
D2.2 FUNDAMENTALS INVOLVED.....	D-3
D3.0 GROUND MAGNETIC SURVEY.....	D-7
D3.1 INTRODUCTION.....	D-7
D3.2 METHODOLOGY.....	D-7
D3.3 COMPUTER MODELING.....	D-8
D3.4 DISCUSSION OF GROUND MAGNETIC PROFILES.....	D-11
D3.4.1 Profiles Across the Thiells Fault....	D-11
D3.4.2 Profiles Across the Letchworth Fault.....	D-11
D3.4.3 Profiles Across the Ramapo Fault....	D-12
D3.5 CONCLUSIONS.....	D-16
D4.0 AEROMAGNETIC SURVEY.....	D-19
D4.1 INTRODUCTION.....	D-19
D4.2 THEORETICAL CONSIDERATIONS.....	D-20
D4.3 INTERPRETATIONS.....	D-22
D4.4 CONCLUSIONS.....	D-26
D5.0 EVALUATION OF GRAVITY DATA.....	D-27
D5.1 INTRODUCTION.....	D-27
D5.2 INTERPRETATIONS.....	D-27
D5.3 CONCLUSIONS.....	D-30
D6.0 RESULTS OF A BATHYMETRIC SURVEY IN THE HUDSON RIVER IN THE VICINITY OF INDIAN POINT.....	D-31
D6.1 INTRODUCTION.....	D-31
D6.2 OPERATIONS.....	D-32
D6.3 RESULTS.....	D-34
D6.3.1 General Bathymetry.....	D-34
D6.3.2 Cultural Effects.....	D-36
D6.3.3 Conclusions.....	D-37
D7.0 SEISMIC REFLECTION PROFILING.....	D-40
D7.1 INTRODUCTION.....	D-40
D7.2 FIELD EQUIPMENT AND PROCEDURES.....	D-40
D7.3 RECORD QUALITY CONTROL AND PROCESSING.....	D-44
D7.3.1 Record Quality.....	D-44
D7.3.2 Tape Transcription and Data Pro- cessing.....	D-45
D7.4 DISCUSSION OF RESULTS.....	D-49
D7.4.1 General.....	D-49
D7.4.2 Line 1.....	D-50
D7.4.3 Line 2.....	D-54
D7.4.4 Line 3.....	D-55
D7.4.5 Line 4.....	D-57
D7.4.6 Line 5.....	D-58
D7.5 CONCLUSIONS.....	D-60

E	GEOCHEMISTRY AND AGE DATING	
E1.0	INTRODUCTION.....	E-1
E2.0	PRESENTATION OF DATA.....	E-3
E3.0	DISCUSSION OF FLUID INCLUSION DATA.....	E-4
E4.0	CONCLUSION.....	E-12
E5.0	DISCUSSION OF POTASSIUM-ARGON (K-Ar) DATA.....	E-13
E5.1	DIABASE AND BASALT.....	E-13
E5.2	ZEOLITES.....	E-14
E5.3	OTHER.....	E-15
ATTACHMENT E-1A	FLUID INCLUSION STUDIES BY DR. BARNES	
ATTACHMENT E-1B	FLUID INCLUSION STUDIES BY DR. BARNES	
ATTACHMENT E-2	POTASSIUM-ARGON ANALYSIS BY GEOCHRON LABORATORIES	

F	INVESTIGATION OF POST-MESOZOIC FEATURES	
F1.0	INTRODUCTION.....	F-1
F2.0	SYNOPSIS OF LATE GLACIAL AND POST-GLACIAL HISTORY OF THE REGION.....	F-3
F3.0	GEOMORPHIC FEATURES AND SURFICIAL DEPOSITS.....	F-7
F4.0	SELECTED INVESTIGATIONS.....	F-12
F4.1	LAKE HUDSON SHORELINE.....	F-12
F4.1.1	Previous Work.....	F-12
F4.1.2	Evidence of Lake Hudson Shoreline....	F-13
F4.1.3	Reliability of Shoreline Elevations..	F-15
F4.1.4	Interpretation.....	F-16
F4.2	GEOMORPHIC FEATURES AT JONES POINT.....	F-17
F4.2.1	Slump Features at 224-2.....	F-20
F4.2.2	Disturbed Features at 226-2.....	F-21
F4.2.3	Interpretation.....	F-21
F4.3	ROCK BENCH.....	F-22
F4.4	MOTT FARM ROAD.....	F-24
F4.4.1	Observations.....	F-24
F4.4.2	Interpretation.....	F-25
F4.5	IMMACULATE CONCEPTION SEMINARY.....	F-27
F4.5.1	Observations.....	F-27
F4.5.2	Interpretation.....	F-29
F4.6	STAG HILL.....	F-30
F4.7	PLEISTOCENE DEPOSITS ALONG THE WESTERN BORDER OF THE NEWARK BASIN IN POMPTON PLAINS, NJ.....	F-31
F4.7.1	Location, Purpose, and Setting.....	F-31
F4.7.2	Geologic Observations.....	F-33
F4.7.3	Interpretation and Conclusions.....	F-36
F4.8	CENTRAL NYACK OUTCROP.....	F-38
F4.8.1	Introduction.....	F-38
F4.8.2	Observations.....	F-38
F4.8.3	Conclusions.....	F-41
F5.0	CONCLUSIONS.....	F-43

G	EVALUATION OF THE RELATIONSHIP BETWEEN SEISMIC EVENTS AND THE RAMAPO SYSTEM OF FAULTS	
G1.0	INTRODUCTION.....	G-1
G2.0	MAXIMUM INTENSITY EARTHQUAKE.....	G-3
G3.0	VELOCITY MODELS AND LOCATION OF EARTHQUAKES.....	G-7
G3.1	VELOCITY MODELS.....	G-7
	G3.1.1 September 3, 1951 - "Rockland County".....	G-9
	G3.1.2 March 11, 1976 - Pompton Plains.....	G-10
G3.2	LOCATIONS OF OTHER EARTHQUAKES.....	G-12
G4.0	FAULT PLANE SOLUTIONS.....	G-13
G5.0	CONCLUSIONS.....	G-16
H	IN SITU STRESS MEASUREMENTS	
H1.0	INTRODUCTION.....	H-1
H1.1	PURPOSE AND SCOPE.....	H-1
H1.2	SITE SELECTION AND DESCRIPTIONS.....	H-1
H2.0	TEST PROCEDURES AND COMPUTATIONS.....	H-4
H2.1	GENERAL.....	H-4
H2.2	FIELD TEST PROCEDURES.....	H-5
H2.3	MODULUS DETERMINATION.....	H-5
H2.4	TEST EQUIPMENT.....	H-6
H2.5	COMPUTATION OF STRESSES.....	H-8
H3.0	TEST DATA AND RESULTS.....	H-11
H3.1	FIELD AND LABORATORY DATA.....	H-11
H3.2	RESULTS.....	H-12
H4.0	REGIONAL CORRELATION.....	H-16
H4.1	GENERAL.....	H-16
H4.2	ORIENTATION OF MAXIMUM HORIZONTAL COMPRESSION IN NORTHEASTERN NORTH AMERICA.....	H-18
H5.0	CONCLUSIONS.....	H-23
J	BIBLIOGRAPHY.....	J-1 to J-13

LIST OF TABLES  
VOLUME I

<u>TABLE NO.</u>		<u>PAGE</u>
<u>APPENDIX A</u>		
A-1	Mineral Assemblages of Rock Samples from Canopus Hollow Fault Zone.....	A-86
A-2	Stress Orientations from Kink Analyses.....	A-87
<u>APPENDIX B</u>		
B.5-1	Selected Observations of Faulting.....	B-37 to B-39
B.5-2	Strikes of Major Subvertical Fracture Sets in Trio-Jurassic Sedimentary Rocks.....	B-40
B.6	Selected Wells in Rockland County.....	B-44 to B-45
B.8-1	Mineral Occurrences by Trend of Sampled Fault or Shear.....	B-58
B.8-2	Mineral Occurrences by Geographic Location.....	B-59
B.8-3	Observed Parageneses.....	B-60 to B-62
<u>APPENDIX C</u>		
C2-1	Interpretation of Ground Magnetic Traverses....	C-13
C2-2	Attitudes of Shears Observed in Exposures Near the Ramapo Fault.....	C-14
C3-1	Analysis of Structural Data at Station CH-37.....	C-23
<u>APPENDIX D</u>		
D3-1	Magnetic Characteristics of Rock Samples.....	D-18

## APPENDIX E

E-1	Fluid Inclusion - Data.....	E-17 to E-22
E-2	Potassium-Argon - Data.....	E-23 to E-25
E-3	Mineral Changes in Formation of Zeolitic Rock..	E-26

## APPENDIX F

F-1	Description of Stations - Gravel Quarry at Riverdale and Pompton Plains, N.J.....	F-45 to F-47
-----	--	--------------------

## APPENDIX G

G-1	Earthquake List 40° to 42°N - 73° to 75°W.....	G-19 to G-22
G-2	List of Epicenters in the Vicinity of the Ramapo Fault.....	G-23
G-3	P and S Arrival Time Data for the September 3, 1951 Earthquake.....	G-24
G-4	Location of the September 3, 1951 Earthquake.....	G-25 to G-26
G-5	P and S Arrival Time Data for the March 11, 1976 Earthquake.....	G-27
G-6	Location of the March 11, 1976 Earthquake.....	G-28 to G-30
G-7	P and S Arrival Time Data for the December 20, 1962 Earthquake.....	G-31
G-8	P and S Arrival Time Data for the March 12, 1976 Earthquake.....	G-32
G-9	P and S Arrival Time Data for the April 13, 1976 Earthquake.....	G-33

G-10	P and S Arrival Time Data for the August 20, 1976 Earthquake.....	G-34
G-11	P and S Arrival Time Data for the September 22, 1976 Earthquake.....	G-35
G-12	P and S Arrival Time Data for the November 22, 1976 Earthquake.....	G-36
G-13	Fault Plane Solutions.....	G-37

#### APPENDIX H

H-1	Definitions.....	H-25
H-2	Uniaxial Compressive Strengths.....	H-26
H-3	Record or Calibration of Borehole Deformation Gauge.....	H-27
H-4	Deformation Calculations, Site 3.....	H-28
H-5	Deformation Calculations, Site 9.....	H-29
H-6	Deformation Calculations, Site 11.....	H-30
H-7	Deformation Calculations, Site 14.....	H-31
H-8	Physical Property Tests, Site 3.....	H-32
H-9	Physical Property Tests, Site 9.....	H-33
H-10	Physical Property Tests, Site 11.....	H-34
H-11	Physical Property Tests, Site 14.....	H-35
H-12	Tabulation of Results, Site 3.....	H-36 to H-37
H-13	Tabulation of Results, Site 9.....	H-38 to H-39
H-14	Tabulation of Results, Site 11.....	H-40 to H-41
H-15	Tabulation of Results, Site 14.....	H-42 to H-43

H-16	Some In-Situ Secondary Principal Stresses in a Horizontal Plane, Eastern North America...	H-44 to H-48
H-17	Some In-Situ Secondary Principal Stresses in a Horizontal Plane, Eastern North America (Hydraulic Fracturing Measurements).....	H-49 to H-50
H-18	Some In-Situ Strain Relief Measurements Recorded at the Surface, Northeastern North America.....	H-51 to H-52

## LIST OF PLATES

### VOLUME II

#### PLATE NO.

- 1A & B      Geologic Map of the Ramapo-Canopus and Croton  
Falls Fault Systems
- 2A & B      Station Location Map to Accompany Geologic Map
- 3            Geographic Location of Various Map Plates

#### APPENDIX A

- A-1            Geologic Map of the Peekskill Area
- A-2            Block Diagram of the Annsville Fault
- A-3            Lower Hemisphere Equal Area Projection - of  
conjugate kink sets in Annsville Formation,  
Annsville, New York (Sets 1&2)
- A-4            Lower Hemisphere Equal Area Projection - of  
conjugate kink sets in Annsville Formation,  
Annsville, New York (Sets 3&4)
- A-5            Geologic Map of Thiells Fault Zone
- A-6            Structural Setting of the Peekskill Pluton
- A-7            Interpreted Ramapo - Canopus Fault System in  
Precambrian Time
- A-8            Interpreted Ramapo - Canopus and Croton Falls  
Fault System in Paleozoic Time
- A-9            Interpreted Ramapo - Croton Falls Fault System  
in Mesozoic Time

#### APPENDIX B

- B-1            Panoramic Profile of Palisades - showing contact  
relationships

#### APPENDIX C

- C-1            Photograph - Granitic pegmatite which has been  
folded during intrusion along the regional  
layering and foliation of Precambrian Paragneiss.  
Located on Gas Line N of SL-136, Pompton Lakes,  
New Jersey.

- C-2            Schematic Diagram - of Diabase Dike near Lake Inez Fault, Pompton Lakes, New Jersey.
- C-3            Geologic Map - of Pompton Lakes Area, New Jersey.
- C-4            Schematic Diagram of Station CH-37 (SL-109) - Showing cross-cutting relationships of exposed faults in conglomerate below Second Watchung Flow.
- C-5            Location Map of Structural Subdivisions in the Pompton Lakes Area, New Jersey.
- C-6            Line Drawing from Photograph - Granitic Gneiss in Western Highlands exhibiting small-scale strike-slip shears sub-parallel to regional trend of Ramapo Fault.
- C-7            Lower Hemisphere Equal Area Projection - Plot of poles to strike-slip and oblique-slip faults. Five faults have inferred dextral movement senses. The faults strike ENE and dip steeply. All faults were observed in Precambrian rocks within deflection zone (B) of Ramapo Fault trace.
- C-8            Lower Hemisphere Equal Area Projection - of poles to Triassic bedding which define a broad fold about an axis oriented (N45W, 9NW) which is approximately normal to the basin margin and the Ramapo fault.
- C-9            Lower Hemisphere Equal Area Projections - Faults in Trio-Jurassic domains of Zones A, B, and C in Pompton Lakes Area, New Jersey.
- C-10           Lower Hemisphere Equal Area Projection - Plot of poles to dip-slip faults in Precambrian domain of deflection zone (B) near Pompton Lakes, New Jersey. Movement senses of faults are both normal and reverse.

#### APPENDIX D

- D.3-1            Ground Magnetic Profiles - Lines 1, 2, and 3
- D.3-2            Ground Magnetic Profiles - Lines 4, 5, 6, 7, 8, and 9
- D.3-3            Ground Magnetic Profiles - Lines 10, 11, 12, and 12A

- D.3-4 Ground Magnetic Profiles - Lines 13, 14, 15, 16, 17, and 18
- D.4-1 Aeromagnetic Map of Area Surrounding the Indian Point Generating Station
- D.5-1 Contoured Bouguer Gravity Map - of a Section of the Northeastern United States
- D.5-2 Contoured Site Bouguer Gravity Map of Peekskill, New York
- D.6-1 Hudson River Bathymetry - vicinity of the Indian Point Generating Station
- D.7-1 Seismic Reflection Profiling Equipment
- D.7-2 High Resolution Seismic Reflection Survey - Shot Point Location Map - Map 1
- D.7-3 High Resolution Seismic Reflection Survey - Shot Point Location Map - Map 2
- D.7-4 High Resolution Seismic Reflection Survey - Shot Point Location Map - Map 3
- D.7-5 High Resolution Seismic Reflection Survey - Shot Point Location Map - Map 4
- D.7-6 High Resolution Seismic Reflection Survey - Shot Point Location Map - Map 5
- D.7-7 High Resolution Seismic Reflection Survey - Shot Point Location Map - Map 6
- D.7-8 High Resolution Seismic Reflection Survey - Shot Point Location Map - Map 7
- D.7-9 High Resolution Seismic Reflection Survey - Shot Point Location Map - Map 8
- D.7-10 High Resolution Seismic Reflection Survey - Shot Point Location Map - Map 9
- D.7-11 High Resolution Seismic Reflection Survey - Shot Point Location Map - Map 10
- D.7-12 High Resolution Seismic Reflection Survey - Shot Point Location Map - Map 11

- D.7-13 High Resolution Seismic Reflection Line - Line 1 - Part 1
- D.7-14 High Resolution Seismic Reflection Line - Line 1 - Part 2
- D.7-15 High Resolution Seismic Reflection Line - Line 2
- D.7-16 High Resolution Seismic Reflection Line - Line 2A
- D.7-17 High Resolution Seismic Reflection Line - Line 2B
- D.7-18 High Resolution Seismic Reflection Line - Line 3
- D.7-19 High Resolution Seismic Reflection Line - Line 4
- D.7-20 High Resolution Seismic Reflection Line - Line 5

#### APPENDIX E

- E-1 Frequency of Occurrence vs. Homogenization Temperature
- E-2 Strike of Fault or Fracture Plane Sampled vs. Homogenization Temperature °C in Paleozoic Host Rock
- E-3 Strike of Fault on Fracture Plane Sampled vs. Homogenization Temperature °C in Mesozoic Rock
- E-4 Mineral Phase vs. Homogenization Temperature
- E-5 Index Map - Showing Onsite Outcrops and References to Detailed Diagrams E-7 through E-9B (which contain F.S. series sample locations)
- E-6 Explanation of Symbols Utilized on Geologic Plans of Site Outcrops
- E-7 Geologic Plan - Outcrop North of Reactor No. 2
- E-8 Geologic Plan - Outcrop Adjacent to Turbogenerator Building No. 1 (Inwood Marble)
- E-9A Geologic Plan - Inwood Marble - Outcrop North of Reactor No. 3
- E-9B Geologic Plan - Inwood Marble - Outcrop North of Reactor No. 3

- DAMES & MOORE**

E-16A Photo A: Outcrop View of Sampling Station MW-106  
Photo B: Close-up of Sampling Stations MW-106-2

E-16B Station MW-106, Mineralization Sampling

E-16C Photomicrograph of Sample MW-106-2

E-17A Photo A: Outcrop View of Sampling Station MW-115  
Photo B: Close-up of Sampling Station MW-115-1

E-17B Photomicrograph of Sample MW-115-1

E-18A Photo A: Outcrop View of Sampling Station GA-1  
Photo B: Closeup of Sample Location GA-1.1

E-18B Station GA-1, Mineralization Sampling

E-18C Photo A: Photomicrograph of Sample GA-1.1  
Photo B: Photomicrograph of Sample GA-1.1

E-19A Photo A: Outcrop View of Sampling Station GA-1  
Photo B: Close-up of Sample Location GA-1.3

E-19B Photomicrograph of Sample GA-1.3

E-20A Photo A: Outcrop View of Sampling Station GA-4

E-20B Station GA-4, Mineralization Sampling

E-20C Photomicrograph of Sample GA-4.1 (quartz phases  
with overgrowth)

E-21A Photo A: Outcrop View of Sampling Station MS-116  
Photo B: Close-up of Sampling Station MS-116-2

E-21B Station MS-116, Mineralization Sampling

E-21C Photomicrograph of Sample MW-116-2

E-22A Photo A: Outcrop North of Reactor No. 2 - Sample  
Location FS-10  
Photo B: Close-up of Sample Location FS-10

E-22B Photomicrographs of Sample FS-10

E-23A Photo A: Outcrop View of Sampling Station GA-9  
Photo B: Close-up of Sample GA-9.1

E-23B Station GA-9, Mineralization Sampling

E-23C Photo A: Photomicrograph of Sample GA-9.1

E-24A Photo A: Outcrop North of Reactor No. 3 - Sample Location FS-11  
Photo B: Close-up of Sample Location FS-11

E-24B Photomicrograph of Sample FS-11

E-25A Photo A: Outcrop North of Reactor No. 2 - Sample Location FS-8  
Photo B: Close-up of Sample Location FS-8

E-25B Photomicrograph of Sample FS-8

E-26A Photo A: Outcrop North of Reactor No. 3 - Sample Locations FS-3 and FS-4  
Photo B: Sample Location FS-3 and FS-4

E-26B Photo A: Close-up of Sample Location FS-3  
Photo B: Close-up of Sample Location FS-4

E-26C Photomicrograph of Sample FS-3

E-26D Photomicrograph of Sample FS-4

E-27A Photo A: Outcrop North of Reactor No. 3 - Sample Location FS-1  
Photo B: Close-up of Sample Location FS-1

E-27B Photomicrograph of Sample FS-1

E-28A Photo A: Outcrop North of Reactor No. 3 - Sample Location FS-5  
Photo B: Close-up of Sample Location FS-5

E-28B Photomicrograph of Sample FS-5

E-29A Photo A: Outcrop Adjacent to Turbogenerator Building No. 1 - Sample Location FS-6  
Photo B: Close-up of Sample Location FS-6

E-29B Photomicrograph of Sample FS-6

E-30A Photo A: Outcrop North of Reactor No. 3 - Sample Location FS-2  
Photo B: Close-up of Sample Location FS-2

E-30B Photomicrograph of Sample FS-2

- E-31A      Photo A: Outcrop View of Sampling Station GA-8  
            Photo B: Close-up of Samples GA-8.1 and GA-8.3
- E-31B      Station GA-8, Mineralization Sampling
- E-31C      Photo A: Photomicrograph of Sample GA-8.1  
            Photo B: Photomicrograph of Sample GA-8.1 -  
                    showing euhedral, undeformed calcite exhibiting  
                    twin lamellae
- E-31D      Photo A: Photomicrograph of Sample GA-8.3
- E-32A      Photo A: Outcrop View of Sampling Station GA-11  
            Photo B: Close-up of Sample GA-11.3  
            Photo C: Close-up of Sample GA-11.4
- E-32B      Photo A: Close-up of Sample GA-11.1  
            Photo B: Close-up of Sample GA-11.2
- E-32C      Station GA-11, Mineralization Sampling
- E-32D      Photo A: Photomicrograph of Sample GA-11.1  
            Photo B: Photomicrograph of Sample GA-11.2
- E-32E      Photo A: Photomicrograph of Sample GA-11.3  
            Photo B: Photomicrograph of Sample GA-11.3  
                    showing undeformed vein calcite
- E-32F      Photo A: Photomicrograph of Sample GA-11.4A
- E-32G      Photo A: Photomicrograph of Sample GA-11.4B  
            Photo B: Close-up of area outlined in Photo A:  
                    showing undeformed vein calcite - note twin  
                    lamellae
- E-33A      Photo A: Outcrop View of Sampling Station GA-12  
            Photo B: Close-up of Sample GA-12.1
- E-33B      Station GA-12, Mineralization Sampling
- E-33C      Photo A: Photomicrograph of Sample GA-12.1
- E-34      Photo A: Outcrop North of Reactor No. 2 - Sample  
            Location FS-9  
            Photo B: Close-up of Sample Location FS-9
- E-35      Photo A: Outcrop Adjacent to Turbogenerator  
            Building No. 1 - Sample Location FS-12  
            Photo B: Close-up of Sample Location FS-12

- E-36A      Photo A: Outcrop North of Reactor No. 2 - Sample Location FS-13  
            Photo B: Close-up of Sample Location FS-13
- E-36B      Photomicrograph of Sample FS-13
- E-37A      Photo A: Outcrop Adjacent to Turbogenerator Building No. 1 - Sample Location FS-7  
            Photo B: Close-up of Sample Location FS-7
- E-37B      Photomicrograph of Sample FS-7
- E-38A      Photo A: Outcrop View of Sampling Location MS-112  
            Photo B: Close-up of Sampling Station MW-112.1
- E-38B      Photomicrograph of Sample MW-112-1

#### APPENDIX F

- F-1A & B      Surficial Geology Reconnaissance Map
- F-2          Diagrammatic Sections Showing Evidence Used to Identify Lake Hudson Shoreline
- F-3          Profile Showing Upwarped Lake Hudson shoreline
- F-4          Map of Pleistocene Deposits, Jones Point
- F-5          Cross-Section of Delta Deposits 225-6, Quarry at Jones Point
- F-6          Sketch of Slump Feature 224-2, Jones Point
- F-7          Slump Feature 224-2, Jones Point
- F-8          Disturbed Lacustrine Deposits 226-2, Jones Point
- F-9          Rock Bench Cross Sections
- F-10        Trench A - Mott Farm Road
- F-11        Photograph Trench A - Mott Farm Road
- F-12        Trench B - Mott Farm Road
- F-13        Photograph Trench B - Mott Farm Road
- F-14        Map: Showing Location of Water Line Breaks at Immaculate Conception

- F-15            Sketches of Trench at Stag Hill
- F-16            Photograph of Trench at Stag Hill
- F-17            Location Map of Sand and Gravel Quarries Contain-  
ing Pleistocene Deposits Along the Ramapo Fault  
Zone, Pequannock, N.J.
- F-18            Photo Mosaic of Pleistocene Deposits in Quarry,  
Pequannock, N.J.
- F-19            Map View of Central Nyack Outcrop
- F-20            Photos:    South End of Central Nyack Outcrop

#### APPENDIX G

- G-1            Epicenter Map of Northeastern United States
- G-2            Seismicity of Southeastern New York and Northern  
New Jersey
- G-3            Different Solutions for the Locations of Septem-  
ber 3, 1951 and March 11, 1976 Earthquakes
- G-4            Focal Mechanism for the July 19, 1975  
Earthquake - Lower Hemisphere Projection
- G-5            Focal Mechanism for the March 11, 1976  
Earthquake - Lower Hemisphere Projection
- G-6            Focal Mechanism for the March 12, 1976  
Earthquake - Lower Hemisphere Projection
- G-7            Focal Mechanism for the April 13, 1976  
Earthquake - Lower Hemisphere Projection
- G-8            Focal Mechanism for the August 20, 1976  
Earthquake - Upper Hemisphere Projection
- G-9            Focal Mechanism for the September 22, 1976  
Earthquake - Upper Hemisphere Projection
- G-10           Focal Mechanism for the November 22, 1976  
Earthquake - Upper Hemisphere Projection
- G-11           Fault Plane Solutions for Earthquakes in the  
Region around the Ramapo Fault

#### APPENDIX H

- H-1            Location of Test Site

H-2	Boring Log, Site 3, Hole 1
H-3	Boring Log, Site 3, Hole 2
H-4	Boring Log, Site 4, Hole 1
H-5	Boring Log, Site 9, Hole 2
H-6	Boring Log, Site 9, Hole 1
H-7	Boring Log, Site 9, Hole 3
H-8	Boring Log, Site 11, Hole 1
H-9	Boring Log, Site 11, Hole 2
H-10	Boring Log, Site 14, Hole 1
H-11	Boring Log, Site 14, Hole 2
H-12	Overcoring Schematic, Borehole Deformation Gauge
H-13	Typical Overcore Results
H-14	Schematic: Bi-Axial Test Apparatus
H-15	Modulus of Deformation, Site 3, Test 2, Axis 1
H-16	Modulus of Deformation, Site 3, Test 2, Axis 2
H-17	Modulus of Deformation, Site 3, Test 2, Axis 3
H-18	Modulus of Deformation, Site 3, Test 3, Axis 1
H-19	Modulus of Deformation, Site 3, Test 3, Axis 2
H-20	Modulus of Deformation, Site 3, Test 3, Axis 3
H-21	Modulus of Deformation, Site 3, Test 4, Axis 1
H-22	Modulus of Deformation, Site 3, Test 4, Axis 2
H-23	Modulus of Deformation, Site 3, Test 4, Axis 3
H-24	Modulus of Deformation, Site 3, Test 5, Axis 1
H-25	Modulus of Deformation, Site 3, Test 5, Axis 2
H-26	Modulus of Deformation, Site 3, Test 5, Axis 3
H-27	Modulus of Deformation, Site 3, Test 6, Axis 1

§

H-28	Modulus of Deformation, Site 3, Test 6, Axis 2
H-29	Modulus of Deformation, Site 3, Test 6, Axis 3
H-30	Modulus of Deformation, Site 3, Test 7, Axis 1
H-31	Modulus of Deformation, Site 3, Test 7, Axis 2
H-32	Modulus of Deformation, Site 3, Test 7, Axis 3
H-33	Modulus of Deformation, Site 3, Test 9, Axis 1
H-34	Modulus of Deformation, Site 3, Test 9, Axis 2
H-35	Modulus of Deformation, Site 3, Test 9, Axis 3
H-36	Modulus of Deformation, Site 3, Test 10, Axis 1
H-37	Modulus of Deformation, Site 3, Test 10, Axis 2
H-38	Modulus of Deformation, Site 3, Test 10, Axis 3
H-39	Modulus of Deformation, Site 9, Test 1, Axis 1
H-40	Modulus of Deformation, Site 9, Test 1, Axis 2
H-41	Modulus of Deformation, Site 9, Test 1, Axis 3
H-42	Modulus of Deformation, Site 9, Test 3, Axis 1
H-43	Modulus of Deformation, Site 9, Test 3, Axis 2
H-44	Modulus of Deformation, Site 9, Test 3, Axis 3
H-45	Modulus of Deformation, Site 9, Test 4, Axis 1
H-46	Modulus of Deformation, Site 9, Test 4, Axis 2
H-47	Modulus of Deformation, Site 9, Test 4, Axis 3
H-48	Modulus of Deformation, Site 9, Test 7, Axis 1
H-49	Modulus of Deformation, Site 9, Test 7, Axis 2
H-50	Modulus of Deformation, Site 9, Test 7, Axis 3
H-51	Modulus of Deformation, Site 11, Test 1, Axis 1
H-52	Modulus of Deformation, Site 11, Test 1, Axis 2
H-53	Modulus of Deformation, Site 11, Test 1, Axis 3

H-54	Modulus of Deformation, Site 11, Test 2, Axis 1
H-55	Modulus of Deformation, Site 11, Test 2, Axis 2
H-56	Modulus of Deformation, Site 11, Test 2, Axis 3
H-57	Modulus of Deformation, Site 11, Test 3, Axis 1
H-58	Modulus of Deformation, Site 11, Test 3, Axis 2
H-59	Modulus of Deformation, Site 11, Test 3, Axis 3
H-60	Modulus of Deformation, Site 11, Test 4, Axis 1
H-61	Modulus of Deformation, Site 11, Test 4, Axis 2
H-62	Modulus of Deformation, Site 11, Test 4, Axis 3
H-63	Modulus of Deformation, Site 11, Test 5, Axis 1
H-64	Modulus of Deformation, Site 11, Test 5, Axis 2
H-65	Modulus of Deformation, Site 11, Test 5, Axis 3
H-66	Modulus of Deformation, Site 11, Test 6, Axis 1
H-67	Modulus of Deformation, Site 11, Test 6, Axis 2
H-68	Modulus of Deformation, Site 11, Test 6, Axis 3
H-69	Modulus of Deformation, Site 11, Test 7, Axis 1
H-70	Modulus of Deformation, Site 11, Test 7, Axis 2
H-71	Modulus of Deformation, Site 11, Test 7, Axis 3
H-72	Modulus of Deformation, Site 11, Test 8, Axis 1
H-73	Modulus of Deformation, Site 11, Test 8, Axis 2
H-74	Modulus of Deformation, Site 11, Test 8, Axis 3
H-75	Modulus of Deformation, Site 11, Test 9, Axis 1
H-76	Modulus of Deformation, Site 11, Test 9, Axis 2
H-77	Modulus of Deformation, Site 11, Test 9, Axis 3
H-78	Modulus of Deformation, Site 11, Test 10, Axis 1

H-79	Modulus of Deformation, Site 11, Test 10, Axis 2
H-80	Modulus of Deformation, Site 11, Test 10, Axis 3
H-81	Modulus of Deformation, Site 11, Test 11, Axis 1
H-82	Modulus of Deformation, Site 11, Test 11, Axis 2
H-83	Modulus of Deformation, Site 11, Test 11, Axis 3
H-84	Modulus of Deformation, Site 11, Test 12, Axis 1
H-85	Modulus of Deformation, Site 11, Test 12, Axis 2
H-86	Modulus of Deformation, Site 11, Test 12, Axis 3
H-87	Modulus of Deformation, Site 11, Test 13, Axis 1
H-88	Modulus of Deformation, Site 11, Test 13, Axis 2
H-89	Modulus of Deformation, Site 11, Test 13, Axis 3
H-90	Modulus of Deformation, Site 14, Test 2, Axis 1
H-93	Modulus of Deformation, Site 14, Test 3, Axis 1
H-94	Modulus of Deformation, Site 14, Test 3, Axis 2
H-95	Modulus of Deformation, Site 14, Test 3, Axis 3
H-96	Modulus of Deformation, Site 14, Test 5, Axis 1
H-97	Modulus of Deformation, Site 14, Test 5, Axis 2
H-98	Modulus of Deformation, Site 14, Test 5, Axis 3
H-99	Modulus of Deformation, Site 14, Test 7, Axis 1
H-100	Modulus of Deformation, Site 14, Test 7, Axis 2
H-101	Modulus of Deformation, Site 14, Test 7, Axis 3
H-102	Overcore Test Results, Site 3, Test 1
H-103	Overcore Test Results, Site 3, Test 2
H-104	Overcore Test Results, Site 3, Test 3
H-105	Overcore Test Results, Site 3, Test 4

H-106	Overcore Test Results, Site 3, Test 5
H-107	Overcore Test Results, Site 3, Test 6
H-108	Overcore Test Results, Site 3, Test 7
H-109	Overcore Test Results, Site 3, Test 8
H-110	Overcore Test Results, Site 3, Test 9
H-111	Overcore Test Results, Site 3, Test 10
H-112	Overcore Test Results, Site 9, Test 1
H-113	Overcore Test Results, Site 9, Test 2
H-114	Overcore Test Results, Site 9, Test 3
H-115	Overcore Test Results, Site 9, Test 4
H-116	Overcore Test Results, Site 9, Test 5
H-117	Overcore Test Results, Site 9, Test 6
H-118	Overcore Test Results, Site 9, Test 7
H-119	Overcore Test Results, Site 11, Test 1
H-120	Overcore Test Results, Site 11, Test 2
H-121	Overcore Test Results, Site 11, Test 3
H-122	Overcore Test Results, Site 11, Test 4
H-123	Overcore Test Results, Site 11, Test 5
H-124	Overcore Test Results, Site 11, Test 6
H-125	Overcore Test Results, Site 11, Test 7
H-126	Overcore Test Results, Site 11, Test 8
H-127	Overcore Test Results, Site 11, Test 9
H-128	Overcore Test Results, Site 11, Test 10
H-129	Overcore Test Results, Site 11, Test 11
H-130	Overcore Test Results, Site 11, Test 12

H-131	Overcore Test Results, Site 11, Test 13
H-132	Overcore Test Results, Site 14, Test 1
H-133	Overcore Test Results, Site 14, Test 2
H-134	Overcore Test Results, Site 14, Test 3
H-135	Overcore Test Results, Site 14, Test 4
H-136	Overcore Test Results, Site 14, Test 5
H-137	Overcore Test Results, Site 14, Test 6
H-138	Overcore Test Results, Site 14, Test 7
H-139	Average Strike of Horizontal Component of Maximum Compression

SECTION 1.0

INTRODUCTION

## 1.0 INTRODUCTION

During the period of January, 1976 to January 1977, Dames & Moore conducted a supplemental geotechnical investigation of the Ramapo Fault System including the region of the Indian Point Generating Station (Plates 1A and 1B, Volume II). The investigation was authorized by Consolidated Edison Company of New York, Inc. The results of previous site geologic investigations have been summarized in the report entitled "Supplemental Geological Investigations of the Indian Point Generating Station", dated November, 1975.

The intent of the investigation, as outlined in our proposal dated January 13, 1976, is to determine, if possible, whether or not evidence exists which is indicative of surface displacement during the past 500,000 years along faults that are herein collectively grouped as members of the Ramapo Fault System.

The immediate objectives of the investigation are to:

- 1) Perform geological mapping in sufficient scope and detail to determine, if possible:
  - a) the main trace of the Ramapo Fault and associated faults of the Ramapo Fault System;
  - b) the structural and tectonic relationship of the Ramapo Fault System with faults at the Indian Point site; and

- c) cross-cutting relationships which might be used to determine the age of last movement on faults of the Ramapo Fault System, and along faults in the area of the 1951 Rockland County, New York earthquake and the 1976 Pompton Lakes, New Jersey earthquake.
- 2) Determine, if possible, the age of most recent movement or minimum age of most recent movement on faults of the Ramapo Fault System by appropriate dating techniques and geologic relationships.
- 3) Attempt to determine the relationship of current and historic seismicity to faults of the Ramapo Fault System.
- 4) Perform stress measurements to assess the current tectonic environment of the area.
- 5) Determine, if possible, additional geochronological age dates and perform fluid inclusion studies on samples taken from faults in the immediate vicinity of the site.

To achieve these objectives, an integrated program of geological and geophysical investigations was conducted. This program included:

- 1) Supplemental and ongoing review of literature.
- 2) Reconnaissance and detailed mapping along the Ramapo Fault System.
- 3) Petrographic studies.

- 4) Ground magnetometer studies.
- 5) Seismic reflection profiling.
- 6) Bathymetric survey of the Hudson River in the vicinity of the site.
- 7) Low level aeromagnetic survey.
- 8) Synthesis and evaluation of gravity data.
- 9) Regional reconnaissance and selected detailed geomorphic investigations.
- 10) Minerologic studies.
- 11) Geochemical (fluid inclusion) and radiometric age dating studies.
- 12) In situ stress measurements.
- 13) Collection and evaluation of "Ramapo" related seismic data.

Consultants with specialized technical skills were retained to supplement the investigation. Principal among these were: Dr. Andreas Haji Vassiliou - consultant in x-ray diffraction mineral identification; Krueger Enterprises, Inc. - radiometric age determinations; Dr. H.L. Barnes - consultant for fluid inclusion analysis; Dr. N. Opdyke - performed measurements on magnetic susceptibility and maximum remanent magnetic intensity; Airmag Surveys, Inc. of Philadelphia, Pennsylvania - conducted the aeromagnetic survey; Atlantic Geophysical Co. of Philadelphia, Pennsylvania - performed the compilation of aeromagnetic survey data; Target Survey, Inc. of Houston, Texas - conducted reflection seismic profiling; Seismograph Services

Corp. of Houston, Texas - performed the data processing and production of seismic profiles.

The remainder of this report is presented in two parts. The first part, Summary (Section 2.0), describes Dames & Moore's conclusions and interpretations in general terms - an overview, not an in-depth evaluation. The second part, which consists of Appendices A through H, is technical and provides the documentation necessary for a thorough evaluation. For convenience the text, attachments, and tables are contained in Volume I and the corresponding plates in Volume II.

SECTION 2.0

SUMMARY

## 2.0 SUMMARY

### 2.1 GENERAL

This investigation was designed to collect all possible data that could be used 1) to define the main trace of the Ramapo Fault and associated faults of the Ramapo Fault System and 2) to establish the geologic history of the Ramapo Fault System. A major effort of the study was the location and description of the Fault System within the area surrounding the Indian Point Generating Station (Plates 1 A&B and 2 A&B). This was done in order to identify the nature and character of the youngest orogenic displacement along the Ramapo Fault or along members of the Ramapo Fault System, and to establish whether or not evidence exists which is indicative of tectonic surface displacement along the Ramapo Fault System during the past 500,000 years.

### 2.2 REGIONAL GEOLOGIC SETTING

The area of this investigation covers portions of Rockland, Westchester and Putnam Counties, New York, and Bergen and Passaic Counties, New Jersey. The rock units which crop out within that area can be classified into three groups: the Hudson Highlands, the Manhattan Prong and the Newark Basin. The Hudson Highlands, which are part of the Reading Prong, consist of paragneisses and orthogneisses of Precambrian age. The Manhattan Prong generally consists of early Paleozoic metasediments that were deposited unconformably on top of Precambrian

rocks. The Newark Basin contains continental sedimentary strata, and intrusive and extrusive diabase and basalt of Triassic age. The fact that the rocks of these three geologic subdivisions are separated by various zones of the Ramapo Fault System illustrates the fundamental importance of that system through geologic time. Where these faults are exposed, they are characterized by intense cataclasis, mylonitization, shearing, sometimes open work breccia, and less frequently, gouge. The field relationships between these different deformational fabrics suggest that these cataclastic effects did not all form simultaneously, but were formed during several deformational episodes and correspond to a cumulative effect of reoccurring tectonism.

### 2.3 PRECAMBRIAN FAULTS

On the basis of field observations made during this investigation, two separate Precambrian episodes of faulting have been recognized (Appendix A). The older episode is represented by the cataclasis of rocks during the Grenville Orogeny, broadly synchronous with the intrusion of local pegmatites and diorite-monzonite rocks of the Canopus Pluton. Ductile deformation during the Grenville Orogeny, which affected gneisses and plutonic rocks alike, recrystallized and healed these cataclastic fault zones. The younger episode of faulting is represented by a late Precambrian phase of cataclasis and diaphoresis, which is marked by the re-utilization of the older, Grenvillian fault zones. This younger episode of faulting probably represents the effects of Late Precambrian rifting along the

continental margin. Faults belonging to the Precambrian Ramapo-Canopus Fault System are shown on a generalized and simplified tectonic map of the system in the Peekskill area, N.Y. (Plate A-7).

#### 2.4 PALEOZOIC FAULTS

During Late Precambrian to Early Ordovician time, the sediments of the Poughquag-Lowerre (quartzite) and the Wappingers-Inwood (limestone/marble) formations were deposited along the stable continental margin (Appendix A). Orogenic uplift of the continent in Middle Ordovician time interrupted sedimentation on the great carbonate bank represented in this area by the Wappingers-Inwood sequence. Block faulting, attendant with uplift, caused the break-up of the carbonate bank resulting in a major unconformity. The Annsville-Manhattan (phyllite/schist) exogeosynclinal sequence was deposited on top of this unconformity.

The next recognizable phase of deformation is characterized by a predominance of crustal shortening, resulting in horizontal translation, development of  $F_1$  and  $F_2$  folds and a westward thrust of the Manhattan Prong. The sharp truncation of the aerial extent of Paleozoic folding by the Ramapo System suggests its participation in reverse faulting. Northeast of the Hudson River, the Annsville, Peekskill Hollow, Canopus Hollow, and Dennytown Faults acted, at that time, as high angle reverse fault zones in which slices of Paleozoic metasediments

are preserved as outliers between upfaulted blocks of Precambrian gneiss. The activity on many of these faults was controlled by the pre-existing members of the Ramapo-Canopus System of faults. This phase of deformation is thought to be both syn- and post-regional metamorphism. This interpretation is based on the character of  $F_1$  folds and the steepness (increasing to the east) of the Taconic metamorphic gradient east of the Ramapo System.

Reverse faulting was followed by regional dextral transcurrent faulting along the Ramapo-Canopus Fault System. This northeast-trending fault system was linked by several synthetic ENE to E-W-trending fault zones to a second en echelon fault system; the Croton Falls Fault System, further east (Plate A-8). Transcurrent fault movements along these fault systems re-utilized and in some instances cross-cut the earlier reverse faults. The most prominent faults involved in this episode of deformation were the Canopus Hollow and Dennytown Faults, the Oscawana-Annsville-Thiells Faults, the Peekskill Hollow Fault, and the Peekskill and Croton Falls Faults. The Cortlandt and Rosetown plutons, lamprophyre dike swarms, the Peekskill Granite and its pegmatitic differentiates, the Croton Falls complex, and the Peach Lake intrusive were emplaced along various fault zones of the fault systems (Plate A-8). The ages of these igneous rocks range from 435 m.y. to 371 m.y. In summary, all the northeast and east-northeast striking fault zones of the Ramapo-Canopus and Croton Falls systems appear to have been active during this dextral transcurrent event (Plate A-8).

## 2.5 MESOZOIC REACTIVATION

The pattern of the faults that were reactivated during Mesozoic time is interpreted to be the result of dip-slip and sinistral movements along the major northeast trending zones of the Ramapo and Croton Falls Fault Systems (Plate A-9). The fault zones of the Canopus System seem to have played a limited role during this reactivation. The deflection of Mesozoic deformation around the Rosetown Pluton was accomplished through the utilization of north-northeast trending synthetic shears and northeast trending major shears (Appendix A). Evidence from within the Newark Basin (Appendices B and C) indicate that northeast sinistral wrench faulting may have occurred during and did occur after the sedimentation and lithification of the Newark strata and the emplacement and cooling of the Triassic-Jurassic diabase and basalt.

Although Mesozoic deformation along the east-northeast trending Letchworth and Mott Farm Road Faults is inconsistent with an idealized model of a northeast sinistral wrench fault, data obtained from Pompton Lakes, N.J. (Appendix C) and Peekskill, N.Y. (Appendix A) suggest that Paleozoic east-northeast zones were utilized for dip-slip adjustments. This left-lateral episode of faulting probably represents the effects of on-going rifting in the central portion of the Appalachian Orogen during the Mesozoic.

## 2.6 WANING OF OROGENIC FAULT MOVEMENTS

The Newark Basin, in Rockland County, developed and was deformed during the Mesozoic Era. The initial subsidence

of the basin was syn-sedimentary (as evidenced by the coarser clastic material along the western margin). This early period of basining and normal faulting was gradually replaced by a period of pervasive left-lateral faulting.

The Palisades and Watchung igneous events appear to have occurred in the transition from basining to strike-slip faulting. In this context, a drastic decrease in the rate of sediment accumulation after the First Watchung flow may reflect the change from predominantly dip-slip to strike-slip faulting along the Ramapo Fault. That the strike-slip movements had begun at least by the time of the intrusion of the Palisades diabase is evidenced by deformed cooling-attendant mineralization in the Rockland Lake Fault, where it passes through the Palisades (Appendix B). Igneous activity, as well as sedimentation, slowed down and eventually stopped altogether before the complete cessation of movements along the fault-members of the left-lateral simple shear system.

By Middle to Upper Cretaceous time, fault movements ceased, as evidenced by the lack of deformation in the low-temperature hydrothermal mineralization which fills faults and shears. The separation of the older mineralization from the wall rock and the crystallization of a new drusy phase may also be indicative of the relaxation of the orogenic stress system in Upper Cretaceous time (Appendix B).

The main trace of the Ramapo Fault in Rockland County, N.Y., follows the northwestern edge of the Newark Basin from

Suffern to Ladentown, N.Y. At Ladentown, the present basin margin swings east-northeasterly away from the Ramapo Fault until it crosses and becomes subparallel to the Thiells Fault branch of the Ramapo Fault System. The Rockland Lake, Trough Hollow, and Hook Mountain Faults are associated with the Croton Falls Fault System (Plate 1 A&B), and are therefore indirectly associated with the Ramapo Fault System.

The tectonic function of the Ramapo Fault during Late Triassic time is interpreted to be primarily as a normal fault with an active role in the development and filling of the Newark Basin. From Late Triassic to Late Jurassic, the Ramapo and Thiells Faults of the Ramapo Fault System and the Long Clove, Trough Hollow, Rockland Lake and Hook Mountain Faults of the Croton Falls Fault System were left-lateral, strike-slip faults. Thus, it is reasonable to conclude that smaller faults in the Indian Point site area (which lies between these two systems) experienced Mesozoic movements related to left-lateral movement on the main faults. Although no faults have been found which cross-cut the Ramapo, Thiells, Trough Hollow, Rockland Lake or Hook Mountain Faults, analysis of mineral samples taken from within the zones of these faults indicates that movement on them had ceased by Late Cretaceous time.

## 2.7 GEOPHYSICAL INVESTIGATIONS

The geophysical surveys helped define, in an indirect way, the tectonic framework of the region. Four sets of aeromagnetic lineaments were identified; these are: a northeast

set, an east-northeast set, a north-south set and a northwest set. Angular intersections and cross-cutting relationships between these sets support the geologic conclusion that a period of right lateral movement preceded a period of left lateral movement (Appendices A, B and C). During the two periods of movements, the northeast trend was the orientation of the major shear. The relationship of the various sets relative to the Rosetown Pluton indicates that right lateral movement generally predates, while left lateral movement postdates the intrusion of the Rosetown Pluton. Left lateral movement along the northeast trend appears to have been deflected westward around the main body of the intrusion. These results, together with the interpretations of the gravity data and the identification and location of fault zones on the seismic reflection and ground magnetometer profiles (Appendix D), support the geologic field observations presented in Appendices A, B and C.

## 2.8 AGE DATING

Where possible, radiometric (K-Ar) age determinations have been made on fault and shear-filling minerals in an attempt to assign an "absolute minimum age" to the most recent movements (Appendix E). This information is particularly useful when evaluated in light of the regional paragenesis and co-genetic mineral assemblages discussed in Appendix B.

As illustrated by an early stage of mineral assemblages (Stage I), the existence of a mixed population of deformed

and undeformed minerals filling faults and shears should be considered as diagnostic of mineralization predating or synchronous with tectonic activity. In this particular case, it is believed that the Stage I mineralization was syntectonic, and that the tectonism was synchronous with igneous activity. On the other hand, the existence of a distinctive mineral assemblage, for which there is a reasonable sampling density and complete absence of any deformation, should be interpreted as representing an event that postdates the last geologically recorded tectonic and fault activity. This is illustrated by a later mineral assemblage (Stage II) which, in the Mesozoic host rocks, is distinguished by the occurrence of analcite, datolite or apophyllite and an average fluid inclusion filling temperature in the 110°C to 150°C temperature range. Since the formation of these mineral assemblages is related to the waning stages of igneous activity in the study area, it is likely that the age of the last tectonic activity is close to that of the Third Watchung flow, or approximately  $142 \pm 10$  m.y. (Appendix E).

Age determination performed on zeolites (primarily stilbite) associated with the Stage II mineralization gave widely varying ages (ranging from  $73.3 \pm 5.1$  m.y. to  $2.1 \pm 0.5$  m.y.). Because of its open crystallographic structure and affinity for cation exchange, stilbite is prone to argon leakage and potassium concentration. Both of these characteristics result in anomalously young ages and therefore, age determinations on stilbite should be considered as minimum ages. The

stilbite associated with the Stage II mineralization is therefore at least 73 m.y. old and probably older (Appendix E).

The apophyllite mineral age of  $92 \pm 5$  m.y. may better approximate the age of the post-tectonic Stage II mineralization.

## 2.9 PLEISTOCENE AND HOLOCENE RECORDS

Along most of its length, the Ramapo Fault is overlain by relatively thick Wisconsinan ground moraine with scattered deposits of stratified drift and Holocene alluvium (Appendix F). In the Pompton Lakes, N.J. area, the deposits are predominantly stratified drift (glacio-fluvial outwash and kame terraces, shoreline deposits of proglacial Lake Passaic and glacially related deltaic deposits). The Letchworth and Thiells Faults are overlain by Wisconsinan ground moraine and Holocene alluvium, while the Annsville Fault (near Peekskill) is overlain by ground moraine and stratified drift. The Peekskill and Peekskill Hollow Faults (near Peekskill) are covered predominantly by stratified drift related to proglacial Lake Hudson. Based on detailed examination, the stratified deposits were not observed to be interrupted by tectonic faulting.

Surveyed shore remnants of proglacial Lake Hudson indicate that the shoreline is presently uniformly upwarped to the north at 4.17 feet/mile, which is in accord with post-glacial regional uplift and local rebound. In areas where the remnants cross the Annsville, Peekskill and Mott Farm Road Faults, no offsets were detected when comparing the elevations of shoreline segments.

Geomorphic features were studied at Jones Point, N.Y., and Mott Farm Road (near the Mott Farm Road Fault). Water line breaks were investigated at the Immaculate Conception Seminary, at Darlington, N.J. (near the Ramapo Fault). These features were determined to be most probably of non-tectonic origin (Appendix F).

A trench at Stag Hill and a large sand and gravel pit wall at Pequannock-Pompton Lakes (adjacent to and across the Ramapo Fault, respectively) were examined for evidence of faulting related to movement on the Ramapo Fault. None was found. The pop-ups and the open fissure at Central Nyack, N.Y., are the only features that appear to have developed post-glacially. These features are discontinuous, of small dimensions, and not associated with mapped regional faults.

## 2.10 CONTEMPORARY SEISMICITY

The distribution of earthquake epicenters in the vicinity of the Ramapo Fault and surrounding region (Plate G-1 and G-2) is irregular and shows no noticeable concentration of earthquakes over the mapped extent of the fault. There may, in fact, be more noticeable concentrations in areas removed from the mapped surface trace of the Ramapo Fault.

Fault plane solutions (Plate G-11) show that the range of focal solutions is wide and the data are few and poorly distributed. It is therefore concluded that based on the existing data, correlation between individual focal mechanisms specifically and between focal mechanisms and fault geometry in general, is speculative at best.

The earthquakes which have occurred near the Ramapo Fault System are small in both number and intensity or magnitude. None of the earthquakes in the vicinity of the Ramapo Fault System is known to have been accompanied by surface faulting or any other observable geological effect. Therefore, no special significance can be ascribed to the Ramapo Fault in relation to contemporary seismicity and tectonics of the region. Although there exist instrumental records from which earthquake locations can be determined with reasonable precision, we conclude that these earthquakes are small in both number and magnitude and that their relationship to the Ramapo Fault is, at best, a matter of speculation.

#### 2.11 IN SITU STRESS MEASUREMENTS

The in situ stresses were measured at four sites, which surround the Indian Point Generating Station. These measurements indicate that there is as much variation in the magnitude of near surface lateral stresses at individual sites as there is from one site to another. The trend of the horizontal component of maximum compression, however, appears to be somewhat more consistent, varying between northeast and east-west.

The stress pattern appears to be complicated in the Appalachian Mountain system because in situ measurements appear to record the resultant of more than one stress component. Several components contribute to the total in-situ stress field measured at any one location. The most important are: a) a gravitational component, b) residual and/or remanent component(s) and c) an applied tectonic component. At present, there

is no quantitative method to separate the effects of remanent and residual components from the applied tectonic component. The correlation between near surface measurements and stress conditions at depth (which presumably generate the earthquakes) is, at best, speculative at the present time.

## 2.12 CONCLUSION

As a result of the investigations presented in the appendices, the following conclusions may be reached relative to the immediate objectives stated in Section 1.0:

- 1) The Ramapo Fault System southwest of Thiells, N.Y., consists of the main, northeast trending trace of the Ramapo Fault and several north trending faults through the Watchung Mountains (Plates 1 A&B). Between Thiells, N.Y. and the Hudson River, the Ramapo Fault System branches on either side of the Rosetown Pluton, with one branch continuing on strike via the Willow Grove, Blanchard Road, Cedar Flats, Ambreys Pond and Timp Pass Faults. The other branch passes southeast of the surface exposure Rosetown Pluton via the Letchworth and Thiells Faults (the latter is en echelon to the Ramapo Fault). North of the Rosetown Pluton, the branches merge with the east northeast-trending Mott Farm Road Fault, which reappears on the eastern shore of the Hudson River as the Peekskill Fault. North of

Peekskill, the Ramapo Fault system continues, as the Canopus and Annsville-Oscawanna Faults, as far as Canopus Lake, where it is joined by the Dennytown Fault (Plate 1A). The Peekskill Fault turns to the east southeast and connects the Ramapo Fault System with the Croton Falls Fault System at Yorktown Heights, N.Y.

Thus, the Indian Point site lies between two en echelon fault systems (the Ramapo-Canopus and Croton Falls Systems) which are connected by the Peekskill Fault. The faulting at the site, therefore, appears to be lesser dislocations between the two major systems.

The Ramapo and Thiells Faults of the Ramapo Fault System and the Long Clove, Trough Hollow, Hook Mountain and Rockland Lake Faults of the Croton Falls Fault System have disrupted the Trio-Jurassic sedimentary and igneous rocks of the Newark Basin (Plates 1 A&B). (Trio-Jurassic, as used herein, refers to the Late Triassic through Late Jurassic time span covered by the Newark Group, as determined from palynologic and radiometric data.) All of these faults, however, are overlain by Wisconsinan deposits (ground moraine, stratified drift and proglacial lake deposits).

No tectonically related offsets of these deposits were determined.

- 2) The minimum age of the most recent movement on faults of the Ramapo and Croton Falls Fault Systems, based on radiometric and fluid inclusion analyses of undeformed mineralization within fault zones on and off site is Late Cretaceous (90 to 70 m.y.).
- 3) No special significance can be ascribed to the Ramapo Fault in relation to the contemporary seismicity and tectonics of the region. The earthquakes which have occurred near the Ramapo Fault System are of small magnitude and none is known to have been accompanied by surface rupture.
- 4) The average trend of the major horizontal compressive stress axis measured at four sites around Indian Point is northeast-southwest. The near surface lateral stresses were quite variable and tensile stresses were noted in at least one measurement at each site. Given the high variability of the stress vectors between different sites and between tests made at any individual site, and the manifestation of tensile stresses at each site, the average magnitudes of lateral stresses are not considered to be representative of the magnitude of principal stresses at depth.

- 5) As noted in 2) above, additional sampling of fault healing mineralization on-site and in the Newark Basin indicates that a Cretaceous episode of hydrothermal mineralization (fluid inclusion filling temperatures 110° to 150°C) occurred throughout the region subsequent to the most recent pervasive tectonic activity.

Therefore, we conclude that a total evaluation of the results of the geotechnical investigations, conducted between January 1976 and January 1977, consistently indicates that the Ramapo Fault System is not capable within the meaning of Appendix A to 10 CFR Part 100.

APPENDIX A

THE RAMAPO SYSTEM IN ROCKLAND,  
WESTCHESTER, AND PUTNAM  
COUNTIES, NEW YORK

APPENDIX A  
THE RAMAPO SYSTEM IN ROCKLAND,  
WESTCHESTER AND PUTNAM COUNTIES  
NEW YORK

A1.0 INTRODUCTION AND GENERAL GEOLOGIC SETTING

The investigation of the Ramapo Fault System north of Ladentown, New York, was instituted because of the uncertainty of the structural and geometric relationships between its many branches.

The data collected pertaining to this problem were used in an effort to establish the geologic history of the Ramapo Fault System and to define whether or not there is any evidence indicative of recent surface displacement along any of the system's various branches. Geologic mapping was undertaken in sufficient scope and detail to define the main trace of the Ramapo Fault and associated faults of the system. In addition, the investigation was aimed at the identification of those features which may be used to determine the age of the most recent movement along the various branches of the Ramapo Fault System.

The area of this investigation covers portions of Rockland, Westchester and Putnam Counties, New York. The rock units which crop out within that area can be classified into three groups: the Hudson Highlands, the Manhattan Prong and the

Newark Basin (Plates 1A and B). The Hudson Highlands, which are the northeast extension of the Reading Prong, consist of paragneisses and orthogneisses of Precambrian age. The Manhattan Prong generally consists of early Paleozoic meta-sediments that were deposited unconformably on top of Precambrian rocks. The Newark Basin contains continental sedimentary strata, intrusive and extrusive diabase and basalt of Triassic-Jurassic age. The fact that the rocks of these three geologic subdivisions are separated by various zones of the Ramapo Fault System illustrates the fundamental importance of that system through geologic time. Where these faults are exposed they are characterized by intense cataclasis, mylonitization, shearing, sometimes open work breccia, and less frequently, gouge. The field relationships between these different deformational fabrics suggest that these cataclastic effects did not all form simultaneously, but were formed during several deformational episodes and correspond to a cumulative effect of recurring tectonism.

The principal results of the field investigation are graphically illustrated on Plates 1A and B. The data station locations are shown on Plates 2A and B.

## A2.0 LITHOLOGIES AND STRATIGRAPHY

### A2.1 HUDSON HIGHLANDS

The varied lithologies of the Hudson Highlands were not mapped in detail; however, several dominant lithologies in the Hudson Highlands were mapped in detail at a scale of 1:24,000. These are described below.

#### A2.1.1 Felsic Gneisses and Associated Intrusives

Four principal lithologies, all of which are Precambrian in age, underlie the Dunderberg-Manitou Mountains area. These consist of: a) quartz-feldspar (plagioclase  $\pm$  microcline)-diopside  $\pm$  epidote  $\pm$  hornblende gneiss, b) quartz-feldspar-biotite  $\pm$  garnet gneiss and its local anatectic derivatives, c) calc-silicate bearing quartz-rich rock and d) gneissic hornblende granite. The first three rock types represent members of the metamorphosed supracrustal suite into which the gneissic granite was emplaced.

Of the supracrustal suite the calc-silicate bearing quartz rock is particularly distinctive and, as such, will be described first. Compositionally it consists of abundant quartz, with orange-brown garnet, dark green clinopyroxene, epidote, scapolite, hornblende and feldspar. This unit crops out east of the Bear Mountain Bridge at the base of Anthony's Nose, and extends southward across the entire western end of Iona Island on to the north-facing slope of Dunderberg Mountain. From there it trends westward and is exposed both at the western end of Dunderberg Mountain and on adjacent Bald Mountain

(Plate 1A). On both mountains this unit is generally less common than white pegmatite. Between the mountains, as well as on top of Dunderberg Mountain, it is the host for pockets of a very coarse-grained, dark-green pyroxene-garnet rock. The pyroxene-garnet rock was also identified in the calc-silicate paragneiss at the northern end of Iona Island and at the base of Anthony's Nose.

The gneissic granite is also distinctive. It is pink and is composed of quartz, microcline, perthite and mesoperthite, and hornblende with or without free plagioclase. Generally the rock is coarse-grained and streaky, although there are textural variations in this intrusive body which range from medium to fine-grained gneiss, to pegmatite. The finer grained variety appears to be more prevalent near the granitic margins than in the interior.

Besides the aforementioned rocks, amphibolite, white granite and pegmatite, and minor quartzite constitute the remaining lithologies. Amphibolite commonly occurs as layers within the light colored quartz-feldspar-biotite paragneiss. The white granite and pegmatite are spatially related to the paragneiss and are interpreted as anatectic in origin. Pegmatite is especially common within and near the axial trace of the Bear Mountain synform and the Timp Pass Fault (Plate 1A), both of which are, in part, coincident.

In the Annsville-Canopus-Peekskill area, the predominant Precambrian lithology is a coarse to medium-grained, pink to gray biotite-quartz-feldspar leucogneiss. Sub-parallel

biotite flakes define foliation, but compositional layering is not clearly developed. Ratcliffe (1976) reports an age date of 1,250 m.y. on the basis of a preliminary whole rock isochron from this unit.

Quartzo-feldspathic pegmatites are often associated with felsic gneisses and are common in the Highlands near Peekskill. The genesis of the pegmatites, whether metamorphic, anatectic or metasomatic, has not been investigated.

#### A2.1.2 Canopus Hollow Marble, Quartzite and Paragneiss

##### A2.1.2.1 Description

The Canopus Hollow marble is part of a sequence of interbedded marble, quartzite and biotite-feldspar gneiss which has been mapped along Canopus Hollow near Cortlandt Lake and Sprout Lake (Plate 1A).

The rock is typically white to gray coarse to medium-grained diopside-calcite marble. Mineral assemblages within the marble consist of calcite, diopside, tremolite, sphene, microcline, phlogopite, graphite, and other minor opaques (Table A-1).

Foliation in the marble is defined by bands of impurities (quartz, phlogopite, diopside, tremolite, etc.) which generally strike N30°E, and dip moderately to the southeast (DF-104, SL-317); however, foliation is undulatory and appears to have flowed around cobble to boulder-size inclusions. These inclusions consist of various lithologies such as pink felsic gneiss, amphibolite, banded quartzo-feldspathic gneiss, dolomite, and pegmatite. Smaller inclusions consist of silicic impurities.

Foliation within the inclusions of metamorphic rock is commonly discordant with foliation in the marble. Large amphibolite inclusions have been elongated, necked, and fractured during boudinage (DF-104). The extension direction of most inclusions appears to be parallel (in two dimensions) to foliation in the marble. Some amphibolite boudins have been folded. Field relationships indicate that foliation in the host marble reflects ductile flowage and shearing during regional metamorphism, probably followed by later cataclasis. Calcite is highly recrystallized and mesoscopic evidence of shearing is not well preserved; however, petrographic evidence of strain in the Canopus marble is exhibited by undulose extinction in quartz, deformed calcite twin lamellae, and a biaxial negative scapolite ( $2V < 10^\circ$ ) which, if unstrained, should be uniaxial (Deer, Howie, & Zussman, 1963).

Reaction rims surround many inclusions and are composed of scapolite, riebeckite, epidote, soda-tremolite, diopside, calcite, and sphene (Table A-1; Ohan, 1964). The mineral assemblages of the reaction rims are evidence to the fact that the host marble and inclusions have together been highly metamorphosed.

The Canopus Hollow marble appears to be a calcareous member of an interbedded paragneiss sequence. Evidence for this interpretation is exposed in outcrops southeast of Cortlandt Lake (SL-317), along the bank of Sprout Brook (DF-108), and probably in the outcrops located at SL-319 (Canopus Hollow, east of

Indian Lake - Plate 1). An interbedded sequence consisting of green to gray-blue, foliated quartzite, feldspathic quartzite, banded biotite-rich gneisses (possible metavolcanics) and calcitic, dolomitic and silicic marble is exposed southeast of Cortlandt Lake (SL-317). The quartzite is not lithologically similar to Paleozoic Poughquag-Lowerre-Hardyston quartzite (Section A2.2.2) but is lithologically similar to other quartzites observed within the Hudson Highlands at Osceola Lake (SL-323: quartzite interbedded with rusty-weathering biotite-feldspar-quartz gneiss and layered feldspathic quartzite; also Berkeley and Rice, 1919). Thin layers of gray quartzite, clearly intercalated with biotite-hornblende schistose gneiss were also observed east of Canopus Lake (SL-328). The paragneiss sequence additionally includes biotite and hornblende feldspar gneisses with diopside calc-silicate rocks apparently interbedded with the Canopus Hollow marble (DF-108, SL-320). Locally, concentrated magnetite occurs in this sequence (DF-110), possibly associated with the occurrence of amphibolite in and adjacent to the marble (DF-104, 105).

#### A2.1.2.2 The Age Problem

The Canopus Hollow marble is lithologically similar to the Franklin marble of the Reading Prong in New Jersey which also contains gneiss and amphibolite inclusions and silicic impurities (Baum, 1957). At several locations, inclusions within the Franklin marble are surrounded by reaction rims containing sphene, pyroxene and scapolite (Hague and others, 1956). Hague and others (1956) believe that the inclusions represent once

continuous lithologic bands which were subsequently deformed and separated by deformation of the less competent marble. As evidence for this, they cite the boudinage of lithologies mapped as stratigraphic markers elsewhere.

The Precambrian age of the Franklin marble is based on stratigraphic, structural and geochronologic data. The Franklin marble is part of a conformable paragneiss sequence including the Hamburg Mountain gneiss series (gradationally below the Franklin), the Median gneiss (within the Franklin), and the Cork Hill gneiss zone (gradationally overlying the Franklin). The Cork Hill gneiss is overlain by the Wildcat marble band (indistinguishable from the Franklin) which in turn is overlain conformably by the Pochuck Mountain gneiss series (Hague and others, 1956). These rocks and others of the New Jersey Highlands were intensely metamorphosed, folded and intruded by syntectonic plutons during the Grenville Orogeny (Hague and others, 1956). A Precambrian age of the marble is further confirmed by three uranium-lead ages ranging from 825 to 915 m.y. (Long, Cobb, and Kulp, 1959, in Long and Kulp, 1962.) Four recent uranium-lead ages from the para- and orthogneisses of the Highlands further establish the age of these rocks between 900 and 1170 m.y. (Mose and Hayes, 1975b). Paleozoic sedimentary rocks overlie the above para- and orthogneisses of the Highlands with angular unconformity (basal Hardyston quartzite overlain by the Kittatinny limestone formation).

The Canopus Hollow marble also appears to be lithologically similar to marbles observed within the Hudson Highlands at Croton Falls (SL-322: very coarse garnet-diopside calcite marble interbedded with quartz-pyroxene gneiss) and at Osceola Lake (SL-323: coarse diopside-calcite marble interbedded with feldspathic quartzite and garnet-biotite-feldspar gneiss). The Canopus, Croton Falls, and Osceola Lake marbles all contain mineral assemblages compatible with the sillimanite-muscovite zone of the Amphibolite facies (Hyndman, 1972), and with the medium grade of metamorphism defined by Winkler (1970), and would be stable under higher temperature-pressure conditions (Granulite facies-Hyndman, 1972) defined for the gneisses of the Hudson Highlands.

Previous investigators have argued for a Paleozoic (Cambro-Ordovician) origin for the Canopus Hollow marble on the following grounds:

- 1) The inclusions within the marble have been interpreted by some as sedimentary clasts of Precambrian and Cambro-Ordovician rock deposited in a younger Ordovician carbonate matrix (Bucher, 1957; Ratcliffe, 1970, 1971). Others have interpreted the inclusions as fragments of once continuous lithologies within or adjacent to the marble, and therefore comprising a tectonic breccia (Schaffel, 1958; Ohan, 1964). The nature of the clasts has been described above. Those who favor the Paleozoic age cite the occurrence of a discordant, foliated rock as a clast within the marble as evidence of a previously metamorphosed rock (the clast) which has been eroded and deposited within a carbonate mud (the marble), subsequently metamorphosed during the Taconic Orogeny. [The discordant foliations between inclusions and host marble are equally easily explained by the formation of foliation during an early phase of ductile deformation during Grenville time when the inclusions were part of layers within or adjacent to the marble, followed by

boudinage, fracturing, and rotation of the boudins during a later phase of Grenvillian deformation. These characteristics have been clearly observed within the Franklin marble of the New Jersey Highlands, which is also Precambrian (Grenvillian)];

- 2) The Canopus Hollow marble has been compositionally and texturally compared with the Cambro-Ordovician Wappinger limestone (Bucher, 1957; Ohan, 1964; Paige, 1956; Ratcliffe, 1970, 1971). [The identification of "cystid fragments" in the marble south of Union Church at Route 9 (Bucher, 1957; near SL-305) is questionable (Finks, 1976 pers. comm.). No fossils have ever been identified in the marble northeast of Annsville. Texturally, the Wappingers and Canopus limestone are in no way similar. Wappinger limestone occurs in gradational contact with Annsville phyllite less than one-half mile from the Canopus marble (DF-103) at Van Cortlandtville. Petrographically, the Wappinger limestone is only slightly recrystallized (Dames & Moore, 1975 - Table B5.4-1, Samples WL-1, 2). Neither limestone nor phyllite at this location contain mineral assemblages indicating P-T conditions above Greenschist facies metamorphism, whereas, high grade metamorphic assemblages, and completely recrystallized textures occur in the Canopus marble]; and,
- 3) The possibility of folding or thrust faulting to emplace high-grade Paleozoic marble west of the chlorite-biotite zone of regional metamorphism has been considered. [No evidence has been found to support isoclinal folding of the Taconic regional metamorphic isograds in the Peekskill area. Reverse faulting has been identified (Section 3.2.2, 4.2.1) within the Canopus Hollow and Dennytown fault zones; however, all of these faults dip 60 to 90 degrees. Balk (1936) disputed the existence of thrust sheets and klippen in Dutchess County, N.Y. He postulated, instead, that basement punched upward through the overlying Paleozoic cover along high angle faults. Recent workers in the same area (Fisher and Warthin, 1976) have identified several possible thrust slices, but there is no apparent shortening of the Taconic metamorphic gradient].

The strongest evidence supporting a Precambrian age for the Canopus marble is a potassium-argon age date of  $893 \pm 10$  m.y. from phlogopite aligned in "cataclastic" foliation from a retrograded shear zone (Ratcliffe and others, 1972). This has been interpreted as a minimum age for the marble because Late Precambrian faulting (Section A4.1.2) has slightly affected the argon retentivity of the phlogopite.

#### A2.1.3 Canopus Pluton

The Canopus Pluton is a highly differentiated igneous intrusive located west of Canopus Hollow, and north of Continental Village (Plate 1A). The pluton contains three mappable units: a generally fine-grained porphyritic hornblende-pyroxene diorite (containing orthopyroxene), a generally coarser-grained porphyritic quartz monzonite, and biotite-feldspar pegmatites (see also Ratcliffe, 1976). The quartz monzonite has intruded the fine-grained diorite (JW-142).

The conclusion that the Canopus Pluton was emplaced prior to the termination of the Grenville Orogeny is based upon the following evidence:

- a) a completely granoblastic fabric in the fine-grained diorite (JW-138);
- b) gently plunging folds seen within, and at the contact between quartz monzonite (intrusive) and amphibolite (country rock); and
- c) the presence of hypersthene and garnet (high grade) within a quartzo-feldspathic phase of the fine-grained diorite.

A Rb/Sr six-point, whole-rock isochron indicates an age of  $1032 \pm 45$  m.y. for this syn-orogenic intrusive (Ratcliffe and others, 1972).

## A2.2 MANHATTAN PRONG

The Manhattan Prong consists of the Yonkers, Fordham and Manhattan formations, Pound Ridge granite, Lowerre quartzite, and Inwood marble (Plate 1A). The Fordham, Lowerre, Inwood and Manhattan are considered to be part of the New York City Group. The stratigraphically lowest units of the New York City Group are the Fordham and Yonkers formations of disputed but probable Late Precambrian age. The Fordham is overlain unconformably (see Section 2.2.1) by the rest of the New York City Group consisting of the following lower Paleozoic units, from oldest to youngest: Lowerre quartzite, Inwood marble and the Manhattan Formation. The Lowerre-Inwood represent a miogeosynclinal, near-shore to carbonate bank or continental shelf, depositional sequence. The overlying Manhattan Formation appears to represent a clastic wedge, part of which may be allocthonous, resting unconformably on the miogeosynclinal sequence.

### A2.2.1 Fordham Gneiss

The Fordham Gneiss is extremely variable. In the White Plains area it consists of five members (Hall, 1968a; 1968b). In the Ossining area it consists of four members (Wissig, 1969). Where the Fordham was seen during this investigation near Montrose and Croton, it is a pink granitic gneiss.

The age of the Fordham is enigmatic, and has been the subject of debate. A probable Grenvillian age for at least part of the Fordham formation is evidenced by the following information:

- a) In the White Plains area, the Fordham formation is overlain unconformably by younger members of the New York City Group (Hall, 1968a; 1968b);
- b) Folds mapped within members of the Fordham do not affect overlying rocks of the New York City Group (Hall, 1968a);
- c) U/Pb dates on zircons have yielded ages of 1000 m.y. (Grauert and Hall, 1973);
- d) Brock (1976, pers. comm.) has identified several occurrences of hypersthene in leuco- and mesocratic gneiss from the Fordham which is overlain unconformably by the Inwood-Manhattan sequence. Similar mineral assemblages have been mapped in gneisses of the Hudson Highlands (Dallmeyer, 1972; Helenek, 1971). These assemblages are indicative of Granulite Facies metamorphism of the Grenvillian Orogeny, and are not present in the overlying Paleozoic rocks. Therefore, a Grenvillian age of at least part of the Fordham Gneiss is indicated; and,
- e) A seven-point Rb/Sr whole rock isochron for the Yonkers Granite Gneiss yielded an age of  $575 \pm 30$  m.y. (Long, 1969). A six-point Rb/Sr whole rock isochron for the Pound Ridge Granite Gneiss (enclosed by the Fordham) yielded an age of  $596 \pm 19$  m.y. Both isochrons had high initial  $^{87}\text{Sr}/^{86}\text{Sr}$  ratios of  $0.725 \pm 0.008$  and  $0.7287 \pm 0.013$  respectively. Scotford (1956) interpreted an anatectic origin for the Pound Ridge body by determining that the migmatite phase of the Fordham is chemically intermediate between the Fordham and Pound Ridge. From additional detailed petrologic study, Lessing (1967) allows for either in situ anatexis or isochemical granitization of a kaolinitic arkose, or intrusion of granitic material into the Fordham as the origin of the Pound Ridge body. A pre-Avalonian age of the Fordham Gneiss is possible for each interpretation.

A Late Precambrian age of part of the Fordham which is younger than the Grenvillian event is postulated on the following grounds:

- a) The Fordham has been mapped in some localities as being conformable with the overlying Inwood-Manhattan sequence (Prucha, 1956; Wissig, 1969). Prucha (1956) suggests that the Lowerre formation may be an upper quartzite facies of the Fordham Gneiss;
- b) U/Pb ages of 1000 m.y. on zircons in the Fordham may represent provenance ages of older zircons from Grenvillian gneisses. Uranium concentrations in zircons from the Yonkers Granite Gneiss (Grauert and Hall, 1973) were the same as or less than those of the Fordham. Thus it is possible that the Yonkers Granite Gneiss may be an Avalonian arkose or volcanic rock within the meta-sedimentary or volcanic rocks (The Fordham Gneiss) which contains zircons of Grenville or older age (Mose and others, 1975); and,
- c) If the Yonkers Gneiss is a metasedimentary rock derived from an arkose, the arkosic protolith may be similar to that suggested for the Pound Ridge body by Lessing (1967). Both formations occur in the nose of an anticlinorium and both yielded similar Rb/Sr isochrons of nearly 600 m.y. Thus the Fordham Gneiss which appears to overlie the Yonkers Gneiss (Hall, 1968 a,b) could be Avalonian.

#### A2.2.2 Poughquag-Lowerre Quartzite

The Poughquag quartzite unconformably overlies Precambrian gneisses along the northern margin of the Hudson Highlands (Berkey and Rice, 1919; Balk, 1936). The quartzite was mapped in Peekskill Hollow, near Lake Peekskill and north of Canopus Lake during this study (see also Berkey and Rice, 1919). Within the Manhattan Prong, the Lowerre is considered the stratigraphic correlative of the Poughquag. Outcrops of Lowerre are sparse, but it does occur above several members of the Fordham

and always below the Inwood Marble (Hall, 1968b; Dames & Moore, 1975).

The Poughquag formation is generally vitreous, micaceous and feldspathic quartzite. The degree of recrystallization varies from moderate (in conglomeratic layers at Canopus Lake--SL-324; Balk, 1936) to well recrystallized (DF-101, SL-300). The quartzite cropping out at the northern end of Canopus Lake (SL-324) consists of a basal conglomeratic facies with blue quartz pebbles and a clean, vitreous facies. The vitreous facies appears lithologically similar to Poughquag-Lowerre in the general vicinity of Peekskill. The pebble-conglomerate facies appears similar to layers mapped by Balk (1936) in Dutchess County, N.Y. These conglomeratic layers may be facies equivalents of the basal Hardyston quartzite which rests with angular unconformity on gneisses of the Reading Prong on Morgans Hill, south of Easton, Pennsylvania.

In the Manhattan Prong, the Lowerre formation is a feldspathic quartzite which varies in composition and becomes locally micaceous. Dark-gray to brown, rusty-weathering beds with interbedded schist have been recognized in the White Plains area (Hall, 1968a).

#### A2.2.3 Wappinger-Inwood Formation

The carbonate sequence which conformably overlies the above clastic sequence consists of Wappinger limestone and the more recrystallized Inwood marble. The Wappinger formation is fine- to medium-grained, dolomite and limestone where it crops out at Tomkins Cove, in Peekskill Hollow and near Lake Peekskill.

Thin sections of samples from Peekskill Hollow at Van Cortlandtville (DF-103; samples WL-1, WL-2 in Dames & Moore, 1975 - Table B5.4-1 also see Table A-1 in this report) indicate that the Wappinger limestone was slightly recrystallized, probably during Greenschist facies regional metamorphism. Pelmatozoan stem plates found at this outcrop (Ratcliffe, 1968) are considered Balmville equivalents and permit correlation of the basal Annsville phyllite and basal Manhattan Formation (Ratcliffe and Knowles, 1969).

The Inwood Marble is more completely recrystallized and appears to represent a southeastern extension of the Wappinger formation which has been metamorphosed under higher temperature-pressure conditions and has been intensely deformed. The Inwood has been subdivided into five members, but is dominantly a coarse-grained, clean, dolomite marble and clean calcite marble (Hall, 1968a; 1968; Dames & Moore, 1975).

#### A2.2.4 Annsville Phyllite - Manhattan Formation

The Annsville phyllite occurs at its type section in Annsville, and underlies most of Gallows Hill. The phyllite consists of fine-grained micas (possibly chlorite and biotite), sericite, and quartz. Discontinuous sandstone layers and quartz stringers are common. A gradational contact between the Annsville phyllite and underlying Wappinger limestone is exposed at Van Cortlandtville (DF-103). Other Wappinger-Annsville contacts were mapped in the Continental Village and Lake Peekskill areas.

The Manhattan Formation has been subdivided into three members in the White Plains area (Hall, 1968a, b) and Indian

Point area (Dames & Moore, 1975). Field mapping in the Croton-Ossining area during this phase of the investigation has confirmed this threefold sub-division (see also Wissig, 1970). The lowermost schist member (A) of the Manhattan locally contains layers of calcite-marble. This unit lies unconformably above clean carbonates of the Inwood Formation and represents the initial stages of uplift at the beginning of the Taconic Orogeny. The middle member (B) contains discontinuous amphibolite, which also occurs locally within members A and C. The amphibolite probably represents metavolcanics, which may indicate the development, at that time, of an island arc shedding volcanic material into a deepening basin filled with pelitic sediments of the Annsville-Manhattan sequence.

### A2.3 PALEOZOIC INTRUSIVE ROCKS

#### A2.3.1 Cortlandt-Type Intrusives

The Cortlandt Complex occurs as a funnel-shaped (in profile) pluton (Balk, 1927) between Peekskill and Croton-on-Hudson, N.Y. The pluton is composed of intermediate, mafic, and ultramafic rocks which have been subdivided into five mappable lithologies (Ratcliffe, 1976). The Cortlandt Complex intruded in Late Ordovician to Early Silurian time, 435 m.y. ago (Long and Kulp, 1962). Ratcliffe (1968) defined a dioritic phase of the Cortlandt Complex occurring as a separate, mappable pluton called the Torment Hill diorite body. This intrusion contains diorite, gabbro, and pegmatitic granite (JT-22) and occurs within the Prickly Pear Shear Zone which is defined in this re-

port (Section A3.2.3). This shear zone served as a pathway for intrusion of this small body from the Cortlandt Complex.

The Croton Falls intrusion is a multiply intruded ultramafic to intermediate pluton which occurs in the Croton Falls Fault near Croton Falls, N.Y. According to Prucha (and others, 1968) and Sneider (1969), these rocks appear to be syntectonic intrusives of the Cortlandt-type that are intruded by younger microcline granites.

#### A2.3.2 The Rosetown Pluton

The surficial exposures of the Rosetown Pluton lie solely within the Precambrian gneisses of the Hudson Highlands. The outline of the complex is irregular and comes to within 500 feet of the Hudson Highlands/Manhattan Prong contact (Thiells Fault) at Stony Point.

The aeromagnetic signature of the Rosetown Pluton is expressed as a high that has the shape of an inverted cone in vertical section. The center of this high coincides with the ultramafic outcrops of the pluton. In addition, a few magnetic contours define a tail to the pluton that extends to the southwest (Appendix D). This tail is not associated with the mapped Rosetown but follows the trace of a fault that projects toward the pluton as shown by Ratcliffe (1971) and Appendix D.

The Rosetown Complex was emplaced as a series of multiple intrusions in Precambrian and Ordovician time. In general, an ultramafic core is surrounded by a variety of mafic to felsic rocks. Intrusive relationships suggest that a sequence of mafic toward felsic rocks is present. Intrusive breccias

are common throughout the complex, but no evidence of proto-clasis was observed. The oldest portion of the Rosetown Complex appears to be a hornblende granite to granodiorite at Lake Boyce (Plate A-5) which has yielded a Rb/Sr whole rock age of  $1061 \pm 12$  m.y. with a low initial ratio of  $0.7026 \pm 0.0008$  (Mose and others, 1975). The youngest portion of the Rosetown Complex, which predominates, has been dated at  $444 \pm 15$  m.y. (Mose and others, 1975). The Late Ordovician age of this portion of the Rosetown is confirmed by the occurrence of xenoliths of early Paleozoic quartzite, limestone, and phyllite within it (Plate A-5).

A dike swarm of intermediate composition occurs in the vicinity of the Rosetown Complex. These dikes are diversely oriented and occur within the Precambrian gneisses and were not found to intrude the Manhattan Prong (Plate 1A). Several dioritic dikes, which were examined, contain plagioclase and hornblende or its alteration products which include biotite, epidote, sphene, chlorite, actinolite, and leucoxene. The dikes are typically aphanitic to weakly porphyritic. These dikes may be related either to the intrusion of the Rosetown, or to the lamprophyric dikes dated by Zartman at  $398 \pm 17$  m.y. in the Monroe Quadrangle (Jaffe and Jaffe, 1973). K/Ar ages on several of the dioritic dikes (Ratcliffe, 1976) ranged from  $386 \pm 14$  m.y. to  $415 \pm 15$  m.y.

The Rosetown Pluton is similar in composition and age to the larger Cortlandt Complex that lies east of the Hudson River. Gravity and magnetic investigations indicated that they were both intruded as a series of pipes located along a line

that the pluton originated as a shallow intrusion which cooled relatively rapidly below the temperature of argon retention.

### A3.0 STRUCTURAL GEOLOGY

#### A3.1 INTRODUCTION AND SUMMARY

From Peapack, New Jersey northeastward to Ladentown, New York, the Ramapo Fault can be easily identified by its prominent topographic expression. A fault line scarp that rises above the Ramapo and Mahwah Valleys marks the western boundary of the Fault Zone. This fault line scarp diminishes north of Ladentown, New York where the Ramapo Fault branches into several individual fault zones that can be traced continuously to the northeast, across the Hudson River (Plate A-1). It is possible that the emplacement of the Rosetown Pluton, in Late Ordovician time, sutured a major fault zone and necessitated the subsequent reactivation of subsidiary faults (Section A3.2.1 and Appendix D). Therefore, from Ladentown northward the problem is largely one of identification of individual fault zones and the characterization and grouping of these zones into systems according to their geologic period of activity.

In Rockland County, New York the Ramapo Fault System forms the northwestern and northern boundary of the Triassic Newark Basin. The Newark Group is not known to be preserved west of the Ramapo or Thiells Fault zones. Thus, present day exposures of the various zones of the system lie entirely within the Precambrian and Paleozoic terrain.

The oldest preserved deformational event within the system is marked by cataclasis, passive flow and healed breccias developed in Precambrian rocks. The next event resulted in the

from Tomkins Cove to Dickerson Hill. This line probably marks an ancient tensional fracture trending approximately east-west (Steeland and Wollard, 1952).

The emplacement of the Rosetown Pluton apparently sutured the fault zones which it intruded. There is no clear evidence of northeast-trending faulting through the center of the body. A wide zone of faulting, trending N30° to 40°E, crosscuts the northwest corner of the complex and possibly offsets the pluton/gneiss contacts in both dextral and sinistral movement senses. North-northeast and north-northwest trending fractures are common within the Rosetown Pluton.

#### A2.3.3 Peekskill Granite

The Peekskill Granite has intruded along the Peekskill Fault that separates the Manhattan Prong from older rocks of the Hudson Highlands (Plates 1A and A-6). This pluton consists of granodiorite and granite phases which are generally massive. Local primary foliation within the pluton is defined by oriented mica flakes and coarse microcline and quartz (Espejo, 1969). Espejo concluded that the pluton represents a single magmatic intrusion of granodiorite. Later in situ differentiation produced the granitic phase which, in places, is contaminated by country rocks. A Rb/Sr, nine-point whole rock isochron dates the intrusion of the Peekskill Pluton at 371±14 m.y. with an initial  $^{87}\text{Sr}/^{86}\text{Sr}$  ratio of 0.7074 (Mose and others, 1976). This date agrees with a potassium-argon mineral age of 356±14 m.y. from a muscovite separate (Long and Kulp, 1962), and indicates

development of mylonitic textures, followed by the development of open-work breccias, intense fracturing and slickensiding. Cross-cutting relationships at several exposures indicate that the youngest movements in the system are exhibited in outcrop as unhealed breccia, commonly with gouge. The fault kinematics observed in the field also indicate polyphase deformation that occurred under different stress regimes. Strike-slip faulting is most pronounced; however, there is considerable evidence of low angle thrusting and high angle dip-slip faulting.

Based on the information presented in this section and in Appendix B, it appears that the unhealed breccia zones delineate the portions of the Ramapo Fault System that were active during the Mesozoic. The unhealed breccia is quite often developed in older healed breccia and/or mylonite. Thus, while it is apparent that these zones were active prior to the Mesozoic, the pre-Mesozoic history is sometimes difficult to decipher in the zones of Mesozoic deformation. The results of fluid inclusion studies and radiometric age determination of minerals sampled throughout the region suggest that there has been no significant orogenic tectonic movement in the area of study since the Late Cretaceous (90 to 70 m.y., Appendix E). Ratcliffe (1976) infers that brecciation in the Mott Farm Road Fault could be dated between 295 to 273 m.y. and 163 m.y.

#### A3.1.1 Ductile Deformation

The rocks of the Hudson Highlands and the Manhattan Prong near Peekskill, N.Y. have been affected by two periods of

ductile deformation and associated metamorphism during the Grenvillian Orogeny (~1.1-1.0 billion years ago) and during the Taconic Orogeny (~470-440 million years ago). Between Route 9 and Canopus Hollow Road, within the Highlands gneisses (as well as within the Canopus Pluton which intruded the gneisses during the Grenvillian event), excellent samples of isoclinal folds, boudinage, and mineral lineation are exposed (SL-311; JW-145, 146, 148).

The Fordham Gneiss of the Manhattan Prong is believed to be composed of metamorphosed clastic sedimentary rocks interbedded with mafic and rhyolitic volcanics (Hall, 1968). The Fordham Gneiss exposed near Montrose and Croton-on-Hudson resembles a metarhyolite or meta-arkose. These rocks are tightly folded and boudined (SL-226, 245). Grauert and Hall (1973) have dated zircons from the Fordham Gneiss at 1 b.y. The problem, however, is that these may be detrital zircons (derived from a 1 b.y. old rock) that were merely deposited within a relatively younger interlayered sequence of sediments and volcanics. This relatively younger sequence may be a Late Precambrian analog of the sequence in the Trio-Jurassic Basin.

The Fordham itself has not been adequately subdivided in this area and parts of it may actually be of Grenvillian age (Section A2.2.1). Hall (1968) indicates that the Fordham Gneiss has been isoclinally folded prior to deposition of the overlying paleozoic sediments.

The Poughquag-Lowerre, Wappingers-Inwood, and Annsville-Manhattan Formations were deposited unconformably on

top of Precambrian Highlands gneisses. At the onset of the Taconic Orogeny, these formations were complexly folded during regional metamorphism, and locally, near Peekskill, two generations of folds were recognized (Dames & Moore, 1975). The second generation of folds ( $F_2$ ) was found to be characterized by a semi-brittle condition of formation.

#### A3.1.2 Brittle Deformation

Precambrian rocks, both in the Hudson Highlands and within the Manhattan Prong, exhibit zones of shearing, some of which are cataclastic in appearance and are typically recrystallized and healed. These zones commonly contain pegmatites which intruded the fault zones. More commonly, the Precambrian rocks are intensely fractured and sheared along zones which are open and unhealed, locally altered, mineralized, and brecciated (SL-303; SL-261, 262; SL-330, 331). Diaphthoresis, or retrogressive metamorphism, is typically exhibited along the major faults which can be mapped in the Hudson Highlands. Many unhealed fault zones have been reactivated during repeated episodes of fault movement. This reactivation is also evidenced by the repeated emplacement, within major fault zones, of large intrusive bodies such as the Canopus Pluton ( $1032 \pm 45$  m.y., Ratcliffe, 1972) and the Lake Boyce Pluton ( $1061 \pm 12$  m.y., Mose and others, 1975), the Cortlandt-Rosetown Complexes ( $\sim 440$  m.y., Long and Kulp, 1962 and Mose and others, 1975), the Croton Falls Complex (Middle Ordovician, Sneider, 1969), the Peekskill Pluton ( $371 \pm 14$  m.y., Mose and others, 1976), and the Mesozoic diabase

and basalt flows (190 m.y. to 136 m.y., Erickson and Kulp, 1961; Dallmeyer, 1975 and Appendix C). Each of these igneous bodies has been affected by younger fault movements (Dames & Moore, 1975 and this report).

### A3.2 DISTRIBUTION AND OCCURRENCE OF FAULTS

The Ramapo Fault System consists of several northeast trending, subparallel fault zones. In Rockland County (Plates 1A and B) the prominent members of the system are the Ramapo, Thiells, Cedar Flats and Ambreys Pond Faults. In addition, there are many fault zones developed in the system which trend north-northeast or east-northeast. In Rockland County, the Blanchard Road, Willow Grove and Timp Pass Faults strike north-northeast and the Letchworth and Mott Farm Road Faults strike east-northeast. In southwestern Rockland County the Ramapo Fault forms the boundary between the Reading Prong (Hudson Highlands) and the Newark Basin. In the northeastern portion of the county, Manhattan Prong strata separate the Reading Prong from the Newark Basin. The Thiells Fault is the western boundary fault of the Newark Basin in that area. East of the Hudson River the Reading and Manhattan prongs are separated by the Peekskill and Croton Falls Faults.

The Canopus Fault System also consists of several northeast-trending subparallel fault zones. Extending north-eastward from the Manitou Mountain-Annsville area, the prominent members are (Plate 1A): The Dennytown, Canopus Hollow, Annsville-Oscawanna and the Peekskill Hollow Faults. In addi-

to these, the Peekskill Fault which strikes east-northeast to east-west between Peekskill Bay and Mohansic Lake, joins the Ramapo-Canopus Fault Systems to the Croton Falls Fault System (Plate A-1).

The Croton Falls Fault System seems to be the eastward en echelon extension of the Ramapo-Canopus Fault System. The importance of this fault system is accentuated by the existence of intrusives along its length and the fact that some of the fault zones are directly aligned with three northeast trending faults mapped in the Newark Basin near Rockland Lake (Appendix B). The major members of the Croton Falls Fault System are: the Croton-Teatown, and Prickly Pear Shear Zones and the Croton Falls Fault (Plate 1A).

#### A3.2.1 The Ramapo Fault System

##### A3.2.1.1 Northeast Trending Faults

##### A3.2.1.1.1 Ramapo Fault

The Ramapo Fault does not crop out where it forms the margin of the Newark Basin in Rockland County, New York. Evidence of significant mass wastage along the southeast front of the Ramapo Mountains suggests that the major zone of deformation lies somewhat further to the southeast beneath the flood plain of the Mahwah and Ramapo Rivers. This is confirmed on seismic reflection line 2, which was run in Mahwah, New Jersey (Plate D.7-15, Appendix D). A small abandoned rock quarry (CH-32) adjacent to line 2, on the west side of the river, lies at the western edge of the fault zone. The Precambrian hornblende

granite gneiss is highly brecciated throughout the quarry and two north-eastward trending zones of quite severe deformation are identifiable. Near the east side of the quarry, one zone (over 20 feet wide) contains healed breccia and mylonite which has been highly fractured. Predominant strikes of subvertical shears within the zone are: N30°E (dip-slip), N30°E (strike-slip), N60°E (strike-slip) and north-northeast to north-northwest (strike-slip). This zone is separated from a similar zone, near the west side of the quarry, by a relatively less deformed zone approximately 100 feet wide. While the above mentioned shear directions are recognizable in the intermediate zone, the predominant trend appears to be west-northwest. The western, highly deformed zone is essentially the same as the eastern, except that the western zone is cut by a north-northeast strike-slip fault. This fault (interpreted as a Mesozoic, synthetic sinistral shear) appears to be the youngest feature at this locality. It strikes N15 to 20°E, dipping 75°S and is filled with 3 to 6 inches of soft gouge. Horizontal grooves and slickensides are visible on both footwall and hanging wall.

At Suffern, New York, a roadcut near Route 202 at the New York Thruway (CH-27), lies at the western edge of the Ramapo Fault. Most of the Precambrian hornblende granite exposed at this location has been brecciated. The breccia is healed and is cut by several mylonites that strike northeast and dip southeast. Both the healed breccia and mylonite have been sheared and faulted in several directions. The dominant brittle fabric strikes east-northeast. Undulatory, polished shear surfaces

strike east-northeast to east-west here, and dip 60 to 90°S, with grooves and slickensides raking west at over 60 degrees.

Thrust faulting is evident in exposures of Precambrian rock immediately west of the Ramapo Fault. At Antrim (CH-34), just north of Suffern, New York, thrust planes strike roughly east-west and dip generally 25°S. The thrusts are cut by basalt dikes (N45°E; 75°S and N40°E; 47°S). Both the dikes and the thrusts are cut by northeast, north-south and north-northwest, near vertical shear fractures. West of Willow Grove, N.Y., (CH-66) north-northeast striking, 15 to 30°E dipping thrust faults contain felsite intrusions which are fractured.

Precambrian exposures at the headwaters of the Mahwah River are characterized by intense brittle fracturing of older healed breccia and mylonite.

#### A3.2.1.1.2 Thiells Fault

The Thiells Fault forms the contact between the Precambrian gneiss and Paleozoic metasedimentary strata. It was mapped between Thiells and Tompkins Cove, N.Y. (Plates 1, A-5). At Tompkins Cove, Wappinger Limestone and Annsville Phyllite of Cambro-Ordovician age crop out along the railroad adjacent to the Lovett Power Plant (N-225, Plate 2). The phyllite is folded and faulted with the limestone, but, in general, lies west of it and east of the Precambrian gneiss. A thrust surface that is subparallel to the near horizontal limestone bedding, dips gently to the southeast and climbs up-section to the northwest. The rock types and the structures are markedly different across this surface. A large N35°E vertical shear plane with a

healed breccia and three sets of slickensides (pitching 0 to 20°, 30°, and 60°SW) forms the southeastern face of this exposure. The near horizontal slickensides are the strongest and most common set. A series of second-order north-south vertical shears extend north from this main shear. These second-order shears crosscut the thrust plane and have breccia "pockets" developed along them, and near-horizontal slickensides. Ratcliffe (1976) noted unhealed breccia in the vicinity of the power plant storage tanks and mapped a north-northeast branch of the fault at that point.

To the southwest, near Route 9W (N-200) the mylonitic fabric in the Precambrian rock is oriented N45°E, 60°SE and has a well developed down-dip lineation. Although relatively intact, the mylonite does exhibit minor brittle deformation in the form of N35°E fractures. These exposures lie along a fault-line scarp extending southwestward from the Lovett Power Plant. The escarpment extends another 2000 feet beyond Route 9W to a point across a small valley from a limestone ridge (N-224, Plate 2). Precambrian gneiss underlies the escarpment along its entire length. A N45°E fault-line scarp defines the northwest side of the limestone ridge which is composed of healed bedding-plane breccias (SL-40, 42, Plate A-5). Minor N10° to 20°E vertical shears, with near horizontal slickensides (raking less than 30°SW), crosscut the N10°E to 10°W and 60° to 80°E bedding plane breccias. These observations suggest that the bedding plane breccias may be related to folding or thrusting. The northeast-trending ridge, valley, and escarpment, in proximity to the

breccias, suggest the presence of a large fault in the valley. The N10° to 20°E vertical shears could be synthetic to a larger fault, implying left-lateral strike-slip faulting along the N45°E main fault.

Five hundred feet further southwest, Precambrian and Paleozoic rocks are exposed, (N-221, Plate 2A) nearly in contact, within a stream that crosses the escarpment (SL-6, 41, Plate A-5). The Precambrian rocks are densely fractured by northeast-trending shears, and a N30°E, 45°SE oriented mylonite in the gneiss occurs near the contact with the phyllite. The phyllite is also deformed. A younger N25°E, vertical shear and many N50°E to EW, 60°SE second order shears crosscut the mylonite. Several hundred feet of phyllite are exposed, followed by limestone further east. The limestone strikes N20°E and dips 40°SE and contains breccia between beds and along east-west fractures. These observations suggest that the mylonite developed after the deposition of the phyllite. The breccia, along with the attitudes of the beds and fractures, suggest that the Paleozoic rocks have been thrust westward onto the Precambrian gneiss.

Three thousand feet southwest of N-221, another limestone ridge is again bordered by a valley on its eastern side (N-209, Plate 2; SL-30, 34, Plate A-5). This ridge, the limestone bedding and fine breccias, and small faults all trend N40°E. In the valley, a N40°E mylonite and breccia occur in contact with Precambrian gneiss. N20° to 40°E-trending vertical shears with oblique and strike-slip slickensides cross the mylo-

nite. The gneiss to the west contains many northeast-trending shears. These observations suggest that a mylonite, which probably pre-dates thrusting, occurs at a thrust fault contact between Precambrian and Paleozoic rocks which has been cut by younger northeast vertical strike-slip faults.

The fault-line scarp intersects the valley of Cedar Pond Brook at Hillside Cemetery in Stony Point. A roadcut on the north side of Old Route 210, about 200 feet west of the church, reveals intense unhealed brittle fracturing of Precambrian gneiss and mafic dikes (CH-76; N-210, Plate 2; SL-29, Plate A-5).

In Cedar Pond Brook, the projection of the Thiells Fault coincides with a sharp deflection of the stream channel (CH-7-9; N-227, Plate 2; SL-7, Plate A-5). Intensely fractured Annsville phyllite crops out at the bend. There are many N40°E, 45°SE fractures present, parallel to foliation, which may be the result of folding or thrusting. These fractures are clearly cross cut by north-south and east-west vertical shears and a N40 to 80°W, 60°NE fault zone with breccia. The outcrop is cut by large N20 to 35°E shears. The northeast and northwest fractures coincide with the trend of the river at the bend. It appears from the geometry and cross-cutting relationships of faults and fractures at this outcrop that high-angle faulting post-dated low-angle faulting.

An alignment of escarpments, swamps, and streams, between scattered outcrops of brecciated quartzite and gneiss,

follows the projection of the previous outcrop southwest to the town of Thiells. Here (N-226, Plate 2) a 10-foot wide zone of healed cataclastic rock trends N20°E and lies at the contact between gneiss on the west and quartzite on the east. These rocks are sheared and the fracture geometry is most clearly expressed in the Cambrian quartzite to the east. N55°E, 60°NW closely spaced fractures with dip-slip slickensides appear to be related to throughgoing N55°E steeply southeast dipping breccias. These observations suggest that cataclasis at N-226 occurred along the contact between gneiss and quartzite striking N20°E. Later N55°E-striking dip-slip shearing has cross cut the N20°E trend.

#### A3.2.1.1.3 Cedar Flats Fault

The Cedar Flats Fault is mapped along a strong topographic lineament extending N30°E from Blanchard Road to Bulsontown, N.Y. (Plate 1A). Brecciated mylonite exposed west of Cedar Flats Road (CH-71, Plate 2A) contains prominent throughgoing fractures oriented N30°E; 60° to 80°NW. A few instances of possible second order fractures at this locality suggest left-lateral movement on the N30°E trend. About a mile to the southwest, the granite gneiss east of Blanchard Road (N-267, Plate 2A) exhibits intense, closely spaced fracturing. Prominent near vertical fractures with horizontal slickensides are oriented N30°E, 50°SE and N60°E. The Cedar Flats Fault can be projected from CH-71 to the southwest to the Blanchard Road Fault Zone, but apparently no further.

#### A3.2.1.1.4 Ambreys Pond Fault

The Ambreys Pond Fault is best exposed along the western escarpment of Buckberg Mountain where it trends about N40°E (Plate 1). A traverse southwest from the summit of Buckberg encounters several sharply defined north-northwest ridges and valleys.

The trend of these valleys appears to be controlled by the dominant fractures; horizontal slickensides occur on the north-northwest shears. These valleys are truncated by a northeast-trending escarpment, which coincides with several exposures of breccia, and N30°E, 50°SE shears with subhorizontal slickensides. Large exposures of breccia and highly fractured rock occur just to the southwest of this escarpment.

A traverse along a northwest bearing, starting from the top of Bensons Point (CH-75, Plate 2), reveals a sharp increase in fracture density. East-northeast fractures are the most dominant, but north-south to northwest shears with dip-slip slickensides are also common. The Ambreys Pond Fault projects just west of Bensons Point, through a well-defined valley, to the projected intersection of the Willow Grove and Cedar Flats Faults (Plate 1). On the east side of the valley lies a north-northeast trending ridge that is closely fractured along N75°E trends. Many N60°E-trending healed shears also occur on this ridge.

### A3.2.1.2 North-Northeast Trending Faults

#### A3.2.1.2.1 Timp Pass Fault

A strong north-northeast topographic and photogrammetric lineament extends from the Cedar Flats Fault, past the Mott Farm Road Fault and through Timp Pass on the west side of Timp Mountain (Plate 1A). Several traverses were made in this area. The intense brecciation and weathering that are characteristic of the Mott Farm Road (Section A3.2.1.4.2), Cedar Flats and Ambreys Pond Faults were not observed except in the extreme southern portion of the area, near the intersection with the Cedar Flats and Mott Farm Road Faults (CH-53). However, several indications of faulting as expressed by cataclasis (healed breccia) do occur in Timp Pass and along the north-northeast linear. Slickensides are rare and the rocks in general, have a massive aspect. Some fracturing oriented N15 to 20°E does occur just north of the Pass adjacent to a north-northeast stream. The exposures on this north flank are more blocky in nature, fractured and contain some microbreccias. Both Dodd (1965) and Ratcliffe (1976) have mapped right-lateral displacements along the Timp Pass Fault.

#### A3.2.1.2.2 Blanchard Road Fault

The exposures on Blanchard Road (DR-34; DR-35, Plate 2) consist of intensely brecciated and weathered Precambrian gneiss. The breccia contains shears and fractures of many orientations but north-south, north-northeast and east-northeast are the most common; all three orientations are horizontally

slickensided, indicating strike-slip movement. Several west-northwest shears also occur. Mylonites and healed shears have been brittly fractured along the same pre-existing trends both within and subparallel to the N15°E-trending zone defined here as the Blanchard Road Fault.

The Blanchard Road Fault can be interpreted to extend as far north as the south slope of Jackie Mountain on the basis of the truncation of  $F_2$  folds mapped by Frimpter (1967). The shape of topography suggests that it extends southward to the Ramapo Fault in the vicinity of CH-18 (Plate 2A).

#### A3.2.1.2.3 Willow Grove Fault

The Willow Grove Fault is mapped on the basis of a topographic lineament between the Cedar Flats and Ramapo Faults and one exposure of unhealed breccia on the lineament (Plate 1A; CH-43, Plate 2A). The Willow Grove exposure consists of intensely fractured unhealed breccia and mylonite. The dominant fracture trends are east-west to east-northeast, north-northeast and northeast. Approximately 500 feet east-southeast of this exposure, an unhealed shear zone (N65 to 70°E; 70 to 80°N) is visible in the Palisades Parkway roadcut (CH-19, Plate 2A).

Between the Willow Grove and Blanchard Road Faults there is coherent but fractured rock (DR-36, CH-42). Small-scale mylonite zones (N30°E) and healed breccia are present. The predominant orientation of open fractures appears to be east-northeast.

### A3.2.1.3 North Trending Faults

#### A3.2.1.3.1 Bald Mountain and Buckberg Mountain Faults

The Bald Mountain Fault is a nearly north-trending structure marked by a much more subtle lineament than either the Timp Pass or Mott Farm Road Faults. Just north of Tomkins Lake, truncated, gneissic, granite-paragneiss contacts on opposite sides of the fault suggest a left lateral offset of approximately 500 feet (Plate 1A), and the valley in which the fault was recognized is marked by weathered, intensely fractured and brecciated gneissic granite. As is the case with rock in the Mott Farm Road Fault, extraction of an intact hand specimen from this fault zone is difficult due to the presence of numerous closely spaced, diversely oriented fractures. In thin section, a narrow pseudotachylite zone was recognized along with highly fractured perthite and internally faulted plagioclase. Secondary biotite and chlorite appear as retrograde products of hornblende, a condition due to diaphoresis attendant upon faulting. Further north in the lineament, between Bald and Dunderberg Mountains, brecciation is also evident.

Ratcliffe (1976) has mapped faults striking roughly north across Bald Mountain and Buckberg Mountain. He also indicates that the intrusion of the Rosetown Pluton post-dates significant left-lateral movement on the Buckberg Mountain Fault. Healed breccia crops out along this fault on the south side of Buckberg Mountain (CH-57).

#### A3.2.1.4 East-Northeast Trending Faults

##### A3.2.1.4.1 Letchworth Fault

The Letchworth Fault has been mapped as striking east-northeast between the Ramapo Fault at Ladentown and the Thiells Fault, at Thiells. It bounds the southeastern side of Cheesecote Mountain, and separates the Reading Prong to the northwest from the Newark Basin on the southeast. Although the actual fault zone does not crop out, its existence is inferred on the basis of a zone of relatively intense fracturing that trends northeast and is dominated by fractures that strike N60°E. Near the summit of Cheesecote Mountain, N50° to 60°E fractures are very abundant. A traverse up the west side of the mountain shows that the intensity of N60°E fractures increases eastward. The only clear relationship between the N60°E fractures and the other two abundant fracture sets (NS and N40°E), can be seen at the summit. The N40°E fractures appear to be the throughgoing structures at this location with the north-south and N60°E fractures occurring subordinately. The N60°E set is inferred to be genetically oldest, since it is offset by the north-south fractures.

Just south of Willow Grove Road on the Palisades Parkway (CH-20, Plate 2A), a large road cut shows an overall increase in the density of N60°E fracturing toward the south. Near the center of the exposure a 10-foot wide zone is densely fractured by predominantly N60°E-trending high-angle fractures. At the south end, the N60°E, 60°SE fractures are throughgoing,

and the N60°E, 60°NW fractures appear to be controlled by, and lie between the N60°E, 60°SE sets.

At Thiells (N-22, Plate 2A), the vast majority of fractures strike N55°E, dip 60°NW, and are closely spaced. Three N55°E, steeply southeast dipping breccia zones have been recognized. The N55°E, 60°NW fractures stop at the breccia zones and frequently bear dip-slip striations. Interpretation of these cross-cutting relationships and the geometry of main and synthetic shears suggest that dip slip movement could have occurred along a N55° to 60°E feature in this area, and locally postdates the N20°E cataclasis (Section A3.2.1.1.2).

#### A3.2.1.4.2 Mott Farm Road Fault

Several outcrops characterized by intense brecciation occur in a N60° to 70°E valley that lies south of the Dunderberg and Timp mountains and north of Buckberg Mountain. The brecciated nature and the scarcity of these outcrops, relative to surrounding exposures, suggest that this valley is the locus of a large fault zone called the Mott Farm Road Fault, which was recognized within and projected along the trend of this valley between Camp Addison Boyce and the Hudson River. The N30°E trend of the Cedar Flats Fault joins the Mott Farm Road Fault south of Camp Addison Boyce. The Ambreys Pond Fault merges with the Mott Farm Road Fault west of Tomkins Lake where the topographic expression of the Mott Farm Road Fault appears to be deflected from N60°E to N70°E (Plate 1A).

Exposures within the Mott Farm Road Fault consist of rusty-weathering, partially decomposed, highly brecciated rocks with innumerable dip-slip, oblique-slip and strike-slip slicken-sided surfaces. Extracting discreet samples from within this zone is difficult because the rocks shatter easily due to the presence of many diversely oriented fractures. There are several fractures within and near this zone which are parallel to the strike of the zone and dip  $60^{\circ}$ - $70^{\circ}$  to the south. Ratcliffe (1976) observed small-scale faults with 1/2 inch of right-lateral strike-separation on the south side of a ravine east of Tomkins Lake.

Dikes of various compositions have been affected by movements along this zone. One of these is a diabase dike (JW-135) which trends  $N70^{\circ}E$  and consists of highly altered augite, urallite, plagioclase and magnetite. It is presently unknown whether the diabase is genetically related to Late Precambrian, Lower Paleozoic or Mesozoic igneous activity. A second dike, which lies amidst a swarm of dikes seen in the abandoned quarry on Mott Farm Road just north of the Rosetown Pluton (Station JW-21), is composed principally of sericitized plagioclase, along with secondary biotite, sphene, chlorite and magnetite (?). The geography and mineralogical composition of the dike suggest that it probably is related to the Rosetown Pluton which was emplaced  $444 \pm 15$  m.y. ago (Mose and Hayes, 1975). The radiometric ages of dikes provided by Ratcliffe (1976) appear to support this contention (Section A2.3.2). Undeformed

zeolite crystals occur on a slickensided surface (N68°E, 88°SE) in a quarry (JW-21) within the fault zone.

#### A3.2.1.5 Dunderberg Fault

The Dunderberg Fault marks the contact between gneissic granite and undifferentiated paragneiss on Dunderberg and Manitou Mountains (Plate 1). Faulting was recognized along this contact at stations JW-75, JW-84, JW-90, JW-110, and JW-116 (Plate 2). As with the other faults, cataclasis along the Dunderberg Fault is marked by crushed and recrystallized quartz, elongate quartz and broken, bent, and internally faulted plagioclase. At JW-90 the granite was intruded by a dark-green colored dike which, like the host rock, has been brecciated. Other dikes occur near the Dunderberg Fault at JW-75 and JW-123 (Plate 2). Both dikes are intensely fractured. Plagioclase in each dike exhibits bent, broken, and internally faulted crystals. Preferential orientation of crystals is also present in each dike. As previously stated (A2.3.2), K/Ar ages of dioritic dikes in this area (Ratcliffe, 1976) range from  $386 \pm 14$  m.y. to  $415 \pm 15$  m.y. The dioritic dikes associated with the Dunderberg Fault have been intensely sheared by the fault. The deformation of the dikes, therefore, post-dates the age of dike formation which appears to be Early Silurian to Early Devonian.

Southwest of the Hudson River, the Dunderberg Fault trends about N35°E, whereas northeast of the river it strikes nearly north, and if followed along strike it swings back again to northeast. Both the lithologic contact and the fault curve westward as they cross the Hudson River.

### A3.2.2 The Canopus Fault System

#### A3.2.2.1 Northeast Trending Faults

##### A3.2.2.1.1 Canopus Hollow Fault

The Canopus Hollow Fault (Plate A-1) is characterized by mylonitization and diaphoresis of Precambrian gneisses and igneous rocks along Sprout Brook and Canopus Hollow. The western edge of the fault zone was intruded by monzo-dioritic rocks of the Canopus Pluton (Plate 1). Cataclasis also affected the rocks of the east edge of the pluton (SL-309, Plate 2). Using Higgins (1971) terminology, quartz monzonitic rocks grade from protomylonite to ultramylonite in a vertical zone striking N25°E. Precambrian gneissic country rock along the west side of Canopus Hollow is mylonitized, altered, and locally sheared. At SL-310 north of Continental Village, the gneiss on the east edge of the pluton has been granulated, altered, and isoclinally folded. Petrographic examination of the rock shows intergranular recrystallization between sheared and granulated feldspar grains. The mortar recrystallization is the healing agent of the mylonite. This granulated rock exhibits tight folding of the mylonitic foliation. The westward plunges of fold axes vary from 18 to 75 degrees, but the folds have consistent counter-clockwise rotation senses (SL-310, JW-145). If these folds formed during fault movements, they can be interpreted as forming during a transition from brittle cataclasis to ductile flowage. An oblique sinistral movement sense with a significant west-side-up component is evident along the mylonite zone ori-

ented N35°E, 75 to 85°NW. Elsewhere in the Canopus Hollow fault zone (JW-145, SL-318), dip-slip movements are evident within mylonites and mylonitic gneisses. At Continental Village (JW-145, SL-310), horizontal boudinage of mylonite and steeply plunging mineral lineations are indications of ductile movement down the dip of layering.

Within the Canopus Pluton, the large plagioclase phenocrysts of the quartz monzonite form a flow lineation parallel to the steep dip of the country rocks (JW-147). The feldspar laths also exhibit an imbrication that suggests a dextral transcurrent movement within the quartz monzonite to form the imbrication. This may be evidence of syn-intrusive fault movements within the Canopus Hollow Fault.

Unhealed faults containing breccia are also present, but not common in the Canopus Hollow Fault. At one such fault (SL-304), rocks of the Canopus Pluton are cut by N45°E and N55°E faults with open-work breccia and vertically raking slickensides.

#### A3.2.2.1.2 Dennytown Fault

The Canopus Hollow Fault merges at a low angle with the Dennytown Fault at Canopus Lake along New York Route 301 in Fahnestock State Park (Plate A-1). A belt of abandoned magnetite mines in Precambrian rocks, known as the Phillips Belt (Colony, 1923), which has been mapped during this investigation (SL-327, 328, 332, Plate 2A), occurs within the Dennytown Fault. The origin of these ores is not certain. Colony (1923) believed

that they were derived from deuteric solutions of concentrated late-stage magmatic products. Prucha (1956) attributes the Brewster (N.Y.) magnetite ores as forming by "replacement of feldspathic country rock in structurally favorable zones close to hornblende-biotite granite bodies from which the iron was derived". Whatever their origin, the Phillipstown mines occur in a 7-mile belt, within iron sulfide rich paragneisses, along a fault zone trending N35 to 40°E. At SL-327 (Plate 2A), the vein of ore occurs in a N35 to 40°E fault which dips 65 to 75°NW; however, at SL-328 the ore occurs in a N40°E fault which dips 50°SE. Thus, it appears that the magnetite ores were deposited in the Dennytown Fault during the Precambrian from Travis Corners (SE corner, West Point, N.Y., 7-1/2' quadrangle) to Canopus Lake where they were deposited within the Canopus Hollow Fault.

The Dennytown Fault has apparently been reutilized after deposition of the ores. At the southwest end of Canopus Lake (SL-331), a zone of sheared mylonites with breccia and gouge are exposed. The main fault zone probably lies in the valley between SL-330 and SL-331; the mylonites at SL-331 are oriented N45°E, 80 to 90°SE. A secondary schistosity within the mylonite appears to be dragged suggesting reverse movements; however, these surfaces are sheared off by strike-slip faulting along the same zone. This brittle zone lies just west of the Phillips ore belt, and projects with the ore belt to the southwest toward Anthony's Nose and Iona Island where other magnetite mines are located. Along strike to the northeast (northeast end

of Canopus Lake) of the mylonite zone, quartzite (Plate 1A) is exposed in a belt 600 ft. wide and bounded on each side by a fault (SL-324, Plate 2). The quartzite consists of two facies: approximately 500 ft. of intensely sheared, vitreous, buff- to gray-weathering, grayish white quartzite, physically overlying (on the southeast side) 50 feet of black-weathering, purplish-gray conglomeratic quartzite with stretched, purple quartz grains and pebbles up to one inch long. The pebble quartzite is more sound than the vitreous quartzite. Within the vitreous quartzite, a secondary planar schistosity with subhorizontal pinch-and-swell structures is developed with increasing intensity westward toward the quartzite-conglomerate contact. Dip-slip slickensides and quartz-filled en echelon gash veins demonstrate that reverse movement occurred on these surfaces, which are oriented N20 to 30°E, 45 to 70°SE. The contact between quartzite and conglomerate (N15°E, 60 to 80°SE) is a major reverse fault. The boundary faults between the quartzite and Precambrian gneisses are not clearly exposed. Berkey and Rice (1919) assigned this quartzite to the Cambrian Poughquag formation and this appears acceptable for the reasons stated previously (Section A2.2.2).

#### A3.2.2.1.3 Annsville-Oscawana Fault

The Annsville-Oscawana Fault in Annsville is the contact between Precambrian granitic gneisses and the Annsville phyllite (Plate 1A). The fault strikes N30°E and follows the west side of Gallows Hill as far as the Westchester-Putnam County line where the gneiss-phyllite contact swings to the

east-northeast. From this point, the main fault strikes N20 to 25°E and passes through the Precambrian gneiss as far north as Oscawana Lake. The east-northeast contact between phyllite and gneiss is also a fault contact (DF-106; SL-315, 316, Plate 2A).

The nature of the Annsville-Oscawana Fault is most clearly seen at the sand pit in Annsville on the east side of Sprout Brook (where access is gained from Highland Avenue). The Annsville Fault is the youngest of many faults exposed in the sand pit. Plate A-2 is a block diagram of the sand pit exposure and the large roadcut in the Annsville phyllite on Highland Avenue. This exposure (SL-303, DF-111, JW-146, Plate 2A) corresponds to station NR-1330 of Ratcliffe (1976). At the south end of the fault (Box A, Plate A-2), there are three distinct lithologic zones which are separated from each other by fault contacts. The westernmost zone (near the base of the hill) is composed of Precambrian mylonitic granitic gneiss. These rocks have a healed cataclastic fabric parallel to foliation which is oriented N-S, 70 to 80°E. Within this unit, the healed mylonite fabric is transected by brittle conjugate shears: N54°E, 70°SE (dextral) and N76°W, 85°NE (sinistral). In general, many N75°W, 77°NE sinistral shears are visible in this zone. The amount of displacement on these faults is less than six inches. These same conjugate shears are seen (SL-303) to be dextrally offset by small scale en echelon shears oriented N25 to 35°E, 70 to 90°SE.

The mylonitic granitic gneiss is in fault contact with the second zone; a mylonitized Precambrian gneiss with zones of

phyllonite or sheared phyllite of the Annsville Formation. The rock of this latter zone has very closely-spaced, pervasive schistosity and is generally sound rock. The fault between the mylonitic gneiss and the mylonite with phyllonite is parallel to the schistosity of the latter, which is oriented N20 to 25°E, 70°SE (SL-303).

The mylonite in turn is in fault contact with the Annsville phyllite. The contact is the Annsville Fault, which truncates the N20 to 25°E schistosity of the mylonite at a very low angle; the orientation of the Annsville Fault being N30 to 35°E, 75°SE. This fault is essentially parallel to the foliation within the Annsville phyllite (SL-303). Little evidence for the movement sense along the Annsville Fault is visible. A steeply plunging mineral lineation is seen in the phyllite, as well as several mesoscopically folded quartz stringers. These minor folds have clockwise rotation senses, and one fold could be measured as having a gentle northward plunge of about 16 degrees. Other folded quartz stringers have been incompletely transposed into the plane of phyllite foliation during passive-slip folding (SL-303). These folds appear to have formed during possible  $F_2$  folding rather than as drag folds due to later movements along the Annsville Fault.

A glacially polished and striated rock surface extends across the Annsville Fault (Box A, Plate A-2) and is not offset by the fault.

Towards the north end of the rock cut at the sand pit (Box B, Plate A-2), a fault wedge of Wappinger dolomitic lime-

stone is exposed between mylonitized Precambrian granitic-gneiss (below) and the Annsville phyllite (above). Within the gneiss there are two zones of intensely sheared and altered gneiss. A phyllonite which grades downward (away from limestone) into a protomylonitic gneiss is in contact with the Wappingers limestone. Below the phyllonite is an intensely sheared fault zone with a biotite-chlorite-tremolite-actinolite assemblage which was apparently produced by retrogressive metamorphism of the hornblende-rich gneisses transected by the fault. Large biotite flakes and related minerals are localized within the shear zone in which the rocks are covered by numerous vertically raking slickensides (SL-303, JW-146). The shear zone is oriented N10 to 20E, 70 to 80SE and appears to be a dip-slip zone. Within the limestone, there are some local en echelon gash veins suggesting apparent dextral movements along the Annsville fault. It was not possible to see them in three dimensions.

Plate A-2 also shows a portion of the Annsville road-cut through the phyllite on Highland Avenue which is dominated by many kink bands and some normal faults (SL-306). The majority of the kink bands are low-angle kinks oriented nearly perpendicular to the plane of the foliation. There are also many smaller scale kink bands and conjugate fold kink sets of variable orientation. The largest kink bands are down-to-the-west in a "normal" sense and are oriented N20 to 40E, 25 to 30 NW. Measurements of the small conjugate fold sets were taken in an attempt to assess the orientation of the axes of strain which

formed the kink bands. Four sets of conjugate folds were measured, and the four solutions obtained (Table A-2, and Plates A-3 and A-4), indicate that the axis of shortening plunges at a steep angle to the south-southeast. The axes of extensional strain plunge at very low angles to the northwest, while the intermediate strain axes are subhorizontal and cluster about the strike of the foliation. Thus, it appears that locally there has been post-metamorphic extension approximately normal to the Annsville-Oscawanna Fault.

Several N-S to N15°W, 65°SE normal faults are also present in the Highland Avenue roadcut. Drag folds of phyllite within the fault planes have nearly horizontal axes and normal movement sense asymmetries. This is corroborated by normal offsetting of some master kink bands which must therefore be older than the normal faults. No evidence that these faults offset the Annsville Fault (Plate A-2) was seen, and it is believed that they do not cross the Annsville Fault.

The Annsville Fault is also exposed on Route 9 approximately 2000 feet southwest of the sandpit (SL-305, Plate 2 and NR-1331 of Ratcliffe, 1976). The phyllite is not seen in contact with Precambrian gneiss on the east side because there is a 25 to 30 foot gap where the fault has been eroded away. In the Precambrian rocks on the east side of Route 9, the gneiss is mylonitized and chlorite, actinolite and sericite are found in the mylonite zones. Marble is also present and strikes approximately N35°E. The orientation of the mylonitic fabric swings from

N60°E to N40°E near the Annsville Fault. The marble is the same as that in which Bucher (1957) reported finding possible cystid fragments (Section A2.1.2.2). On the west side of Route 9, Precambrian gneisses are sheared by very prominent N25 to 35°E, 40 to 45°SE faults. These surfaces exhibit slickensides raking nearly vertically. It is important to note that these faults dip toward the Annsville Fault, which dips more steeply, but their relationship to the Annsville Fault is not discernable from the exposure. Additionally, these low angle dip-slip faults resemble similar features seen along the Thiells fault at the Lovett Power Plant, approximately 4 to 4-1/2 miles to the southwest (N-225, Plate 2, A.3.2.1.1.2).

Along strike to the northeast from the Annsville Fault, the Oscawana Fault is exposed at two places near Oscawana Lake (SL-314, 315, Plate 2A). At these exposures, granitic gneisses of the Precambrian Hudson Highlands exhibit cataclastic texture and the rocks are brittly sheared. At SL-314, nearly horizontal lineations are present on the shear surface which strikes N30°E, 75°SE; however, at SL-315, slickensides along a N20°W, 45 to 60°NE fault zone exhibit dip-slip slickensides and breccia. No slickensides were seen on N30°E shears at SL-315.

#### A3.2.2.1.4 Peekskill Hollow Fault

Peekskill Hollow trends N45°E from the Hudson River (Peekskill Bay) northeast toward Carmel (Plate A-1). This is the largest valley emerging from the southern margin of the Highlands (Berkey, 1911). The only conclusive evidence for a

wide fault zone in Peekskill Hollow are the data from borings and tunnelling along the line of the Catskill aqueduct across the hollow (Berkey, 1911). This fault zone is actually three faults: a mylonitized fault contact between the Highlands gneisses and the Poughquag quartzite on the southeast side of the hollow, and two crushed zones in the Wappinger limestone encountered in borings for the aqueduct.

The gneiss-quartzite contact is described by Berkey (1911) as a fault contact in which the rock is of sound quality. Field evidence confirms this conclusion (SL-300, 325, 326; DF-116, Plate 2A). It is important to note at this point that field mapping during this investigation demonstrated (SL-325, 326; DF-116) that the gneiss-quartzite contact is not offset sinistrally by four north-south faults as mapped by Berkey and Rice (1919) and depicted on the N.Y. State Geologic Map (Fisher and others, 1970). The contact strikes N30 to 45°E, and dips 50 to 60°SE (SL-325; DF-116). The apparent deflections in the contact are caused by the shape of topography; furthermore, no evidence of N-S faulting is exhibited in the rocks along the contact.

Berkey (1911) reports a crushed zone in the Wappinger limestone "nearly central in the valley.....where the rock shows a finely brecciated condition; some portions of the drill cores being literally crushed to bits." The orientation, movement nature, and continuity of this fault zone are unknown. Berkey further reported that the contact between the Wappinger lime-

stone and Annsville phyllite in Peekskill Hollow is not a fault. This is supported by field observations at Van Cortlandtville (DF-103, Plate 2A).

#### A3.2.2.2 North-Northeast Trending Faults

##### A3.2.2.2.1 Manitou Mountain Fault

The Timp Pass Fault projects from Timp Pass northward into the Hudson River just west of Iona Island (Plate 1A). North of the river, at Manitou Mountain, the fault appears to coincide with a topographic lineament stretching along the east shore. Ratcliffe (1976) implied that the Timp Pass Fault lies within the River and "reappears along the east shore of the Hudson River at Manitou Chapel".

Exposures of this fault zone were examined at the eastern end of Bear Mountain Bridge. The rocks are Precambrian, coarse-grained, gneisses consisting dominantly of diopside, quartz, plagioclase, and garnet with localized concentrations of garnet, diopside, pyrite, and calcite. The calcite layers and lenses have weathered deeply, and the pyrite-rich rocks are easily recognized since they weather to a very rusty surface.

Locally, the rock is fractured and faulted and a large shear zone is seen in three outcrops. This shear zone, the largest structure observed, is well exposed 150 feet north of the northern abutment, along Route 9D. At this location, the zone is six feet wide and deeply weathered. The compositional layering at this location is oriented N30°W 30°NE. Many closely spaced fractures within the weathered shear zone are oriented

N30°E and are nearly vertical. Slickensides on these surfaces rake 45°SW. The zone itself strikes approximately N20°E. The first large exposure southwest of Route 9D occurs at the eastern end of the southern bridge buttress. At this exposure, a four-foot wide fracture zone containing discrete shear surfaces with horizontal slickensides was recognized. The zone strikes N20°E and dips 80°NW.

About 20 feet to the southwest, a large, well exposed NNE to NS-trending shear zone is encountered along Route 6/202. This zone is extremely rusty in appearance due to the pyrite content of the host rock in this area. It consists of a major plane that strikes N10°E and several subordinate splaying surfaces with strikes between N30°E and N10°W, and dips from 65 to 85°W. The sheared zone is roughly 6 feet wide. It contains many N40° to 60°E fractures as well as the main curvilinear shears. Two sets of slickensides occur on the shear planes. One set is indicative of strike-slip movement, and the other set rakes more steeply, suggesting dip-slip movement. No strong evidence for age relations between the two sets was found.

The three large shear zones that were recognized, and which occur near the eastern buttress of the Bear Mountain Bridge, are believed to constitute a continuous zone. This zone is oriented north-northeast and could be related to the Timp Pass Fault. The dominant sense of movement on this fault is interpreted to be right-lateral strike-slip. The geometric relationship of the fractures to the main shears support this inter-

pretation. The one occurrence of dip slip slickensides along this shear may have developed either as the result of earlier reverse faulting or a later adjustment to the strike-slip movement. The curvilinear trace of the fault in this area is a reflection of the curvilinear style of the fault plane. This is seen on a small scale in the exposure 75 to 100 feet south of the bridge.

#### A3.2.2.2.2 The Roa Hook Fault

North of the northwest segment of the Hudson River, the rock units, which define a north-northeast plunging antiform, terminate abruptly against the N20°E-trending Roa Hook Fault. West of the fault the rocks strike about northeast, whereas east of this structure they are oriented north-northeast. Deformation along the fault is characterized by: local mylonitization of the rocks, pseudotachylite, shattered and bent plagioclase, and crushed and recrystallized quartz in the gneissic granite. On the north side of the river, the fault marks the contact between gneissic granite on the west, and interlayered amphibolite and quartz-feldspar-biotite paragneiss on the east. To date this structure has not been positively identified on the south side of the river, but at the eastern end of Dunderberg Mountain, near Jones Point, gneissic granite and incorporated amphibolite are brecciated. The amphibolite is also weathered and cut by fairly, tightly spaced fractures. Petrographically, hornblende, in the gneissic granite, is either totally preserved or has been incompletely altered to a mosaic

of several, small, brown biotite crystals. Mortar texture and bent, broken and internally faulted plagioclase crystals were also recognized. These features all indicate that the rocks here are at the edge of and/or within a fault zone. The width of the gneissic granite, near Jones Point, is slightly greater than on the north side of the river suggesting that perhaps the cataclasis, described above, is due to movement on the Roa Hook Fault. This is not unequivocal though because: a) the inter-layered sequence seen east of the fault on the north side of the river has not yet been recognized near Jones Point, although Ratcliffe (1976) has recorded it on his map, and b) the outcrop here lies fairly close to the projection of the Thiells, Canopus and Dickiebush Lake Faults.

#### A3.2.2.2.3 The Dickiebush Lake Fault

East of the Roa Hook Fault is a fairly prominent N15°E trending lineament which passes northward from the river through the Camp Smith Military Reservation. This lineament marks the position of the Dickiebush Lake Fault. According to Ratcliffe (1976) gneissic layering shows left-lateral strike separation of 3 cm, indicating either left-lateral slip or oblique slip, with the west side up relative to the east side. At a second exposure Ratcliffe noted "down to the east separation" across micro-faults oriented N15°W;85°SW and concluded that this is consistent with "left lateral west-up thrust motion on shallow north-plunging slip lines". One outcrop along this fault consists of a light gray to off-white, intensely granulated gneissic granite

with many hematite-stained slickensided surfaces. The host rock is cut by a dark gray-green, finely porphyritic dike. Petrographically the country rock consists of ribbon quartz, elongate, bent, broken and internally faulted plagioclase and abundant intergranular recrystallization. The dike has also been affected by cataclasis.

No other outcrops were seen along this zone although an exposure of mylonitized amphibolite (Station JW-AG, Plate 2) was identified along a N30 to 35°E trending fault, which is probably a splay off the Dickiebusch Lake Fault. This fault was named independently in this report and by Ratcliffe (1976) as the Wallace Pond Fault. According to Ratcliffe (1976), diabase dikes are offset right laterally about 4,000 feet across the Wallace Pond Fault.

#### A3.2.2.3 Peekskill Fault

The Peekskill Fault zone was mapped by Berkey and Rice (1919) as the contact between Precambrian gneisses and the Manhattan Prong, striking east-northeast from Peekskill Bay to Mohegan Lake. The fault occurs along a deeply incised valley which runs through the city of Peekskill (Plate A-1). Very few outcrops are preserved along the fault, but field mapping of this feature has revealed that there is a fault zone along the contact between the Hudson Highlands and the Manhattan Prong. Shearing is visible in isolated outcrops along the fault, and is generally oriented between N55°E and N80°E (SL-339, 342, 343, 345, Plate 2). Nearly a mile east of Peekskill, the western

edge of the Peekskill granite intrusion truncates the Highlands - Prong fault contact. The fault contact emerges from the eastern edge of the Peekskill granite, near the Cortlandt-Yorktown line on Route 202, and appears to merge with the Croton Falls Fault at Mohansic Lake. Field mapping has also revealed that the Peekskill Fault appears to splay at the western end of the Peekskill pluton. One fault zone follows the northwestern edge of the pluton; the other transects the southern edge. The contact of the granite and Manhattan schist is exposed in a spectacular outcrop on the Bear Mountain Parkway near Locust Avenue (SL-343, Plate 2A) where intense shearing, with some unhealed brecciation, is developed both within the granite and the schist. Two faults oriented N84 to 90°E, 50°S, with prominent strike-slip slickensides, border a block containing the east-west trending contact between granite and schist. Two granite dikes occur within the schist and are in close proximity with N30°E, 60 to 90°E strike-slip faults. Slickensides raking 0 to 30° were measured on one of the dike-schist contacts. Within the granite at this outcrop, several small shears are oriented N55°E, 85°SE. The intensity of shearing in the granite increases toward the fault contact with the schist. Additional shears are visible in the granite on Locust Avenue (SL-344; JT-90) which are oriented N50°E, 90° with strike-slip slickensides. Outcrops in Precambrian gneiss on Locust Avenue (SL-345; JT-88) exhibit a strong cataclastic texture, with foliation and shearing oriented N80°E, 80 to 90°SE. Strongly developed mineral lineations rake 40° east.

Excellent exposures of the Peekskill granodiorite occur at the abandoned quarry (SL-337, Plate 2A), located on Millstone Hill near the southwest edge of the Peekskill pluton. The rocks of the quarry exhibit a dominant east-west fracture fabric which appears to have been the "rift" direction for quarrying. The south wall of the quarry exposes two pronounced fault zones. One fault is oriented N75 to 85°W, 90°, and contains openwork breccia and weakly developed slickensides, which rake 0 and 15°NW. No mineralization was found along the fault. The other fault is oriented E-W, 75°N and is intersected by a low-angle E-W, 40°S fault, which contains openwork breccia. The low-angle fault truncates a N25 to 30°E, 60°W brecciated zone. The west wall of the quarry contains a wide zone of N0 to 20°E, 65 to 75°W shear joints which brecciate the granite at the intersection of the E-W faults. In the northwest corner of the quarry, a large N75°W, vertical fault with slickensides raking 5 to 10°NW, truncates a 5 foot thick N25°E, 80°NW brecciated zone. A series of N60°W, 55°NE strike-slip shears also appears to merge at a low angle with the N75°W fault. The general east-west to west-northwest trend of faulting at the southern edge of the Peekskill Granite projects eastward to Lake Mohansic where the Croton Falls Fault is exposed. Previous workers (Espejo, 1969; Mose, et al., 1976) did not observe evidence for faulting in the granite because these same exposures were cited as exhibiting no faults. Careful examination of the granite has shown that faults are present as previously described, and that these

faults are clear evidence for post-cooling disruption of the Peekskill Pluton. It further appears that the Peekskill Fault zone intersects the Croton Falls Fault System at Mohansic Lake, based on the projection of the Millstone Hill faults east-southeast toward Mohansic Lake, and the occurrence of faults and shears at the southeastern contact of the pluton (SL-269, Plate 2A).

### A3.2.3 The Croton Falls Fault System

The Croton Falls Fault System, as defined in this investigation, refers to a series of shear zones which pass from Croton-on-Hudson, N.Y. to Amawalk, N.Y. and beyond (Plate A-1). Berkey and Rice (1919) mapped two northeast-trending faults in the area north of the New Croton Reservoir (Turkey Mountain). Sneider (1962) reported several shear zones adjacent to the border between the Hudson Highlands and the Manhattan Prong at Croton Falls. Prucha and others (1968) published a map of this fault boundary, calling it the Southern Border Fault which they described as a high angle reverse fault based on an exposure near Somers, N.Y. The Southern Border Fault has been subdivided in this report into the Croton Falls Fault described below and the Peekskill Fault described in Section A3.2.2.3. Mose and others (1976) show a major regional fault extending northeast from Croton-on-Hudson to the Brewster, N.Y. area, within 5 miles of Connecticut. Two ultramafic to granitic intrusive bodies occur in the fault zone near Croton Falls - the Croton Falls Pluton and the Peach Lake Pluton (Sneider 1962, Prucha and

others, 1968). The importance of this fault system is underscored by its tectonic function as a border fault, the existence and location of these mantle derived intrusive bodies and by the fact that the Croton Falls System is directly aligned with northeast faults mapped in the Newark Basin near Rockland Lake and Long Clove (Appendix B; Plate A-1).

Field mapping of the area between Amawalk and Croton-on-Hudson has shown that the trace of the Hudson Highlands - Manhattan Prong contact diverges westward from this system of intensive shearing near Mohansic Lake. The contact swings from NE-SW through E-W to WNW-ESE, where it is truncated by the Peekskill granite approximately 1 mile west of Yorktown (see Plate A-1). From Mohansic Lake southwest to Croton-on-Hudson, three subparallel shear zones have been mapped in the rocks of the Manhattan Prong. They are named, from northwest to southeast, the Prickly Pear, Croton, and Teatown shear zones (Plate A-2).

#### A3.2.3.1 Northeast Trending Faults

##### A3.2.3.1.1 The Croton Falls Fault

The Croton Falls Fault (Plate 1A; A3.2.3) is not directly exposed at the surface in the area between Amawalk Reservoir and Mohansic Lake; however, evidence for the fault is exposed at the southern end of Amawalk Reservoir (SL-257, 258, Plate 2A) where a large fold structure and healed fault zones within Precambrian gneisses of the Hudson Highlands are exhibited at the northwest bank of the reservoir. These structures,

however, are absent in highly contorted and metamorphosed Manhattan schist on the southeast bank of the reservoir. Within the Manhattan schist (SL-258) a prominent shear zone occurs along the plane of foliation and strikes N80°W, 80°N. Slickensides on the shear surface rake 60 to 75°E. Schist in a nearby quarry (SL-259) is intensely faulted in several directions. Many faults are oriented N50 to 60°W, 60 to 65°NE and show oblique dextral movements. These northwest-trending faults, which consistently offset east-west vertical faults, show brecciation and strike-slip movements. On N.Y. Route 35, west of the Amawalk dam, a prominent N55°E, vertical strike-slip fault zone truncates an east-west strike-slip shear (SL-260).

At Mohansic Lake, Precambrian gneisses are exposed on the north side (JT-52; SL-254), and on the south side, rocks of the Manhattan schist are exposed along the Taconic State Parkway (SL-261, 262). Little can be said about the fault here since it is covered by the lake. The rocks on each side of the fault, however, are intensely sheared.

#### A3.2.3.1.2 The Prickly Pear Shear Zone

The Prickly Pear Shear Zone is named for exposures of intensely sheared Manhattan schist occurring on the southeastern flank of Prickly Pear Hill between Croton-on-Hudson and Chimney Corners (Plate 1A; SL-228, 229, 230, Plate 2A). A roadcut on Route 9 North (SL-229) has exposed, at its south end, a 10 foot thick, vertical fault zone containing brecciated schist and fine gouge. The fault is oriented N40°E and exhibits horizontal

slickensides. The movement sense of this fault is uncertain. A paved road to the top of Prickly Pear Hill has exposed the fault again in a roadcut east of the summit (SL-230). The fault is in Manhattan schist and is oriented N40°E, 90° with prominent horizontal slickensides. The shear zone apparently swings to N55 to 60°E, parallel to the regional foliation, northeast of SL-230. The trace of the fault appears to contain the Torment Hill body of biotite-hornblende diorite and gabbro with minor pegmatitic granite (JT-22), located southwest of the end of Torment Hill. The origin and occurrence of the body has been discussed previously (Section A2.3.1). The trace of the Prickly Pear zone, east-northeast of Torment Hill is poorly exposed. Faulting along the trace is exposed again near Hunters Brook Bridge (SL-233) on Route 129 at New Croton Reservoir, but is not seen again to the northeast until the Mohansic Lake area (SL-261, 262, 265). Outcrops along the Taconic State Parkway (south) between Baldwin Road and Mohansic State Park exhibit several through-going N40°E, vertical, strike-slip faults with breccia and gouge that range from 5 to 20 feet thick. These faults cross cut older, high angle reverse faults with NE and NW strikes. The largest fault (SL-262) is 15 to 20 feet thick, and exhibits smeared and powdered mineral deposits, which appear to be zeolites. Individual shear surfaces within the fault zone vary from N30°E to N55°E. Precambrian rocks on strike to the northeast of this fault (JT-52; SL-254) are also intensely sheared.

From Route 9 near Montrose, the southwest projection of the Prickley Pear Shear Zone aligns with the probable fault through Long Clove in the Palisades diabase of the Newark Basin (Plates 1A and B).

#### A3.2.3.1.3 Croton-Teatown Shear Zones

Southeast of the Prickly Pear shear zone, two additional shear zones of the Croton Falls Fault System have been mapped (Plate 1A). These shear zones - the Croton Shear Zone and Teatown Shear Zone - are poorly exposed in the area between the New Croton Reservoir and the Hudson River. Some overlap of these zones is likely.

The existence of the Croton Shear Zone was suspected because Berkey and Rice (1919) had mapped a large fault along the northwest flank of Turkey Mt. north of the reservoir. Field mapping has confirmed the existence of this shear zone (SL-241, 242, 244, 245, 253, 264; JT-20, Plate 2A). Along the Taconic State Parkway, near Underhill Avenue, two large N35 to 40°E vertical faults containing breccia and gouge are exposed. It appears that both dextral and sinistral strike-slip fracture geometries are present, however, the area of rock between the faults contains many north-south fractures that cut across the east-northeast faults which are interpreted as dextral synthetic slices. The N-S fractures stop at the N30 to 40°E faults, suggesting a post-dextral, sinistral strike-slip movement plan. Additional faults of similar character are exposed on the northern bank of the reservoir, on Route 129.

The southwest end of the Croton Shear Zone is poorly exposed. A large fold (possibly  $F_2$ ) in the Inwood-Manhattan contact has been mapped in Croton-on-Hudson, which extends the mapping of Wissig (1970) from the Ossining quadrangle into the Haverstraw quadrangle. Strike-slip faulting occurs along the limbs of this fold in Croton (SL-203, 208; JT-32; SL-223, Plate 2A). The  $F_2$  fold in Croton has a clockwise rotation sense (Z-shape) and the short limb is oriented roughly north-south. Thus, it appears that the limbs of the fold are favorably oriented so as to experience sinistral strike-slip fault movements along both the long limbs (en echelon, northeast-trending main shears) as well as along the short limb (N-S synthetic shear).

The Teatown Shear Zone (Plate 1A) is the least well exposed of the Croton Falls Fault System. Berkey and Rice (1919) mapped a fault in this zone along the southeastern flank of Turkey Mt. This fault passes through New Croton Reservoir very close to a 700 foot wide brecciated zone reported by Berkey (1911) from borings along the line of the Catskill Aqueduct. Roadcuts along the Taconic State Parkway, south of the reservoir (JT-49, JT-50, Plate 2A), exhibit a series of N-S and N40°E, 75 to 90°SE faults with strike-slip to oblique-slip slickensides. The south end of JT-49 shows that a N-S, 65°E strike-slip fault, which projects toward the aqueduct crushed zone, is truncated by a N35°E, 70°SE strike-slip fault. This N35°E fault is nearly coincident with Berkey and Rices' fault located southeast of Turkey Mt. Although no conclusive movement sense is visible,

this pattern strongly resembles the sinistral fault geometries described at Indian Point (Dames & Moore, 1975). The Teatown Shear Zone appears to pass to the southwest along the flanks of the Teatown anticline of Wissig (1970). The anticline is cored by pink granitic gneiss of the Fordham Gneiss and is flanked by deeply incised valleys which are underlain by eroded Inwood marble. Some brecciated N30°E and N40°E, 75 to 90°SE strike-slip faults are present in the Fordham Gneiss on Route 9 north in Croton-on-Hudson (SL-240).

In general, the southwestern portion of the Croton Falls Fault System exhibits a decrease in the intensity of strike-slip faulting toward the southeast. The Prickly Pear zone is the most intense and the Teatown zone is the least intense. Low-angle shears and ductile folds appear to increase in intensity toward the southeast. Across the Hudson River to the southwest, the Rockland Lake Fault, the Hook Mt. Fault, and the Trough Hollow Fault strike N40°E, and appear to be sinistral strike-slip faults (Plate A-1). The northeast projection of these faults aligns them with the Croton-Teatown shear zones.

#### A3.2.4 Popolopen Brook Structure

The segment of the Hudson River, between Jones Point and the Bear Mountain Bridge trends about N60°W and is an area where lithological contacts curve westward as they cross the river between Dunderberg Mountain and Manitou Mountain. In addition, the Dunderberg Fault and possibly the Roa Hook Fault appear to be similarly rotated. This portion of the river is

aligned with Popolopen Brook, which occurs within a topographic depression trending N50 to 60°W (Plate 1). Further northwest, Dodd (1965) mapped a shear zone on strike of this northwest trending lineament; however, he indicated neither deflections nor offsets of the rock units across the shear zone.

Adjacent to the river bend, small scale faulting with recognizable offsets was observed at only one exposure (Station JW-126 N). Several closely spaced small scale faults, ranging in strike from about N60°E to N60°W and dipping from 50°N to nearly 90°, were identified. In plan view it appears that the N60°E and N60°W faults define a conjugate strike-slip system, with the former showing right-lateral separation and the latter displaying left-lateral movement; however, most of these faults dip toward the north at about 60°. Furthermore both right and left-lateral strike separations occur across similarly oriented small scale faults. Since a three-dimensional kinematic analysis was impossible on the outcrop, several oriented samples were removed and cut in the laboratory. The results show that both normal and reverse dip-separations are larger than strike-separations. Right-lateral separation is associated with normal movement and left-lateral separation is related to high angle reverse faulting. Drag along faults showing left-lateral separation indicates that, at least, these structures are oblique-slip faults with both dip-slip and strike-slip components. In plan view, the small scale geometry across some of the faults reflects the much larger scale geometry across the river.

The Popolopen Brook Structure is expressed as a large topographic lineament trending N60°W; the portion of this lineament which has been investigated is approximately 9 miles long. The lineament is pronounced in the gneiss of the Highlands and the metasediments of the Manhattan Prong, but it is weakly expressed and discontinuous where it passes through the Cortlandt Complex.

Two faults, the Dunderberg and the Roa Hook Faults, appear to be deflected, along with the lithologies and foliations, across the lineament, which coincides with the northwest segment of the Hudson River. The Dunderberg Fault deforms Siluro-Devonian dikes, and was active at that time. Other prominent faults, such as the Timp Pass Fault and the Thiells-Annsville Fault, do not appear to be noticeably deflected by this structure. No offsets of lithologies have been observed in the area of investigation west of the river bend (Dodd, 1965). As stated previously, laboratory analysis of oriented rock samples suggested that dip-slip movement exceeds strike-slip movement along small-scale faults. This may represent the movement sense of larger scale faults along this lineament.

The time of origin of the Popolopen Brook Structure can be interpreted in two general ways: 1) that it formed in Precambrian time and was reactivated through time due to tectonic adjustments, and 2) that it formed after the Paleozoic metamorphism and intrusion of the Cortlandt Complex. This could explain the offsetting of the Dunderberg Fault which is seen to

deform Paleozoic dikes. A Precambrian time of origin is preferred to a Paleozoic origin. It can be interpreted that this is a fundamental adjustment feature which formed during orogeny in Precambrian time. Throughout the ensuing complex geologic history, this, and perhaps other northwest-trending features experienced considerable reactivation in adjustments, which may account for these features in the Cortlandt Complex, Rosetown Complex and the Newark Basin.

#### A3.2.5 Topographic Expression of Some Faults

A marked topographic difference, based on peak elevations, occurs across the Mott Farm Road Fault, a feature especially evident on aerial photographs. To the north, the Timp, Bald Mountain and Dunderberg Mountain show respective elevations of 1060, 1100, and 900 feet, whereas to the south, Buckberg Mountain, the tallest peak, shows an elevation of 793 feet. Thus there is an elevation difference of about 110 to 310 feet across the Mott Farm Road Fault.

Across the northeast trending Cedar Flats Fault, which is the southern continuation of the lineament extending from the Timp Pass Fault, the maximum elevations, in the Precambrian terrain, are 1023 feet, west of the lineament (on the Pingyp) and about 534 feet, east of the lineament. Interestingly, the Mott Farm and Cedar Flats Faults intersect, and the Cedar Flats Fault extends southwestward, to the Ramapo Fault. These zones and the Willow Grove and Ambreys Pond Faults then combine to define the boundaries of a block that is topographically lower than the

northern and western counterparts (i.e. the area north of the Mott Farm Road Fault and west of the Cedar Flats, Blanchard Road and Ramapo Faults).

Gneissic granite and paragneiss crop out at peak elevations on both sides of the two major lineaments which mark the aforementioned elevation difference (i.e. Cedar Flats - Timp Pass and the Mott Farm Faults). Specifically, the Timp and Buckberg Mountains which occur on opposite sides of the lineaments are both cored by biotite gneiss (Dodd, 1965; Ratcliffe, 1976). Other prominent peak elevations such as Bear Mountain, West Mountain, Bald Mountain, and Dunderberg Mountain are cored by gneissic granite and paragneiss. Thus, it does not appear that the elevation differences can be readily explained by differential resistance to erosion as a function of differences in bulk composition. It is also difficult to imagine that these elevation differences were produced by glacial action. While glaciation would enhance negative relief in the downflow direction, it is not likely to create it.

The area underlying the Newark Basin, and bounded on the west by the Ramapo Fault, was downdropped to the east relative to the exposed Precambrian crystalline rocks to the west, during formation of the basin and possibly later as well. The senses of topographic displacement, noted in the preceeding paragraph, agree with this relative tectonic movement, which suggests that the recorded elevation differences may be a geomorphic expression of Mesozoic faulting. The presence of numer-

ous fractures which parallel the strike of the Mott Farm Road Fault and dip to the south at about 60 to 70°, the intensely fractured and rusty weathering rock characteristic of the Ramapo Fault, and the agreement of tectonic and topographic displacement all favor this interpretation.

#### A4.0 CONCLUSIONS AND INTERPRETED HISTORY OF FAULT MOVEMENTS

##### A4.1 PRECAMBRIAN FAULTS

On the basis of field observations made during this investigation, two separate episodes of faulting have been recognized. The older episode is represented by the cataclasis of rocks during the Grenville Orogeny, broadly synchronous with the intrusion of local pegmatites and diorite-monzonite rocks of the Canopus Pluton. Ductile deformation during the Grenville Orogeny, which affected gneisses and plutonic rocks alike, recrystallized and healed these cataclastic fault zones. The younger episode of faulting appears to be represented by a late Precambrian phase of cataclasis and diaphthoresis, which is marked by the re-utilization of the older, Grenvillian fault zones. Faults belonging to the Precambrian Ramapo-Canopus Fault System are shown on a generalized and simplified tectonic map of the system in the Peekskill area, N.Y. (Plate A-7).

##### A4.1.1 Grenvillian Faults

During the Grenville event, an extensive, continuous, deeply rooted fault zone was active. The Dennytown and Canopus Hollow Faults compose this zone north of the bend in the Hudson River. The lineament that coincides with the Dennytown Fault and strikes N30 to 40°E can be traced southwestward to Travis Corners and can be projected from there, through South Mountain Pass, toward the Timp and the Ramapo Fault. The Canopus Hollow Fault extends southwestward from Canopus Lake to Annsville, and extends across the Hudson River to Lake Boyce and the Ramapo

Fault. These fault zones probably represent part of the ancestral Ramapo-Canopus Fault System (Plate A-7). The Canopus Pluton intruded into the Canopus Hollow Fault System during the Grenville Orogeny, and differentiated into fine-grained diorite to coarse-grained quartz monzonite (JW-142, Plate 2A). The igneous intrusives and the country rocks were both affected by ductile deformation during the Grenville event. Ratcliffe and others, (1972) interpret the emplacement of the pluton as synchronous with  $F_2$  folding in the Precambrian gneisses. Ductile folding of the pluton and the country rock are exposed at JW-148. Flow lineations in the pluton, defined by feldspar phenocrysts, suggest upward flow of the magma with some dextral rotation (JW-147). Ratcliffe and others (1972) interpret the emplacement as occurring during dextral strike-slip faulting. Limited evidence, such as minor fold asymmetry and rotated phenocrysts, within the pluton lend support to this interpretation.

The Lake Boyce hornblende-granite intruded the southwest segment of the Canopus Hollow Fault, west of the Hudson River (Plate A-5, A-7). Rb/Sr whole rock studies indicate that the intrusion is  $1061 \pm 12$  m.y. old (Mose and others, 1975). The granitic and dioritic intrusions along the Canopus Hollow Fault, and the many iron ore deposits that occur along the faults of the system, characterize its members and suggest that they were all active during the Grenville event.

Other minor faults, which trend N40 to 55°E and are preserved in Precambrian gneisses between Peekskill and Mohegan

Lake, were probably also (Plate A-7) active during the Grenville event (SL-303, JT-81, SL-336, Plate 2A).

#### A4.1.2 Post-Grenville Precambrian Faults

Recurrent fault movements, along the eastern edge of the Canopus Pluton, in the Canopus Fault granulated and altered both plutonic and country rocks during Late Precambrian time. The geometry of minor scale folds, which fold the granulated gneisses (SL-310), suggest a sinistral strike-slip movement sense along the fault zone. Additionally, these rocks are altered by diaphoresis within the fault zone to assemblages indicative of temperature-pressure conditions below hornblende granulite facies.

Helenek and Mose (1976) have identified several late tectonic zoned plutons within Grenvillian paragneiss, collectively called the Canada Hill Granite. They have shown that the Canada Hill Granite formed by a partial melting of the paragneiss. Isotopic studies yielded a Rb/Sr age of 914 m.y. (Helenek and Mose, 1976). K/Ar and Rb/Sr mineral ages from the Canopus Pluton yielded ages of 700 to 524 m.y. and a K/Ar age on phlogopite from the Canopus Hollow Marble yielded an age of  $893 \pm 10$  m.y. (Ratcliffe and others, 1972).

The K/Ar ages can be interpreted as representing the age of crystallization or the age of the last significant thermal event. This suggests that the Precambrian rocks were kept at a temperature greater than that of argon retention until 800 to 900 m.y. ago. It is also possible to interpret an episode of

post-Grenville, Late Precambrian deformation along the Canopus Hollow Fault. Sinistral minor folds (SL-310, Plate 2) in an altered, healed mylonite which deforms the Canopus Pluton, together with previously mapped cross-shears in the pluton (Ratcliffe 1970, 1972), and sinistral offsets and healed breccias along the Buckberg Mountain Fault, suggest an episode of post-Grenvillian, sinistral transcurrent faulting. This interpretation may serve to explain the late Precambrian age dates discussed above. This episode of faulting probably represents the effects of rifting (Stewart, 1976), which may have initiated Late Precambrian orogenic deformation of continental margin type sediments (deposited as a result of rifting). These effects have been recognized in Newfoundland by Kennedy (1976).

#### A4.2 PALEOZOIC FAULTS

During Late Precambrian to Early Ordovician time, the rocks of the Poughquag-Lowerre and the Wappinger-Inwood formations were deposited along the stable continental margin. Orogenic uplift of the continent in Middle Ordovician time interrupted sedimentation on the carbonate bank represented in this area by the Inwood-Wappingers sequence. Block faulting, attendant with uplift, caused the break-up of the carbonate bank resulting in a major unconformity. The Annsville-Manhattan exogeosynclinal sequence was deposited unconformably on top of this.

The next recognizable phase of deformation is characterized by a predominance of crustal shortening, resulting in horizontal translation, development of  $F_1$  and  $F_2$  folds and a

Transcurrent fault movements along these fault systems re-utilized and cross cut the earlier reverse faults formed during the early stages of the Taconic Orogeny. The most prominent fault zones involved in this episode of deformation were the Canopus Hollow and Dennytown Faults, the Oscawana-Annsville-Thiells Faults, the Peekskill Hollow Fault, and the Peekskill and Croton Falls Faults. The Cortlandt and Rosetown plutons, lamprophyre dike swarms, the Peekskill Granite and its pegmatic differentiates, the Peach Lake intrusive and the Croton Falls complex were emplaced along various fault zones of the fault systems (Plate A-8). The age of these igneous rocks ranges from 435 m.y. to 371 m.y. In summary, it may be interpreted that the northeast and east-northeast striking fault zones of the Ramapo-Canopus and Croton Falls systems were active during this transcurrent event (Plate A-8).

#### A4.2.1 Dennytown-Canopus Hollow Faults

It is evident from the best exposures that the healed and diaphthoretic Precambrian faults were reutilized (SL-304, 310, 324, 328, Plate 2). Both fault zones exhibit predominantly dip-slip movement. The inlier of Cambro-Ordovician Poughquag quartzite at the north end of Canopus Lake contains well developed quartz-filled gash veins indicative of reverse movement sense along a NE-trending thrust fault dipping 45 to 64°SE. The quartzite also exhibits a well-developed schistosity, parallel to the quartzite-geniss fault contact, with strongly developed, vertically raking slickensides. This clearly resembles the

"thrust-structure" described in Dutchess County, N.Y. by Balk (1936, pp. 737-744).

At the southwest corner of Canopus Lake (SL-330, 331) a large NE-striking fault zone exhibits strike-slip shearing of mylonite with some gouge present. This wide fault zone is the most convincing example of Paleozoic or younger strike-slip deformation along the Canopus Hollow and Denntown Faults.

#### A4.2.2 The Annsville - Oscawana Fault

At Annsville, a fault truncates older Precambrian mylonites (SL-303, 305, Plate 2A). Small wedges of Wappinger limestone are preserved along the fault between the Annsville phyllite and the Precambrian gneiss (Plate A-2, SL-303, SL-313). The high-grade metamorphic assemblages of the gneiss along the fault zone have retrogressed to lower grade assemblages (SL-303). The movement, as indicated by slickensides at Annsville, is predominantly dip-slip. Locally, a phyllonitic mylonite, subparallel to the phyllite-gneiss contact, is developed.

The older mylonite, the dip-slip surfaces in Precambrian gneiss at Annsville (SL-305), and the phyllonitic mylonite (SL-303) are truncated by later movements along the Annsville Fault. Although not compelling, both the exposure of the fault at Oscawana Lake (SL-314), and the eastward bend in the phyllite-gneiss fault contact north of Annsville, near Continental Village, strongly suggest that dextral strike-slip movements contributed to the map pattern. Thus it appears that the re-

verse movements were followed by dextral transcurrent movements along the Annsville fault.

#### A4.2.3 Peekskill Hollow Fault

Very little is known about the nature or extent of the Peekskill Hollow Fault. The Wappinger limestone is intensely brecciated at the aqueduct crossing, indicating that movement must have occurred along the fault in post-Middle Ordovician time. Along the east side of the valley, between Peekskill and Adams Corners (South Putnam Valley), the Poughquag quartzite-Precambrian gneiss contact is exclusively a mylonite (SL-300, 325 Plate 2A; Berkey, 1911). This mylonite appears to have formed during dip-slip movement, as evidenced by the schistose nature of the mylonite, the down-dip slickensides on the quartzite bedding (SL-325, 326), and a fault wedge of quartzite within the gneiss (SL-300). At two locations (SL-300, 325) the mylonite is sheared by strike-slip faults, one of which exhibits clear dextral offset of bedding along northeast fractures (SL-325). These observations demonstrate the multiple nature of the Paleozoic movements along this fault, in which dip-slip movements were followed by strike-slip movements.

#### A4.2.4 Peekskill Fault

Cambro-Ordovician metasediments of the Manhattan Prong were brought into fault contact with gneisses of the Hudson Highlands along the east-striking Peekskill Fault. Although no direct evidence for the movement sense is present, due to the paucity of outcrops, it appears that dip-slip movement occurred

on the fault. The foliation of the meta-sediments is sub-parallel to the fault, dips steeply northwest, and exhibits vertical mineral lineations. Strike-slip shears subsequently deformed the meta-sediments, gneisses, and the Peekskill granite intrusion, which is situated within the fault zone (SL-339, 342, 343, 337, Plate 2).

#### A4.2.5 Croton Falls Fault

The southeastern edge of the Hudson Highlands was brought into fault contact with Cambro-Ordovician meta-sediments of the Manhattan Prong during Middle Ordovician time. The fault dips northwest (Prucha et al., 1968; JT-1) beneath the Precambrian. The Manhattan schist near the fault south of Lake Mohansic (SL-261) is intensely sheared and folded. The geometry of a large-scale fold within the schist suggests that the Highlands moved upward relative to the schist. Smaller scale, high-angle, north-dipping reverse faults are exposed in the same area (SL-261). The fact that these features are cross cut by low-angle, north and south dipping fractures, and large northeast trending strike-slip faults (SL-261, 262, 264) indicates that the earlier vertical movements along the Croton Falls Fault were replaced by younger strike-slip movements. These younger movements were associated with the displacements along the many east-west trending faults that formed or were reactivated during and after the intrusion of the Cortlandt Complex (Ordovician-Silurian) (Dames & Moore, 1975).

#### A4.3 MESOZOIC FAULTS

The map scale geometry of the fault zones that were reactivated during Mesozoic time is interpreted to be the result of sinistral movements along the major northeast trending zones of the Ramapo and Croton Falls Fault Systems (Plate A-9). The fault zones of the Canopus System seem to have played a limited role during this reactivation. The deflection of Mesozoic deformation around the Rosetown Pluton was accomplished through the utilization of north-northeast trending synthetic shears and northeast trending major shears. Evidence from within the Newark Basin (Appendices B and C) indicates that northeast sinistral strike-slip faulting occurred during and after the sedimentation and lithification of the Newark strata and the emplacement and cooling of the Trio-Jurassic diabase and basalt.

Although Mesozoic deformation along the east-northeast trending Letchworth and Mott Farm Road Faults is inconsistent with an idealized model of a northeast sinistral wrench fault, data obtained from Pompton Lakes, N.J. (Appendix C) and Peekskill, N.Y. (Appendix A) indicate that Paleozoic east-northeast zones were utilized for dip-slip adjustments between en echelon major northeast sinistral fault systems. The Mott Farm-Peekskill Fault and the Letchworth Fault are favorably oriented to experience compressive deformation during Mesozoic, sinistral, transcurrent faulting along N40°E faults. Thrust fault movement across older east-northeast to west-northwest trending faults can be postulated. This may explain the dip-slip

adjustments observed in the areas of Peekskill, N.Y. and Pompton Lakes, N.J. (Appendix C), and may also explain the northern termination of the Newark Basin. Dip-slip adjustments that were observed along the aforementioned fault zones may also be attributed, in part, to differential uplift.

Additionally, exposures of Wappinger limestone on Park Road (SL-45, CH-9, Plate A-5), Route 9W (SL-40, 43), and the limestone quarry in Tomkins Cove, N.Y. are stained with red mud; and fractures in the limestone are filled with Trio-Jurassic sedimentary limestone breccia with a red mud matrix containing siltstone fragments (SL-45). This evidence, which occurs north of the present Newark Basin terminus, strongly suggests that the Newark Basin at one time extended farther north. Late Mesozoic and younger epeirogenesis may explain the differential erosion of the north end of the Newark Basin, and may likewise account for some of the dip-slip adjustments seen along east-northeast trending faults.

#### A4.3.1 Dennytown Fault

Strike-slip shears across older mylonites occur on Route 301, at the southwest end of Canopus Lake (SL-330, 331, Plate 2A). The presence of gouge and sinistral strike-slip fracture geometry suggest that the Dennytown Fault experienced some Mesozoic movement. Fracture geometry likewise suggests sinistral strike-slip movement along the fault zone at SL-327 in Fahnestock Park. The fact that these occurrences were the only ones seen along the fault zone indicates that strike-slip move-

ments, if present in the Mesozoic, were neither extensive nor intense (Plate A-9).

#### A4.3.2 Annsville-Oscawana Fault

Very little evidence exists to suggest Mesozoic movement on the Annsville-Oscawana Fault. The roadcut in the phyllite at Annsville exhibits several normal faults striking approximately north-south (SL-306, Plate A-2). These faults were not found to cross the Annsville Fault in the Annsville sandpit (SL-303). Additionally, kink bands in the phyllite indicate extensional strain approximately normal to the Annsville-Oscawana Fault (Plates A-3 and A-4). The angular relationship between the north-south faults and the Annsville Fault may suggest that the Annsville moved sinistrally during Mesozoic time; subsequent movements along the north-south faults were normal, producing well-developed drag folds. This possibility, however, is highly conjectural, and the last movements of the fault may either be Paleozoic or Mesozoic. The fact that a polished and striated glacial surface is not offset by the fault indicates that it has not moved since the Wisconsinan glaciation (15,000 to 17,000 years before present).

#### A4.3.3 Peekskill Fault

Evidence for possible Mesozoic movement along the Peekskill Fault is limited to a few key exposures. Post-crystallization fault deformation of the Peekskill Granite is clearly visible at the contacts (SL-343, 269, Plate 2A), and in the Millstone Hill quarry (SL-337). The faults are strike-slip

and are oriented approximately north-south and east-west. The quarry also contains a set of low-angle faults and shear fractures, which strike east-west and dip north and south. One of these faults contained open-work breccia that was sheared by a N25 to 30°E, 60°NW fault, which also contained open work breccia. These faults may represent local dip-slip faults that formed along the Peekskill Fault when the Croton Falls and Ramapo Systems were moving sinistrally during Mesozoic time. This phenomenon was observed on similar east-northeast trending fault zones at Pompton Lakes, N.J.; and on the Mott Farm Road Fault north of Tomkins Cove, N.Y. (Appendix C and A3.2.1.4.2). These faults may equally represent local dip-slip adjustments that occurred as a result of uplift. Since several of these low-angle faults truncate or cross-cut north-northeast and east-northeast strike-slip faults, these features could be associated with Mesozoic or younger uplift. Well-formed sprays of zeolite crystals are present along the Peekskill Fault (SL-335, Plate A-9). Studies of similar minerals (Appendix E) have shown that they formed as a late stage of Mesozoic mineralization.

#### A4.3.4. Croton Falls Fault System

As with the faults described above, there is only circumstantial evidence to indicate that the faults of the Croton Falls Fault System were active during Mesozoic time north of the Hudson River (Plate A-9). The faults exposed south of Mohansic Lake, along the Taconic Parkway (SL-261, 262, 264, 265; JT-203, Plate 2A), trend N30-40°E, and are vertical strike-slip faults

in which breccia and gouge are present. The small-scale fracture geometries on these faults suggest a sinistral movement sense, and they appear to transect zones of N30°E faults with dextral strike-slip fracture geometry (SL-264). At one fault (SL-262) it appears that zeolite mineralization on the N35 to 40°E fault is smeared. This fault is in close proximity to the Peekskill Fault, the west end of which contains zeolites as described above. Sinistral fault geometry is also expressed along the N35°E faults, which are exposed along the Taconic State Parkway (JT-20, SL-264). Sinistral strike-slip fault movements can be interpreted as being localized along the limbs of the Croton fold (see Section A3.2.3).

The occurrence of sinistral N40°E strike-slip faults at Rockland Lake Gap, Trough Hollow and Hook Mtn. and Long Clove, within the Triassic-Jurassic Newark Basin directly southwest of, and aligned with the Croton Falls System, appears to support the geometric evidence for sinistral strike-slip fault movement along the Croton Falls System during the Mesozoic.

#### A4.4 CONCLUSIONS

As a result of the investigations presented in this Appendix, the following conclusions may be reached relative to the general objectives of this study:

- 1) The Ramapo Fault System between Suffern and Ladentown, N.Y., consists of the northeast trending Ramapo Fault which forms the boundary between the Hudson Highlands and the Newark Basin (Plates 1A & B). North of Ladentown, N.Y.,

the Ramapo Fault branches on either side of the Rosetown Pluton, with one branch continuing northeastward via the Willow Grove, Blanchard Road, Cedar Flats, Ambreys Pond and Timp Pass Faults. The other branch passes southeast of the surface exposures of the Rosetown Pluton via the Letchworth and Thiells Faults (the latter is en echelon to the Ramapo Fault). North of the Rosetown Pluton, the branches merge with the east northeast-trending Mott Farm Road Fault, which reappears on the eastern shore of the Hudson River as the Peekskill Fault. North of Peekskill, N.Y., the Ramapo Fault System continues, as the Canopus and Annsville-Oscawanna Faults, as far as Canopus Lake, where they are joined by the Dennytown Fault (Plate 1A). The Peekskill Fault turns to the east-southeast near the Peekskill Pluton and connects the Ramapo Fault System with the Croton Falls Fault System at Yorktown Heights, N.Y. To the northeast of Yorktown Heights, the Croton Falls Fault System (which is en echelon to the Ramapo Fault System) is composed of the Croton Falls Fault; to the southwest it branches into the Prickly Pear, Croton and Teatown Shear Zones.

2. The faults which were active during the Precambrian are 1) the colinear Ramapo, Timp Pass and Dennytown Faults, 2) the Thiells, Canopus Hollow and Annsville-Oscawanna Faults, as well as 3) several smaller faults, such as the Buckberg Mountain, Bald Mountain and Dunderberg Faults.
3. Paleozoic fault activity occurred along all the northeast, east-northeast and east-west striking members of the Ramapo and Croton Falls Fault Systems (Plate 1A and B).
4. The youngest fault activity in the area occurred during the Mesozoic on 1) the Ramapo, Cedar Flats, Blanchard Road, Willow Grove, Ambreys Pond, Letchworth and Thiells, Annsville Faults of the Ramapo Fault System, 2) the Prickly Pear, Croton and Teatown Shear Zones and Croton Falls Faults of the Croton Falls Fault System, and 3) the Mott Farm Road and Peekskill Faults which join the Ramapo and Croton Falls Fault Systems.

TABLE A-1

## MINERAL ASSEMBLAGES OF ROCK SAMPLES FROM CANOPUS HOLLOW FAULT

Samples											
DF-104B (marble with inclusion)	microcline	quartz	plagioclase	sodic hornblende	scapolite	riebeckite (crossite)	epidote	soda- tremolite	sphene	calcite	zircon
DF-104C (marble)	calcite	diopside	tremolite	phlogopite	sphene						
DF-113A (protomylonite)	quartz	plagioclase	epidote	opaque	sericite	chlorite					
SL-310A (protomylonite)	quartz	plagioclase	muscovite	epidote	sericite	chlorite					
SL-319A (marble)	calcite	phlogopite	quartz	talc	cummingtonite						
SL-319B (calc-silicate protomylonite)	diopside	plagioclase	microcline	quartz	epidote	allanite	opaque				
SL-319C (greenschist)	quartz	plagioclase	biotite	epidote	muscovite	chlorite	zircon				
SL-321 (marble)	calcite	talc	tremolite	opaque	zircon						
SL-322A (calc-silicate)	quartz	microcline	plagioclase	calcite	sphene	opaque	chlorite				
SL-322B (marble)	sodic diopside	calcite	plagioclase	microcline	sphene	biotite	opaque				
SL-325A (mylonite gneiss)	quartz	biotite	muscovite	opaque							

TABLE A-2

STRAIN ORIENTATIONS FROM KINK ANALYSES

Set	Kink Planes	Shortening Axis	Intermediate Axis	Lengthening Axis	Foliation
1	S <u>N76W 8SW</u> D <u>N75E 40NW</u>	S19E, 74°	S79W, 3°	N 9W, 16°	N55E, 70SE
2	S <u>N32W 28NE</u> D <u>N42E 31NW</u>	S 4E, 70°	N 8E, 19°	N83W, 4°	N55E, 75SE
3	S <u>N34W 8NE</u> D <u>N21E 30NW</u>	S56E, 76°	N11E, 6°	N80W, 13°	N55E, 75SE
4	S <u>N05E 10SE</u> D <u>N75E 38NW</u>	S23E, 72°	N64E, 8°	N26W, 15°	N55E, 70SE

S = Sinistral

D = Dextral

(Rotation senses are apparent movements as viewed on the southern wall of an approximately east-west road cut.)

Sample Orientations of  
Master Kink Set

N40E 27NW (dextral  
N36E 28NW (dextral)

APPENDIX B

ASSESSMENT OF THE DEFORMATION OF THE NORTHERN END  
OF THE NEWARK-GETTYSBURG BASIN

APPENDIX B  
ASSESSMENT OF THE DEFORMATION OF THE NORTHERN END  
OF THE NEWARK-GETTYSBURG BASIN

B1.0 INTRODUCTION

B1.1 PURPOSE

This appendix presents the results of geologic investigations performed in the northern end of the Newark-Gettysburg Basin. The area of investigation is shown on Plates 1A & B. Station locations are shown on Plates 2A & B. These investigations were performed in order to:

1. Define the main trace of the Ramapo Fault and the associated faults of the Ramapo Fault System within the Trio-Jurassic Basin;
2. Assist in determining the tectonic relationship of faults at the Indian Point site to the Ramapo Fault System; and
3. Attempt to determine the age of most recent surface rupture on the Ramapo Fault and the Ramapo Fault System by appropriate age dating techniques and relationships to cross-cutting features.

B1.2 GEOLOGIC SETTING

The Newark-Gettysburg Basin extends southwestward from Rockland County, New York, to York County, Pennsylvania; a distance of about 140 miles. Its maximum width, along the

the Delaware River, is about 32 miles (Van Houten, 1969). Along the south and southeast margins of the basin, the sedimentary strata unconformably overlap a complex of Precambrian and Paleozoic rocks of the Appalachian Piedmont. To the southeast, the strata are overlain by Cretaceous and younger deposits of the Coastal Plain (Glaeser, 1966). The northeastern edge of the basin lies beneath the Hudson River where the Trio-Jurassic strata disconformably overlie early Paleozoic metamorphic rocks (Worzel and Drake, 1959). Trio-Jurassic, as used herein, refers to the Late Triassic through Late Jurassic time span covered by the Newark Group (as determined by palynological and radiometric data). This usage varies from some older references which refer to the Newark Group as Triassic. The northwestern margin of the basin is marked by a series of steeply dipping faults that separate the strata from Precambrian rocks of the Reading Prong and Hudson Highlands (Van Houten, 1969).

The basin's continental sedimentary strata and associated intrusive and extrusive igneous rocks are estimated to be between 16,000 and 20,000 feet thick in the central part of the basin (Van Houten, 1969). Deposition of these strata began in Triassic time and continued into the Upper Jurassic Period. The major intrusive body in Rockland County, the Palisades diabase, has been dated at approximately 190 m.y. (Dallmeyer, 1975). The First, Second and Third Watchung Flows, in New Jersey, have been

dated at approximately 186, 170 and 142 m.y., respectively (Appendix E). Therefore, the Palisades diabase and the First Watchung Flow are contemporaneous.

In New Jersey and Pennsylvania, four formations of sedimentary rock that have been recognized in the basin constitute the subdivisions of the Newark Group. The conglomerate (Hammer Creek Formation of Glaeser, 1966) that occurs along the basin's margin is thought to be time equivalent to the other three units which are the Stockton (predominantly arkose), Lockatong (argillite) and Brunswick (predominantly shale and sandstone) formations (Kummel, 1898). The greatest part of the area studied is underlain by the Brunswick formation. The Brunswick formation contains major deposits of conglomerate and sedimentary breccia that are limited to the northwestern and northern margins of the basin. However, conglomeratic beds and pebbly sandstone (within sand-siltstone sequences) occur across the entire basin in Rockland County, New York.

Early workers (Darton, 1890 and Kummel, 1898) recognized the presence of a major fault along the basin's northwestern margin and the general absence of major faulting along the southern and eastern margins. Structure within the basin (at least compared to that in the adjacent Reading and Manhattan Prongs) is relatively simple. Low relief anticlines and synclines, with axes transverse to the major fault trends, have been mapped through much of the basin in New Jersey and Pennsylvania. Wheeler (1939) postulated that these folds developed

during fault movement, while Faill (1973) described them as cross-folds that formed during monoclinal rotation of the entire basin.

Aside from the border faults, no major structures have previously been mapped within the Newark Basin of Rockland County. Several minor faults had been postulated (Darton, 1890; Kummel, 1898; Lowe, 1959, Thompson, 1959) and small-scale east-northeast left-lateral and northwest dip-slip faults have been described (Dames & Moore, 1975). Similar movement plans had been observed in Pennsylvania (Dames & Moore, 1974). Therefore, it appears that north-northeast to east-northeast strike-slip faults are pervasive and maintain constant orientations despite the curvature of the basin.

## B2.0 LITHOLOGIES OF THE NEWARK BASIN IN ROCKLAND COUNTY

### B2.1 TRIO-JURASSIC SEDIMENTARY ROCKS

The sedimentary strata of the Newark-Gettysburg Basin in Rockland County can be divided into four lithosomes:

(1) calcareous conglomerate (locally sedimentary breccia); (2) shale; (3) conglomerate; and (4) sandstone. These are interpreted to have originated under two sedimentary regimes. The calcareous conglomerate/shale facies appears to have been deposited during a stage of immature drainage development, while the conglomerate/sandstone facies is the result of deposition within a mature fluvial system.

The immature facies, which crops out only in the northern portion of the study area, consists of a calcareous conglomerate lithosome, interfingered with an interbedded shale and limestone lithosome. The conglomerate consists of pebble to cobble size, subangular to subrounded clasts in a reddish-brown calcareous sand matrix. The pebbles and cobbles are predominantly dolomite and limestone with some quartzite and sandstone (Paleozoic sedimentary lithologies). The calcareous conglomerate crops out north and west of the town of Stony Point, and it interfingers southward and westward with the shale lithosome exposed in the valley of Cedar Pond Brook. The latter lithosome consists predominantly of reddish-brown shale with occasional thick beds of grey limestone (exhibiting algal structures). The shale often contains burrows, carbonate nodules, and green reduction spots. Toward the zone of interfingering, sandy beds

occur along with a few beds of caliche. The coexistence of coarse clastic carbonate debris and fine-grained, sub-aqueous deposits (in part carbonate) may be interpreted as the result of immature drainage, with isolated standing bodies of water receiving occasional influxes of coarse detritus.

The mature facies crops out on the north slope of South Mountain and south of the diabase, throughout the remainder of Rockland County. The conglomerate lithosome occurs throughout the western third of the basin in Rockland County, south of Ladentown. It consists of subrounded to rounded, pebble to boulder size quartzite, sandstone and carbonate rock clasts in a reddish-brown medium-to-coarse sand matrix. Interbeds of medium-to-coarse grained sandstone and pebbly sandstone are frequent. The conglomerate interfingers eastward with a lithosome consisting of reddish-brown medium-to-coarse grained sandstone interbedded with frequent pebbly sandstones, pebble to cobble size conglomerate and a few beds of siltstone. Both lithosomes; conglomerate and sandstone, are medium-to-thick bedded with frequent channel cross-bedding and cut and fill structures. These deposits are characteristic of deposition during the mature stage of the fluvial cycle.

## B2.2 DIABASE

The above sedimentary strata have been intruded by: the Palisades diabase sill and associated dikes, a diabase body between Ladentown and Pomona Heights (Ladentown Body, probably extrusive), and a plug at Union Hill, near Suffern, New York. A

small plug at Turtle Hill, west of Darlington, New Jersey intruded the Ramapo Fault. The major intrusive body, the Palisades diabase, is a sill in New Jersey and southern Rockland County; however, along the Hudson River in Rockland County the intrusive body begins to migrate up the stratigraphic section within the host sedimentary strata. At Haverstraw, New York, the diabase outcrop makes an abrupt turn to the northwest and then turns southwest to its termination near Mt. Ivy, New York.

The Palisades diabase consists of plagioclase, clinopyroxene and orthopyroxene, olivine, biotite and other less abundant minerals (hornblende, magnetite, ilmenite, etc.). Extensive subophitic texture indicates that plagioclase and pyroxene crystallized simultaneously throughout the cooling history of the intrusive. A magnesium olivine zone (discussed below) and late crystallization stages within the diabase have a coarse-grained texture.

Walker (1969) defined a diabase stratigraphy for the Palisades based on textural and mineralogical variations within the intrusive. This vertical variation is the result of chilling of the upper and lower contacts, chemical differentiation and, to a lesser extent, gravitational differentiation.

Both lower and upper diabase contacts (chilled zones) can be recognized by a fine-grained to very fine-grained texture. In some locations chilled diabase and severely baked hornfels (see below) appeared to be similar in hand sample, and petrographic confirmation of the field identification was

required. Along Verdrietege Hook, the westward dipping diabase-sediment contact generally occurs near or below the base of the north and/or south quarry face.

The magnesium (Mg)-olivine zone rests on the lower chilled zone (early dolerite of Walker, 1969). The diabase texture is fine- to medium-grained and the Mg-olivine zone (up to 25% Forsterite) is recognizable in the field by its marked preferential weathering. This zone usually produces a ledge-like feature and a coarse, sandy disintegration product. The olivine can be recognized in the field by its differential weathering and subsequent pitting-out. The Mg-olivine zone usually occurs 25 to 60 feet above the lower diabase contact, and its thickness is variable. This stratigraphic unit was mapped at: Nyack Beach State Park (DF-34B; see also Walker, 1969), in the south wall of the old Rockland Lake Gap quarry (DF-37), and along Route 9W between Long and Short Clove (DF-64). The petrogenesis of the Mg-olivine zone has been the subject of debate (Van Houten, 1969; Walker, 1940; Walker, 1969), but this problem is not relevant to the current investigation.

Most stratigraphic units occurring between the olivine zone and the upper chilled zone can be mapped only with the aid of a microscope and were not utilized in the present study. These diabase units are characterized by coarse subophitic to gabbroic texture.

### B2.3 HORNFELS

The contact between the Palisades Diabase and Newark Group sediments is characterized by varying degrees of thermal alteration (contact metamorphism). The shaly layers, within the Brunswick formation, exhibit a greater intensity of baking to hornfels while the more porous and permeable sandstone and conglomeratic sandstone exhibit varying degrees of alteration. The quartzo-feldspathic rocks are not as sensitive to thermal mineralogical alteration as clay-rich aluminous shale. Hornfels can be recognized in the field by changes in texture from clastic (sedimentary) to granoblastic or granoblastic-polygonal (contact metamorphosed).

### B3.0 CONFIGURATION OF THE DIABASE BODIES

#### B3.1 GENERAL

The Palisades intrusion can be visualized in map view, as occurring along several relatively discrete segments (Plates 1A & B). South of Hook Mountain, the main body of the Palisades forms a small arc, open to the east, which encircles the town of Nyack. Several outcrops, water wells, and geophysical data indicate that a belt of diabase extends from Nyack, northwestward to New City Park. Another belt extends northward from the arc into Hook Mountain and as far as Verdrietege Hook, where it suddenly curves to the northwest. The northwest-trending segment persists to Little Tor, where the diabase again changes trend, to west-southwest, toward Mt. Ivy. The Ladentown diabase body occurs approximately at the intersection of the Little Tor - Mt. Ivy trend with the Ramapo Fault. The Union Hill and Turtle Hill bodies are plugs within the Ramapo Fault zone.

In general, the trend of the Palisades diabase outcrop is concordant with sedimentary bedding from south of Nyack to Verdrietege Hook. The outcrop is discordant along South Mountain, and along the spur extending northwestward from Central Nyack to New City Park. Darton (1890) and Kummel (1898) attribute the map pattern of the Palisades to the intrusion changing from a sill to a dike, or a sill-dike-sill sequence that migrates up-section to the north and northwest. Lowe (1959) postulates a ring-dike type configuration. Thompson (1959) believes the intrusion remains a sill and is faulted. Kummel

noted that the Ladentown and Union Hill (Suffern) bodies could be extrusive and intrusive, respectively.

### B3.2 PALISADES DIABASE

#### B3.2.1 Lower Contact

Lower concordant contacts have been observed in: Upper Nyack (DF-33, Plate B-1), in an old quarry at Nyack Beach State Park (DF-34a) and in the south wall at the Rockland Lake Gap quarry (DF-37). On the basis of observations made close to the contact (see Sections B2.2 and B2.3), concordant contacts were inferred at Nyack (DF-61) and along Verdrietege Hook, from Rockland Lake Gap (DF-35) northward to DF-31 (below the diabase quarry, south of Trough Hollow). A possible concordant lower contact was observed in a quarry along Route 303, in Central Nyack, (DF-65) on the west side of the main Palisades ridge (Plates 1 and 2). This location had previously been interpreted as the upper contact (Kummel, 1898), however, more recent quarrying has exposed hornfels beneath the diabase.

Northward, along the east side of the Palisades, the lower diabase contact is locally discordant between DF-34a (contact at elevation 250') and DF-39 (contact at Hudson River level). within Nyack Beach State Park. Diabase crops out along the Hudson River between DF-39 and DF-38. North of DF-38, the contact rises discordantly to approximately 75 to 80 feet above the river level. To explain this change in elevation, Sanders (1974) infers the presence of a near vertical fault trending N10°W along this discordant contact. He assumes a downthrow of at least 70 feet to the west. His criteria are: the absence of an

olivine zone in the abandoned Rockland Lake Gap quarry, the absence of a chill zone in the diabase and the absence of contact metamorphic effects in the sediments. The present investigation revealed: 1) the presence of a chilled to very fine-grained diabase zone, 2) the presence of contact metamorphic effects expressed by very slight recrystallization of sandstone and the occurrence of hornfels 50 feet above DF-38, and 3) the presence of the Mg-olivine zone and an unfaulted contact in the south wall of the Rockland Lake Gap quarry (DF-37). Both the Mg-olivine zone and the contact dip under the talus slope along the west wall of the quarry. In addition, no faults or fractures indicative of N10°W faulting were identified in the zone (at DF-38) where Sanders postulated the fault. The diabase-sediment contact occurs above the elevation of DF-40, but drops down to the 50 foot level at DF-37, where it is conformable below the olivine zone. Diabase crops out at river-level from just north of Rockland Lake quarry to south of Rockland Lake Gap (GA-162, Plate B-1). This decrease in elevation may be accounted for by the northwestward apparent dip component along the concordant contact at DF-37 (Plate B-1). The diabase outcrop at river level ends at the Rockland Lake Fault, discussed in Section B5.

Traverses along the Hudson River between Trough Hollow and Long Clove indicate that the sediments have an apparent dip component to the north. Consequently, the stratigraphic section rises northward along the river. Diabase, however, is not encountered at river level along these traverses. Therefore, it

can be concluded that diabase is migrating upward in the stratigraphic section with a gradient steep enough to keep it above the river level, and even above the 75 to 80 foot park trail level, until a descending contact is again inferred at the 100 foot quarry level north of DF-53. An elevation change of the lower diabase contact north of DF-53, in the vicinity of the two northern-most quarries along Verdreitege Hook, may be accounted for by the northward apparent dip component of a conformable contact (DF-53, elevation 100 feet to DF-54, elevation 20 to 30 feet).

Northwest of DF-54, the contact rises abruptly to an elevation of about 240 feet near Long Clove (MW-18, 20, Plate B-1; and Lowe, 1959). The cause of this sudden rise is interpreted to be fault-related (see Section B5.4.3). On the basis of several borings, Lowe (1959) concluded that the lower contact in this area dips  $11^{\circ}$  to  $14^{\circ}$  to the southwest, which is generally concordant to the dip of bedding along Route 9W. In keeping with this general concordance, the contact descends northward from 240 feet near Long Clove to less than 110 feet in elevation at Short Clove (Lowe, 1959).

The lower contact is not exposed further west, but it may be inferred beneath the talus below Little Tor at an elevation of 320 feet (MW-12, CH-25, DF-30; see Plates 1A and 2A). There, the sedimentary strata beneath or north of the diabase contain numerous apophyses (with rounded bulbous ends) intruded along and across bedding. These forms, together with the

presence of vesicles in the disturbed sediments, suggest that the intrusion (or extrusion) occurred when the sediments were still wet and uncemented. A similar contact, with fingers of diabase intruding the sediments occurs east of Mt. Ivy, but may be inferred to occur there at an elevation of about 540 feet. At Mt. Ivy, a seismic profile indicates that the diabase is a dike (see Appendix D).

#### B3.2.2 Upper Contact

A conformable upper diabase contact was not observed along the main ridge of the Palisades diabase in Rockland County, however, an upper conformable contact can be observed in New Jersey along Interstate-80, west of the George Washington Bridge.

Where it is exposed at the south portal of the West Shore railroad tunnel (DF-8, MW-14, CH-5-4, Plate 2A), near Lake Lucille (DF-11, MW-11, CH-6-8) and in the Martin-Marietta Haverstraw quarry (MW-67, CH-5-6), the upper contact is sharply discordant, displays dike-like characteristics (Plate 1A), and is in part faulted (see Section B5.3 for discussion of faulting). A cross-section along Little Tor Road (Walker, 1969) indicates that the upper contact is discordant and dips to the south. Based on borings in the Martin-Marietta Haverstraw quarry, Lowe (1959) concluded that the Palisades diabase has a dike-like configuration, the upper margin of which is discordant and dips to the southwest at 40°.

West of Lake Lucille, the upper contact is exposed at only two locations which are along South Mountain Road. At one location (MW-57, Plate 2A), the contact appears to be concordant with the diabase occurring below the sedimentary rocks; at the other (MW-60), the diabase occurs above the sedimentary rocks. Therefore, the diabase may be partly a dike in this area.

### B3.2.3 New City Park Dike

The northwest trending extension of the Palisades body was mapped by the New York State Geological Survey (Fisher and others, 1970) on the basis of aeromagnetic anomalies and water well data. This diabase body crops out at DF-17, DF-19, DF-20 and DF-21 (Plates 1B and 2B). Sedimentary rock is baked to hornfels at DF-14 (town of Germonds). Elsewhere, along the trend of the diabase body, sedimentary rock, red residual soil and/or till is exposed at the surface. The aeromagnetic anomaly pattern is parallel to the strike of bedding, but the magnetic gradient is steep suggesting that this, mainly subsurface, diabase body may be a dike extending from West Nyack (N45°W) toward New City Park. Additionally, low level aeromagnetic coverage flown during this investigation suggests that a system of subsurface diabase dikes persists as far northwest as Pomona (see Appendix D).

At DF-14 (Plate 2B), along the southwest side of the diabase body, diabase crops out above the sediments. At DF-17 and DF-18, on the northeast side of the diabase body, the diabase is seen below the sediments. Therefore, the diabase body is

interpreted as a dike. This dike is generally discordant to the southwest dip of bedding and probably dips to the northeast.

### B3.3 LADENTOWN AND UNION HILL BODIES

The Ladentown and Union Hill bodies (Plate 1B) occur immediately to the southeast of the Ramapo Fault at Pomona Heights and Suffern, respectively. Kummel (1898) noted that the Ladentown body was characteristically vesicular as seen at several outcrops, and at one location appeared to have pahoehoe texture. He concluded that the Ladentown body is extrusive. This conclusion is compatible with the radial pattern of cooling joints observed in that body along Route 202. Similarly, Kummel concluded, from a lack of scoriaceous texture, that the Union Hill body is intrusive. However, the operations of the Plaza Materials quarry at Union Hill (MW-38) have exposed a highly vesicular layer near the surface of the plug, so the presently exposed level may have been near the surface at the time of emplacement.

### B3.4 INTERPRETATION

From the above observations, it appears that the main body of the Palisades diabase in Rockland County (i.e. Hook Mountain-South Mountain) is generally discordant to bedding and has the structure of a dike. This dike has an intermediate dip to the south or southwest and lies along the inner side of the Hook Mountain-South Mountain arc. On the outer edge of the arc, the body is locally sill-like, however, in a gross sense the sill-like aspect is discordant (rising very gently to the northwest while the sediments dip to the west).

In the Central Nyack area, the dike appears to bifurcate with a smaller branch that trends northwest, toward New City Park. Aeromagnetic data suggest that this feature may extend, in subcrop, as far as Pomona (Appendix D).

The Ladentown body is interpreted to be predominantly extrusive, but regardless of whether it is intrusive or extrusive, it can easily be derived from either the main arcuate dike at Mt. Ivy, from the New City Park dike or from the Ramapo Fault. Ground magnetic profiles (Profiles 3 and 4, Appendix D) have indicated that diabase occurs below the Pleistocene sedimentary cover within the Ramapo Fault immediately west of the Ladentown body. The signature of aeromagnetic highs (Appendix D) suggest that the Palisades Diabase, at Mt. Ivy, and the Ladentown Diabase are connected and extend into the Ramapo Fault. The Union Hill and Turtle Hill bodies seem to be small plugs that are isolated from the Palisades and emplaced along the Ramapo Fault.

## B4.0 NEWARK BASIN FORM AND RATES OF SEDIMENTATION

### B4.1 BEDDING ATTITUDES

Within Rockland County, the Trio-Jurassic strata form a shallow half-basin that is truncated along its northwestern side by the Ramapo Fault (Plate 1). In the area north of South Mountain, bedding generally strikes northwest and dips toward the southwest. The dip is normally about  $10^{\circ}$ , although it locally steepens to approximately  $25^{\circ}$ . In the area south of South Mountain, including Long Clove and Verdrietege Hook, bedding strikes between north-south and northeast and dips at an average of  $9^{\circ}$  to the west.

On either side of the New City Park Dike, bedding strikes northwest and dips to the southwest. Dips are gentle on the northeast side of the dike and are steeper on the southwest side. Southwest of New City, the strike of bedding is quite variable; however, the low dips are predominantly toward the north or northwest. The approximate center of this half basin is Ladentown. The bedding dips an average of  $7^{\circ}$  NW on the southeastern limb and reaches  $26^{\circ}$  to the southeast on the northwestern limb, close to the Ramapo Fault.

Although the sedimentary units are generally cross-bedded and the dips are usually gentle, making accurate measurements difficult, the following points should be made:

- 1) The Ramapo Fault prominently defines the northwest margin of the basin. Generally bedding dips

toward the fault, however, near it dip reversals are noted. Faults within the basin do not control the form of the basin.

- 2) Changes in bedding attitudes seem to coincide with the outcrop of the Palisades diabase. These may be drag phenomena, rather than folds, and may be related to dip-slip movements along faults or to the emplacement of the body.
- 3) No major folds were recognized within the basin.

#### B4.2 BASIN SUBSIDENCE

Van Houten (1969) has estimated the rate of initial deposition for the Brunswick Formation to be 1000 feet/million years. He calculated the average rate of basin subsidence as ranging between 700 to 1070 feet/million years by assuming that all of the Newark rocks are of upper Triassic age. However, on the basis of palynological data, Cornet and Traverse (1973) assigned the Brunswick Formation of the Newark Basin to the Early Jurassic. Additionally, the Third Watchung flow has also been radiometrically dated as Jurassic (see Appendix E). Therefore, it is presently appropriate to reconsider these rates of basin subsidence. The pertinent data for this recalculation are as follow:

- . approximate age of the Third Watchung Flow:  
142 m.y. (Appendix E);
- . approximate age of the First Watchung Flow:  
186 m.y. (Appendix E);

- . thicknesses of the First and Second Watchung Flows: 600 feet and 750 feet, respectively (Faust, 1976);
- . thickness of the sedimentary rocks between the First and Third Watchung Flows: 2100 feet (Faust, 1976);
- . thickness of the Palisades Intrusion: 1000 feet (Van Houten, 1969);
- . age of the Palisades: about 190 m.y. (Dallmeyer, 1975);
- . start of Newark sedimentation; pre-Karnian (Van Houten, 1969) or approximately 210 m.y.; and
- . thickness of the pre-First Watchung sedimentary rocks: 13600 feet (Faust, 1976 after Van Houten, 1969).

Calculation of the rate of subsidence and basin filling subsequent to the First Watchung Flow may follow two extremes:

1. If we assume that the intrusion of the Palisades and the extrusion of the Watchungs did not raise the land surface significantly above the contemporary level of deposition, then the 2100 feet of sedimentary rocks within the Watchungs accumulated in the 44 million years, between the First and Third flows, at a rate of 46.6 feet/million years.

2. Alternatively, if we assume that the relief of the Palisades and the First and Second Watchungs were additive, and raised the land surface above the level of deposition by their cumulative thickness (2350 feet); then the subsidence of this relief, plus the accumulation of the sediments, occurred between 190 and 142 m.y. at a rate of 88.5 feet/million years.

In light of the apparent absence of extensive dissection of the Watchung Flows, an intermediate rate of sedimentation, between the two extremes mentioned above, appears more appropriate. Interestingly, however, both of these rates are an order of magnitude lower than those calculated by Van Houten.

The rate of subsidence and accumulation of the pre-Palisades (Pre-First Watchung) sedimentary rocks, on the other hand, would have been on the order of 680 feet/million years (total accumulation of 13,600 feet in 20 m.y.). This is close to Van Houten's (1969) estimate of the initial rate of Lockatong deposition (based on varve counts) and would be comparable to his estimates of Brunswick and Stockton accumulation with bypassing. Nonetheless, Van Houten notes that this higher rate is still an order of magnitude lower than those of flysch and molasse basins, which are representative of rates of sedimentation in tectonically active areas. What is most interesting, however, is that the subsidence prior to the Palisades-First Watchung event was an order of magnitude greater than that after

these events. It is postulated that this change in the rate of subsidence reflects the waning level of dip-slip movement along the Ramapo Fault during syn- and post-Palisades times.

## B5.0 FAULTING AND FRACTURING

The investigation of faulting in the northern portion of the Newark Basin was concentrated in the vicinity of the Palisades, Ladentown and Union Hill intrusions. Rock exposure in these areas is much more abundant than in any other portion of the basin. In addition, the bases of locally concordant portions of the Palisades intrusion provide stratigraphic markers from which to determine the existence as well as the movement sense of large faults.

Faulting in the study area is dominated by northeast trending faults (see Table B5-1), of which the Ramapo Fault and the Rockland Lake Fault are the best defined (Plate 1). Several instances of dip-slip faulting were observed on the inner edge of the Palisades dike. Additionally, faulting was noted in the Little Tor and Thiells areas.

### B5.1 THE RAMAPO FAULT

South of Ladentown, the Ramapo Fault Zone forms the northwestern border of the Newark-Gettysburg Basin. It is the most profound structure in the basin, but its trace is completely obscured by the deposits and bed of the Mahwah River. The observations that can be made come from scattered outcrops, a few wells and some geophysical traverses performed during this study (Plate 1; Appendix D).

The Trio-Jurassic sediments exposed adjacent to the Ramapo Fault are cemented fluvial conglomerates (as opposed to fanglomerates) composed almost entirely of Paleozoic lithologies. Thus, 1) the absence of fans indicates that the Ramapo Fault did not have a particularly pronounced scarp during the pre-Palisades stages of basin sedimentation, and 2) the throw on the fault during Pre-Palisades sedimentation was not sufficient to greatly expose the Precambrian basement of the Highlands. Presently, the thickness of the northern Newark Basin, adjacent to the fault, is at least 718 feet (from a well at Suffern) and probably exceeds 1000 feet (as indicated by modelling of ground magnetometer traverses). The prominent fault line scarp has a differential relief on the order of 500 to 700 feet. This geometry of vertical displacement has commonly been interpreted as the result of normal faulting. Observations in the Trio-Jurassic and Precambrian rocks adjacent to the fault indicate that the driving mechanism for much of the deformation was strike-slip faulting.

Observations along the Ramapo Fault at Ladentown have already been discussed in Sections B3.3 and B4.0. A second outcrop adjacent to the Ramapo Fault occurs in the Plaza Materials Quarry at Union Hill (Suffern, New York; Plate 1). Here, the deformation of the diabase plug appears to have been in two stages. The first stage is represented by kinked diabase columns. The kink zones were found to dip at low to intermediate angles and to have highly variable strikes. This geometry of deformation is indicative of flattening in a vertical direction.

In some instances the kink zones are mineralized (quartz, calcite, chlorite and zeolites). Three samples of this mineralization (GA19.1, GA20.1 and GA20.2) were taken for study (see Table B8.3 and Appendix E) and were found to consist of cooling attendant minerals. Thus, the kinking appears to be a cooling attendant phenomenon.

The second stage of deformation is represented by several vertical zones of shearing and brecciation. In two cases, these were observed to offset the kink zones. The shear zones vary in width from 0.5 to 2 feet and occasionally have fillings of quartz, calcite and chlorite, which show evidence of multiple deformations. These zones vary in strike from N20°E to N40°W, but may fall into two sets with maxima at N24°W and N3°E (antithetic and synthetic, respectively, to sinistral movement on the Ramapo Fault). Where present, slickensides on these surfaces rake at low angles to the north.

#### B5.2 FAULTS IN THE AREA OF ROCKLAND AND DEFOREST LAKES

Four faults trending approximately N40°E have been mapped in the vicinity of Rockland and DeForest Lakes. These faults are along the southwestward projection of several shear zones of the Croton Falls Fault System (Plate 1; Appendix A). The Rockland Lake Fault is the largest and can be mapped over a distance of 5 miles. The smaller Trough Hollow and Hook Mountain Faults lie north and south of the Rockland Lake Fault, respectively. The Long Clove Fault is suspected to extend through the notch in the Palisades, north of DeForest Lake.

#### B5.2.1 Rockland Lake Fault

The Rockland Lake Fault has been mapped from the gap at Rockland Lake, southwestward to an outcrop south of the New York State Thruway. This fault trends about N40°E and appears to dip steeply to the southeast. It is best defined at Route 303 south of Valley Cottage (GA-154; Plate 2)), west of Nyack (GA-157; Plate 2), and at river level along Verdrietege Hook (DF-35; Plates 2 and B1). The geometry of associated secondary faulting (with which the offset of the intrusive contact is consistent) defines the movement sense along this fault as primarily sinistral. A component of dip-slip movement is also indicated to a lesser degree by the small scale faults at GA-157.

At GA-154, the southeast side of the roadcut is within the fault zone and the rock is consequently reduced to rubble. The northwest side of the roadcut consists of reasonably coherent but highly sheared (N40°E, subvertical) diabase. Closely spaced subsidiary shears, trending north-south to north-northeast, with strike-slip slickensides, support the interpretation of sinistral movement along the main N40°E trending fault zone. Two samples of quartz and chlorite mineralization (MW-114-1 and MW-114-2) were obtained from the north-northeast trending synthetic shears for petrographic study.

The diabase exposure in the gravel quarry at GA-157 (west of Nyack) demonstrates that some dip-slip movement has also occurred along this fault. Three small fault zones trending N30°E to N50°E and dipping 70 to 90 degrees to the southeast

exhibit dip-slip slickensides. The fracture geometry associated with these zones is interpreted to indicate normal movement senses. The diabase within these subparallel zones is almost completely reduced to gouge. Three samples of quartz, calcite, stilbite and chlorite mineralization were taken from these shears (MW-116-1, MW-116-2 and MW-116-3; see Section B8).

At Rockland Lake Gap (DF-35), along the Hudson River, the apparent vertical offset of the lower diabase contact can be estimated to be between 50 and 100 feet.

#### B5.2.2 Trough Hollow Fault

The Trough Hollow Fault is exposed only at Trough Hollow (MW-106; Plate B-1) as a 2-foot wide shear zone, oriented N46°E, 78°SE. To the southwest, it is expressed as a gap in the diabase ridge. Within the main shear zone, minor shears are oriented N10°W, 64°E and N80°W, 62°S. Slickensides within the shear zone are subhorizontal. The center of the shear zone is filled with a 3 to 6 inch thick septum of large, intergrown calcite crystals that are oriented normal to the fault plane. Locally, this septum has been brecciated by subsequent shearing, and the calcite crystals are visibly deformed. Samples of this mineralization (MW106-1 and MW106-2) also contain chlorite and zeolites (see Section B8).

In the quarry north of Trough Hollow (MW-101, 102, 103, 104; Plate B-1), the Palisades diabase is broken by numerous subvertical shears striking N40 to 65°E (with horizontal and southwest raking, oblique-slip slickensides) and N10 to 25°W

shears (with horizontal slickensides). The overall impression gained from these observations is that the N40 to 60°E and the N10 to 25°W are main and synthetic shears, respectively. Mineralization samples from several of these shears (MW-102-1 to -3, and MW-103-1 to -5) contain calcite, chlorite and a wide variety of zeolites. In the quarry there are also several large shears trending N40 to 60°W and dipping at intermediate angles to the south (with dip-slip and oblique-slip slickensides). These northwest shears are probably related to the faults described in Section B5.3.

At river level, below the quarry (MW-68; Plate 2), the sedimentary strata below the diabase are strongly fractured by two sets of vertical fractures with maxima at N15°E and N50°E. The geometry of these fracture sets suggests that they may be a conjugate pair.

#### B5.2.3 Hook Mountain Fault

The Hook Mountain Fault is inferred to exist on the basis of northeast-trending zone of intense shearing that lies to the southeast of the Rockland Lake Fault. This shearing is most evident in the southwest corner of the Rockland Lake diabase quarry which lies due east of Romic School (GA-158 and MW-111; Plate B-1). There the major vertical shears strike N30 to 50°E (slickensides are horizontal). Progressing southwestward through a notch in the Palisades ridge, the shearing is again observed in the hornfels at the southern end of the Rockland Lake (MW-23 and GA-17; Plate 2). The main fault at this

location trends N26°E (with horizontal slickensides). Shear filling mineralization at MW-111 consists of pectolite and prehnite (MW-111-1 to -3), while at GA-17 it consists of calcite and stilbite (GA-17.1 and GA-17.2; see Section B8).

#### B5.2.4 Long Clove Fault

At Long Clove, the northern contact of the diabase rises abruptly from an elevation of 20 to 30 feet on the south side of the notch to 240 feet north of the notch (see Section B3.2.1). This sudden change in elevation has been the cause of debate regarding the existence of a fault through Long Clove (Darton, 1890; Kummel, 1898; Lowe, 1959; Thompson, 1959).

Although this fault was not observed in the field, the following information is considered sufficient to postulate the presence of a N30°E to N40°E trending fault through Long Clove.

1. The outcrop (MW-19; Plate 2) on the east side of Route 9W, at the intersection with Route 304, exhibits several northeast trending shears with strike-slip slickensides.
2. Several N25°E and N40°E shear surfaces were observed in the diabase, along an abandoned section of Route 9W, just east of MW-110 (Plate B-1).
3. A seismic reflection profile (Line 5, Plate D.7-20) indicates the presence of a fault about 600 feet north of the north portal of the railroad tunnel.

4. Aeromagnetic contours in the Long Clove area suggest a left-lateral offset of the Palisades diabase.

The intrusive contact at Long Clove is interpreted to be offset left laterally by this fault.

### B5.3 FAULTS PARALLELING THE SOUTH MOUNTAIN DIKE

Faults roughly parallel to the inner edge of the South Mountain dike have been recognized at the south portal of the west shore railroad tunnel, in the Martin Marietta Haverstraw quarry, and at Lake Lucille (Plate 1). These are predominantly dip-slip faults that have affected the Palisades diabase and Brunswick formation.

#### B5.3.1 South Portal Fault

At the south portal of the West Shore railroad tunnel (DF-8, MW-14, CH-5-4; Plate 2), the contact between the Palisades diabase and the Trio-Jurassic hornfels is a N60°W-trending fault, which dips 50 to 70° to the south. As previously noted (Section B3), the diabase in this area is either a dike or a dike-like feeder to a higher sill. The fault lies primarily within the diabase, but the undulating contact is also faulted. Both the diabase and the hornfels are strongly fractured (N60°W, 55°NE and N60°W, 55°SW), and the fractures commonly have both dip-slip and strike-slip slickensides. A few of the fractures have a normal component of displacement of up to 5 inches.

The diabase/hornfels contact in the Martin-Marietta Quarry (MW-67, CH-5-6, CH-5-7; Plate 2) is also faulted (this

outcrop lies along strike of the railroad portal fault zone). As noted in the previous study (Dames & Moore, 1975), this fault has an average strike of N65°W and dips steeply to the south. Slickensides on the fault rake nearly verically to the east-southeast.

Further to the northwest, along South Mountain Road, a small, mineralized shear zone oriented N60°W, 64°NE was noted in the Palisades diabase. Slickensides on the fractures are sub-horizontal. A sample of calcite and chlorite (GA-7.1) was taken for petrographic study (see Table B8.3).

The southeastward extension of the South Portal Fault is obscured by till on the southwest flank of South Mountain but may extend as far as Verdrietege Hook. In the quarry, northwest of Trough Hollow (MW-101, 104, and 105; Plate B-1), shear zones striking N40° to 55°W and dipping vertically to 50°SW occur on strike with each other at each end of the quarry and along the path southeast of the quarry. Slickensides on the shears are oblique or dip-slip. Fracture geometry suggests that the shear zone movement was reverse. In one case, one of these shears is crosscut by N40-65°E trending shears that are parallel to and associated with the Trough Hollow Fault.

#### B5.3.2 Lake Lucille Fault

At Lake Lucille, along South Mountain Road (DF-11, CH-8), a normal fault oriented N60°E, 62°SE parallels the intrusive contact of a discordant apophysis with the sedimentary rocks. The fault is characterized by a 5 to 6 foot wide brec-

ciated zone. The sedimentary rock (red clay-shale) southeast of the fault zone is not metamorphosed, although fragments of hornfels were found adhering to the diabase northwest of the fault. No accurate estimate of the amount of displacement is possible, however, the unmetamorphosed character of the southeastern wall suggests that the displacement along this fault is significantly greater than that on the South Portal Fault. It is interesting to note that since the Lake Lucille and South Portal Faults follow the inner intrusive contact of the Palisades, they may have controlled the emplacement of this portion of the dike (see also Appendix D). It is certain, however, that post-intrusive movement has also occurred along these faults.

#### B5.4 FAULTS AT STONY POINT, MT. IVY, AND LITTLE TOR

##### B5.4.1 Shearing Near the Thiells Fault

Shearing was noted at two locations adjacent to and on the projection of the Thiells Fault in the Trio-Jurassic Basin (Plate 1). At Cedar Pond in Stony Point (DF-2, MW-66, MW-113 and CH-7-2; Plate 2), the calcarous Trio-Jurassic conglomerate adjacent to the Thiells Fault is broken by numerous shears with predominant east-northeast to east-west strikes. Slickensides on these shears are horizontal and displaced beds indicate left-lateral motion. Two samples of calcite mineralization (MW-113-1 and MW-113-2) were taken from one of the faults for further analysis.

The Palisades diabase quarry at Mt. Ivy lies near the projection of the Thiells Fault (Plate 1). Along the western

border of the quarry, a 50-foot wide zone of closely spaced shears occurs, consisting of N-S and N50°E vertical fractures with horizontal slickensides. Brecciated rock occurs in shears trending N25°E within this zone.

#### B5.4.2 Faulting in the Little Tor Area

On the north slope of South Mountain, near Little Tor (CH-25; Plate 2), two prominent N50°E-striking shear zones are visible in the sandstone underlying the diabase. Small-scale offsets indicate N50°E left-lateral movement and north-northeast right-lateral movement. Within one of the shear zones, a fault plane (N52°E, 83°SE) contains 1 to 3 inches of clay and gouge. Slickensided surfaces are visible within the gouge. The foot-wall is highly polished with grooves and slickensides raking 22°SW. There are also faint, horizontal slickensides superimposed on the polished surface.

#### B5.5 FRACTURING

During this investigation, 10 measurements of fracture orientations were taken from each of 42 outcrops of Triassic-Jurassic sedimentary strata throughout the northern end of the Newark-Gettysburg Basin. This effort was directed toward obtaining a regional picture of the fracture geometry within the Basin. The readings were collected from outcrops of various sizes and orientations. The results of this study revealed the existence of three vertical sets of fractures with maxima striking N5° to 20°E, N60° to 70°E, and N65°W. Of the three, the N65°W-trending set is the least well developed, and the N5° to

20°E set is the best developed. Each of the faults described in this section (B5.0) can be related to one of these maxima.

Additionally, 100 fracture attitudes were taken at Verdrietege Hook, Route 304 and the south portal of the Penn-Central Railroad tunnel. The strikes of the major subvertical fracture sets at these locations are presented in Table B.5-2, along with the results of additional fracture studies conducted in the Newark Basin (Dames & Moore, 1975). In general, these larger samples show the same maxima as the regional study, with the exception of the introduction of N15°E to N25°W and east-west striking sets adjacent to the Thiells and Ramapo Faults.

#### B5.6 INTERPRETATION

The above observations on faulting in the northern portion of the Newark Basin can be interpreted and summarized as follows:

Basin-marginal faulting along the Ramapo Fault has resulted in the subsidence of the sediments and the formation of the half basin structure (Section B4.0). This deformation may be interpreted largely as an effect of regional extension with the major extensional axis oriented at a high angle to the Ramapo Fault. Compression parallel to the Ramapo Fault is suggested by conjugate north-northeast and east-northeast trending shear fractures (e.g. Section B5.2.2) in the Brunswick sedimentary rocks (see also Dames & Moore, 1975 and DeBoer, 1967) and by the large component of dip-slip movement along the Ramapo Fault.

The persistence of the Newark depocenter (and a source area for its sediments) through a long period of time suggests that basin-marginal faulting was active throughout sedimentation. From a study of sedimentation rates, it was interpreted that subsidence prior to the Palisades-First Watchung event was an order of magnitude greater than that after these events. It was also interpreted that the decrease in the rate of subsidence during syn- and post-Watchung times was indicative of the waning level of dip-slip movement along the Ramapo Fault (Section B4.0). Therefore, it can be concluded that a large portion of the downdropping of the basin occurred during the period of dip-slip movement. Toward the end of this period, the emplacement of diabase seems to have been initiated. The trends of prominent segments of the Palisades sill suggest that igneous emplacement was facilitated along northeast and northwest oriented faults. The South Portal (B5.3.1) and Lake Lucille (B5.3.2) Faults, for example, appear to have provided pathways for diabase intrusion at stratigraphic levels above the main body of the Palisades sill. These faults have clearly been reactivated after crystallization of the diabase.

Left-lateral strike-slip faulting appears to be the most pervasive mode of deformation of the Newark Basin. It has occurred on the Ramapo and Thiells Faults (of the Ramapo Fault System) and on the Rockland Lake, Hook Mountain, Trough Hollow and Long Clove Faults (of the Croton Falls Fault System). Repeated intrusion and extrusion of diabase and basalt decreased

and eventually stopped altogether during the late stages of left-lateral simple shear deformation. The transition from normal faulting to strike-slip faulting seems to have occurred by the time of crystallization of the Palisades and First Watchung diabase and basalt (~190 m.y.). This transition coincides with the decrease in the rate of sedimentation within the basin. Strike-slip faulting was left-lateral on N40°E faults. Within the basin, the South Portal and Lake Lucille Faults, were favorably oriented for reactivation as antithetic shears, as evidenced by the subhorizontal rake of slickensides on these faults within the diabase.

TABLE B.5-1 (Continued)

Rockland Lake Area

<u>Sta. #</u>	<u>Fault Trend &amp; Movement Sense</u>	<u>Criteria</u>
D.F.-54	N70°E, ?                      Sinistral	Stratigraphy
D.F.-62	Possibility of two similarly oriented faults based on out-crop pattern between DF-54 & DF-62 and DF-62 & DF-63 Topographic expression supportive only of former.	Elevation change in position of igneous contact and topography.
	Minor Strike-slip Faulting and Shearing	
G.A.-164	N20°W, 90° 1-3 foot wide intensely sheared zone N40-50°E, sub vertical              sub-horizontal slicks N70-80°E, sub vertical              sub-horizontal slicks	
G.A.-166	N-S to NNW, sub vertical              sub-horizontal slicks	
G.A.-158	N40°E, sub vertical Valley of similar trend	Sub-horizontal slickensides
G.A.-151	N40-60°E, 70-90°SE (major trend)  N70°E-N80°W, sub-vertical (scatter) Interpreted as dextral on N40-60°E producing scatter further to east.	Fracture study interpretation
G.A.-163	N10-20°E, 80°SE                      Sinistral N20-30°W, 80-90°NE                  Dextral	Fracture geometry Fracture geometry

TABLE B.5-1 (Continued)

Rockland Lake Area

<u>Sta. #</u>	<u>Fault Trend &amp; Movement Sense</u>		<u>Criteria</u>
MW-106	N42°E, 78°N	Slickensides rake 9°SW	
D.F.-23	N22°W, 75°NE	Sinistral	Slickensides rake 10°S Fracture geometry
	N13°W, 55°NE	Dextral	Slickensides rake 25°S Stratigraphy Offset
	N-S, 75°E	Dextral	1 foot vert. strati-
	N20°E, 70°SE	Normal	graphic offset, dragged beds, Fracture geometry
	N30°E, 80°SE	Sinistral	Slickensides rake 20°SW Fracture geometry
D.F.-8	N35°E, 82°NW	Sinistral	Slickensides rake 45°SW Stratigraphic Offset
	N60°W, 56°SW	Normal & Dextral	Vertical and horizon- tal slickensides, minor faults of similar trend show normal
	N30-40°E, 80°NW		Slickensides rake 70°NE
D.F.-11	N60°E, 62°SE 5-6 foot wide brecciated zone	Normal	Fracture geometry

TABLE B.5-2STRIKES OF MAJOR SUBVERTICAL FRACTURE  
SETS IN TRIO-JURASSIC SEDIMENTARY ROCKS

<u>Station</u>	<u>Location</u>	<u>N</u>	<u>Strikes of Sets</u>
	Small Samples from Whole Area	420	N 5°E to N20°E, N60°E to N70°E, N65°W
MW-1	Route 304	100	N10°E, N45°E
CH-4	Wesley Chapel	40	N45°E, N50°W
TR3	Wesley Chapel	120	N15°W, N85°E
CH 3-4	Pomona Heights	60	N27°E, N60°W
TR3	Pomona Heights	100	N35°E, N65°W
CH-25	Dowd Apts.	48	N 5°E, N45°E, N55°W
MW-14	Penn Central R.R. Portal	100	N 5°E, N30°E, N60°W
CH-7	Cedar Pond Brook	180	N25°W, N35°E
TR1	Cedar Pond Brook	200	N20°W, N45°E
MW-68	Verdrietege Hook	100	N20°E, N50°E
CH-10	Hook Mtn. Park	200	N40°E, N85°W
TR2	Hook Mtn. Park	200	N40°E, E-W

## B6.0 WATER WELL DATA

### B6.1 DATA BASE

In order to obtain better subsurface control of bed-rock lithologies, a search was made of available water well data for Rockland County. The data obtained are listed by Perlmutter (1959) in "Geology and Ground-Water Resources of Rockland County, New York", which remains the most comprehensive publication for boring data in Rockland County. The locations of the most informative wells are shown on Plate 1, and the pertinent information is summarized in Table B.6. The well records that were reviewed included:

1. locations on or adjacent to the Ramapo Fault;
2. locations on or adjacent to other fault zones within the Newark Basin;
3. locations along the border of the Newark Basin;
4. locations adjacent to the diabase outcrops; and
5. locations where borings penetrated both Newark Series sedimentary rocks and diabase intrusives.

The depths noted in Table B6 are only minimum depths for the mapped geologic formations (i.e. the depth at which drilling was stopped). The data presented by Perlmutter is not uniform with respect to quality of lithologic descriptions, subdivision of lithostratigraphic units, or completeness. Well location, owner, altitude, depth, geologic unit and other parameters are tabulated for 540 borings in Rockland County (Perlmutter, 1959, Table 17). Of these 540 water wells and test borings, only

99 logs were published (Perlmutter, 1959, Table 16). All logs were obtained from the drillers except where otherwise noted. None of the logs list intervals of fracturing, or characteristics of fracture zones (i.e. presence of slickensides, mineralization, bedding plane cleavage, offsets, dikes or vein fillings), and no structural geology has been noted on the logs (attitude of bedding, foliation, fracture planes, etc.). The well logs are not uniform, and the lithologic characteristics of the Newark Series are too variable for these logs to be useful in stratigraphic correlation.

#### B6.2 INTERPRETATIONS

None of the deep wells located adjacent to the Ramapo Fault in Rockland County intercepts the fault zone. Similarly, none of the wells which started within the Newark Series pass into the underlying crystalline rocks. Boring R193 (R for Rockland County) indicates that the Newark Series is more than 718 feet deep on the Avon Allied Products property, west of the Union Hill Quarry and south of an exposed fault, in Precambrian rocks, at the intersection of U.S. Route 202 and the New York State Thruway in Suffern, New York (CH-27, Plate 2). This minimum depth of 718 feet is located at a maximum distance of 800 feet from the Ramapo Fault zone.

The wells located just southeast of the northwestern margin of the Newark Basin reach depths of 400 feet at Ladentown, 357 feet north of Mount Ivy, 435 feet south of Thiells, 300 feet northeast of Thiells, and approximately 220 feet at Stony Point. All borings penetrated Newark Series strata; none

penetrate underlying Precambrian or Paleozoic rocks. This indicates a moderately to steeply dipping western contact between the Newark Series and older rocks.

The thickness of unconsolidated material along the Mahwah River Valley is variable and ranges from 0 to 57 feet west of Mount Ivy, New York to between 108 and 116 feet at Suffern, New York.

The borings at the Martin-Marietta Haverstraw quarry (R537 and R538) have already been noted as indicating that the Palisades diabase is discordant with bedding (see Section B3.2). Other deep wells (122 to 329 feet) located west or south of the outcropping diabase do not penetrate diabase. On the other hand, well R262 (Central Nyack) penetrates 120 feet of the Newark Series, then 15 feet of diabase. This fact and the outcrop pattern suggest a more tabular configuration for the diabase at this location. North of Bardonia, New York, well R291 penetrates two diabase bodies within the Newark Series, and well R292 penetrates one diabase body. Wells R291 and R292 lie southwest of, and within the New City Park dike, respectively. Additionally, well R21, which lies just east of station DF-65 (Plate 2), starts in diabase but passes into Newark Series rocks at 750 feet. This supports the interpretation that DF-65 is a lower contact (see Section B3.2.1).

TABLE B6

## SELECTED WELLS IN ROCKLAND COUNTY

Well Number	Location*	elevation (feet)	total depth (feet)	depth to bedrock	Bedrock Unit
R21	Central Nyack	350	770	-	0-750:diabase 750-770:Newark series
R22	Long Clove	200	200	18	diabase
R44	Valley Cottage	210	175	17	0-120:Newark series 120-170:diabase
R45	Upper Nyack	300	258	45	Newark series
R47	Central Nyack	70	131	23	Newark series
R68	Orangetown	312	718	-	Newark series
R149	Thiells	360	127	0.5	Precambrian gneiss
R173	Haverstraw	25	350	90	Newark series
R193	Suffern	310	718	108	Newark series
R205	Ladentown	400	120	42	Newark series
R251	Valley Cottage	210	122	17	Newark series
R255	Rockland Lake	170	329	53	Newark series
R262	Central Nyack	70	135	60	60-120:Newark series 120-135:diabase
R263	Cedar Pond	170	194	0	Ordovician shale
R264	Cedar Pond	220	34	-	Ordovician shale
R271	Thiells	360	265	241	Newark series
R272	Mt. Ivy	525	357	-	Newark series
R279	Suffern	340	200	-	Precambrian gneiss
R285	Nyack	231	40	40?	Newark series
R289	Bardonia	286	477	23	Newark series
R291	Bardonia	300	601	17	17-436:Newark series 436-473:diabase & Newark series 473-601:Newark series
R292	Germonds	260	156	15	15-55:Newark series 55-85:diabase & Newark series 85-126:Newark series 126-156:diabase
R296	Stony Point	120	100	0	Cambro-Ordovician limestone
R341	Centenary	190	93	42	Newark series
R347	Centenary	110	89	4	Newark series
R349	Centenary	160	96	24	Newark series
R355	Congers	170	140	-	Newark series
R361	Congers	180	221	18	Newark series
R368	Rockland Lake	160	123	15	Newark series
R381	Rockland Lake	220	141	49	Newark series
R388	Rockland Lake	230	170	15	diabase
R428	Suffern	340	278	20	Newark series
R433	Wesley Chapel	430	140	36	Precambrian granite
R434	Wesley Chapel	390	125	40	Newark series
R441	Ladentown	440	91	2	diabase

\*Shown on Plate 1A &amp; B

TABLE B6 (Continued)

Well Number	Location	elevation (feet)	total depth (feet)	depth to bed- rock	Bedrock Unit
R442	Ladentown	440	34	5	diabase
R443	Ladentown	440	185	100	diabase
R446	Ladentown	430	143	40	Newark series
R450	Mt. Ivy	480	60	7	Precambrian gneiss
R458	Mt. Ivy	415	300	70	Newark series
R459	Cedar Pond	140	175	45	Newark series
R464	Mt. Ivy	500	317	0	diabase & Newark series
R468	Stony Point	15	220	31	Newark series
R469	Mt. Ivy	440	159	135	Newark series
R470	Mt. Ivy	460	221	200	Newark series
R471	Thiells	440	435	325	Newark series
R474	Thiells	310	130	30	Paleozoic limestone or quartzite
R476	Ladentown	410	98	0	Diabase
R477	Mt. Ivy	440	175	146	Newark series
R480	Suffern	330	181	65	Newark series
R485	Mt. Ivy	460	162	120	Newark series
R509	Suffern	270	121	116	Precambrian granite
R511	Thiells	260	133	82	Newark series
R512	Stony Point	240	345	0	Cambro-Ordovician limestone
R523	Wesley Chapel	380	80	20	Newark series
R524	Wesley Chapel	390	201	80	Newark series
R525	Suffern	340	225	40	Newark series
R537	Long Clove	270	54	20	20-44: diabase 44-54: sandstone
R538	Long Clove	151	140	34	34-115: Newark series 115-140: diabase
R539	Long Clove	166	219	56	Newark series

Note: this table is condensed from Perlmutter (1959)

## B7.0 SEISMIC REFLECTION PROFILING

Coincident with the geologic mapping, several seismic reflection profiles were run within the Newark Basin in Rockland County. These are reported in detail in Appendix D, however, two of the lines, which are pertinent to the emplacement of the diabase, are discussed here.

### B7.1 LINE 1 PART 1

Line 1, Part 1 was run along the Palisades Interstate Parkway from south of Mt. Ivy to Thiells, N.Y. (Plate 2). A portion of the line crosses known outcrops of the Palisades diabase, between shot points 98 and 109 (Plate D.7-13), and indicates that the diabase is a nearly vertical dike. Disruption of the otherwise horizontal layering on the northern side of the dike, suggests that the diabase intruded along a fault.

South of shot point 98, there are no known outcrops of diabase, although low level aeromagnetic coverage (Appendix D) suggests that the main extent of the Palisades diabase lies to the south of South Mountain. The reflection profile did, however, reveal the presence of two possible dikes, one at shot point 63 to 66 and one at shot point 69 to 74, and a splaying fault at shot point 75 to 88. (Curvature of the reflectors, believed to be bedding, adjacent to the dikes, suggests that the dike margins are faulted.) Thus, it appears that the seismic reflection profiles confirm the conclusion that the Palisades diabase body is increasingly dike-like northwestward from Verdrietege Hook.

Line 1 Part 1 also crossed the probable extension of the Thiells Fault at shot point 118 to 142 (Plate D.7-13). South of the vertical Thiells Fault (between shot points 106 and 118), the Brunswick/basement contact has been interpreted as an unconformity dipping to the south at about 25°. The unconformity is truncated by the fault, and may be up-thrown to the north (between shot points 109 and 118). At shot point 118 the Brunswick sedimentary rocks appear to be broken by a steeply north-dipping, apparently reverse fault that may be synthetic to the main Thiells Fault. These interpretations support the conclusion that the Thiells Fault has broken the Trio-Jurassic sedimentary rocks. The geometry appears to be that of a subvertical fault zone displacing a buried fault line scarp.

#### B7.2 LINE 5

Line 5 was run along the west shore railroad grade from Samsondale to the south of Long Clove (Plate 2). The portion of the profile between shot point 10 and shot point 65 (Plate D.7-20) is of particular interest to this discussion since it crosses the Long Clove and South Portal Faults, as well as the Palisades Diabase at Long Clove.

The most probable interpretation (see Appendix D.7) of this data suggests that the Palisades Diabase, as exposed between shot point 24 (the South Portal Fault) and shot point 51, is a discordant, sill-like body, completely underlain by Brunswick sedimentary rocks. The source of the sill, which is defined as a broad, fault bounded dike between shot point 13

and 27, has been down-dropped to the south and separated from the sill by the South Portal Fault. The southward tilt of the sedimentary reflectors on the north side of the South Portal Fault is compatible with the southward down-dropping, and with surface observations of normal movement. It appears, then, that the source of the Palisades Diabase at Long Clove is a fault bounded dike, and that the South Portal Fault has at least 500 feet of normal displacement. The Long Clove Fault is shown on the profile of Line 5 at shot point 56.

## B8.0 FAULT AND SHEAR FILLING MINERALIZATION

Most of the major faults within the study area contain fracture-filling mineralization, either along their length, or along associated shears. All significant occurrences of mineralization observed in the field were sampled, analyzed and are discussed in this section and in Appendix E. In addition to 35 samples taken from the Newark Basin in Rockland County, New York, two mineral samples were taken from the Turtle Hill diabase body and one from the Second Watchung Flow in New Jersey. As such, the analysis includes samples from faults and shears related to 1) the Ramapo Fault 2) the faults at Rockland Lake 3) the faults at Long Clove and 4) the Thiells Fault. Because the Trio-Jurassic sedimentary rocks in this area crop out rather poorly, the majority of specimens were obtained from the Palisades and Watchung igneous rocks.

### B8.1 DISTRIBUTION OF MINERAL PHASES AND DEFORMATION

The mineral phases observed during this study include: quartz, calcite, stilbite, chlorite, analcite, datolite, apophyllite, prehnite, opaques, pectolite, chabazite, natrolite and other undifferentiated zeolites. Additionally, albite is common in the country rock immediately adjacent to the mineral veins. Because of its commonness, as well as its affinity to the wall rock rather than to vein mineralization, albite has not been studied in detail. The distribution of these phases is presented in terms of the trend of the sampled fault or shear in Table B8-1 and in terms of geographic location in Table B8-2.

In both tables it is apparent that calcite, stilbite and chlorite are the most commonly occurring phases and that quartz and analcite, although less common, are still significant. These mineral phases occur within faults of all trends, and in the vicinity of all major fault systems (with the exception of stilbite, which was not noted on the possible trace of the Thiells Fault). Datolite, apophyllite, prehnite and pectolite were not noted in faults or shears trending N60° to 90°E or in the vicinity of the Thiells Fault. However, because of their relative scarcity, this is not considered to be significant. Although the common phases are present on all fault trends and fault systems, they are not present at all locations. For example, analcite occurs in the Verdrietege Hook area, but is absent at other locations in the vicinity of the Rockland Lake, Trough Hollow and Hook Mountain Faults. This is probably a function of local variation in the host rock or mineralizing fluid chemistry.

It should also be noted that deformed mineralization occurs in the majority of cases and that it is not unusual for deformed and undeformed examples of the same phase to occur in the same sample. Analcite, datolite, apophyllite and prehnite were not observed to be deformed.

Thus, based on the distribution of minerals and observations of deformation it appears that:

1. deformation subsequent to some of the mineralization occurred on all trends of faults and shears and on all major fault systems;

2. the observed varieties of mineralization are not restricted to particular fault trends or systems;
3. some mineral phases are not deformed, regardless of fault system, shear trend or geographic location, and thus, may be assumed to be post-tectonic,
4. the total sample is an adequate base for analysis of the regional pattern of mineralization and deformation.

#### B8.2 INTERPRETED REGIONAL PARAGENESIS

As a result of microscopic studies, it is possible to develop a history (or paragenesis) of mineralizing and deforming events for each sample. The resulting parageneses are presented in Table B8-3. For convenience, they have been placed in five groups (A through E) to illustrate five pertinent observations relative to the interpretation of what may be termed the "regional paragenesis". These observations are as follows:

1. Quartz, calcite, stilbite and chlorite are commonly cogenetic. This may be seen throughout the parageneses of group A and in the early portions of group B. Additionally, the assemblage quartz + calcite + stilbite + chlorite appears before the last deforming event.
2. Analcite, datolite, apophyllite, calcite, stilbite and chlorite are commonly cogenetic. This assemblage is evident in the latter portions of the group B and C parageneses and all of the parageneses of group D.

- 3) The assemblage ·analcite + datolite + apophyllite + calcite + stilbite + chlorite· occurs after the assemblage ·quartz + calcite + stilbite + chlorite· (as shown in group B) and after the last deforming event (as may be seen in the parageneses of groups B and C). Schaller (1932), on the basis of microscopic and mesoscopic studies of mineralization in the Watchung Flows, also concluded that quartz (and albite) were precipitated before the crystallization of analcite, datolite and apophyllite (Section B8.4 and Table E-3).
- 4) Calcite, chlorite and stilbite occur both deformed and undeformed. This is evident in all five groups.
- 5) In all but two samples, there are one or more undeformed phases at the younger end of the paragenesis.

Thus, it appears that the regional paragenesis consists of an early assemblage ·quartz + calcite + stilbite + chlorite· which was more or less synchronous with the last stages of the deforming events, and a later assemblage ·analcite + datolite + apophyllite + calcite + stilbite + chlorite· which clearly post-dates the last tectonic activity.

#### B8.3 RADIOMETRIC DATING AND ANALYSES OF FLUID INCLUSION FILLING TEMPERATURES

On the basis of the analyses described above, 13 samples were selected for determination of fluid inclusion filling

temperatures and 3 samples were radiometrically dated (K/Ar method). The samples used, and the phases specified for analysis are indicated on Table B8-3 along with the results (see also Appendix E). The samples were selected on the basis of material quality and to represent a wide range of geographic locations, fault trends, associated major structures and mineral varieties in the final data set. In one instance (GA 17.3), it was possible to extract a dateable phase (stilbite) and a phase suitable for fluid inclusion study (calcite) from the same sample.

The results of the analyses indicate that primary fluid inclusion filling temperatures on phases of the assemblage ·quartz + calcite + stilbite + chlorite· commonly exceeded 150°C (samples GA4.1, GA19.1, MW114-1, MW115-1, MW116-2, MW103-2, GA7.1, MW67d-1 and MW106-2), while the primary inclusion filling temperatures on phases of the later assemblage ·analcite + datolite + apophyllite + calcite + stilbite + chlorite· are all below 150°C (samples GA1.3, GA1.1, MW103-2, MW103-3, and probably GA17.3). The three radiometric ages ( $92 \pm 5$ ,  $73 \pm 5$ ,  $< 1.2$  m.y.), all of which are from phases of the later assemblage, should be taken as minimum ages (see Appendix E for a discussion of age dates) so that the older,  $92 \pm 5$  m.y. age of apophyllite in MW112-1, most closely approaches the true age of the assemblage. Thus, it appears that the early mineral assemblage formed at a distinctly higher temperature than the later, and that both assemblages formed prior to 92 m.y.

TABLE B.5-1

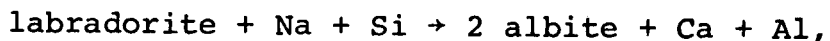
SELECTED OBSERVATIONS OF FAULTING

Rockland Lake Area

<u>Sta. #</u>	<u>Fault Trend &amp; Movement Sense</u>	<u>Criteria</u>
G.A.-157	N45°E, 75°SE	Slickensides rake 90° Slickensides rake 73° SW & Fracture geometry
	N30-50°E, 80°SE	
	N45-50°E, 85°NW	Slickensides rake 35°NW Fracture geometry
	N25°W, 70°SW	
G.A.-154	N40°E, 85°NW	Slickensides rake 40°N Fracture geometry Slickensides rake 40°N Fracture geometry Horizontal slickensides Fracture geometry Slickensides rake 35°N Strike-slip Slickensides Fracture geometry
	N39°E, 85°NW	
	N16°E, 20°NW (Several planes)	
	N28°E, 45°NW	
	N-S, 90° (several zones)	
D.F.-35 & G.A.-162	Valley between two outcrops trends N35-40°E and contains sinistral fault, which displaces basal contact of Palisades "Sill"	Stratigraphy Diabase exposed on south side of valley (G.A.-162) Hornfels exposed on north side of valley D.F.-35.
MW-23	N26°E, 83°E	Slickensides rake 2° SE

#### B8.4 DISCUSSION AND CONCLUSIONS

Differentiation trends and chemical analyses of the Palisades sill (Walker, 1969) indicate that the intrusion fractionated from early to late stages toward Fe-enrichment with only slight alkali enrichment. In the very late stages, the trend changed and moved exclusively toward alkali-enrichment. Black (1972) concluded that the Watchung flow units followed a differentiation sequence similar to Hawaiian tholeiites and that in at least one location an increasing partial pressure of oxygen produced a silica enriched, iron depleted diabase. Thus, late-stage concentrations of silica and alkalies may be common in the Palisade and Watchung bodies. The albite and quartz veins noted by Walker in the top and bottom of the Palisades sill probably formed when these residual liquids penetrated cooling fissures. Based on these observations, it is suggested here that silica and sodium rich solutions derived from these residual liquids caused albitization of the wallrock along fractures and thereby contributed to the early phase of mineralization. The general reaction for this process would be:



with Ca, Al and free silica involved in the crystallization of calcite, stilbite and free quartz. The alternative possibility that the reaction is isochemical, with labradorite breaking down to albite, quartz and calcite in the presence of  $\text{CO}_2$ , is not considered likely since the albitization appears to be restricted to the region of the mineralized fractures.

Implicit in this interpretation of the early assemblage as a product of late cooling residuals is the conclusion that the mineralization was localized, in space and time, to the intrusion within which it occurs. Additionally, the formation temperature of the mineralization could be high.

This process of albitization appears to have been followed by an episode of hydrothermal mineralization, which occurred subsequent to the final cooling of the intrusive bodies and subsequent to the strike-slip faulting. The hydrothermal episode is characterized by the crystallization of zeolites and associated minerals from circulating fluids in the fault and fracture system. Mesoscopic and microscopic observations of textural relationships show that the persisting post-tectonic assemblage consists of analcite, apophyllite, datolite, zeolites (stilbite) and calcite. Although hydrothermal, this episode does not appear to have been above 150°C in temperature, which is consistent with Dallmeyers' (1975) observation that there has been no argon loss from the Palisades diabase.

The only effects in the later episode of mineralization, which may be construed as tectonic are the dilatational events which occur throughout (Table B8-3). These are recorded by separation of the older mineralization from the wall rock and crystallization of new; generally drusy, phases in the void (so that the vein has a sandwich-like appearance). If, as suggested, the age of this episode is approximated by the 92 m.y. radiometric age, then the dilatational events would be compatible

with the relaxation of the Trio-Jurassic stress system and the downwarping of the Coastal Plain.

At this point, it is worth noting two earlier studies of mineralization in the Watchung flows. Schaller (1932) discussed in considerable detail the sequence of formation of the different minerals and their paragenesis in the First Watchung Flow near Paterson, N.J. His observed sequence is as follows:

- |             |  |
|-------------|--|
| Period I:   | Labradorite, Augite, Olivine, Magnetite;   |
| Period II:  | Anhydrite, Glauberite;   |
| Period III: | Albite, Quartz, Babingtonite;  |
| Period IV:  | Calcite, Prehnite, Datolite, Pectolite, Babingtonite;  |
| Period V:   | Analcite, Apophyllite, Chabazite, Gmelinite, Heulandite, Stilbite, Natrolite, Calcite, Babingtonite; |
| Period VI:  | Gypsum, Thaumassite, Calcite, Goethite, Malachite.   |

Regarding the chemistry of these parageneses, Schaller suggested that the constituents of the saline minerals of the lake beds, over which the lava of First Watchung flowed, were brought into solution and reacted with the lava. The albitization, which is one of the first mineral changes that took place, may have been accelerated by the increase in the percentage of sodium in solution when the calcium crystallized as anhydrite. The solution that formed the zeolites, thus contained a complex mixture of various elements and the order of crystallization was dependent on the solubility of the compounds.

Mason (1960) cites Schaller's sequence of the principal minerals and adds that in other areas of the Watchung basalt,

no glauberite or anhydrite crystallized, and therefore no crystal cavities were formed. In these areas, Period II of Schaller did not occur and there are no gypsum and thaumasite in Period VI, (since there is no anhydrite to provide the necessary sulphate ions). In general, Schaller's and Mason's observations regarding the relative timing of albite-quartz mineralization and analcite-zeolite mineralization are similar to those made in this study.

Based on the preceding discussions and observations, it appears that the mineralization of faults and shears in the Newark basin rocks is dominated by two episodes. The first episode is dependent on the age of the diabase or basalt body in which it occurs and is characterized by their late-stage albitization. This first episode is considered to be syntectonic. The second episode appears to be a strictly hydrothermal, low-temperature event and is concluded to be post-tectonic. The age of this second event, although not precisely defined, is taken to be Middle to Upper Cretaceous.

TABLE B8-1

MINERAL OCCURRENCES BY TREND OF SAMPLED FAULT OR SHEAR

Trend	Sample	quartz	calcite	stilbite	chlorite	analcite	datolite	apophyllite	prehnite	undetermined zeolite	opaque	iron stain	Other
N0°-30°E	GA 17.2		u	u							u		
	GA 17.3		u	u									
	MW 67d-1		d&u	u	u								
	MW 67d-2		d&u	u	d								
	MW 112-1		u		u		u	u	u				pectolite
	MW 112-2		u	u	u	u	u	u	u				
	MW 114-2	d			u							u	
	MW 116-3	d	d&u	u	d&u						d		
N30°-60°E	MW 102-1			u	u	u	u						chabazite
	MW 102-2		u	u	u		u						
	MW 106-1		d	u	u	u	u				u		
	MW 106-2		d&u	d	u								
	MW 111-1				u								natrolite, pectolite
	MW 111-2		d							d			natrolite
	MW 111-3								u	u			pectolite
	MW 115-1	u	d		d								
	MW 115-2	u			d&u						u		
	MW 116-1	d	d&u	d	d						d		
N60°-90°E	GA 1.1		d&u		u	u							
	GA 1.2		d&u			u							
	GA 1.3	d	d&u			u						d	
	GA 3.1					u							
	GA 4.1	u											
	MW 103-1		u	u	u								
	MW 103-2		d&u	u	d&u	u							
	MW 103-4		u	u	d&u	u							
	MW 113-1		d&u										
	MW 113-2		u										
	MW 116-2	d	d		d						d		
N0°-90°W	CHd-1				u				u			u	amphibole, pectolite
	GA 7.1		d		d						d		
	MW 103-3		d&u	u	d&u	u							
	MW 103-5		d&u	u	d&u						u	u	
	MW 114-1	d&u			d							u	
Sub-horizantal	GA 19.1	d&u	d&u	u	d&u								
	GA 20.1		u	u	d	u	u						
	GA 20.2	d	u		d	u	u						

u = undeformed

d = deformed or cogenetic with deformed phase

Table B8-2 Mineral Occurrences by Geographic Location

	Location	Sample	Fault or Shear Orientation	Plunge of Slickensides	Quartz	Calcite	Stilbite	Chlorite	Analcite	Datolite	Apophyllite	Prehnite	Undetermined Zeolite	Opaque	Iron stain	Other
General Vicinity of the System of Faults at Rockland Lake	Rockland Lake	GA17.2	N20E85E	5S		u	u							u		
		GA17.3	N30E85E	5S		u	u									
	Verdrietege Hook	MW102-1	N49E84S	dip		u	u	u	u	u						Chabazite
		MW102-2	N51E82E	35W		d	u	u	u	u				d		Scolecite
		MW102-3	float						u							
		MW103-1	N65E90	57W		u	u	u								
		MW103-2	N65E90	57W		d+u	u	d+u	u							
		MW103-3	N10W62W	1S		d+u	u	d+u	u							
		MW103-4	N83E82N	25W		u	u	d+u	u							
		MW103-5	N15W57W	3S		d+u	u	d+u						u	u	
		MW106-1	N42E78E	9S		d	u	u	u	u				u		
		MW106-2	N42E78E	21S		d+u	d	u								
		MW112-1	N10E65E	14S		u		u		u	u	u				Pectolite
		MW112-2	N10E65E	14S		u	u	u	u	u	u	u				
	Romic School	MW111-1	N52E82N	10W				u								Natrolite, Pectolite
		MW111-2	N52E82N	10W		d							d			Natrolite
		MW111-3	N38E79E	2N								u	u			Pectolite
	Valley Cottage	MW114-1	N15W87E	46N 5S	d+u			d							u	
	West Nyack	MW114-2	N25E84E	dip	d			u							u	
	Nyack	MW116-1	N59E65S	dip	d	d+u	d	d						d		
		MW116-2	N66E78N	65E	d	d		d						d		
		MW116-3	N14E80W	54S	d	d+u	u	d+u						d		
Vicinity of Thiells Fault	Long Clove - Short Clove area	GA7.1	N60W64N	strike		d		d								
		MW67d-1	N21E80E	16-31S		d+u	u	u								
		MW67d-2	N21E80E	16-31S		d+u	u	d								
	Mt. Ivy	GA1.1	N65E85N	50-60E		d+u		u	u							
		GA1.2	N65E85N	50-60E		d+u			u							
		GA1.3	N65E85N	50-60E	d	d+u			u						d	
		GA3.1	E-W 50N	---					u							
	Cedar Pond	MW113-1	N78E73S	4W		d+u										
		MW113-2	N78E73S	4W		u										
	Indian Road	CHd-1	N20W90	strike				u				u			u	Amphibole, Pectolite
Vicinity of Ramapo Fault	Ladentown	GA4.1	N66E46S	---	u											
	Union Hill	GA19.1	N70W30N	---	d+u	d+u	u	d+u								
	Hill	GA20.1	N65E20S	---		u	u	d	u	u						
		GA20.2	N70W20S	---	d	u		d	u	u						
	Turtle Hill	MW115-1	N47E87S	72W	u	d		d								
		NW115-2	N42E73E	71S	u			d+u							u	

u = undeformed

d = deformed or cogenetic with deformed phase

Note: GA17.2, GA17.3, NW113-1 and MW113-2 are from sedimentary rocks,  
all others are from diabase

TABLE B8-3  
OBSERVED PARAGENESES

<u>GROUP A</u>	<u>Paragenesis</u>
GA4.1	(Qtz*) # D (Qtz*) Tp ~ 200°C
GA19.1	(Chl) # S (Cc*+Qtz*) # S (Stil+Qtz+Cc+Chl) Tp = 308°C      Tp = 99°C
MW114-1	(Chl) # S (Qtz*+Chl) # S (Qtz) # S (Qtz+L) Tp = > 300°C, ~ 215°C, Ts = 135°C
MW114-2	(Qtz*) # S (Chl+L)
MW115-1	(Cc+Chl) # S (Qtz*) Tp ~ 168°C
MW115-2	(Chl) # S (Chl+Qtz) # D (Qtz*+0)
MW116-1	(Chl+0+Cc) # S (Qtz+Cc+Chl+Stil) # S (Cc)
MW116-2	(Chl+Cc) # S (Qtz+Cc+Chl+0) # S Tp = 148°C, Ts = 102°C
MW116-3	(Cc+0+Chl+Qtz) # S (Stil+Cc+Chl)
<u>GROUP B</u>	
GA1.3	(Qtz) # S (Cc+L) # S (Cc+Anal) Tp ~ 100°C
GA20.2	(Chl) # S (Qtz) # S (Anal+Dato+Cc) age < 1.2 m.y.
<u>GROUP C</u>	
GA1.1	(Cc) # S (Cc+Chl+Anal) # D (Anal*+Cc*) Tp = 80°C
GA1.2	(Cc) # S (Cc+Anal*)
GA20.1	(Chl) # S (Stil*+Dato*+Cc+Anal*)
MW102-3	(Cc+Sco+0) # S (Anal+Sco)
MW103-2	(Chl) # S (Cc) # S (Anal*+Cc*+Chl+Stil*) Tp = 271°C, 180°C      Tp = 114°C, Ts = low
MW103-3	(Chl+Cc) # S (Chl+Anal+Cc*) # D (Cc+Stil*) Tp = 135°C, Ts = 99°C
MW103-4	(Chl) # S (Anal*+Chl+Cc*) # D (Chl+Cc+Stil*)
MW106-1	(Cc*) # S (Cc) # S (0+Chl+Stil+Anal)
MW112-1	(?+Pect) # S (Apo*+Chl+Dato*+Cc+Prehn*+Pect) age = 92±5 m.y.

TABLE B8-3 (Continued)

<u>GROUP D</u>	<u>Paragenesis</u>
GA3.1	(Anal*)#D(Anal)
MW102-1	(Anal*+Dato+Chl+Chab*)#D(Anal*+Stil*)
MW102-2	(Chl+Stil+Dato+Cc)(Stil*)
MW112-2	(Cc*+Anal+Apo*+Stil*)(Chl+Dato+Prehn*)
<u>GROUP E</u>	
ChD-1	(chl+Amph+Pect*)#D(Prehn*)(L)
GA7.1	(Chl)#S( <u>Cc+0+Chl</u> )#S Tp = 215°C
GA17.2	(Cc*+Stil*+0) age = 73+5 m.y.
GA17.3	( <u>Cc*+Stil*</u> ) Tp = 124°C
MW67d-1	( <u>Cc*</u> )#S(Stil+Cc+Chl) Tp = 128°C, Ts = 110°C
MW67d-2	(Cc+Chl)#S(Stil*+Cc)
MW103-1	(Cc+Chl)#D(Cc*+Stil*)
MW103-5	(Cc+Chl)#S(Cc*+Stil*+Chl+L+0)
MW111-1	(Chl*+Pect*+Natro*)
MW111-2	(Cc+Zeo)#S(Natro)
MW111-3	(Zeo+Pect*)#D(Prehn*)
MW113-1	(Cc)#S(Cc*)
MW113-2	(Cc)(Cc*)
MW106-2	<div style="text-align: right;">Tp = 114°C, Ts = low</div> (Cc*)#S( <u>Stil+Cc</u> )#S( <u>Chl+Cc</u> ) Tp = 192°C,

Example of Notation:

(Qtz\*)#S(Cc+L)#S(Cc+Anal); means first episode of sparry quartz mineralization followed by shearing, followed by a second episode of calcite mineralization and iron staining, which in turn is sheared. The third and final episode of mineralization consists of calcite and analcite. The other symbols are explained on the accompanying key.

TABLE B8-3 (Continued)

## KEY TO SYMBOLS

Qtz	=	quartz
Chl	=	chlorite
Cc	=	calcite
Stil	=	stilbite
L	=	iron staining
O	=	opaque
Anal	=	analcite
Dato	=	datolite
Sco	=	scolecite
Pect	=	pectolite
Apo	=	apophyllite
Prehn	=	prehnite
Chab	=	chabazite
Amph	=	amphibole
Natro	=	natrolite
Zeo	=	undetermined zeolite
*	=	drusy or sparry phase
( )	=	cogenetic phases
#S	=	deforming event
#D	=	dilatational event
_____	=	submitted for fluid inclusion filling temperature analysis
Tp	=	average primary inclusion homogenization temperature
Ts	=	average secondary inclusion homogenization temperature
-----	=	submitted for age dating, radiometric age given

## B9.0 CONCLUSIONS

From the preceeding observations it can be concluded that the Newark Basin in Rockland County developed and was deformed during the Mesozoic Era. The initial subsidence of the basin was syn-sedimentary (as evidenced by the coarser clastic material along the western margin). This early period of basining and normal faulting was gradually replaced by a period of pervasive left-lateral strike-slip faulting.

The Palisades and Watchung igneous events appear to have occurred in the transition from dip-slip to strike-slip faulting. In this context, the drastic decrease in the rate of sediment accumulation during the Watchung Flows may reflect the change from predominantly dip-slip to strike-slip faulting along the Ramapo Fault. That the strike-slip movements had begun at least by the time of the intrusion of the Palisades diabase is evidenced by deformed cooling-attendant mineralization in the Rockland Lake Fault, where it passes through the Palisades (the same is true of the Ramapo Fault and the undated Union Hill Diabase). Igneous activity, as well as sedimentation, slowed down and eventually stopped altogether before the complete cessation of movements along the fault-members of the left-lateral simple shear system.

In Middle to Upper Cretaceous time, fault movements ceased, as recorded by the lack of deformation in the low-temperature hydrothermal mineralization. The separation of the

older mineralization from the wall rock and the crystallization of a new drusy phase may also be indicative of the relaxation of the stress system in Upper Cretaceous time.

Thus, the following specific conclusions may be reached relative to the purposes noted in Section B1.1:

- 1) The main trace of the Ramapo Fault in Rockland County follows the northwestern edge of the Newark Basin from Suffern to Ladentown, N.Y. At Ladentown, the present basin margin swings east-northeasterly away from the Ramapo Fault until it crosses and becomes subparallel to the Thiells Fault branch of the Ramapo Fault System. The Rockland Lake, Trough Hollow, and Hook Mountain Faults are associated with the Croton Falls Fault System, and are therefore indirectly associated with the Ramapo Fault System.
- 2) The tectonic function of the Ramapo Fault during Late Triassic time is interpreted to be primarily as a normal fault with an active role in the development and filling of the Newark Basin. From Late Triassic to Late Jurassic, the Ramapo and Thiells Faults of the Ramapo Fault System and the Trough Hollow, Rockland Lake and Hook Mountain Faults of the Croton Falls Fault System were left-lateral, strike-slip faults. Thus, it is reasonable to conclude, as has been done in

Appendix A, that faults in the Indian Point site area (which lies between these two systems) have had Mesozoic movements related to left-lateral movement on these faults; and

- 3) Within the Newark Basin, no faults have been found which cross-cut the Ramapo, Thiells, Trough Hollow, Rockland Lake or Hook Mountain Faults. The Ramapo Fault cross-cuts the Union Hill Diabase, and the others cross-cut the Palisades Diabase. The only materials overlying these faults are Pleistocene (Wisconsinan) deposits, which are discussed elsewhere (Appendix F). However, analysis of mineral samples taken from within the zones of these faults indicates that movement on these faults had ceased by Late Cretaceous time.

APPENDIX C

DEFORMATION ALONG THE RAMAPO FAULT IN THE  
VICINITY OF POMPTON LAKES, NEW JERSEY

## APPENDIX C

### DEFORMATION ALONG THE RAMAPO FAULT IN THE VICINITY OF POMPTON LAKES, NEW JERSEY

#### C1.0 INTRODUCTION AND OBJECTIVES

Field reconnaissance and geologic mapping were performed in the vicinity of Pompton Lakes and Oakland, New Jersey, along a narrow belt extending between southern Mahwah Township and Montville Township (6 miles north and 5 miles south of the Pompton Lakes area respectively). This area was investigated for the following reasons:

- 1) to define the nature of the deflection in the main trace of the Ramapo Fault System at Pompton Lakes;
- 2) to identify cross-cutting features and faults which might be used to determine the age of most recent movement on faults of the Ramapo system; and
- 3) to examine the exposed faults in the vicinity of the 1976 Pompton Lakes earthquake.

In addition to field mapping (stations located on Plate 2), geophysical (Appendix D) and geochronological (Appendix E) studies were conducted in order to help define the location and geometry of the Ramapo Fault Zone and to determine the ages of movement and igneous activity along the Ramapo Fault.

## C2.0 STRUCTURAL GEOLOGY

### C2.1 REGIONAL GEOLOGIC SETTING

The rocks in this area can be grouped into the Precambrian ortho- and paragneisses of the Reading Prong (west of the Ramapo Fault trace), and the Trio-Jurassic sedimentary and igneous rocks of the Newark Basin (east of the Ramapo Fault trace). The quality of Precambrian exposure is good, whereas that of the Mesozoic exposure is poor. The bedrock of the area has been eroded and covered by extensive unconsolidated deposits ranging in age from Pleistocene (Wisconsinan) to recent.

### C2.2 READING PRONG

The ortho- and paragneiss of the Reading Prong show evidence of both ductile and brittle deformation. The compositional layering ( $S_0$ ) of the paragneiss has been isoclinally folded during a Precambrian event. The regional foliation ( $S_1$ ) is generally parallel to the compositional layering and is axial planar to the isoclinal folds. Locally, the regional layering and foliation were seen to be re-folded and intruded by numerous igneous dikes ranging in composition from granite to diorite. Many of these intrusive bodies were emplaced during a period of ductile deformation. At one locality a pegmatite dike was observed to be co-axially folded with the layering due to rock flowage along the path of intrusion (Plate C.1). This example plus abundant exposures of boudinage or pinch-and-swell structures are evidence of the polyphase nature of the early ductile deformations seen in Precambrian rocks in the Pompton Lakes area.

The Reading Prong rocks are also intensely faulted and sheared along and near the Ramapo Fault. Many of the smaller fault zones appear to have been re-utilized during repeated episodes of deformation. In general, the faults in the Pompton Lakes area fall into three groups: 1) N-S to NE high angle faults, which are generally parallel to the regional foliation (these are typically mylonitic fault zones and exhibit intense diaphoresis); 2) ENE, E-W, and WNW high and low angle faults, which are commonly brecciated and have cataclastic textures (diaphoresis is less common); and 3) NW high angle faults, which are typically distinct, closely spaced, open fractures with unhealed breccias.

The north-south to northeast-trending group consists of high-angle strike-slip faults, which are the most pervasive in the area. Several of them have been mapped for long distances. The largest of these faults is exposed in the south wall of the Riverdale Quarry (SL-131; Plate 2). The fault here is oriented approximately N30 to 40°E, 70 to 80°NW and is mylonitized. The fault is exposed along strike to the northeast in the Passaic Quarry (SL-136) where it is oriented N40 to 65°E, 90° and exhibits slickensides raking 20°N.

North-south and N15°E-trending, small fault zones are exposed in Riverdale and Pompton Lakes along the walls of the valleys containing Lake Inez and Twin Lakes. These are interpreted to reflect the presence of a larger fault along the valley bottom, here termed the Lake Inez Fault (Plate 1). Along

the ridge crest, on the east side of Lake Inez, a 50 to 60 foot, vertical diabase dike is exposed for nearly one mile (Plate 1; SL-126, 127, and 128, Plate 2). The dike is sub-parallel to the Lake Inez Fault.

The diabase is fine-grained, porphyritic and crystalline. Petrographically, the rock contains phenocrysts of pyroxene and opaque minerals with a fine-grained feldspar groundmass. Opaque minerals comprise up to 25 percent of the rock. Additionally, the pyroxene exhibits pervasive edge-alteration to a greenish mineral which resembles chlorite. These petrographic constituents do not resemble the tholeiitic, olivine-poor basalt and diabase of the Trio-Jurassic basin described by Van Houten (1969).

Near the southern end of the dike (SL-126), the margin of the diabase (oriented N20°E, 90°) is chilled and sheared. In the country rock, small discontinuous fractures occur which stop at the contact (SL-126, Plate C-2). Further north (SL-128), the dike splits into two 10 to 15 foot thick dikes oriented N15 to 20°E, 90°. The gneiss between the two branches of the dike appears to be a very large xenolith caught within the large dike. At this exposure (Plate C-2), many fractures occur within the diabase, but do not affect the gneiss. Small second order synthetic-like shears occur at the margins of the dikes suggesting that sinistral strike-slip movement occurred along the contact. Additionally, a small stringer of diabase fills a N20°E

fracture in the gneiss xenolith. This stringer of diabase is offset less than an inch by a dip-slip open fracture, oriented N05°W, 67°E. This fracture appears to be a later feature since it was not filled with diabase.

One K/Ar whole-rock and two K/Ar mineral age dates (on pyroxene and feldspar), were obtained from this diabase dike (samples SL-127A and SL-PLd, Appendix E). The dike yielded concordant ages of  $439 \pm 18$  m.y. for the whole-rock, as well as  $424 \pm 22$  and  $458 \pm 17$  m.y. for pyroxene and feldspar separates, respectively. These results indicate that the dike is Late Ordovician and time equivalent to the Rosetown intrusive event ( $444 \pm 15$  m.y., Mose and others, 1975). It can be interpreted that this dike intruded parallel to the N20°E-trending Lake Inez Fault during Paleozoic movement along the Ramapo Fault. At the time of intrusion, the margins of the dike were sheared and locally a fine foliation developed within the chilled margin (Plate C-2). The sinistral strike-slip fracture geometries probably developed during a later episode of sinistral shearing.

Many shears and faults in the Reading Prong near Pompton Lakes exhibit dip-slip movement senses. At SL-101 (Plate 2) a complex fault zone is exposed in which the predominant faults are oriented N65 to 80°E, 70 to 80°SE. Although these faults also show evidence of strike-slip movement, the majority of the faults have slickensides raking 60 to 70°SW. Similar structural features are exposed in the Passaic Crushed

Stone quarry in Pompton Lakes (SL-136). At this locality, many north-south to northeast-striking faults in the gneiss are cross-cut and in many cases offset by generally east-west striking, low to intermediate angle, dip-slip faults. The west wall of the quarry exposes several of these dip-slip faults which dip both north and south in a horst and graben configuration. The faults appear to offset a north-south shear zone along the west wall. The significance of these faults will be discussed in Section C3.0.

Aside from the dike described above, only one other outcrop of possible Paleozoic rock was encountered (SL-102; Plate 2). The outcrop, a dark gray to black quartz-feldspar phyllite-like rock, is located in the north-central ninth of the Pompton Plains 7 1/2-minute Quadrangle, N.J., in a creek at the foot of the highlands on Mountain Avenue in Pompton Plains. Ratcliffe (1971; Figure 1, p. 127) illustrates the occurrence in Pompton, N.J. of "Cambrian and Ordovician metasediments, including shelf and eugeosynclinal rocks in the Manhattan Prong". However, he does not give any more information. Thin section examination of the phyllite-like rock reveals that its texture resembles that of a phyllonite. The rock exhibits a crude form of slip cleavage and contains secondary calcite. Vertical foliation strikes N15 to 30°E. Thus it appears that while the rock resembles the Annsville phyllite, it may instead be mylonitized rock, interlayered with cataclastic gneiss and thus related to shearing along the trace of the Ramapo Fault.

### C2.3 NEWARK BASIN

The rocks of the Newark Basin consist of interlayered shale, sandstone, and conglomerate with extrusive basalt flows. The sedimentary rocks belong to the Brunswick Formation (Triassic-Jurassic), and the basalts comprise three Watchung flows. Six potassium-argon age dates, two from each flow, were obtained from the Watchungs (see Appendix E). The First Watchung gave ages of  $193 \pm 10$  and  $179 \pm 9$  m.y.; the Second Watchung  $180 \pm 8$  and  $159 \pm 8$  m.y.; and the Third Watchung  $147 \pm 9$  and  $136 \pm 9$  m.y.

The clasts of the Brunswick conglomerate consist of quartzite, dolomite and sandstone in every exposure examined except one (SL-116), near Sunset Valley golf course in Lincoln Park, which contains abundant cobbles of pink granitic gneiss from the Reading Prong. Conglomerates occur at the base of the First and Second Watchung flows. Rounded, vesicular boulders of the First Watchung are contained in the conglomerate beneath the Second flow at Oakland, N.J. (CH-37; Plate 2).

The New Jersey Geological Survey (N.J.G.S.) has mapped eight faults in the Watchung basalts of the Oakland area. Seven of these transect the Second Watchung Flow and one fault cuts a portion of the First Watchung. These faults have been mapped through topographic breaks in the basalt ridges, and strike roughly north-south.

Field mapping during this investigation has shown that the Breakneck Road Fault strikes north-south (Plates 1, C-3). The outcrop pattern of the base of the Second Watchung suggests

a sinistral displacement along the fault. In addition, the density of north-south to north-northeast oriented fractures increases at the base of the flow. The Breakneck Road Fault is apparently cross-cut at Indian Road (CH-36, Plate 2) by a wide shear zone striking N30°W (Plate C-3). Shears within the zone are generally oriented N10°E to N20°W, 60-90° with low angle slickensides indicating strike-slip movement. Undeformed zeolite crystals were collected from a N10°E slickensided shear surface at this locality (sample CHd-1). This cross-cutting shear zone, the Indian Road Fault (Plates 1, C-3), is exposed to the northwest, at the northwestern extremity of the Second Watchung. The trace of the Indian Road Fault is therefore interpreted to trend N30°W rather than north-south as mapped by the New Jersey Geological Survey.

The Franklin Lake Fault was mapped by the N.J.G.S. in the Second Watchung (Plates 1, C-3). The trace of the fault trends N10°E paralleling deeply weathered valleys carved through the flow. The Indian Trail Fault, a smaller zone farther west, also exhibits a series of deeply eroded vertical fractures trending N40 to 50°W (CH-38, Plate 2). These northwest trending fractures do not appear to cross the valley and can be interpreted as synthetic shears associated with sinistral movement along the north-northeast trending Indian Trail Fault.

East of the Franklin Lake Fault, the N.J.G.S. has mapped two faults in the basalt through large valleys in High Mountain between Franklin Lake and Haledon Reservoir (Plates 1, C-3). At locality CH-39 a 3 foot wide, N10°W, 90° shear zone

with three 4-inch thick gouge zones is exposed. Zeolite crystals are present at the margins of the shear zone. The movement sense along these faults is uncertain. Elsewhere in the valley, glacial striae are present on the valley floor, suggesting that these fault-controlled, topographic valleys existed prior to Pleistocene glaciation.

Very little evidence for faulting was found along the east side of the Fyke Brook Fault (Plate C-3) as mapped by the N.J.G.S. in the First Watchung (Plate 1). One outcrop of basalt exhibited a high fracture density, but no faults were found.

Faults in the Brunswick formation (sedimentary rocks) were also seen in two other outcrops - CH-37 (SL-109) and SL-116. At CH-37, faulted conglomerate beneath the Second Watchung is exposed behind the Long Hill Mall on Route 202 in Oakland. At this exposure three faults were identified (A, B, C; Plate C-4) and a fourth fracture trace may be either a large joint or a fault (D; Plate C-4).

Three small faults are exposed in an outcrop of interbedded conglomerate, sandstone, and shale at the entrance to Sunset Valley golf course (SL-116, Lincoln Park Township). Two of the faults strike  $N40^{\circ}E$  and  $N60^{\circ}E$  and dip 80 to  $90^{\circ}N$ . The third is oriented  $N35^{\circ}W$ ,  $80^{\circ}W$  and offsets the other faults with an apparent dextral movement sense. The two offset faults appear to be conjugate shears.

#### C2.4 RAMAPO FAULT

The Ramapo Fault in the Pompton Lakes area is the contact between the Reading Prong and the Newark Basin. The

fault is not exposed at the surface, but field mapping along its trace has demonstrated that the fault strikes N35 to 40°E, except in the vicinity of Pompton Lakes and Riverdale where it swings to a N60°E strike for a distance of 3.3 miles. Additional support for mapping the position of the fault trace has been gained from the logs of borings reported by Vechiolli and Miller (1973). These borings are designated on Plate 1 by the letter U. Mapping has also shown that at two localities, Turtle Hill (SL-THd) in Mahwah and Indian Lane (SL-121) in Montville, New Jersey, the fault zone is intruded by aphanitic diabase which has been intensely sheared (N35°E, subvertical strike-slip and N45°W, subvertical oblique slip), brecciated, and mineralized. Two potassium-argon dates obtained on diabase from these two bodies yielded ages of  $156 \pm 7$  and  $149 \pm 7$  m.y. respectively (See Appendix E).

Both ground magnetic and regional aeromagnetic data indicate that the Ramapo Fault is intruded by diabase in this area. The occurrence of the Union Hill plug in the fault at Suffern, N.Y. north of this area further supports these observations. At SL-116, thin section examination of a sandstone bed near the fault zone has revealed a high concentration of pyroxene, olivine, biotite and chlorite in addition to quartz and feldspar. This detrital assemblage is most likely derived from from diabase. The regional aeromagnetic map of the Pompton Plains 7-1/2 minute quadrangle, N.J. (Henderson et al, 1957) reveals a positive magnetic anomaly of 8050 gammas in the fault zone, some 2000 feet north of this sandstone outcrop. Therefore,

it is interpreted that diabase, which is the probable source of this anomaly, may also be the source of the detritus at SL-116.

Eleven ground magnetic traverses were conducted in the Pompton Lakes area. Nine of these traverses provided enough data to model the measured magnetic profiles. Table C2.1 gives a generalized interpretation of the results, while Appendix D discusses each traverse in greater detail. In general, it can be interpreted that the Ramapo Fault is intruded by basaltic material, and that the fault is subvertical or dips steeply to the southeast.

Table C2.2 shows the orientation of faults in Precambrian exposures found nearest to the Ramapo Fault. The shears that were measured are vertical to steeply dipping toward the southeast and show evidence of predominantly oblique-slip movement.

Comparison of the information in Tables C2.1 and C2.2 reveals consistency between the surface exposures and subsurface information. It appears that much of the Ramapo Fault is intruded by diabase and that the fault zone dips steeply southeast or is subvertical.

#### C2.5 QUATERNARY DEPOSITS

Field mapping in the Pompton Lakes area revealed that much of the bedrock was covered with unconsolidated sedimentary deposits of glacial and post-glacial origin. These deposits consist of both stratified and non-stratified glacial drift and outwash, and finely laminated lake bed silts were found at one locality.

No structural features related to brittle deformation of the bedrock were found in the Quaternary deposits. In one case, an apparent post-glacial terrace, approximately 15 feet above the flood plain of the Wanaque River in Hershfeld Park of Pompton Lakes (SL-134; Plate 2) showed no noticeable difference in elevation across the river. This observation is significant because the terrace is situated within 2000 feet from the Ramapo Fault. A detailed report on the origin and occurrence of Pleistocene deposits is given in Appendix F.

TABLE C2-1INTERPRETATION OF GROUND MAGNETIC TRAVERSES

<u>Line</u>	<u>Location</u>	<u>Nature of Fault Contact</u>	<u>Geometry of Fault Contact</u>
8	Turtle Hill (Mahwah)	diabase (continuous)	?
9	Fyke Brook (Mahwah)	diabase (continuous)	?
10	Campgaw Mt. (Oakland)	diabase (2 dikes)	steep dip to SE at contact
11D	Oakland	diabase (continuous)	vertical
12	Pompton Lakes	magnetite or diabase	?
14	Riverdale	diabase (two dikes contin. at depth)	?
15	Riverdale	diabase (two dikes, contin. at depth)	sub-vertical
17	Pompton Lakes (SL-102)	diabase (dike, phyl- lonite at surface may be in fault zone)	steep dip to SE
18	Indian Lane (Montville)	diabase (continuous)	sub-vertical

TABLE C2-2

ATTITUDES OF SHEARS OBSERVED IN EXPOSURES  
NEAR THE RAMAPO FAULT

<u>Station</u>	<u>Shear Attitude</u>	<u>Rake of Slickensides</u>	<u>Remarks</u>
SL-100	N45°E 60°SE	30°SW	
SL-101	N40°E 90°	25°SW	
SL-102	N30°E 90°		phyllonite
SL-117	N40°E 65°SE	-	
	N50°E 70°SE	-	
	N60°E 70°SE	-	
SL-122	N45°E 40°SE	70°NE	diabase outcrops
	N60°E 70°SE	-	200 ft to east (SL-121)
SL-THd	N40°E 80°SE	0°	diabase in Ramapo Fault

### C3.0 SEQUENCE OF DEFORMATION

#### C3.1 GENERAL STATEMENT

There is ample field evidence of repeated movements along faults and shears within and parallel to the Ramapo Fault (generally trending N30 to 40°E, and dipping 60 to 90°SE). Protomylonites, mylonites, and ultramylonites have all been fractured or sheared, and in some cases show evidence of multiple movement senses, brecciation, and alteration. Many of the shears within the mylonite zones are curved both along strike and down dip. Splaying main shears and cross-cutting shears are common. The intersection and spacing of fractures and shear zones is typically dense so that few marker horizons are visible to determine the direction or amount of offset. Slickensides are typically the only movement sense indicators that are present.

The sequence of deformation in the Pompton Lakes area has been interpreted using field geologic mapping in conjunction with stereographic analysis. In order to understand the kinematics and deformational sequence along the Ramapo Fault, the orientation, movement sense and geographic location of associated faults should be taken into account. The trace of the Ramapo Fault is topographically expressed as a straight fault-line scarp trending N35 to 40°E between Mahwah and Oakland (Plate 1). At Oakland, the trace of the fault swings to the trend N65°E-S65°W for 3.3 miles, south of which (at Pompton Plains) the trace of the Ramapo Fault is again sharply expressed as a N35 to

40°E fault-line scarp. With this in mind, the structural elements collected from the various outcrops were grouped into three zones (Plate C-5): Zone A, covering the area north of the "deflection" of the Ramapo Fault trace; Zone B, covering the area of the "deflection" of the fault trace and Zone C, covering the area south of the "deflection" of the fault trace. Within each zone observations were collected from two domains: 1) Precambrian gneisses and 2) Trio-Jurassic rocks.

### C3.2 PALEOZOIC DEXTRAL TRANSCURRENT FAULTING

Fracture geometry along several steeply dipping faults oriented N30 to 40°E indicate that dextral transcurrent movement occurred on many of them. A clear example of dextral geometry is exposed in the Highlands along Skyline Drive, east-northeast of Wanaque, N.J., one mile west of the Ramapo Fault. At this locality (SL-133) the small-scale fracture geometry suggests that the N30 to 40°E shears experienced a component of dextral strike-slip movement. Plate C-6 is a sketch of a portion of the outcrop at Station SL-133 illustrating the evidence of dextral movement. This diagram also suggests that the C-set may be considered left-lateral synthetic to the A-set, and from cross-cutting relationships may post-date the right-lateral event.

Many faults and shear zones were mapped with N60 to 85°E strikes and sub-vertical dips. If any or all of these faults formed as synthetic shears in response to dextral displacement along the Ramapo, then the 60°E trend of the "deflection" of the Ramapo fault trace reflects the effect of this

period of deformation. Plate C-7 is a plot of poles to the east-northeast oriented faults that were recognized in the Highlands gneisses of Zone B (Plate C-5). Five of these faults were interpreted to have experienced right-lateral movement. The inferred sense of movement is based on fracture geometry and slickensides, rather than offset marker horizons. Additional evidence for dextral shearing has been reported in the Paleozoic rocks north of the Newark Basin (Ratcliffe, 1971; Dames & Moore, 1975, and Appendix A). The controlled emplacement of Paleozoic igneous plutons along east-northeast to east-west trends within the Ramapo Fault System (Appendices A and D), and the many dextral offsets recorded along northeast-trending faults in the area of Indian Point (Dames & Moore, 1975) indicate that the dextral movements are most likely Paleozoic, post-Taconic in age.

### C3.3 MESOZOIC WRENCH TECTONICS

Relative to the Precambrian gneisses, the rocks of the Brunswick formation are much less deformed in the Pompton Lakes area. Several outcrops of sediments were altogether free of faults and joints. Where deformational features were observed, they were widely spaced, and brecciation, gouge and mineralization were not consistently present. The faults observed in the Brunswick formation clearly post-date lithification. In some instances cobbles and clasts within the conglomerates have been clearly offset. In some outcrops, poorly developed sedimentary structures such as channels, cross-bedding, and pebble imbrication have been tilted, as evidenced by a 15 to 30 degree westward

dip toward the Ramapo Fault. Near Pompton Lakes bedding strikes generally north-northwest to northwest and dips 15 to 30 degrees southwest. At Pompton Plains, however, bedding in a large outcrop (several hundred feet long, exposing approximately 150 ft. of sediments) strikes east-northeast and dips gently northwest (Plate C-8). The spread of poles to bedding suggests that bedding is gently folded about an axis approximately oriented N45°W, 9NW. This fold axis is approximately normal to the basin margin and Ramapo Fault, and seems to be similar to other folds described within the Basin in Pennsylvania (Faill, 1973).

All of the faults observed in the Mesozoic rocks of Zones A, B and C (Plate C-5) are plotted on stereograms (Plate C-9). All three faults observed in Zone C were small, occurring within one outcrop (SL-116). Because of the paucity of Mesozoic outcrop in this domain, it is not certain whether these faults are representative of the regional deformation throughout Zone C. The stereograms on Plate C-9 reveal that in these zones there are: 1) high-angle strike-slip faults striking north-northeast to northeast, except for one fault that strikes northwest in Zone C; 2) high-angle dip-slip faults striking northeast and northwest; and 3) high-angle strike-slip and dip-slip faults oriented east-northeast. The interpretation of the sequence of movements on these faults is based primarily on data and observations made in the Pompton Lakes area, which is supported by the observations made and conclusions reached in Appendix B.

The gentle synclinal fold, the axis of which is nearly normal to the basin margin and the Ramapo Fault (Plate C-8) has affected rocks both above and below the Third Watchung Flow. Analysis of cooling-attendant mineralization in the Palisades diabase elsewhere in the Basin indicates that strike-slip movement along northeast-striking faults had begun by Palisades - First Watchung time (~190 m.y.a., Appendices B and E). This would coincide with the transition from an early phase of greater sediment accumulation (possibly a result of a normal fault regime) to a late phase of strike-slip deformation with lesser sediment accumulation. Therefore it can be concluded that the syncline formed during the strike-slip phase, in the deflection zone of the Ramapo Fault. This conclusion is consistent with the local compression that would affect this portion of the Trio-Jurassic Basin during left-lateral strike-slip movement along the northeast-striking segments of the Ramapo Fault. The northeast dip-slip faults (Zone C; Plate C-9) probably formed during the early normal faulting. However, the northwest-striking dip-slip faults in Zone A, and possibly the northwest-striking faults of unknown movement sense in Zone B, may have formed as normal faults parallel to the axial plane of the fold.

Although there is no direct evidence to this effect in the Pompton Lakes area, the several north-northeast to northeast-striking transcurrent faults (Zones A and B, Plate C-9) may be interpreted as members of the later phase of Mesozoic sinistral

wrench tectonics that affected the Newark Basin (Appendix B). Additional supporting evidence of sinistral movement is provided by observations made in Zone B. Within this zone, the trace of the Ramapo Fault strikes N60°E and has been interpreted to have developed as a Paleozoic synthetic shear during dextral strike-slip movement (Section C3.2). During sinistral strike-slip movement, along the northeast-striking segments of the Ramapo Fault, the N60°E striking segment would be favorably oriented to experience compressional deformation. Excellent examples of east-northeast, east-west and west-northwest-striking faults with dominant components of dip-slip movement are exposed in local quarries within the Precambrian gneiss of Zone B. Plate C-10 is a stereogram showing 18 of these faults. The observed movement sense is normal on some and reverse on others. These generally east-west-striking faults are the best developed, throughgoing faults in the quarries and cross-cut N30 to 40°E-striking mylonitized and brecciated shear zones. Because of the sparse exposure in the Trio-Jurassic Basin only two generally east-west-striking faults were observed, one of which showed evidence of dip-slip movement. This dip-slip fault was observed in the Second Watchung (Zone B, Plate C-9; Indian Trail). These observations suggest that many of the dip-slip faults shown on Plate C-10 have been reactivated in the Mesozoic during strike-slip deformation.

#### C3.4 REGIONAL ROTATION OF BEDDING

Within the Newark Basin, faults of the later phase described above, appear to have been rotated downward toward the

west. Evidence for this rotation is best exhibited at CH-37 in Oakland, N.J. (Section C2.3; Plate C-4). At this locality tilted pebble imbrication suggests an anomalous "up-slope" current flow direction (Section C2.3). The faults exposed at this outcrop dip very gently, yet appear to be strike-slip, as evidenced by slickensides. Stereographic analysis was used to compensate for the rotation of bedding in order to examine the original geometry of the faults at CH-37. Since it is not known whether the axis of rotation trends at right angles to the fold axis or whether it is parallel to the strike of bedding at CH-37, these two rotations were performed (Table 3-1).

A nine degree rotation, bringing the axis of folding to a horizontal position, has little effect on the orientation of faults and slickensides. However, a rotation of 25 degrees about the strike of bedding at CH-37 results in significantly different orientations for faults and slickensides (Table 3-1). Rotated faults A, B, and C all strike N20-40°E. Faults A and C are clearly strike-slip, whereas B, the most gently dipping, is actually a dip-slip fault with a strong element of rotational displacement as evidenced by 55° and 90° raking slickensides on the same fault plane. Therefore, it can be concluded that faults A, B, C and D, which formed after lithification (fault B slices a cobble in the conglomerate), were rotated downward and to the west along with bedding. By restoring the bedding to horizontal, the effects of folding have been removed, and the faults are restored to nearly pre-folding orientations.

Faill (1973) recognized a final episode of monoclinial rotation in the Gettysburg Basin of Pennsylvania. Sanders (1963) suggested that a period of broad arching occurred late in the deformation of the Newark and Connecticut Basins. Thus the present tilted configuration of the structural elements at CH-37 may be the result of compound rotation (due to folding and due to arching). The component of rotation due to regional arching may be contemporaneous with the relaxation of the Triassic-Jurassic stress regime which appears to be coincident with the Late Cretaceous hydrothermal event (Appendix B and E).

TABLE C3-1

ANLAYSIS OF STRUCTURAL DATA AT STATION CH-37

	Orientation after Rotation around Axis trending <u>N45°E</u>	Orientation after Rotation around Axis trending <u>N25°W</u>
<u>Fault A</u>		
N40°E 40°SE	N41°E 49°SE	N20°E 66°SE
slicks rake 5°NE	4°NE	34°NE
<u>Fault B</u>		
N55°E 35°SE	N54°E 44°SE	N27°E 46°SE
slicks rake 20°NE	22°NE	55°NE
N60°E 30°SE	N57°E 39°SE	N26°E 40°SE
slicks rake 50°NE	54°NE	90°
<u>Fault C</u>		
N55°E 50°SE	N54°E 59°SE	N38°E 58°SE
slicks rake 0°	2°NE	30°NE
<u>Joint or Fault D</u>		
N60°E 90°	N60°E 81°NW	N61°E 87°NW

Synclinal fold axis N45°W, 9°NW

Average orientation of bedding at CH-37, N25°W, 25°SW.

#### C4.0 CONCLUSIONS

The east-northeast striking segment of the Ramapo Fault at Pompton Lakes developed during right-lateral strike-slip movement along the northeast-striking sections of the fault farther north and south. The controlled emplacement of Paleozoic Plutons, such as the Rosetown and Cortlandt Complexes, along the Fault System (Appendices A and D) is represented in the Pompton Lakes area by the vertical diabase sill near Lake Inez (Section C2.2).

Igneous activity accompanied sedimentation during the formation of the Newark Basin in Triassic-Jurassic time. The three Watchung basalt flows were extruded approximately 186, 170, and 142 m.y.b.p. Igneous rocks intruded the Ramapo Fault zone at Turtle Hill and Indian Lane (Plate C-5, approximately 150 m.y. b.p., Section C2.4).

Within the Newark Basin the main period of sediment accumulation was succeeded by a phase of strike-slip faulting. This phase is well expressed as strike-slip faults with a left-lateral sense of displacement along the N40°E-striking segments of the Ramapo Fault. The sub-ordinate north-northeast faults are interpreted as synthetic to the main shear orientation (N40°E). The generally east-west-oriented shears, in the deflection zone, experienced dip-slip adjustments in response to the local compression that developed in this area. This local compression was also responsible for the folding of the rocks of the Newark

Basin about a northwest axis at a high angle to the basin margin and the Ramapo Fault. At Oakland, New Jersey field relationships suggest that both strike-slip and dip-slip faults are rotated downward toward the west along with the bedding (Section C3.4).

Mineralization studies suggest that relaxation of the Trio-Jurassic stress regime occurred in Late Cretaceous time (Appendix B). This relaxation may be contemporaneous with the regional monoclinal rotation of Faill (1973) and broad arching of Sanders (1963).

APPENDIX D

GEOPHYSICAL INVESTIGATIONS

## APPENDIX D

### GEOPHYSICAL INVESTIGATIONS

#### D1.0 INTRODUCTION

The primary purpose of the geophysical investigations is:

- 1) to provide subsurface information in critical areas where surface exposure was lacking;
- 2) to assist in the subsurface definition of the main trace of the Ramapo Fault and associated faults of the Ramapo Fault System; and
- 3) to develop a bathymetric map and seismic profiles of the Hudson River bottom, between the areas of Jones Point and the town of Verplanck, in order to evaluate the nature of previously observed irregularities in the Hudson River bottom.

All of the basic characteristic differences in the physical properties of the various materials within the study area were exploited. Differences in magnetic susceptibility (magnetic data), material density (gravity data), and acoustic impedance (seismic reflection) were each used where applicable to aid in understanding and correlating the surface and subsurface geology.

The geophysical surveys help define, in an indirect way, the tectonic framework of the area under investigation and assist in defining the boundary between crustal blocks at depth.

It should be realized at the onset that the usefulness of these explorational surveys is dependent on the quality of the interpretation that can be abstracted from the data. Interpretations were made on the basis of a thorough understanding of field relationships. Although this may be considered a largely subjective process, in so far as geophysical data appear to complement the field investigation, they should be treated as supportive evidence.

## D2.0 GROUND MAGNETIC AND AEROMAGNETIC

### INVESTIGATION - GENERAL

#### D2.1 INTRODUCTION

The objective of any magnetic investigation is the identification and description of spatial variations in the earth's magnetic field. Once a variation is detected, and its character identified, it is possible to interpret its significance relative to the geologic problem under consideration. In this study the specific purpose of studying variations in the earth's magnetic field was to assist in the evaluation of the geometry and location of the system of faults which is herein collectively referred to as the Ramapo Fault System.

#### D2.2 FUNDAMENTALS INVOLVED

In general the earth's magnetic field can be thought of as a bar magnet that is approximately coincident with the earth's rotational axis. The origin of the field is not well understood, but is thought to be due to currents in a fluid conductive core. The fact that the distribution of the earth's total field intensity is not perfectly symmetrical about the geographic poles, and that there exist very large scale anomalous features distorting its symmetry, simply reflects the unknown characteristics of the generating mechanism in the earth's core. These large scale distortions, however, need not be considered, since they are very large relative to the scale of the area of the subject magnetic investigation. Therefore, for the purpose

of this investigation, the interpretations presented reflect factors that alter a uniform total magnetic field.

The primary factors which must be considered are:

- 1) the flux of particles and electric currents from the sun that distort the magnetic lines of force as the earth rotates (i.e., diurnal variation) and variations in the solar flux (i.e., sun spots, solar flares), and;
- 2) distortions of the earth's local magnetic field caused by variations in the distribution of magnetic minerals in the earth's crust.

Of the two, the latter is the most relevant in the evaluation of geologic problems. The former can be corrected for by determining the diurnal variation, or precluded by not conducting an investigation during periods of high magnetic variation (i.e., magnetic storms).

Therefore, by considering 1) the study area to be under the influence of a constant magnetic field, and 2) corrections to negate the effect of variations of the sun's electromagnetic radiation, all that is necessary to make geologic interpretations is an understanding of the nature of crustal materials that can cause variations in the earth's total field.

For the most part the variations in the total magnetic field result from variations in the content of magnetic minerals contained within the rocks. The most common magnetic miner-

al is magnetite. This mineral can alter the earth's magnetic field in two ways:

- 1) by induced magnetization whereby the mineral responds to the ambient magnetic field and itself acts as a magnet enhancing the ambient magnetic field, or;
- 2) by remanent or permanent magnetization which is independent of the earth's ambient field and depends only on the magnetic mineral's metallurgical properties and its thermal, mechanical and magnetic history. Remanent magnetization in minerals can either add to or subtract from the total ambient field, depending on the orientation of the mineral's magnetic poles. The effect is primarily additive if the mineral cooled to a temperature below its Curie point in a normal earth's magnetic field and subtractive if the mineral cooled below its Curie point in a reversed earth's magnetic field.

In this investigation, the effect of remanent magnetization is negligible except for basic igneous rocks. Table D3-1 shows that for rock types other than basic igneous, the intensity of the remanent component is small relative to the intensity from induced magnetization. Therefore, the extent to which these rocks enhance the earth's ambient magnetic field is pro-

portional to their content of magnetic minerals, which in turn is proportional to a value referred to as the rock's magnetic susceptibility, such that:

$$I_i = kF$$

where,  $I_i$  is the induced magnetization per unit volume or mass in cgs electromagnetic units,  $F$  is the ambient field intensity in gauss (0.5-0.6 gauss in study area) and  $k$  is the magnetic susceptibility per unit volume or mass.

For basic igneous rock however, the relative contribution of induced versus remnant magnetization must be considered. For a more detailed discussion of the earth's total magnetic field and rock magnetization refer to Dobrin (1976), Breiner (1973), and Grant and West (1965).

### D3.0 GROUND MAGNETIC SURVEY

#### D3.1 INTRODUCTION

Eighteen ground magnetic profiles were obtained between Stony Point, New York and Montville, New Jersey. Profiles are numbered consecutively from north to south. Profiles 1 and 2, cross the trace of the Thiells Fault, Profile 3, crosses the trace of the Letchworth Fault and Profiles 4 to 18, cross the trace of the Ramapo Fault (Plates 1 and 2). The ground magnetic survey was conducted to assist in the evaluation of the nature and location of the system of faults which is collectively referred to as the Ramapo Fault System.

#### D3.2 METHODOLOGY

The survey was conducted using a total field proton precession magnetometer (Geometrics Model G816). This instrument measures the total intensity of the earth's magnetic field at a point. A base station located at Mt. Ivy, New York, monitored the total field intensity at 15 minute intervals. This data was used to determine the diurnal variation which in turn was used to correct all field measurements to a common datum.

Distance along the magnetic profiles was measured with a "Rolatape" which is a device that gives the distance travelled by a wheel along the ground surface. Total magnetic intensity readings were taken, generally at 100 foot spacings along the measured lines. Existing roads were used to provide easy access,

therefore, erroneous measurements due to cultural "noise" such as power lines, pipes, etc. (which are concentrated along roads), were considered on an individual basis. Many of these features were identified during the course of the study and are labelled directly on the profiles.

During the early stages of the ground magnetic investigations, representative values for the magnetic susceptibilities of the various rock types were used in modelling. At the same time, 17 samples were sent to Dr. N. Opdyke of Lamont-Doherty Geological Observatory for measurement of magnetic susceptibility and maximum remanent intensity. Oriented samples for determining the direction of the remanent magnetization were not taken. The results of these analyses are contained in Table D3-1.

### D3.3 COMPUTER MODELING

The ground magnetic profiles were modeled using the Dames & Moore computer program MAGNETX, which utilizes the methods of Talwani and Heirtzler (1965). This two-dimensional program makes use of up to 10 polygons of 20 sides each to produce a given magnetic anomaly.

The shape of the two-dimensional magnetic profile is a function of the magnetic characteristics of the underlying materials, the nature of the earth's magnetic field along the profile, and the azimuth of the survey line.

The earth's magnetic field was assumed to be constant throughout the study area. Although, in fact, there may be some

minor variations, these were not sufficiently large to affect the analysis. The azimuth and location of the lines is known from the field survey.

Representative magnetic susceptibilities for each of the typical lithologies have been used in modeling. With the exception of a few rocks such as Trio-Jurassic diabase and the Rosetown gabbro, the ratio of maximum remanent intensity to susceptibility is low. Therefore, the use of only induced magnetization is appropriate. Discussion of possible effects of remanent magnetization is made in a few cases for specific profiles. Values of magnetic susceptibility used for computer modeling are listed below:

<u>Rock Type</u>	<u>Susceptibility (emu/gm)</u>
Trio-Jurassic sedimentary	$0.4 \times 10^{-4}$
Trio-Jurassic diabase	$12.0 \times 10^{-4}$
Precambrian Gneisses	$0.1 \times 10^{-4}$
Paleozoic meta-sediments	$0.2 \times 10^{-4}$
gabbro	$20.0 \times 10^{-4}$
cataclastic rock	$0.1 \times 10^{-4}$
river alluvium	$0.01 \times 10^{-4}$
glacial till	$0.05 \times 10^{-4}$

The principal purpose of computer-modeling the magnetic profiles was to assist in the evaluation of the configuration of the subsurface bodies, particularly those associated with the Ramapo and related faults.

A basic model for each of the profiles was sketched manually. The choice of lithologies and boundaries was constrained in most cases by field exposures. The basic model was run through the program, producing an anomaly. An iterative process of computer runs for each profile was conducted to obtain an acceptable fit between modelled and smoothed observed values. No attempt was made to model each observed peak or to exactly match amplitudes. On the average, each line was modified five times, with a few requiring as many as 12 to 15 runs. Special emphasis was given to the orientation of igneous bodies along faults, as this could provide information regarding the orientation of the fault itself.

Parametric studies were conducted on the effect of depth. It was found that increasing the depth from 1000 feet to 5000 feet increased the size and amplitude of the anomalies only about 10%. Therefore, a depth constraint of 1000 feet was used in modeling (Plates D3-1 to D3-4).

Additionally, since no attempt was made to exactly fit the measured profiles, and the only correction applied was that for diurnal variations, the computer models should be considered as simplified illustrations showing the probable orientation of the underlying rock. Each profile was modeled separately, and although an attempt was made to correlate all lines to a single datum, the shape rather than the absolute value of the anomalies was most closely modeled.

#### D3.4 DISCUSSION OF GROUND MAGNETIC PROFILES

##### D3.4.1 Profiles Across the Thiells Fault

Along Profiles 1 and 2 (Plates D3-1 and 2A), the Precambrian and Trio-Jurassic rocks are separated at the surface by a small section of Paleozoic metasediments. On the basis of assigned susceptibilities, the fairly large positive anomaly cannot be produced by the metasediments themselves. Therefore, the presence of a mafic intrusion (gabbro-type), similar to the nearby Rosetown or Cortlandt intrusion (at Stony Point), is proposed to occur beneath the Paleozoic metasediments. The mafic intrusion is subvertical or steeply dipping to the east on Model 1 (Plate D3-1). Model 2 appears to favor a westerly dip for the body. Based on the amplitude, symmetry and short wavelength of the observed anomalies, a steeper and easterly dip (Model 1) is favored. This interpretation is supported by the seismic profiling (Section D7.0).

##### D3.4.2 Profile Across the Letchworth Fault

Profile 3, is oriented approximately north-south along the Palisades Parkway (Plate 2). Diabase is exposed at the south end of the line, near Mt. Ivy, New York (distance 10,000 to 11,000 feet, Plate D3-1). A positive magnetic anomaly between distances 2700 and 3700 feet on the profile separates Precambrian and Trio-Jurassic rocks. This positive anomaly was modeled as a vertical mafic intrusion (gabbro-type). However, no indication of its presence can be inferred from the seismic profile. Although the full ground magnetic signature of the

diabase outcropping at the southern end of the profile was not recorded, it was modeled to have a steep southerly dip (Plate D3-1). Seismic profiling indicates the contact between Trio-Jurassic sediments and diabase to be near vertical.

#### D3.4.3 Profiles Across the Ramapo Fault

Profile 4, crosses the Mahwah Valley, southwest of Ladentown. The profile starts just east of the Precambrian-Trio-Jurassic contact. Although the Trio-Jurassic rocks in the valley are covered by river alluvium, the magnetic high indicates that diabase is present under the alluvium (Plate D3-2). Diabase is exposed towards the eastern end of this profile (Plates 1 and 2). This profile was not modeled.

Profile 5, just south of Profile 4, crosses the northern portion of the Ladentown diabase exposure (Plates 1 and 2). The magnetic profile indicates that diabase occurs at shallow depth under the river alluvium in the Mahwah Valley, and extends past the eastern end of the line, under the Trio-Jurassic sediments (Plate D3-2). The analysis of Profiles 4 and 5, support the conclusion that the Ladentown diabase body extends westward into the Ramapo Fault. This profile was not modeled.

Profile 6, lies along the Stag Hill Road, southwest of Suffern (Plate 2). Numerous cultural objects may have distorted many of the magnetic signatures along this profile (Plate D3-2).

Profile 7, is just south of Profile 6, and does not extend into the Precambrian to the west (Plates 1 and 2). The model indicates that the line may start over a shallow diabase body that extends eastward, under the alluvium for a distance of 800 feet (Plate D3-2). Since the entire extent of the anomaly was not measured, it is difficult to make an accurate dip estimate. However, the model presented shows that the eastern margin of the diabase may be dipping steeply to the east.

Profile 8 runs, in part, over the diabase outcrop at Turtle Hill (Plates 1 and 2). The magnetic low at distance 0-400 feet is complementary to the magnetic high over the diabase (Plate D3-2).

Profile 9, is a near north-south profile that crossed the Ramapo Valley. The line begins at the Turtle Hill diabase outcrop and ends near the Immaculate Conception Seminary, which is also located on a diabase outcrop (Plates 1 and 2). The level of the magnetic anomaly indicates the presence of basaltic material between the line ends as well, which may even be continuous. A modelling problem occurs near the basaltic outcrops near the southern end of the line (Plate D3-2). A magnetic low, on the order of 700 gammas, occurs before the basalt outcrop is reached. With the azimuth of the line and the susceptibilities used, this large low cannot be modeled. This anomaly may be partially due to terrain effects or more likely to the presence of a significant component of remanent magnetism in a direction different from that of the normal field (reverse polarity).

Profile 10, (Plate D3-3) is a long profile running approximately east-west, south of the Immaculate Conception Seminary and north of Campgaw Mountain (First Watchung). This line is continuous from the Precambrian into the Trio-Jurassic sedimentary rocks (Plates 1 and 2). A diabase dike, which appears to have a steep easterly dip, occurs at the junction of these rock types. Various other bodies of basaltic material occur to the east of this dike, including the exposures of Campgaw Mountain. As with other lines further south, this basalt may represent parts of a continuous flow.

Profile 11, is a long discontinuous profile, northeast of Pompton Lakes, extending from the Precambrian into the Trio-Jurassic sedimentary rocks (Plates 1 and 2). Segments 11A, B and C, were not used in the model and any anomaly present represents cultural noise or lithologic subdivisions in the Precambrian.

The model for Profile 11D, (Plate D3-3) shows that the whole profile is underlain by basaltic material (Second Watchung) east of the Precambrian contact. The dip of that contact appears to be vertical. The various highs along Profile 11A and 11B may represent variations in Precambrian lithologies.

Profile 12, is oriented approximately north-south through the town of Pompton Lakes, New Jersey (Plate 2). Because of the uncertainty as to whether the anomalies recorded through town are real or represent cultural noise, this line was not modelled.

Profile 13, is just west of Profile 12 and oriented approximately north-south. Because of cultural noise and because none of the anomalies appear to be reliable, this line was not modeled (Plate D3-4).

Profile 14, is located south of Riverdale, N.J., trends approximately north-south and overlaps with the southern end of Profile 13 (Plate 2). The profile shows two separate peaks that are interpreted as diabase dikes, centered at a distance of 750 feet and 1450 feet (Plate D3-4). Although this is not a unique interpretation, it is compatible with observed occurrences of diabase near the Precambrian gneiss - Trio-Jurassic sedimentary rocks contact.

Profile 15, is located south of Riverdale, N.J. and trends generally east-west. The line extends from the Precambrian gneisses into the Trio-Jurassic sedimentary rocks (Plates 1 and 2). The gneiss-sedimentary rock contact was fixed by field mapping. East of distance 2,000 feet, the continuous, general increase of the magnetic intensity suggests the presence of diabase gradually approaching the surface (Plate D3-4). Profile 16, which may be considered an eastern extension of profile 15, approaches outcrops of the Third Watchung (Plates 1B and 2B).

Profile 16, located just east of Profile 14, reflects the same general level of magnetic intensity as the eastern end of Profile 15, and in fact, may be considered an eastern extension of that profile (Plate D3-4).

Profile 17, is located just south of the western end of Profile 15 (Plate 2). Because this line changes azimuth near its center, it was not modeled.

Profile 18, located north of Montville, N.J., is generally oriented northwest-southeast. A sizeable portion of this line lies in Precambrian terrain. A magnetic anomaly on the order of 1200 gammas indicates the presence of a magnetically rich layer in the gneisses. A diabase body was modelled between the distances 3500 and 3900 feet to coincide with the exposure of the Indian Lane Diabase (Plate D3-4 and Plate 1-B). This body is near-vertical, but an accurate dip cannot be determined due to the presence of the large, adjacent magnetic low. Diabase crops out at the distance 4,600 feet and a diabase body is believed to occur between the distance of 4800 and 6400 feet (Third Watchung) (Plate D3-4). The large magnetic low, located between distance of 3700 and 5000 feet is problematical. Based on the azimuth of the line and the assumed susceptibilities, no configuration of adjacent basaltic bodies could generate such a low. However, the exact properties of the shear zone materials are not known and the effects of remanent magnetization have not been taken into account (Plate D3-4).

### D3.5 CONCLUSIONS

Most of the profiles are characterized by a positive magnetic anomaly that is coincident with or close to the fault zones that were investigated. In the case of the Ramapo Fault, these anomalies were modeled as diabase on the basis of the many

intermittent outcrops of diabase that were encountered near and within the fault zone. The diabase within the fault zones appears subvertical or steeply dipping to the east.

The magnetic highs that are associated with the Letchworth and Thiells Faults were modeled as gabbroic intrusions because the survey lines cross either exposed gabbro or the interpreted subsurface extension of the Rosetown Pluton (see Section D-4). Although the orientations of these intrusions are variable, they may be connected at depth to the exposed Rosetown Pluton nearby.

TABLE D3-1

MAGNETIC CHARACTERISTICS OF ROCK SAMPLES

<u>Sample No.</u>	<u>Rock Type</u>	<u>Susceptibility (emu/gm)</u>	<u>Maximum Remanent Intensity (emu/gm)</u>
CH-M-1	Trio-Jurassic sandstone	$0.3931 \cdot 10^{-4}$	$0.2080 \cdot 10^{-5}$
CH-M-2	cataclastic rock	$0.1279 \cdot 10^{-4}$	$0.1325 \cdot 10^{-5}$
CH-M-3	Precambrian gneiss	$0.1353 \cdot 10^{-4}$	$0.2023 \cdot 10^{-5}$
CH-M-4	Trio-Jurassic shale	$0.2581 \cdot 10^{-4}$	$0.8115 \cdot 10^{-5}$
CH-M-5	Trio-Jurassic diabase	$0.7039 \cdot 10^{-3}$	$0.2027 \cdot 10^{-3}$
CH-M-6	Precambrian cataclastic rock	$0.1273 \cdot 10^{-4}$	$0.1259 \cdot 10^{-6}$
CH-M-7	Precambrian gneiss	$0.7352 \cdot 10^{-5}$	$0.5466 \cdot 10^{-6}$
CH-M-8	Trio-Jurassic diabase	$0.9851 \cdot 10^{-3}$	$0.4144 \cdot 10^{-3}$
CH-M-9	Cambro-Ordovician quartzite	0	$0.5319 \cdot 10^{-6}$
CH-M-10	Cambro-Ordovician dolomite	weak & viscous	$0.54 \cdot 10^{-5}$
CH-M-11	Rosetown Gabbro	$0.1297 \cdot 10^{-2}$	$0.1489 \cdot 10^{-2}$
JW-MS-1A	mylonite (sheared amphibolite)	extremely viscous	$0.1177 \cdot 10^{-4}$
JW-MS-1B	less sheared amphibolite	$0.1791 \cdot 10^{-4}$	$0.1737 \cdot 10^{-5}$
JW-MS-2	fractured - no measurement possible	---	---
JW-MS-3	Cambro-Ordovician phyllite	$0.1218 \cdot 10^{-4}$	$0.9702 \cdot 10^{-6}$
JW-MS-4	Cambro-Ordovician quartzite	extremely viscous	$0.5437 \cdot 10^{-5}$
JW-MS-5	amphibolite	$0.4379 \cdot 10^{-4}$	$0.9466 \cdot 10^{-6}$

## D4.0 AEROMAGNETIC SURVEY

### D4.1 INTRODUCTION

In March, 1976, an airborne magnetometer survey was flown in the southeastern part of New York State, encompassing portions of Putnam, Orange, Rockland and Westchester counties. The City of Peekskill is located in the northeastern part of the survey area.

The geophysical survey was conducted by Airmag Surveys, Inc., of Philadelphia, Pennsylvania and the compilation of the survey data was performed by Atlantic Geophysical Company of Philadelphia. The purpose of the aeromagnetic survey was to study variations in the earth's magnetic field to obtain additional data to assist in the evaluation of the nature and location of the system of faults which is collectively referred to as the Ramapo Fault System. The advantage of an aeromagnetic survey over a ground magnetic survey is the ability to study larger areas. The disadvantage is a corresponding loss of resolution.

The survey area is sixteen miles long and slightly more than seven miles wide; the long dimension of the area is oriented northeast-southwest. The traverse direction was northwest-southeast, with an average spacing of one-tenth mile (528 feet) between adjacent parallel traverses. One hundred sixty-one traverses, and three tie lines normal to the traverses were flown. A total of one thousand one hundred seventy-five linear operational miles were flown during the course of the survey.

The average elevation above the terrain level was five hundred feet.

The total magnetic intensity was recorded digitally. The analog record was recorded at a sensitivity of one thousand gammas full scale (ten inches) deflection, and a horizontal scale averaging two thousand feet per inch.

The total magnetic intensity over the area flown was compiled on a series of three contour maps at a scale of 1:12,000. These three map sheets were reduced to a scale of 1:48,000 for presentation in this report (Plate D.4-1). The contour interval is ten gammas, except where it is precluded by steepness of gradient.

The survey aircraft was a Cessna 320 equipped with a Airmag Mark IV continuously recording fluxgate magnetometer. Ancillary equipment included a continuously recording radar altimeter and a continuous exposure 35 mm camera.

In the area of the aeromagnetic survey, the magnetic inclination is about seventy-two degrees, directed northward and below the horizon. The general strength of the earth's undisturbed magnetic field is about 57,000 gammas. The declination of the field is approximately eleven degrees west of geographic north.

#### D4.2 THEORETICAL CONSIDERATIONS

The earth's surface magnetic field would presumably follow a bar magnet distribution if the planet was perfectly homogeneous in composition and magnetic property. Departures from this ideal condition are caused by inhomogeneities in the

upper mantle and crust and by variations in the distribution of magnetic minerals, primarily magnetite, in the rock units that are near the surface. Local magnetic variations are the diagnostic features in most magnetometer surveys. Their shape and intensity are determined by many factors. Of these factors, the intensity and inclination of the regional field are of critical importance. The remaining factors are properties of the causative body itself; composition, shape, size, orientation, etc.

The proportion and direction of remanence in the causative body, as compared to induced magnetization, is another important factor in the determination of the characteristics of the magnetic anomaly. This, however, cannot be assessed without laboratory study of oriented samples of the body causing an anomaly; therefore, induced conditions are normally assumed in magnetic surveys.

With few exceptions, sedimentary rocks are virtually non-magnetic. The local distortions in the natural magnetic field are considered to arise primarily from the igneous and metamorphic bedrock. In general, the stronger the magnetic relief and intensity, the greater the proportion of magnetic minerals that is in the rock unit influencing the magnetic pattern. By further inference, the more likely it is to have a basic composition.

Faults may be manifested magnetically by dislocations or disruptions in a magnetic pattern or by persistent changes in

pattern over long distances or by the presence of pronounced linear patterns. Plugs, dikes, and other igneous bodies are inferred from the shape and intensities of the associated magnetic features. Recognition of such features is to some extent subjective in nature. The recognition of magnetic lineaments in this investigation was based on the identification of one or more of the following elements: linear patterns of contours, changes in gradient, alignments of magnetic lows and/or highs, and termination of highs and/or lows (Gay, 1972 and Dobrin, 1976). The aeromagnetic lineaments identified on Plate D4-1 are drawn at the base of pronounced magnetic gradients. These lineaments can be moved parallel to themselves within the zone of the linear gradient. It is the orientation of the lineaments, rather than their exact position, that reflects the probable tectonic framework of the area. The aeromagnetic map is (Plate D4-1) printed to overlay the central portion of the geologic map (Plate 1A and B). Therefore, a direct comparison can be made between exposed lithologies and magnetic signatures.

#### D4.3 INTERPRETATIONS

Aeromagnetic lineaments are commonly indicative of faults; therefore special attention was given to the major aeromagnetic lineaments to better understand the fundamental tectonic framework of the area. It should be remembered, however, that not all aeromagnetic lineaments are indicative of faulting. Metamorphic layering, and normal depositional, intrusive and extrusive contacts are also common causes of magnetic lineaments.

The most fundamental lineament through the area is the one that extends in a northeasterly direction, between A and D (Plate D.4-1). Exposures of the Rosetown Pluton were recognized in the area of the conical magnetic high that occurs between B and C. The magnetic pattern, which includes the elongated extension of the magnetic high between lineaments HG and JI, delineates the shape of the pluton at depth. Prior to the emplacement of the pluton, it seems likely that lineament AD was continuous between B and C. Therefore, it can be concluded that this lineament predates and, to some extent, controlled the emplacement of the pluton. Segment CD of this lineament coincides with the trace of the Ramapo Fault (Plate 1).

Several other lineaments, parallel to AD can be easily identified in the area of coverage. The longest and most conspicuous of these occur to the northwest of lineament AD and are truncated by lineament KL. Lineament KL trends east-northeast, and its segment LM coincides with the Mott Farm Road Fault Zone. KL is cross-cut by AB in the vicinity of L. Lineament NO coincides with the Peekskill Fault and is curved near N, as if dragged along AB. This apparent drag, however, may have been exaggerated by the effect of the nearby circular Cortlandt Pluton. The alignment of lows, which identify this prominent lineament, can also be considered complementary to the magnetic highs associated with the pluton and would tend, therefore, to follow its outline (Plate D.4-1).

Lineament PQ appears to be the extension of NO but is apparently displaced left laterally between P and O, along a

north-trending lineament. Similarly, if KL is considered to be the extension of NO, it is also displaced left laterally along lineament AB. A tangent to the curve at N intersects lineament AB at N'. The displacement between L and N', measured along AB, is on the order of 2,000 feet.

Steenland and Woollard (1952) determined that the emplacement of the main funnels of the Rosetown and Cortlandt Plutons were controlled by east-northeast trending fractures. The Cortlandt Complex occurs south of lineament NO-PQ and east of lineament JI, and is cross-cut by lineaments of similar orientation. Lineament RS, marked by the alignment of magnetic lows that are complementary to the magnetic highs associated with a linear segment of the Palisade diabase, is also parallel to this same east-northeast trend (Plate 1).

Several north-south to north-northeast trending lineaments have been identified, especially in the area surrounding the Rosetown Pluton. Lineaments HG and JI affect the western and eastern boundaries of the pluton, while lineament EF connects two major, northeast trending lineaments (Plate D.4-1).

The angular relationship between the east-northeast and the northeast trending lineaments is suggestive of a right-lateral geometry produced by movement along the northeast lineaments. In a similar fashion, the angular relationship between the north-south and northeast trending lineaments is suggestive of a left lateral geometry produced by movement along the northeast lineaments. The apparent displacement of the east-northeast lineaments by north-south and northeast lineaments (PO and

NL) indicates that right lateral movement preceded left lateral movement. In addition, the controlled emplacement of the Rosetown and Cortlandt funnels along an east-northeast trend (Steenland and Wollard, 1952) and the subsequent truncation of the western and eastern margins of the pluton by north-south lineaments supports this conclusion. It is possible, however, that this left-lateral geometry was inherited from the Precambrian and was merely reactivated during a period of deformation that post-dates the emplacement of the early Paleozoic Rosetown Pluton. The course of left-lateral movement (or reactivation of movement) along the major northeast trending lineaments appears to have contoured the Rosetown Pluton along EF, FM and ML (Plate D.4-1).

Several short and discontinuous northwest trending lineaments can be recognized throughout the survey area. Many of these may have been artificially generated because they are parallel to the flight lines of the survey. Lineament TU, however, the longest and best developed of this set, is defined not only by the deflection of magnetic contours, but also by the termination of magnetic patterns and, is therefore considered to be real. Lineament TU also appears to be aligned in the general direction of lineament VW, which parallels South Mountain, a linear segment of the Palisades diabase (Plate 1). Because of the possible artificial enhancement of this trend, it is difficult to establish the relative age of this lineament with respect to the others.

Finally, it may be useful to point out that the asymmetric nature of the magnetic anomalies over the diabase, south of lineament RS, indicates that it dips generally to the south. Also, the magnetic pattern of the Precambrian slice, north of lineament KM, appears to be different from that of the remaining Precambrian terrain, west of lineament AD (Plate D.4-1).

#### D4.4 CONCLUSIONS

Four major sets of lineaments were identified; these are: a northeast set, an east-northeast set, a north-south set and a northwest set. Angular intersections and cross-cutting relationships between these sets support the geologic conclusion that a period of right lateral movement preceded a period of left lateral movement (Appendices A, B and C). The relationship of the various sets relative to the Rosetown Pluton indicates that right lateral movement generally predates, while left lateral movement postdates the intrusion of the Rosetown Pluton. Left lateral movement along the northeast trend appears to have been deflected westward around the main body of the intrusion. Again, it should be stressed that not all of the magnetic lineaments are necessarily indicative of faulting.

## D5.0 EVALUATION OF GRAVITY DATA

### D5.1 INTRODUCTION

The National Oceanographic and Atmospheric Administration (NOAA) maintains a general data file of gravity measurements for the continental United States. Bouguer values obtained from this file were plotted on base maps at a scale of 1:250,000 and contoured at five milligal intervals. The area of evaluated coverage surrounds the mapped Ramapo Fault and is enclosed by latitudes 40°N to 43°N and longitudes 70°W to 76°W. The Bouguer values are based on a reduction density of 2.67 gm/cm<sup>3</sup>. Station spacing, in general, is about three to five kilometers. Detailed information about particular geologic features is not usually obtainable with this large spacing. However, regional features may be identified and the data may be used in large-scale generalized interpretations.

### D5.2 INTERPRETATIONS

In general, the anomalous gravity trends are nearly parallel to the structural trends of the Appalachians. The most prominent feature of the map is a gradient of 5 to 10 milligals per mile that separates an area of predominantly positive anomalies from an area of negative anomalies (Plate D5-1). This gradient is part of the feature that was traced from the Gaspe Peninsula to Alabama by Griscom (1963). Zietz, et. al. (1966), recognized that this "gravity feature" is a combination of a linear gravity high of about 40 milligals and a parallel linear

gradient of from 0 to -50 milligals along most of its length. Although, in New Jersey, this high occurs over the Coastal Plain, it is clearly associated with the Piedmont to the north and south (Bonini, 1965).

Wollard (1943a) examined the portion of the high that crosses New Jersey and concluded that the maximum depth to the center of mass of the source is 16 miles (26 km) with a depth of 11 miles (18 km) to its top. Ewing, Wollard and Vine (1939) reported high seismic velocities of up to 22,000 ft/sec. (6.71 km/sec) near the New Jersey gravity high, suggesting that the pre-Cretaceous basement may be basic in composition. Johnson (1956) found that basement topography may explain residual anomalies on the order of one or two milligals on the crest of the high, but most of the high itself was caused by high density basement.

Wollard (1943b) determined that the Appalachian Mountains (Valley and Ridge) have a 50 milligal negative isostatic anomaly associated with them, indicating a deficiency of mass at depth. Bonini (1965) computed the isostatic anomalies along a trans-New Jersey profile oriented northwest-southeast, between Phillipsburg and Barnegat Bay. The rocks of the Valley and Ridge and the Mesozoic Newark Basin, Bonini concluded, are associated with a negative isostatic anomaly, indicating a mass deficiency at depth; while the rocks under the Coastal Plain (Piedmont equivalent), east of Trenton are associated with a positive anomaly, indicating a mass excess at depth. Therefore,

he concluded that "for New Jersey, isostatic adjustment has not been perfect." These same regional gravity relationships hold for eastern New York State, where the site is located. Therefore, it can also be concluded that the isostatic adjustment of the Appalachians is not complete.

On a local scale, the most prominent gravity feature is a 25 milligal positive anomaly associated with the Cortlandt Complex. This anomaly, which disrupts the regional gravity gradient, has a well defined peak at latitude  $41.25^{\circ}\text{N}$ , longitude  $73.85^{\circ}\text{W}$ . The deflections of the gravity contours around the Cortlandt Complex extend to the western side of the Hudson River and into the Hudson Highlands. This is indicative of the connection between the Rosetown Pluton and the Cortlandt Complex at depth (Appendix A). In a detailed gravity study over the Cortlandt Complex, Steenland and Woollard (1952) identified a series of gravity highs corresponding to funnel-shaped mafic and ultramafic bodies within the plutons. This series of highs, between the Rosetown and the Cortlandt, line-up along an east-northeast to east-west trend. Similarly, the axial trace of the deflections of the gravity contours is also oriented east-northeast to east-west, confirming a controlled emplacement along that trend (Plate D5-1).

Whereas the gravity contours over the center of the Cortlandt Complex are circular, those along the northeast, northwest and southwest margins of the Pluton (on the east side of the Hudson River) tend to be rectilinear (Plate D5-1 and 2).

It is interesting to speculate that this rectilinear outline may reflect the effect of post-intrusive faulting. The faults affecting the western flank of the Cortlandt Complex are part of the Ramapo Fault System, while those affecting its eastern flank are part of the Croton Falls Fault System (Plate 1; see also Appendix A).

#### D5.3 CONCLUSIONS

The interpretation of the gravity data indicates that the isostatic adjustment of the Appalachians may not be complete. In terms of vertical crustal movements, the Piedmont and Coastal Plains, associated with a mass excess, will tend to move down; while the Highlands, Triassic Basin and Valley and Ridge, associated with a mass deficiency, will tend to move up.

The emplacement of the Cortlandt Complex was controlled along an east-northeast to east-west trend. The Rosetown Pluton appears to be connected to the Cortlandt Complex at depth. The northeast, northwest and southwest margins of the Cortlandt Complex appear to be rectilinear. This rectilinear outline may reflect the effect of post-intrusive faulting.

D6.0 RESULTS OF A BATHYMETRIC SURVEY IN THE HUDSON RIVER  
IN THE VICINITY OF INDIAN POINT

D6.1 INTRODUCTION

Bathymetric and seismic reflection data obtained from a brief reconnaissance geophysical survey in August 1975 (Dames & Moore, 1975) suggested a number of apparently anomalous features on the river bottom. These irregularities appeared to fall within a N35°E aligned zone, near the western bank of the river and parallel to its trend at that point. This trend corresponded to the geologic grain in the area and the trend of the Ramapo Fault System. Concern was expressed that this apparently anomalous zone might be evidence of recent faulting. A second "anomalous condition" on the river bottom was reported to occur on the eastern side of the river, near the mouth of Lent's Cove. Due to the limited coverage of the survey lines, the continuity of these bathymetric irregularities could only be postulated.

A second survey was conducted in March 1976 to provide better coverage of the Hudson River, between the areas of Jones Point and the town of Verplanck, to evaluate if the previously observed bathymetric and seismic reflection irregularities formed a continuous linear feature(s). A second objective was to develop a bathymetric map of the area to provide data on bathymetric expression of other previously unrecognized river bottom features.

## D6.2 OPERATIONS

The bathymetric survey was conducted during March 4 and 5, 1976. The primary survey tracklines were oriented roughly normal to the river axis with an average line spacing of 500 feet. Crossing tie lines were normal to the primary lines and spaced 1000 to 1500 feet apart.

Bathymetric data were measured and recorded with a Raytheon DE719 Precision Survey Fathometer. Bar checks<sup>(1)</sup> were performed at least twice daily to correct for variations in the speed of sound through the water. Based on repeated bar checks the accuracy of the bathymetric measurements is estimated to be +1 foot.

Positions were determined with a Motorola Mini Ranger I, electronic positioning system. Shore stations used, with one exception, were those surveyed in previous operations at the site. One new location was established (entitled "Ladder") for this survey, and coordinates were determined by Consolidated Edison surveyors. The shore reference stations are indicated on Plate D6-1.

A field measurement, of a calculated baseline, was made on the first survey day to check instrument calibration. Position accuracy for the survey is estimated at +10 feet. Position "fixes" were measured and recorded at an average spacing of 250 feet along each survey line.

---

(1) Bar check is a procedure where by a bar is suspended at a known depth beneath the fathometer transducer. The known depth is then compared to the depth recorded on the fathometer strip chart.

Water-level control was provided by a Weather Measure Corporation water-level recorder. This instrument is located on Consolidated Edison's docks and is maintained by personnel of Texas Instruments Incorporated. The gauge was leveled to Mean Standard Sea Level (MSSL) at Sandy Hook, and all records are relative to that datum. Two daily measurements of water level, to that datum, were also made to provide calibration and a check on the continuous recording gauge.

Data reduction consisted of:

- 1) Reduction of all field-recorded range-range positions to the local coordinate system and plotting to appropriate scale. A computer data reduction and plotting routine was used.
- 2) Correction of recorded bathymetric data to the MSSL datum, using the recorded water levels. This was done manually, at approximately 1/2-hour intervals.
- 3) Picking, plotting and contouring of corrected bathymetric data on the final position plot sheet was done manually. Water depths were plotted at each position-fix point and at locations of significant bathymetric variations (i.e. slope break points, channel axis, anomolous bottom relief, etc.).

The final bathymetric values developed through the above procedures are estimated to have a horizontal accuracy of +10 feet and a vertical accuracy of +1.5 feet.

Plate D6-1 presents a bathymetric contour map of the entire survey area. The depths shown on Plate D6-1 represent a small portion of the total data base from which the bathymetric contours were drawn.

A high resolution seismic reflection survey of the river bottom was attempted concurrently with the above bathymetric survey, but was terminated, after a trial run, because the analog record of this trial run indicated a lack of penetration. It is believed that the lack of penetration is the consequence of the high organic content of the river sediments. It was later determined that a resurvey, using a different energy source and/or electronic recording parameters, had only a marginal likelihood of providing useable results. Because of this and the logic presented in Section D6.3.3 it was decided not to attempt additional seismic profiling.

### D6.3 RESULTS

#### D6.3.1 General Bathymetry

The bathymetry across the survey area (Plate D6-1) appears to conform to the shape and character of an upper-estuarine river valley. Water depths along the thalweg<sup>(1)</sup> range from 50 to 92 feet. The thalweg of the river is only slightly more sinuous than the overall shape of the river through the area. The greatest depths occur in two closed depressions along the thalweg; at 88 and 92 feet, in the northern half of the area.

---

<sup>(1)</sup> The line joining the deepest points of a channel.

Two large shoals are present within the survey area. One is in the northeast corner of the area at Peekskill Bay, with an average water depth of 6 feet across the shoal. The second is on the west side of the river, south of Jones Point. Water depths generally range from 23 to 30 feet across the Jones Point Shoal.

Relatively steep slopes are evident at several locations along both sides of the river. The steepest slope is at the northern extreme of Jones Point, where rocky bluffs above the river dip steeply to water depths of 50 to 70 feet. Gradients could not be calculated precisely, but they appear to exceed 45°.

A narrow steep slope is present on the west-side of the river, from approximately 1/2 mile north to 1/2 mile south of the reference station "Lovett" (Plate D6-1). Maximum slope observed on this feature is approximately 20°.

On the eastern side of the river, steep slopes are present at two locations: at the point immediately south of the Georgia-Pacific loading docks, and at an area immediately north of the Indian Point Generating Station. At these locations, the river bottom drops steeply off into water depths of 40 to 45 feet with slopes of up to approximately 25°.

South of Jones Point, a narrow shelf is present along most of the western side of the river. This shelf ranges in width from approximately 100 to 500 feet, and is generally contained by the shoreline and the 10 foot bathymetric contour. In

the southern portion, several large boulders are present on this shelf and extend above the water surface.

Minor channels can be defined at several locations along, and roughly parallel to, the western side of the river. Several of the channels appear to be associated with the relatively steep bottom slopes. The most continuous channel lies along the base of the steep slope near "Lovett", and dips gently to the south (downstream) from the Jones Point Shoal. Minor and discontinuous channels appear to, also, lie along or near, and parallel to, the upper portion of this slope. Minor north-dipping channels are also present on the northern portion of the Jones Point Shoal.

#### D6.3.2 Cultural Effects

Three types of cultural or "man-made" operations appear to have affected the bathymetry. These are:

- a) a pipeline crossing;
- b) navigation and construction dredging; and
- c) vessel propeller tracks.

A gas pipeline extends across the river immediately south of the Indian Point Generating Station. The dredging and backfilling associated with the placement of this pipeline has resulted in a curving 200 to 500-foot wide zone of very irregular water depths. These irregular depths are most distinctive in the deeper portions of the river, and less apparent at the more shallow ends.

The uniform 45-foot water depth along the front of the Georgia-Pacific loading docks suggests previous dredging for vessel navigation purposes.

Likewise, the irregular, but deep water (averaging about 30 feet) along the front of the Indian Point Generating Station suggests dredging and/or bottom disturbance during plant construction.

A minimum draft 7-foot navigation channel has been dredged around the perimeter of Peekskill Bay.

In water depths of 35 feet or less, particularly at the river bend around Jones Point, discontinuous shallow troughs are common in the river bottom. These are evident on the bathymetric record as isolated 2 to 3-foot deep depressions or pot-holes, and may represent propeller tracks of vessels wandering beyond the deeper water channels, or localized minor current scouring.

#### D6.3.3 Conclusions

Repeated bathymetric measurements across the previously suspected "anomalous zone" do not reveal evidence of N35°E trending bathymetric irregularities. The linear trends of bathymetric relief which are visible, such as the steeper slopes along the margins of the river, generally cross-cut at a small angle rather than parallel regional geologic structural trends.

The principal feature<sup>(1)</sup> of the previously suspected anomolous trend is a portion of the pipeline corridor. The

---

<sup>(1)</sup> In the initial survey, it was this single feature that generated a level of concern from which speculation on a NE trending alignment of anomolous features was initiated.

limited number of reconnaissance tracklines run during the previous survey (Dames & Moore, 1975) was insufficient to identify the "anomaly" as a "crossing" over a construction area. During the previous survey (Dames & Moore, 1975), four lines crossed the pipeline. Two crossings (fixes 1445 to 1446 and 1604 to 1606), happen to intersect directly over the zone in mid-river, thus not identifying the pipeline as a linear feature. The other two crossings occurred close to shore in shallow waters where the pipeline construction irregularities are not as distinct.

The other anomalous features, previously reported as part of the N35°E trend, were not distinguished as unique features during this survey. Numerous small bottom irregularities are evident in the records. These occur at a number of locations in the study area, and, as far as can be presently discerned, can be interpreted as natural features.

The anomaly previously identified at Lent's Cove was not detected during this survey. It is known from diver reconnaissance that the river bottom in the Lent's Cove area is composed of loose muddy sediments. Tree stumps and other debris were also detected by divers during an earlier investigation. Therefore due to currents and the nature of the river bottom it is unlikely that the feature initially detected as an apparent 3 to 4 foot offset could have persisted and accordingly must have been newly formed at or near the time of the original survey. Since this feature is either of small linear extent, or

is so transient that it could not be detected in the second survey, it is illogical to ascribe any tectonic significance to it. Furthermore a fault offset of this magnitude (3 to 4 feet) would have produced noticeable effects on land, both geologic and seismic, and none have been detected or recorded (Appendix A, Appendix G). It is therefore concluded that the 3 to 4 foot offset recorded near Lent's Cove was transient in nature, lacked continuity and probably resulted from current action undercutting bottom debris.

## D7.0 SEISMIC REFLECTION PROFILING

### D7.1 INTRODUCTION

A seismic reflection survey, consisting of approximately 25 line miles of shallow "high resolution" profiling, was conducted in Rockland County, New York and Bergen County, New Jersey. Target Survey, Incorporated, of Houston, Texas, performed the field work under contract to Dames & Moore and under the direct supervision of Dames & Moore geophysicists. Processing of field data and the production of final seismic sections was accomplished by Seismograph Services Corporation of Houston, Texas under the guidance of Dames & Moore geophysicists. The interpretation of the seismic profiles was performed by Dames & Moore geophysicists and geologists.

### D7.2 FIELD EQUIPMENT AND PROCEDURES

Target Survey, Inc., of Houston, Texas, provided all equipment and personnel needed to accomplish the field phase of the program. The following is the list of equipment used:

- a) One GMC Suburban 4-wheel drive vehicle.
- b) Two Varipulse land high-resolution seismic non-explosive energy sources.
- c) One S.I.E. RA-49R 12 channel amplifier system.
- d) One S.I.E. RM-49S 12 channel stacker with dual RAM cards.
- e) One S.I.E. R-6AB recording oscillograph with 26 each 7s galvanometers.

- f) One S.I.E. RU-49R digital tape deck and power supply.
- g) A total of 36 strings of Walker-Hall-Sears geophones, in groups of 6 geophones per string.
- h) Six land recording cables with four geophone take-out positions per cable.
- i) One Varipulse trigger and firing system.

The amplifying and recording components were housed in the GMC Suburban 4-wheel drive vehicle and the energy source was mounted on its front bumper. Field equipment, geophone spread arrangement, signal recording and general field procedures are diagrammatically illustrated on Plate D7-1.

Ground motion from reflected seismic waves was recorded on 12 channels connected to 12 groups of geophones that are spread out along the line of survey. With this arrangement, each shot yields information on the configuration of a subsurface reflecting interface at twelve positions distributed along the line.

Six land recording cables, each with four take-out positions for recording seismic signals, were laid out along the line of survey. These cables were linked together by connectors. At each take-out position a string of 6 geophones, spaced approximately 10 feet apart, was laid-out parallel to the line of survey. Adjacent take-out positions were spaced 70 feet apart and the geophones of successive strings did not overlap (Plate D7-1).

The use of multiple geophones per geophone position tends to improve the signal to noise ratio and helps cancel the low-velocity, low-frequency surface waves (ground roll). Surface waves, with an amplitude level that is high compared to subsurface reflections, tend to override useful reflection information. On the first day of field operation, the records from noise spread shots were analyzed. On the basis of this analysis, the groups of parallel-series-connected geophones were laid-out with spacings (approximately 10 feet between geophones) that were compatible with the wavelengths of the ground roll. Such an arrangement resulted in the suppression of horizontally traveling ground roll and enhancement of vertically traveling reflections.

A non-explosive seismic energy source was used to eliminate the problem of obtaining permission to use explosives, and also to eliminate the need to drill shot holes. The non-explosive energy source used is called the Varipulse. The Varipulse consists of a chamber into which is metered precise amounts of propane and oxygen. The resultant mixture is fired by a spark plug. The Varipulse unit is mounted on the front bumper of the recording truck and is coupled to the ground by hydraulic rams.

The common-depth-point shooting technique (C.D.P.) was used in the field to cancel out-of-phase signal (Dobrin, 1976). A six hundred percent subsurface coverage was used after analyzing the records from the noise spreads shot on the first day of

field operation. By shooting at each geophone take-out position and using a 12 channel recording system, reflections from the same subsurface reflecting point are obtained six times. When the reflection data is computer processed and the six common reflections are stacked together, a 600% C.D.P. overlap is obtained. This stacking of corrected traces recording the same reflection enhances in-phase reflected arrivals and attenuates the out-of-phase noise.

A unique property of the recording system used is its ability to stack or add together multiple shots before the data is recorded on magnetic tape. Any number of shots can be added together and a playback from memory can be obtained for quality control. It is possible, therefore, to cancel noise and enhance real events, thereby improving the signal to noise ratio. This feature makes it possible to work in areas where high seismic noise is prevalent, such as along highways and through urban areas.

With the exception of a portion of Line 1, Part 1, a 0.0005 second (0.5 millisecond) sample rate was used. This means that in converting the analog signal to digital language, the signal is sampled at 0.5 millisecond intervals. This short sample rate is necessary when recording high seismic frequencies. In high resolution recording, the higher the frequency recorded, the greater the near surface resolution achieved. A total record length of 680 milliseconds is possible when recording at 0.5 millisecond sample rate using the S.I.E. RM-49S

recording system. If a greater depth of investigation is desired, a one millisecond sample rate must be used as was done on Line 1, Part 1.

The land survey was conducted by Target Survey, Inc. Geophone locations were established using a Rol-a-Tape measuring wheel and elevations were obtained using a transit and stadia rod. Both horizontal and vertical accuracy is within  $\pm$  one foot.

### D7.3 RECORD QUALITY CONTROL AND PROCESSING

#### D7.3.1 Record Quality

The quality of the data obtained as seen on the monitor records, is considered to be good for high resolution reflection recording in the environment (such as the type of terrain and cultural noise) in which the recording was accomplished. However, as a rule, monitor records taken in the field do not show clear reflections. This is due to the effects of topography and the zone of seismic weathering on high frequency shallow reflections, particularly when the energy source is located at the surface of the ground. Seismic weathering is usually different from "geologic weathering" and refers to the near surface low velocity layer (see Sheriff, 1973). In addition, shallow reflections will also be affected, to a greater extent, by normal move-out (apparent curving of uncorrected reflections) than are deeper events. This is because the effect of normal move-out decreases with increasing time as measured from shot time (time zero). The effect of normal move-out has

been minimized by maintaining a short spread length of geophones in the field.

Two monitor records were taken in the field. First, a "read after write" record was taken at each shot point. This record is taken after the data is recorded on the magnetic tape and shows exactly what is on the tape. Thus, it is important in quality control. It should be noted that the real time between timing lines on the "read after write" playbacks is two and one half milliseconds.

Because of the expanded nature of the "read and write" playbacks, a second playback was taken from the memory of the RAM stacker. This playback was not expanded and shows the real time of recorded events. This form of playback was normally taken at every fourth shot point.

The playback from the memory of the RAM stacker was used to assess the effectiveness of the RAM stacker in improving the signal to noise ratio on records in high seismic noise areas, and were examined to see if legitimate reflections could be recognized. This record was very important in the attempt to maximize the data obtained from the field recording.

#### D7.3.2 Tape Transcription and Data Processing

The data obtained in the field were recorded on one quarter inch, four-track tape. However, since seismic data processing centers use one half inch, nine-track tape, it was necessary to transcribe the data to a tape compatible with the computers. This was accomplished by S.I.E., Houston, Texas (the

manufacturers of the recording instruments). The transcribed one half inch tape was delivered to Seismograph Service, Corp. (SSC) Houston, Texas, for processing.

In processing, the digitized data on the magnetic tapes were corrected for static effect (seismic weathering and elevation corrections) and normal moveout. Initially, a trial run (brute stack) was made to see the general quality of the data. A more sophisticated static program (C-Stat) was then run to improve the stack. At this point, the reflected events became clearer and a final program was run to improve the signal to noise ratio (Spacon) and the final seismic sections were produced.

A detailed list of the processing needed to produce the final record sections follows:

- a) Demultiplex - change the tape digital language to a language compatible with the computers used.
- b) Sort and Datum Statics - sort works out the spread geometry (the shot point interval, geophone spacing, spread directions, etc.). Datum statics corrects the elevation differences along the line-of-survey to the chosen datum elevation (in this case, 20 feet below actual ground surface).
- c) Filter - at this point in the processing, the following filters were applied to the data: Line 1, 90 hertz low cut, 240 htz high cut and a 180 htz notch filter. All other lines used a 60 htz

low cut, a 240 htz high cut and a 120 htz notch filter.

- d) Velocity Analysis - a range of velocities, in this case 6000 feet to 10,000 feet per second was chosen. The computer then assigned incremental velocities to the data (at 50 feet per second intervals) within the chosen range. The results of this analysis were judged by the ability of the data to stack and generate meaningful reflections. The velocities that improve the stack the most were run through Step C). This is strictly a statistical process.
- e) Normal Moveout - normal moveout is defined by Sheriff (1973) as, "the variation of reflection arrival time because of the variation in the shot point-to-geophone distance". Normal moveout is primarily a function of velocity. The velocities arrived at in Step (d) were applied to the data and the normal move-out correction was computed.
- f) Brute Stack - after all of the above corrections are accomplished the data were stacked and rough preliminary sections were produced. At this point, the decision was made as to what additional processing was needed.
- g) CSTAT - the CSTAT is a sophisticated static program. CSTAT enhances sections by applying static

refinements to all the traces of a CDP. Each trace is statically corrected to align with a pilot trace. The pilot trace is a tapered mix of the stacked CDP data, centered on the CDP being processed.

Having generated a pilot trace, the data were cross-correlated with it over a specified window in which the desired event was known to exist. Great care must be exercised in applying this program so that too heavy a mix, in generating the pilot trace, is not used and that the search window is not too large. It is possible to distort and even create data by improperly applying this program.

- h) SPACON - SPACON suppresses random noise and/or filters out unwanted events separable on a step-out basis (velocity filters). The basic mode of this program is spatial deconvolution. It is designed to strongly discriminate against random noise and improve the signal to noise ratio. Care again must be exercised in applying this program. It is possible to distort events and the final SPACON section should be compared with the CSTAT section to be sure this has not happened before the interpretation is finalized.

- i) Time sections were lastly converted to depth sections by applying an 8000 foot per second velocity to the data. Since there are no direct velocity measurements (borehole velocity survey or sonic logs), the depth sections provides approximate estimates only.

#### D7.4 DISCUSSION OF RESULTS

##### D7.4.1 General

The reflection profiles which are located on Plates 2A and B and are presented on Plates D7-13 through D7-20 are depth sections. The selected velocity used in generating these profiles was 8,000 feet per second. This is the velocity from which the best stacking of the data was obtained. The choice of prominent reflectors was based on the subhorizontal line-up of similar peaks (positive) and troughs (negative) deflections of the sine wave on the record section. Similarity was established on the basis of the estimated amplitude and wave length of the signal.

Short, near-surface refraction lines were run over outcrops of Precambrian gneiss and Triassic sediments. The resulting velocities were nearly the same (to within 1000 feet per second). Reflections from an interface between the two rock types would be expected to be poorly defined on the record. Therefore, an estimate of the accuracy of the depths to the reflecting interface on the depth sections Plates D7-13 through D7-20 is very difficult to determine. There is no velocity in-

formation except the above-mentioned refraction lines and the velocities determined in the data processing.

Because of their expanded vertical scale, the time sections were used in many cases to identify reflections and trace their continuity. The interpretation was then transferred onto the appropriate depth section. Every second trace on the depth section represents a shot point. Shot point numbers are indicated above the topographic profiles and shot point locations are shown on Plates D7-2 through D7-12. The file numbers of data on the magnetic tapes are marked below the seismic profiles.

#### D7.4.2 Line 1

Line 1 runs along the Palisades Parkway from a point 2870 feet south of the Route 45 overpass to a point 8760 feet north of the Tiorati Brook Road intersection (Plates D7-2 to D7-6). This line was shot in two parts: Part 1, approximately 2.2 miles long, was sampled every one millisecond over a 1360 millisecond sample interval; Part 2, approximately 7.8 miles long was sampled every one-half millisecond over a 680 millisecond sample interval. Part 1 extends from shot point 0 to 166, while Part 2 extends from shot point 150 to 585, giving an 1,120-foot overlap in coverage. Part 1 was sampled at one millisecond to obtain deeper penetration into the Triassic-Jurassic rocks of the Newark Basin; Part 2 was sampled at one-half millisecond to achieve greater resolution at shallower depth, since this portion of the line was underlain by Precambrian metamorphic rocks.

Several distinct and gently curving reflectors can be traced continuously between shot points 0 to 63. These reflectors, which are defined by waves of higher amplitude and longer wavelength than the discontinuous reflectors within the interpreted diabase dikes, can be easily recognized to a depth of 1250 feet (Plate D7-13). The reflectors are discontinuous between shot points 63 and 80, but the reflectors between the two interpreted dikes (shot points 65 to 69) have the same character as those between shot points 0 to 60. Between shot points 99 and 109 the seismic line crosses exposed Palisades diabase. The exposed diabase contains subhorizontal joints. The signature of diabase on the reflection profile is made up of poorly defined discontinuous reflectors that are defined by waves of lower amplitude and shorter wavelength than those on either side of the body. The signature of the reflectors within the diabase body appears to be similar to that within the interpreted diabase dikes between shot points 63 to 80. The Palisades diabase cuts through the reflectors on either side of the body and can be extrapolated easily to a depth in excess of 1,000 ft. The Palisades diabase is interpreted to be a dike (not a sill) between shot points 99 to 109 (Plate D7-13, see also Appendix B). On the basis of similarity in the reflection pattern, two smaller diabase dikes were interpreted between shot points 63 to 66 and shot points 69 to 74. The reflectors are clearly truncated at shot point 79, which is interpreted as the position of a

subvertical fault extending at least to a depth of 1250 ft. Some of the reflectors are also displaced across shot point 79. This fault has two splays, one of which (the northern splay) does not reach the surface (Plate D7-13).

Between shot points 118 and 143 truncated and discontinuous reflectors indicate the presence of a wide fault zone; here interpreted as the Thiells Fault because of its close proximity to the mapped field location (Plate 1 and Plates D7-3 and D7-13). The fault traces that are shown on Plate D7-13 delineate the interpreted maximum width of the fault zones. This procedure was followed in interpreting all other seismic profiles (Plates D7-14 to D7-20). North of the Palisades diabase dike and south of the Thiells Fault, a faint, gently dipping (to the south) boundary may be interpreted as the Trio-Jurassic-Paleozoic contact. North of the Thiells Fault, a suggested south dipping boundary may also be interpreted as the Trio-Jurassic-Paleozoic (or Precambrian) contact (Plates D7-13 and 14).

The subvertical fault zone between shot points 169 to 202 is consistent with the presence of the Letchworth Fault at this location, as interpreted from geological mapping. The character of the reflectors north of the fault zone and within it suggests that the fault affected Precambrian gneiss (Plate 1 and Plate D7-14). The presence of flat or gently dipping prominent reflectors in the Precambrian metamorphic rocks is coincident with the observed gently dipping lithologic layering

that is very well developed along the survey line (see Plate 1-A). In addition, the reflectors may have also been enhanced by the gently dipping jointing that is parallel to that layering. It may also be interpreted that the same character of Precambrian reflectors extends further south, to the lower side of the interpreted lithological contact north of the Thiells Fault. In this case, both the Trio-Jurassic rocks and the Paleozoic metasediments will be above that contact (Plate D7-13). The Thiells Fault separates Precambrian gneisses from Paleozoic metasediments between Thiells and Tomkins Cove (Plate 1). It may be that along strike, to the southwest, the Paleozoic section is greatly reduced.

Except for a short loss of signal between shot points 238 to 244, two fault zones were identified along the remainder of Line 1, Part 2. The fault zone between shot points 279 to 300 corresponds to the Willow Grove Fault, while that between shot points 414 to 441 corresponds to the Cedar Flats Fault (Plate 1 and Plate D7-14).

Signal penetration between shot points 0 to 99 indicates that the Trio-Jurassic basin is at least 1250 feet deep south of the Palisades diabase. North of the diabase dike, between shot points 99 to 109, the Trio-Jurassic basin appears to shallow quite rapidly (Plate D7-13). This rapid thinning of sediments within the basin, north of the diabase dike, suggest that the diabase contacts are faulted (see also Appendix B).

#### D7.4.3 Line 2

Line 2 is located in Bergen County, New Jersey, near the town of West Mahwah. This line was shot in three parts and the signal was sampled every one-half millisecond. Line 2, approximately 1.3 miles long, starts on Stag Hill Road, runs southeast across the Ramapo River and extends towards Route 202. Line 2A, approximately 0.3 miles long trends northeast-southwest along Route 202 and serves as a tie line between Lines 2 and 2B. Line 2B, approximately 0.4 miles long, runs east-west from Route 202 to a point just west of Route 17 (Plates D7-2 and 12).

Line 2 crosses the Ramapo Fault approximately at a right angle. The fault can be easily identified as a zone of short discontinuous and unmatched reflectors between shot points 72 to 99 (Plate D7-15). The amplitude and wavelength of the signal that characterizes the reflectors between shot points 0 to 27 is similar to that between shot points 72 to 99, suggesting that the subvertical fault zone affects Precambrian gneiss. The reflectors between shot points 0 to 72 are more continuous and can be seen to overlap without displacement at different depths (Plate D7-15). The change in character, lower amplitude and longer wave length, of the near surface reflections, down to a depth of 200 feet, over the fault zone may represent the signature of the Pleistocene deposits within the Ramapo River Valley (Plate D7-15).

There is no clear indication of a lithologic change from Precambrian gneiss to Tertiary-Jurassic sedimentary rock on

record sections 2A and 2B (Plates D7-16 and 17). However, these lines suggest the reflection of higher frequencies and the presence of somewhat thinner layering at depth. It is possible that this change in character of the reflections may indicate a change in lithology. Although the northwestern boundary of the fault zone can be easily located at shot point 72 (Plate D7-15), the southeastern boundary is not clearly identifiable on the records.

#### D7.4.4 Line 3

Line 3 is approximately 2.9 miles long and runs generally east-west along State Route 210 (Plates D7-2, D7-5 and D7-7). This line starts over Precambrian gneiss and ends over Trio-Jurassic sedimentary rock, connecting Lines 1 and 4. Because of the topographic drop along Highway 9W, as it crosses Cedar Pond Brook, Line 3 was terminated just west of its intersection with Line 4, and Line 4 was deflected around a short segment of Highway 9W (Plate D7-7). The seismic signal along this line was sampled every one-half millisecond.

A subvertical fault zone was identified between shot points 5 to 18 (Plate D7-18). The western limit of the fault zone was identified by the alignment of the termination of reflectors at the depth of 200 and 500 feet. The eastern limit was identified by the displacement of the reflector at the 175 foot depth and the abrupt termination of the prominent reflector at the 300 foot depth. This fault zone corresponds to the mapped Cedar Flats Fault (Plate 1). Between shot points 26 to

55, there is a significant down-warping of the reflections above a depth of 300 feet. Below 300 feet, the warping is still evident but much less pronounced, which may be the result of the reflectors being discontinuous and some signal resolution being lost immediately below a high power transmission line (between shot points 45 to 49). While the reflections are definitely disturbed within the western portion of the zone, they gradually regain their definition and continuity toward the eastern portion of the zone. This graben-like feature, with moderately dipping sides, is along the northeastern-strike extension of the Willow Grove Fault, or may also represent an eastern extension of the Ambreys Pond Fault. The section, between shot points 5 to 55, probably represents a crossing over several members of the Ramapo Fault System (Plate 1 and Plate D7-18; see also Appendix A).

A change in the character of the reflections, between shot points 101 to 128, represents the outline of a funnel-shaped intrusion that extends to a depth below effective energy penetration. At a depth of 500 feet, a dike-like feeder can be identified between shot points 110 to 113 (Plate D7-18). It is interpreted that this feature is a portion of the Rosetown Pluton, which is exposed at this location in the field, and extends on either side of the survey line (Plate D7-5 and Plates 1, 2 and A-5). The weak layering that can be picked-up within the pluton may reflect a cryptic igneous layering within this intrusive body.

At about shot point 130, an interruption in the pattern of reflections is interpreted to represent the eastern edge of the Thiells Fault. The main Thiells Fault appears to extend between shot points 137 to 153. None of the prominent reflectors on either side of this interval can be carried clearly across it. Within this interval, the reflections are completely disturbed (Plate D7-18). Between shot points 153 to 216 an identifiable, irregular faint reflector can be picked-up continuously between a depth of 700 feet (at shot point 153) to a depth of 1,000 feet (at shot point 216). This reflector abuts against the eastern margin of the Thiells Fault (Plate D7-18) and may represent the top of "basement" below the Trio-Jurassic sedimentary rock. Below this faint reflector the signal appears to be too noisy to extract any meaningful interpretation.

#### D7.4.5 Line 4

Line 4 is approximately 5.2 miles long and trends generally north-south. The line circles Tomkins Lake and then runs south on Buckberg Road to Highway 9W. It continues south on Highway 9W to shot point 387, or for approximately 12,390 feet (Plates D7-2 and D7-7, 8 and 9). The seismic signal along this line was sampled every one-half millisecond.

Since Line 4 was laid out to circle Tomkins Lake, shot points 0 and 83 are common. This was done because it was believed that the trace of the Mott Farm Road Fault (see Appendix A) passes under the lake. The seismic section seems to confirm this. The reflections between shot points 0 to 83 appear to

terminate abruptly against and are displaced across a series of subvertical fault traces. However, since the line is over Precambrian gneiss, care must be taken in assuming that the apparent offset of events represent total displacement across faults.

The change in the character of the reflections between shot points 200 and 227 is interpreted to be the result of faulting. The lack of reflector continuity across this section coincides with the mapped position of the Thiells Fault (Plate D7-19 and Plates 1 and 2). A change in lithology is also interpreted to occur across the Thiells Fault. On the north side Precambrian gneiss is exposed, whereas Trio-Jurassic sedimentary rocks are exposed to the south along the survey line. Several minor faults were identified south of the Thiells Fault and one to the north (Plate D7-19). Between shot points 227 and 387 an irregular faint reflector can be picked-up at a depth of 750 feet. This reflector abuts against the southeastern side of the Thiells Fault (Plate D7-19) and may represent the top of "basement" below the Trio-Jurassic sedimentary rocks. Below this faint reflector the signal appears to be too noisy to extract any meaningful interpretation.

#### D7.4.6 Line 5

Line 5 is approximately 4.2 miles long and was run along the Penn Central Railroad right-of-way from a point approximately 1750 feet south of the railroad tunnel near Long Clove, north to Gurnee Avenue, in Haverstraw, New York (Plates D7-2 and D7-9, 10 and 11). The seismic signal along this line was sampled every one-half millisecond.

The railroad tunnel lies between shot points 25 and 49. The blank spot on the section between these shot points indicates that there was no useable data here. It is known from surface geological investigations that there is a suspected fault at the north portal and a known fault at the south portal of the tunnel (South Portal Fault, Appendix B). Also, diabase is exposed both north and south of the portal, as well as within the tunnel. Unfortunately, neither the faults nor the diabase show-up clearly on the record. A possible interpretation is presented on the record showing the diabase downdropped to the south along the trace of the South Portal Fault at shot point 24 (Plate D7-20).

On the north side of the railroad tunnel the line of survey crosses the suspected position of the Long Clove Fault (Appendix B). The seismic record supports the presence of a fault and extends the zone of faulting between shot points 56 to 71. A small displacement of the reflector at 200 feet and the abrupt termination of the prominent reflector at 950 feet mark the position of the fault trace at shot point 56 (Plate D7-20). A minor fault was identified at shot point 91 and a small fault zone recognized between shot points 285 to 293 (Plate D7-20).

The irregular "basement" reflector that was recognized on Line 4 can be picked-up at the same depth and followed on Line 5. This reflector, which is interpreted to represent the base of sedimentary rocks on Line 5 is shown on Plate D7-20.

Between shot points 175 to 257 a channel-like depression in this "basement" reflector can be easily identified. However, since the section has not been corrected for apparent dips of reflectors, it would be difficult to estimate the actual differential relief of this channel. Below this reflector, the signal appears to be too noisy to extract any meaningful interpretation.

#### D7.5 CONCLUSIONS

Areas of faulting, as interpreted from the seismic profiles are shown on Plate 1. Most of these faults are members of the Ramapo Fault System. The most important fault zones are: The Thiells Fault identified on Line 1, Part 1; the Letchworth Fault, the Willow Grove Fault and the Cedar Flats Fault identified on Line 1, Part 2; the Ramapo Fault identified on Line 2; the Cedar Flats Fault, the Thiells Fault identified on Line 3; the Mott Farm Road Fault, the Thiells Fault identified on Line 4 and the South Portal Fault and the Long Clove Fault identified on Line 5.

In general, lithologic boundaries were not clearly indicated on the seismic profiles. The identification of the diabase dikes on Line 1 and the portion of the Rosetown Pluton, on Line 3, was facilitated by the outcrops that were noted along the line of survey. The identification of the lithologic contacts on Line 1, Part 1 and Line 1, Part 2 were based on interpreted transitions in the character of the reflections. The irregular "basement" reflector recognized along Line 3, 4 and 5 is also interpreted as the base of the Trio-Jurassic sediments

at the northern end of the Newark Basin. The Basin is at least 750 to 1,000 feet deep on the southeast side of the Thiells Fault and along the west shore of the Hudson River in the vicinity of Haverstraw, New York.

APPENDIX E

GEOCHEMISTRY AND AGE DATING

## APPENDIX E

### GEOCHEMISTRY AND AGE DATING

#### E1.0 INTRODUCTION

The purpose of this investigation was to 1) evaluate the nature of fault and fracture filling materials in the region and immediate vicinity of the Indian Point Generating Station, and 2) through the use of appropriate geochemical techniques, to determine the minimum age of last movement along faults within the Ramapo Fault System. This investigation increased the data base in the immediate vicinity of the site and extended the regional sampling effort to better define the extent of the proposed hydrothermal event (Dames & Moore, 1975, Appendix K).

The largest body of data contained herein is related to fluid inclusion studies, primarily on calcite, performed by Dr. H.L. Barnes (Attachment E-1A&B). This is the result of the widespread distribution of calcite mineralization within the study area, and the limited occurrence of other usable vein filling minerals.

Where possible, radiometric (K-Ar) age determinations have been made in an attempt to assign an "absolute minimum age" to the most recent movements. This information is particularly useful when evaluated in light of the regional paragenesis and co-genetic mineral assemblages discussed in Appendix B. Additionally, K-Ar age determinations were performed on selected igneous and metamorphic whole-rocks and/or mineral separates for the specific purpose of determining time markers and assessing the nature of the thermal history of the study area.

Fluid inclusion sample preparation procedures, fluid inclusion calibration procedures, fluid inclusion examination procedures and the fundamentals of fluid inclusion analysis have previously been discussed in Appendix K of Dames & Moore (1975).

## E2.0 PRESENTATION OF DATA

For each sample studied for fluid inclusions, the sample number, sample location, petrographic description, structural significance and fluid inclusion analysis are presented in Table E-1, Fluid Inclusion-Data. This table also contains appropriate references to plates.

For each sample submitted for potassium-argon analysis, the sample number, sample location, petrographic description, structural significance and results of the K-Ar analysis are presented in Table E-2, Potassium-Argon Data. This table also contains appropriate references to plates.

### E3.0 DISCUSSION OF FLUID INCLUSION DATA

Plate E-1 shows a histogram of the Frequency of Occurrences vs. Homogenization Temperature for individual fluid inclusion observations. The total number of observations or homogenization measures performed was 297, of which 200 were measurements done on primary or pseudosecondary fluid inclusions and 97 measures were done on secondary or late stage fluid inclusions. The total number of samples studied was 44, of which 13 were obtained from Mesozoic host rock and 31 were obtained from Paleozoic host rock.

In Plate E-1, 18 measurements are classified as having homogenization temperatures equal to or greater than 270°C and less than 360°C. Of the 18 measurements, 6 were estimated or interpreted to have formed at "high temperatures" and were assigned a temperature of 300°C. In other words, 6% of all the measurements indicated that the homogenization temperature lies between 270° and 360°C of these, one third were not actually measured, but were interpreted to be high temperature. This is the only temperature grouping for which a significant portion of the group (one third of the group, or 2% of the total data base) is inferred, and not obtained by actual physical measurements.

Similarly, in Plate E-1, 19 measurements (or approximately 6% of the total data) were classified as having homogenization temperatures equal to or greater than 220°C and less than 270°C. Of these 19 measurements, 9 (or approximately one half) were derived from one sample. It should therefore be noted that

the combination of the above two groups (220°C to 360°C) represents 37 measurements or approximately 12% of the total number of fluid inclusion measurements performed. Of this 220° to 360°C group, 15 measurements (approximately 40% of the data set or 5% of the total data base) are either inferred or representative of a single sample. It is obvious that the statistical basis for this temperature range is weak and although some discussions on this group will be presented, the major portion of this text is directed toward the remaining distribution shown on Plate E-1, which includes approximately 90% of the data and is representative of homogenization temperatures that are lower than 220°C. For this temperature interval, the samples studied were obtained from one of two broad classifications:

- 1) Host Rock - Mesozoic (Plate E-3)
- 2) Host Rock - Paleozoic (Plate E-2)

The paragenesis of the vein filling materials is discussed in Appendix B and summarized in Table E-3 (taken from Schaller, 1932).

For samples obtained from Mesozoic host rock, Plate E-3 shows a plot of homogenization temperature versus the fault or fracture orientation from which the individual sample was taken. Plate E-3 illustrates the absence of a preferred orientation, from which it is concluded that the mineralization associated with the basic igneous activity of the Palisades and/or Watchung events occurred randomly, along existing faults and fractures that served to facilitate the transport of magmatic and/or hydrothermal solutions.

Plate E-3 shows that there are six samples that contain minerals whose average fluid inclusion filling temperature is 200°C or greater, and that from these six samples 16 measurements of the fluid inclusion homogenization temperatures were made. All of these temperature determinations except one (MW 103-2) were performed on quartz crystals. This observation is consistent with the interpretation that quartz mineralization resulted from late stage magmatic or early stage high temperature hydrothermal fluids and preceeded, at least in time, the major phase of hydrothermal mineralization as shown on Plate E-1 and Table E-3. The remaining temperature distribution shown on Plate E-3 was obtained from crystals, primarily calcite, that are petrologically associated with the formation of zeolites (i.e. Periods 4, 5 and 6 of Table E-3) by the action of hydrothermal solutions.

Plate E-2 gives a presentation of data identical to that in Plate E-3 except that the vein filling minerals studied were obtained from Paleozoic host rocks in the immediate vicinity of the site. This plot, like Plate E-3, illustrates that the occurrence of vein filling mineralization is random and not concentrated along a preferred orientation. The conclusion that, in both the Mesozoic and Paleozoic rocks, there is no preferred concentration or noticeable absence of vein filling mineralization along any of the observed fault or fracture orientations, is compatible with the conclusion reached in Appendix B, that the observed mineral assemblages are genetically related and

that their development was syn and/or post the last geologically recorded significant tectonic deformational event.

In Plate E-2 there are 10 samples for which the average fluid inclusion filling temperature is equal to or greater than 200°C. For these ten samples only four represent actual measurements of the homogenization temperature. The temperature for the other six samples is inferred to be "high temperature" probably metamorphic in origin. This inference is made on the basis of the fluid inclusion morphology. This interpretation is not inconsistent with the past history of the Paleozoic rocks. It is reasonable to expect that the thermal effects of the Taconic Orogeny were sufficient to generate "high temperature" calcite vein filling mineralization. This interpretation is strengthened by 14 homogenization measurements on four samples whose average filling temperature is in excess of 200°C. In particular, three of the four samples studied were taken from generally east-west trending faults that are observed to have been annealed.

Therefore, it is concluded that the high temperatures (greater than 200°C), whether measured or inferred, are the result of localized late stage magmatic fluids in the Mesozoic host rocks or regional metamorphic effects associated with the Taconic Orogeny in the Paleozoic host rocks.

Plate E-4 shows a plot of distinctive samples representative of mineral assemblages referenced in Appendix B. In

summary, the assemblages observed in the Mesozoic host rock were interpreted to have a regional paragenesis, consisting of an early assemblage of quartz + calcite + stilbite + chlorite, which was more or less synchronous with the last deforming events, and a later assemblage of analcite + datolite + apophyllite + calcite + stilbite + chlorite which clearly post-dates the last tectonic activity. The two groups have here been termed Stage I and Stage II respectively. In general, Stage I can be equated to Period 3 and early Period 4, and Stage II can be equated to the late portion of Period 4, Period 5, and possibly Period 6 of Table E-3. The diagnostic features of the Stage I assemblage are the existence of quartz and/or the occurrence of deformed minerals, particularly calcite. When samples with these distinctive characteristics are grouped and plotted relative to temperature (Plate E-4, Stage I) it can be seen that high temperature quartz mineralization (i.e. above ~200°C) grades into lower temperature (less than 200°C) Stage I zeolite mineralizations. This later portion of Stage I mineralization is most likely hydrothermal in nature and related to an elevated regional geothermal gradient. Therefore, the distinction of high temperature Stage I assemblages and lower temperature Stage I assemblages is primarily a function of proximity to the magmatic bodies (and their localized high temperature environments), which are superimposed on already elevated regional temperatures (that are themselves adequate to support the circulation of hydrothermal fluids). Because Stage I represents a continuum,

and given only the information in Plate E-4, it is difficult to assign a temperature that is representative of a purely hydrothermal regional condition. If, however, Plates E-4 and E-2 are considered together, the following observations in Plate E-2 become significant:

- 1) Samples taken from Paleozoic host rock in the vicinity of the site are far enough away from most Mesozoic igneous activity so as to minimize the effects of localized high temperatures and, therefore, probably reflect temperatures representative of the actual regional hydrothermal conditions.
- 2) Samples taken from Paleozoic host rock in the vicinity of the site show two distinctive temperature groupings. One from approximately 200°C to 150°C and the other approximately 150°C to 110°C.

These observations agree closely with the data presented in Plate E-4, in that the bulk of the temperatures representative of zeolite mineralization in Stage I are between 200°C and 150°C, and similarly the temperatures representative of Stage II mineralization (Plate E-4) can reasonably be grouped in a 150°C to 110°C temperature range. It is therefore, likely that the maximum temperature that can reasonably be associated with Mesozoic regional hydrothermal activity is approximately 200°C.

In Plate E-4, the diagnostic features of the Stage II assemblage are the occurrence of analcite, datolite or apophyllite and the absence of deformed minerals. When samples with these distinctive minerals are grouped and are plotted relative to temperature, it can be seen that the average filling temperature is distinctively lower than that of the Stage I zeolite phase. As a result of the lower temperature of formation and in view of the generic relationship expressed in Table E-3, it is logical to conclude that the Stage II mineralization post-dates the Stage I mineralization. This supports the petrographic observations presented in Appendix B.

The determination of temperature groupings adds an additional characteristic which can be used to distinguish between syn-, and post-tectonic mineralization. This is particularly useful in the absence of diagnostic Stage I and Stage II minerals.

It should be noted that the mineral assemblages associated with the regional hydrothermal activity generated by the Watchung and Palisades events, are a function primarily of hydrothermal fluids acting on a particular host rock. The hydrothermal minerals should not be thought of as being derived directly from late stage magmatic fluids, and transported throughout the region. Rather, heat is the driving force as it relates to the development of hydrothermal fluids. The hydrothermal fluids then react with the host rock (by alteration and solution) to generate mineralizing solutions from which vein filling minerals are deposited as pressure, temperature and concentration

conditions change. In the Mesozoic host rocks, hydrothermal solution and alteration have resulted in a progressive sequence of mineral assemblages, since the hydrothermal fluids acted directly on the causative heat source. In the Paleozoic limestones, hydrothermal solutions simply reworked existing calcite and deposited it as vein filling hydrothermal calcite. In the Precambrian gneiss, it appears that the reactivity of the hydrothermal solutions was low, since vein filling mineralization is extremely rare in Precambrian host rocks.

#### E4.0 CONCLUSION

Reference to Plate E-4 and Appendix B clearly illustrates that the existence of a single undeformed vein filling mineral does not preclude the possibility of later tectonic activity elsewhere. As illustrated by the Stage I mineral assemblages, the existence of a mixed population of deformed and undeformed minerals should be considered as diagnostic of mineralization predating or synchronous with tectonic activity in general and fault activity specifically. In this particular case, it is believed that the Stage I mineralization was syntectonic, and that the tectonism was synchronous with igneous activity. On the other hand, the existence of a distinctive mineral assemblage for which there is a reasonable sampling density and complete absence of any deformation should be interpreted as representing an event that postdates the last geologically recorded faulting activity. This occurrence is illustrated by the Stage II mineral assemblage which, in the Mesozoic host rocks, is distinguished by the occurrence of analcite, datolite or apophyllite and an average fluid inclusion filling temperature in the 150°C-110°C temperature range. Since the formation of these mineral assemblages is related to the waning stages of igneous activity in the study area, it is likely that the age of the last faulting activity is close to that of the Third Watchung Flow, or approximately 142 $\pm$ 10 m.y. (Section E.5).

## E5.0 DISCUSSION OF POTASSIUM-ARGON (K-Ar) DATA

### E5.1 DIABASE AND BASALT

A sampling of the basic igneous activity associated with the Watchung Mountains clearly shows that the duration of successive events occupied a larger time frame than previously suspected. All three Watchung flows were dated; and individual samples dated within a given flow were obtained from different geographic locations (Plate 2B). A summary of the results is presented below:

<u>WATCHUNG MOUNTAINS</u>				
<u>Event</u>	<u>Ages Determined</u>	<u>Average Age</u>	<u>% K</u>	<u>Avg % K</u>
Flow I	179 + 9	186 ± 15	0.47	0.48
	193 ± 10		0.49	
Flow II	159 + 8	170 ± 10	0.64	0.66
	180 ± 8		0.68	
Flow III	147 + 8	142 ± 10	0.25	0.24
	136 ± 9		0.23	

The above summary shows that each flow has a distinctive potassium content; and that the total duration of the igneous activity was from approximately Late Triassic (190 m.y.) to Late Jurassic (140 m.y.) or approximate 50 million years.

Other Mesozoic dikes dated in this study give ages of 149±7 m.y., 156±7 m.y. and 175±8 m.y. (Table E-2). These ages and the generally accepted age of the Palisades diabase of about 190± m.y. (Dallmeyer, 1975) indicate that igneous activity in the study area commenced with the Palisades and Watchung

Flow I approximately 190 m.y. ago and concluded with the Watchung Flow III approximately 140 m.y. ago. This period of time was therefore one of appreciable igneous activity for which an associated higher geothermal gradient would be expected. The increased geothermal gradient is in turn responsible for at least the initial high temperature (150 to 200°C) regional hydrothermal fluids.

## E5.2 ZEOLITES

Age determinations performed on zeolites associated with the Stage II mineralization gave widely varying ages. In order to assess the magnitude of expected variation, a series of replicate control samples were submitted for dating. The results are given in Table E-2 and summarized below:

<u>Sample No.</u>	<u>Age (m.y.)</u>	<u>% K</u>	<u>Comments</u>
HO 1-1	2.1 + 0.5	0.27	Stilbite crystal as handpicked from same parent sample
HO 2-2	63 ± 5	0.46	
GA 17.3	73.3 ± 5.1	0.26	
FS-15	8.3 ± 1.7	0.76	Submitted because well developed and easily hand picked stilbite crystals.

It can be seen that the spread in ages makes the mineral (stilbite) unsuitable for use in the determination of absolute ages. Because of stilbite's open crystallographic structure and affinity for cation exchange, stilbite is prone to argon leakage and potassium concentration. Both of these characteristics result in anomalously young ages and therefore age determination on stilbite should be considered as minimum ages.

The stilbite associated with the Stage II mineralization is therefore at least 73 m.y. old and probably older.

The apophyllite mineral age determined on Sample No. MW-112-1 of  $92 \pm 5$  m.y. may better approximate the age of actual crystal formation. Apophyllite is unusual in that it was originally classified as a framework silicate and placed in the zeolite group and later changed to a phyllo or sheet silicate and placed in the mica group. Therefore, because of its "border-line" status, it can be expected to possess some properties and characteristics that are detrimental to its use for the determination of absolute ages. On the other hand, it would also be expected to inherit some of the properties of the mica group, which is considered to be a "reliable" mineral for use in K-Ar dating. Overall, one would expect that the K-Ar apophyllite age more closely approximates the absolute age of mineral formation, although it too can be considered a minimum age. Therefore, it is concluded that the apophyllite associated with the Stage II mineralization is at least 92 m.y. old.

### E5.3 OTHER

Other samples dated during this study (JT-111, JT-121, JT-122) are listed in Table E-2 and referenced in other portions of this report. The K-Ar age determinations performed on a separated mineral appear to reflect a degree of thermal resetting. These age data should also be considered as minimum ages.

Whole-rock diabase sample SL-127A gave a potassium-argon age of  $439 \pm 18$  m.y. This age was considered suspect and

K-Ar age determinations were performed on pyroxene (SL-Pld) and plagioclase (SL-PLd) mineral separates from the same sample. The mineral ages (pyroxene 424 m.y.±22, plagioclase 458 m.y.±17) are concordant to the K-Ar whole-rock age minimizing the likelihood of thermal resetting. Therefore, it is concluded that this age probably represents the age of emplacement and solidification for the dike from which the sample was taken.

TABLE E-1

## FLUID INCLUSION - DATA

SAMPLE NUMBER	SAMPLE LOCATION- COUNTRY ROCK	PETROGRAPHIC DESCRIPTION	STRUCTURAL SIGNIFICANCE	FLUID INCLUSION ANALYSIS		COMMENTS
				PRIMARY	SECONDARY OR LATE PHASE	
<u>MESOZOIC</u>						
GA19.1	Union Hill Quarry, East Corner @ North End (Triassic Diabase) Plates 2, E-10A and E-10B	Chlorite (Fe-Rich) aggregates line fracture, with some calcite, stilbite and comb structure quartz (syn & post to euhedral calcite crystals showing well developed cleavage traces & deformation lamellae) (Chl)#S(Cc*+Qtz*)#S(Stil+Qtz+Cc+Chl) Plate E-10C	Sample from N70°W, zone fracture 295-318(3) 308°C(quartz) sample taken 2 ft north of a fault oriented N29°W, 78°W. Although this fracture extends into the fault zone, no displacement was observed.	295-318(3) 308°C(quartz)	90-109(7) 99°C(calcite)	
GA7.1	Martin-Marietta's Long Clove Quarry @ Haverstraw Near Conveyor (Triassic Diabase) Plates 2, E-11A and E-11B	Large calcite crystals with deformation lamellae (Chl)#S(Cc+O+Chl)#S Plate E-11C	Sampled N60°W, 64°NE, shear zone with nearly horizontal slickensides. Shear zone contains 1/2"-2" of green chloritic material. Nearby subparallel fractures contain sheared green material and calcite.	195-229(9) 215°C(quartz)	----	
MW114-1	Route 303 - South of Valley Cottage, 250 ft North of Casper Hill Road. Plates 2, E-12A and E-12B	Strained quartz crystals with numerous inclusions. (Chl)#S(Qtz*+Chl)#S(Qtz)#S (Qtz+L) Plate E-12C	Taken from N15°W, 87°E shear zone (slickensides plunge 46°N & 55°N) near intersection with N25°E, 84°SE, shear in Rockland Lake Fault Zone. More steeply plunging slickensides crosscut vein.	~300°C(quartz) ~215(1) (quartz)	130-142(3) 135°C(quartz)	
MW103-3	Verdrietege Hook Quarry north of Trough Hollow, Palisades sill. (Triassic Diabase) Plates 2, E-13A, E-13B and E-13C	I. Alteration - albite, calcite, chlorite, sulfides? II. Calcite and analcite. III. Stilbite, calcite. (Chl+Cc)#S(Chl+anal+Cc*)#D (Cc+Stil*) Plate E-13D	Taken from N10°W, 62°W Shear (slickensides plunge 1°S) near intersection with N83°E, 82°N shear. N10°W, 62°W shear appears to be younger.	130-145(6) 135°C(calcite)	93-103(3) 99°C(calcite)	
MW67d-1	Martin-Marietta Quarry @ Haverstraw, Center of NE wall (Triassic Diabase) Plate 2	Large euhedral calcite crystals with deformation lamellae overgrown by tabular stilbite, much smaller and displaying twinning patterns (Cc*)#S(Stil+Cc+Chl) Plate E-14	Sampled shear (N55°E, 74°SE, slickensides plunge 25°S) within larger shear zone, N21°E, 80°SE. Zone post-dates but utilized low-angle shears. Other shears in same zone.	123-138(4) 128°C(calcite)	110-111(2) 110°C(calcite)	

TABLE E-1 (Continued)

SAMPLE NUMBER	SAMPLE LOCATION-COUNTRY ROCK	PETROGRAPHIC DESCRIPTION	STRUCTURAL SIGNIFICANCE	FLUID INCLUSION ANALYSIS		COMMENTS
				PRIMARY	SECONDARY OR LATE PHASE	
GA17.3	Southern end of Rockland Lake SE corner of Soccer Field (Triassic Sediments and Intrusives) Plates 2, E-15A and E-15B	Large euhedral calcite crystals and stilbite. Some calcite crystals exhibit twin lamellae. (C <sub>c</sub> *+Stil*) Plate E-15C	Sample adjacent to N30°E, Vert. Fault. No relationship between the mineralization and subhorizontal slickensides was apparent.	100-150(3)124°C(calcite)	----	K/Ar age 73.3 m.y. $\pm$ 5 Stilbite
MW106-2	Same as MW103-3 (Triassic Diabase) Plates 2, E-16A, and E-16B	I. Large crystals of calcite. Fracture marked by chlorite. II. Stilbite and calcite crystals. (C <sub>c</sub> *)#S(Stil+C <sub>c</sub> )#S(Chl+C <sub>c</sub> ) Plate E-16C	Taken from shear surface just west of major fault, N42°E, 78°E. Shear surface oriented N44°E, 88°E, slickensides plunge 21°SW.	165-220(4)192°C(calcite)	99-136(7)114°C(calcite)	
MW115-1	South End of Turtle Hill in Ramapo Reservation. (Triassic Diabase) Plates 2 and E-17A	Quartz filling cavities and fractures. Some sheared calcite. Chlorite occurs along what appears to be older fractures. (C <sub>c</sub> +Chl)#S(Qtz*) Plate E-17B	Taken from shear zone, 8" wide, oriented N47°E, 87°SE, slickensides plunge 72°SW.	~168°C(quartz)	----	
GA1.1	Mt. Ivy, N.Y. South Wall of Quarry (Triassic Diabase) Plates 2, E-18A, and E-18B	Analcite enclosing secondary products of diabase alteration over thin layer of calcite which displays curved deformation lamellae. (C <sub>c</sub> )#S(C <sub>c</sub> +Chl+Anal)#D(Anal+C <sub>c</sub> *) Plate E-18C	Sample taken from a plane located just behind 65°E, 80°NW fault. Slickensides rake 50°-60°N.	High T ~300°C(NG) (calcite)	99(7),80(calcite)	
GA1.3	Mt. Ivy, N.Y. South Wall of Quarry (Triassic Diabase) Plates 2, E-18B and E-19A	Strained calcite separated from strained quartz by iron oxides. Later analcite (Qtz)#S(C <sub>c</sub> +L)#S(C <sub>c</sub> +Anal) Plate E-19B	Sample taken from a plane located just behind 65°E, 80°NW fault. Slickensides rake 50°-60°N.	~100°C(analcite)	----	
MW103-2	Same as MW103-3 (Triassic Diabase) Plates 2, E-13A, E-13B, and E-13C	Euhedral calcite overgrown by well developed crystals of stilbite, radially arranged & analcite with chlorite overgrowth structures plus stilbite. (Chl)#S(C <sub>c</sub> )#S(Anal+C <sub>c</sub> *+Chl+Stil*) Plate E-13D	Taken from northside of 1 ft wide N65°E, Vert., shear (slickensides plunge 57°W)	271(1) (calcite) 151-207(5)180°C(calcite)	99-130(14)114°C(calcite)	

TABLE E-1 (Continued)

SAMPLE NUMBER	SAMPLE LOCATION-COUNTRY ROCK	PETROGRAPHIC DESCRIPTION	STRUCTURAL SIGNIFICANCE	FLUID INCLUSION ANALYSIS		COMMENTS
				PRIMARY	SECONDARY OR LATE PHASE	
GA4.1	Eastside Rt #202 200 ft north of Limekiln Road. Wesley Chapel, N.Y. (Triassic Diabase) Plates 2, E-20A and E-20B	Quartz phases; comb structure. Subparallel orientation normal to fragment surfaces; well developed crystals arranged perp. to others; overgrowths separated by iron oxides, etc. (Qtz*)#D(Qtz*) Plate E-20C	Sampled N66°E, 46°S, fracture Quartz vein 1/4"-1/2" thick fills fracture.	~200°C(quartz)	----	
MW116-2	Abandoned Quarry, East Side of hill to WSW of Thruway, Ext. 12. West Nyack. (Trias- sic Diabase) Plates 2, E-21A and E-21B	Calcite mineralization, deformed crystals. Chlorite aggregates, and quartz. (Chl+Cc)#S(Qtz+Cc+Chl+O)#S Plate E-21C	Example from shear zone, N66°E 78°N. Slickensides plunge 65°NE.	129-168(8)148°C(calcite)	98-111(4)102°C(calcite)	
<u>PALEOZOIC</u>						
FS-10	Outcrop North of Reactor No.2 (Inwood Marble) Plates 2, E-5, E-7 and E-22A	Thin section contains deformed minerals (microcline, phyllo- silicates, aggregate of quartz) cemented by strained calcite mineralization plus sulfides. Last phase of calcite in form of euhedral crystals. (Cc+O)#S(Cc*) Plate E-22B	Sample from N83°W, 82°S Fault	190-220(3)205°C(calcite) 138-168(8)156°C(calcite)	115-119(2)117°C(calcite)	
B-35	(Reference: Dames & Moore; 1975)			141-195(3)171°C(calcite)	93(1)(calcite)	
GA9.1	Verplank Quarry, East Wall, 200 ft. South of NE Corner. (Manhattan Schist) Plate 2, E-23A, and E-23B	Plate E-23C	Sample taken from a N15°W, 65°SW, Joint	----	113(1)(calcite)	
FS-11	Outcrop north of Reactor No. 3 (Inwood Marble) Plates 2, E-5, E-9A and E-24A	Large calcite crystals with fragments of Host Rock. (Cc*+O)#S(Cc*) Plate E-24B	Sampled N11°W, 70°E, Fault Sample suggested by Dr. Barnes on his visit to the site.	----	92-129(6)114°C(calcite)	

TABLE E-1 (Continued)

SAMPLE NUMBER	SAMPLE LOCATION-COUNTRY ROCK	PETROGRAPHIC DESCRIPTION	STRUCTURAL SIGNIFICANCE	FLUID INCLUSION ANALYSIS		COMMENTS
				PRIMARY	SECONDARY OR LATE PHASE	
FS-8	Outcrop North of Reactor No. 2 (Inwood Marble) Plates 2, E-5, E-7 and E-25A	Calcite crystals - deformed ( $C_c^*$ )#S Plate E-25B	Sample from N5°W, 80°E fault	~300(1)(calcite) 175-220°C (calcite) 132-143(4)137°C(calcite)	94(1)(calcite)	
FS-4	Outcrop North of Reactor No. 3 (Inwood Marble) Plates 2, E-5, E-9A, E-26A and E-26B	Calcite, euhedral crystals in cavity. ( $C_c^*$ ) Plate E-26D	Sample approximately 1 ft away from FS-3 taken on same fault, however, trend curves to be N4°W, 70°E	133(1) (calcite)	----	
B-4	(Reference: Dames & Moore; 1975)			171-187(7)177°C(calcite)	----	
B-31	(Reference: Dames & Moore; 1975)			159-169(7)161°C(calcite)	69-98(5)82°C(calcite)	
C-5	(Reference: Dames & Moore; 1975)			159-201(5)174°C(calcite)	83-119(3)106°C(calcite)	
FS-1	Outcrop North of Reactor No. 3 (Inwood Marble) Plates 2, E-5, E-9B, and E-27A	Calcite crystals ( $C_c^*$ ) Plate E-27B	Taken from N-S, 63°E fault. This is the fault first emphasized by Dr. Ratcliffe.	~150-250(calcite)	83-119(3)106°C(calcite)	
FS-5	Same as FS-1 (Inwood Marble) Plates 2, E-5, E-9A and E-28A	Euhedral calcite crystals, aggregate of quartz - recrystallized silicon from earlier phase? + new oxides... oriented texture of host rock disturbed by recrystallization. (Qtz)#S( $C_c^*$ ) Plate E-28B	Sample taken from fault oriented N-S, 64°E. Sample within orange healed breccia which is cut by N-S fault.	125-150(6)141°C(calcite)	86-106(3)99°C(calcite)	
FS-6	Outcrop Adjacent to Turbogenerator Building No. 1 (Inwood Marble) Plates 2, E-5, E-8 and E-29A	Calcite crystals, brecciated host rock. Last euhedral phase of calcite (subhedral to euhedral) appears to be undeformed although many crystals show twin lamellae ( $C_c$ )#S( $C_c^*$ ) Plate E-29B	Sample from N-S, 70°E, fault	135-172(5)145°C(calcite)	----	
FS-2	Same as FS-1 (Inwood Marble) Plates 2, E-5, E-9B and E-30A	Calcite crystals with deformation lamellae ( $C_c$ )#S Plate E-30B	Sample taken from N2°E, 64°E fault	163-173(3)170°C(calcite)	----	

TABLE E-1 (Continued)

SAMPLE NUMBER	SAMPLE LOCATION-COUNTRY ROCK	PETROGRAPHIC DESCRIPTION	STRUCTURAL SIGNIFICANCE	FLUID INCLUSION ANALYSIS		COMMENTS
				PRIMARY	SECONDARY OR LATE PHASE	
FS-3	Same as FS-1 (Inwood Marble) Plates 2, E-5, E-9A, E-26A and E-26B	Recrystallization of mica, quartz and K-spar along fracture. I. Hydrothermal metamorphic crystallization. II. Calcite phase. (C <sub>c</sub> *)#S(C <sub>c</sub> ) Plate E-26C	N6°E, 70°E Fault. Calcite crystals approximately 2" from fault plane within mineralized vug.	127-162(6)145°C(calcite)	~90(?) (calcite)	
GAS.1	Croton-on-Hudson Rear of Chevrolet Dealer Parking Lot (Inwood Marble) Plate 2, E-31A and E-31B	Plate E-31C	Sample from irregular deposit trending generally northeast near N10°, 76 SE fault	High T metamorphic origin ~300°C(?) (calcite)	125-144(2)134°C(calcite)	
GAll.1	Railroad cut west of Lovett Generating Station, Tomkins Cove. (Wappinger Limestone) Plates 2, E-32A, E-32B and E-32C	Plate E-32D	Taken from within a N10° to 20°E, dipping steeply northwest, healed breccia. A suggestion of both dextral & sinistral movement (strike-slip) is indicated by tensional fractures.	High T metamorphic origin ~300°C(?) (calcite)	----	
GAll.2	Same as GAll.1 Plates 2, E-32A, E-32B and E-32C	Plate E-32D	Same as GAll.1	126-130(3)128°C(calcite)	----	
GAll.3	Same as GAll.1 Plates 2, E-32A, and E-32C	Plate E-32E	Same as GAll.1	237-298(9)277°C(calcite)	----	
GAll.4A	Same as GAll.1 Plates 2, E-32A, and E-32C	Plate E-32F	Same as GAll.1	107-157(8)133°C(calcite)	----	
GAll.4B	Same as GAll.1 Plates 2, E-32A, and E-32C	Plate E-31G	Same as GAll.1	<171-187(5)181°C(calcite)	----	
GAS.3	Croton-on-Hudson Rear of Chevrolet Dealer Parking Lot (Inwood Marble) Plates 2, E-31A and E-31B	Plate E-31D	Sample from classical tension gash trending N20°E, 85°SE. Gash related to N10°E, 76°SE fault (right lateral)	High T ~169-202°C(calcite)	83-98(6)94°C(calcite) 117-125(3)121°C(calcite)	

TABLE E-1 (Continued)

SAMPLE NUMBER	SAMPLE LOCATION-COUNTRY ROCK	PETROGRAPHIC DESCRIPTION	STRUCTURAL SIGNIFICANCE	FLUID INCLUSION ANALYSIS		COMMENTS
				PRIMARY	SECONDARY OR LATE PHASE	
GAL2.1	Railroad cut West of Lovett Generating Station, about 50 ft north of GALL (Wappinger Limestone) Plates 2, E-33A and E-33B	Plate E-33C	Sample from N20°E, 85°SE, fault. (Strike-Slip) Slickensides on layer immediately adjacent to fault plane rake 80°S, on next layer, slickensides rake 20°S. Second layer truncates the first, suggesting it the younger of the two. Deposited above this is a third layer composed of undeformed calcite about 3/8" thick.	High T ~300°C(?) (calcite)	----	
D-1	(Reference: Dames & Moore; 1975)			171-226(12) 194°C (calcite)	----	
FS-9	Outcrop North of Reactor No. 2 (Inwood Marble) Plates 2, E-5, E-7 and E-34A	Attachment 1A - Fluid Inclusion Studies	Sample from N25°E, 85°NW	~300(1) (calcite) 168-208(6) 190°C (calcite) 127-139(4) 132°C (calcite) (pseudosecondary?)	<100 (calcite)	
FS-12	Outcrop adjacent to Turbogenerator Building No. 1 (Inwood Marble) Plates 2, E-5, E-8 and E-35A	Calcite crystals. Large vein calcite appears to be deformed (C <sub>c</sub> ) Attachment 1B - Fluid Inclusion Studies	Sample from within large weathered shear zone which strikes approximately N30°E. Sample suggested by Dr. Barnes.	172-197(3) 181°C (calcite) 129-159(10) 140°C (calcite)	---- ----	
FS-13	Outcrop North of Reactor No. 2 (Inwood Marble) Plates 2, E-5, E-7 and E-36A	Euhedral calcite crystals with overgrowth marking (O+C <sub>c</sub> *) Plate E-36B	Sample from E-W, 85°S Fault	143-216(5) 178°C (calcite)	90-100(4) 97°C (calcite)	
D-6	(Reference: Dames & Moore; 1975)			274-352(3) 317°C (calcite)	106-209(3) 171°C (calcite)	
A-1	(Reference: Dames & Moore; 1975)			131-188(8) 168°C (calcite)	----	
A-2	(Reference: Dames & Moore; 1975)			92-167(5) 139°C (calcite)	50-72(3) 62°C (calcite)	
FS-7	Same as FS-6 (Inwood Marble) Plates 2, E-5, E-8 and E-37A	Calcite crystals - deformed. Most rock cut by calcite veins with deformation lamelle and curved cleavage traces. (C <sub>c</sub> )#S(C <sub>c</sub> ) Plate E-37B	Sample taken from small exposure of E-W, 82°S, Fault	-----	95-118(7) 105°C (calcite)	

TABLE E-2

Potassium-Argon - Data

Sample No.	Location	Petrographic Description	Structural Significance	Results of Analysis	Comments
Z-76-81a	Watchung: Flow I Sneider La., Campgaw Ramsey Quad Elev ≈450' Plate 2	Basalt	1st Flow, Watchung Mtns.	Avg % K = .469; Age = 179 MY <sub>+9</sub> Whole Rock: Basalt	
Z-76-81b	Watchung: Flow I Same as 2-76-81a Elev ≈470' Plate 2	Basalt	1st Flow, Watchung Mtns.	Avg % K = .486; Age = 193 MY <sub>+10</sub> Whole Rock: Basalt	
Z-76-82a	Watchung: Flow II Indian Rd #470 ≈10'N of Bridge Pompton Plains Quad Elev ≈280' Plate 2	Basalt	2nd Flow, Watchung Mtns.	Avg % K = .643; Age = 159 MY <sub>+8</sub> Whole Rock: Basalt	
Z-76-82b	Watchung: Flow II Breakneck Rd. NW Corner of Paterson Quad. Elev ≈520' Plate 2	Basalt	2nd Flow, Watchung Mtns.	Avg % K = .675; Age = 180 MY <sub>+8</sub> Whole Rock: Basalt	
Z-76-83a	Watchung: Flow III Route 202, Pompton ≈30'N of Dam; Pompton Plains Quad Elev ≈220' Plate 2	Basalt	3rd Flow, Watchung Mtns.	Avg % K = .250; Age = 147 MY <sub>+9</sub> Whole Rock: Basalt	
Z-76-83b	Watchung: Flow III Pompton From Rock Ledge Facing North Pompton Plains Quad Elev ≈380' Plate 2	Basalt	3rd Flow, Watchung Mtns. Elevation ≈380'	Avg % K = .231; Age = 136 MY <sub>+9</sub> Whole Rock: Basalt	
FS-14	Route 303, Central Nyack Across from Nyack Drive-in Plate 2	Basalt	Chilled diabase dike trending N80°E, Vert. in T-J hornfels	Avg % K = .900; Age = 175 MY <sub>+8</sub> Whole Rock: Basalt	
SL-121I	Indian Lake, east flank of Waughaw Mt., Montville, NJ Plate 2	Aphanitic Diabase	Sheared plug in trace of Ramapo Fault	Avg % K = 1.089; Age = 156 MY <sub>+7</sub> Whole Rock: Basalt	

TABLE E-2 (Continued)

Sample No.	Location	Petrographic Description	Structural Significance	Results of Analysis	Comments
SL-THD	Turtle Hill, Ramapo River Reservation, Rte. 202, Mahwah, NJ Plate 2	Aphanitic Diabase	Sheared plug in trace of Ramapo Fault	Avg % K = .631; Age = 149 MY <sup>+7</sup> Whole Rock: Basalt	
SL-127A	Hill east of Lake Inez, DuPont Works, Pompton Lakes, NJ Plate 2	Finely Crystalline Diabase	Intruded along N15-20°E fault in Precambrian highlands	Avg % K = .887; Age = 439 MY <sup>+18</sup> Whole Rock: Basalt	
SL-PLd	Same Sample as SL-127A Plate 2	----	----	Avg % K = .355; Age = 424 MY <sup>+22</sup> Pyroxene Avg % K = 1.809; Age = 458 MY <sup>+17</sup> Feldspar	Concordant mineral and whole-rock age
FS-15	Float Sample from Mott Farm Road Quarry Stony Point Plate 2	Aggregates of coarse bladed Stilbite	none - control sample	Avg % K = .761; Age = 8.3MY <sup>+1.7</sup> Stilbite	
HO 1-1	Single Float Sample from Rockland Lake Plate 2	Radial aggregates of Stilbite on fracture surface	none - control sample	Avg % K = .270; Age = 2.1MY <sup>+0.5</sup> Stilbite	Same sample as GA-17.3
HO 2-2	Single Float Sample from Rockland Lake Plate 2	Radial aggregates of Stilbite on fracture surface	none - control sample	Avg % K = .462; Age = 63MY <sup>+5</sup> Stilbite	Same sample as GA-17.3
GA-17.3	Soccer Field @ Southern End of Rockland Lake Plates 2, E-15A and E-15B	Large Euhedral Calcite (I&II?) some crystals exhibit twin lamellae (?) and stilbite coating (C <sub>c</sub> *+stil*) Plate E-15C	Sample from large shear; N30°E, 85°S slickensides rake 5°S	Avg % K = .256; Age = 73.3 MY <sup>+5.1</sup> Stilbite	Stilbite
GA 20.2	Union Hill Quarry 100 Ft. from NW corner Plate 2	Altered diabase cut by veinlet of wavy quartz parallel to fracture with datolite and analcite mineralization (Chl)#S(Qtz)#S(Anal+Dato+C <sub>c</sub> )	From N70°W, 20°S breccia zone, appears to be kink zone. Breccia zone off-set by N28°E, 2°W Shear	Avg % K = .1142; Age = <1.2 MY Analcite	Analysis meaning - less and not used

TABLE E-2 (Continued)

Sample No.	Location	Petrographic Description	Structural Significance	Results of Analysis	Comments
MW-112-1	Palisades, Verdrietege Hook; Quarry just South of Trough Hollow Plates 2 and E-38A	Calcite, pectolite (or prehnite impregnation) datolite, fibrous zeolite, apophyllite (overgrown BFeO & Stilbite, prehnite, needles of pectolite in apophyllite (?+Pect) #S (Apo*+Chl+Dato*+C <sub>c</sub> +Prehn*+Pect) Plate E-38B	From shear zone @ N10°E, 65°E, slickensides plunge 14°S	Avg % K = 3.921; Age = 92MY+5 Apophyllite	
JT-111	Camp Bullowa, Crickettown Road, Stony Point Plate 2	Bullowa Granite	To define the Mid-Paleozoic extent of the major crustal break of the dextral wrench system	Avg % K = 6.964; Age = 432 MY+15 K - Feldspar Avg % K = 5.204; Age = 364MY+13 Biotite	
JT-121	Just uphill on north side of town of Croton Falls Plate 2	Croton Microcline Granite	same as JT-111 above	Avg % K = 5.535; Age = 321 MY+11 Biotite Avg % K = 12.268; Age = 261 MY+9 Microcline Avg % K = 8.708; Age = 344MY+12 Muscovite	
JT-122	Just uphill (north) from town of Croton Falls Plate 2	Croton Gabbro	same as JT-111 above	Avg % K = .346; Age = 367 MY+19 Hornblende Avg % K = 6.079; Age = 335 MY+12 Biotite	

## MINERAL CHANGES IN FORMATION OF ZEOLITIC ROCK

	PERIOD 1	PERIOD 2	PERIOD 3	PERIOD 4	PERIOD 5	PERIOD 6
Lava minerals	Labradorite Diopside Olivine Magnetite		Albite → Quartz Albite { Quartz Amphiboles. Albite Garnet Chlorite Hematite.	Prehnite Prehnite	Zeolites Zeolites Zeolites Serpentine.	Calcite. Calcite. Calcite.
Saline minerals	Lava Lava Lava	Anhydrite Glauberite Calcite (lamellar) (?)	Quartz. Rectangular and lamellar cavities. Quartz. Rhombic cavities		Rectangular cavities.	Gypsum { Rectangular cavities. Thaumasite.
Zoelitic rock minerals			Albite Quartz Garnet Babingtonite (?) Green amphibole → garnet.	{ Prehnite Datolite Pectolite } { Prehnite Datolite Pectolite } { Prehnite, Green amphibole.  Prehnite { Datolite Pectolite } Datolite Pectolite	{ Apophyllite, Chabazite, Natrolite, Stilbite. Apophyllite } { Chabazite Heulandite } { Apophyllite Chabazite, Natrolite.  Analcite { Chabazite Heulandite Natrolite Stilbite } Apophyllite Chabazite { Heulandite Laumontite Natrolite Stilbite } Heulandite { Laumontite Natrolite Stilbite } Laumontite → Natrolite Natrolite Scolecite → Natrolite Stilbite → Natrolite  Chalcopyrite Pyrite (?) Babingtonite	Calcite. Calcite. Calcite. Calcite. Calcite. Calcite. Calcite. Calcite. Calcite. Calcite. Calcite. Azurite, Chrysocolla, Malachite. Limonite. Fibrous amphibole (?) Gypsum → Thaumasite.

TABLE FROM SHALLER, "THE CRYSTAL CAVITIES OF THE N.J. ZEOLITE REGION",  
U.S. GEOL. SURVEY BULLETIN NO. 832 (1932).

ATTACHMENT NO. 1A

TO APPENDIX E

Report of Fluid Inclusion

Studies by Dr. Barnes

Fluid Inclusion Analysis

for

Dames and Moore, Inc.

Job #0874 - 062 - 10

Submitted by:

Robert J. Pottorf, Graduate Assistant  
H. L. Barnes, Professor of Geochemistry

H. L. Barnes

September 27, 1976

PART I (Indian Point Site)

Summary (Range, (no. of measured inclusions), average, in °C)

Part I

<u>Sample</u>	<u>Primary Inclusions</u> (and pseudosecondary)	<u>Secondary Inclusions</u> (latest stage)	<u>Notes</u>
FS-1	150-250 (?)	83-119 (3) <u>106</u>	Many inclusions but leak easily.
FS-2	163-173 (3) <u>170</u>	minor	Incl. rare; pyrite present
FS-3	127-162 (6) <u>145</u>	(~90)	Abundant
FS-4	133 (1)	minor	Very rare; minor sulfides
FS-5	125-150 (6) <u>141</u>	<sup>6</sup> 86-103 (3) <u>99</u>	Good negative crystals
FS-6	<sup>5</sup> 137-172 (5) <u>145</u>	--	Slightly deformed
FS-7	--	95-118 (7) <u>105</u>	Parallel to cleavage
FS-8	<sup>1</sup> ~300 (Ø) ~175-200 132-143 (4) <u>137</u>	94 (1)	Several populations; sulfides present
FS-9	~300 168-208 (6) <u>190</u> 127-139 (4) <u>132</u>	<u>&lt;100</u>	Several populations; sulfides present
FS-10	190-220 (3) <u>205</u> 138-168 (8) <u>156</u>	115-119 (2) <u>117</u>	Abundant, slightly deformed; sulfides present
FS-11	--	92-129 (6) <u>114</u>	Deformed
FS-12	172-197 (3) <u>181</u> 129-159 (10) <u>140</u>	--	Deformed; secondary too small to resolve
FS-13	143-216 (5) <u>178</u>	90-100 (4) <u>97</u>	Sulfides present.

### Discussion

Samples FS-1 to FS-13 are very similar to those previously analyzed from the Indian Point Reactor site. Those samples containing sulfides tend to have slightly higher homogenization temperatures for primary inclusions. Secondary, low temperature inclusions are relatively rare compared to those having temperatures above 130-140°C. Although evidence of deformation of the inclusions is not uncommon; nevertheless, inclusions showing such features maintain their comparatively high homogenization temperatures in nearly all cases. This implies that the dominant faulting occurred while these rocks were at temperatures above 130-140°C.

Comparison of analyses on the following table for four sets of samples allows evaluation of the consistency of the homogenization temperatures. Because the number of measurements is limited to a small population by practical constraints, the limits to each range are not well established. However, the overlap in the ranges for related samples is extensive.

### Comparison of Related Samples

<u>Sample</u>	<u>Primary Inclusion</u>	<u>Secondary Inclusions</u>	<u>Notes</u>
1. FS-1 FS-11	150-200 (?) --	83-119 (3) <u>106</u> 96-129 (6) <u>114</u>	On nearly parallel faults with roughly parallel slickensiding
2. FS-2 B-31	163-175 (3) <u>170</u> 151-169 (7) <u>161</u>	minor 69-98 (5) <u>82</u>	Close and apparently on the same fault
3. FS-5 B-35	125-150 (6) <u>141</u> 141-195 (3) <u>171</u>	86-103 (3) <u>99</u> 93 (1)	In same breccia zone
4. FS-8 FS-9 FS-10 ND-2 ND-6	132-200 (5); ~300 (6) 127-208 (10); ~300 (1+) 138-220 (11) 171-250 (17) 159-232 (11); 274-352 (3)	94 (1) <u>≤ 100</u> 115-119 (2) <u>117</u> -- 106 (1)	These samples are all along fault 1 and most contain visible sulfides. Each also apparently multiple stages of "primary" inclusions.

## Sample FS-1

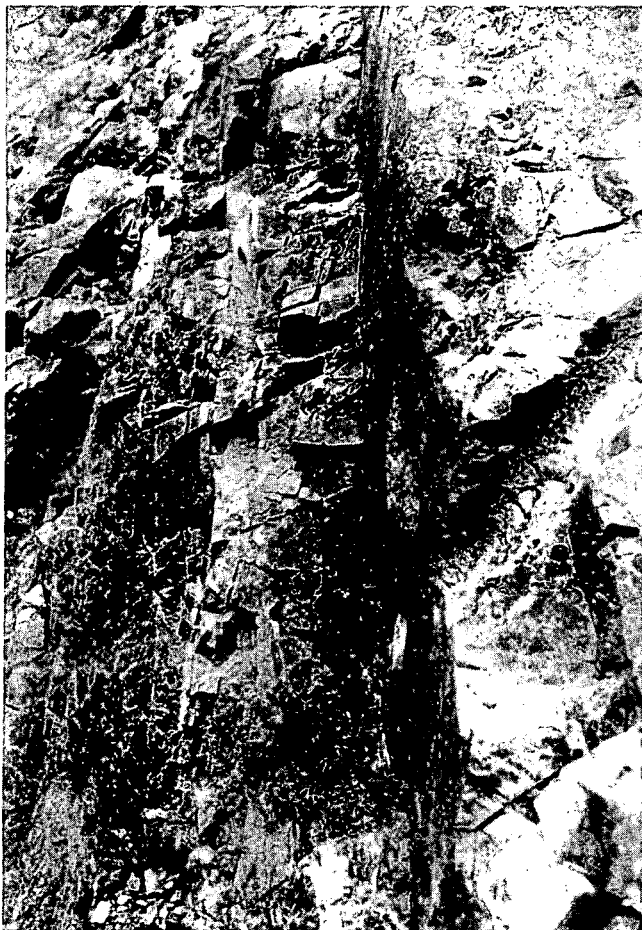
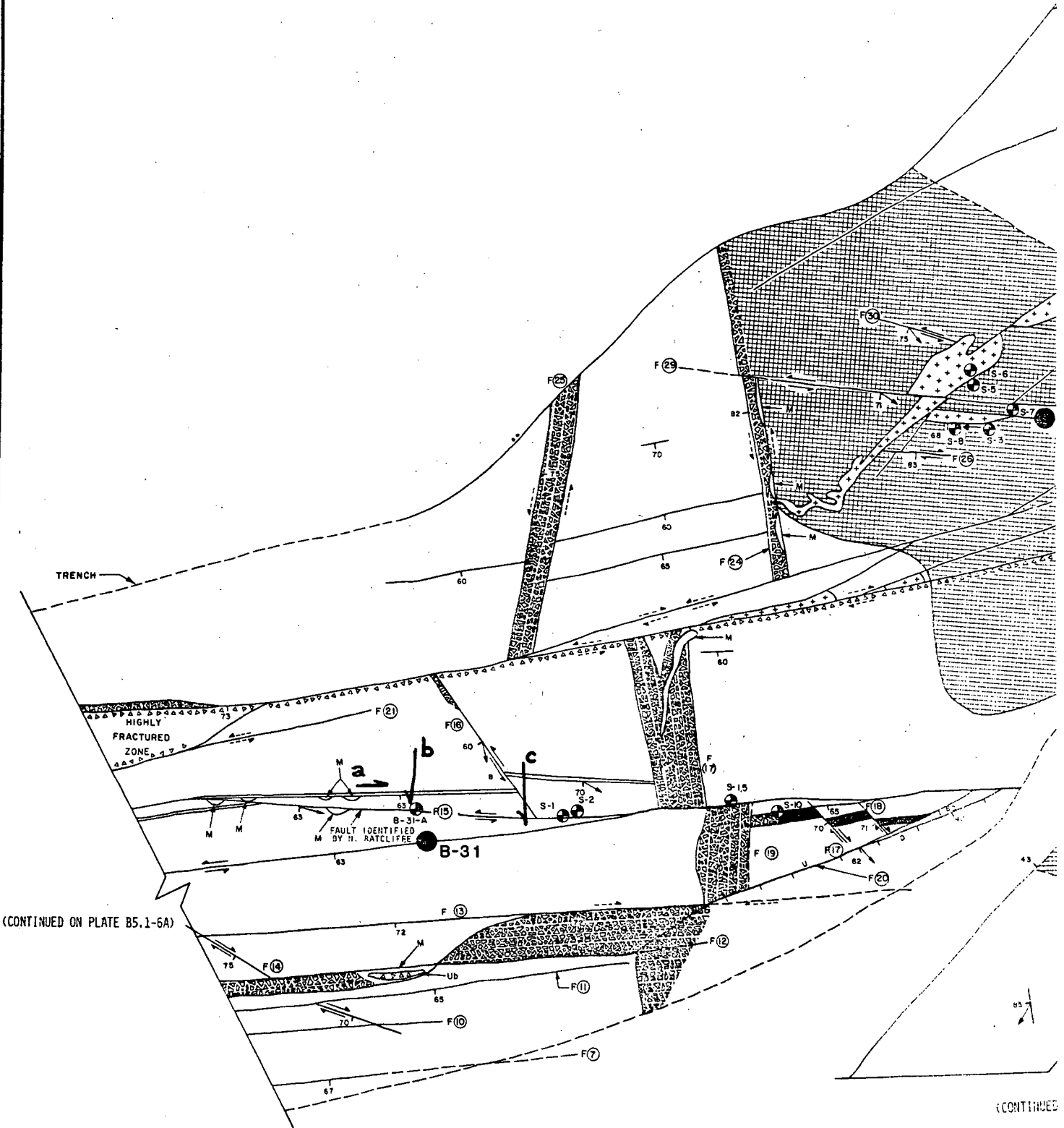


Photo (a), left, looking north along fault 15 as shown on Plate K-6. The sample was collected near the white painted spot just to the right of the jackknife.

Photo (b), below, looking east at fault 15 as shown on Plate K-6. The sample was collected just to the left of the painted spot. Note that the slickensiding dips about  $25^\circ$  to the left and is parallel on both sides of the sampled wedge. This indicates that wedge was involved in one dominant direction of fault movement which was followed by growth of calcite crystals on the wedge.





(CONTINUED ON PLATE B5.1-6A)

(CONTINUED)

NOTE: KEY TO SYMBOLS ON PLATE B5.1-2

Sample FS-1 - Small Calcite Crystals

Extremely easy leakage occurred because nearly all inclusions are necked or display spurs and tails. There are also large numbers of solid inclusions present. Of 16 inclusions heated, 13 leaked.

The three inclusions for which filling temperatures were obtained are large and essentially isolated but are not necessarily primary. From the behavior of smaller (primary?) inclusions during heating, before leakage occurred, there is the possibility that there is a large population of inclusions which formed at higher temperatures, approximately between 150°-250°. However, the separation of this population must be viewed as tentative in the absence of more homogenization temperatures.

Population 1(?)

Range 150-250°C

Population 2

Range 83-119°C (3)

Average 106°C

ANALYST: RJ POTTORF

FLUID INCLUSION SKETCHES

CON EDISON

SAMPLE No. FSI

CHIP No. 7-8

MINERAL: CALCITE

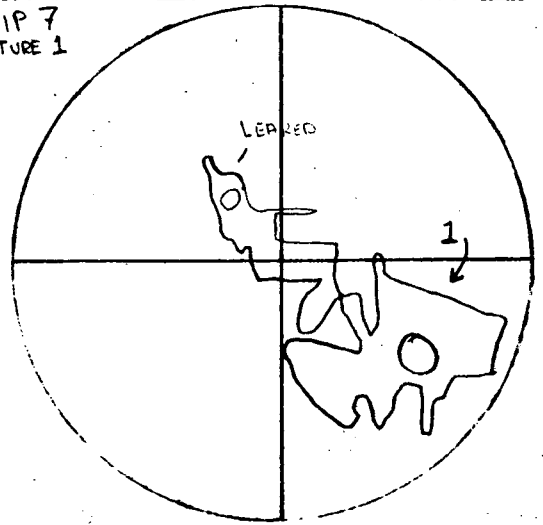
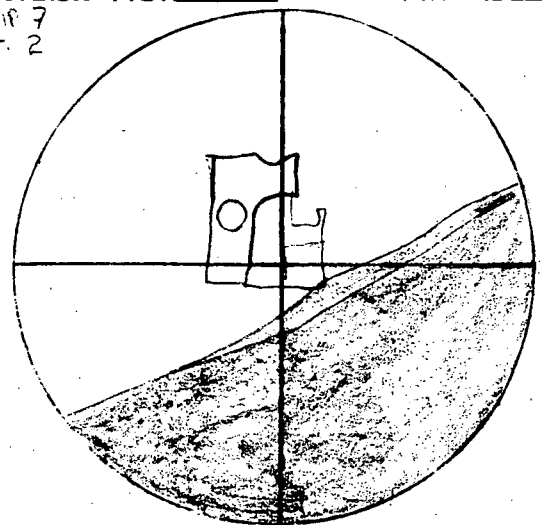
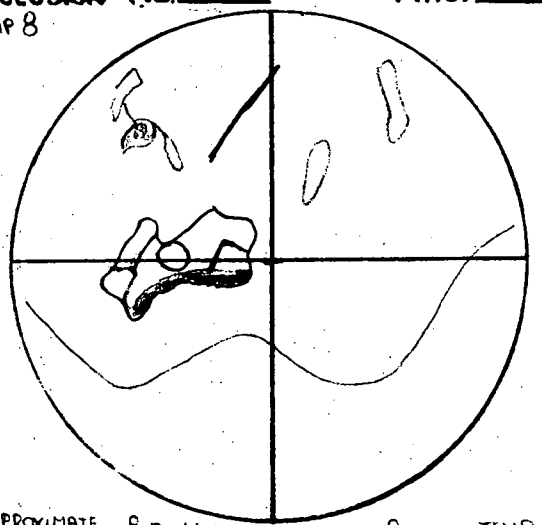
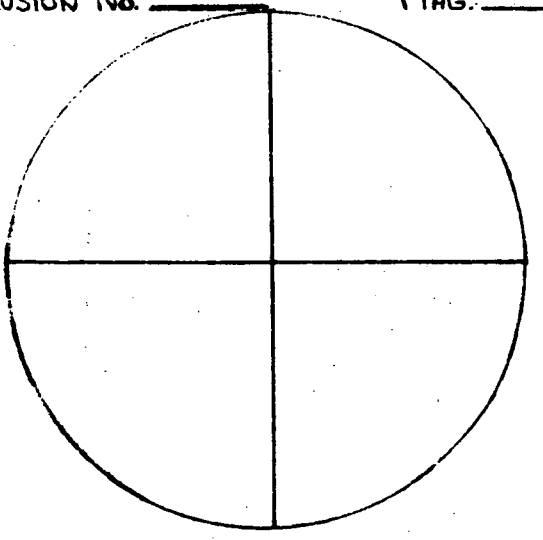
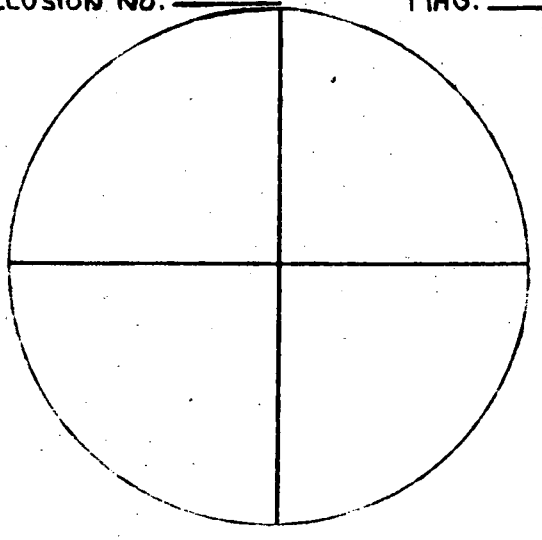
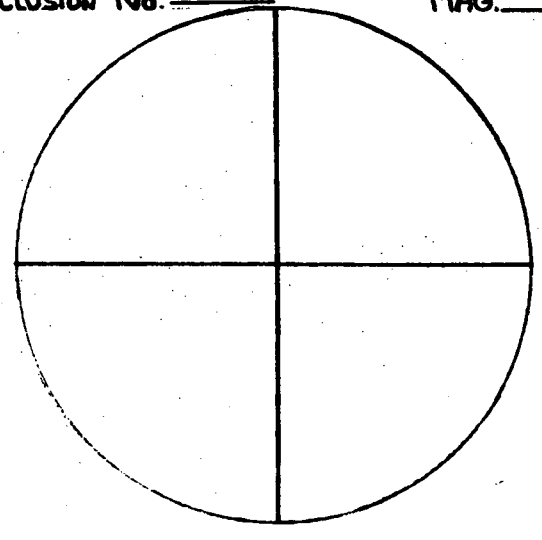
Inclusion No. <u>1</u> MAG. _____	Inclusion No. <u>2</u> MAG. _____	Inclusion No. <u>3</u> MAG. _____
<p>CHIP 7 PICTURE 1</p>  <p>1) 4.90, 4.88 119°, 119°</p>	<p>CHIP 7 PICT. 2</p>  <p>2) 4.80, 4.80 117°, 117°</p>	<p>CHIP 8</p>  <p>APPROXIMATE, BUT VERY CLOSE TO ACTUAL TEMP. BUBBLE COULD NOT BE SEEN AS HOMOGENIZATION WAS CLOSELY APPROACHED</p> <p>3) 3.40, 3.40 83°</p>
<p>Inclusion No. _____ MAG. _____</p> 	<p>Inclusion No. _____ MAG. _____</p> 	<p>Inclusion No. _____ MAG. _____</p> 

PHOTO 1, FS-1, CHIP 7,  
INCLUSION No. 1; SEE  
SKETCH.



PHOTO 2, FS-1, CHIP 7  
INCLUSION No. 2; SEE  
SKETCH.



## Sample FS-2

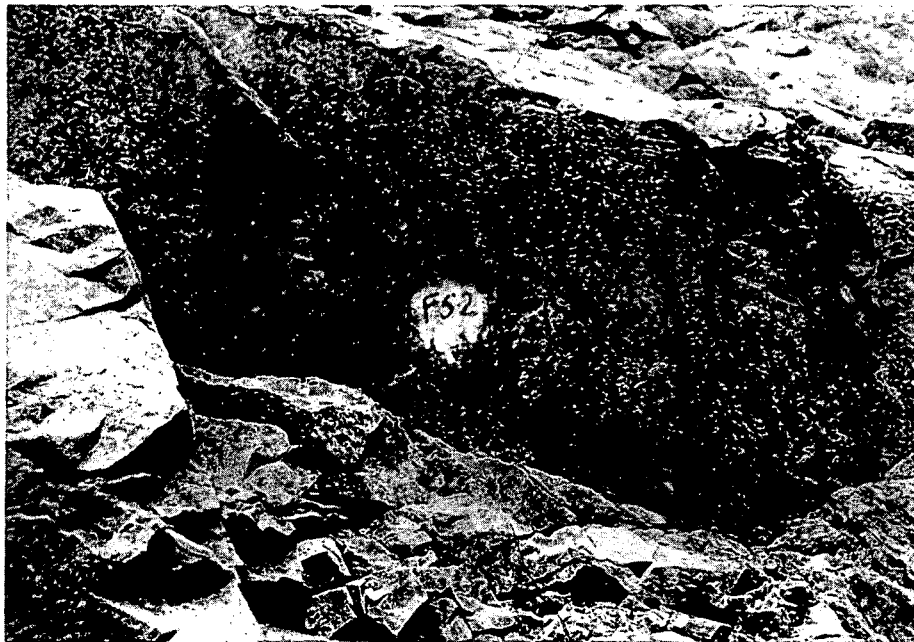


Photo (c) looking east as shown on Plate K-6. The sample was collected just to the left of the painted spot. Slickensiding dips steeply (about  $80^\circ$ ) to the right.

Sample FS-2 - Calcite Crystals

Inclusions are rare; 10 were measured among which 7 leaded before the filling temperature was reached. Minor secondary inclusions were present along healed fractures. Pyrite was present.

Range:  $163-175^\circ\text{C}$  for 3 inclusions

Average:  $170^\circ\text{C}$

ANALYST: RJ POTTORF

SAMPLE No. FS2

FLUID INCLUSION SKETCHES

CHIP No. 1-2

CON EDISON

MINERAL: CALCITE

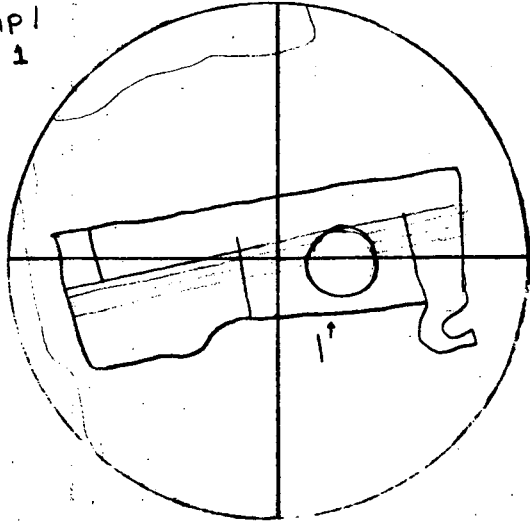
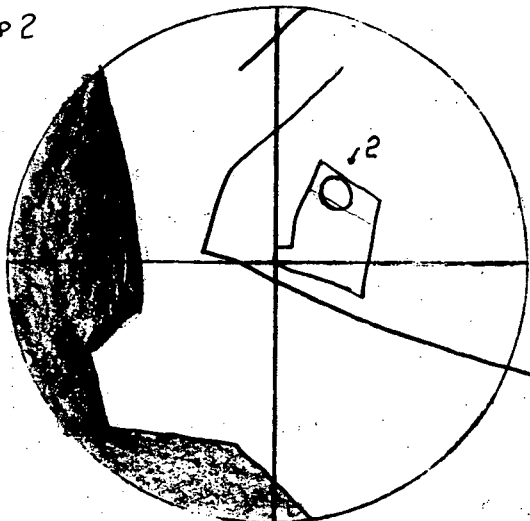
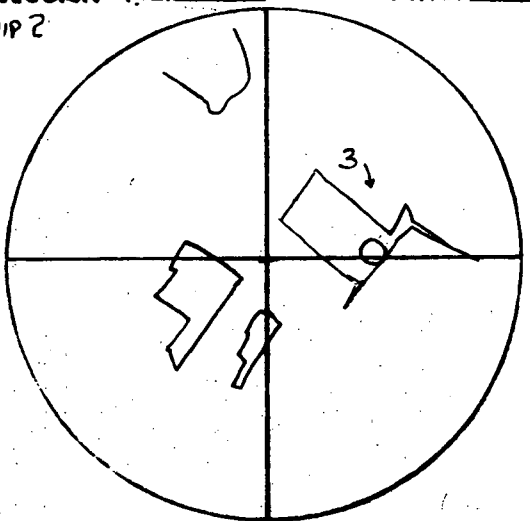
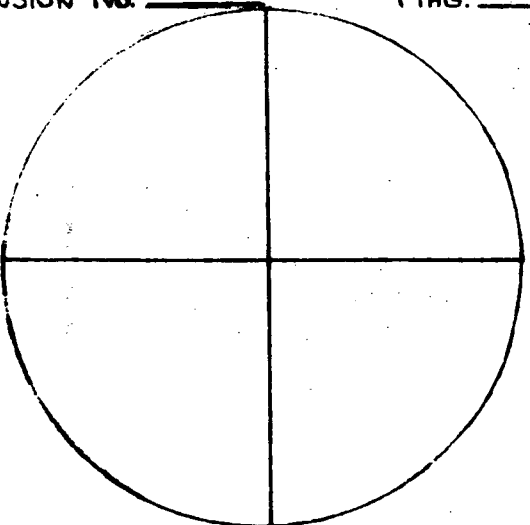
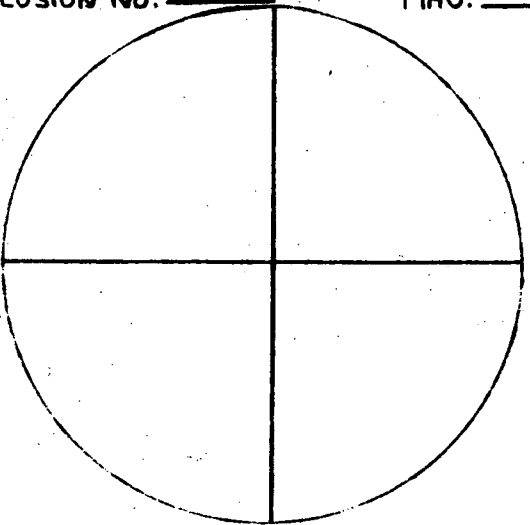
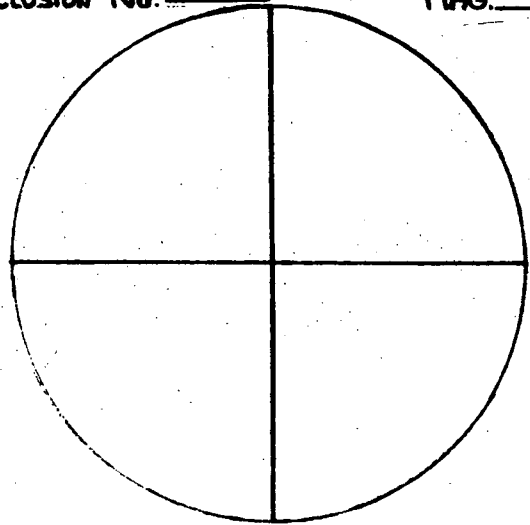
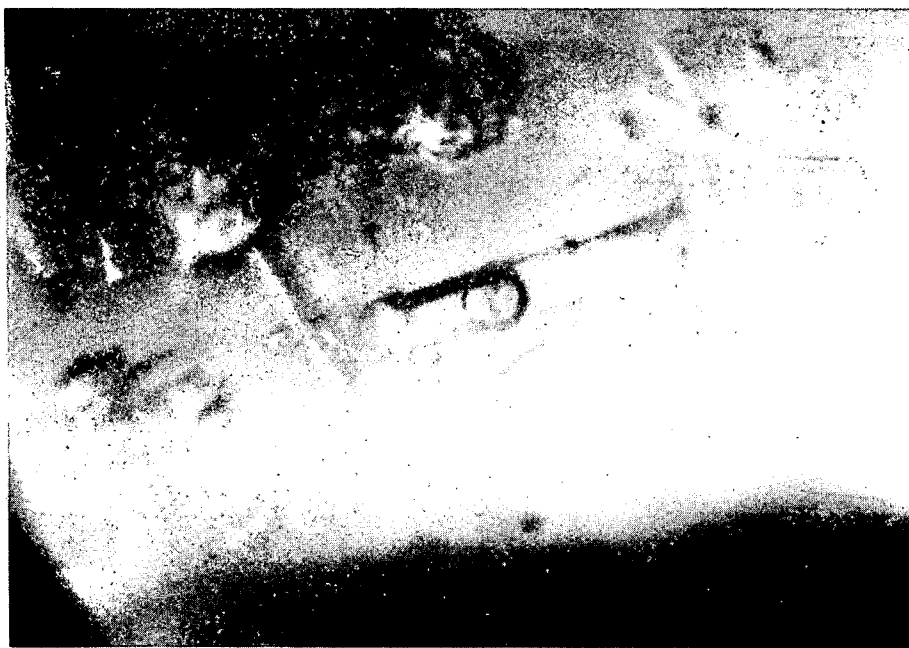
Inclusion No. 1	MAG. _____	Inclusion No. 2	MAG. _____	Inclusion No. 3	MAG. _____
CHIP 1 PICT 1 		CHIP 2 		CHIP 2 	
07.15	175°	2) 6.95, 7.01	171° 172°	3) 6.65, LEAK (SUSPECT)	163°
Inclusion No. _____	MAG. _____	Inclusion No. _____	MAG. _____	Inclusion No. _____	MAG. _____
					

PHOTO 1, FS-2, CHIP 1

INCLUSION 1: SEE

SKETCH.



### Sample FS-3 - Calcite Crystals

Inclusions are relatively abundant; 18 heated, 12 leaked.

Primary inclusions nearly always display tails and/or are stretched or necked and leak upon heating. Secondary inclusions are very small and appear as patches or clusters along rehealed fractures. The vapor phase was either too small to resolve with the heating stage optics or larger secondaries, which could be resolved, leaked when heated. From the vapor/liquid ratios it is estimated that these inclusions would homogenize at  $\sim 90^{\circ}\text{C}$ .

#### Primary inclusions

Range  $127\text{--}162^{\circ}\text{C}$  (6)

Average  $145^{\circ}$

#### Secondary inclusions

Average  $\sim 90^{\circ}(?)$

ANALYST: RJ POTTOFF

# FLUID INCLUSION SKETCHES

CON EDISON

SAMPLE No. FS-3

CHIP No. 2

MINERAL: CALCITE

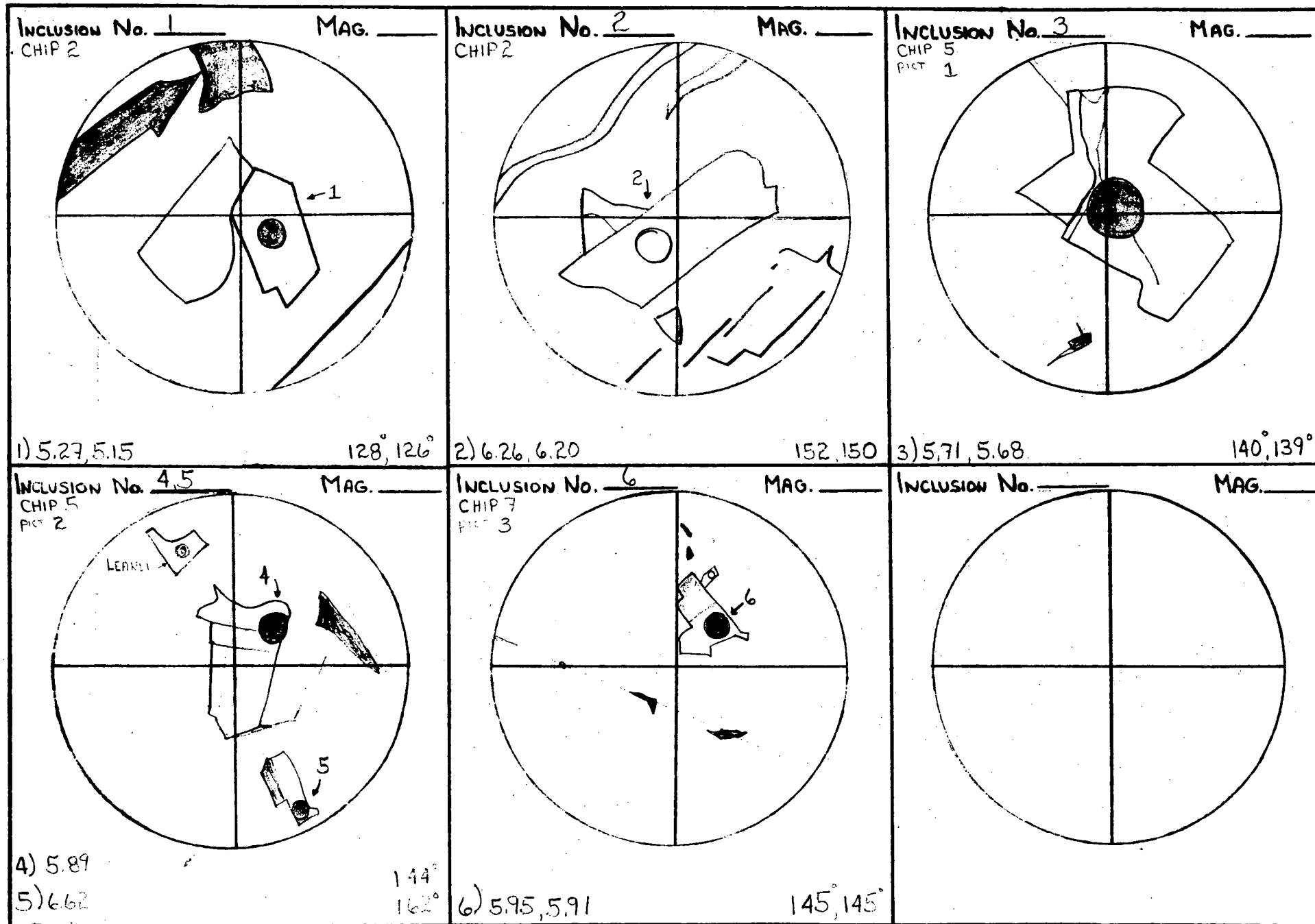


PHOTO 1, FS-3, CHIP 5  
INCLUSION No. 3; SEE  
SKETCH

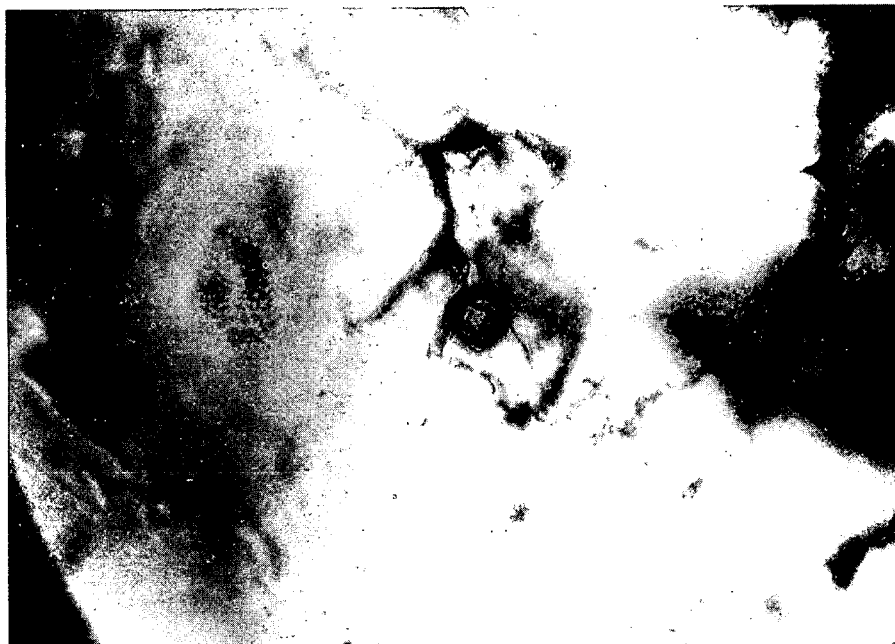
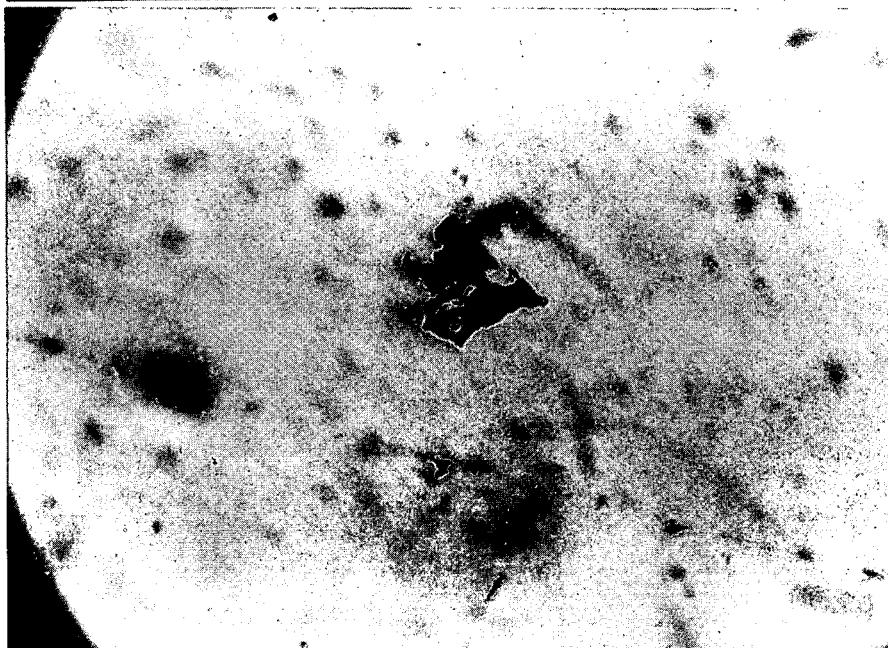


PHOTO 2, FS-3, CHIP 5.  
INCLUSIONS 4 AND 5;  
SEE SKETCH.

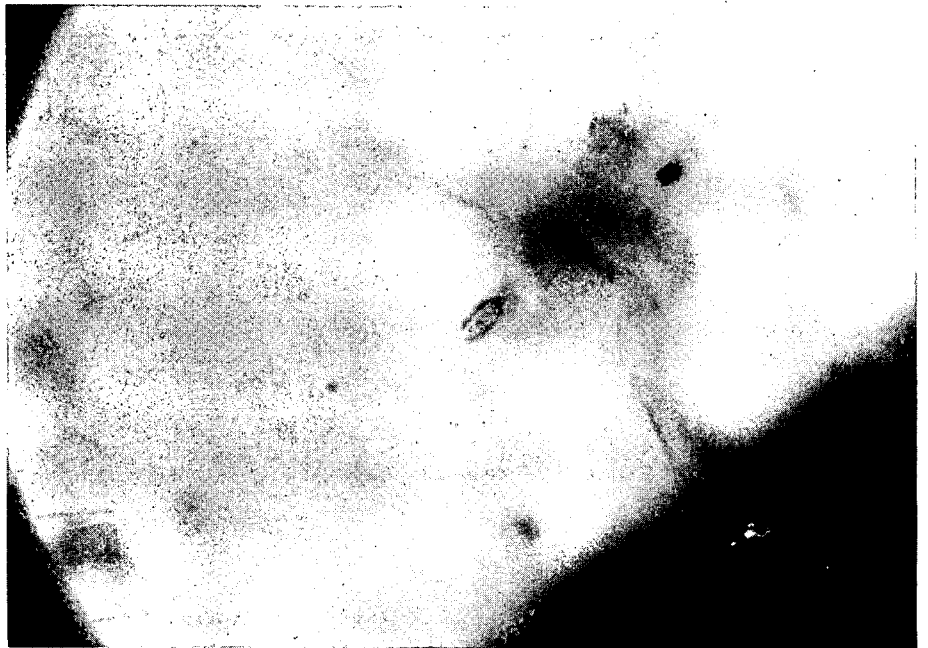


PHOTO 3, FS-3, CHIP 7.  
INCLUSION No. 6; SEE  
SKETCH.





PHOTOS 4,5 AND 6 , FS-3.  
THESE INCLUSIONS LEAKED  
BEFORE AN HOMOGENIZATION  
TEMP. COULD BE REACHED.



Sample FS-4 - Calcite Crystals

Inclusions are very rare in the material sampled. Secondary inclusions are present in elongated stringers parallel to rehealed cleavage planes. No successful temperature measurements were made on these secondaries. Minor sulfides noted.

Only one temperature was obtained for the entire sample (133°). Without further study it is difficult to ascertain the significance of this value.

Average 133° (1)

ANALYST: RJ POTTOFF

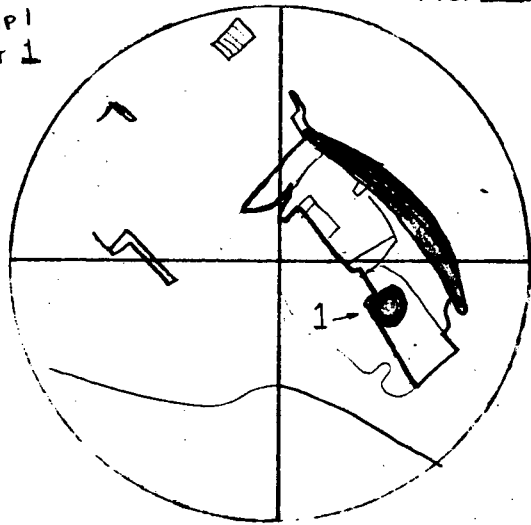
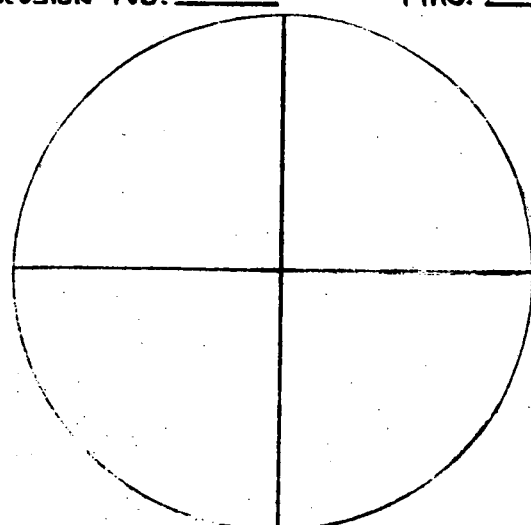
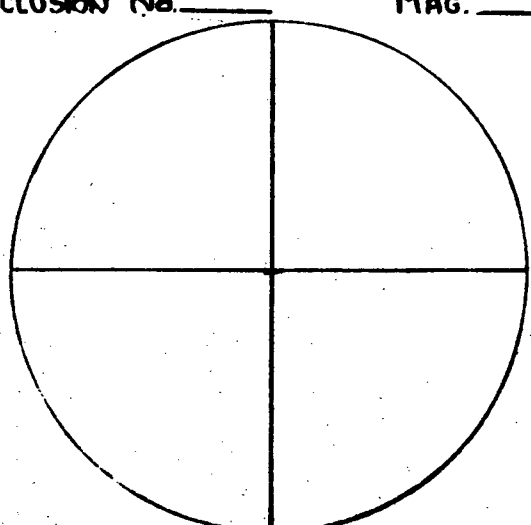
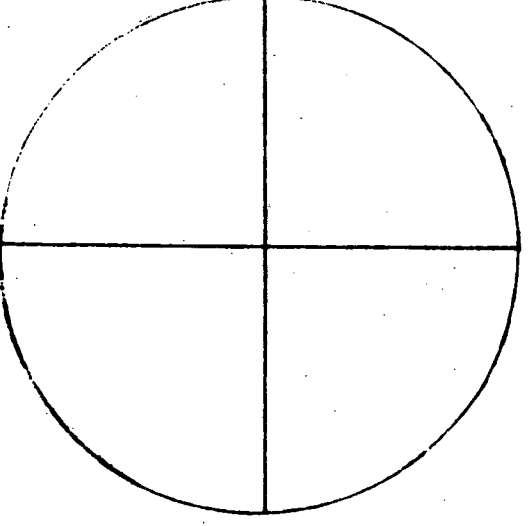
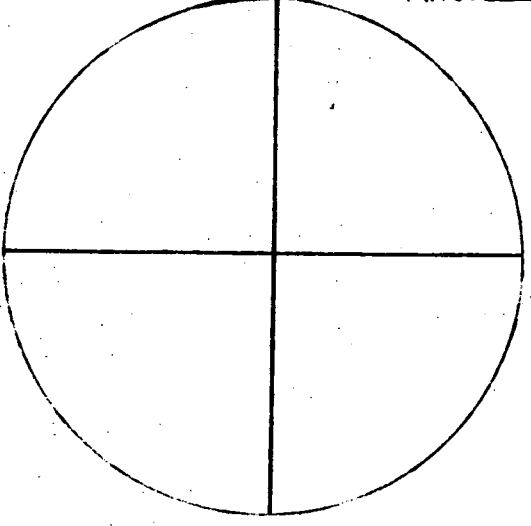
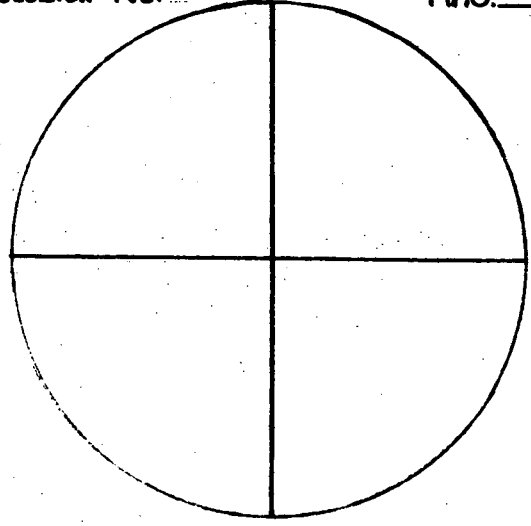
# FLUID INCLUSION SKETCHES

CON EDISON

SAMPLE No. FS4

CHIP No. 1

MINERAL: CALCITE

<p>Inclusion No. <u>1</u> MAG. _____</p> <p>CHIP 1 PICT 1</p>  <p>5.44, LEAKED (SUSPECT) 133°</p>	<p>Inclusion No. _____ MAG. _____</p> 	<p>Inclusion No. _____ MAG. _____</p> 
<p>Inclusion No. _____ MAG. _____</p> 	<p>Inclusion No. _____ MAG. _____</p> 	<p>Inclusion No. _____ MAG. _____</p> 

LEAKS II

PHOTO 1, FS-4, CHIP 1,  
INCLUSION No. 1; SEE  
SKETCH.



PHOTOS 2 AND 3; FS-4;  
EXAMPLES OF INCLUSIONS  
WHICH LEAKED BEFORE  
HOMOGENIZATION.



Sample FS-5



Photo (h) looking east at fault 7 as shown on Plate K-5. This sample of an oxidized breccia zone was collected from close to the jackknife.

#### Sample FS-5 - Calcite Crystals

Many of the larger inclusions exhibit negative crystal shapes (photos 1, 2, 5). Tails and spurs occur on most inclusions and are oriented parallel to cleavage directions (photo 4). Based solely on morphology, it is not obvious that two populations are present; however, homogenization temperatures separate clearly to two populations.

#### Primary inclusions:

Range 125-150°C for 6 inclusions

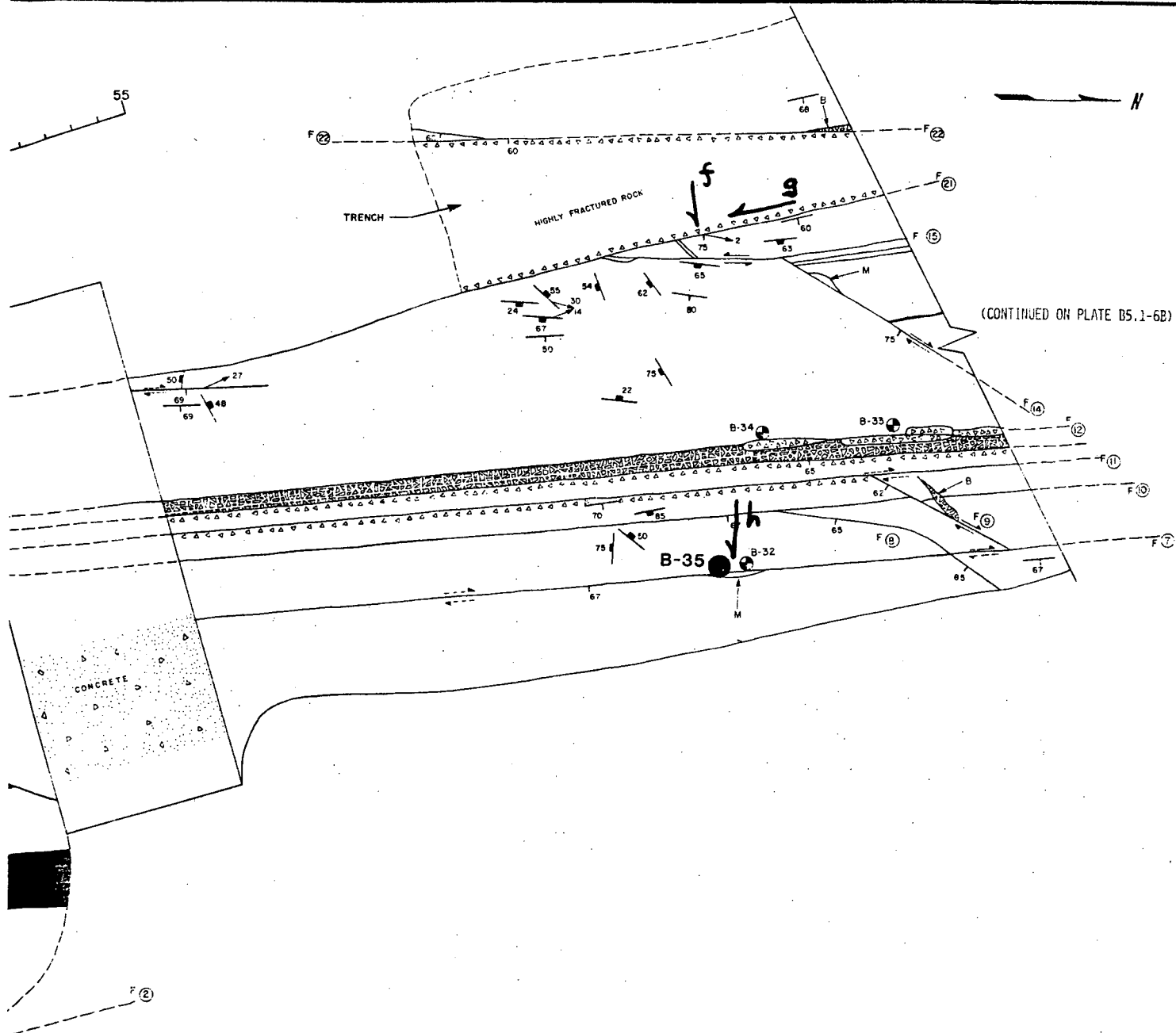
Average 141°C

#### Secondary inclusions:

Range 86-106°C for 3 inclusions

Average 99°C

## Plate K-5



## GEOLOGICAL PLAN

INWOOD MARBLE: OUTCROP NORTH OF REACTOR NUMBER 3

ANALYST: RJ POTTORF

FLUID INCLUSION SKETCHES

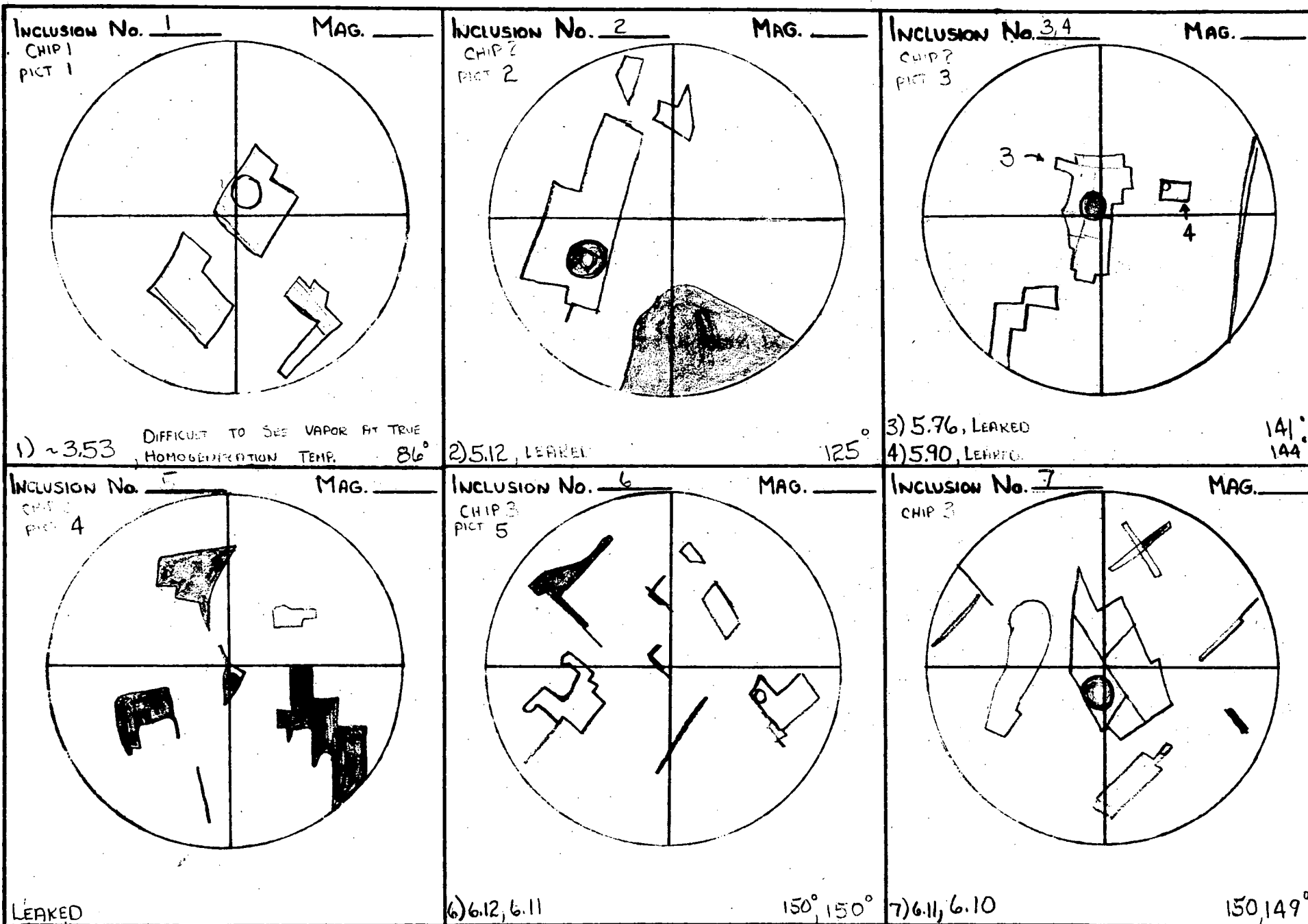
CON EDISON

SAMPLE No. FS5

CHIP No. 1-3

MINERAL: CALCITE

22



22

ANALYST: R.J. POTTOFF

FLUID INCLUSION SKETCHES

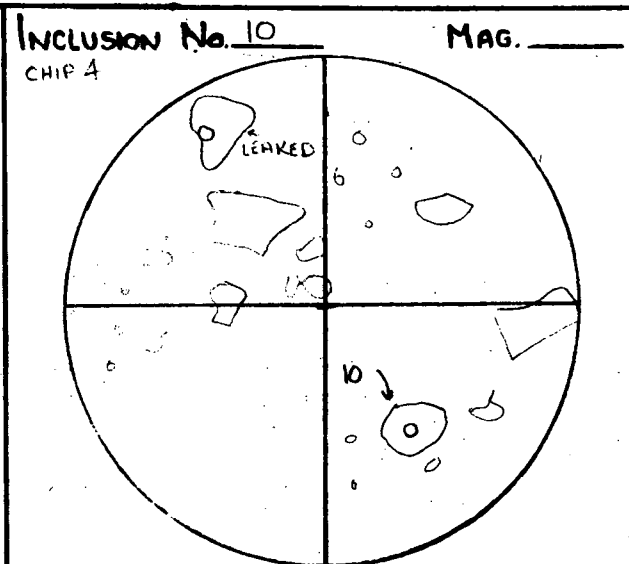
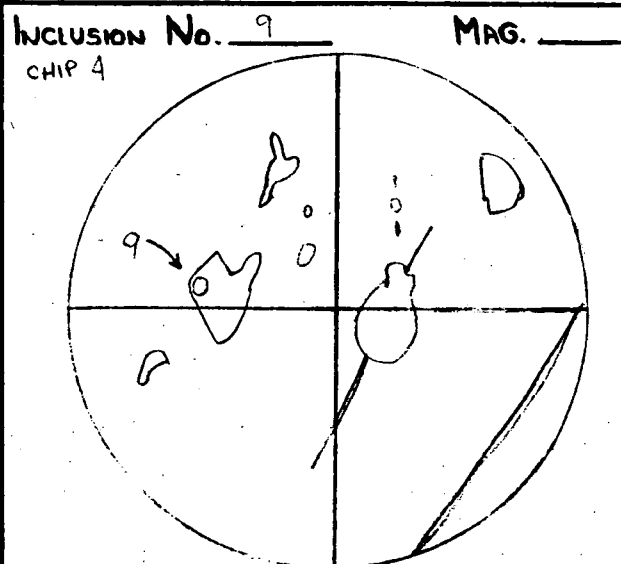
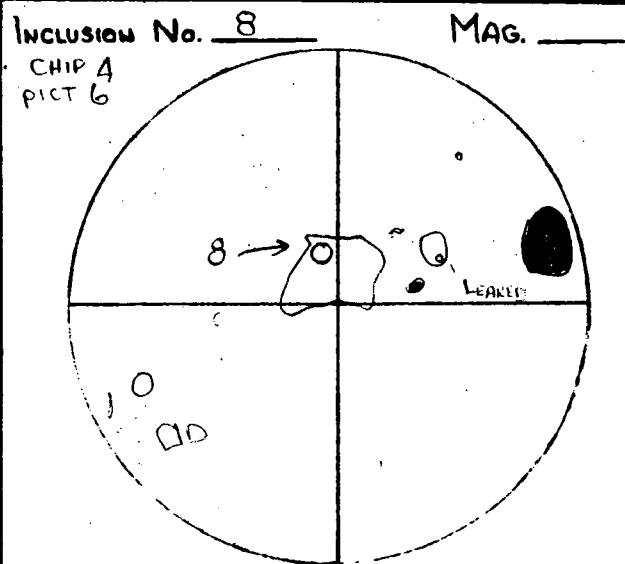
CON EDISON

SAMPLE No. FS5

CHIP No. 4

MINERAL: CALCITE

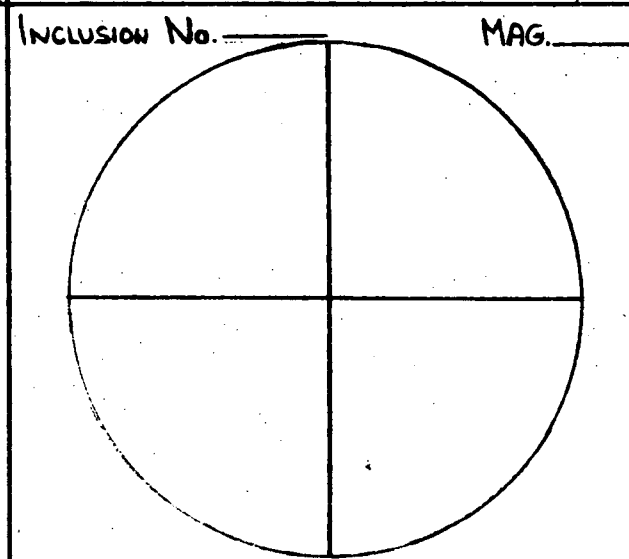
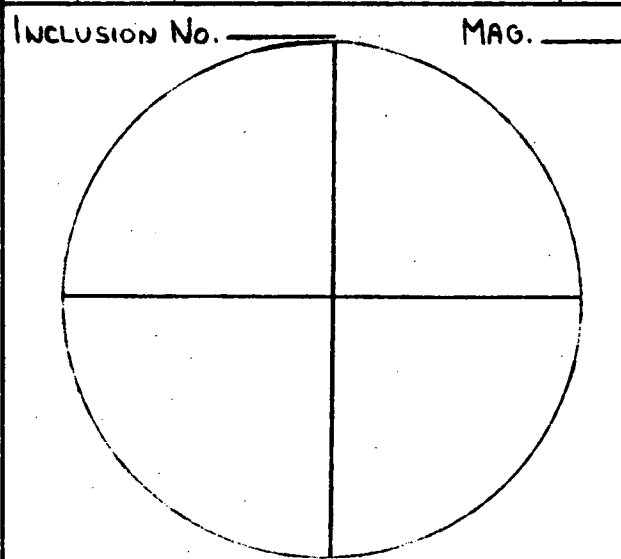
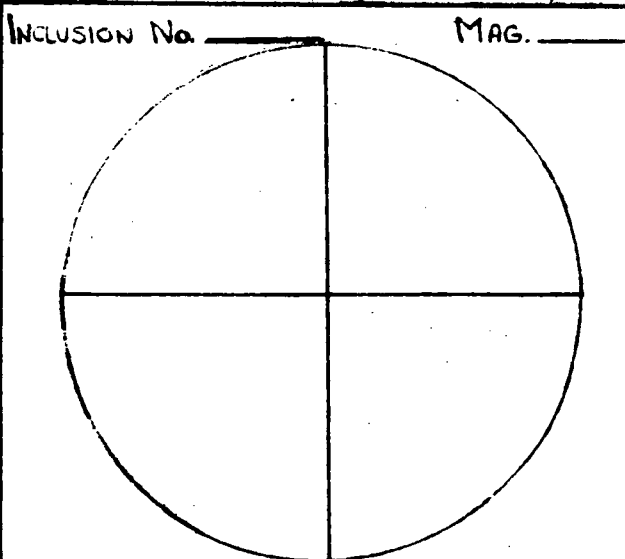
23



5.68, 5.67 139, 138

4.34, 4.36 106, 106

4.29, 4.26 105, 104



23

PHOTO 1, FS-5, CHIP 1,  
INCLUSION No. 1; SEE  
TEXT AND SKETCH. NEGATIVE  
CRYSTAL INCLUSION.



PHOTO 2, FS-5, CHIP 2,  
INCLUSION 2; NEGATIVE  
CRYSTAL INCLUSION; SEE TEXT  
AND SKETCH



PHOTO 3, FS-5, CHIP 2,  
INCLUSION No. 3 (No. 4 NOT  
IN FOCUS); SEE SKETCH.

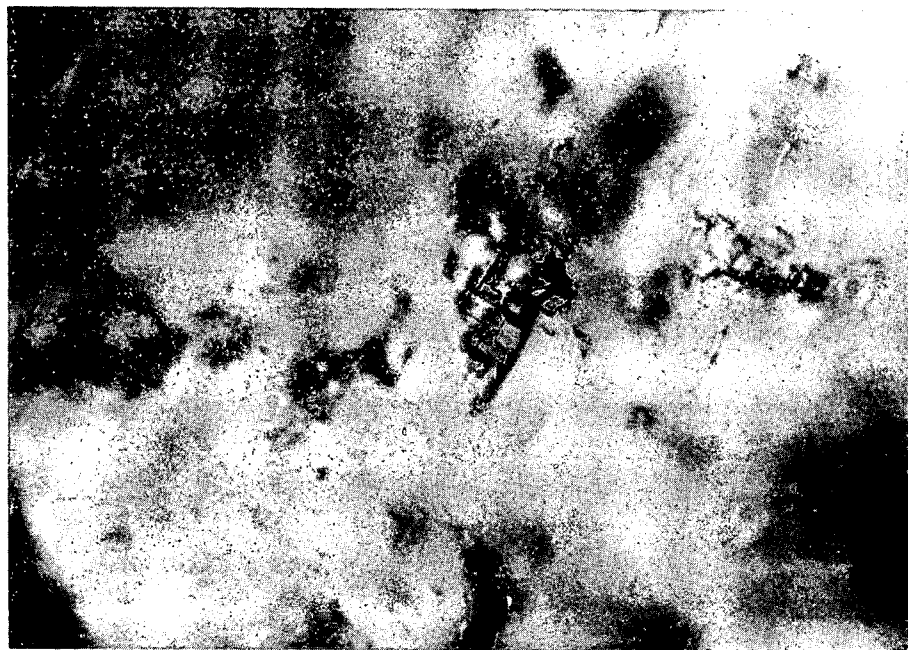


PHOTO 4, FS-5, CHIP 2,  
INCLUSION No. 5; INCLUSIONS  
SHOWING TAILS AND SPURS  
PARALLEL TO CLEAVAGE DIRECTIONS.  
SEE TEXT AND SKETCH.



PHOTO 5, FS-5, CHIP 3,  
INCLUSION No. 6; NEGATIVE  
CRYSTAL INCLUSION; SEE  
TEXT AND SKETCH.

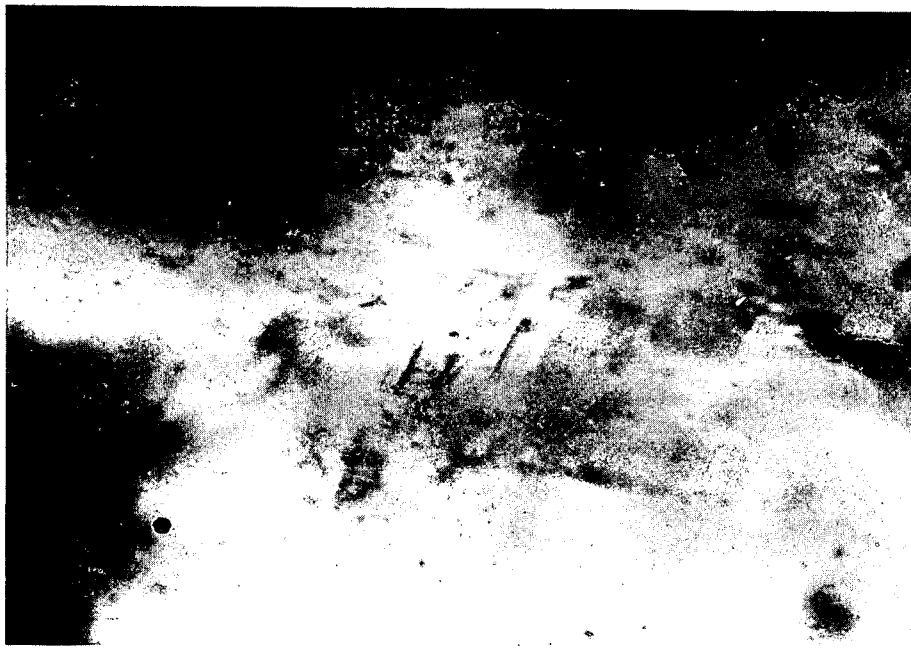


PHOTO 6, FS-5, CHIP 4,  
INCLUSION No. 8; SEE  
SKETCH.



## Sample FS-6 and FS-7



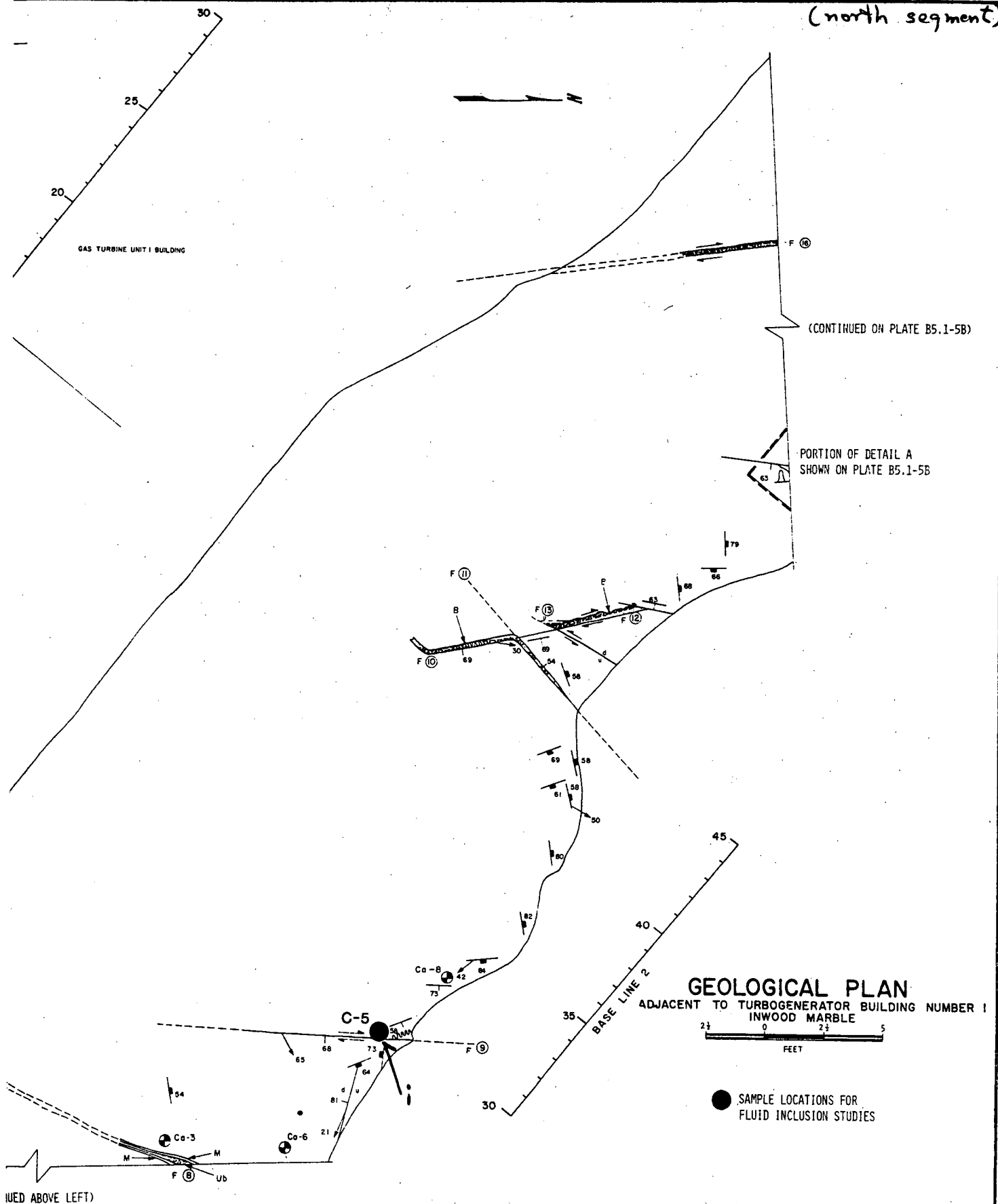
Photo (i) looking west at fault 9 as shown on Plate K-4, north segment. Sample FS-6 was collected about 40 cm to the right of the jackknife and close to the white painted spot just above the nearly horizontal painted black line. The location of sample FS-7 is close to the painted white spot slightly to left of the middle of the photo and 1 cm below its top edge.

## Sample FS-6 - Calcite Crystals

The inclusions are generally stretched and/or exhibit tails parallel to cleavages (photos 3-6). This leads to an extreme leaking problem; of 18 inclusions measured, 13 leaked.

Range 137-172° (5)

Average 145°



ANALYST: RJ POTTORF

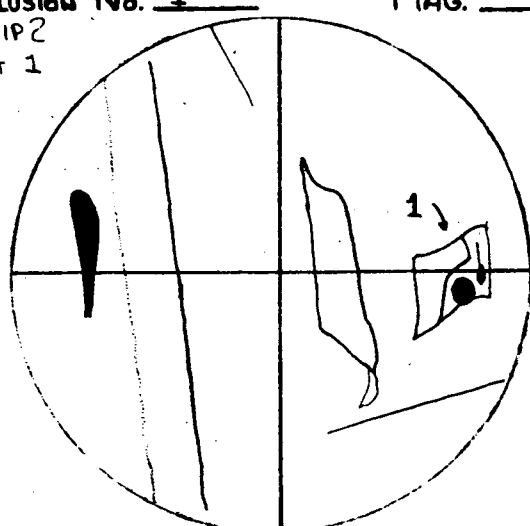
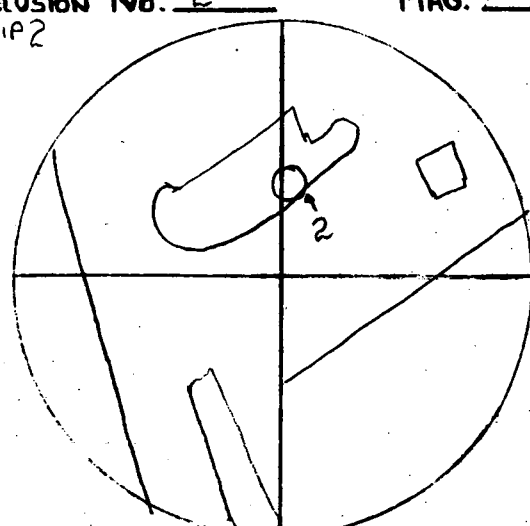
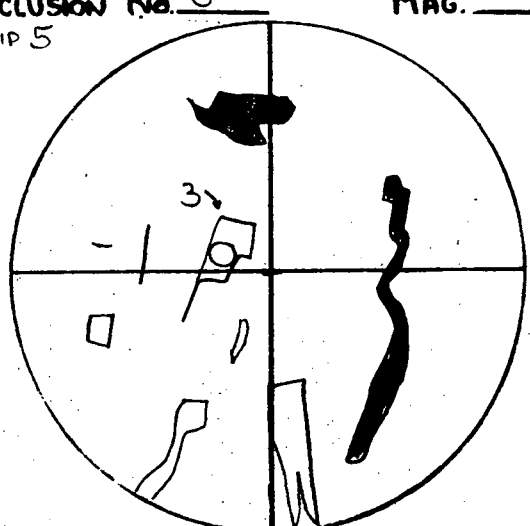
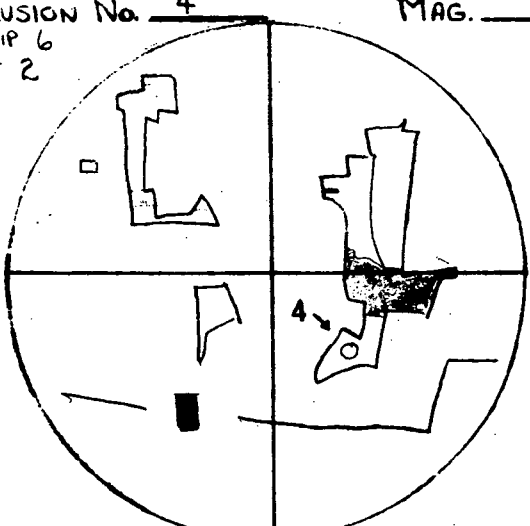
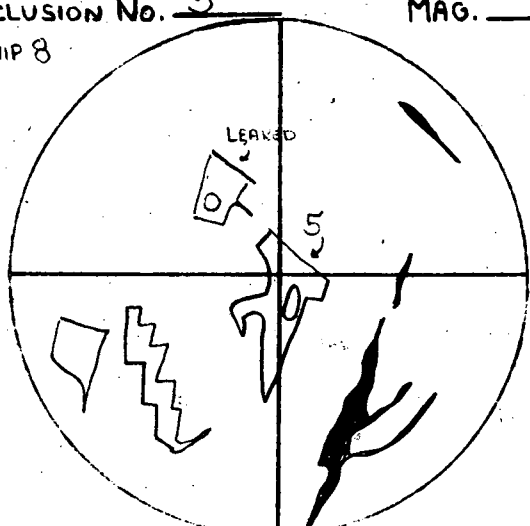
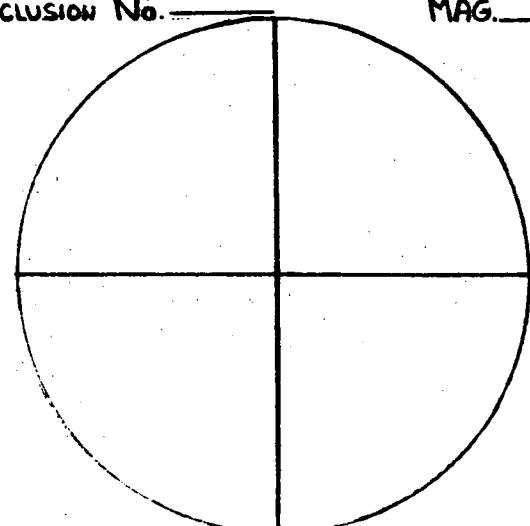
# FLUID INCLUSION SKETCHES

CON EDISON

SAMPLE No. FS 6

CHIP No. 2, 5, 6, 8

MINERAL: CALCITE

<p>Inclusion No. <u>1</u> MAG. _____</p> <p>CHIP 2 PICT 1</p>  <p>15.59, 5.59 137°, 137°</p>	<p>Inclusion No. <u>2</u> MAG. _____</p> <p>CHIP 2</p>  <p>2) 5.52, LEAKED 135°</p>	<p>Inclusion No. <u>3</u> MAG. _____</p> <p>CHIP 5</p>  <p>3) 6.99 172°</p>
<p>Inclusion No. <u>4</u> MAG. _____</p> <p>CHIP 6 PICT 2</p>  <p>4) 25.93, LEAK 145°</p>	<p>Inclusion No. <u>5</u> MAG. _____</p> <p>CHIP 8</p>  <p>LEAKED</p> <p>LEAK? 5.65, 5.95 138°, 145°</p>	<p>Inclusion No. _____ MAG. _____</p> 

● PHOTO 1, FS-6, CHIP 2,  
INCLUSION No. 1; SEE  
SKETCH.

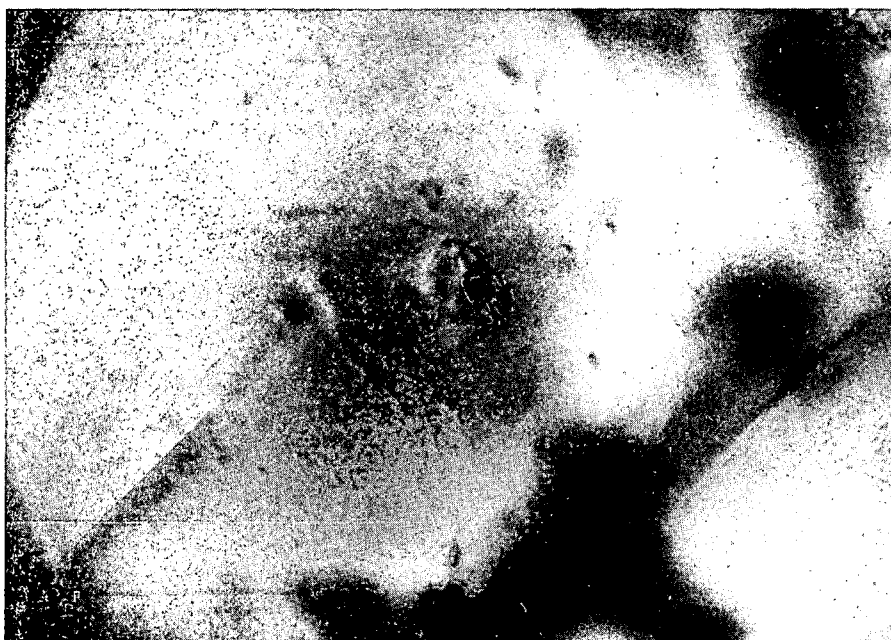


PHOTO 2, FS-6, CHIP 6,  
INCLUSION No. 4; SEE  
● SKETCH.



PHOTO 3, FS-6; PHOTOS 3-6  
ILLUSTRATE INCLUSIONS WHICH  
LEAKED WHEN HEATED. NOTE  
THE CLEAVAGE DIRECTIONS AND  
THEIR EFFECTS ON THE  
INDIVIDUAL INCLUSIONS.

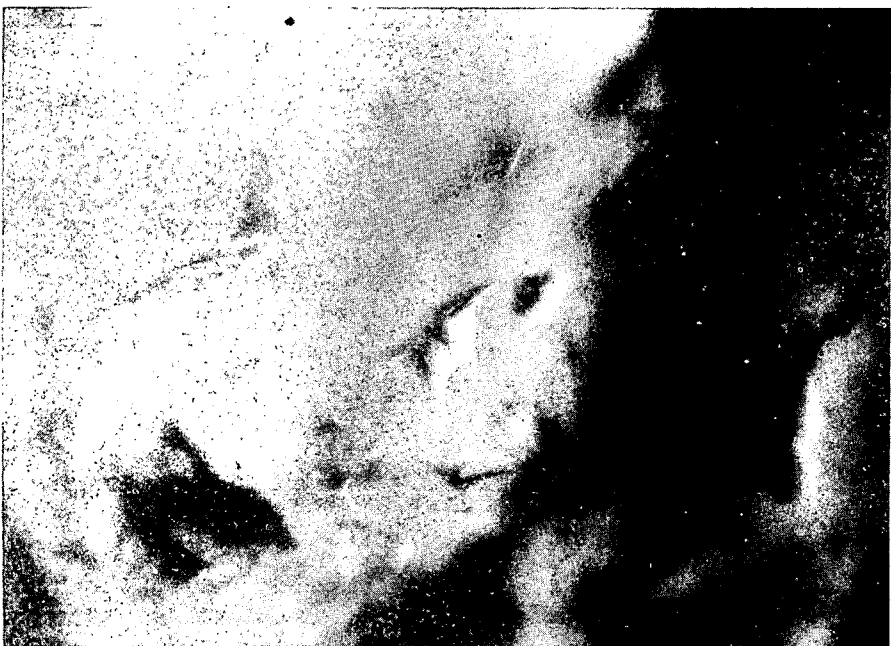


PHOTO 4, FS-6; INCLUSIONS  
ALIGNED PARALLEL TO REHEALED  
CLEAVAGE PLANE.

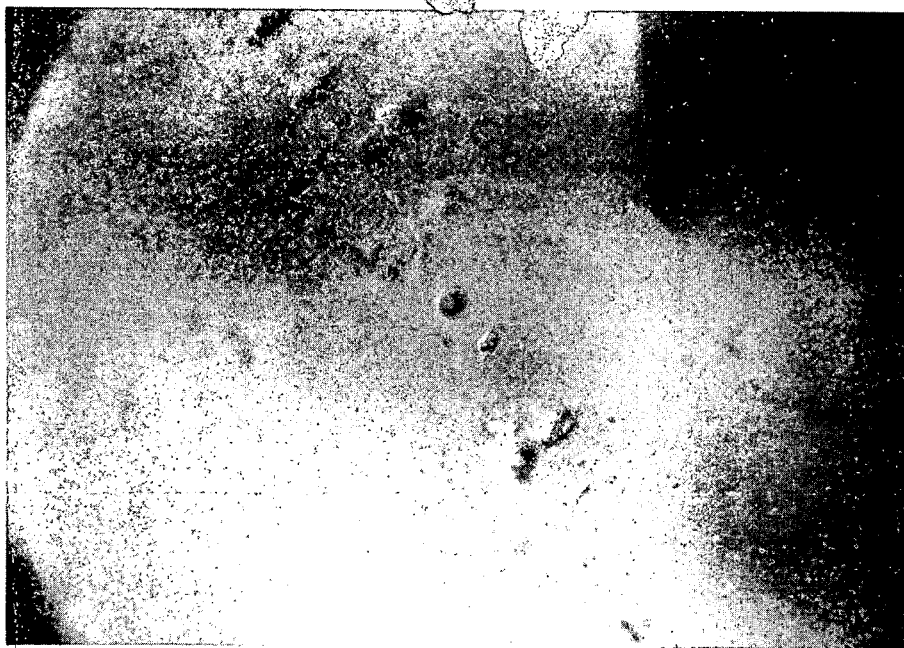


PHOTO 5, FS-6

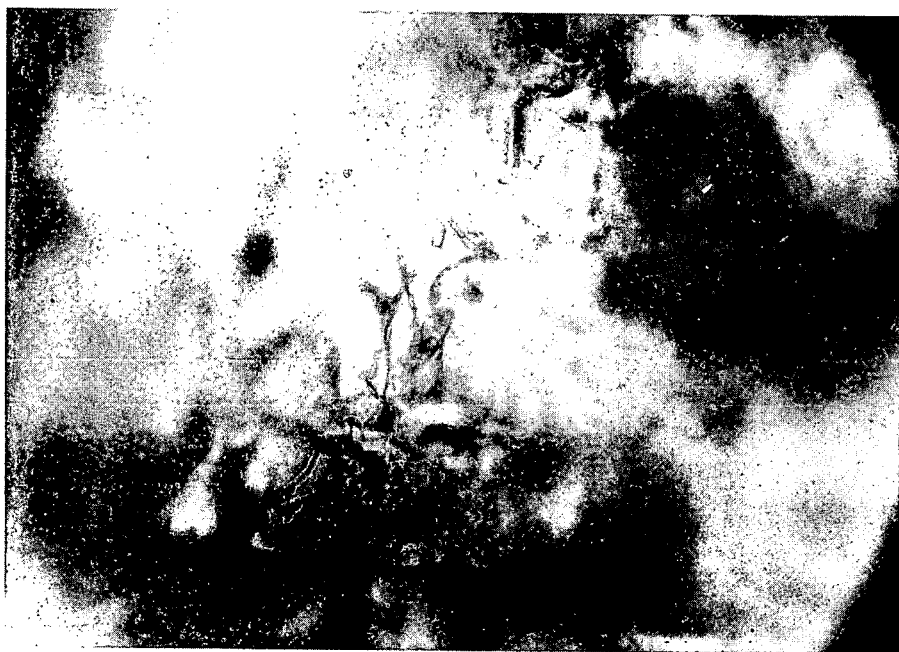
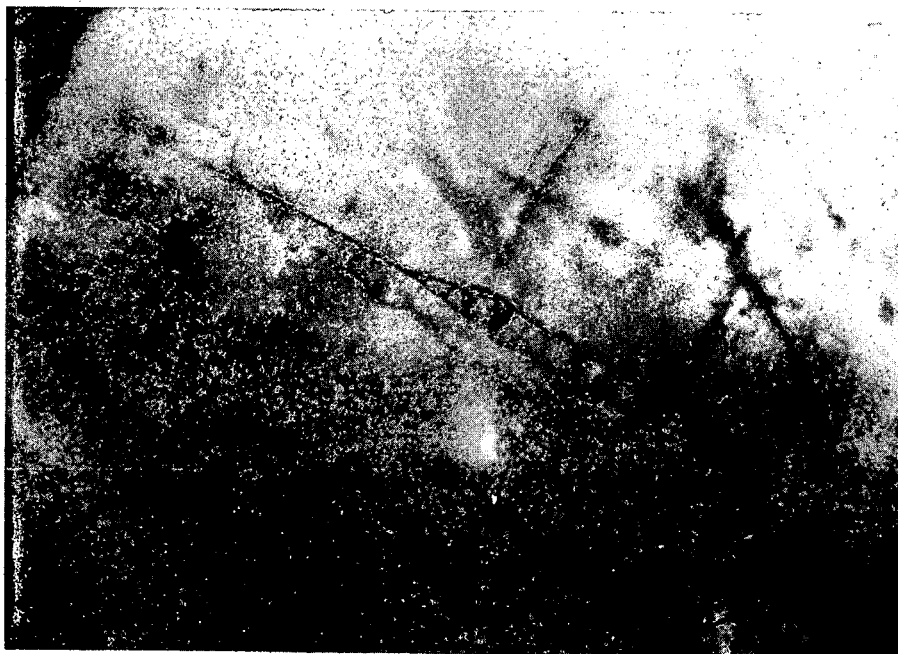


PHOTO 6, FS-6:



Sample FS-7 - Calcite Crystals

Inclusions morphologically could be primary, but give relatively low temperatures. Most inclusions are elongated parallel to cleavage planes and display tails and spurs. Small clusters of secondary inclusions are also present.

Range 95-118° (7)

Average 105°

ANALYST: RJ POTTORF

SAMPLE No. FS7

FLUID INCLUSION SKETCHES

CHIP No. 1,2,3,5,6

CON EDISON

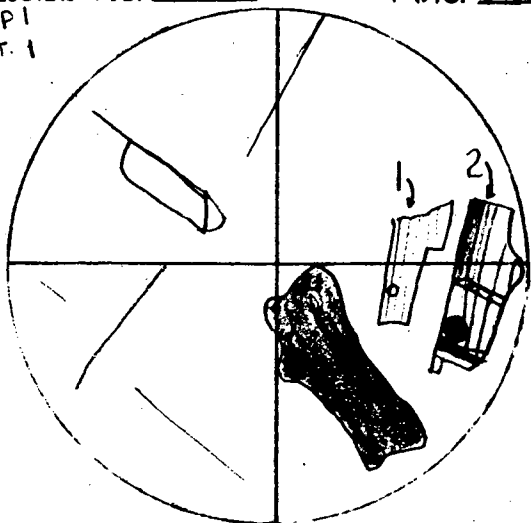
MINERAL: CALCITE

32

Inclusion No. 1,2

MAG. \_\_\_\_\_

CHIP 1  
PICT. 1



1) 3.85 3.91

96°, 96°

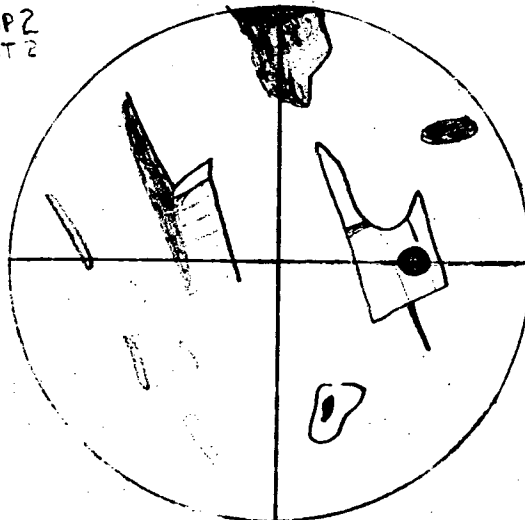
2) 3.89 3.85

95°, 94°

Inclusion No. 3

MAG. \_\_\_\_\_

CHIP 2  
PICT. 2



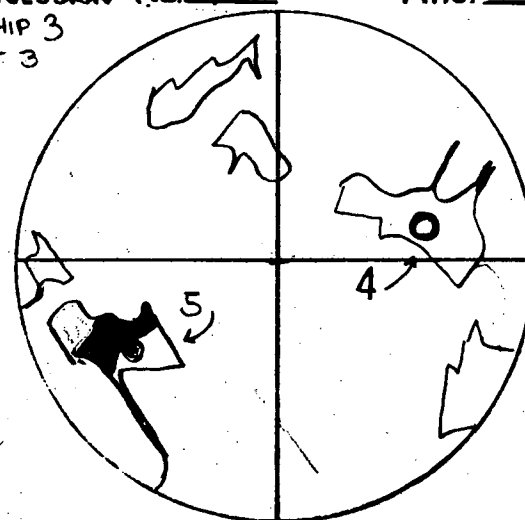
3) 4.85 LEAKED

118°

Inclusion No. 4,5

MAG. \_\_\_\_\_

CHIP 3  
PICT. 3



4) 4.05, 4.11

99, 100

5) ~ 4.60?

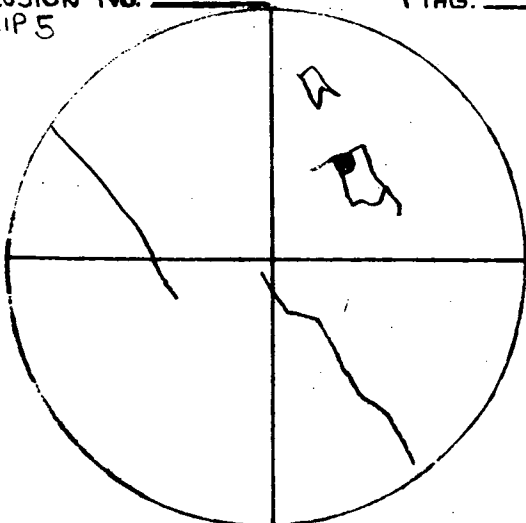
OPTICAL CLARITY

112

Inclusion No. 6

MAG. \_\_\_\_\_

CHIP 5



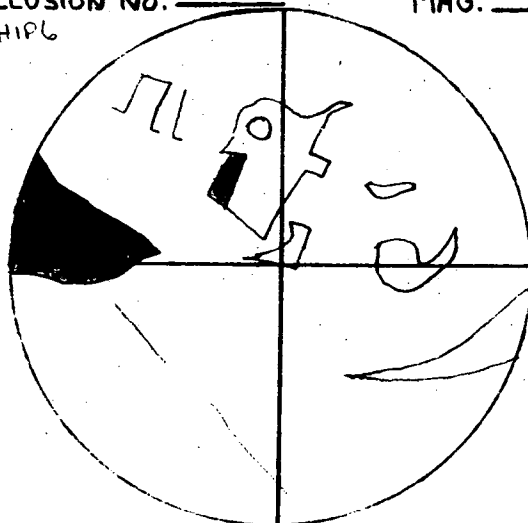
6) 4.28, OPT. CLAR.

104°

Inclusion No. \_\_\_\_\_

MAG. \_\_\_\_\_

CHIP 6

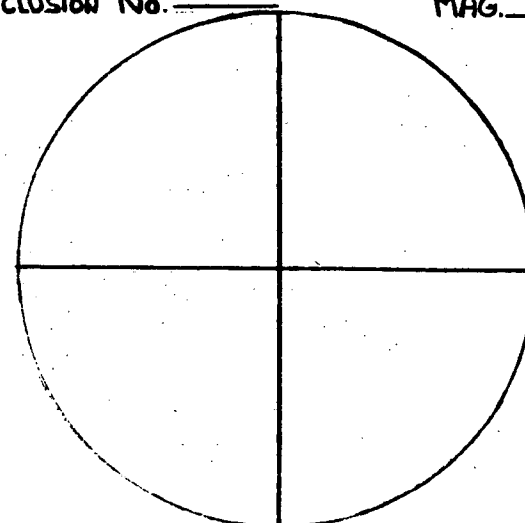


7) 4.56, 4.55

111°, 111°

Inclusion No. \_\_\_\_\_

MAG. \_\_\_\_\_



32

PHOTO 1, FS-7, CHIP 1  
INCLUSION 1; NEGATIVE  
CRYSTAL; SEE SKETCH.



PHOTO 2, FS-7, CHIP 2  
INCLUSION No. 3; SEE  
SKETCH.

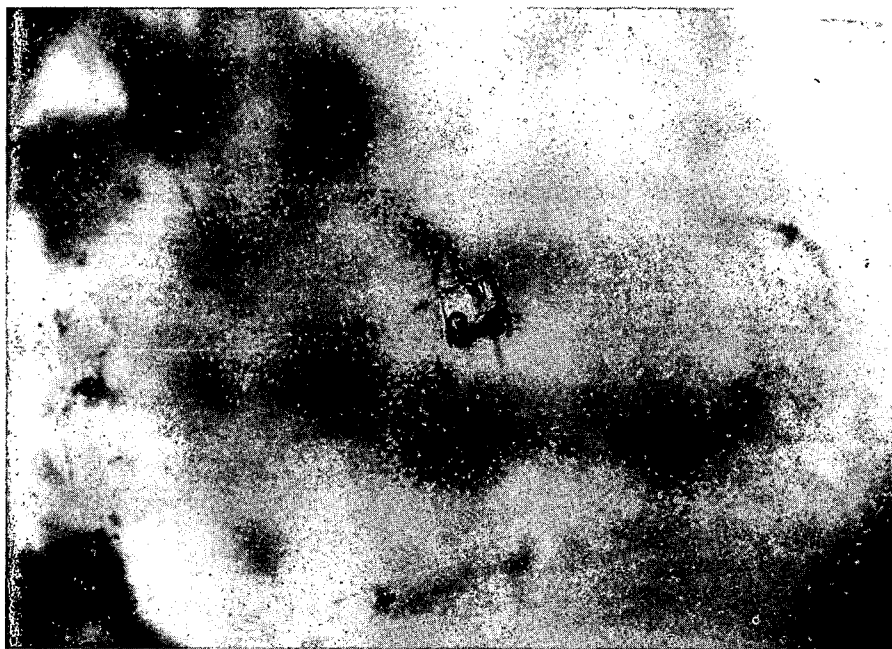


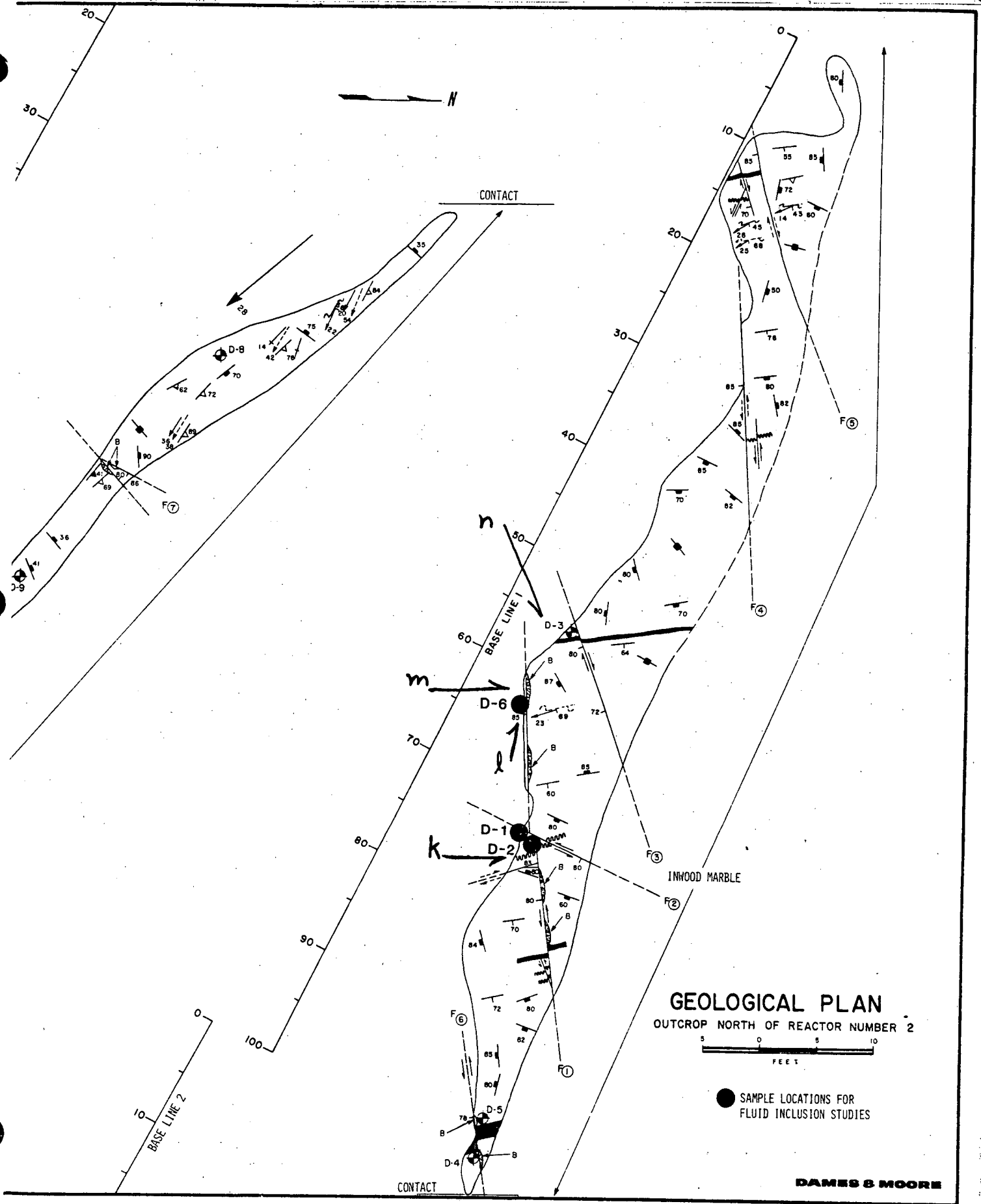
PHOTO 3, FS-7, CHIP 3  
INCLUSION No. 4, SEE  
SKETCH.



## Sample FS-8 and FS-9



Photo (k) looking north at the intersection of faults 1 and 2 as shown on Plate K-3. Sample FS-8 at the painted white spot in the lower center of the photo. Sample FS-9 was collected from within the fault just to the left of the pen in the upper center of the photo.



GEOLOGICAL PLAN  
OUTCROP NORTH OF REACTOR NUMBER 2

● SAMPLE LOCATIONS FOR  
FLUID INCLUSION STUDIES

DAMES & MOORE

### Sample FS-8 - Calcite Crystals

Although several different populations may be present, most inclusions exhibit numerous spurs and tails, and leakage is very common. 24 inclusions were heated and 18 leaked. Sulfides (generally euhedral pyrite) are commonly found in linear arrays which appear to follow cleavage. Secondary inclusions are extremely abundant along healed cleavage planes.

On the basis of inclusion morphology and liquid/vapor ratios four tentative populations are suggested:

- 1) A very high temperature population consisting of inclusions with "rounded" shapes and very high vapor/liquid ratios (see inclusion 6). This population was observed but not common. Homogenization temperatures obtained on 6 inclusions gave about 317°. These samples decrepitated at about 250°C.
- 2) This population appears to be moderately common but the inclusions invariably leak when heated (e.g., see inclusion 1). Based on the "behavior" of inclusions during heating before leakage, and on the approximate temperature of inclusion number one (189°), filling temperatures are estimated to be about 175-200°.
- 3) Population of inclusions found in clusters and linear arrays, such as cleavage planes. Nearly all of these inclusions are totally fluid-filled and thought to be secondary (see photo 3). In many of these clusters, one or two examples of inclusions with two phases can be found (e.g., inclusions 2, 3,4,5; (see sketches and photos 1 and 2). While these

inclusions give similar homogenization temperature, it is not known whether this temperature is significant or simply represents inclusions which leaked fluid at some time resulting in vapor + fluid-filled inclusions.

- 4) Population consisting of groups of small negative crystals and irregular shaped inclusions which are low temperature and secondary (e.g., inclusion 7, see sketch and photo 4).

Population 1 (?)

~300°

1  
(8)

Population 2 (?)

Range ~175-200° (1+)

Population 3

Range 132-143° (4)

Average 137°

Secondary inclusions

Average 94° (1)

ANALYST: RJ POTTORF

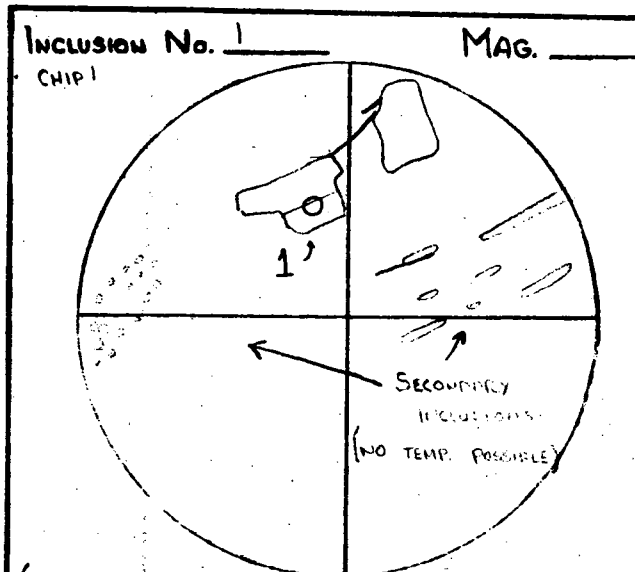
SAMPLE No. FS8

# FLUID INCLUSION SKETCHES

CHIP No. 1,3,4,5

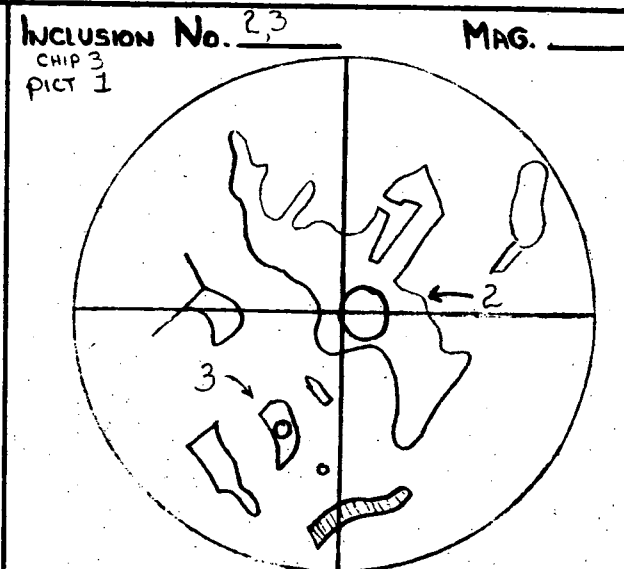
CON EDISON

MINERAL: CALCITE



(189° IS A MAXIMUM BECAUSE OF LEAKAGE)

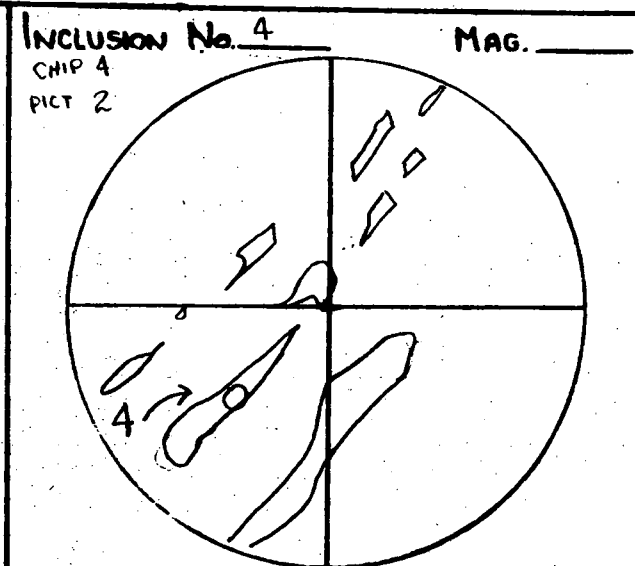
1) 7.70, 8.10 (POSSIBLE LEAK) 489°, 199°



2) ~5.39, LEAKED

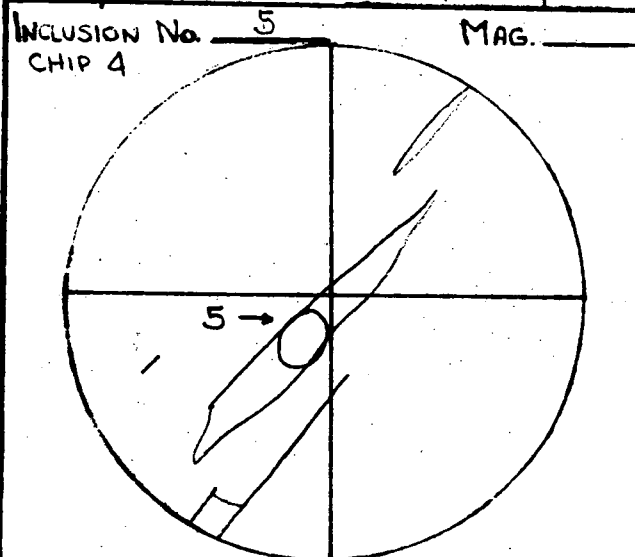
3) ~5.85, LEAKED

132°  
143°



4) 5.47, LEAK

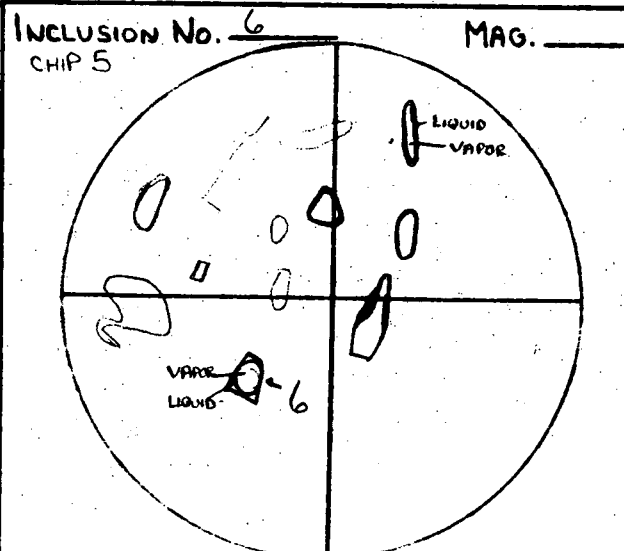
134°



ALONG THE CLEAVAGE(?) PLANE AS NO. 4

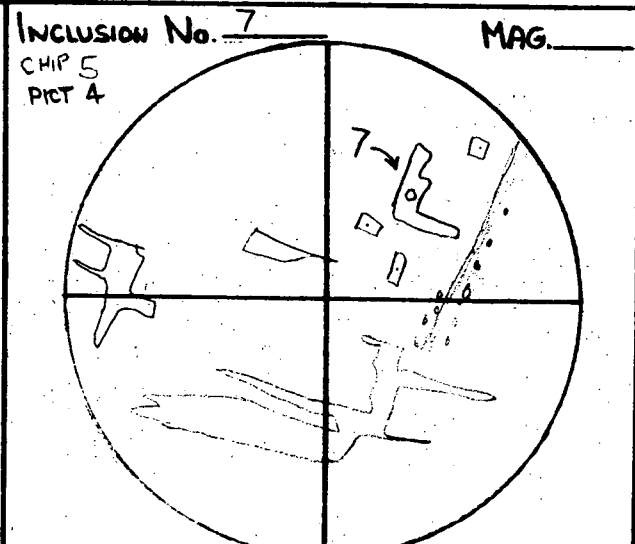
5) 5.60, 5.59

137°



DECEPITATED AT 347°

6) HOMOGENIZED AT 317° (?) [DIFFICULT TO DETERMINE HOMOGENIZATION POINT]



OTHER SMALL INCLUSIONS SURROUNDING # 7 TEND TO SUPPORT THESE NUMBERS, ALTHOUGH THE HOMO. TEMP. COULD NOT BE MEASURED

7) 3.75, 3.92

92°, 96°

PHOTO 1. FS-8, CHIP 3  
INCLUSION No. 2; SEE  
TEXT AND SKETCH.

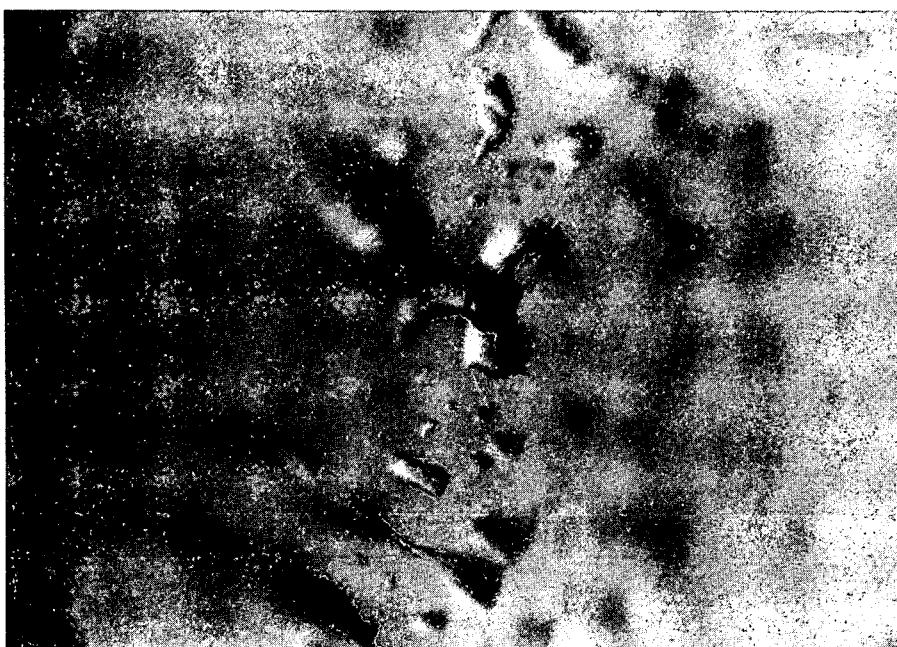


PHOTO 2. FS-8, CHIP 4,  
INCLUSION No. 4, SEE  
TEXT AND SKETCH.

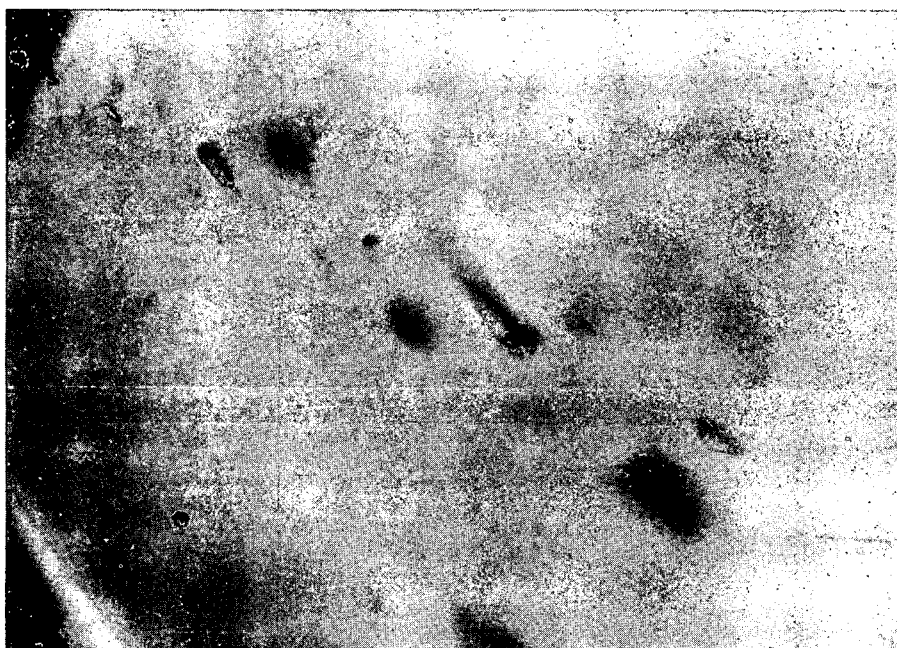
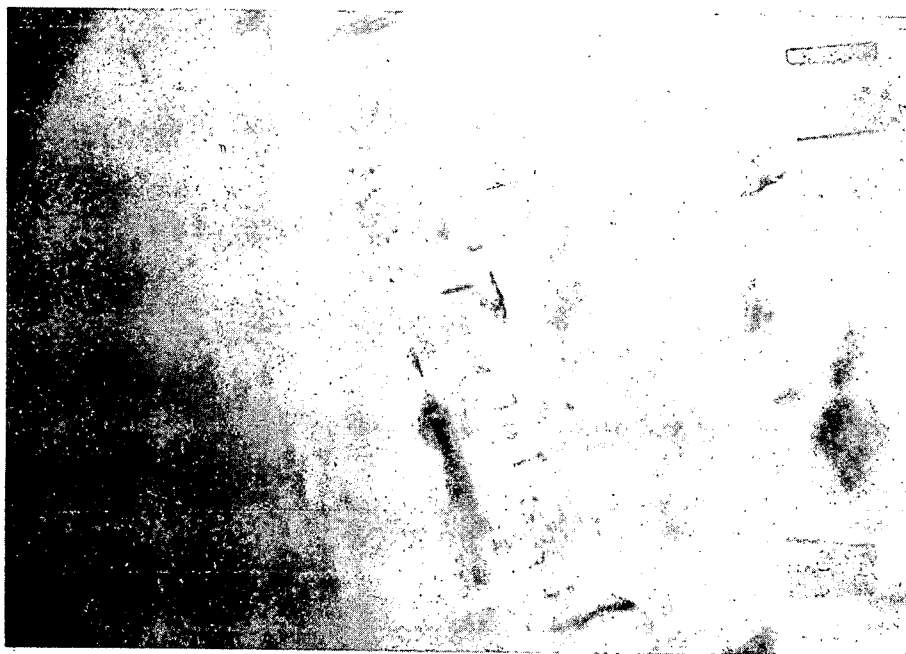


PHOTO 3. FS-8, CHIP 5  
POPULATION OF TOTALLY  
FLUID-FILLED INCLUSIONS;  
SEE TEXT.



PHOTO 4. FS-8, CHIP 5,  
INCLUSION No. 7; SECONDARY  
INCLUSIONS. SEE TEXT  
AND SKETCH.



### Sample FS-9 - Calcite Crystals

This sample appears to have a complicated history which is further obscured by large numbers of visible and rehealed fractures. Of 25 inclusions heated, 13 leaked; Sulfides generally present in linear arrays. Appearance is similar to FS-8.

There is some evidence for a very high temperature population ( $\sim 300^\circ$ ). Some inclusions don't homogenize at very high temperatures and vapor/fluid ratios don't increase when brought to room temperature ( $\text{CO}_2$  filled?). Inclusion number 6 gave  $327^\circ$ , but is probably necked.

On the basis of temperature (not morphology), two other populations are proposed, averaging  $190^\circ$  and  $132^\circ$ . It is possible that the  $190^\circ$  population is primary while the  $132^\circ$  population is pseudo-secondary.

Small secondary inclusions are present along rehealed cleavages or in "curved" arrays. These display tails parallel to cleavage. Four inclusions were heated but all leaked. Temperatures are probably  $\leq 100^\circ$ .

Population 1 (?)

Average  $\sim 300^\circ$  (1+)

Population 2 (Primary (?) inclusions)

Range  $168-208^\circ$  for 6 inclusions

Average  $190^\circ\text{C}$

Population 3 (Pseudo-secondary (?) inclusions)

Range  $127-139^\circ$  (4)

Average  $132^\circ$

Population 4 (Secondary inclusions)

Range probably  $\leq 100^\circ$

SAMPLE No. FS 9

CHIP No. 1, 2, 3, 5, 6

MINERAL: CALCITE

42

2) ~5.20, LEAK

3) LEAK

PROBABLY NECKED GIVING ANOMALOUSLY  
HIGH TEMPERATURE; DISCARD  
13.32, 13.27

8.48, LEAKED 208°

5.40 5.30 132.129°

42

ANALYST: RJ POTTORF

# FLUID INCLUSION SKETCHES

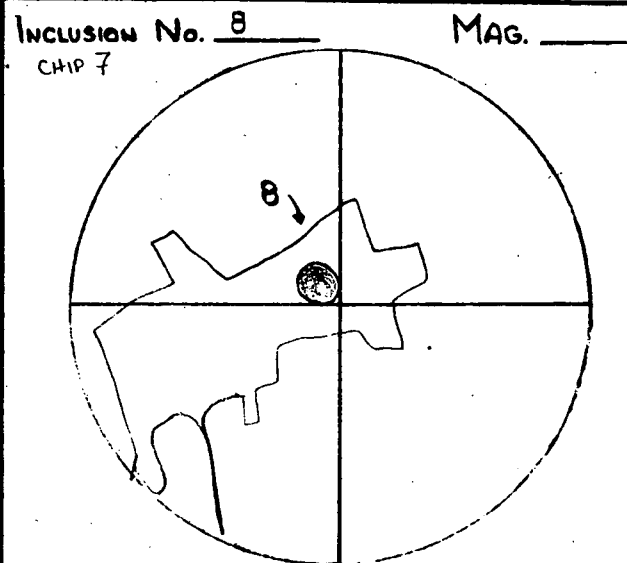
CON EDISON

SAMPLE No. FS9

CHIP No. 7-10

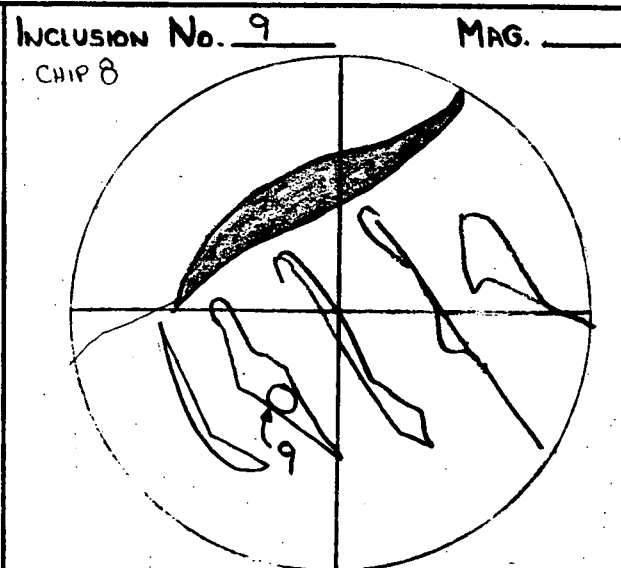
MINERAL: CALCITE

57



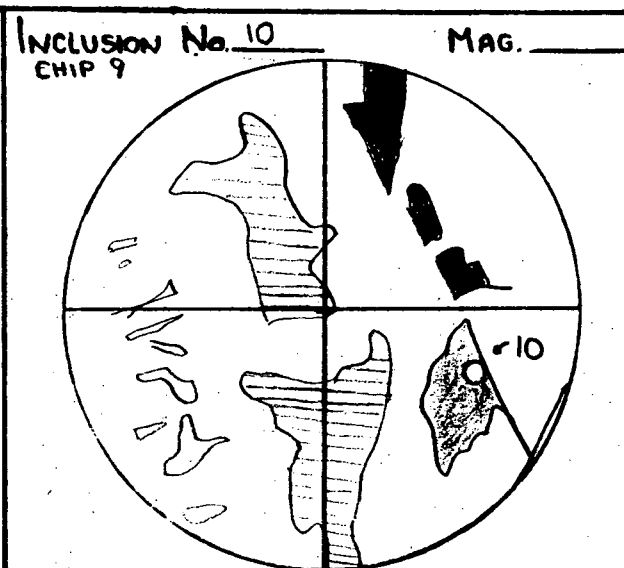
HOMOG. ~7.50 - 184°

8) LEAKED AT 179° VERY NEAR HOMOGENIZATION



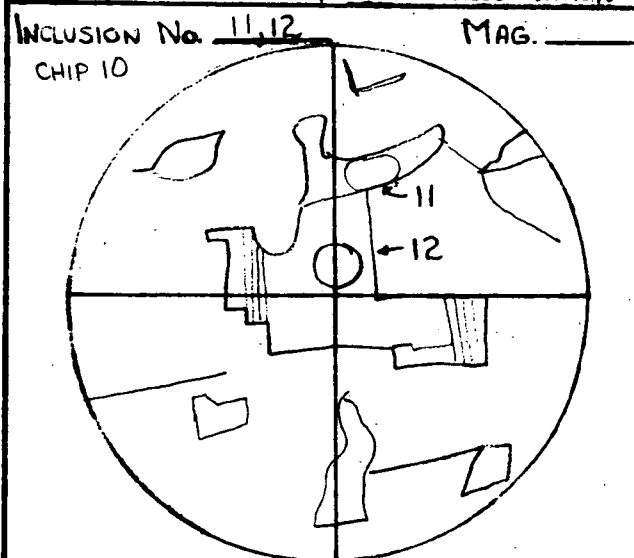
9) 5.70, 5.71

139°, 139°



10) ~8.30, LEAKED

~204°

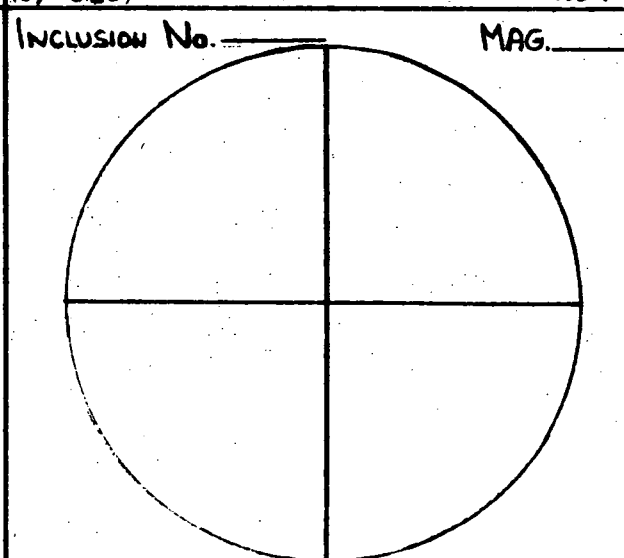
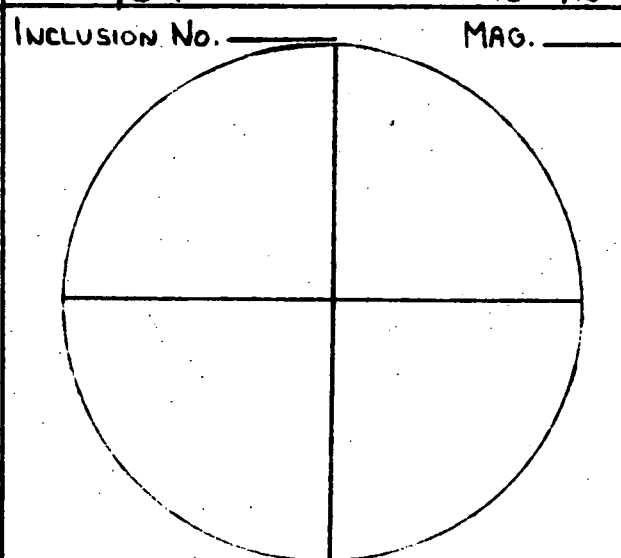


11) 7.26, LEAK

178°

12) 6.85, 6.85

168°, 168°



43

174

PHOTO 1, FS-9, CHIP 1  
INCLUSION 1 ; SEE TEXT  
AND SKETCH.



PHOTO 2, FS-9, CHIP 2  
INCLUSION 4 ; SEE TEXT  
AND SKETCH

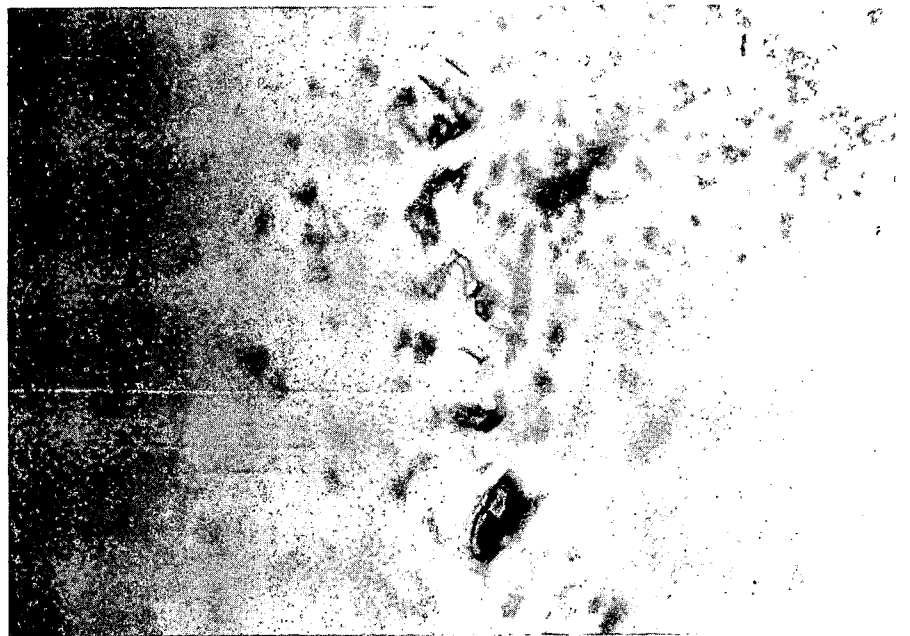


PHOTO 3, FS-9, CHIP 2;  
SAME AREA AS PHOTO 2,  
DIFFERENT DEPTH OF FOCUS.

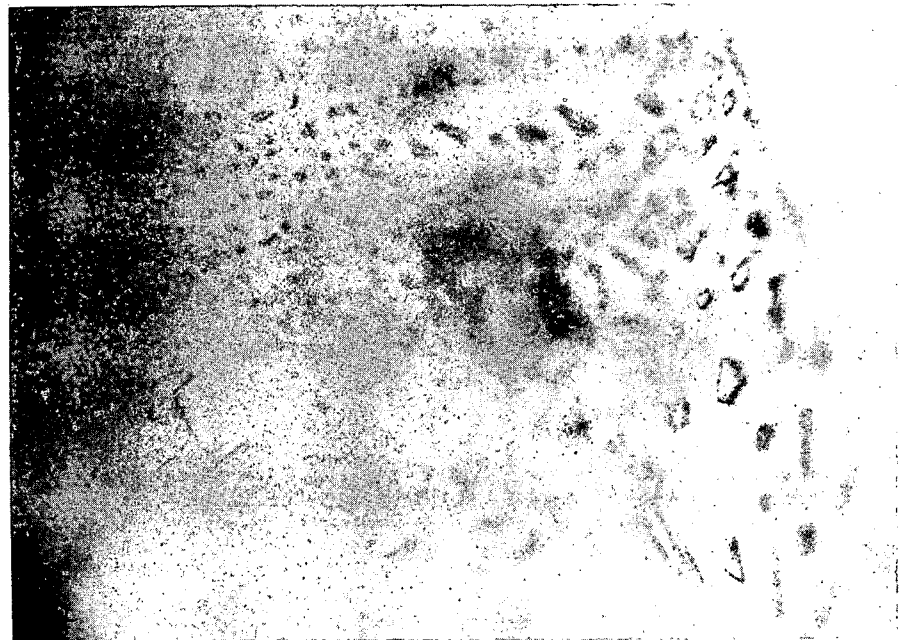
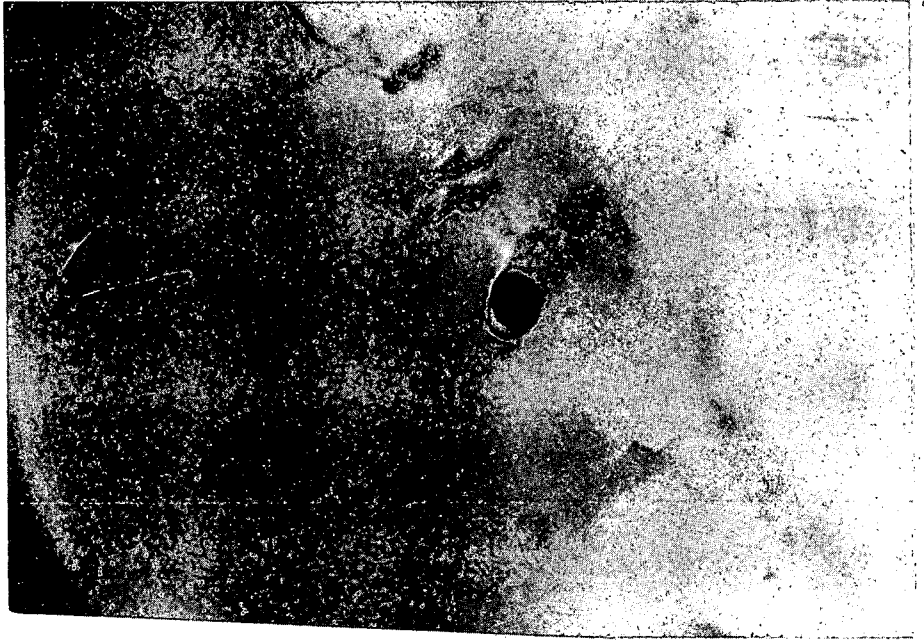


PHOTO 4, FS-9, CHIP 3,  
INCLUSION No. 5; SEE SKETCH  
AND TEXT.



## Sample FS-10



Photo (1), left, looking west along fault 1 as shown on Plate K-3.

Photo (m), below, showing the collection of sample FS-10 by removing block containing calcite crystals on surface within the plane of fault 1.

(See also the photo of the location of FS-13).



### Sample FS-10 - Calcite Crystals

Inclusions are relatively abundant and display spurs and tails parallel to the cleavage planes. Euhedral opaque minerals, mostly pyrite, and small solid inclusions are also abundant. Very small solid inclusions are also abundant. Very small secondary inclusions are present but not abundant and are too small for resolving homogenization temperatures.

As shown on the following frequency plot, there are clearly three populations present.

#### Population 1

Range 191-220°C for 3 inclusions

Average 205°C

#### Population 2

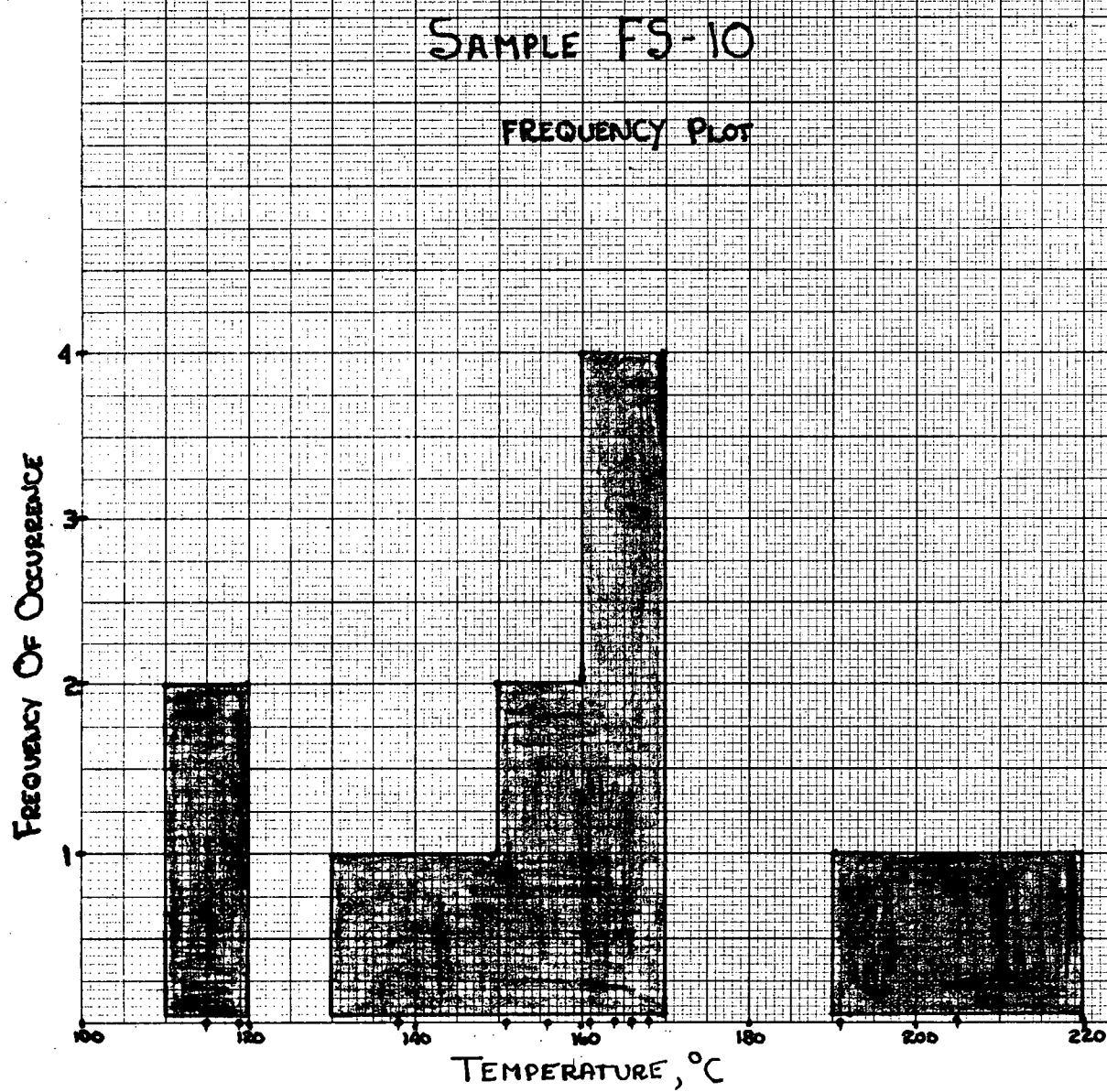
Range 138-168°C for 8 inclusions

Average 156°C

#### Population 3 (Secondary)

Range 115-119°C for 2 inclusions

Average 117°C



ANALYST: RJ POTTORF

SAMPLE No. FS 10

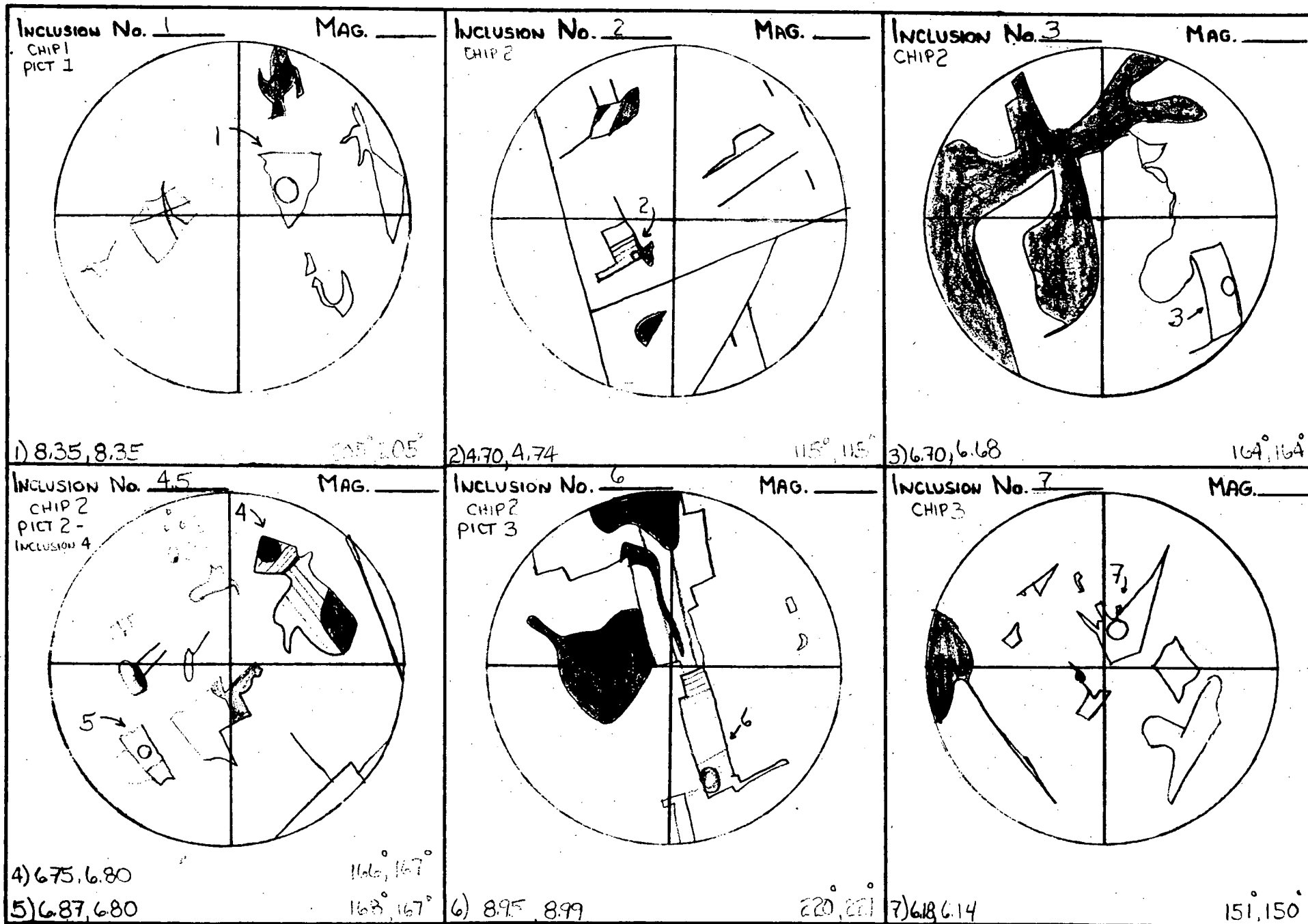
FLUID INCLUSION SKETCHES

CHIP No. 1-3

CON EDISON

MINERAL: CALCITE

64



49

ANALYST: RJ POTTORF

SAMPLE No. FS 10

FLUID INCLUSION SKETCHES

CHIP No. 3-7

CON EDISON

MINERAL: CALCITE

Inclusion No. <u>8</u> CHIP 3	MAG. _____	Inclusion No. <u>9</u> CHIP 4	MAG. _____	Inclusion No. <u>10</u> CHIP 5	MAG. _____
8) 6.57, 6.63 161°, 162°		9) 5.64, 5.54 138°, 135°		10) 7.77 LEAK 191°	
Inclusion No. <u>11</u> CHIP 6 PICT 4	MAG. _____	Inclusion No. <u>12, 13</u> CHIP 7 PICT 5	MAG. _____	Inclusion No. _____	MAG. _____
11) 5.75, 5.70 140°, 139°		12) 4.88 LEAK 119° 13) 6.37, 6.38 156°, 156°			

51

PHOTO 1, FS-10, CHIP 1  
INCLUSION 1; SEE SKETCH.



PHOTO 2, FS-10, CHIP 2  
INCLUSION 4; SEE SKETCH

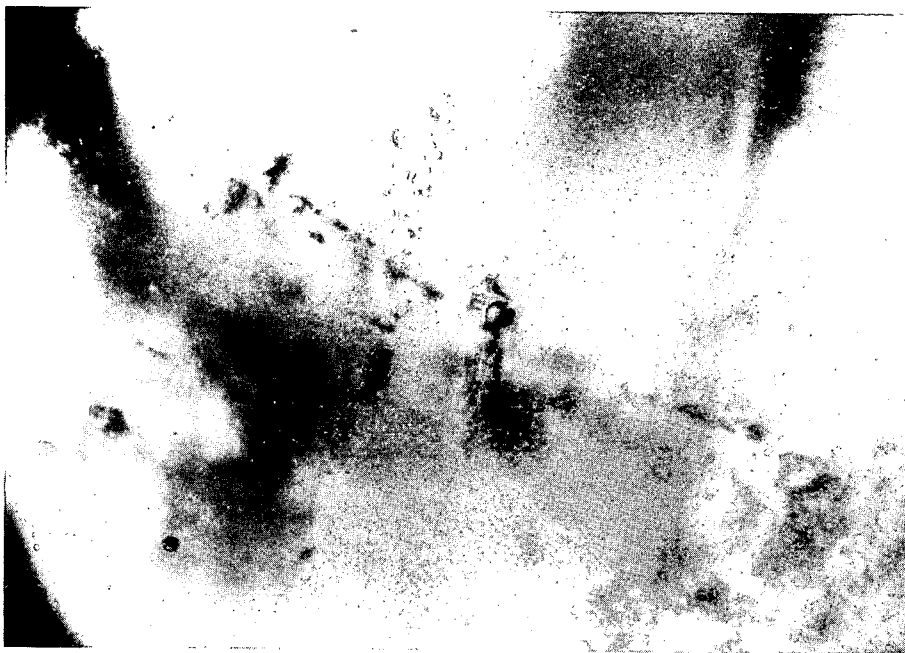


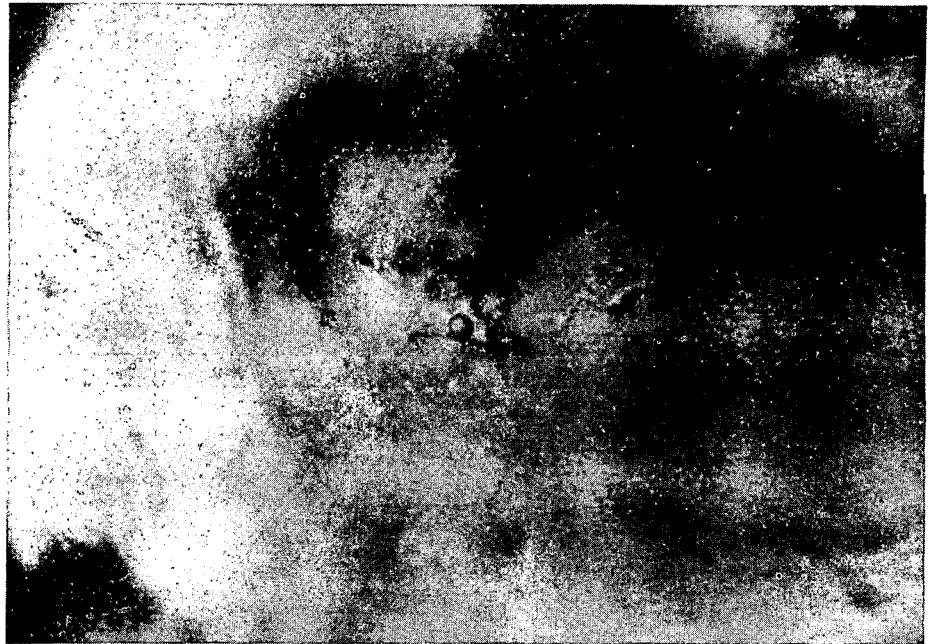
PHOTO 3, FS-10, CHIP 2  
INCLUSION 6; SEE SKETCH.



PHOTO 4, FS-10, CHIP 6  
INCLUSION 11; SEE SKETCH



PHOTO 5, FS-10, CHIP 7  
INCLUSION 12; SEE SKETCH



## Sample FS-11



Photo (g) looking south along fault 21 as shown on Plate K-5 (see sample FS-5). The painted black arrow indicates the orientation of slickensiding.



Photo (8) enlarges the center of the above photo. The sample was collected near the painted white spot and toward the jackknife.

Sample FS-11 - Calcite Crystals

Nearly all inclusions display spurs and tails; of 14 heated, 7 leaked. Obvious secondary inclusions are present along cleavages and in clusters, commonly without visible vapor.

Consistent temperatures were observed for a population of inclusions but their morphology suggests that they represent late stage deformation.

One high temperature (275°) was recorded for inclusion 7 which may represent a higher temperature population. There is, however, textural evidence that this inclusion may have been necked down during recrystallization and will be neglected for this reason.

Range 96-129° (6)

Average 114°

ANALYST: RJ POTTORF

SAMPLE No. FS11

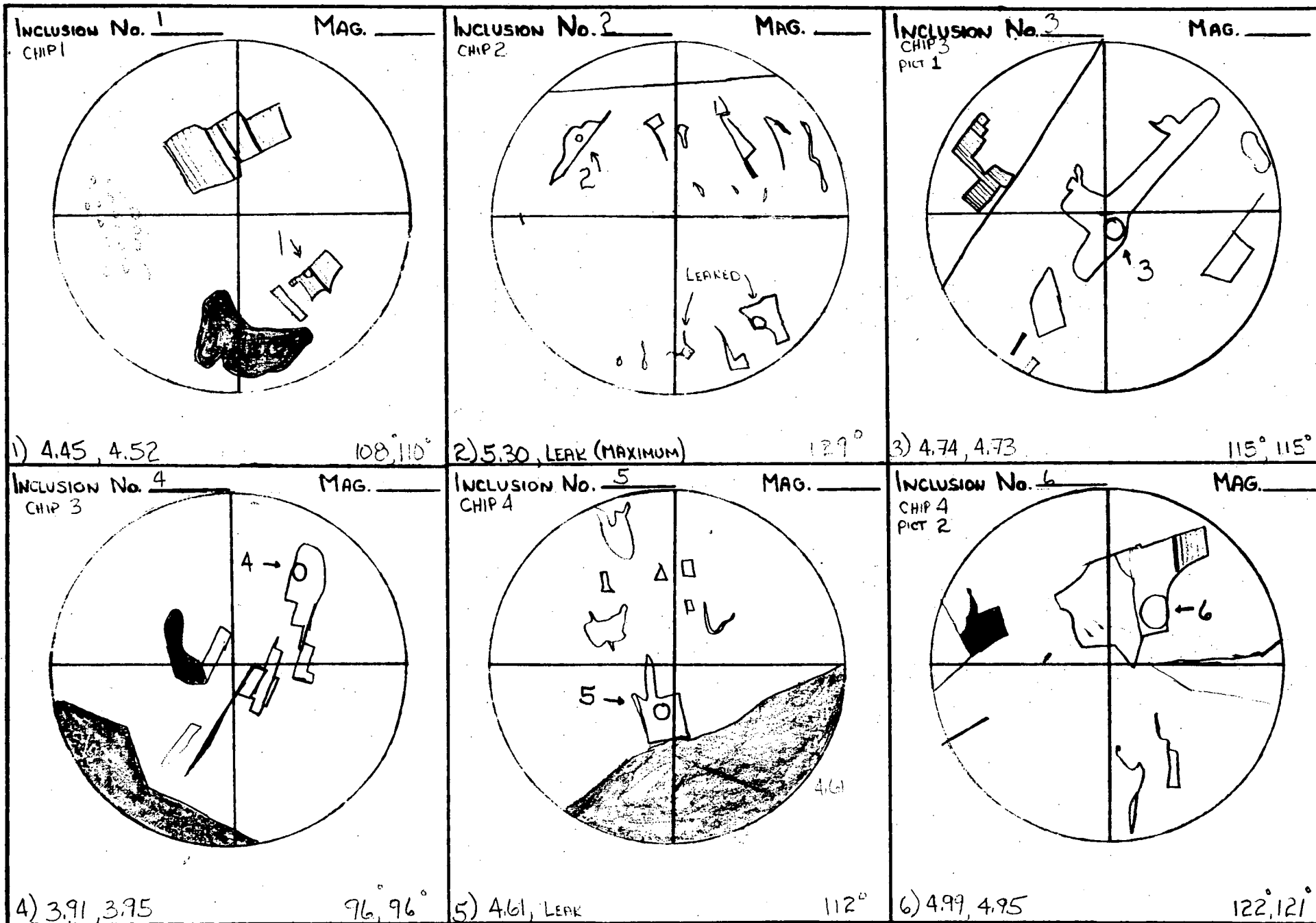
FLUID INCLUSION SKETCHES

CHIP No. 1-4

CON EDISON

MINERAL: CALCITE

55



55

ANALYST: RJ POTTORF

SAMPLE No. FS11

FLUID INCLUSION SKETCHES

CHIP No. 5

CON EDISON

MINERAL: CALCITE

27

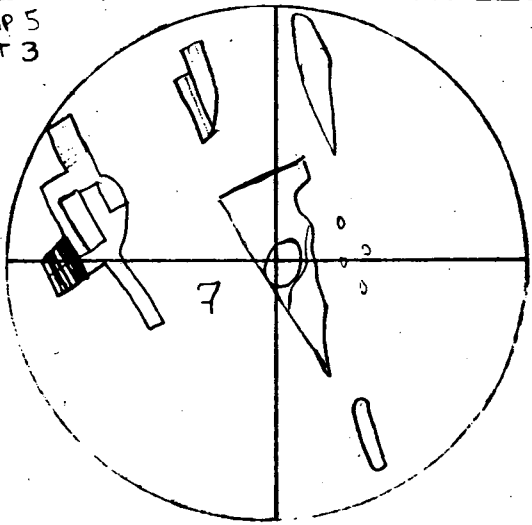
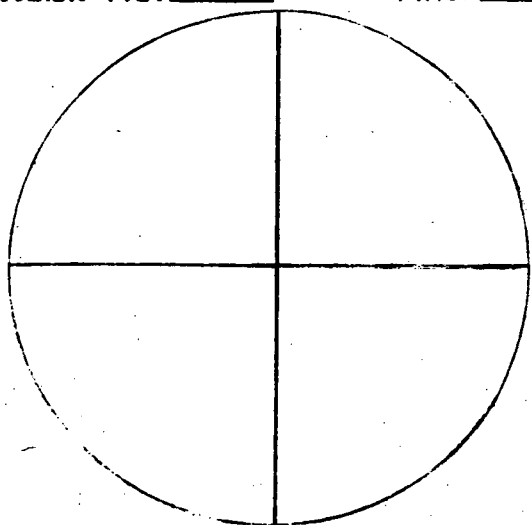
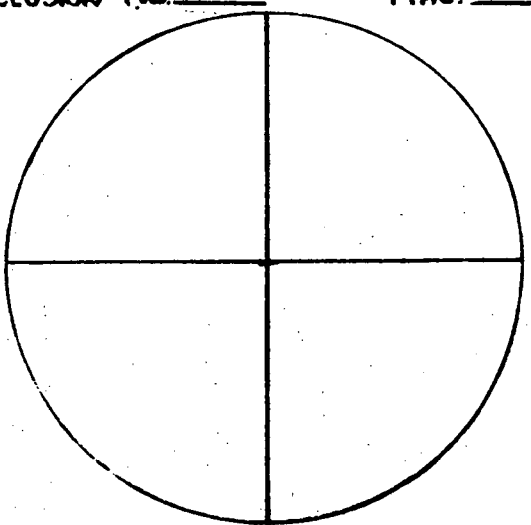
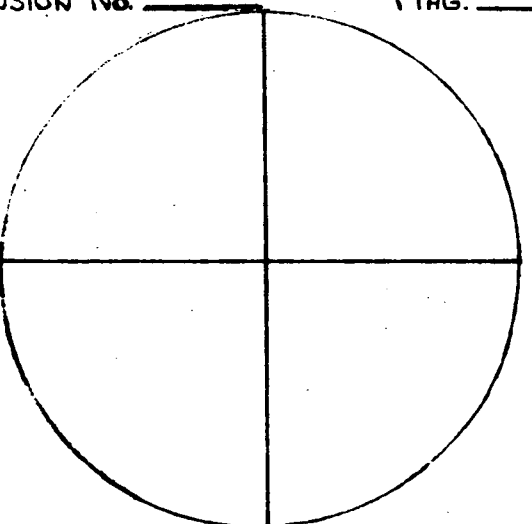
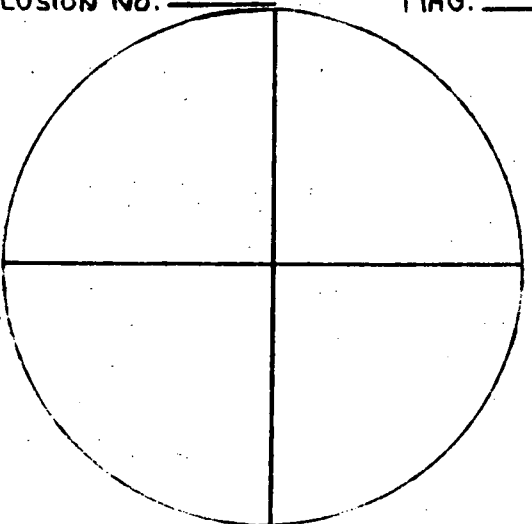
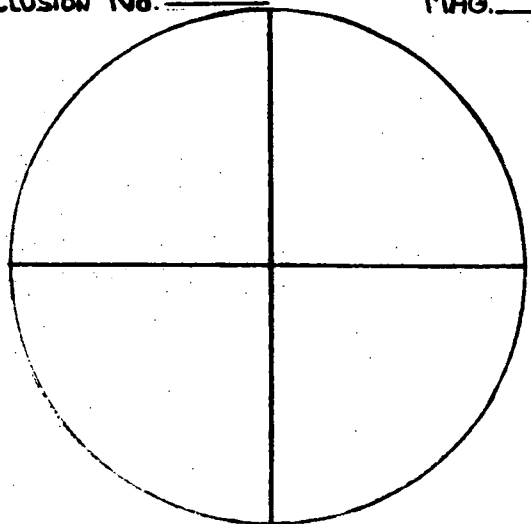
<p>INCLUSION No. <u>7</u> MAG. _____</p> <p>CHIP 5 PICT 3</p>  <p>11.17, 11.17 275° 275°</p>	<p>INCLUSION No. _____ MAG. _____</p> 	<p>INCLUSION No. _____ MAG. _____</p> 
<p>INCLUSION No. _____ MAG. _____</p> 	<p>INCLUSION No. _____ MAG. _____</p> 	<p>INCLUSION No. _____ MAG. _____</p> 

PHOTO 1, FS-11, CHIP 3  
INCLUSION 3; SEE SKETCH

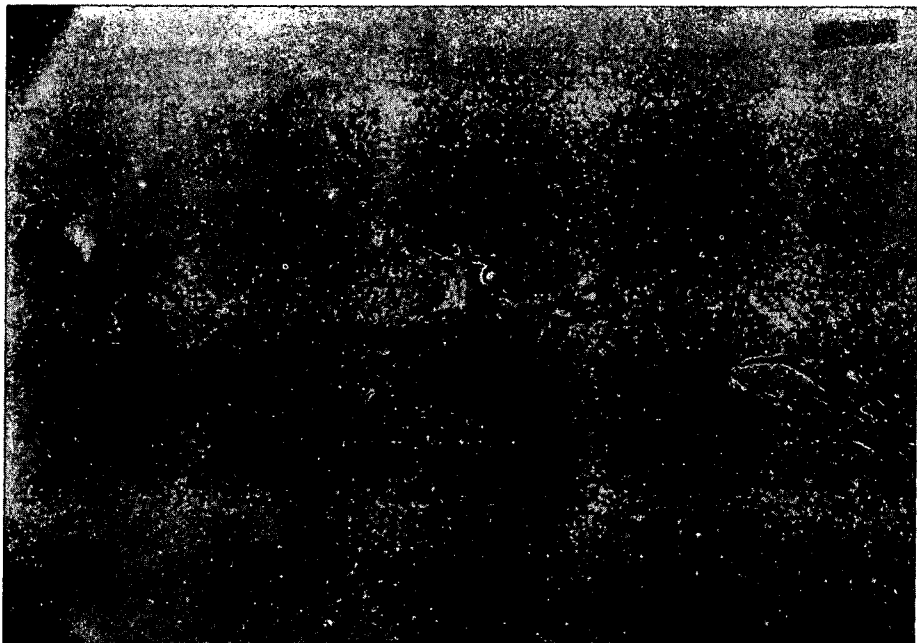


PHOTO 2, FS-11, CHIP 4,  
INCLUSION 6; SEE SKETCH.

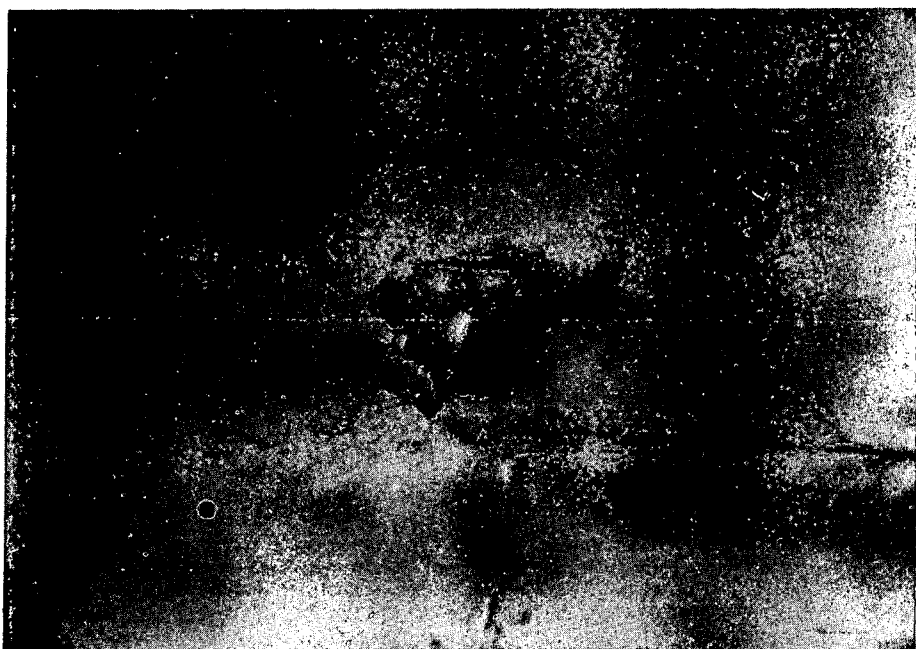
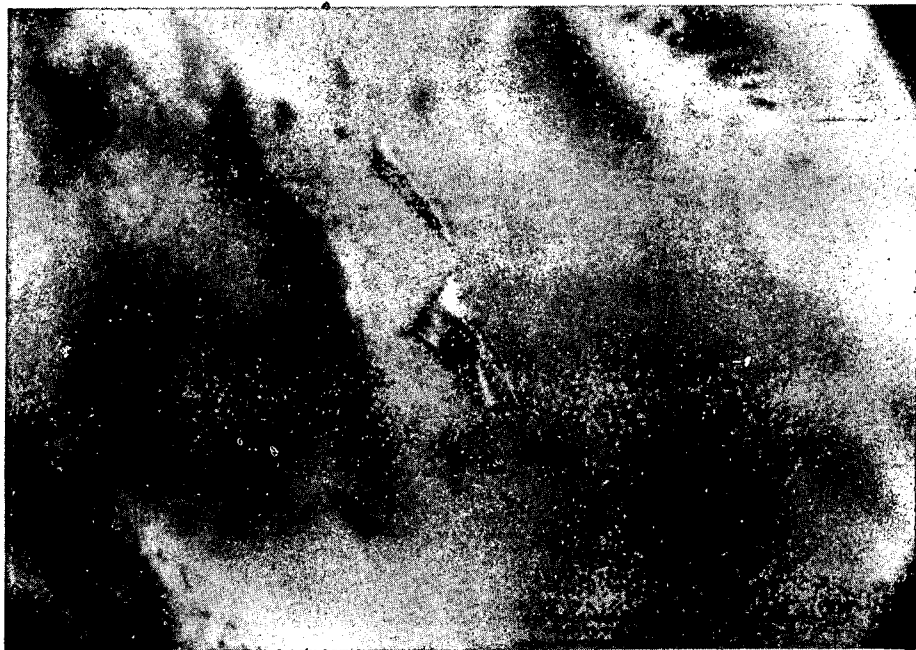


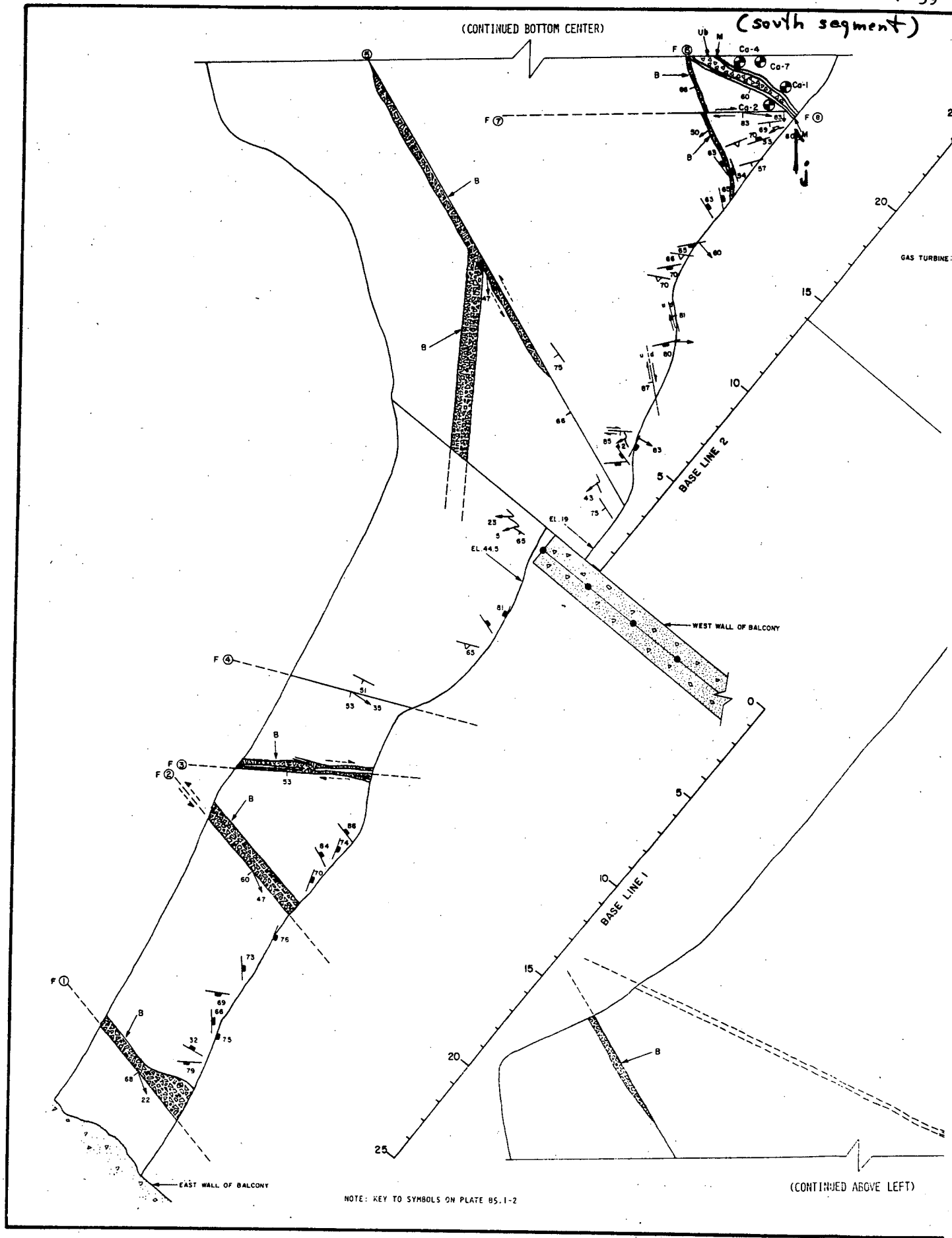
PHOTO 3, FS-11, CHIP 5,  
INCLUSION 7; SEE TEXT  
AND SKETCH.



Sample FS-12



Photo (j) looking west at an oxidized area at the intersection of faults 7 and 8 as shown on Plate K-4, south segment. The sample was collected about 10 cm to the right of the vertical pen, in the lower right corner of the photo, and near the painted white spot.



### Sample FS-12 - Calcite Crystals

Large numbers of solid inclusions are present. Nearly all fluid inclusions are "deformed" in some way (spurs, tails, necking); of 24 heated, 9 leaked. Inclusions are relatively abundant; very small secondary inclusions are present but could not be optically resolved for heating.

From the frequency plot for these samples, two tentative populations are suggested on the basis of temperature:

#### Population 1

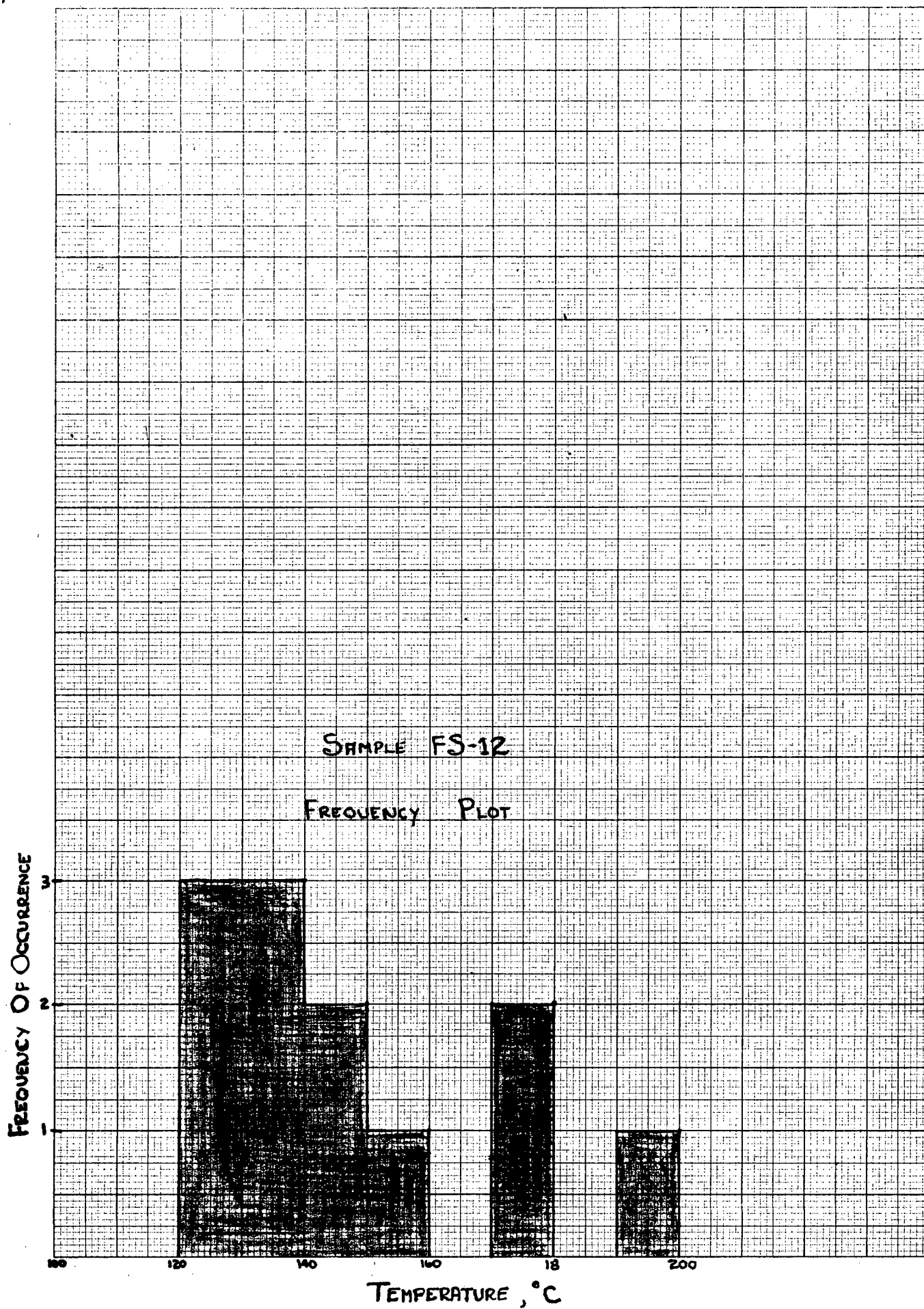
Range 172-197° (3)

Average 181°

#### Population 2

Range 129-159 (10)

Average 140°



ANALYST: RJ POTTORF

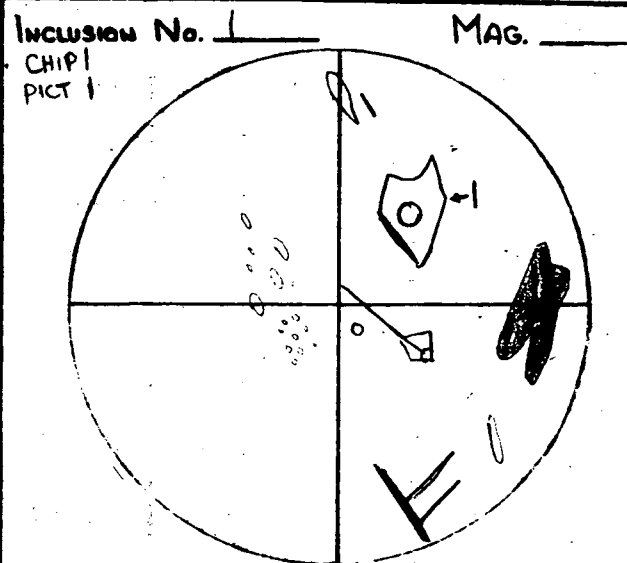
SAMPLE No. FS12

FLUID INCLUSION SKETCHES

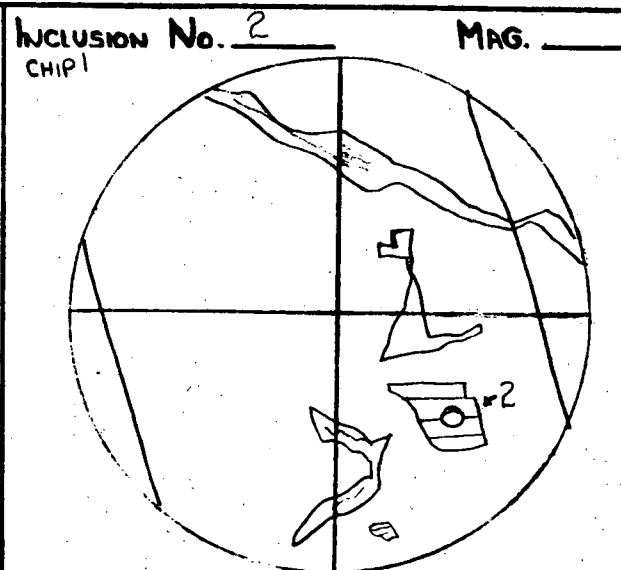
CHIP No. 1-4

CON EDISON

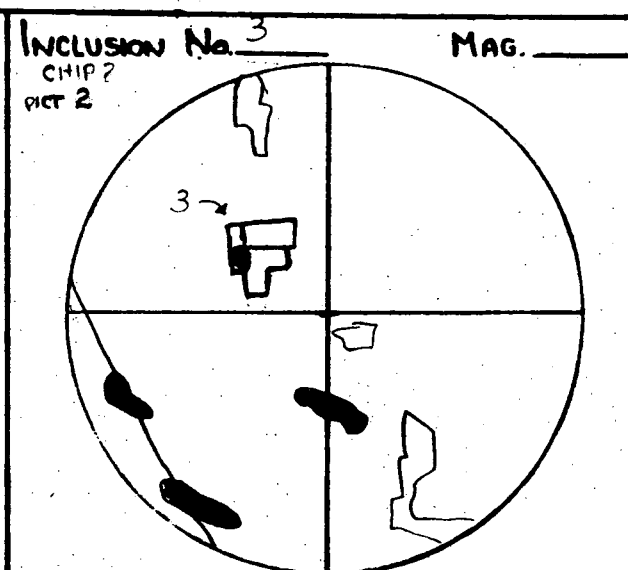
MINERAL: CALCITE



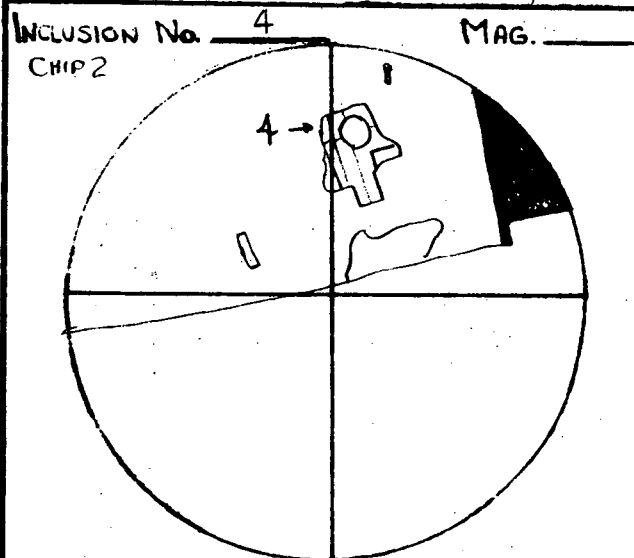
1) 7.00, 6.97 172°, 171°



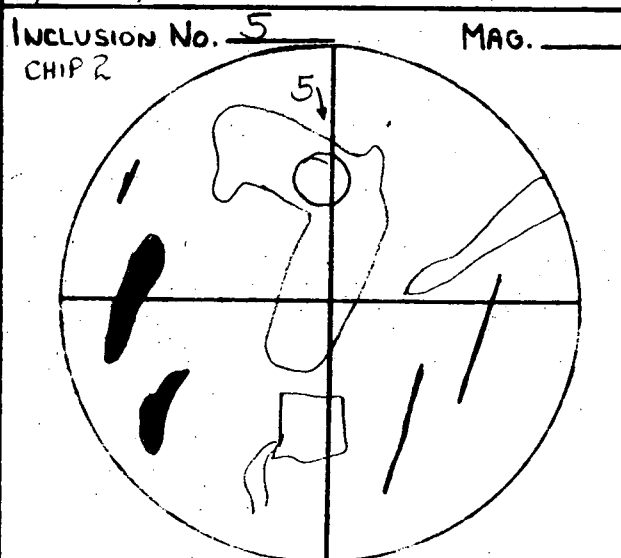
2) 8.03, 8.02 197°, 197°



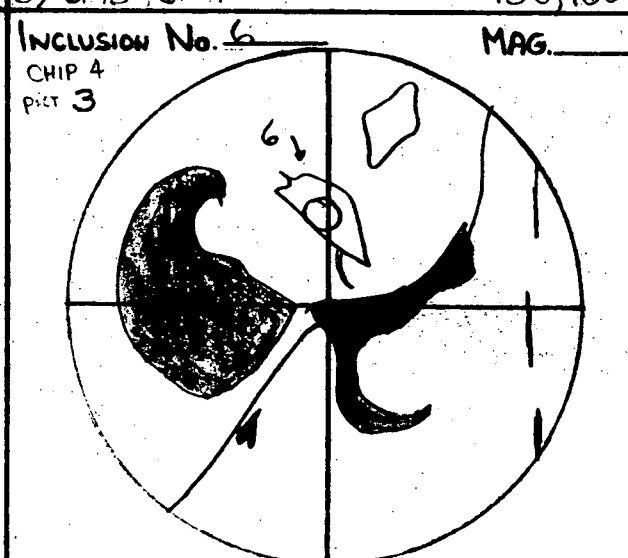
3) 6.43, 6.54 158°, 160°



4) 6.05, 5.98 148°, 146°



5) 7.09, 7.17 174°, 176°



PROBABLY LEAKED, UNRELIABLE - DISCARD

6) 10.97, 11.49 270°, 282°

ANALYST: RJ POTTORF

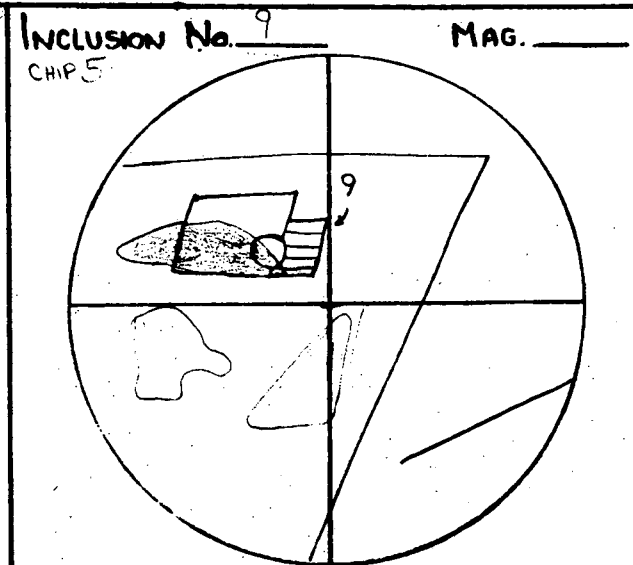
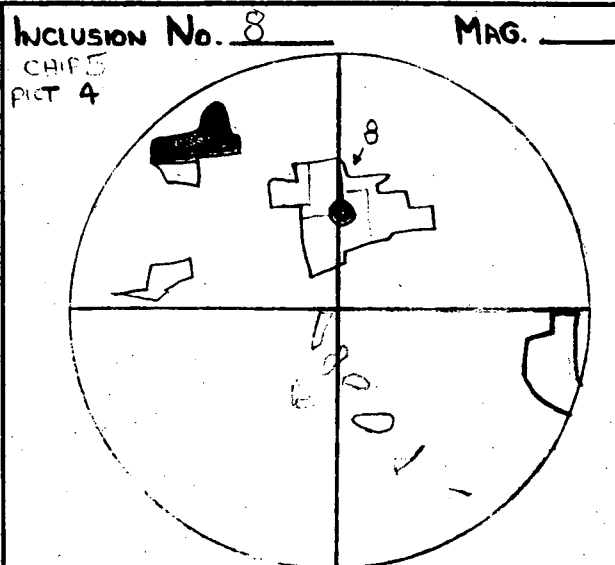
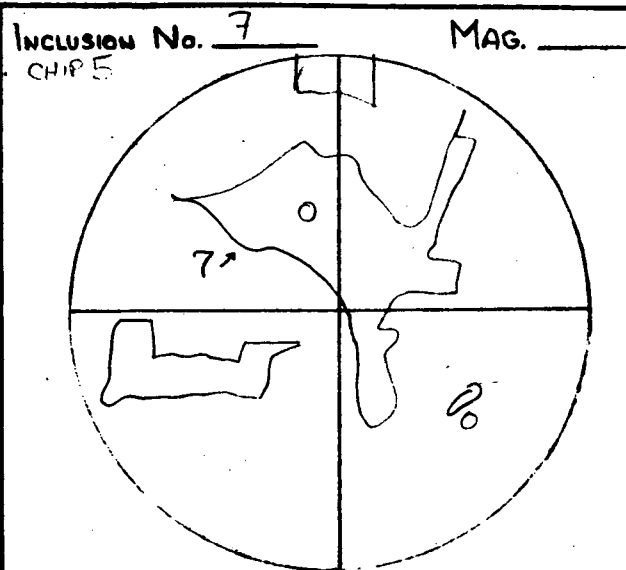
SAMPLE No. FS12

# FLUID INCLUSION SKETCHES

CHIP No. 5-6

CON EDISON

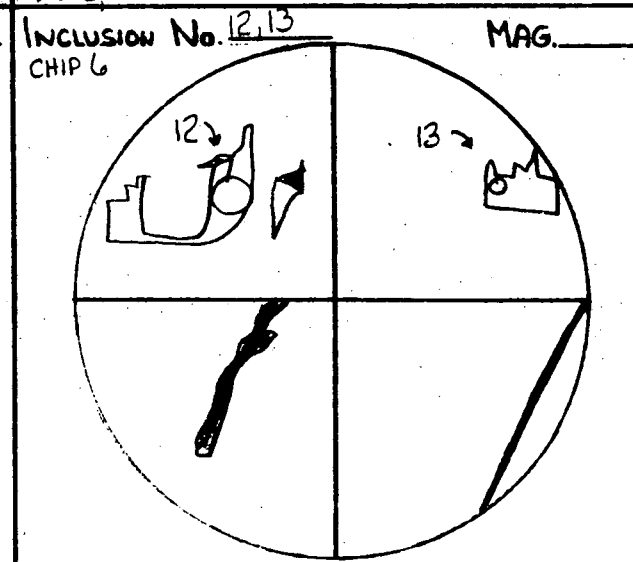
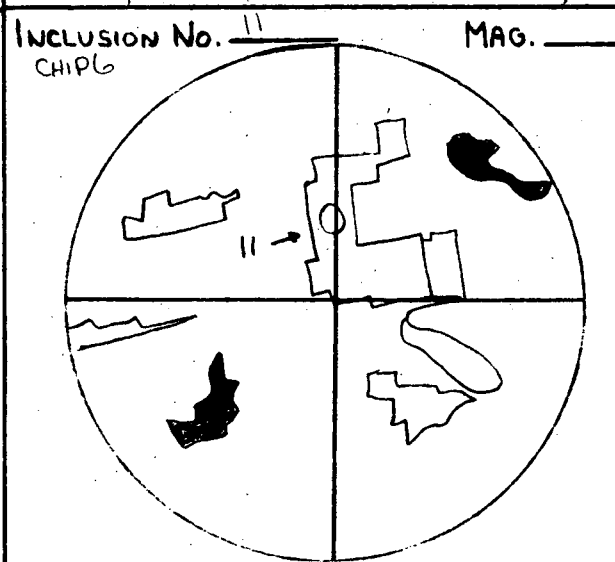
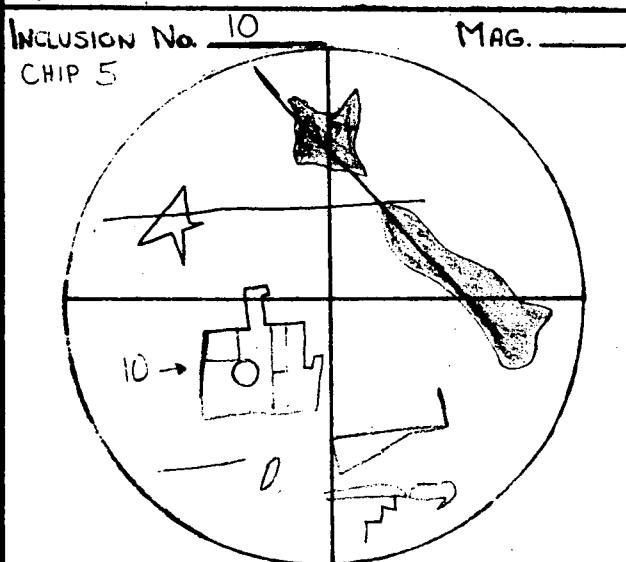
MINERAL: CALCITE



7) 3.89 LEAKED (UNREPRODUCIBLE) 95°

8) 5.29, 5.34 129°, 130°

9) 5.95, 6.01 145°, 147°



10) 6.02, 5.97 145°, 146°

11) 5.29, 5.34 129°

12) 5.68, LEAK 139°  
13) 5.30, LEAK 129°

ANALYST: RJ POTTORF

SAMPLE No. FS 12

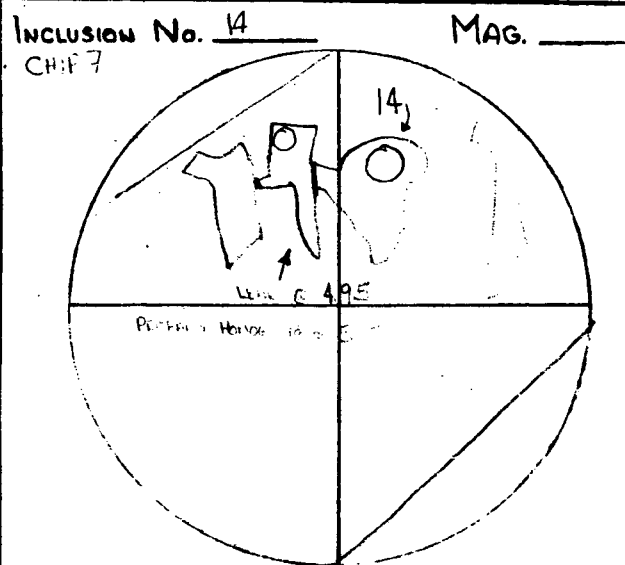
FLUID INCLUSION SKETCHES

CHIP No. 7-8

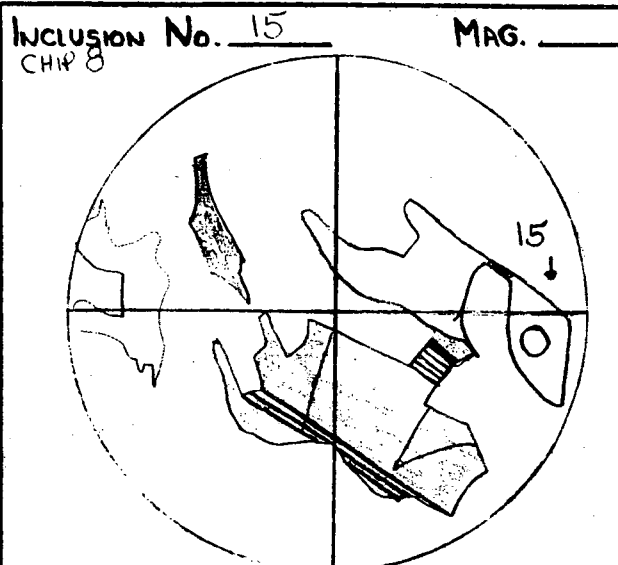
CON EDISON

MINERAL: CALCITE

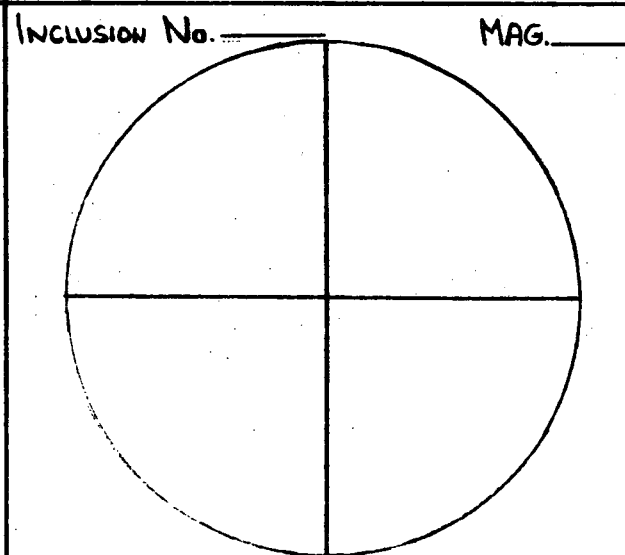
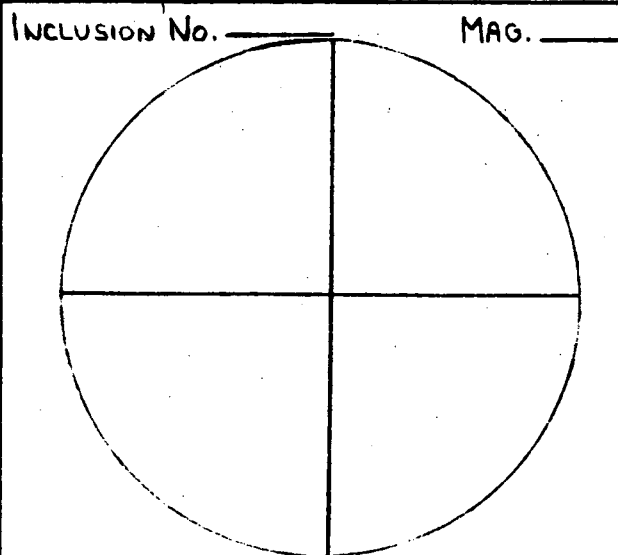
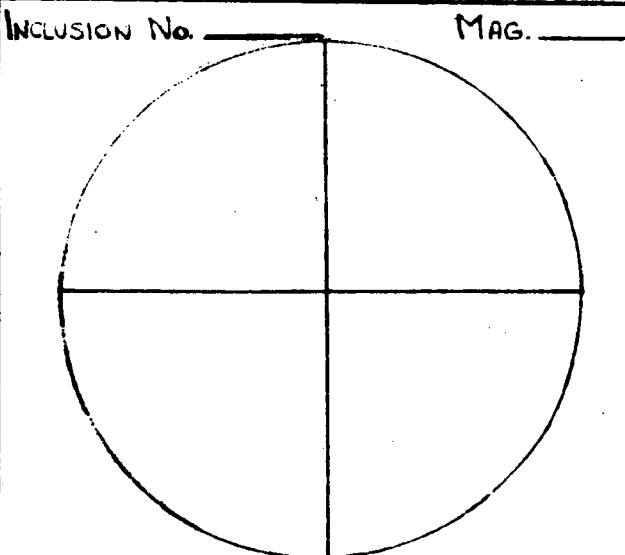
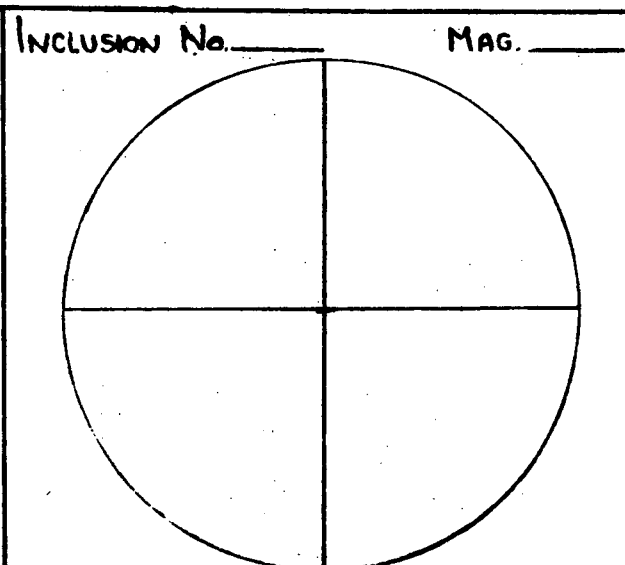
64



14) 5.75, LEAK 140°



15) 5.58, 5.61 136, 137°



64

PHOTO 1, FS-12, CHIP 1,  
INCLUSION 1; SEE SKETCH.

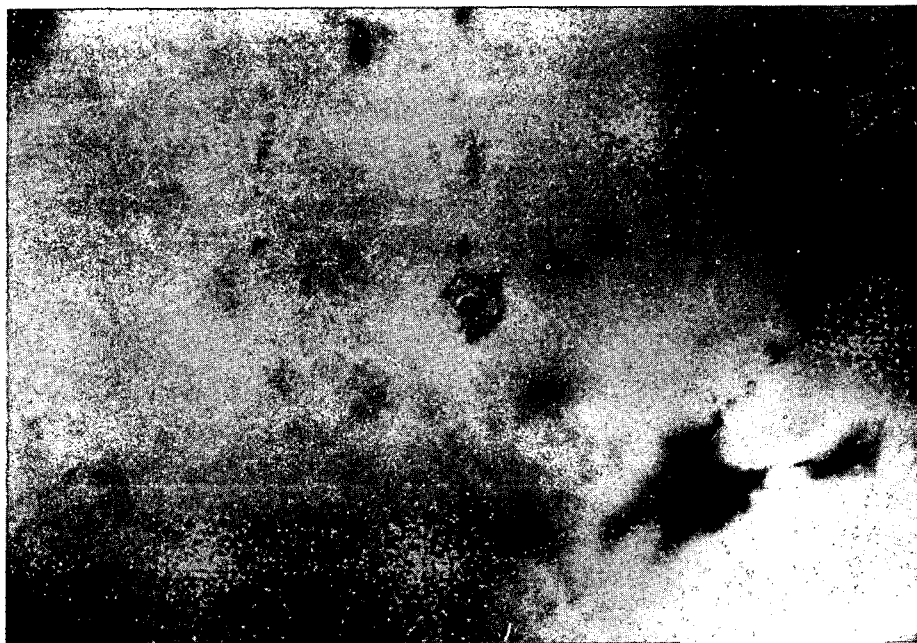


PHOTO 2, FS-12, CHIP 2,  
INCLUSION 3; SEE SKETCH.



PHOTO 3, FS-12, CHIP 4,  
INCLUSION 6; SEE SKETCH.

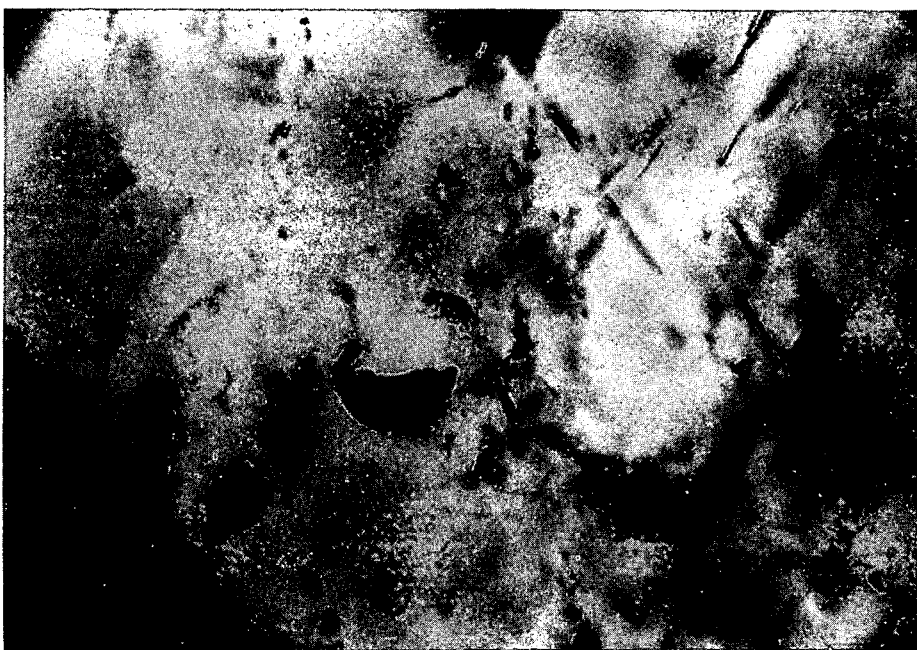


PHOTO 4, FS-12, CHIP 5,  
INCLUSION 8; SEE SKETCH



PHOTOS 5 AND 6, FS-12;  
TWO TYPICAL EXAMPLES OF  
INCLUSIONS WHICH LEAKED  
UPON HEATING.



Sample FS-13



Photo (n) looking northeast at fault 3, in upper left center, and fault 1, in lower right corner, as shown on Plate K-3 (with samples FS-8 and FS-9). Sample FS-13 was collected at the circled point at top left center of the photo; sample FS-10 was collected at the circled point in the lower right corner of the photo. The black notebook, slightly below and to the right of the center of the photo, is 15 cm long.

### Sample FS-13 - Calcite Crystals

Sulfides are present. Probably there is only one population of primary inclusions but several minute secondary inclusions are found along rehealed cleavage planes. The secondary inclusions measured were much larger than the majority of the population. One phase, fluid-filled inclusions were observed and assumed to be very low temperature secondaries formed in fractures. Of 14 inclusions measured, 5 leaked.

#### Primary inclusions

Range 143-216° (5)

Average 178°

#### Secondary inclusions

Range 90-100° (4)

Average 97°

ANALYST: RJ POTTORF

SAMPLE No. FS 13

FLUID INCLUSION SKETCHES

CHIP No. 1-6

CON EDISON

MINERAL: CALCITE

67

Inclusion No. 1 CHIP 1 PICT 1	MAG. _____	Inclusion No. 2 CHIP 2 PICT 2	MAG. _____	Inclusion No. 3 CHIP 3	MAG. _____
1) 6.78, 6.81 166°, 167°		2) 5.86, 5.82 143°, 142°		UNRELIABLE - DISCARD 3) 5.08, LEAK 124°	
Inclusion No. 4 CHIP 4	MAG. _____	Inclusion No. 5 CHIP 5 PICT 3	MAG. _____	Inclusion No. 6, 7, 8, 9 CHIP 6 PICT 4 SECONDARY INCLUSIONS	MAG. _____
4) 8.80 LEAK 216°		5) 6.75, 6.75 166°, 166°		6) 4.09 7) 4.04 8) 3.98 9) 3.67 THE INCLUSIONS MEASURED HAD THE LARGEST VAPOR/ FLUID RATIO AND THEREFORE REPRESENT THE MAXIMUM TEMPERATURES. 100° 99° 97° 90°	

69

ANALYST : RJ POTTORF

FLUID INCLUSION SKETCHES

CON EDISON

SAMPLE No. FS 13

CHIP No. 7

MINERAL: CALCITE

04

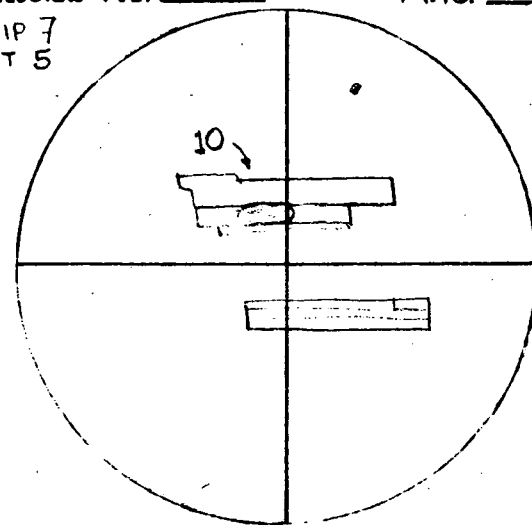
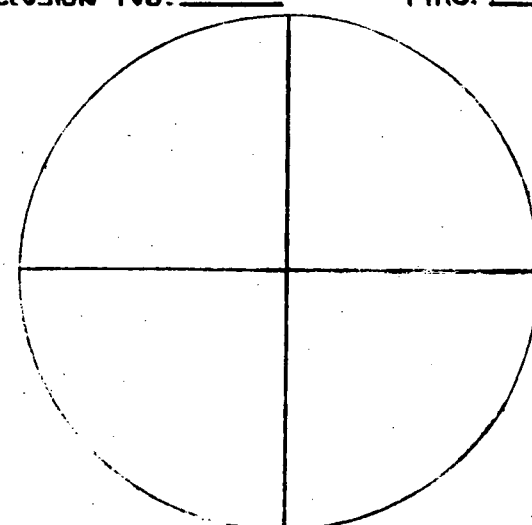
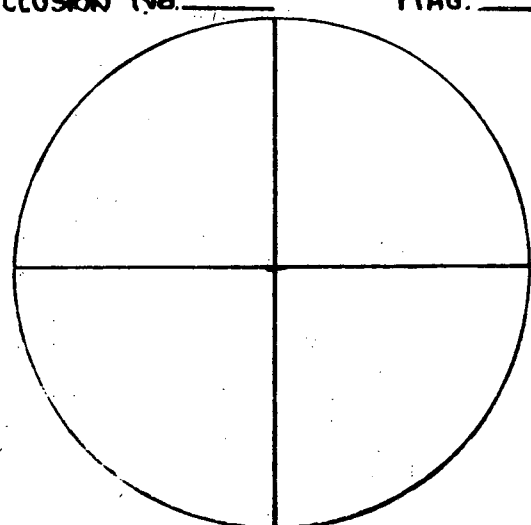
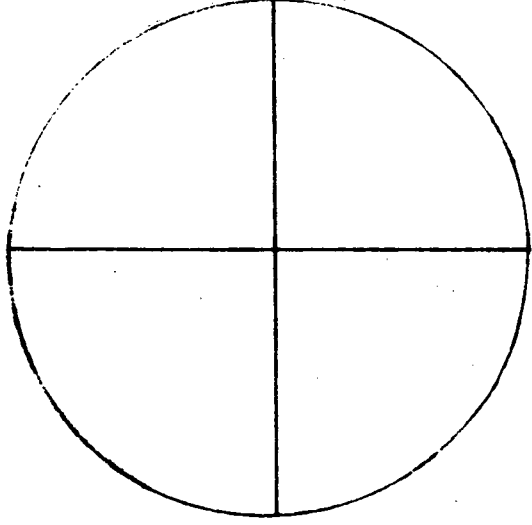
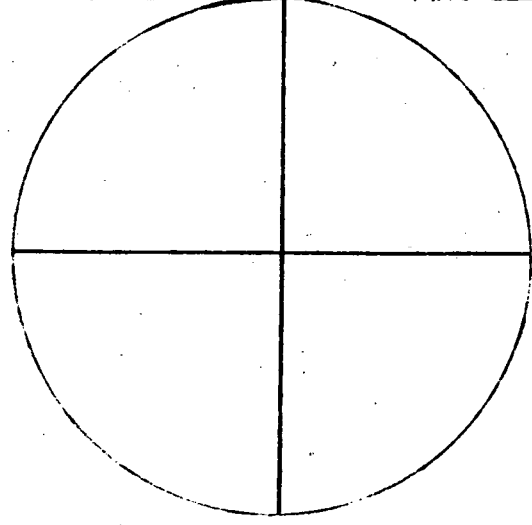
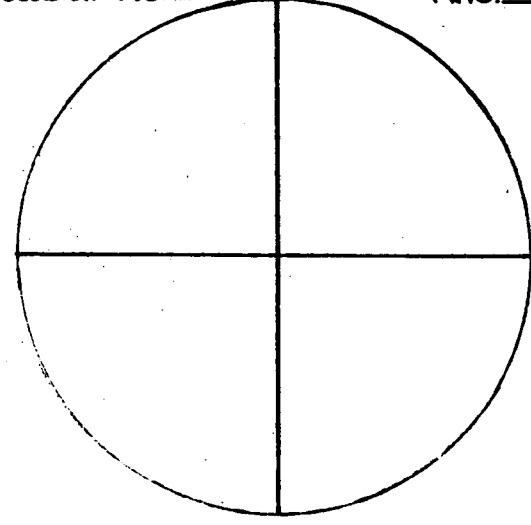
<p>Inclusion No. <u>10</u> MAG. _____</p> <p>CHIP 7 PICT 5</p>  <p>10) 7.91, 7.99 195, 196</p>	<p>Inclusion No. _____ MAG. _____</p> 	<p>Inclusion No. _____ MAG. _____</p> 
<p>Inclusion No. _____ MAG. _____</p> 	<p>Inclusion No. _____ MAG. _____</p> 	<p>Inclusion No. _____ MAG. _____</p> 

PHOTO 1, FS-13, CHIP 1.  
INCLUSION 1 ; SEE SKETCH



PHOTO 2, FS-13, CHIP 2.  
INCLUSION 2 ; SEE SKETCH



PHOTO 3, FS-13, CHIP 5,  
INCLUSION 5 ; SEE SKETCH.

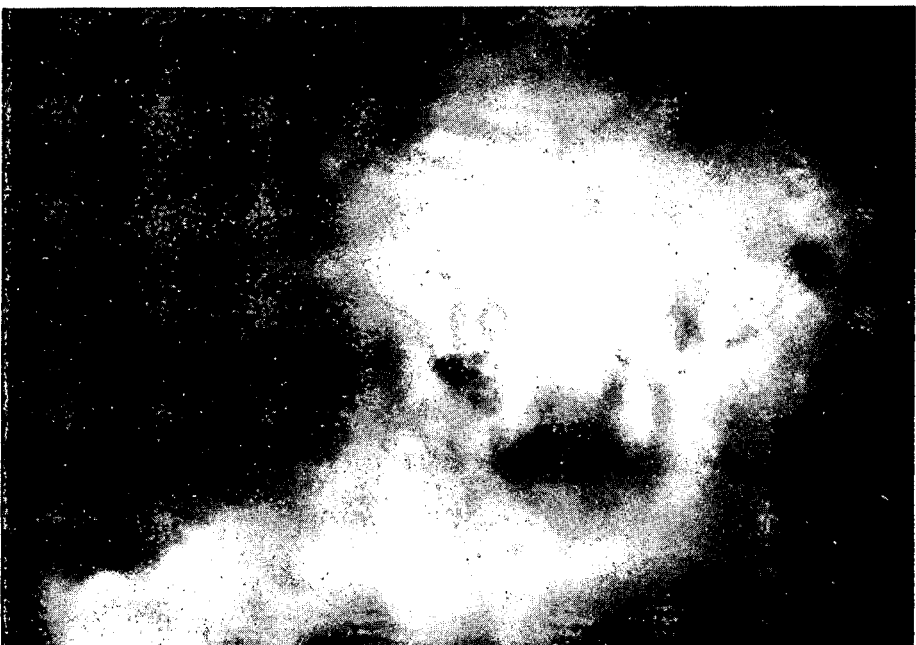


PHOTO 4, FS-13, CHIP 6,  
INCLUSIONS 6-9 (SOME  
NOT IN FOCUS); SECONDARY  
INCLUSIONS. SEE SKETCH.

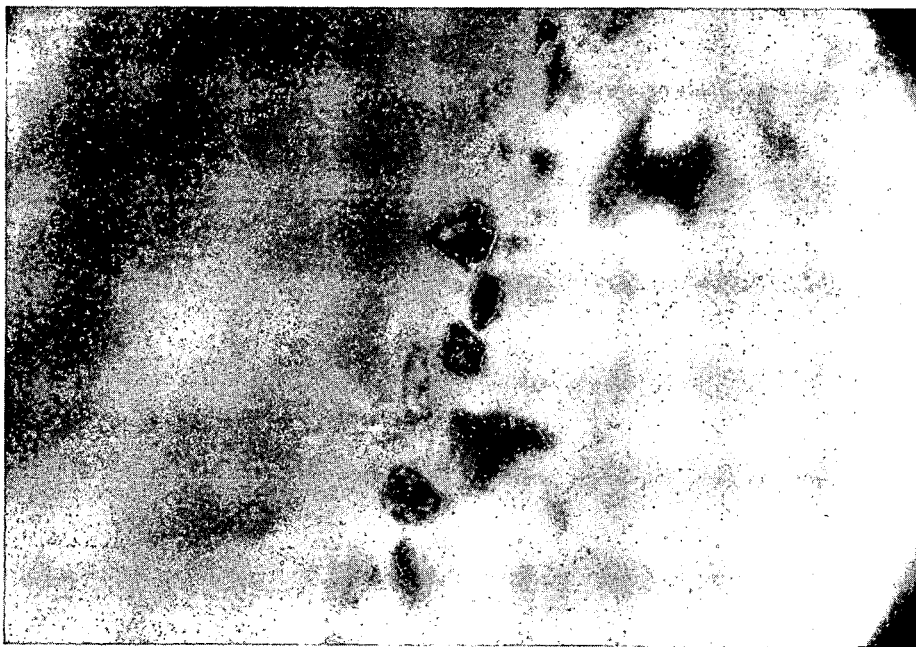


PHOTO 5, FS-13, CHIP 7,  
INCLUSION 10; SEE SKETCH;  
NEGATIVE CRYSTAL



## PART II (Triassic Host Rocks)

Summary (Range, (no. of measured inclusions), average, in °C; \* Previously reported values)

<u>Sample</u>	<u>Primary Inclusions</u>	<u>Secondary Inclusions</u>	<u>Notes</u>
GA 1.3	~100	---	Analcite
GA 4.1	~200	---	Quartz, fractured
GA 19.1	295-318 (3) <u>308</u>	90-98 (3) <u>94</u> *(96-109 (4) <u>104</u> )	Quartz with zeolites and calcite
MW 67d-1	123-138 (4) <u>128</u>	110-111 (2) <u>110</u>	Deformed calcite
MW 103-2	151-271 (6) <u>195</u>	99-130 (14) <u>114</u>	Calcite, a very low temperature group also present
MW 103-3	130-145 (6) <u>135</u>	93-103 (3) <u>99</u>	Deformed calcite
MW 106-2	165-220 (4) <u>192</u>	99-136 (7) <u>114</u>	Late, clear calcite; a very low temperature population also present
MW 114-1	~300+ ~215 (1)	130-142 (3) <u>135</u>	Quartz, three groups of temperatures
MW 115-1	~168?	---	Quartz, fractured
MW 116-2	129-168 (8) <u>148</u>	98-111 (4) <u>102</u>	Calcite

Sample GA 1.3 - Analcite

Analcite shows weak birefringence and minor twinning. All inclusions are necked or stretched and all (13 inclusions heated) leaked to some extent when heated. Leaks at temperatures less than 100° are common; the entire sample decrepitates at ~200°. Small irregular fractures are very common.

From the behavior of the inclusions when heated it is estimated that the average true homogenization temperature is probably close to 100°, or slightly higher.

Crystallization temperature ~100°C (?)

ANALYST: RJ POTTORF

SAMPLE No. GA1.3

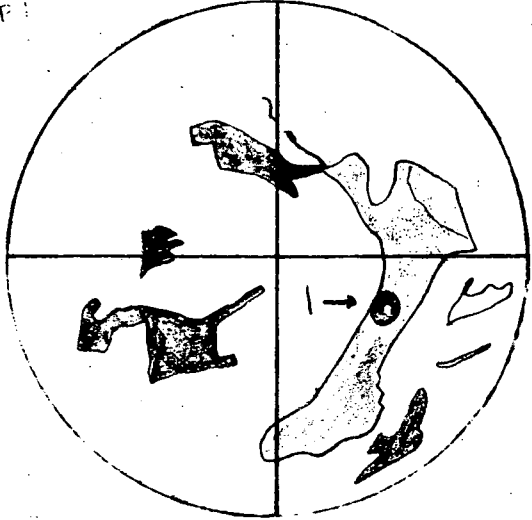
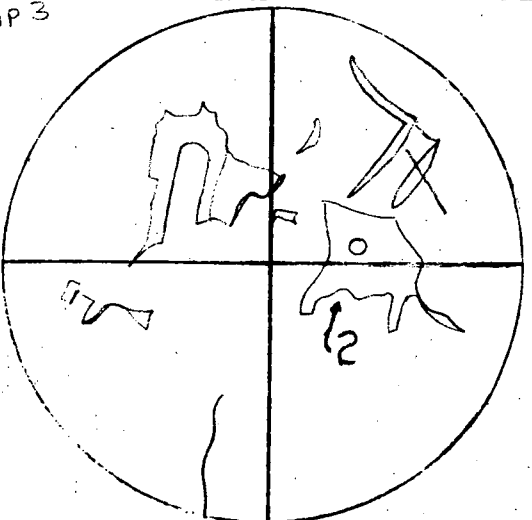
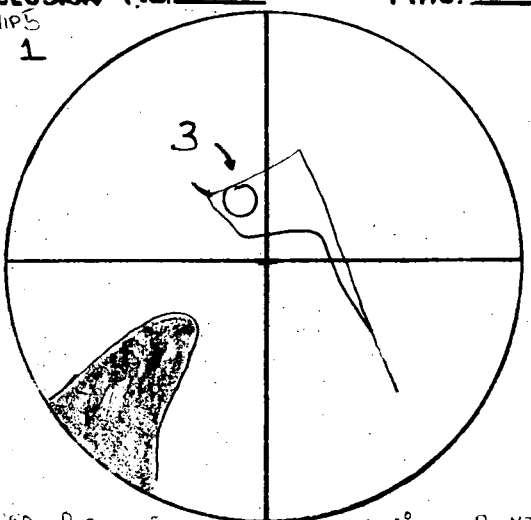
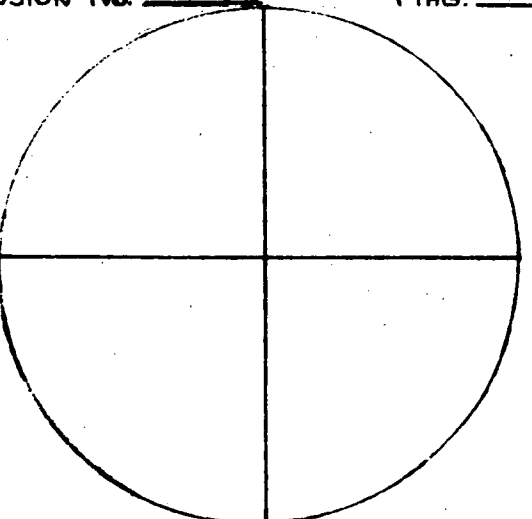
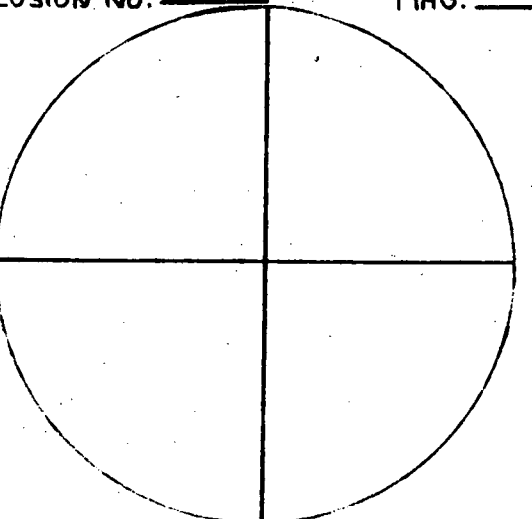
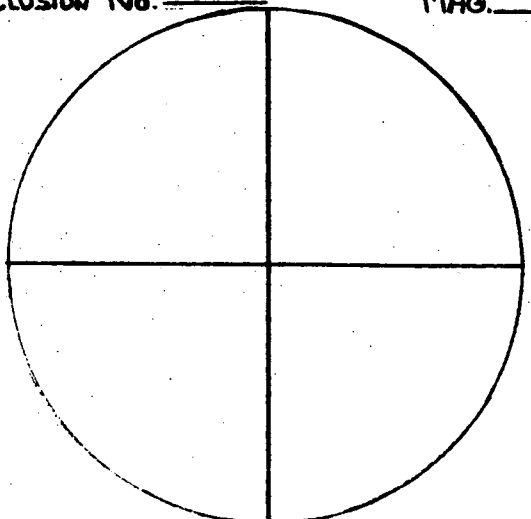
FLUID INCLUSION SKETCHES

CHIP No. 13,5

CON EDISON

MINERAL: ANALCITE

45

Inclusion No. 1 CHIP 1	MAG. _____	Inclusion No. 2 CHIP 3	MAG. _____	Inclusion No. 3 CHIPS PICT 1	MAG. _____
					
1) 5.02, LEAKED 122°		MUST BE CORRELATED A MAXIMUM TEMP. VISUALLY LEAKED DURING HEATING 2) 6.42, LEAKED 157°		LEAKED DURING FIRST HEATING, 165° IS A MAXIMUM 3) ~6.75, DECEASED 8.33 165°, 205°	
Inclusion No. _____ MAG. _____		Inclusion No. _____ MAG. _____		Inclusion No. _____ MAG. _____	
					

75

PHOTO 1; GA 1.3, CHIP 5  
INCLUSION 3; SEE SKETCH.

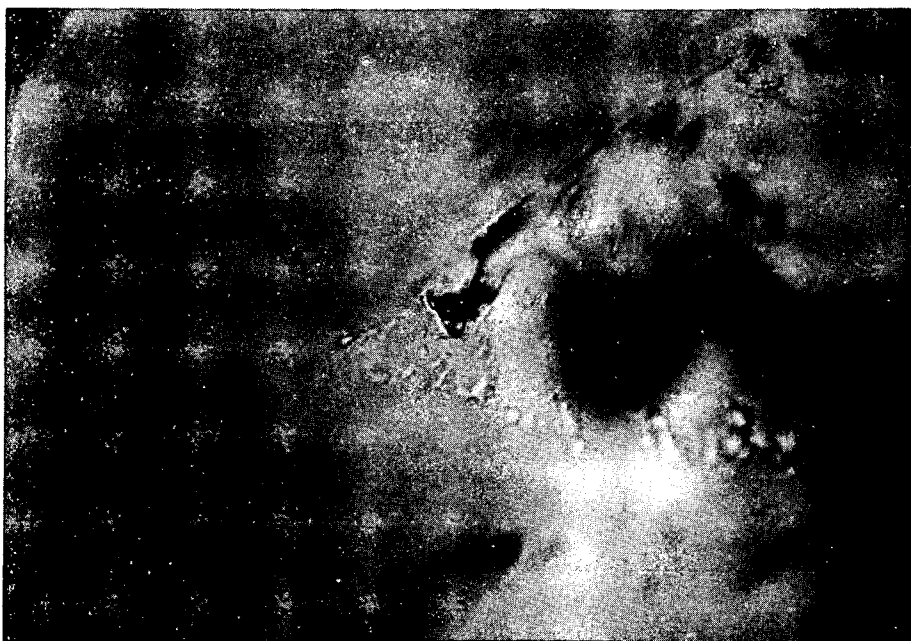


PHOTO 2, GA 1.3; INCLUSION  
WITH LARGE VAPOR/LIQUID  
RATIO RESULTING FROM LIQUID  
LEAKAGE. NOT SUITABLE FOR  
FILLING TEMP.



Sample GA 4.1 - Quartz

Pyramidal shaped negative crystals are fairly common (see photos). These inclusions always have tails found at some or all corners of the inclusion. Often the inclusion is found at intersections of fractures and is generally empty. Some two-phase inclusions (photo 2 and 3) were observed but leaked when heated.

Secondary inclusions have elongated and irregular shapes generally controlled and intersected by fractures while other very small secondaries appear in clusters.

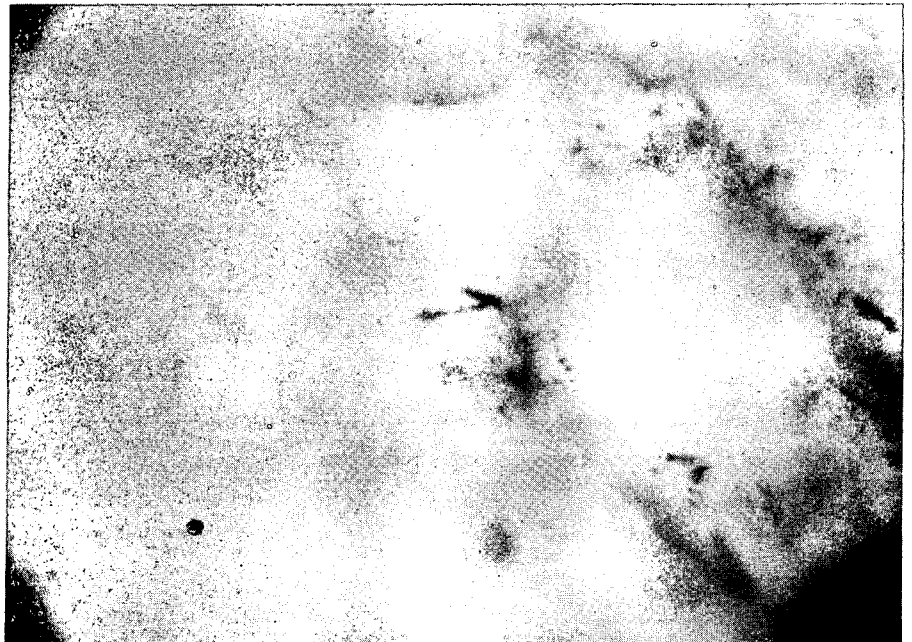
All of the inclusions heated leaked. From the vapor/fluid ratios observed in negative crystals, it is estimated that the homogenization temperature is approximately 200°.

Homogenization temperature ~200° (?)

PHOTO 1 , GA 4.1, EMPTY  
NEGATIVE CRYSTAL



PHOTOS 2 AND 3 , GA 4.1;  
NEGATIVE CRYSTALS CONTAINING  
TWO PHASES ; NOTE TAILS  
AT CORNERS OF INCLUSIONS.



Sample GA 19.1 - Quartz (amethyst) and Calcite Crystals;  
(minor zeolites present)

Small secondary inclusions are concentrated along numerous rehealed, curved fractures and show extreme tails and spurs in quartz. Secondary inclusions have a similar appearance in calcite. Leakage predominately occurs in these inclusions along the fractures.

"Primary" inclusions in both quartz and calcite are exceedingly rare. The few high temperature inclusions found always had a pseudo-secondary appearance (e.g., photos 1 and 2). After heating these inclusions to homogenization and returning to room temperature, several "new" inclusions were formed in the chip, apparently from leakage of fluid-filled inclusions. When these inclusions are heated they surprisingly give consistent temperatures (see inclusions 6, 8, 10, 11), but always less than the original "primary" inclusion temperature. In all cases these measurements were discarded. It is also possible that inclusions 4, 5, and 9 are the result of leakage of fluid-filled inclusions at some time in the geologic past. For these reasons, the "primary" temperatures obtained must be viewed with reservation.

Inclusions 1-3 give very low temperatures (90-98°) but do not have the appearance of secondary inclusion and may actually be close to the true crystallization temperature.

Population 1 (Primary (?) inclusions in quartz)

Range 295-318° (3)

Average 308°

Population 2 (Secondary (?) inclusions in calcite)

Range 90-98° (3)

Average 94°

ANALYST: RJ POTTORF

SAMPLE No. GA 19.1

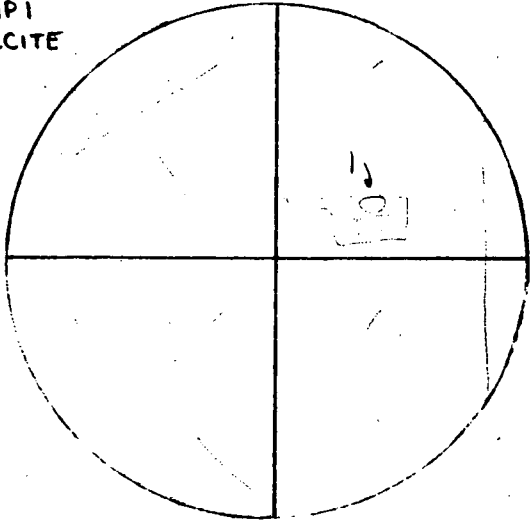
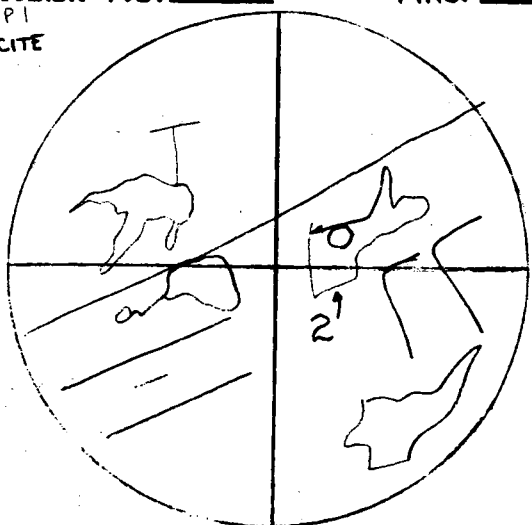
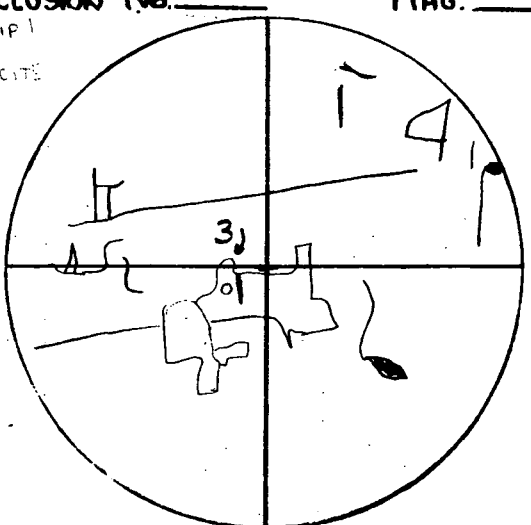
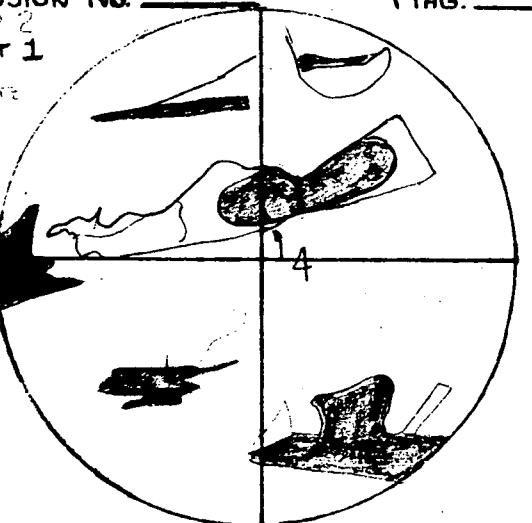
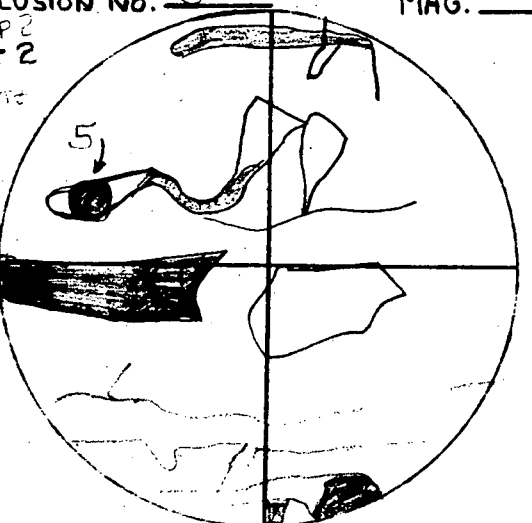
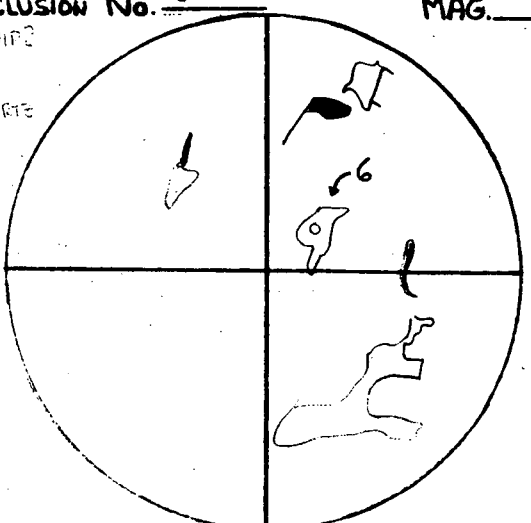
FLUID INCLUSION SKETCHES

CHIP No. 1-2

CON EDISON

MINERAL: QUARTZ, CALCITE

28

Inclusion No. 1 CHIP 1 CALCITE MAG. _____  1) 3.85, LEAK 94°	Inclusion No. 2 CHIP 1 CALCITE MAG. _____  2) 3.61, 3.68 90°, 90°	Inclusion No. 3 CHIP 1 CALCITE MAG. _____  3) ~ 4.03 LEAK 98°
Inclusion No. 4 CHIP 2 PICT 1 QUARTZ MAG. _____  4) 13.03, 12.95 320°, 317°	Inclusion No. 5 CHIP 2 PICT 2 QUARTZ MAG. _____  5) 12.03, 12.00 295°, 295°	Inclusion No. 6 CHIP 2 QUARTZ MAG. _____  OBSERVED ONLY AFTER HEATING 6) 9.56, 9.45 235°, 235°

88

ANALYST: RJ POTTORF

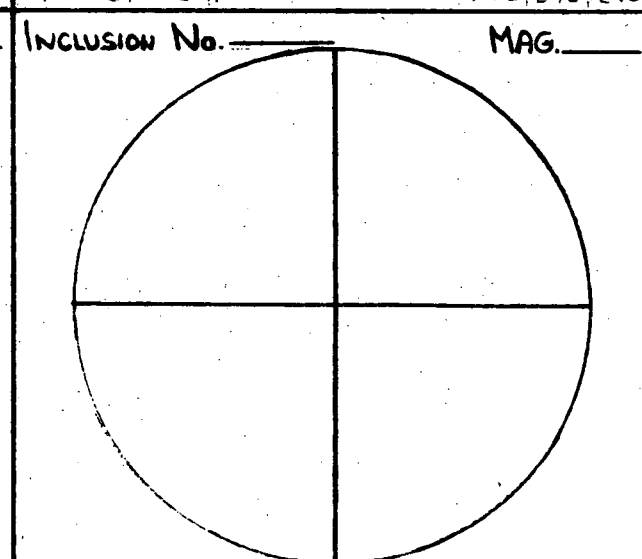
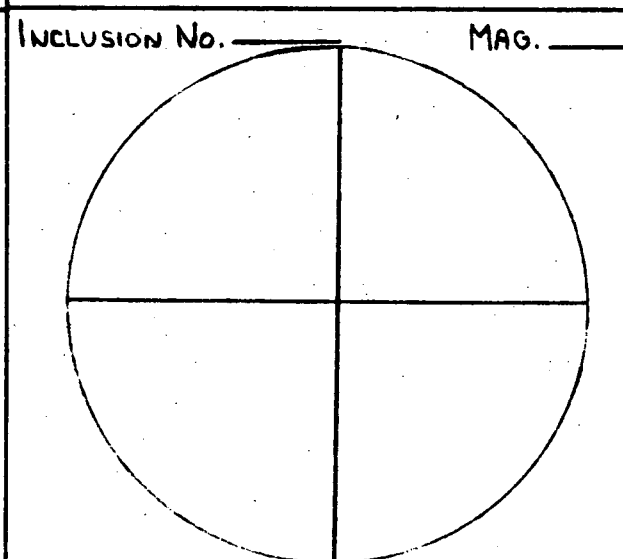
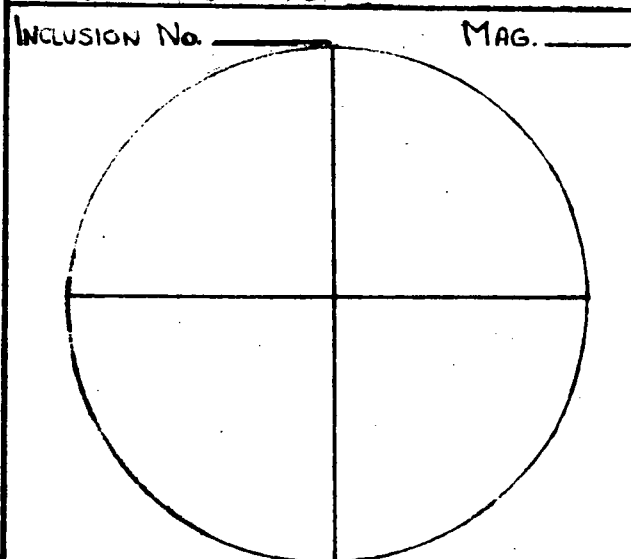
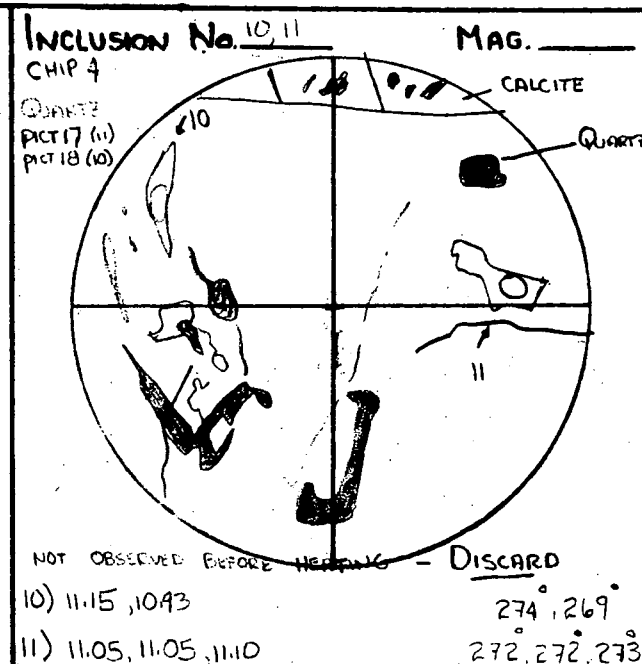
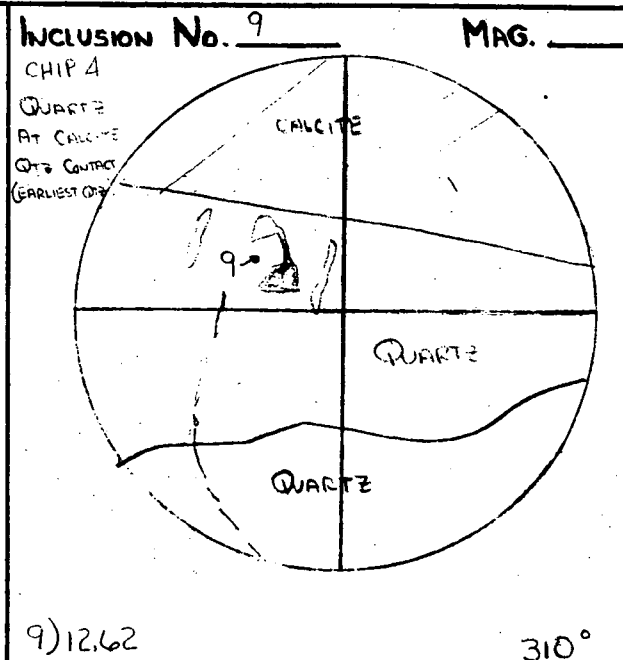
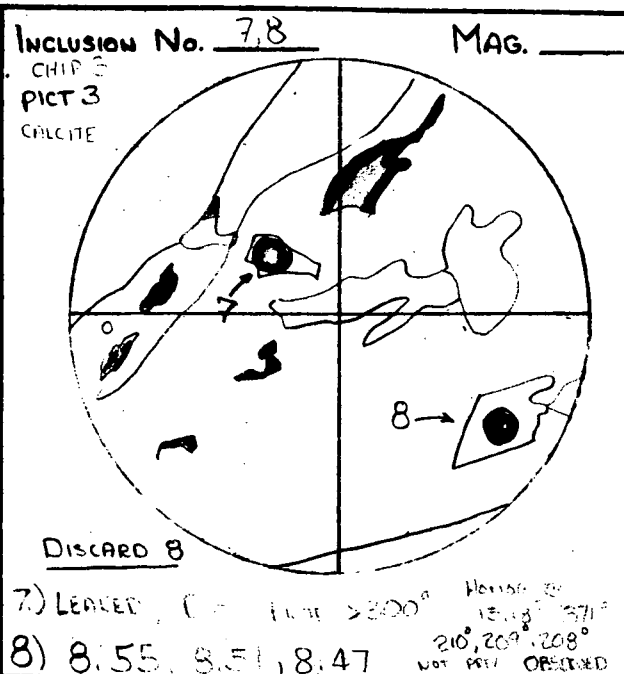
SAMPLE No. GA19.1

# FLUID INCLUSION SKETCHES

CHIP No. 3-4

CON EDISON

MINERAL: CALCITE + QUARTZ



87

PHOTO 1, GR 19.1, CHIP 2,  
INCLUSION 4; SEE TEXT  
AND SKETCH. (QUARTZ)



PHOTO 2, GR 19.1, CHIP 2  
INCLUSION 5; SEE TEXT  
AND SKETCH. (QUARTZ)

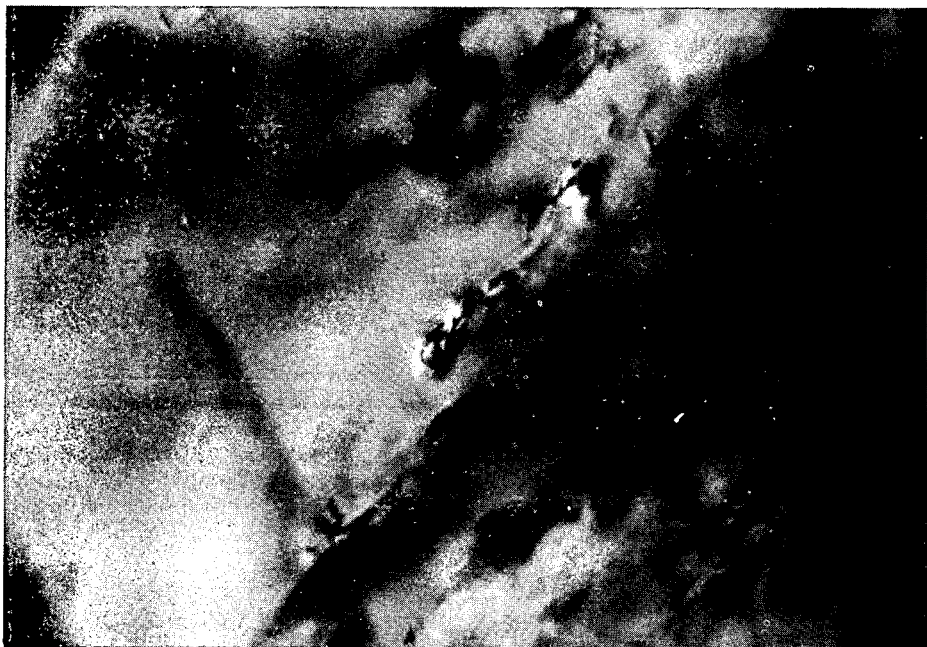
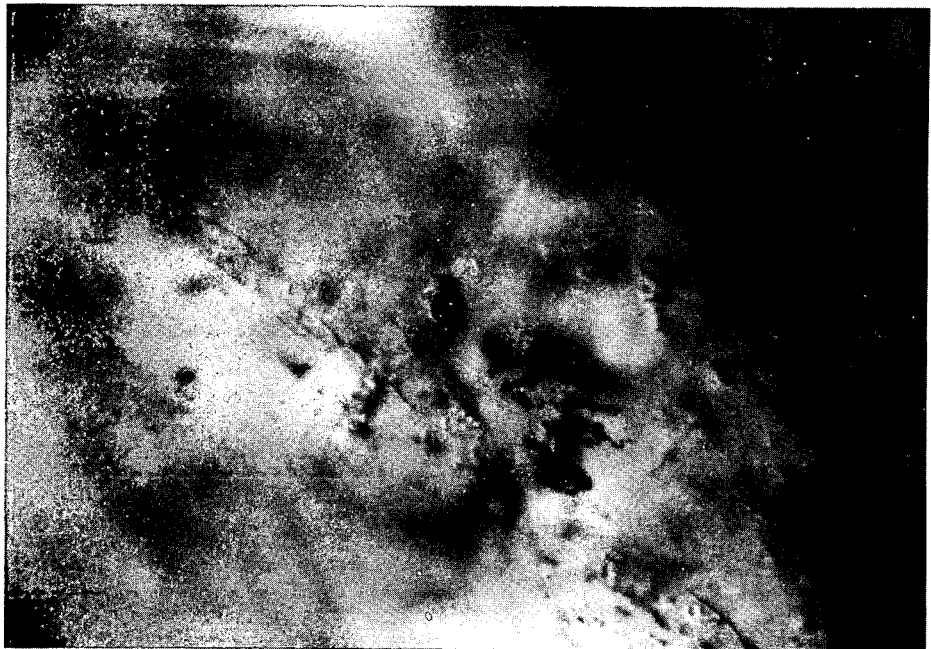


PHOTO 3, GR 19.1, CHIP 3,  
INCLUSION 7; SEE SKETCH  
(CALCITE)



Sample MW 67D-1 - Sparry Calcite

Nearly all inclusions are "deformed" (tails and spurs very abundant) leading to extreme leakage; of 26 heated, 19 leaked. Due to leakage, a general association with fluid-filled inclusions thought to be secondary, and similarity in temperatures, it is difficult to distinguish between primary, pseudo-secondary, and secondary inclusions. Inclusion 4 is isolated, undeformed, and thought to best represent a primary population. The following interpretation is suggested:

Primary or pseudo-primary inclusions

Range 123-138 (4)

Average 128°

Secondary inclusions

Range 110-111 (2)

Average 110°

ANALYST: RJ POTTORF

SAMPLE No. MW67D-1

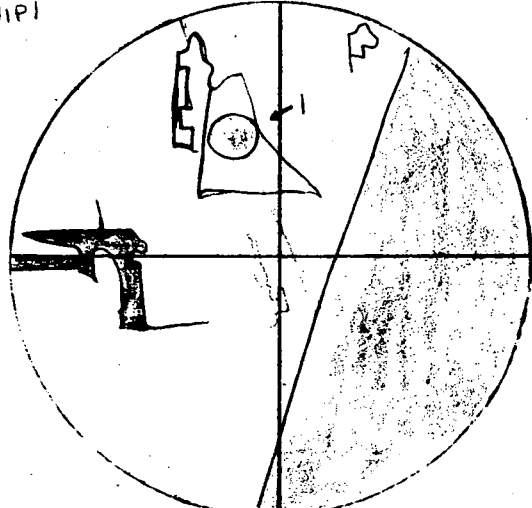
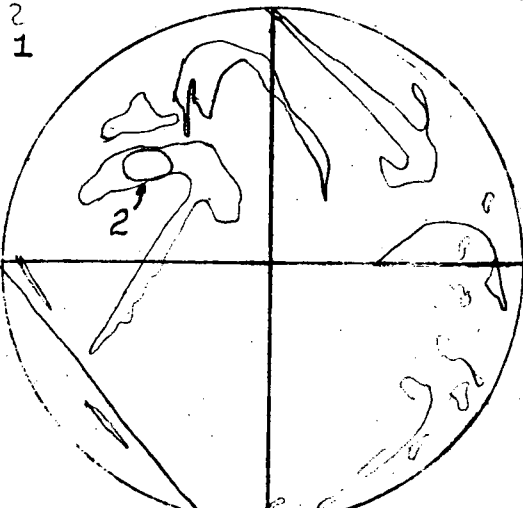
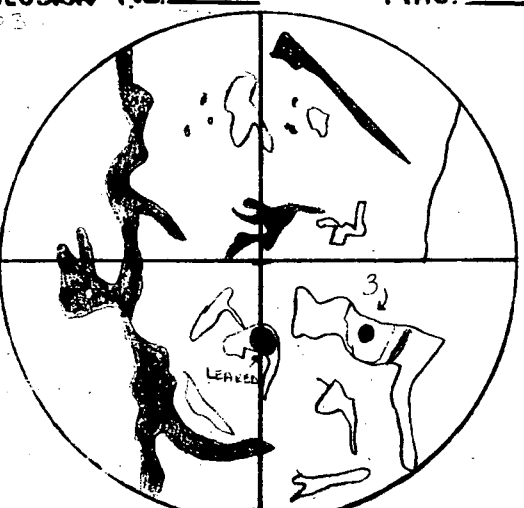
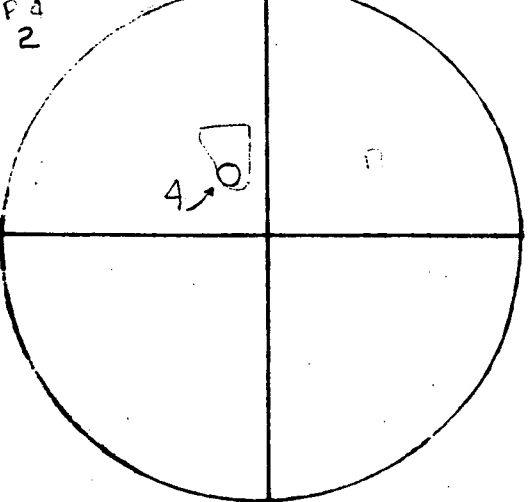
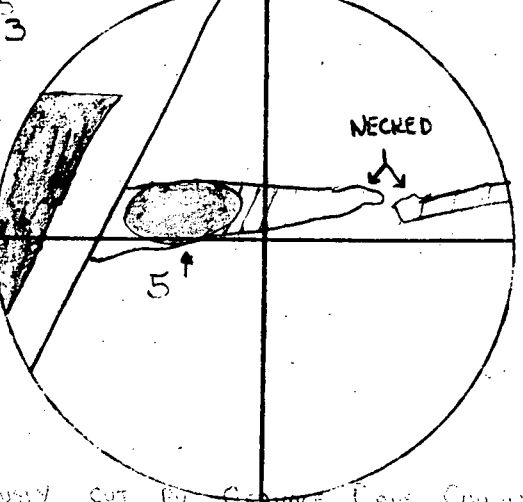
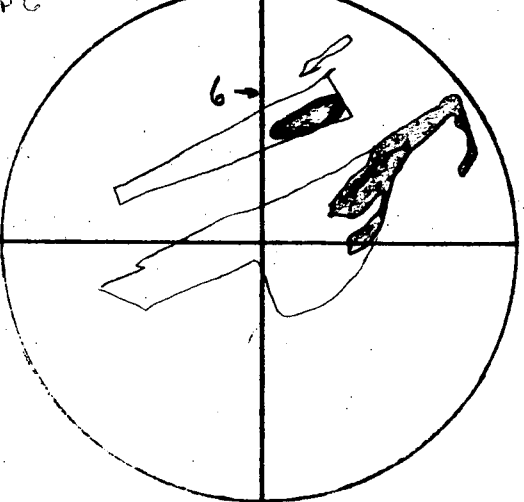
FLUID INCLUSION SKETCHES

CHIP No. 1-6

CON EDISON

MINERAL: CALCITE

48

Inclusion No. <u>1</u> MAG. _____	Inclusion No. <u>2</u> MAG. _____	Inclusion No. <u>3</u> MAG. _____
<p>CHIP 1</p>  <p>OBVIOUS LEAK - DISCARD</p> <p>1) 9.63, 10.30 237°, 253°</p>	<p>CHIP 2 PICT 1</p>  <p>2) 4.57, 4.53 111°, 111°</p>	<p>CHIP 3</p>  <p>3) 4.08, LEAK 100°</p>
Inclusion No. <u>4</u> MAG. _____	Inclusion No. <u>5</u> MAG. _____	Inclusion No. <u>6</u> MAG. _____
<p>CHIP 4 PICT 2</p>  <p>FROM LARGE SINGLE CRYSTAL</p> <p>4) 5.63, 5.64 138°, 138°</p>	<p>CHIP 5 PICT 3</p>  <p>OBVIOUSLY CUT BY CLEARANCE PLANE (NO INCL. TO LEAK, BUT TAIL TOO HIGH AND TAIL TOO THIN)</p> <p>5) 15.86, LEAK 397°</p>	<p>CHIP 6</p>  <p>6) 5.26, LEAK 128°</p>

48

ANALYST: RJ PATTORF

FLUID INCLUSION SKETCHES

CON EDISON

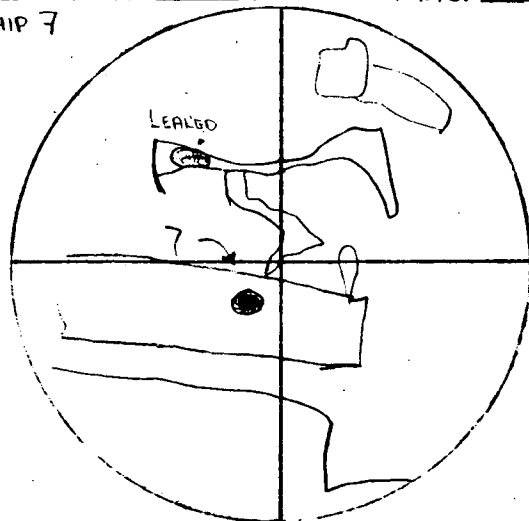
SAMPLE No. MW 67D-1

CHIP No. 7-8

MINERAL: CALCITE

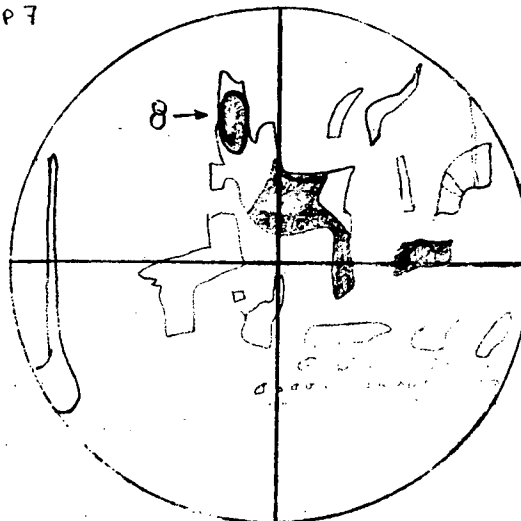
Inclusion No. 7 MAG. \_\_\_\_\_

CHIP 7

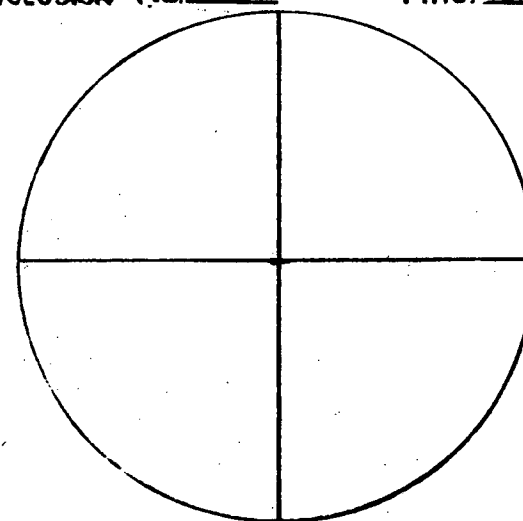


Inclusion No. 8 MAG. \_\_\_\_\_

CHIP 7



Inclusion No. \_\_\_\_\_ MAG. \_\_\_\_\_



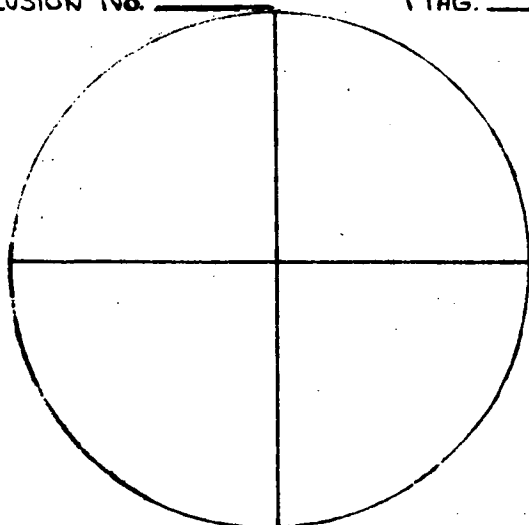
7) 5.06, LEAK

123°

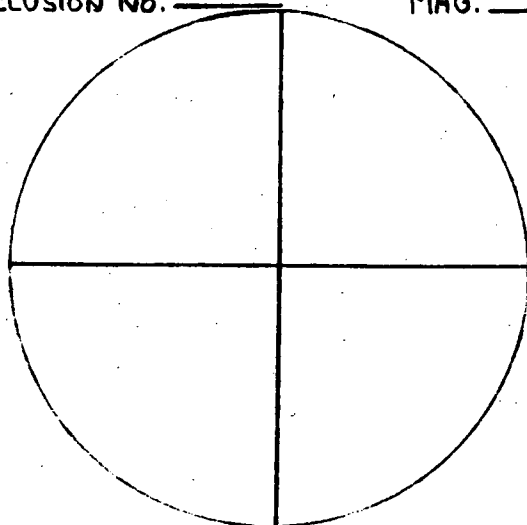
8) 5.08, LEAK

123°

Inclusion No. \_\_\_\_\_ MAG. \_\_\_\_\_



Inclusion No. \_\_\_\_\_ MAG. \_\_\_\_\_



Inclusion No. \_\_\_\_\_ MAG. \_\_\_\_\_

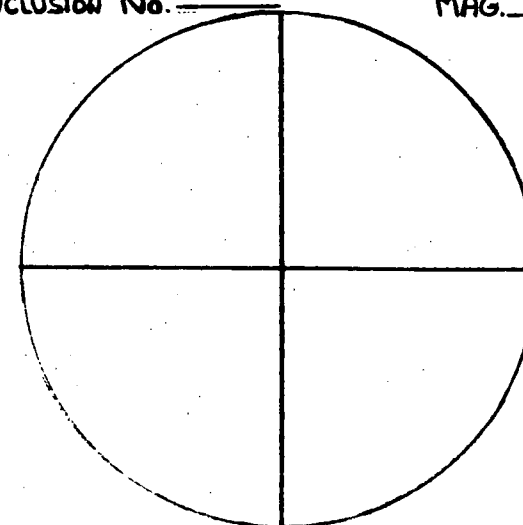


PHOTO 1, MW67D-1, CHIP 2.  
INCLUSION 2; SECONDARY?  
INCLUSION, SEE SKETCH.



PHOTO 2, MW67D-1, CHIP 4.  
INCLUSION 4: PRIMARY  
INCLUSION, SEE TEXT AND SKETCH.

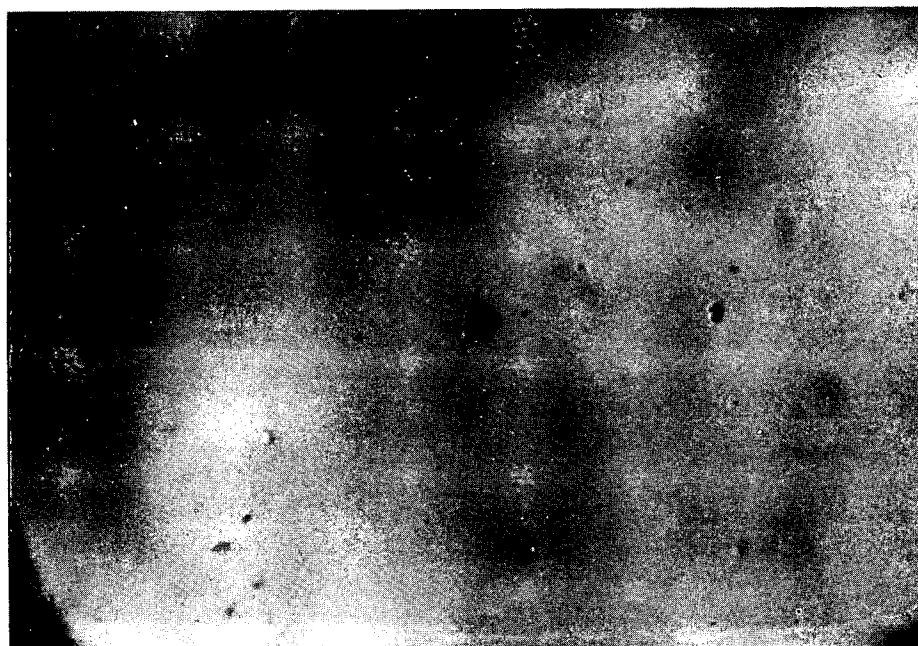
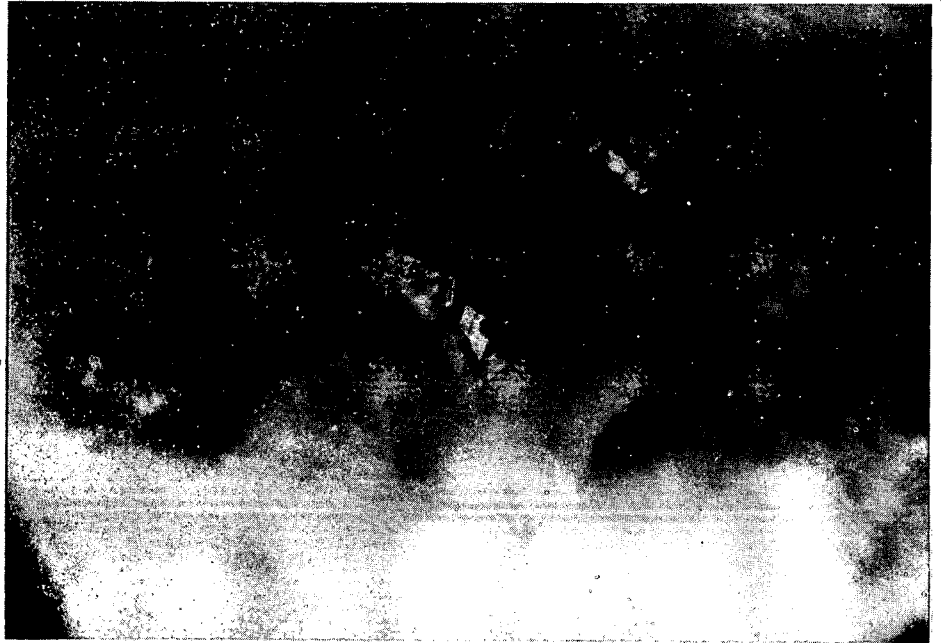


PHOTO 3, MW67D-1, CHIP 5.  
INCLUSION 5; NOT SUITABLE  
FOR HOMOGENIZATION TEMP.;  
SEE SKETCH.



PHOTO 4, MW67D-1; NEGATIVE  
CRYSTAL THOUGHT TO BE  
PRIMARY. THIS INCLUSION LEAKED,  
BUT VAPOR/LIQUID RATIO INDICATES  
TEMP. SIMILAR TO INCLUSION 4.



Sample MW 103-2 - Sparry Calcite

Inclusions are abundant; of 25 heated, 5 leaked. Totally fluid-filled inclusions are present (see photo 12). When these inclusions are heated and brought back to room temperature, two phases are present indicating leakage of fluid. It is concluded that these must be very low-temperature secondary inclusions.

There is a wide temperature variation among the inclusions measured, and populations can not be divided according to their morphologies. The frequency plot serves as a means to visualize differences in populations on the basis of temperature. There appears to be a low temperature population (secondary) ranging from 99-130°. It is not obvious if one or more populations (primary, pseudo-secondary) are present from 151-271°. Tentatively, only one population is suggested.

Primary inclusions

Range 151-271° (6)

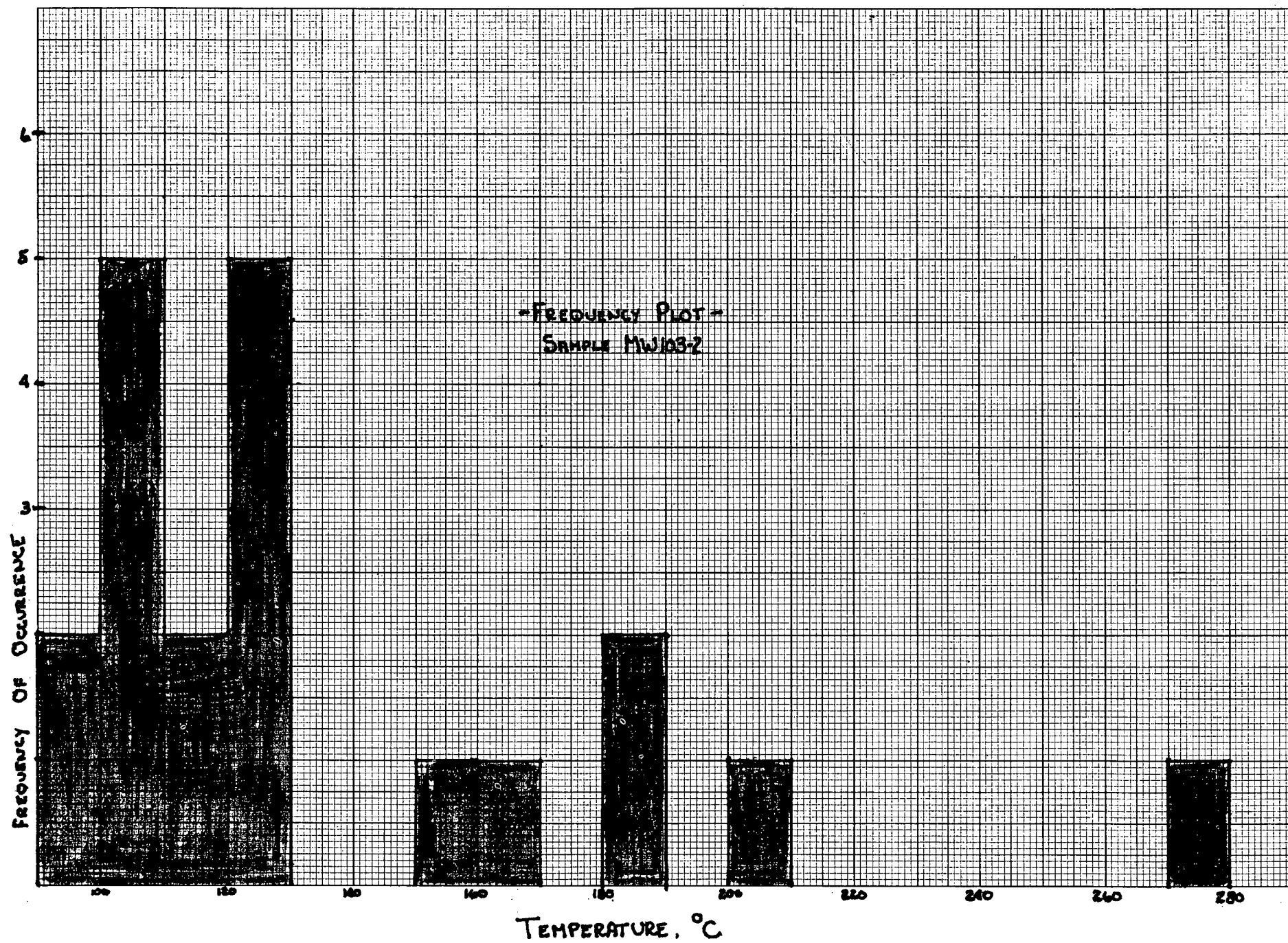
Average 195°

Secondary inclusions

Range 99-130° (14)

Average 114°

Very low temperature fluid-filled secondary inclusions



ANALYST: RJ POTTORF

# FLUID INCLUSION SKETCHES

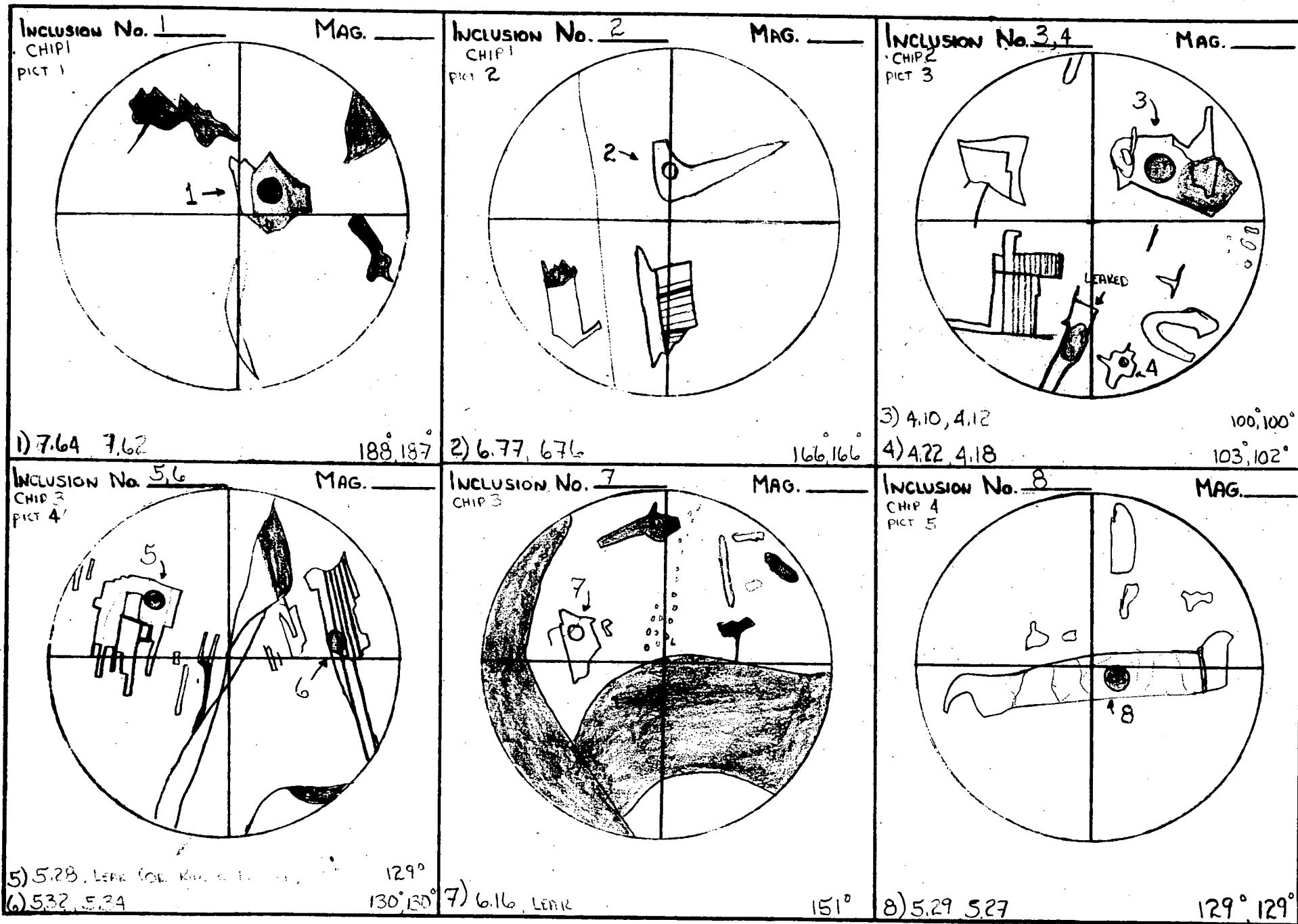
CON EDISON

06

SAMPLE No. MW103-2

CHIP No. 1-4

MINERAL: CALCITE



06

ANALYST: RJ POTTORF

FLUID INCLUSION SKETCHES

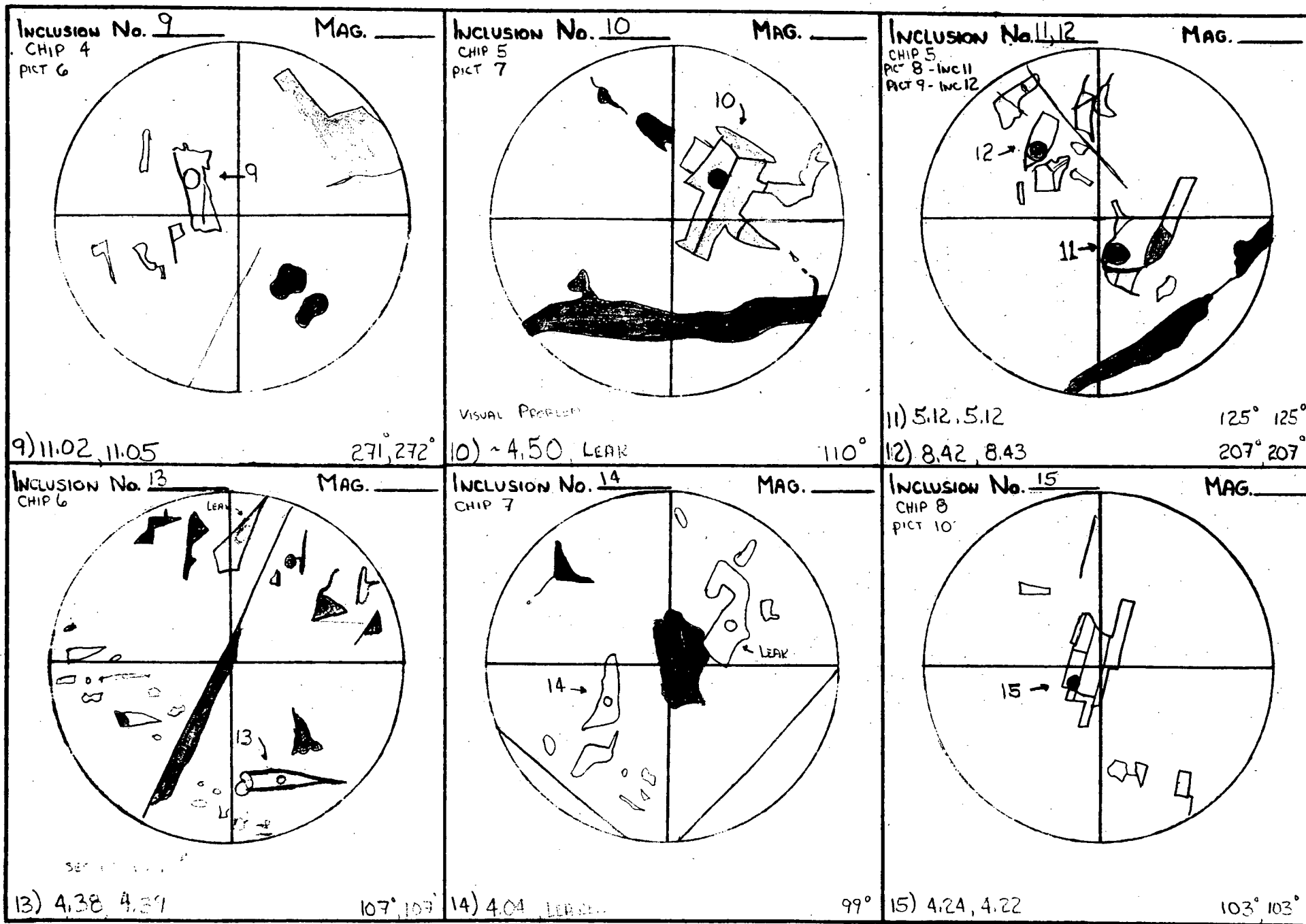
CON EDISON

SAMPLE No. MW 103-2

CHIP No. 4-8

MINERAL: CALCITE

16



16

ANALYST: RJ POTTORF

FLUID INCLUSION SKETCHES

CON EDISON

92

SAMPLE No. MW103-2

CHIP No. 9

MINERAL: CALCITE

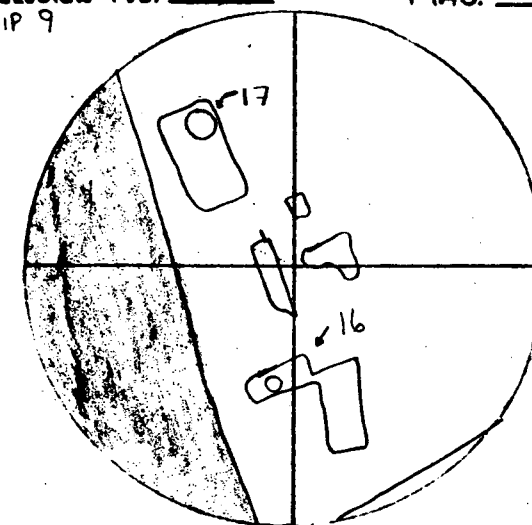
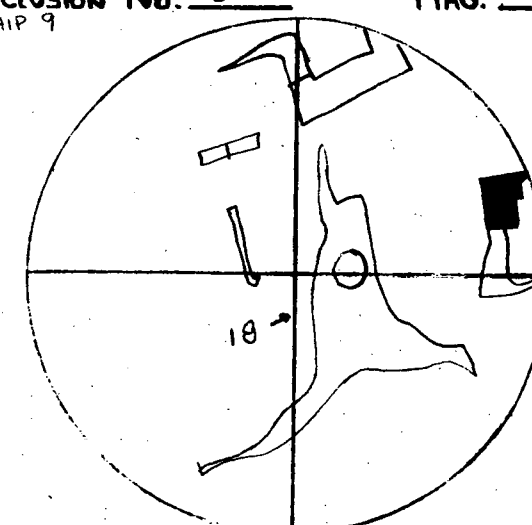
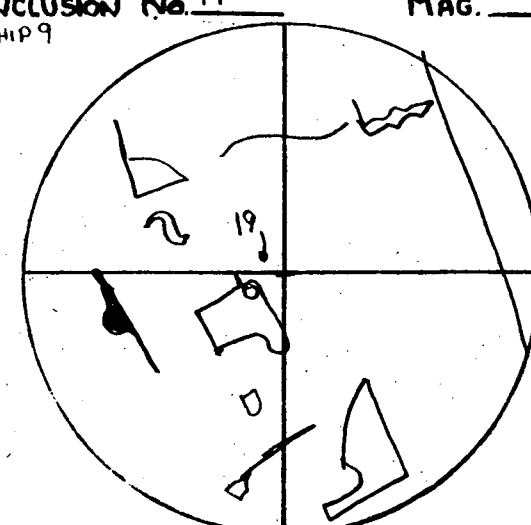
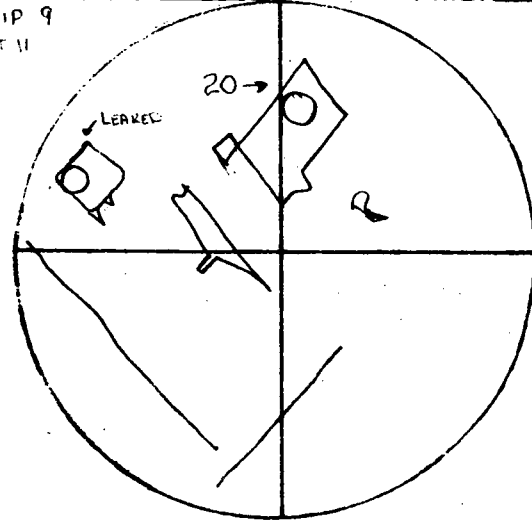
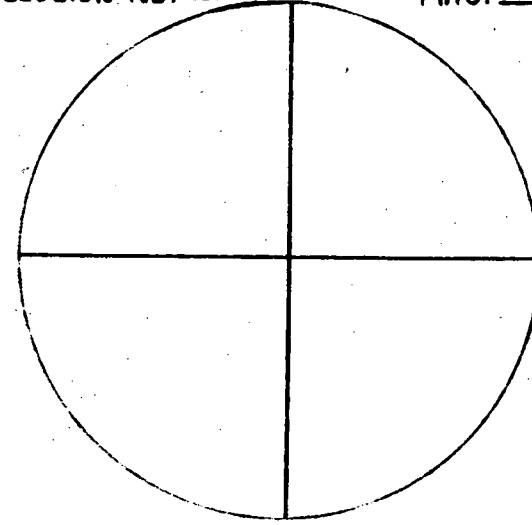
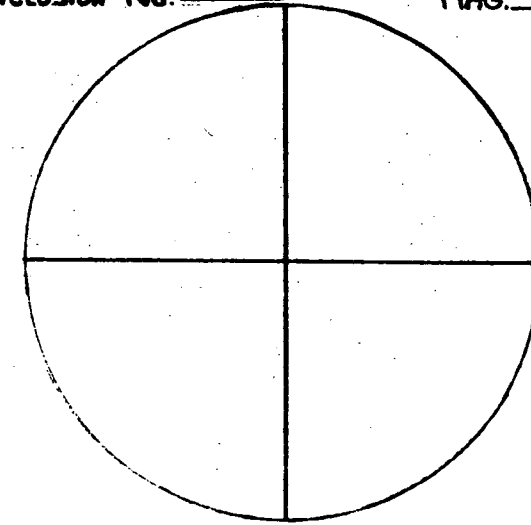
<p>Inclusion No. <u>16, 17</u> CHIP 9</p>  <p>16) 4.15, LEAK 17) 5.10, 5.11</p> <p>MAG. _____</p> <p>101° 124°, 124°</p>	<p>Inclusion No. <u>18</u> CHIP 9</p>  <p>18) 4.90, LEAK</p> <p>MAG. _____</p> <p>120°</p>	<p>Inclusion No. <u>19</u> CHIP 9</p>  <p>19) 4.66, 4.67</p> <p>MAG. _____</p> <p>114°, 114°</p>
<p>Inclusion No. <u>20</u> CHIP 9 PIT II</p>  <p>20) 7.58, 7.60</p> <p>MAG. _____</p> <p>186°, 187°</p>	<p>Inclusion No. _____</p>  <p>MAG. _____</p>	<p>Inclusion No. _____</p>  <p>MAG. _____</p>

PHOTO 1, MW103-2, CHIP1  
INCLUSION 1 ; SEE SKETCH.



PHOTO 2, MW103-2, CHIP1.  
INCLUSION 2 ; SEE SKETCH.

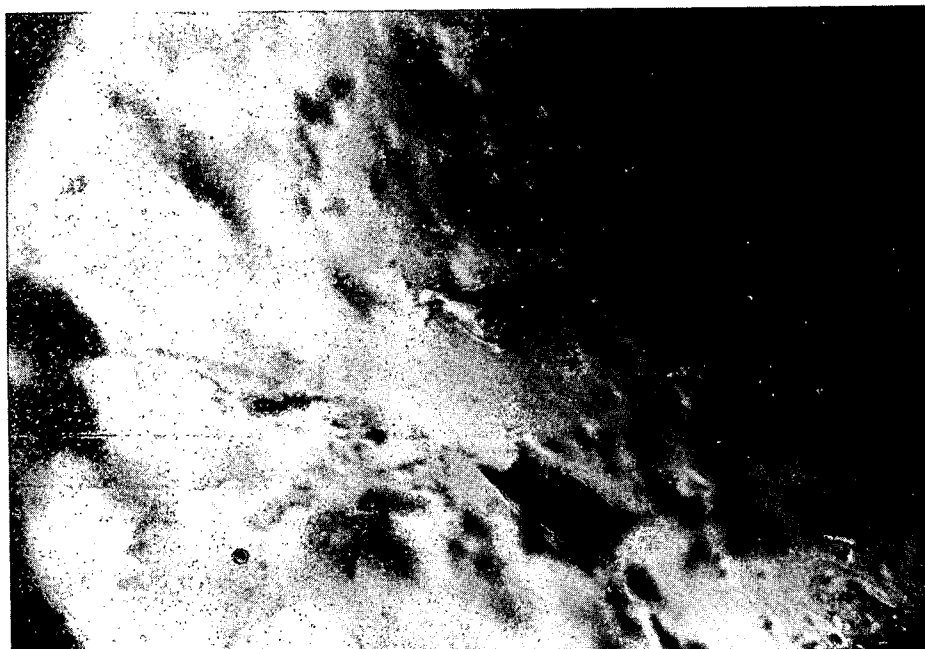


PHOTO 3, MW103-2, CHIP2  
INCLUSION 3 ; SEE SKETCH.

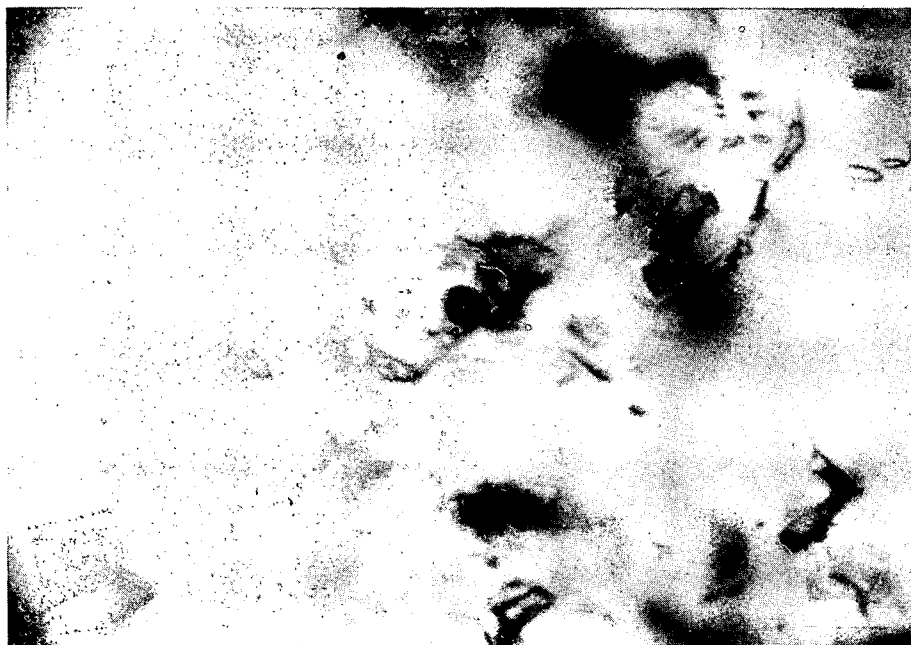


PHOTO 4, MW103-2, CHIP 3,  
INCLUSION 5 ; SEE SKETCH.



PHOTO 5, MW103-2, CHIP 4,  
INCLUSION 8 ; SEE SKETCH.

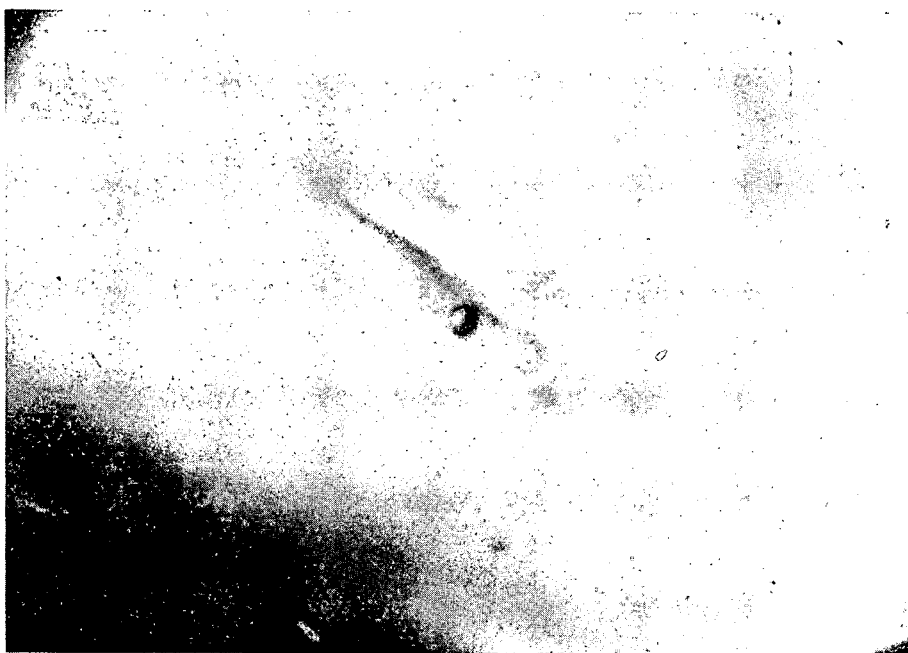


PHOTO 6, MW103-2, CHIP 4,  
INCLUSION 9 ; SEE SKETCH



75  
PHOTO 7, MW103-2, CHIP 5,  
INCLUSION 10; SEE SKETCH.



PHOTO 8, MW103-2, CHIP 5  
INCLUSION 11; SEE SKETCH

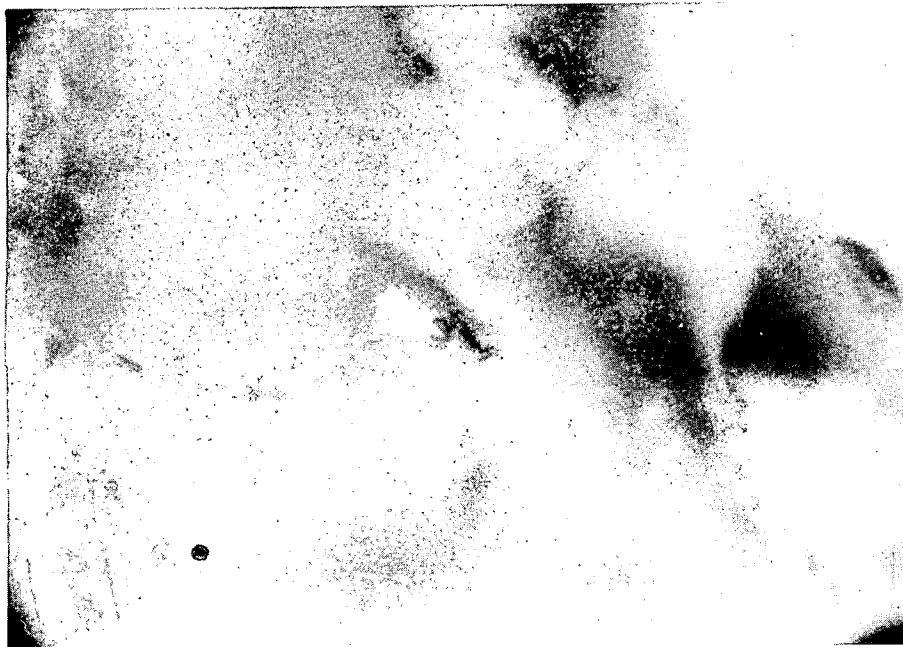


PHOTO 9, MW103-2, CHIP 5,  
INCLUSION 12; SEE SKETCH

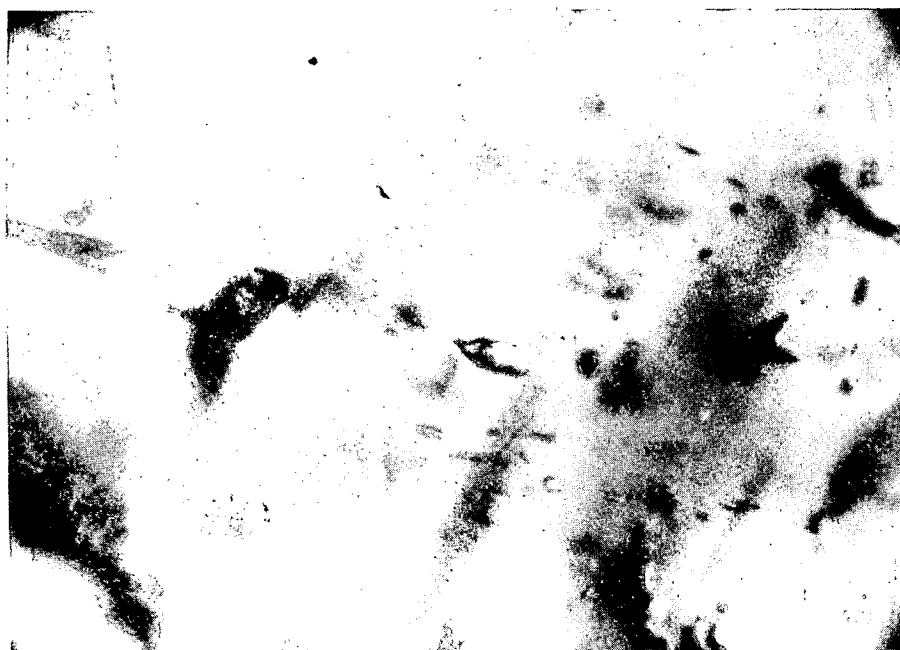


PHOTO 10, MW103-2, CHIP 8,  
INCLUSION 15; SEE SKETCH.

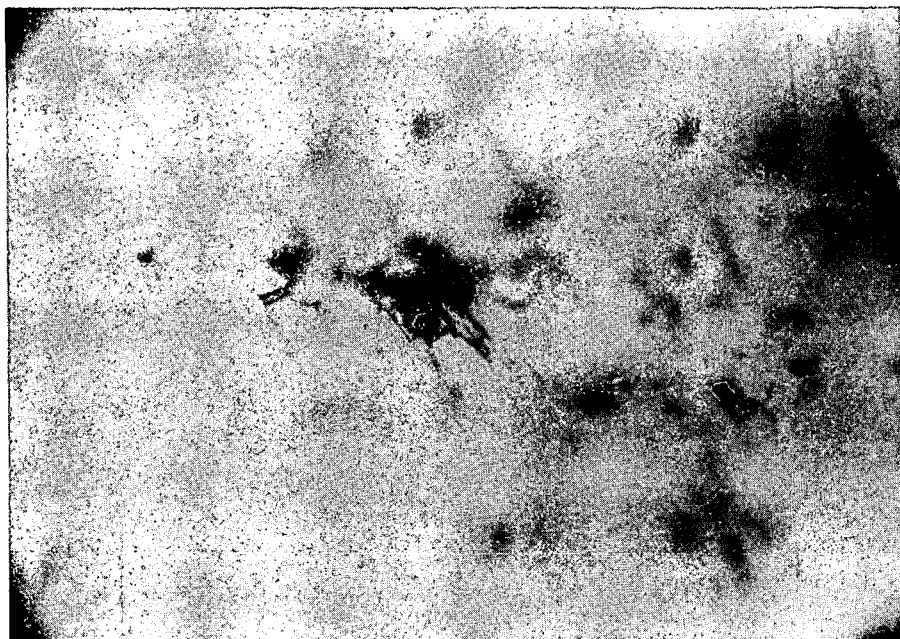
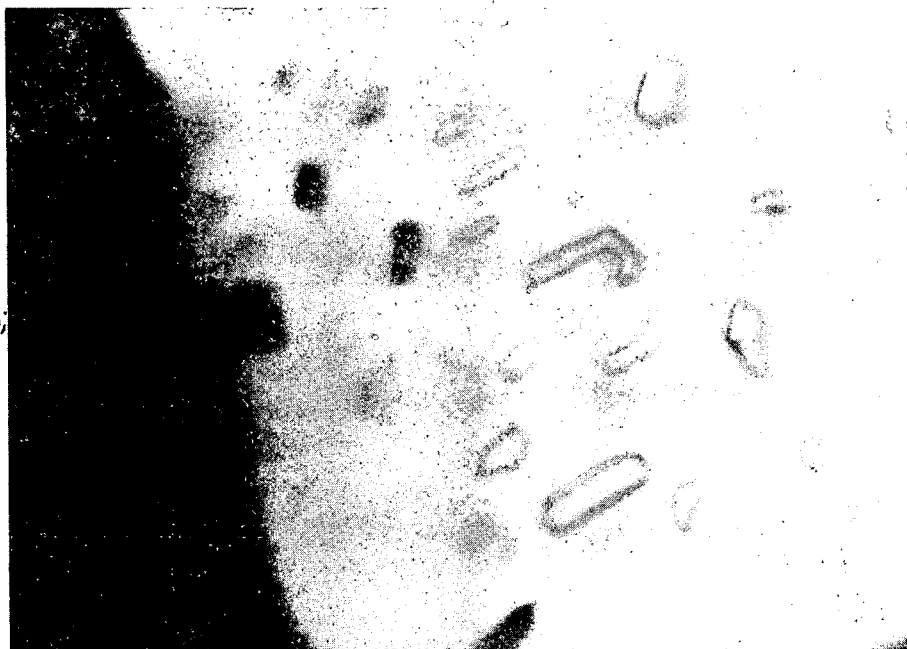


PHOTO 11, MW103-2, CHIP 9,  
INCLUSION 20; SEE SKETCH.



PHOTO 12, MW103-2; FLUID-  
FILLED SECONDARY INCLUSIONS;  
SEE TEXT.



Sample MW 103-3 - Sparry Calcite

Large numbers of secondary inclusions with spurs and tails are present along rehealed cleavage surfaces.

Primary (or pseudo-secondary) inclusions also generally have irregular shapes with tails. Of 17 inclusions heated, 8 leaked.

Primary (?) inclusions

Range 130-145° (6)

Average 135°

Secondary inclusions

Range 93-103° (3)

Average 99°

ANALYST: RJ POTTORF

SAMPLE No. MW 103-3

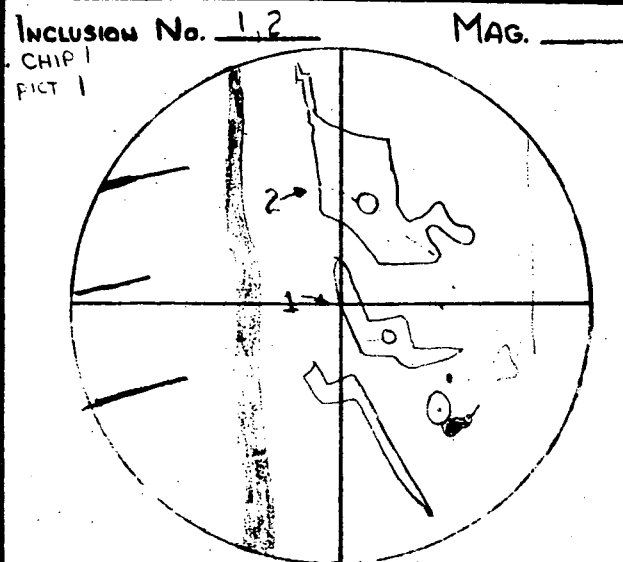
# FLUID INCLUSION SKETCHES

CHIP No. 1-6

CON EDISON

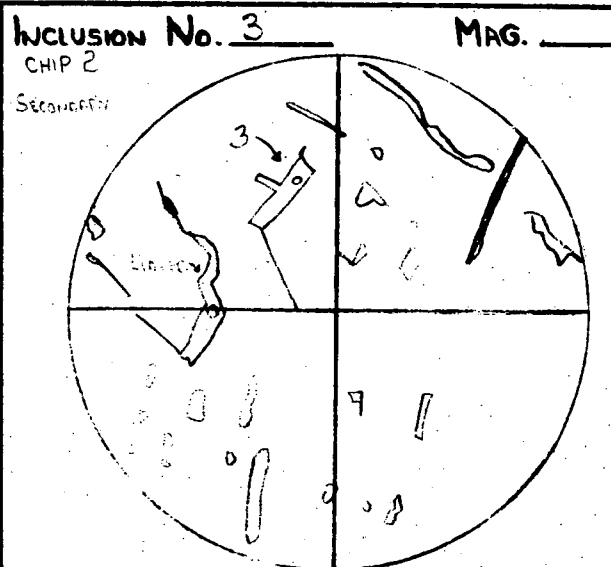
MINERAL: CALCITE

26



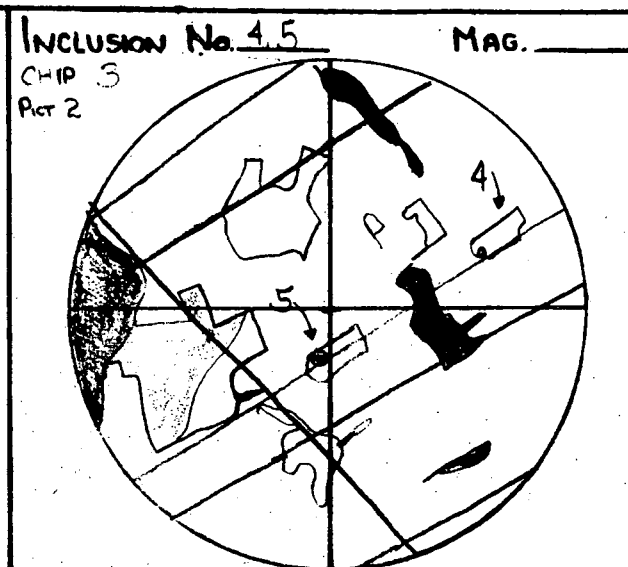
1) 5.35, LEAKED  
2) 5.95, 6.77, (4.595 & 6.77)

131°  
145°



3) 4.13, LEAK

101°

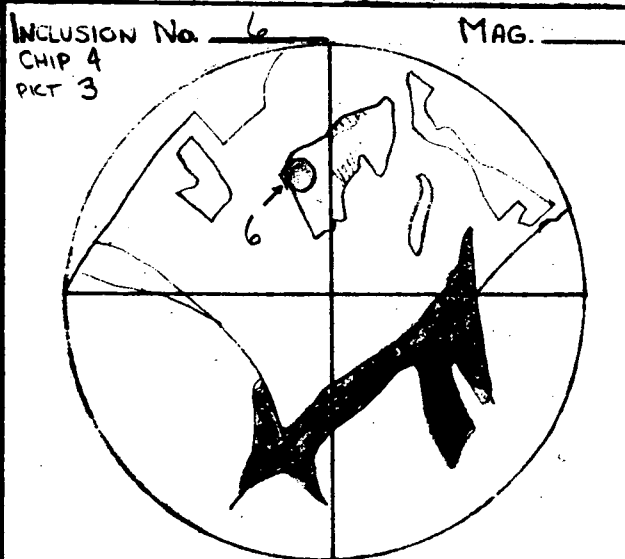


4) 4.22, LEAK

103°

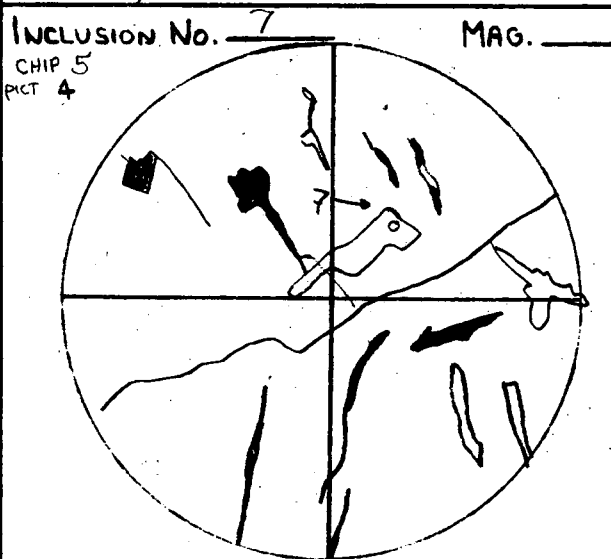
5) 5.33, LEAK

130°



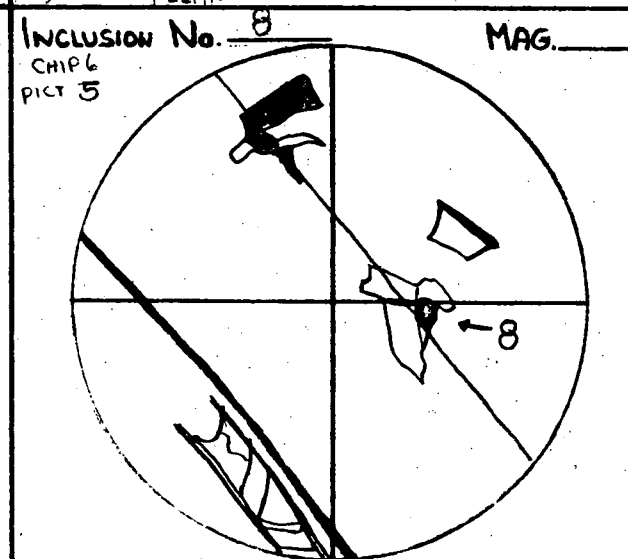
6) 3.85, 3.76

94°, 92°



7) 5.65, 5.62

138°, 137°



8) 5.56, 5.68

136°, 139°

86

ANALYST: RJ POTTORF

FLUID INCLUSION SKETCHES

CON EDISON

66

SAMPLE No. MW 103-3

CHIP No. 7

MINERAL: CALCITE

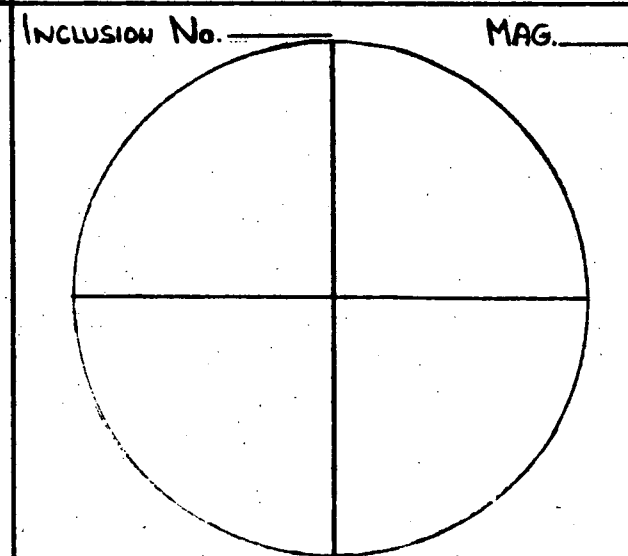
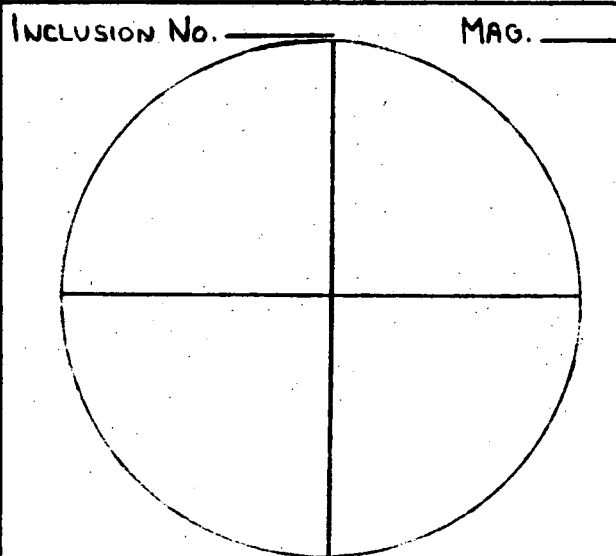
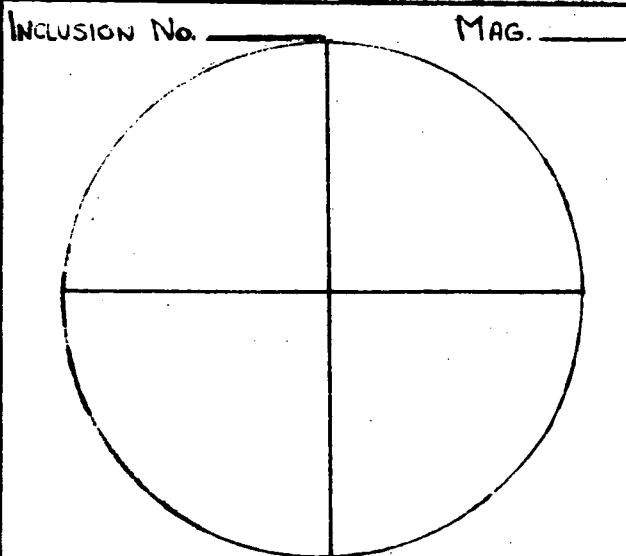
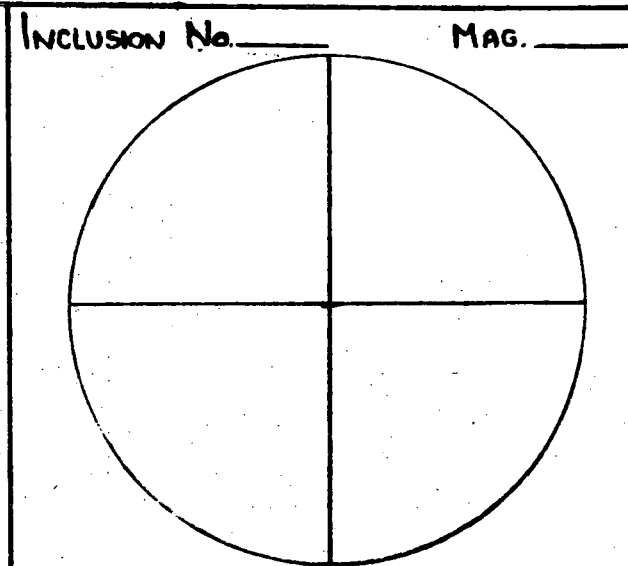
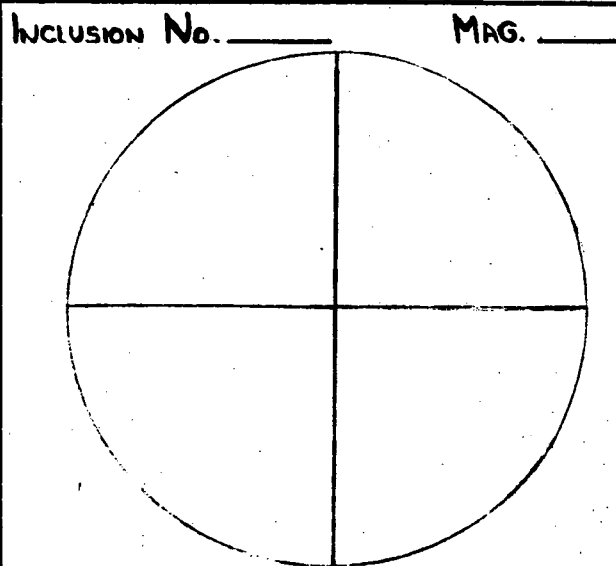
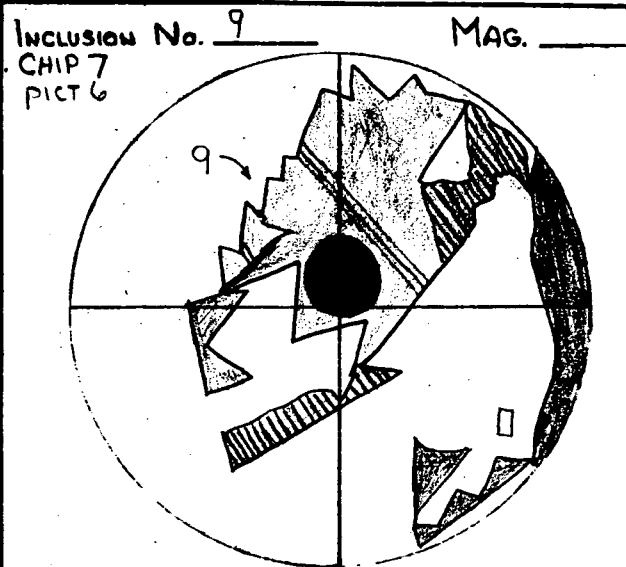


PHOTO 1, MW103-3, CHIP 1,  
INCLUSION 1 AND 2; SEE  
SKETCH.



PHOTO 2, MW103-3, CHIP 3,  
INCLUSION 5; SEE SKETCH

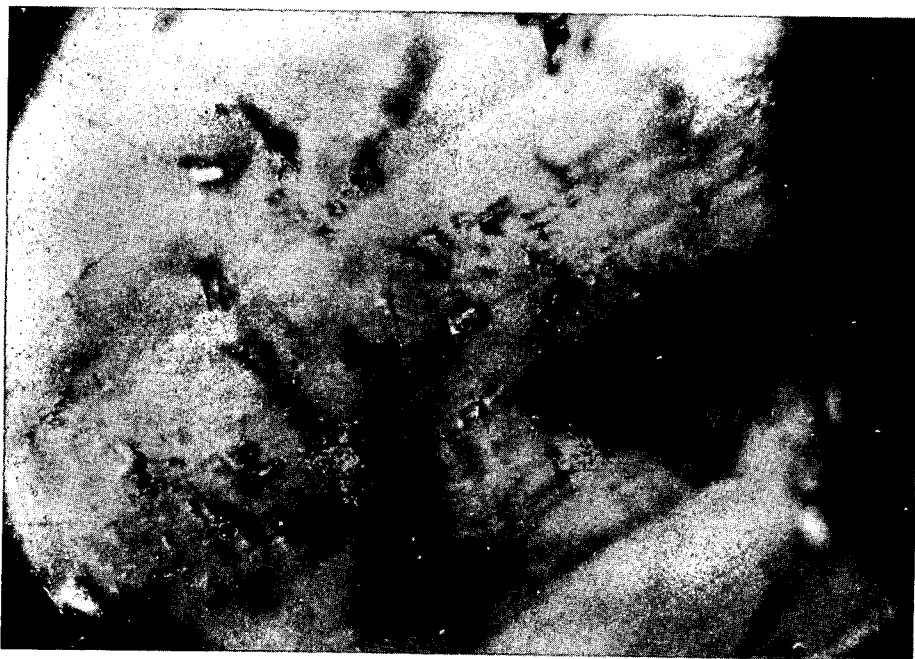


PHOTO 3, MW103-3, CHIP 4,  
INCLUSION 6; SEE SKETCH.



PHOTO 4, MW103-3, CHIP 5.  
INCLUSION 7; SEE SKETCH.

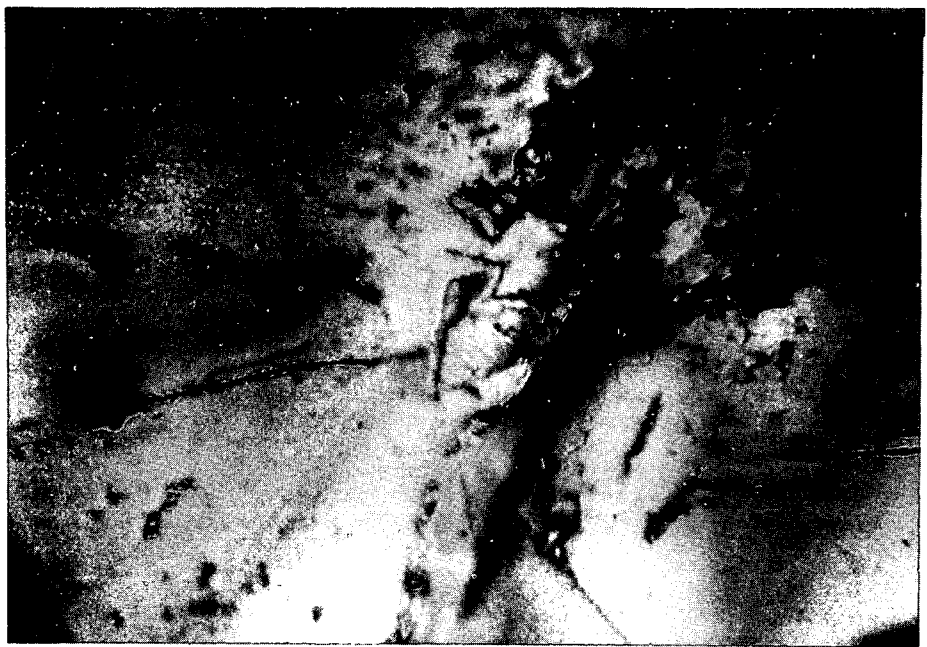


PHOTO 5, MW103-3, CHIP 6  
INCLUSION 8, SEE SKETCH.

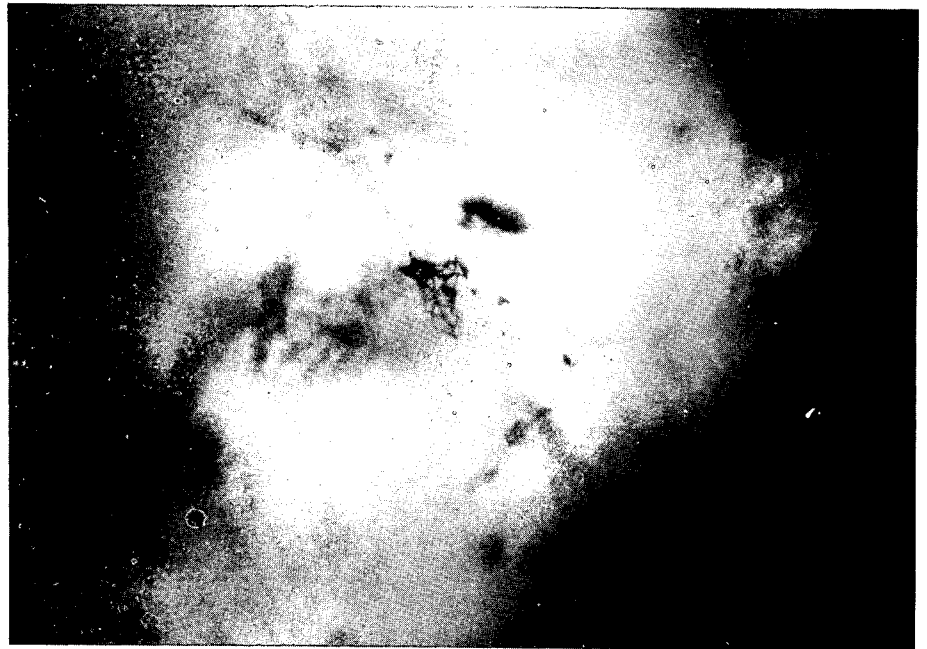


PHOTO 6, MW103-3, CHIP 7  
INCLUSION 9; SEE SKETCH.



Sample MW 106-2 - Calcite Crystals (cogenetic with stilbite)

Two generations of calcite are present in the sample: an early, deformed gray calcite and a later undeformed clear calcite stage.

1) Gray calcite: Inclusions are greatly necked and/or display spurs and tails. Rhombohedral cleavage traces are very prevalent, which contribute to leakage. Only a few inclusions were heated, but all leaked. It was decided little useful information could be gained from further study of the gray phase.

2) Clear calcite: Inclusions fairly abundant; low temperature, fluid-filled inclusions are very common. The inclusion populations are not well-defined either by morphology or temperature. Three populations are tentatively suggested (see frequency plot):

Primary (?) inclusions

Range 165-220° (4)

Average 192°

Secondary (?) inclusions

Range 99-136° (7)

Average 114°

Low temperature fluid-filled secondary inclusions.

ANALYST: RJ POTTORF

# FLUID INCLUSION SKETCHES

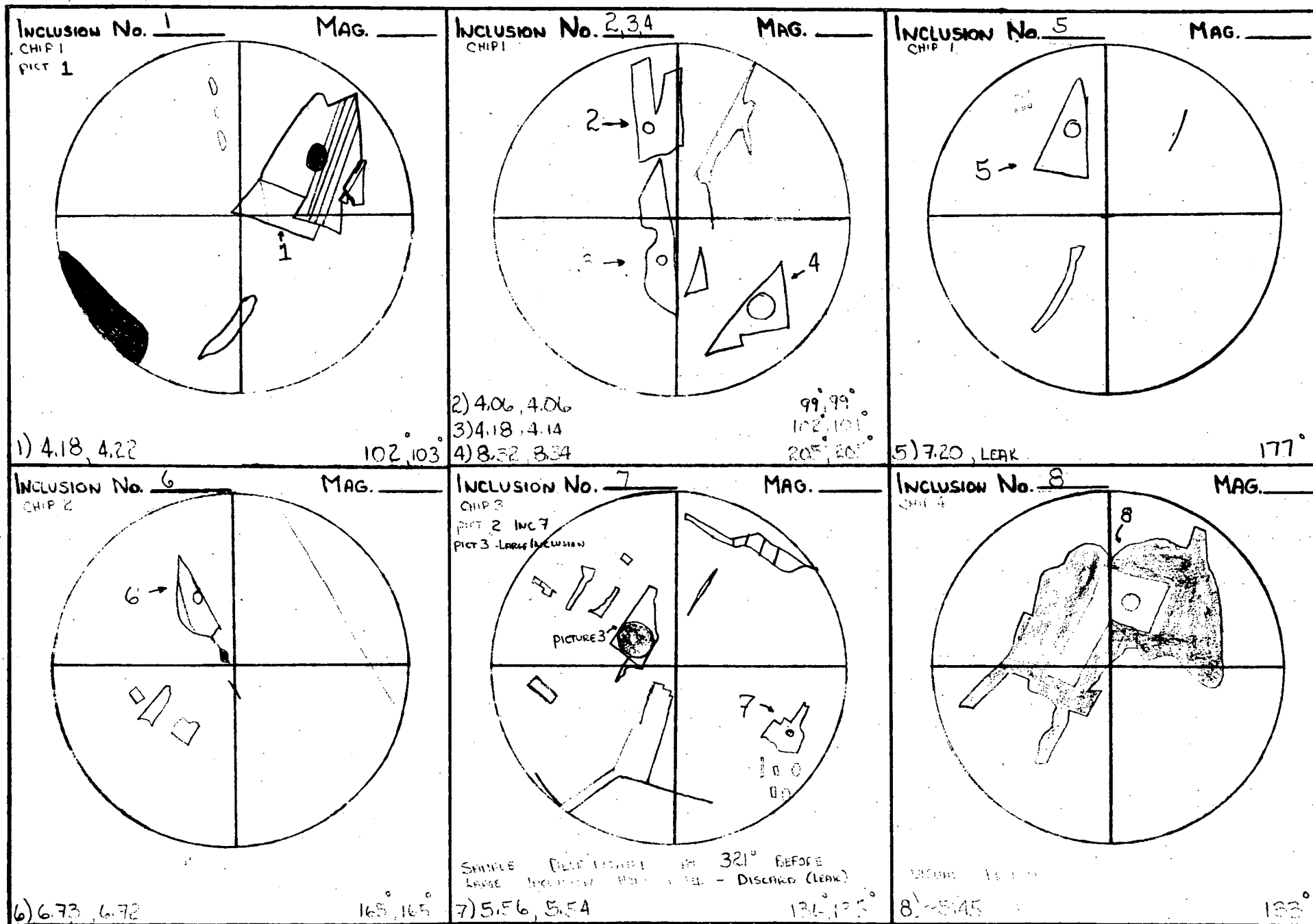
CON EDISON

SAMPLE No. MW 106-2

CHIP No. 1-4

MINERAL: CALCITE

103



104

ANALYST: RJ POTTORF

FLUID INCLUSION SKETCHES

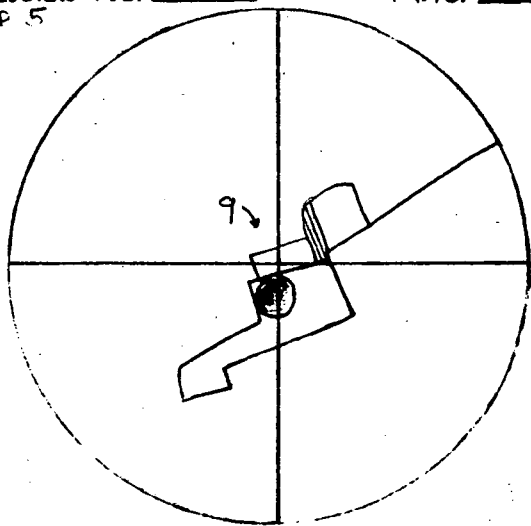
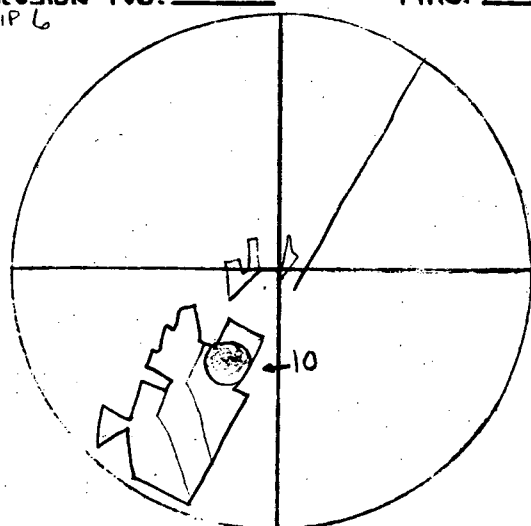
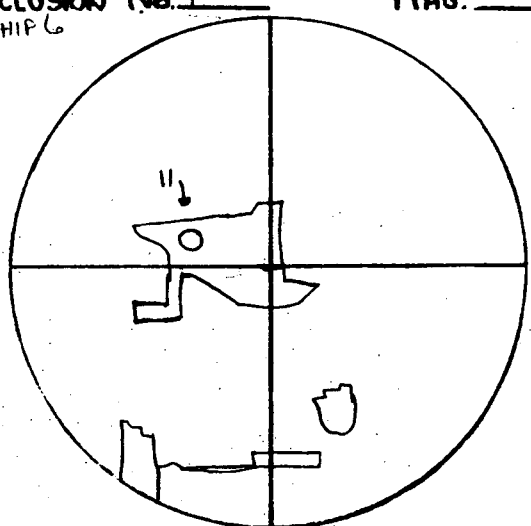
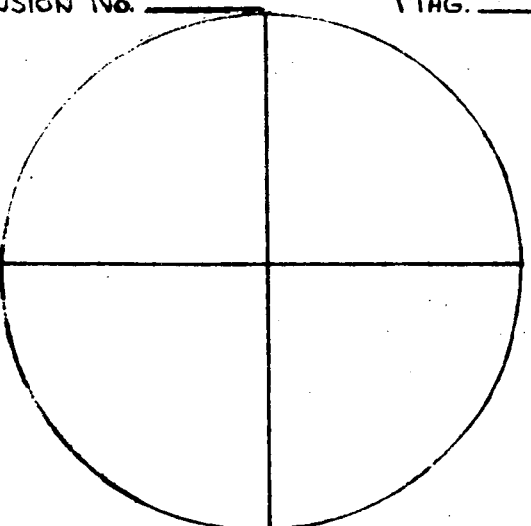
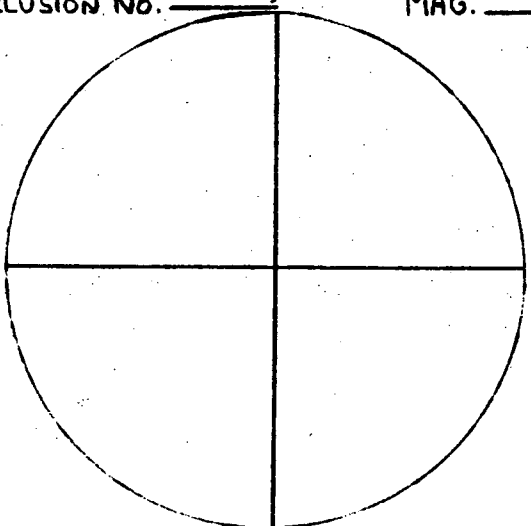
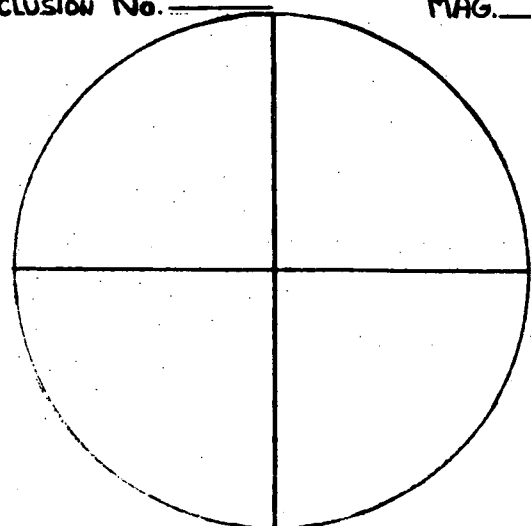
CON EDISON

SAMPLE No. MW 106-2

CHIP No. 5-6

MINERAL: CALCITE

104

<p>Inclusion No. <u>9</u> MAG. _____ CHIP 5</p>  <p>9) 8.99, 8.96 221° 220°</p>	<p>Inclusion No. <u>10</u> MAG. _____ CHIP 6</p>  <p>10) 4.10, 4.13 100° 101°</p>	<p>Inclusion No. <u>11</u> MAG. _____ CHIP 6</p>  <p>11) -5.15, LEAK + VISUAL PROBLEM 125°</p>
<p>Inclusion No. _____ MAG. _____</p> 	<p>Inclusion No. _____ MAG. _____</p> 	<p>Inclusion No. _____ MAG. _____</p> 

105

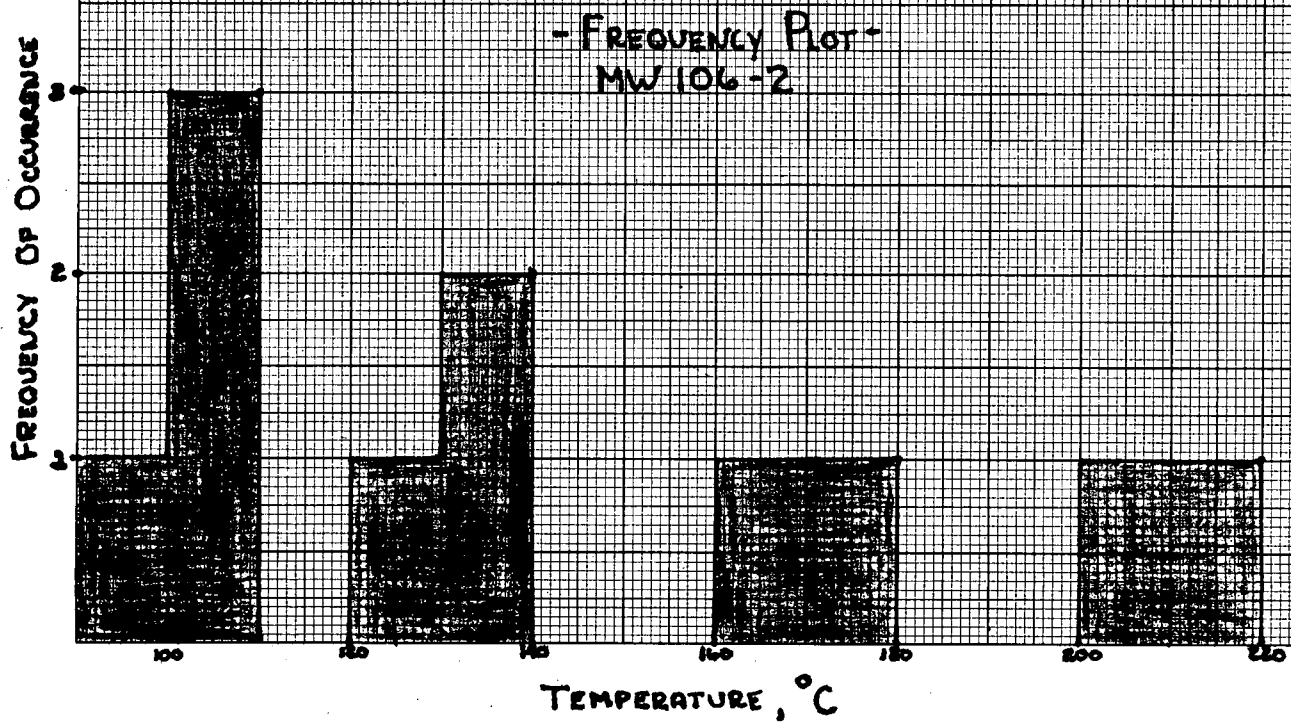


PHOTO 1, MW106-2, CHIP1,  
INCLUSION 1 ; SEE SKETCH.

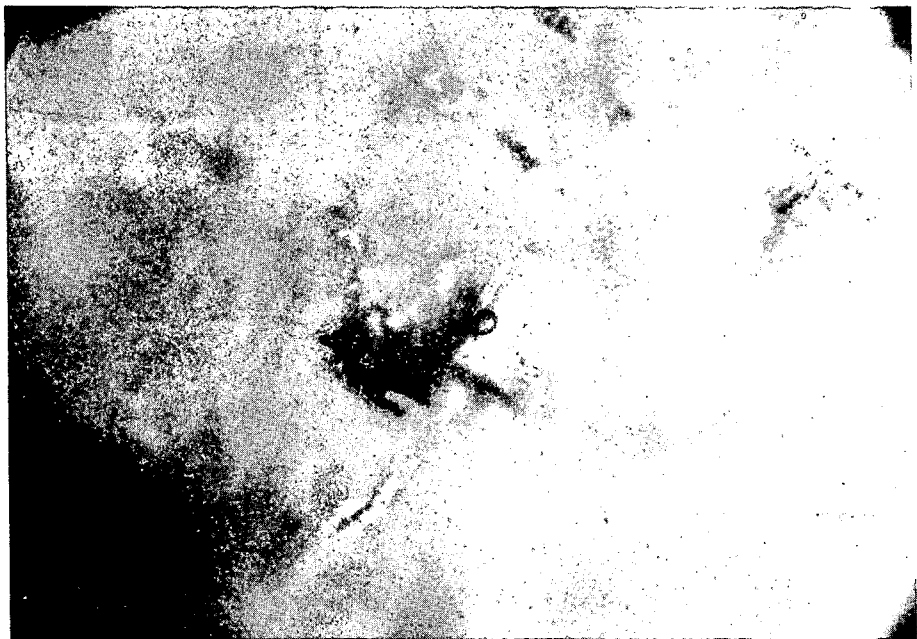
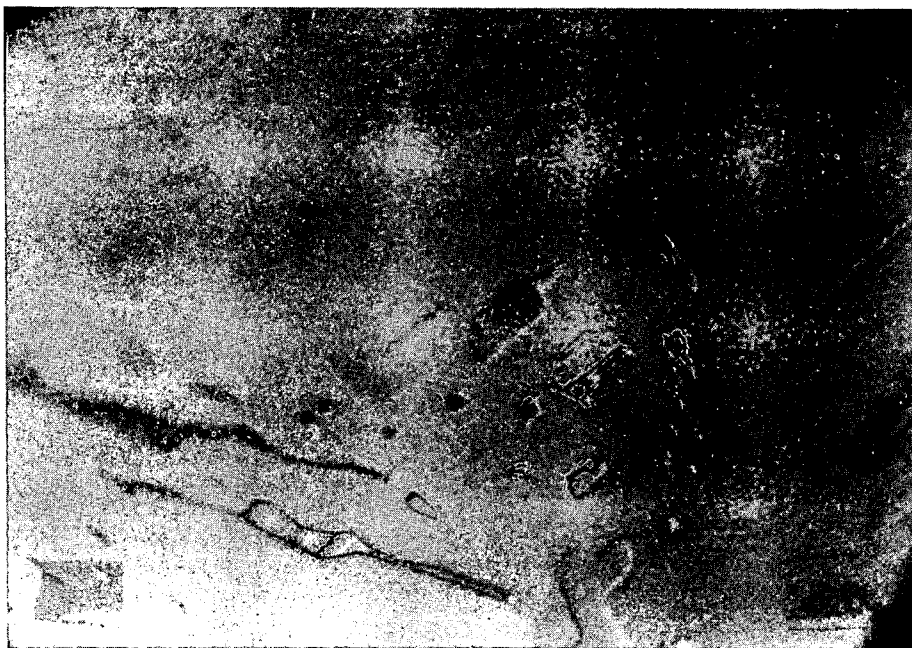


PHOTO 2, MW106-2, CHIP3,  
INCLUSION 7 ; SEE SKETCH



PHOTO 3, MW106-2, CHIP3,  
SAME AREA AS PHOTO 2,  
DIFFERENT DEPTH OF FOCUS;  
LARGE INCLUSION WAS PROBABLY  
ORIGINALLY A FLUID-FILLED  
INCLUSION WHICH LEAKED.



## Sample MW 114-1 - Quartz

Inclusions generally have large and irregular shapes with varying liquid/vapor ratios. Most of these inclusions display tails and many have large vapor/liquid ratios, possibly as a result of leakage at some time. These generally homogenize at temperatures  $>300^{\circ}\text{C}$ , or the sample decrepitates before homogenization. Their association with totally fluid-filled inclusions also suggests that these two-phase inclusions are products of leakage and don't represent a high temperature population. However, their consistent temperatures, greater than  $300^{\circ}$ , may be meaningful and must be considered.

Inclusion 2 does not exhibit noticeable tails and may approximate the primary temperature. Inclusions 1, 4, and 5 are probably pseudo-secondary or secondary.

Three possible populations:

- 1)  $\sim 300^{\circ}$
- 2) Primary (?) inclusions  
Average  $\sim 215^{\circ}$  (1)
- 3) Pseudo-secondary (?) inclusions  
Range  $130-142^{\circ}$  (3)  
Average  $135^{\circ}$

ANALYST: RJ POTTORF

SAMPLE No. MW 114-1

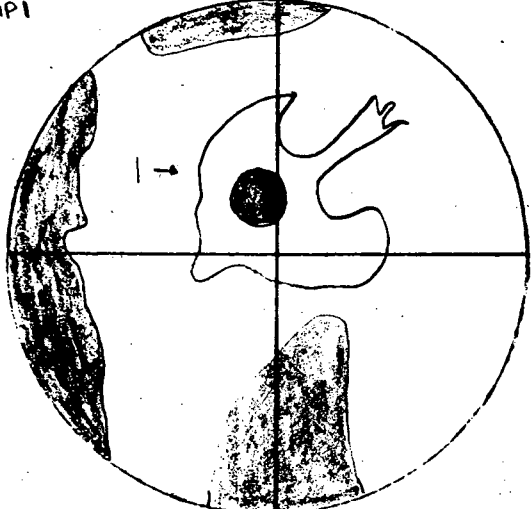
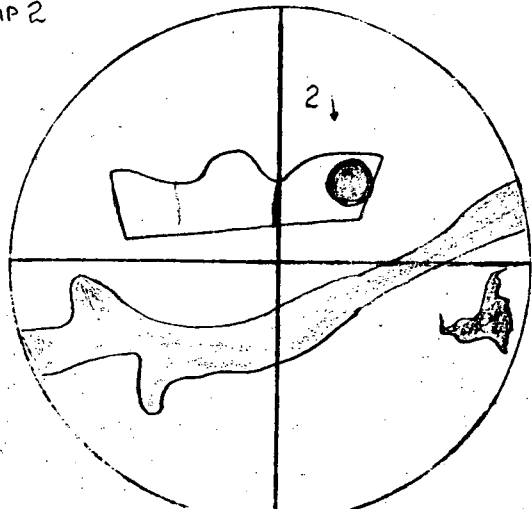
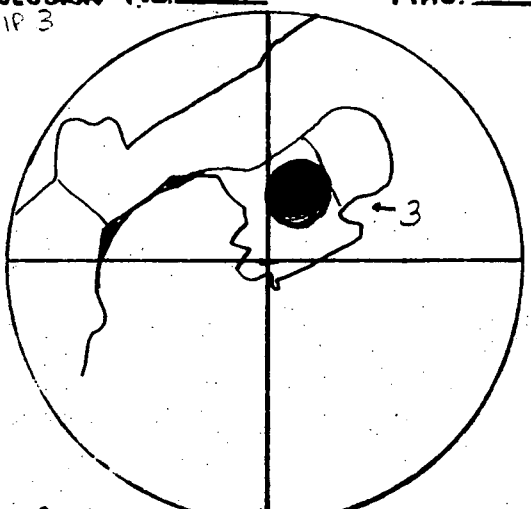
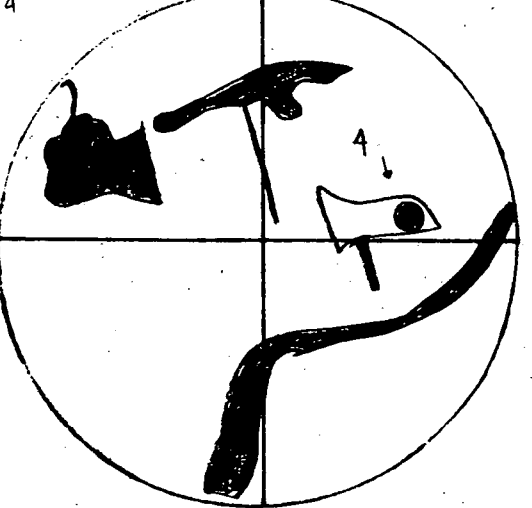
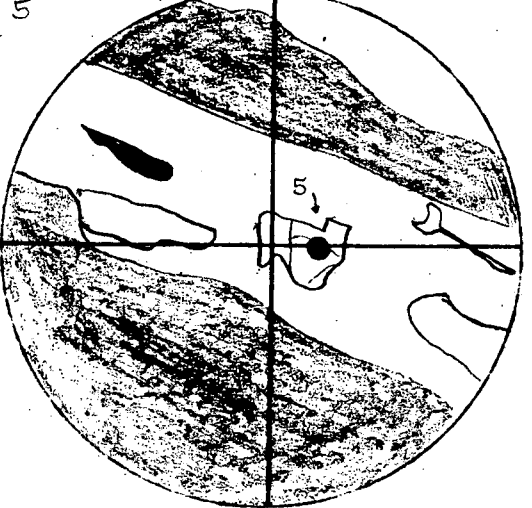
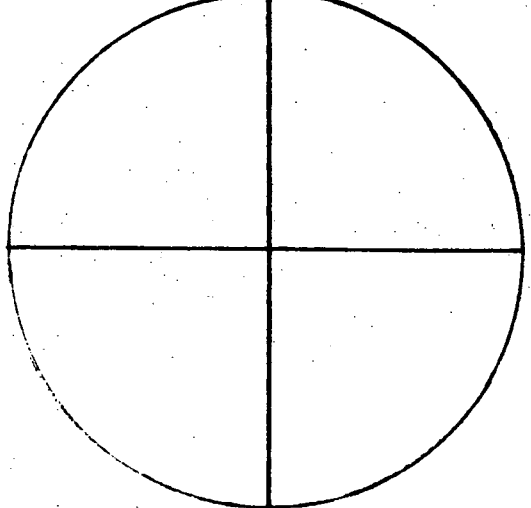
# FLUID INCLUSION SKETCHES

CHIP No. 1-5

CON EDISON

MINERAL: QUARTZ

101

Inclusion No. 1 CHIP 1	Inclusion No. 2 CHIP 2	Inclusion No. 3 CHIP 3
		 <p data-bbox="1361 795 1915 860">COULD BE NECKED OR FORMED BY LEAKAGE OF FLUID FILLED INCLUSION.</p>
1) 5.33, 5.35 130°, 130°	2) 8.92, 9.18 (SLIGHT LEAK, 219° MAXIMUM) 219°, 226°	3) 12.34, 12.35, 12.28 303°, 303°, 302°
Inclusion No. 4 CHIP 4	Inclusion No. 5 CHIP 5	Inclusion No. 6 CHIP 6
		
4) 5.81, LEAK 142°	5) 5.45, 5.75 (LEAK, 133° MAXIMUM) 133°, 140°	

Sample MW 115-1 - Sparry Quartz

Primary inclusions are rare; irregular fractures are common. Pyramid-shaped negative crystals are present, generally displaying tails at their corners, and nearly all are empty (see sketch, inclusion 1 and 2). Those with two phases observed (8 inclusions) leaked when heated. One inclusion (no. 3) darkened and homogenized at  $\sim 168^{\circ}\text{C}$ . This temperature must be viewed with reservation.

Very small, irregularly shaped secondary inclusions are present; 3 were heated but all leaked. The appearance of this sample is very similar to GA 4.1.

Homogenization temperature  $\sim 168^{\circ}(\text{?})$

ANALYST: RJ POTTORF

FLUID INCLUSION SKETCHES

CON EDISON

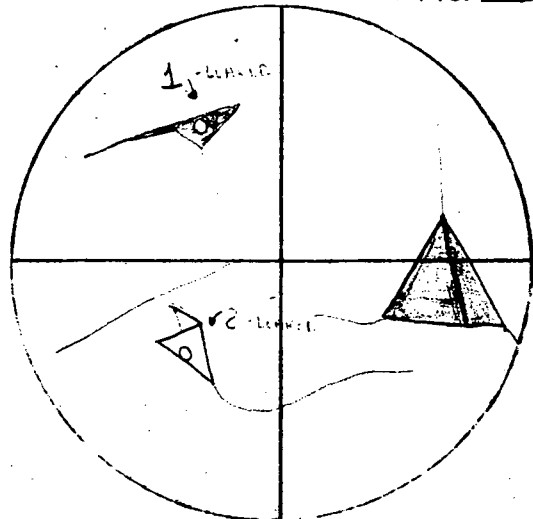
SAMPLE No. HW 115-1

CHIP No. 1

MINERAL: QUARTZ

Inclusion No. 1, 2

MAG. \_\_\_\_\_

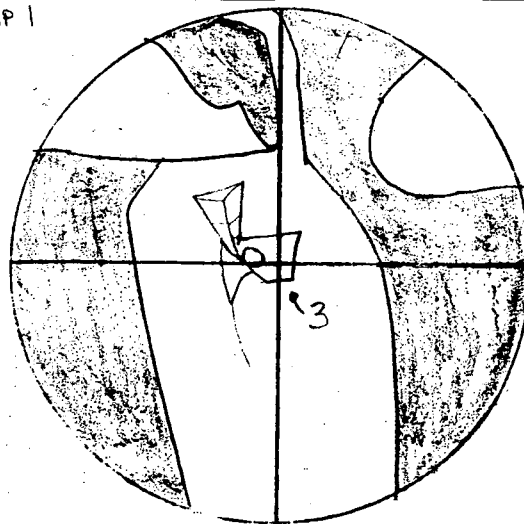


TYPICAL NEGATIVE CRYSTALS SHOWING TAILS AT CORNERS. BOTH INCLUSIONS 1 AND 2 LEAKED.

Inclusion No. 3

MAG. \_\_\_\_\_

CHIP 1

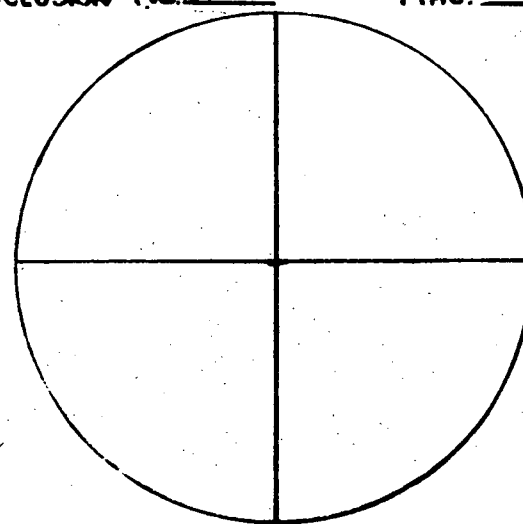


1) ~285, DRYING AND LEAKED, TEMP. TENTATIVE

~168°

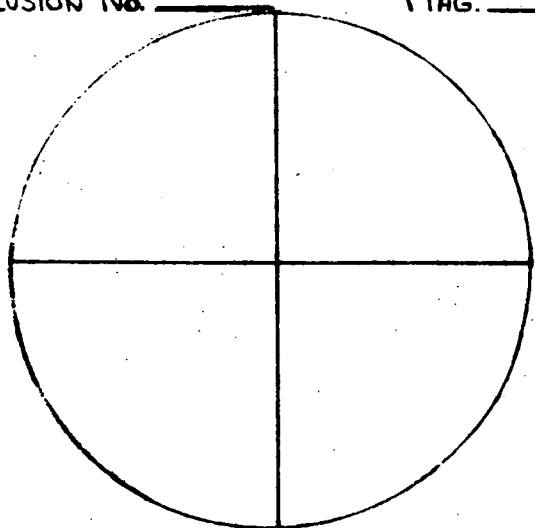
Inclusion No. \_\_\_\_\_

MAG. \_\_\_\_\_



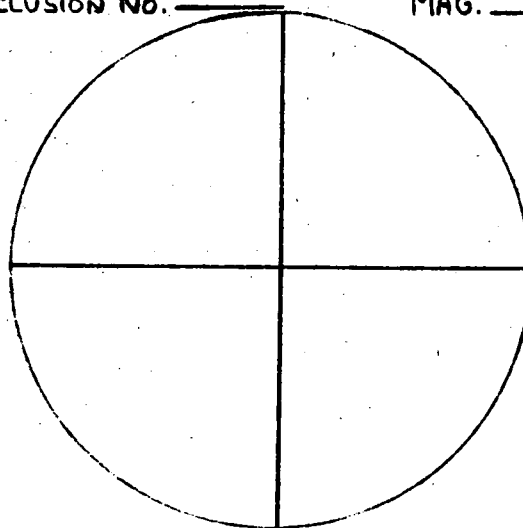
Inclusion No. \_\_\_\_\_

MAG. \_\_\_\_\_



Inclusion No. \_\_\_\_\_

MAG. \_\_\_\_\_



Inclusion No. \_\_\_\_\_

MAG. \_\_\_\_\_

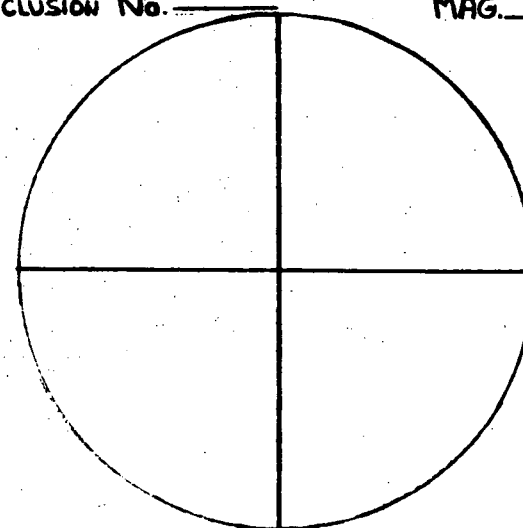
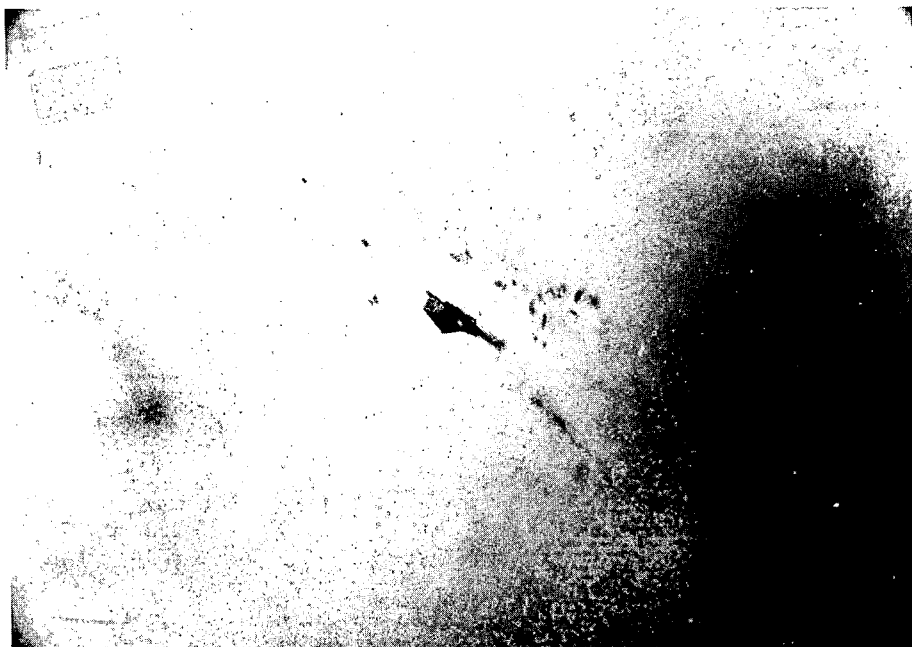


PHOTO 1, MW115-1;  
NEGATIVE CRYSTAL CON-  
TAINING TWO PHASES WHICH  
LEAKED WHEN HEATED.



## Sample MW 116-2 - Sparry Calcite

Minor to moderate amounts of fractures and rehealed fractures occur along cleavage planes. Small, dark, secondary inclusions are commonly found in these areas. Totally fluid-filled negative crystals are fairly common in the coarsest, clear calcite (latest stage calcite).

## Primary inclusions

Range 129-160° (8)

Average 148°

## Secondary inclusions

Range 98-111° (4)

Average 102°

ANALYST: RJ POTTORF

# FLUID INCLUSION SKETCHES

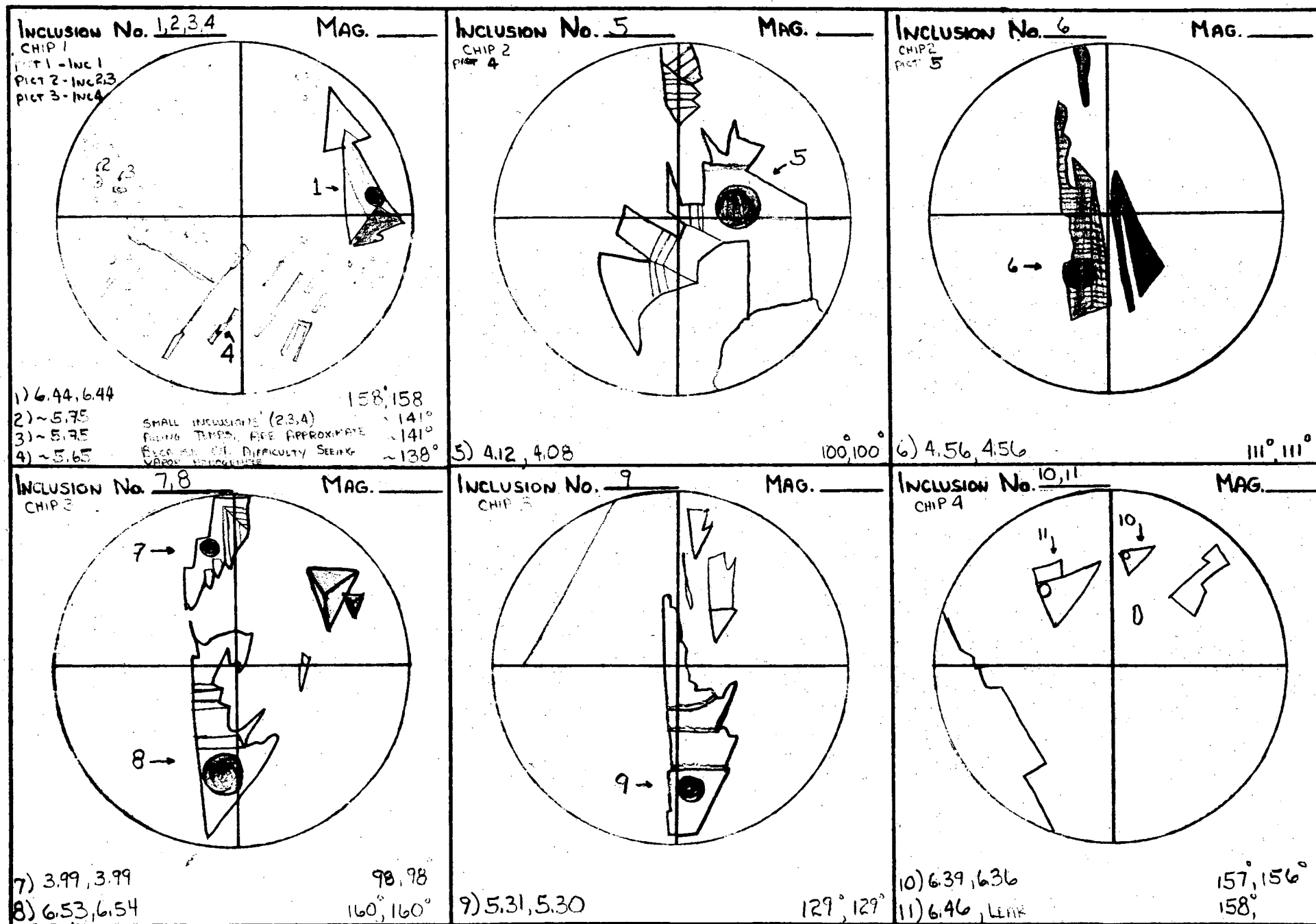
CON EDISON

SAMPLE No. MW 116-2

CHIP No. 1-4

MINERAL: CALCITE

113



113

ANALYST: RJ POTTORF

SAMPLE No. MW 116-2

# FLUID INCLUSION SKETCHES

CHIP No. 4

CON EDISON

MINERAL: CALCITE

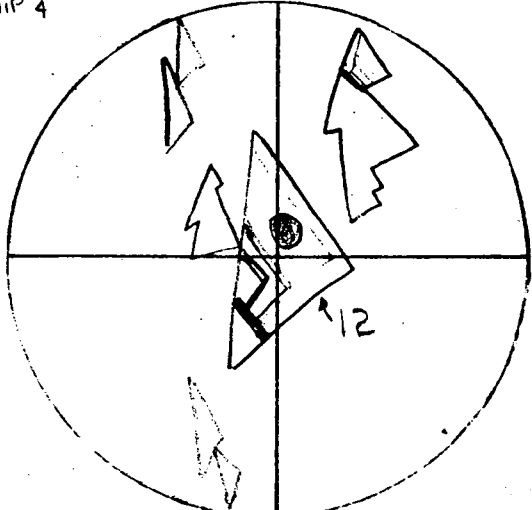
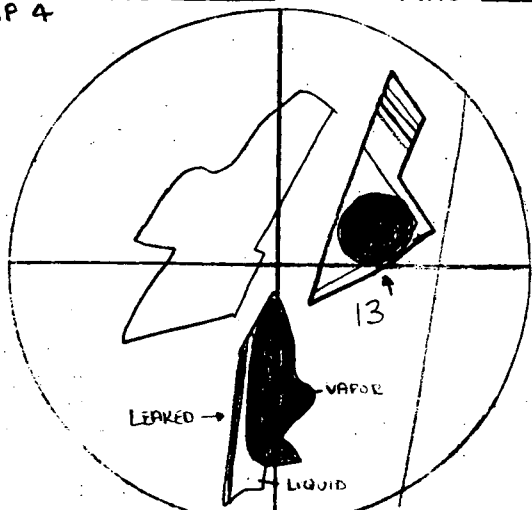
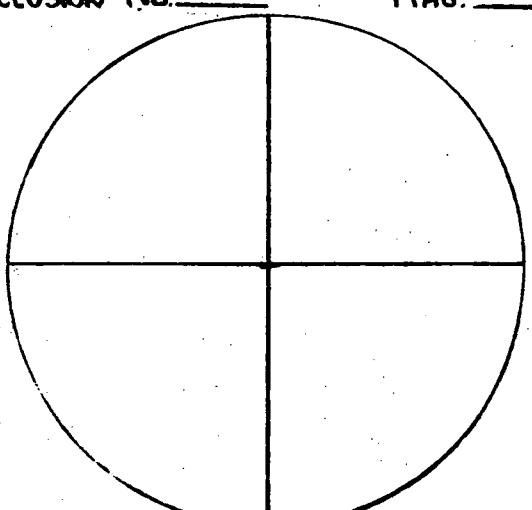
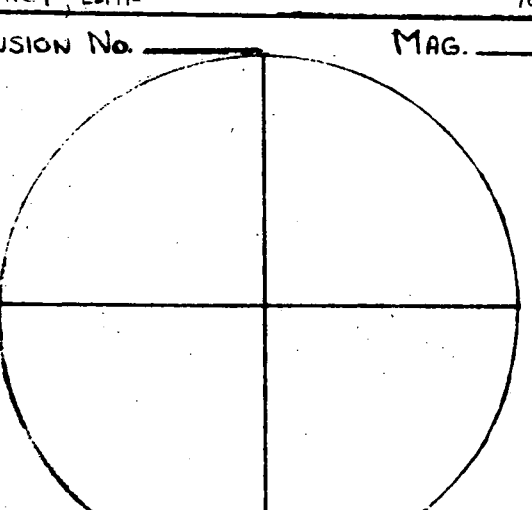
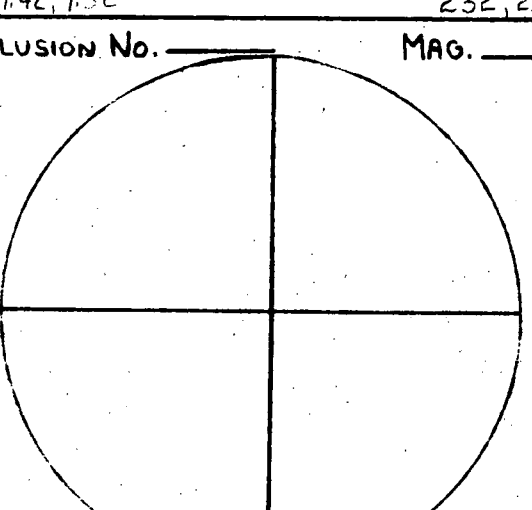
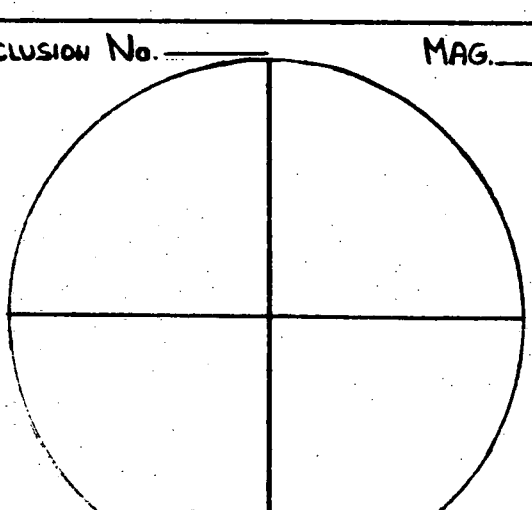
Inclusion No. <u>12</u> CHIP 4	Inclusion No. <u>13</u> CHIP 4	Inclusion No. _____ MAG. _____
 <p>12) 4.01, LEAK 98°</p>	 <p>PROBABLY LIQUID FILLED INCLUSIONS WHICH PARTIALLY LEAKED AT SOME TIME LEAVING LARGE VAPOR/LIQUID RATIOS, CONSIDERED UNRELIABLE (SURROUNDED BY LIQUID FILLED INCLUSIONS)</p> <p>13) 9.42, 9.32 232°, 230°</p>	
		

PHOTO 1, MW116-2, CHIP1,  
INCLUSION 1; NEGATIVE  
CRYSTAL; SEE SKETCH.



PHOTO 2, MW116-2, CHIP1  
INCLUSIONS 2 AND 3; SEE  
SKETCH.

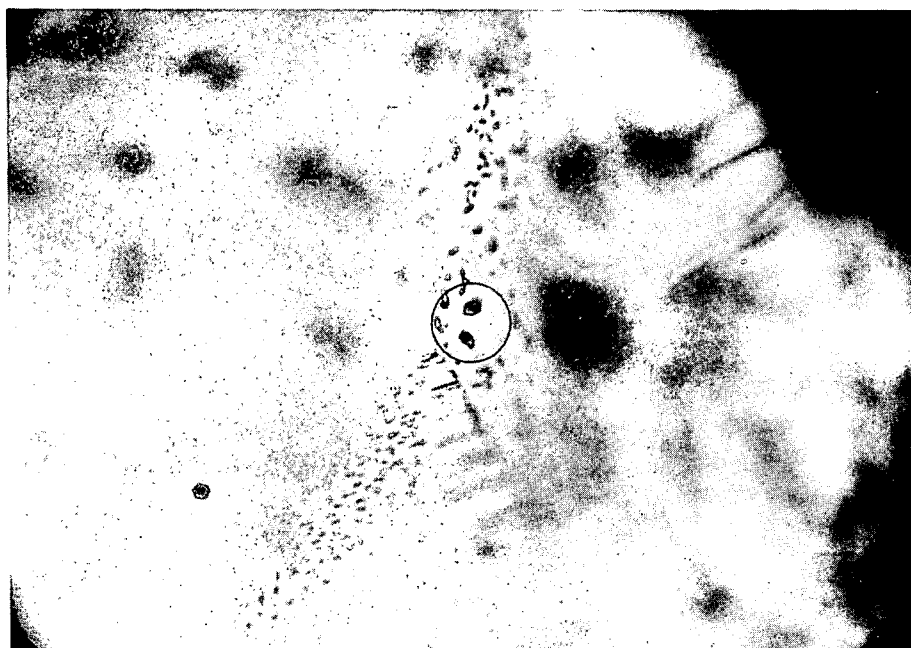


PHOTO 3, MW116-2, CHIP1  
INCLUSION 4; SEE SKETCH.

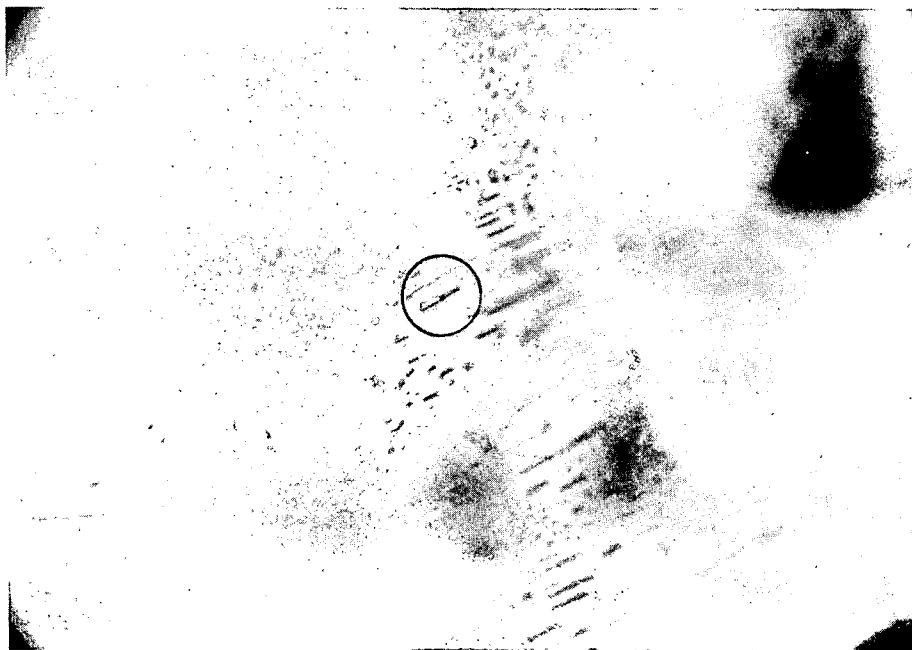


PHOTO 4, MW116-2, CHIP 2,  
INCLUSION 5; SEE SKETCH.



PHOTO 5, MW116-2, CHIP 2,  
INCLUSION 6; SEE SKETCH.



ATTACHMENT NO. 1B

TO APPENDIX E

Report of Fluid Inclusion

Studies by Dr. Barnes

# Summary

Job. 0874-062: 12 samples

<u>Sample</u>	<u>Primary</u>	<u>Secondary</u>	<u>Notes</u>
GA 1.1	"high T"	---	epidote, CO <sub>2</sub> (l)
GA 3.1	---	---	analcime (no inclus.)
GA 7.1	195-229(9) <u>215</u>	---	Cu-Fe sulfides: many inclus.
GA 8.1	"high T"	125-144(2) <u>134</u>	early w. CO <sub>2</sub> (l): v. rare inclus.
GA 8.3	"high T" >169-202(spurs)	83-98(6) <u>94</u> 117-125(3) <u>121</u>	epidote, CO <sub>2</sub> (l): gives low values due to split along spurs.
GA 9.1	---	113(1) <u>113</u>	deformed & then rexl., spurs, tails, w. foreign solids, all leak!
GA 11.1	"high T"	vapor-filled	epidote, CO <sub>2</sub> (l): inclus. rare.
GA 11.2	126-130(3) <u>128</u>	vapor filled	v. rare inclus.
GA 11.3	237-298(9) <u>277</u>	not measurable	
GA 11.4A	197-157(8) <u>133</u>	vapor-filled	irreg. vapor/liq. in sec. inclus. from H <sub>2</sub> O(l) + CO <sub>2</sub> (v) irreg. trapping??
GA 11.4B	171-187(5) <u>181</u>		inclus. rare.
GA 12.1	"hi T"	vapor-filled	CO <sub>2</sub> (l) + H <sub>2</sub> O(l) ? >300°C.

-----  
Job. 0874-062-10: 3 samples

GA 16.1	---	w. necking & tails (too small to resolve)	quartz; rehealed shattering; bad geom. of spurs, tails, + zeolites, calcite
GA 17.3	100-150(3) <u>124</u>	vapor only	spurs & tails; most leaked.
GA 19.1	96-109(4) <u>104</u>	along cleavages	spurs & necking; primary rare. (not measurable)

Job. # 0874-062

Summary (range (no. samples) average, in °C)

<u>Sample</u>	<u>Primary Inclusions</u>	<u>Secondary Inclusions</u>
GA 3.1		
GA 8.3	High Temperature (?)	83-98 (6) <u>94°</u> 117-125 (3) <u>121°</u>
GA 9.1		113° (1) <u>113°</u>
GA 11.1	High Temperature (metamorphic)	
GA 11.2	126 - 130 (3) 128°	
GA 11.4A	107 - 157 (8) 133°	
GA 12.1	High Temperature	

3

Sample GA 3.1 - Analcime

The material designated for study was incorrectly identified as calcite in the field description. An X-ray diffraction analysis indicates the sample is analcime ( $\text{NaAl}(\text{SiO}_3)_2 \cdot \text{H}_2\text{O}$ ). The analcime was examined for fluid inclusions, but none suitable for homogenization were found.

Sample GA 8.3 - Calcite

Appears to have a complicated history, several populations of inclusions noted; 14 inclusions measured.

Two inclusions were located at the contact between host rock and vein calcite where epidote was noted to occur. These inclusions did not homogenize at  $300^\circ$  and are probably composed of an aqueous fluid phase and aqueous carbon dioxide (inclusion 6, 16).

Inclusions 1-3 gave temperatures between  $169-202^\circ$ . These inclusions appear to be crystallographically controlled, possibly of metamorphic origin after crystallization, characteristically displaying spurs. Due to the poor morphologic characteristics of these inclusions, the homogenization temperatures must be viewed with reservation.

Range  $169-202^\circ$

Average  $184^\circ$

Two sets of secondary inclusions were noted on the basis of texture. These commonly occur in trains along fracture fillings.

Set 1 (inclusions 7-12)

Range  $83-98^\circ$

Average  $94^\circ$

4  
Set 2 (inclusions 13-15)

Range 117-125°

Average 121°

Some inclusions leaked upon heating and could not be homogenized. This is a common problem when working with calcite. After leaking an inclusion will commonly have a larger vapor/liquid ratio and will give a temperature higher than its true filling temperature. Care must be taken to avoid measuring these inclusions.

ANALYST: RJ POTTORF

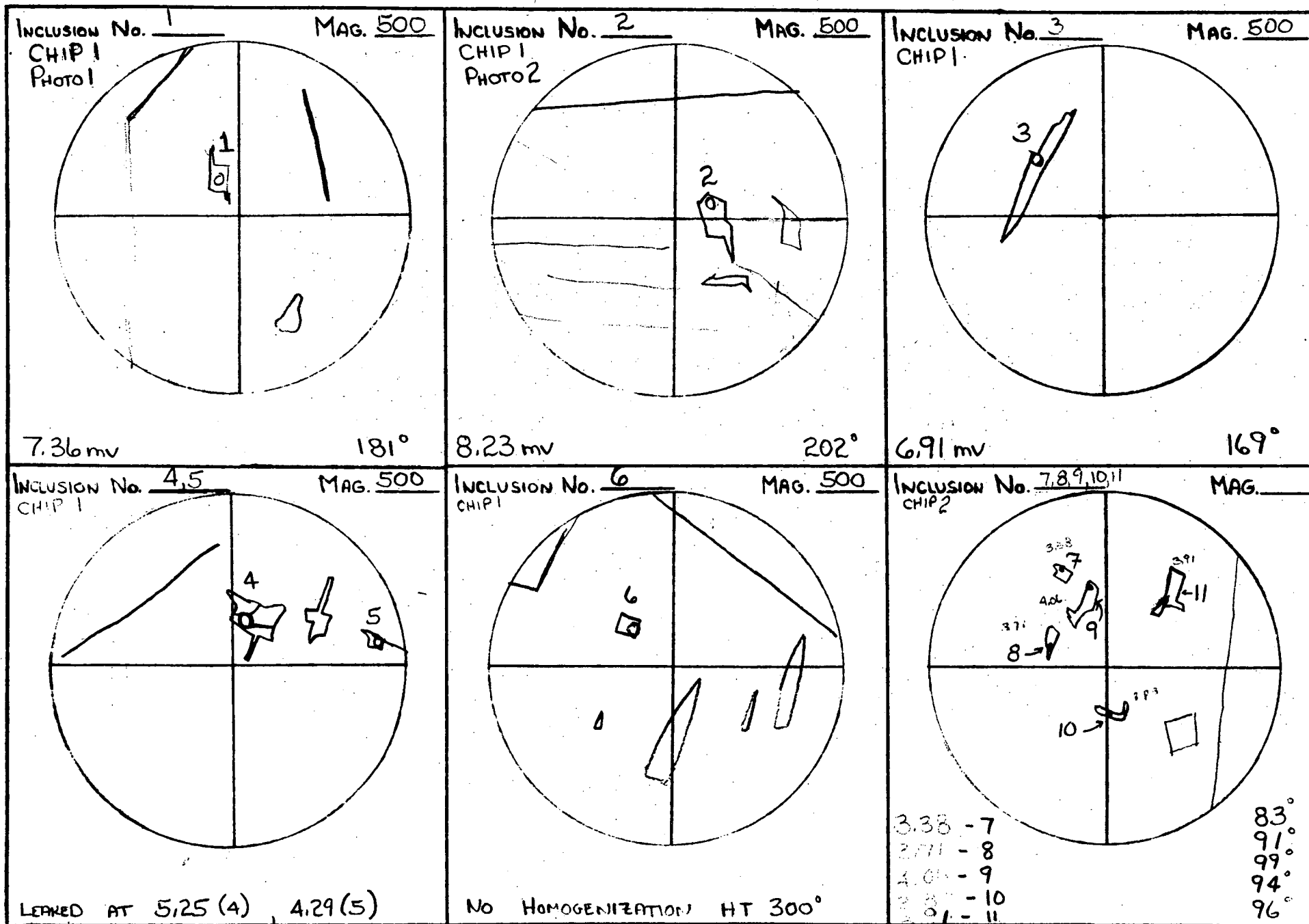
SAMPLE No. GA 8.3

FLUID INCLUSION SKETCHES

CHIP No. 1-2

CON EDISON

MINERAL: CALCITE



ANALYST : RJ POTTORF

SAMPLE No. GA 8,3

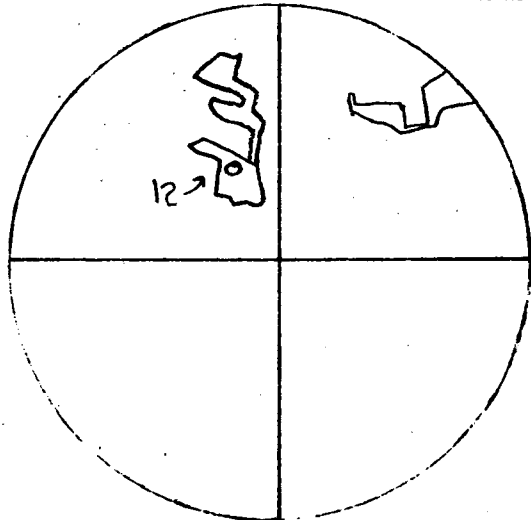
FLUID INCLUSION SKETCHES

CHIP No. 2

CON EDISON

MINERAL: CALCITE

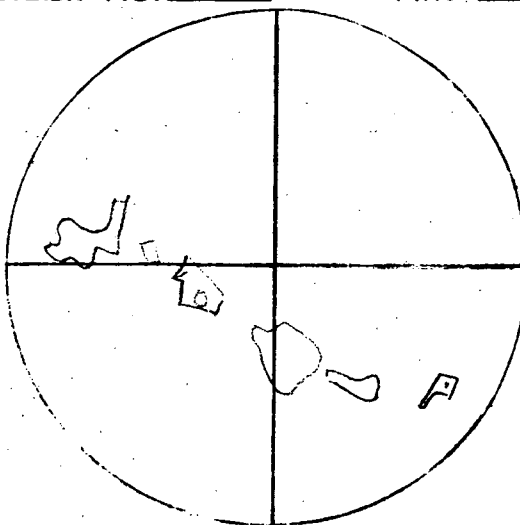
INCLUSION No. 12 MAG. 500



4.00, 4.06 mv

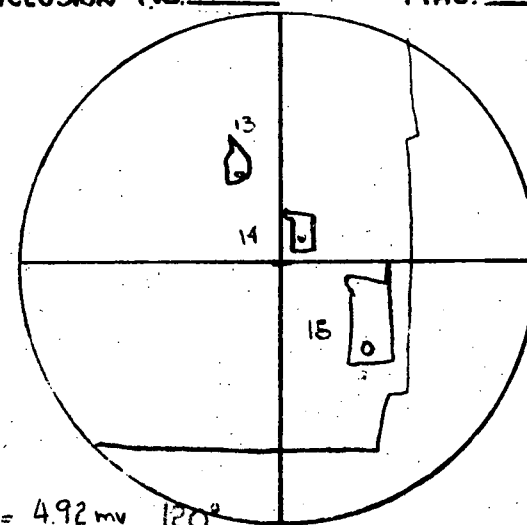
98°

INCLUSION No. 17 MAG. 500



LEAKED ; STOPPED AT 153°

INCLUSION No. 13, 14, 15 MAG. 500

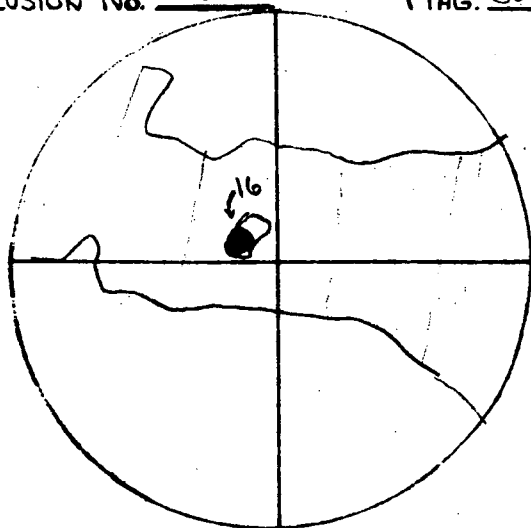


13 = 4.92 mv 120°

14 = 5.12 mv 125°

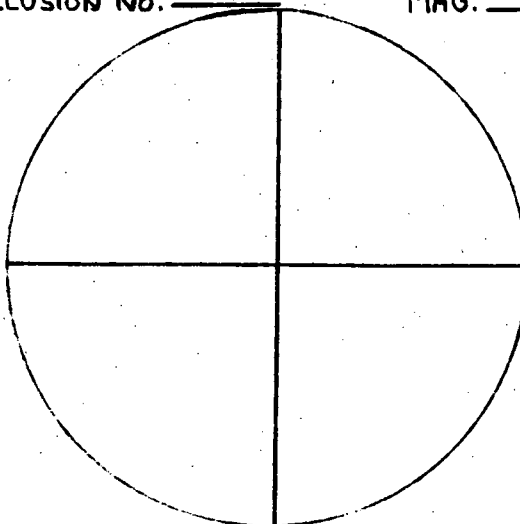
15 = 4.79 mv 117°

INCLUSION No. 16 MAG. 500



No HOMOGENIZATION AT 300°

INCLUSION No. \_\_\_\_\_ MAG. \_\_\_\_\_



INCLUSION No. \_\_\_\_\_ MAG. \_\_\_\_\_

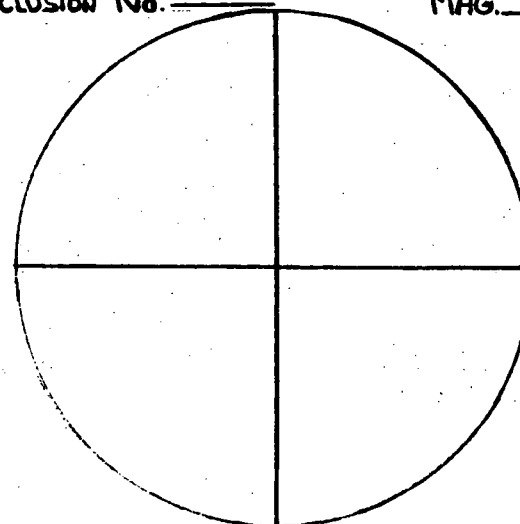


PHOTO 1, GA 8.3, CHIP 1  
INCLUSION 1, SEE SKETCH.  
ALL PHOTOGRAPHS IN THIS  
REPORT ARE 0.24mm X 0.16mm

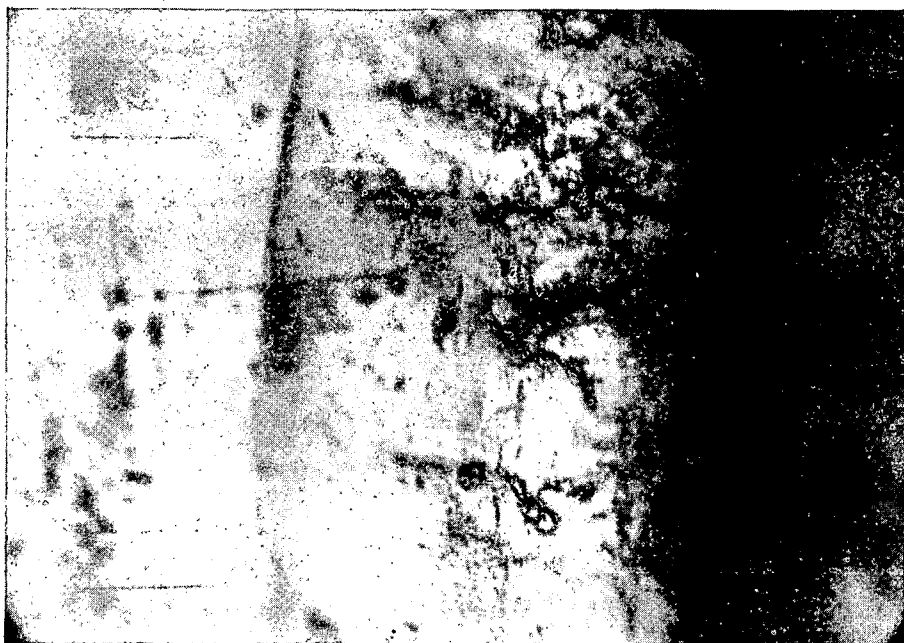


PHOTO 2, GA 8.3, CHIP 1,  
INCLUSION 2, SEE SKETCH  
AND TEXT.



8

Sample GA 9.1 - Calcite

Inclusions fairly abundant, nearly all display spurs and tails; several follow healed or unhealed fractures; 12 inclusions heated, all leaked without homogenizing except inclusion 1.

The calcite contains a large amount of opaque included material which occasionally acts as loci for deformation. Some fluid inclusions contain this solid included material (not to be confused with daughter minerals which are precipitated from the fluid upon cooling) and this tends to increase the leakage problem. The textural appearance of the calcite seems to indicate partial recrystallization after deformation.

1 Secondary (?) inclusion:  $113^{\circ}$

ANALYST: RJ POTTORF

SAMPLE No. GA 9.1

FLUID INCLUSION SKETCHES

CHIP No. 3

CON EDISON

MINERAL: CALCITE

6

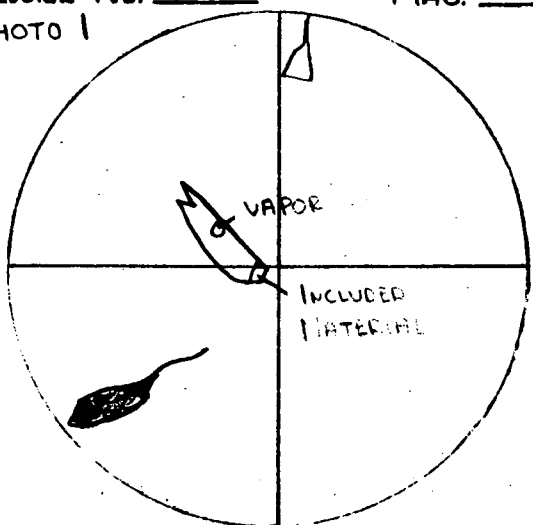
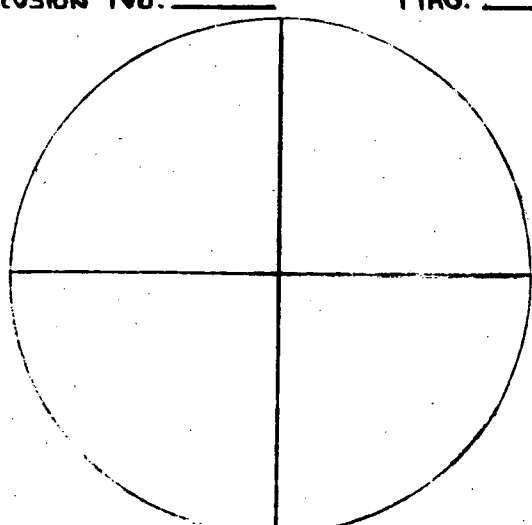
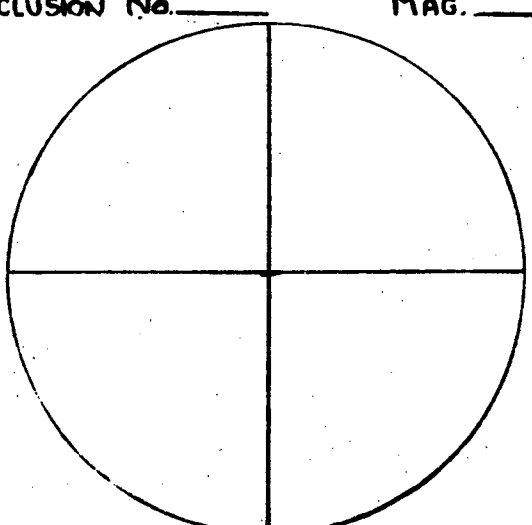
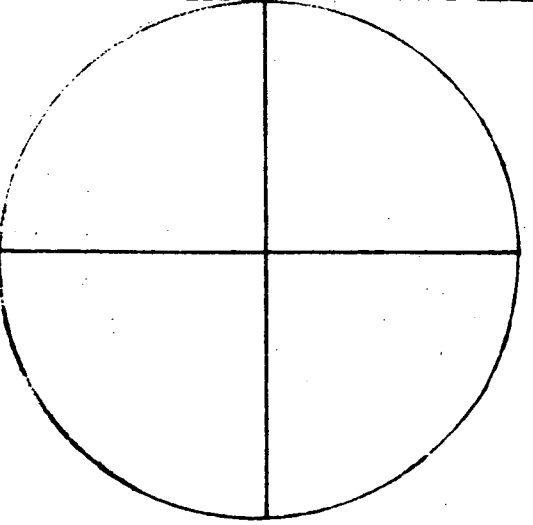
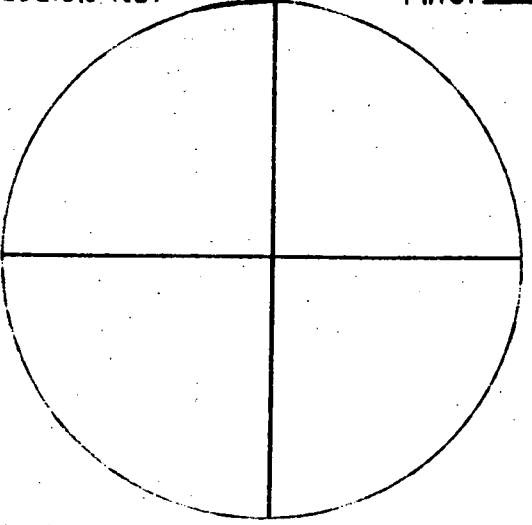
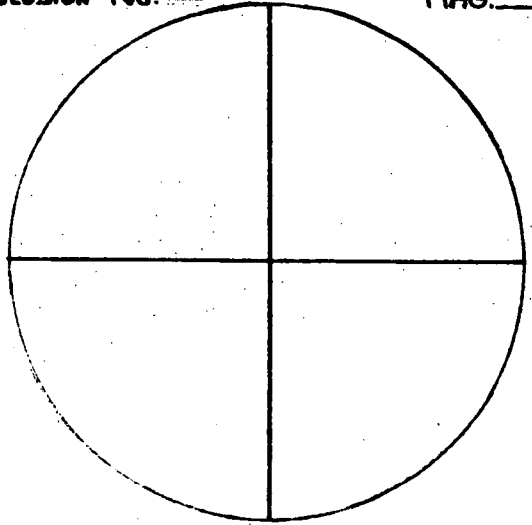
<p>Inclusion No. <u>1</u> MAG. <u>500</u></p> <p>PHOTO 1</p>  <p>4.65 113°</p>	<p>Inclusion No. _____ MAG. _____</p> 	<p>Inclusion No. _____ MAG. _____</p> 
<p>Inclusion No. _____ MAG. _____</p> 	<p>Inclusion No. _____ MAG. _____</p> 	<p>Inclusion No. _____ MAG. _____</p> 

PHOTO 1, GA 9.1, CHIP 3  
INCLUSION 1; SEE SKETCH



ANALYST: RJ POTTORF

SAMPLE No. GA 11.1

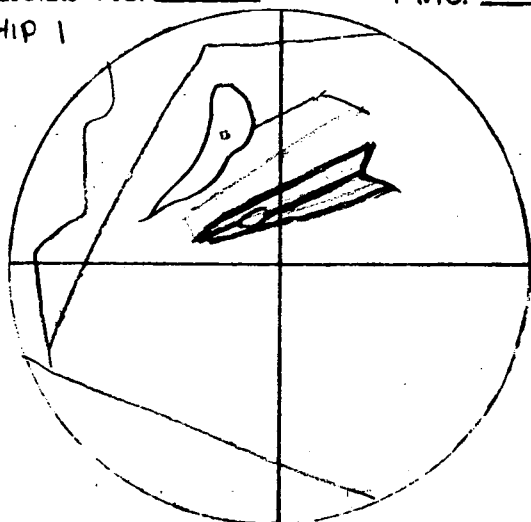
FLUID INCLUSION SKETCHES

CHIP No. 1-2

MINERAL: CALCITE

Inclusion No. 1 MAG. 500

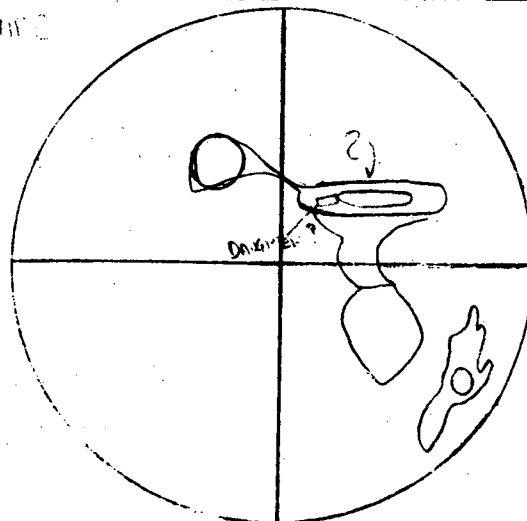
CHIP 1



STOPPED AT 300° TENDS TO HOMOG.  
P.H. DUE TO

Inclusion No. 2,3 MAG. 500

CHIP 2

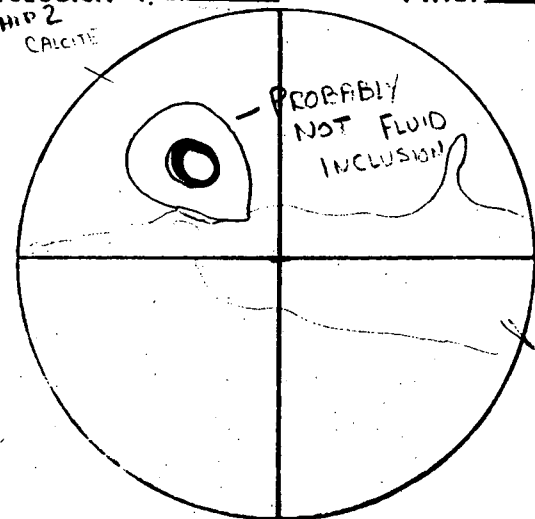


>300°

NO HOMOG.

Inclusion No. 4 MAG. 500

CHIP 2  
CALCITE



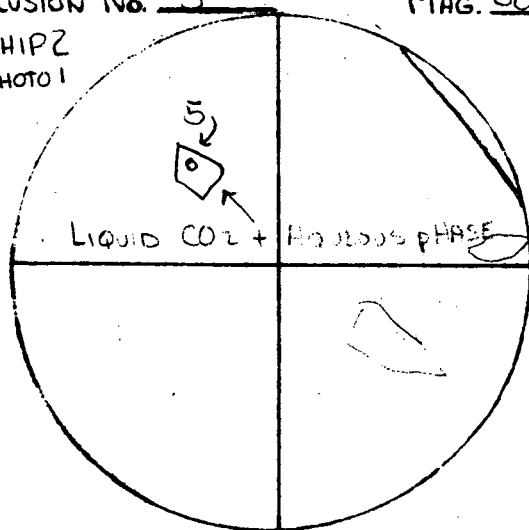
PROBABLY  
NOT FLUID  
INCLUSION

>300°

NO HOMOG.

Inclusion No. 5 MAG. 500

CHIP 2  
PHOTO 1



LIQUID CO<sub>2</sub> + AQUEOUS PHASE

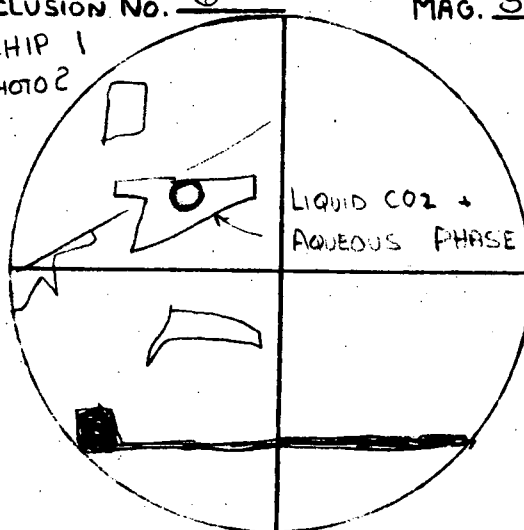
Inclusion

>300°

NO HOMOG.

Inclusion No. 6 MAG. 500

CHIP 1  
PHOTO 2

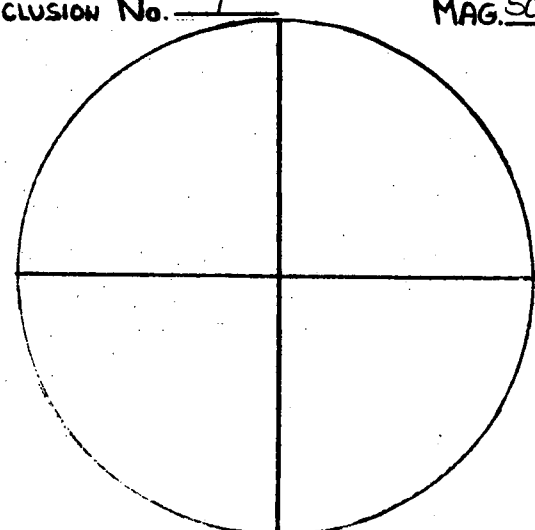


LIQUID CO<sub>2</sub> +  
AQUEOUS PHASE

>300°

NO HOMOG.

Inclusion No. 7 MAG. 500



SEVERAL OTHERS HEATED WITH  
THE SAME RESULT

PHOTO 1, GA 11.1, CHIP 2,  
INCLUSION 5; SEE SKETCH



GA 11.1, PHOTO 2, CHIP 1  
INCLUSION 6; SEE SKETCH



PHOTO 3, GA 11.1, CHIP 1  
SEE TEXT (SECONDARY INCLUSIONS)



Sample GA 11.1 - Calcite

Inclusions rare; primary inclusions commonly are necked or display spurs, some contain daughter minerals; alteration minerals (epidote ?) along veins. In all cases the inclusions did not homogenize at  $300^{\circ}$ . This is attributed to inclusions containing liquid  $\text{CO}_2$  and an aqueous fluid phase (see photos and sketches). These inclusions are therefore high temperature (metamorphic).

Secondary inclusions are present, sometimes necked, and appear to be filled with a vapor phase which is probably  $\text{CO}_2$  (see photo 3).

Sample GA 11.2 - Calcite

Primary inclusions extremely rare. 3 inclusions.

Range 126 - 130°

Average 128°

Secondary inclusions are present generally in linear arrays along cleavage planes. These contain only a vapor phase (see photo 3) and can not be measured.

ANALYST: RJ POTTORF

SAMPLE No. GA 11.2

FLUID INCLUSION SKETCHES

CHIP No. 1-3

CON EDISON

MINERAL: CALCITE

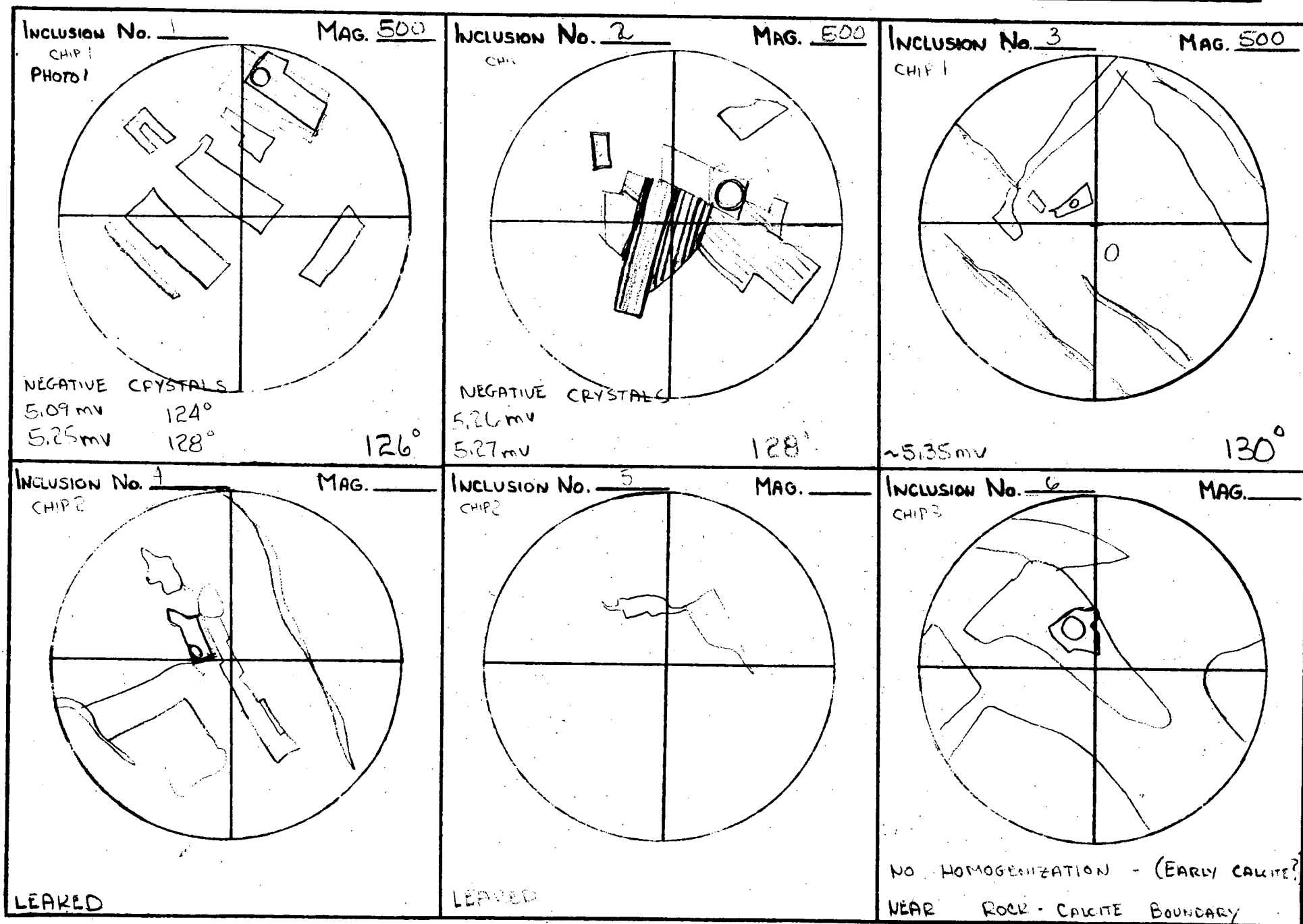


PHOTO 1, GA 11.2, CHIP 1,  
INCLUSION 1, SEE SKETCH;  
LARGE PRIMARY INCLUSION  
(NEGATIVE CRYSTAL)

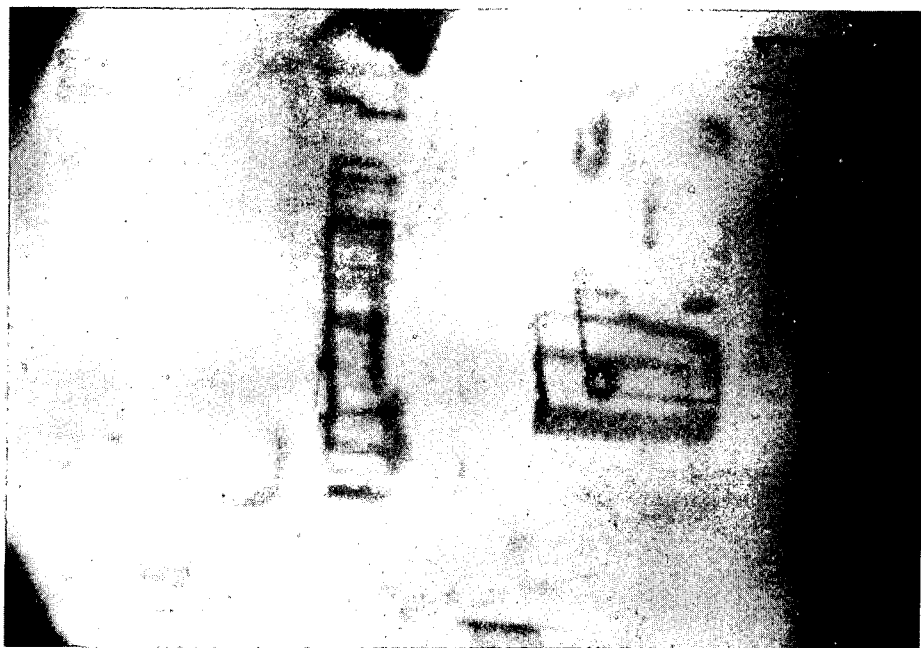


PHOTO 2, GA 11.2, CHIP 1,  
NEGATIVE CRYSTALS



PHOTO 3, GA 11.2, CHIP 2;  
SERIES OF SECONDARY  
INCLUSIONS CONTAINING ONLY  
A VAPOR PHASE; LARGE DARK  
PATCHES ARE PYRITE.



Sample GA 11.4A - Calcite

Primary inclusions probably belong to one population. 10 inclusions, 2 disregarded because of probable partial leakage upon heating (inclusion 5, 14). At higher temperatures fluid inclusions with lower filling temperatures leaked, therefore higher anomalous homogenization temperatures occur if overheated.

Range 107 - 157°

Average 133°

Large numbers of small secondary inclusions occur in long linear trains. Most contain only vapor, but some show widely variable vapor/fluid ratios possibly due to irregular trapping of two immiscible fluids. These inclusions are not suitable for measurements.

Sample GA 12.1 - Calcite

Inclusions in all cases did not homogenize at 300° and are assumed to contain two immiscible fluids consisting of liquid CO<sub>2</sub> and an aqueous fluid phase. Minor secondary inclusions present.

ANALYST: RJ POTTORF

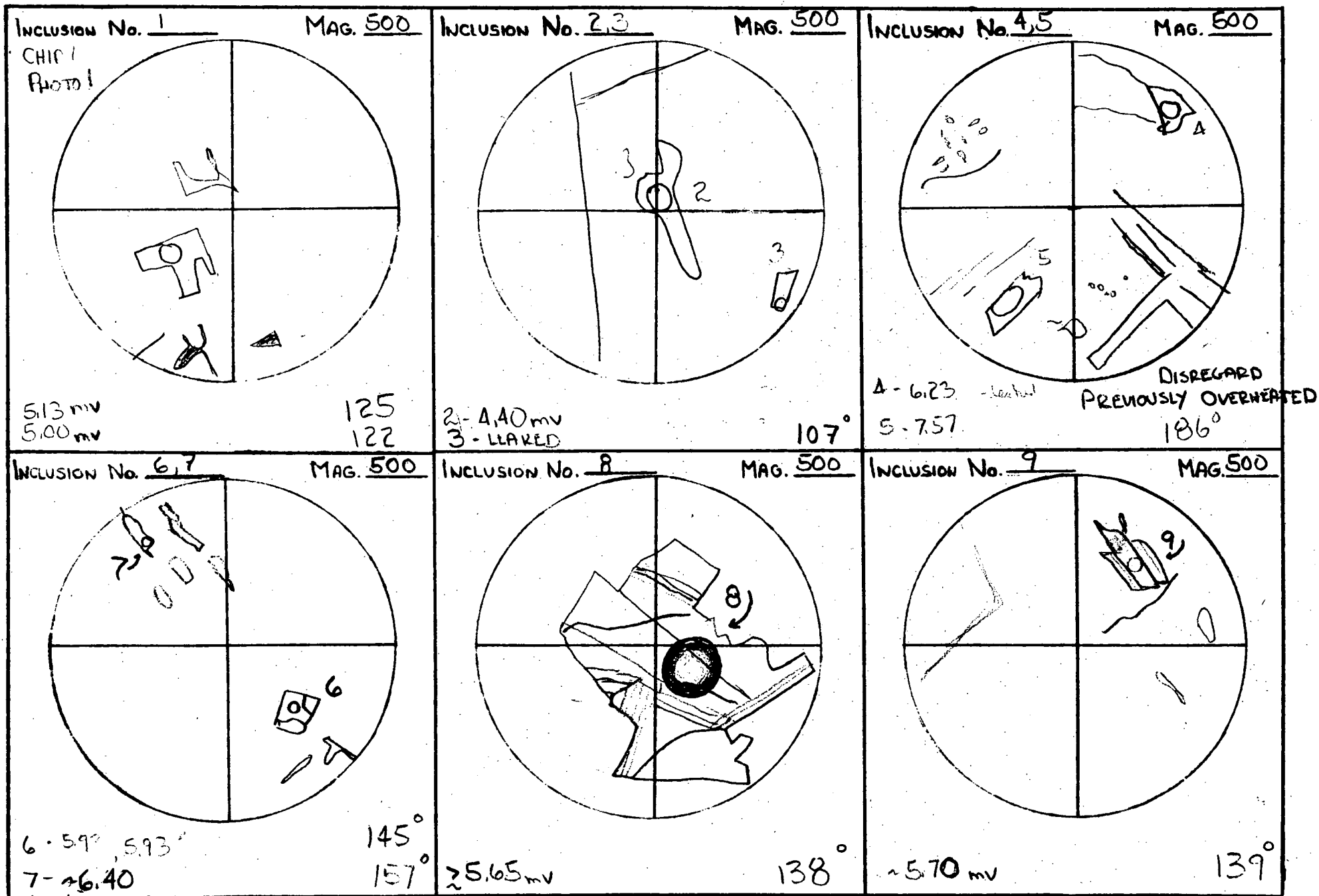
SAMPLE No. GA 11.4 A

FLUID INCLUSION SKETCHES

CHIP No. 1

CON EDISON

MINERAL: CALCITE



ANALYST: RJ POTTORF

SAMPLE No. GA 11.4A

FLUID INCLUSION SKETCHES

CHIP No. 2

CON EDISON

MINERAL: CALCITE

19

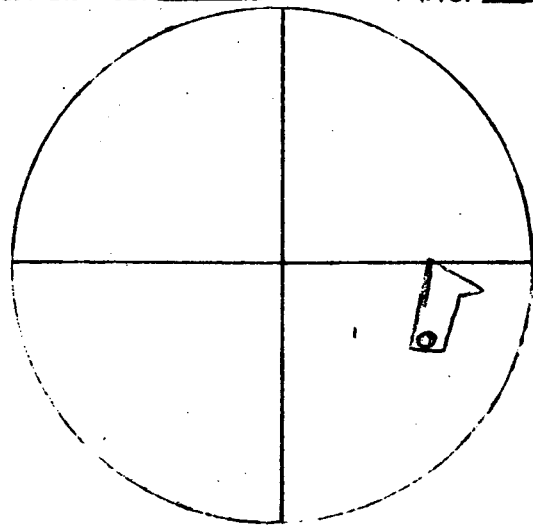
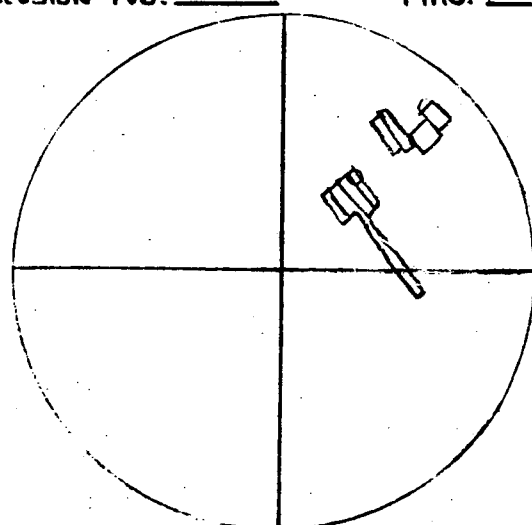
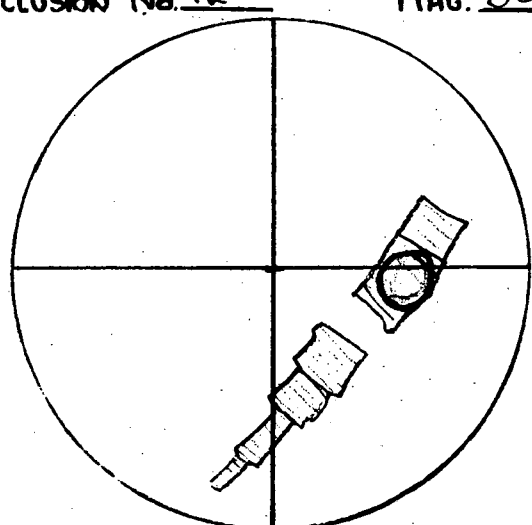
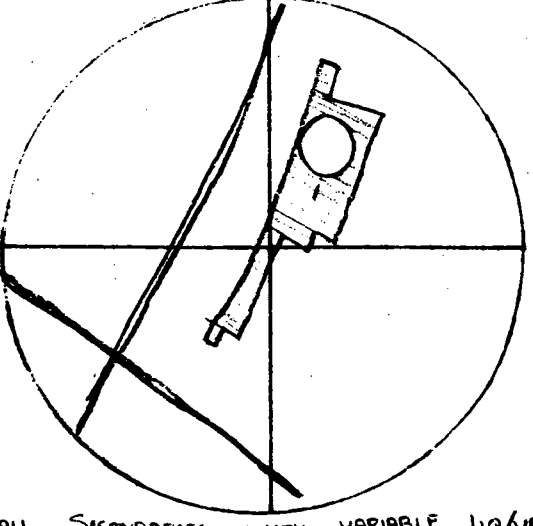
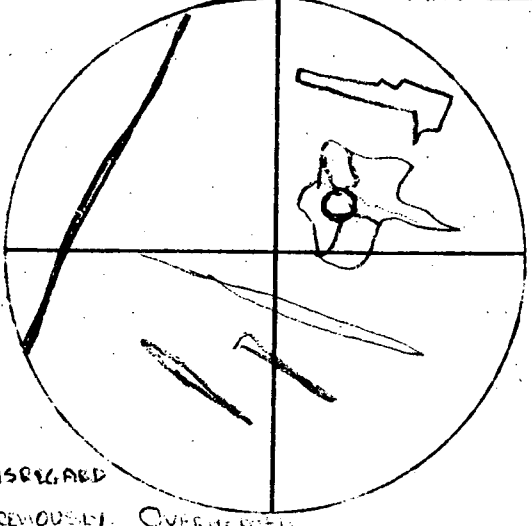
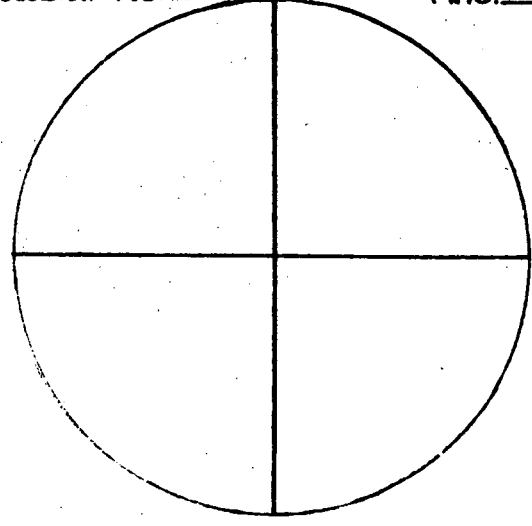
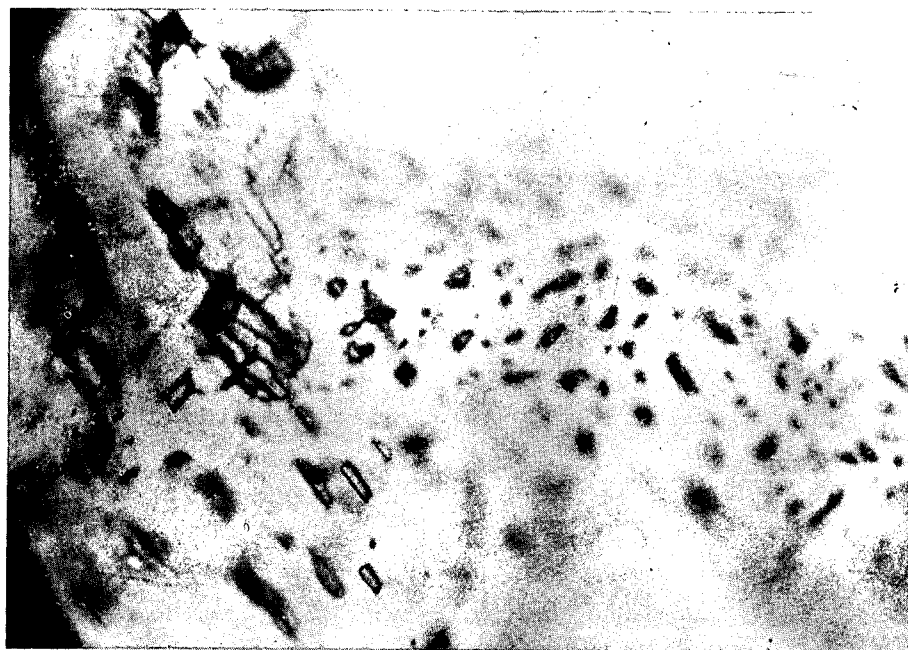
<p>Inclusion No. <u>10</u> MAG. <u>500</u></p>  <p>4.77 116</p>	<p>Inclusion No. <u>11</u> MAG. <u>500</u></p>  <p>LEAKED</p>	<p>Inclusion No. <u>12</u> MAG. <u>500</u></p>  <p>NECKED NO HOMOGENIZATION AT HI TEMP</p>
<p>Inclusion No. <u>13</u> MAG. <u>500</u></p>  <p>SMALL SECONDARIES WITH VARIABLE LIQ/VAPOR PHASING</p> <p>5.82 142</p>	<p>Inclusion No. <u>14</u> MAG. <u>500</u></p>  <p>DISREGARD PREVIOUSLY OVERHEATED</p> <p>8.75 215°</p>	<p>Inclusion No. _____ MAG. _____</p> 

PHOTO 1, GA 11.4A, CHIP 1,  
INCLUSION 1, SEE SKETCH;  
PRIMARY INCLUSION



PHOTO 2, GA 11.4A, CHIP 1,  
SEE TEXT; SECONDARY INCLUSIONS



ANALYST: RT POTTORF

SAMPLE No. GA 12.1

FLUID INCLUSION SKETCHES

CHIP No. 1-2

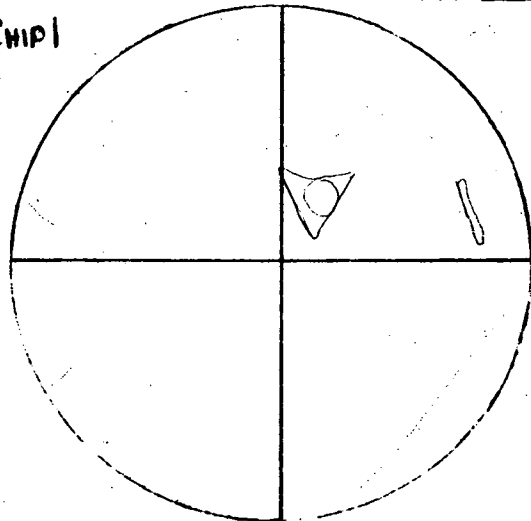
CON EDISON

MINERAL: CALCITE

2

Inclusion No. 1 MAG. 500

CHIP1

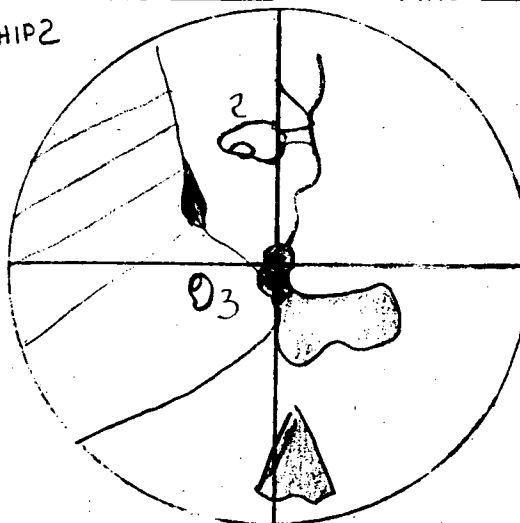


DAUGHTER MINERAL?  
PRESENT

NO HOMOGENIZATION @ 300°

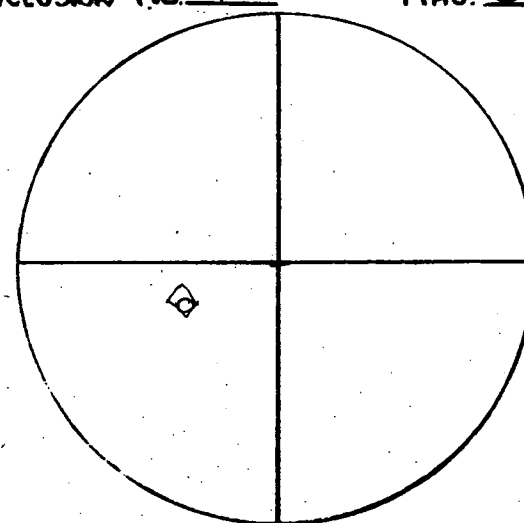
Inclusion No. 2,3 MAG. 500

CHIP2



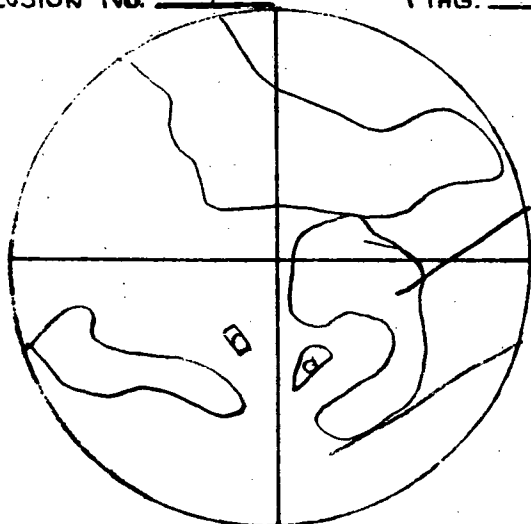
NO HOMOGENIZATION @ 300°

Inclusion No. 4 MAG. 500



NO HOMOG - 300°

Inclusion No. 5,6 MAG. 500

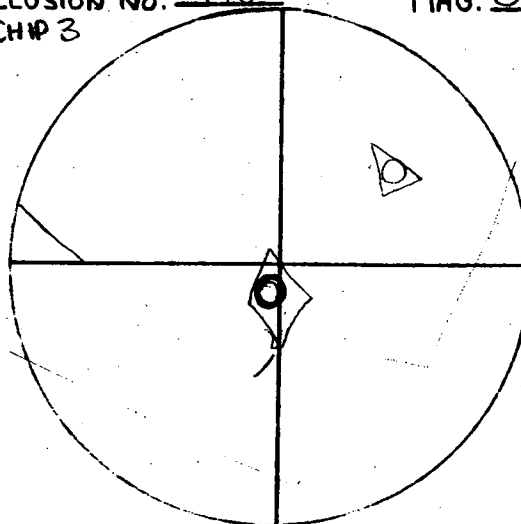


NO HOMOG

300°

Inclusion No. 7,8 MAG. 500

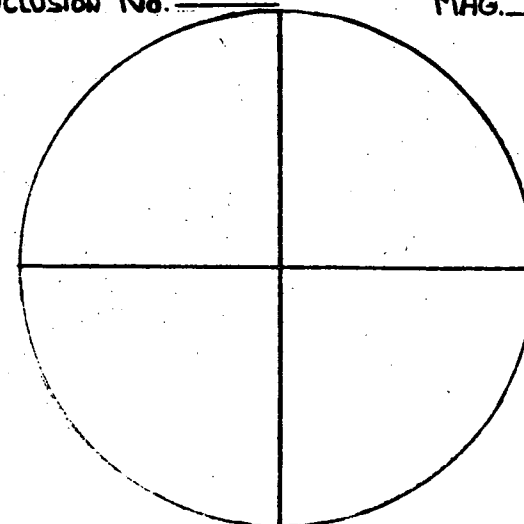
CHIP 3



NO HOMOG

300°

Inclusion No. \_\_\_\_\_ MAG. \_\_\_\_\_



Job. # 0874-062-10

Summary (range (no. samples) average, in °C)

<u>Sample</u>	<u>Primary Inclusions</u>	<u>Secondary Inclusions</u>
GA 16.1		
GA 17.3	100 - 150 (3) <u>124°</u>	
GA 19.1	96 - 109 (4) <u>104°</u>	

Sample GA 16.1 - Quartz (gray and white); field description identified as calcite

The entire sample is filled with extremely small dark inclusions (probably solids or vapor) which occur in linear arrays as healed fracture fillings. The healed fractures show several cross cutting relationships. Much larger inclusions also occur in trains and display necking and tails. These inclusions are not suitable for measurements. The relationships indicate a complex history of alternate vein shattering, filling and reopening.

The quartz commonly contains zeolites and minor calcite rhombohedra.

Sample GA 17.3 - Calcite

Primary inclusions rare, 3 measured; several others heated but leaked. Secondary inclusions present, particularly along fractures, containing only vapor. Nearly all inclusions display spurs and tails.

Range 100 - 150°

Average 124°

Sample GA 19.1 - Calcite

Primary inclusions rare, 4 measured; secondary inclusions common along cleavage planes. Inclusions showing spurs or necking occur almost without exception.

Range 96 - 109°

Average 104°

ANALYST: RJ POTTORF

SAMPLE No. GA 16.1

FLUID INCLUSION SKETCHES

CHIP No. 4

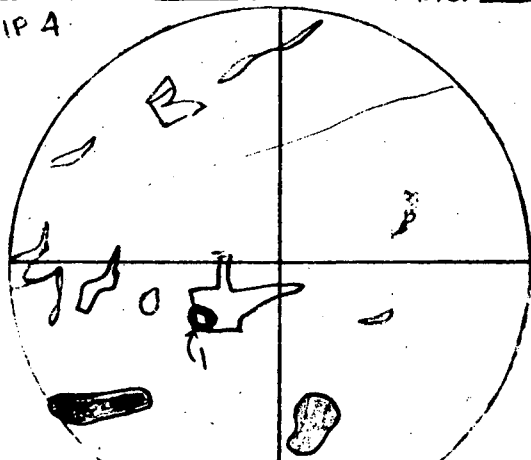
CON EDISON

MINERAL: QUARTZ

24

Inclusion No. 1 MAG. 500

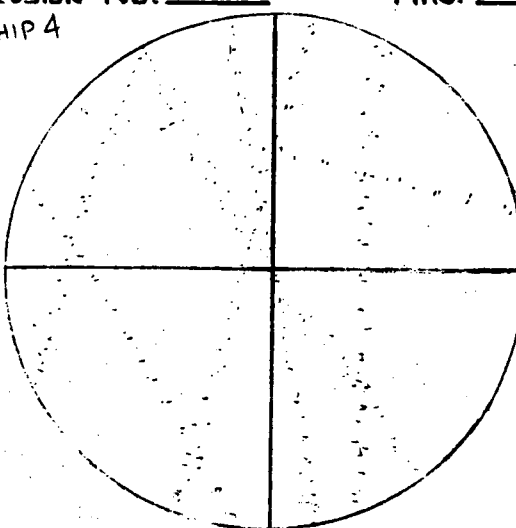
CHIP 4



THIS INCLUSION IS TYPICAL OF LARGER INCLUSIONS WHICH ARE ALWAYS NECKED OR DISPLAY SPURS. THESE HAVE VERY DIFFERENT  $> 7.5$  MV  $185^\circ$  VAPOR/FLUID RATIOS AND AREN'T SUITABLE FOR MEASUREMENT.

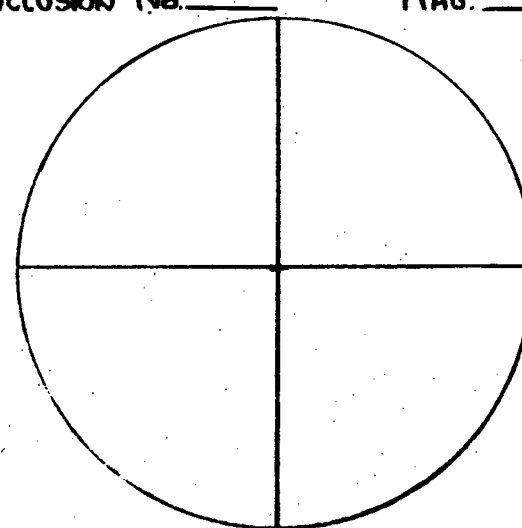
Inclusion No. 2 MAG. 500

CHIP 4

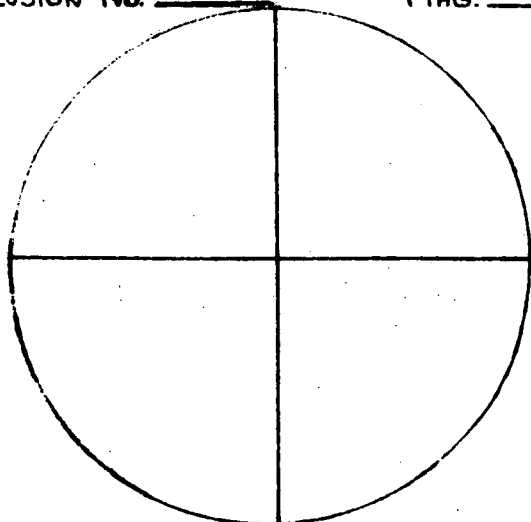


THE ENTIRE SAMPLE IS FILLED WITH INCLUSIONS ALONG REVEALED FRACTURES.

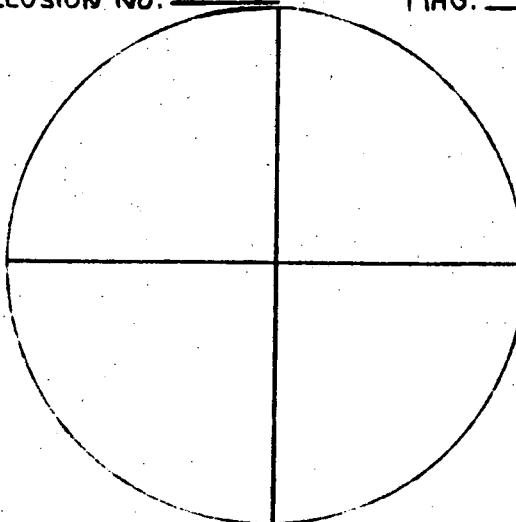
Inclusion No. MAG.



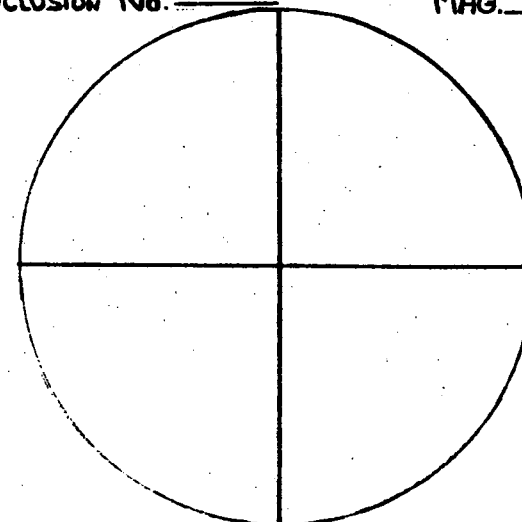
Inclusion No. MAG.



Inclusion No. MAG.



Inclusion No. MAG.



ANALYST: RJ POTTORF

SAMPLE No. GA17.3

FLUID INCLUSION SKETCHES

CHIP No. 1-3

CON EDISON

MINERAL: CALCITE

25

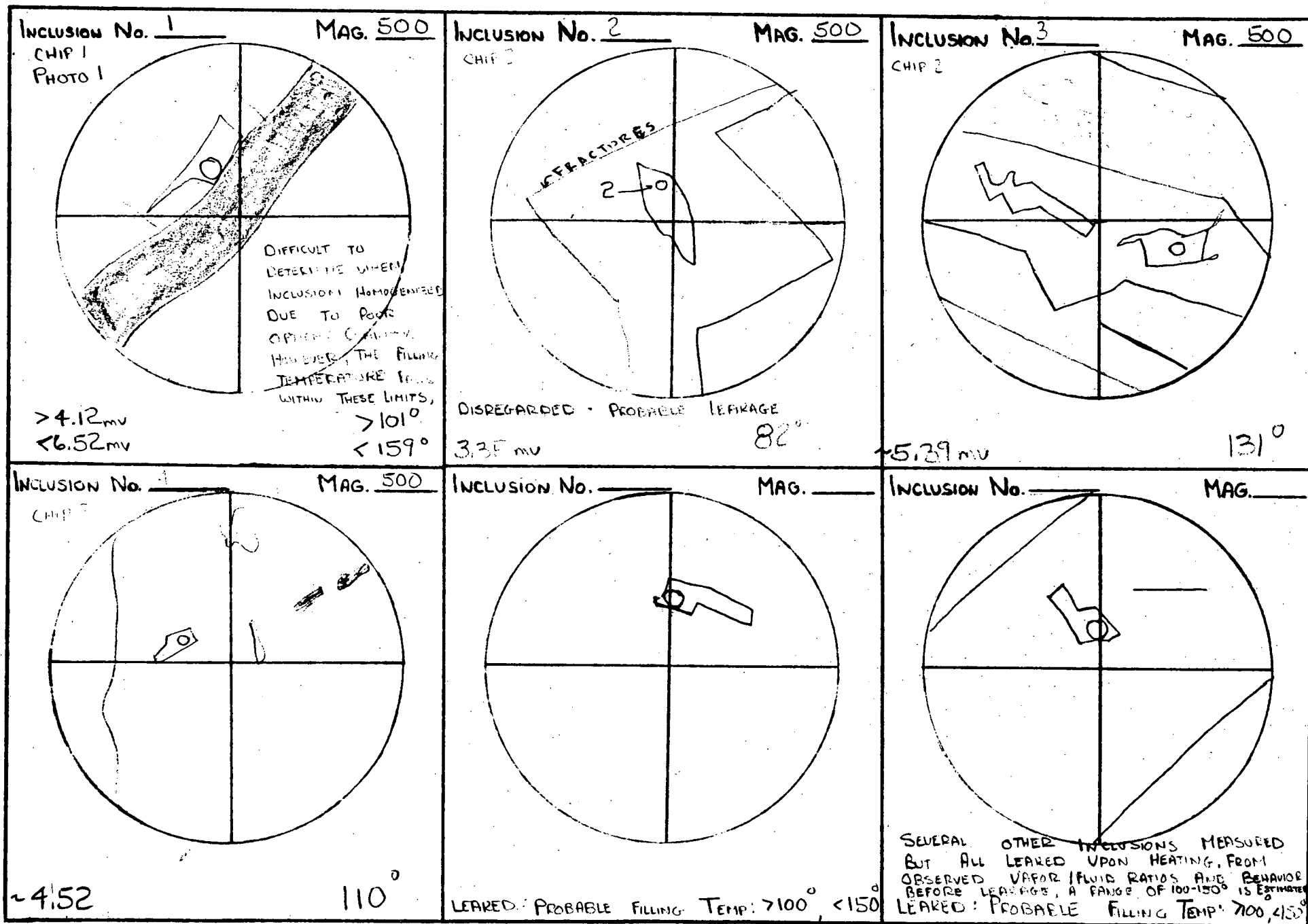
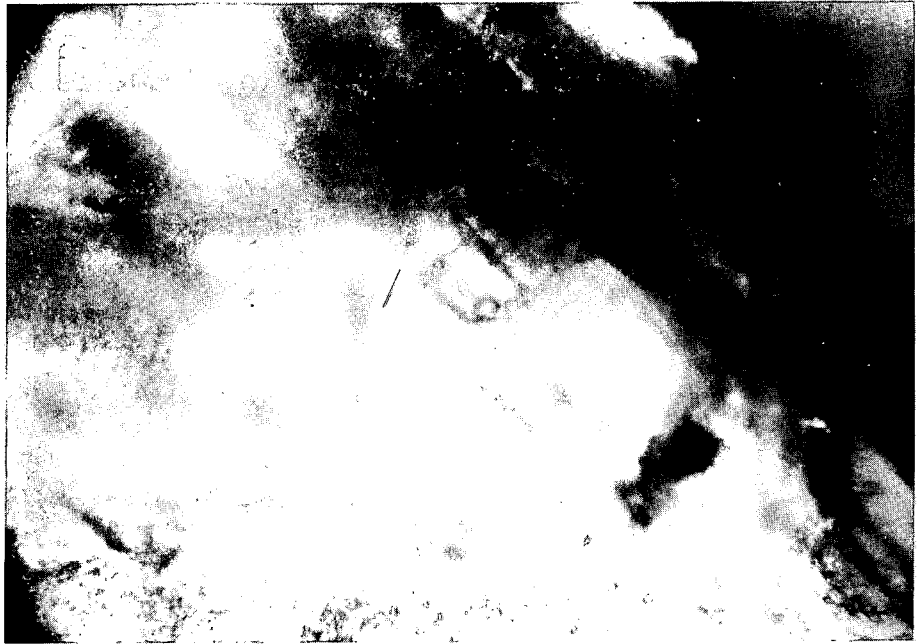


PHOTO 1, GA 17.3, CHIP 1,  
INCLUSION 1; SEE SKETCH;  
PRIMARY INCLUSION



PHOTOS 3 AND 4; GA 17.3  
CHIP 2 AND 3; PRIMARY INCLUSIONS  
WHICH LEAKED UPON HEATING.  
FROM THE VAPOR / FLUID RATIOS  
AND BEHAVIOR BEFORE LEAKAGE  
OCCURRED, IT IS ESTIMATED THAT  
THESE WOULD HOMOGENIZE BETWEEN  
100 - 150 °C.



ANALYST: RJ POTTORF

FLUID INCLUSION SKETCHES

CON EDISON

27

SAMPLE No. GA 19.1

CHIP No. 1,2,4,6

MINERAL: CALCITE

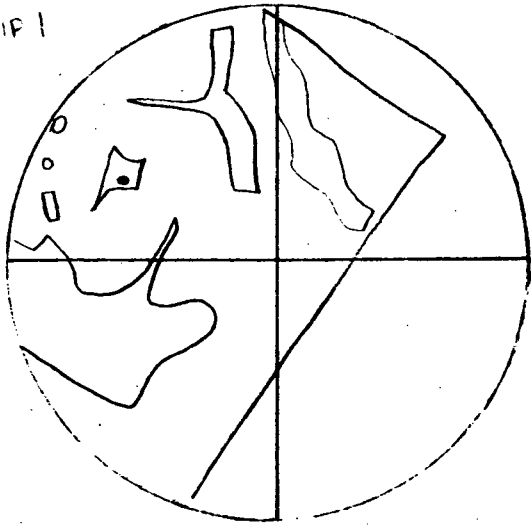
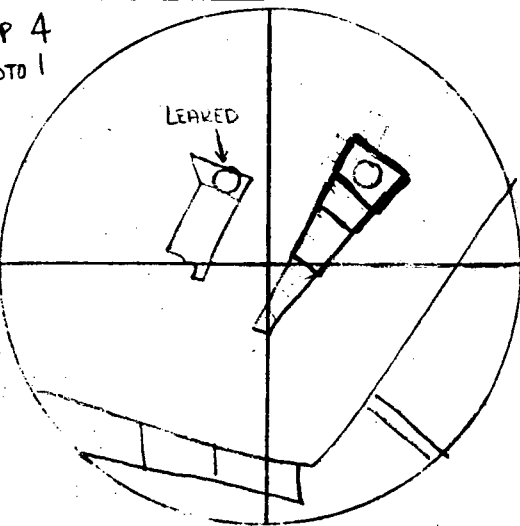
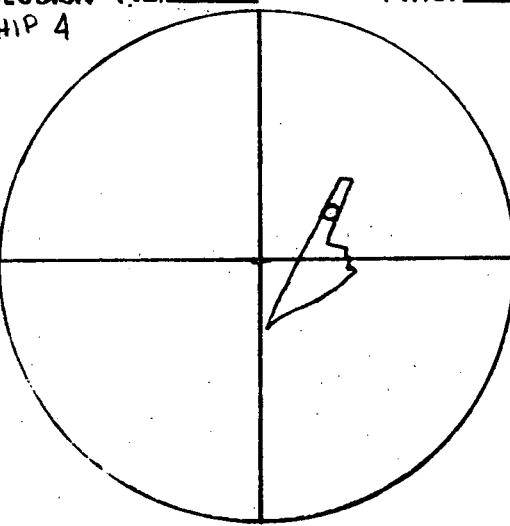
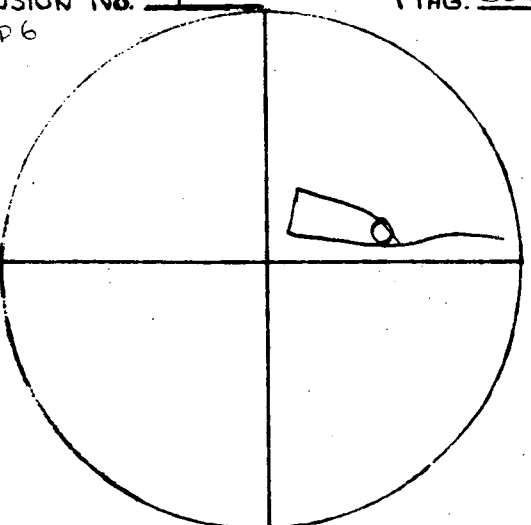
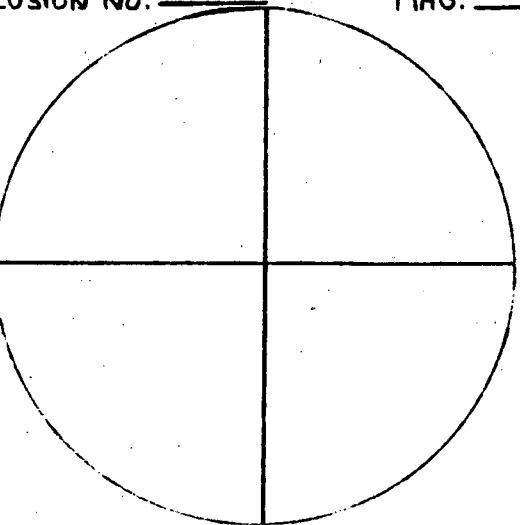
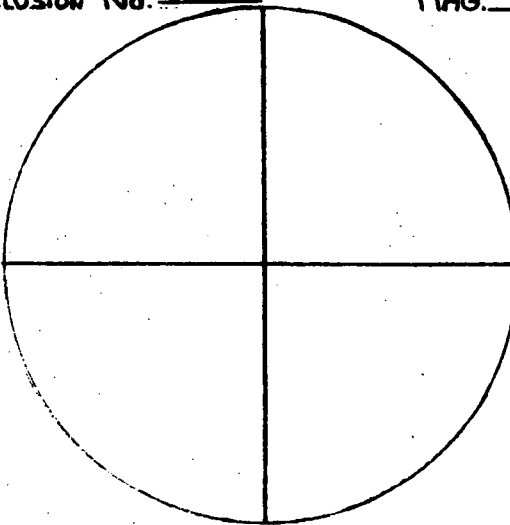
<p>Inclusion No. <u>1</u> MAG. <u>500</u> CHIP 1</p>  <p>3.88, 4.04 mv 95°, 98°</p>	<p>Inclusion No. <u>2</u> MAG. <u>500</u> CHIP 4 PHOTO 1</p>  <p>4.36, 4.56 mv 106°, 111°</p>	<p>Inclusion No. <u>3</u> MAG. <u>500</u> CHIP 4</p>  <p>~ 4.46 mv 109°</p>
<p>Inclusion No. <u>4</u> MAG. <u>500</u> CHIP 6</p>  <p>4.22 mv 103°</p>	<p>Inclusion No. _____ MAG. _____</p> 	<p>Inclusion No. _____ MAG. _____</p> 

PHOTO 1, GA 19.1, CHIP 4,  
INCLUSION 2 ; SEE SKETCH ;  
PRIMARY INCLUSION (NEGATIVE  
CRYSTAL)



Sample GA 1.1 - Vein calcite

Inclusions rare, commonly necked and unsuitable for homogenization temperatures; only a small quantity of material available.

Although the data are limited, inclusions in this sample have significant differences in vapor/liquid ratios or appear to contain two fluids and no vapor. Upon heating some of the inclusions to temperatures approaching 300°C no shrinkage of the "vapor" phase was observed (eg. sketch of inclusion 5 and photo 3). This behavior indicates two fluid phases rather than vapor and liquid. Epidote was noted in some of the fractures and surrounds inclusion 5 (see dark patches surrounding inclusion in photo 3). Carbon dioxide is a product of epidote formation in calcite, and liquid carbon dioxide could be expected to form. It is then proposed that an aqueous fluid phase, a liquid carbon dioxide phase, and a carbon dioxide vapor phase can exist in varying proportions in any given inclusion. This negates the possibility of any meaningful formation temperatures from homogenization studies of the inclusions in this sample. However, the processes involved are of a metamorphic nature and the temperatures involved must have been correspondingly high.

The temperatures given below are for those inclusions containing vapor plus one or two fluids and probably have no real significance.

1 - 325°C (necked)

2 - 99°C

3 - 80°C

ANALYST: RJ POTTORF

SAMPLE No. <sup>GA-1.1</sup>

FLUID INCLUSION SKETCHES

CHIP No. 1-3

CONN EDISON

MINERAL: CALCITE

30

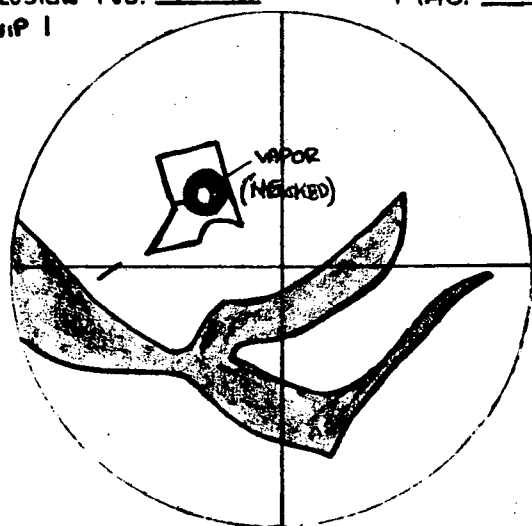
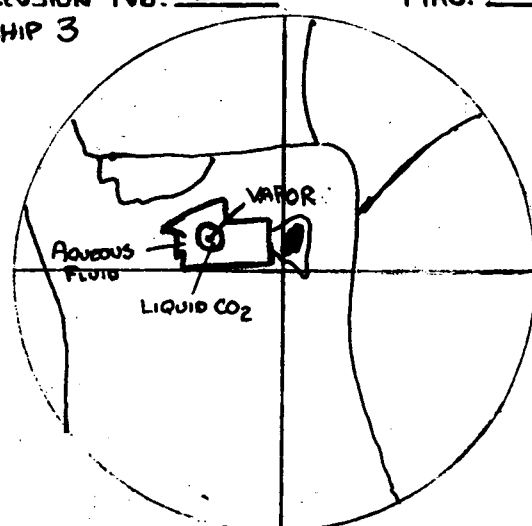
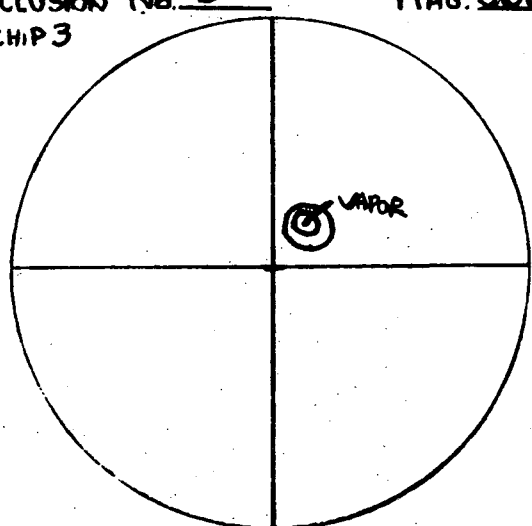
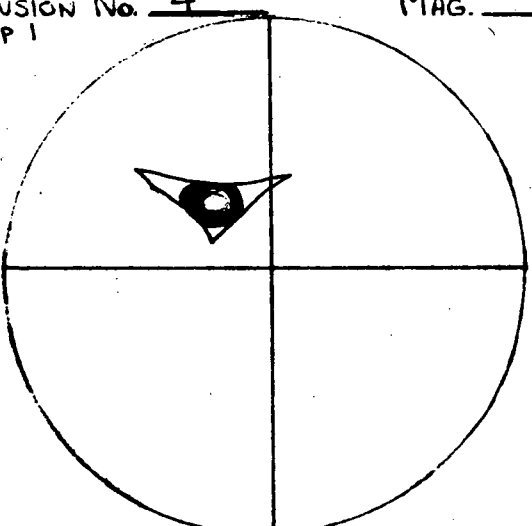
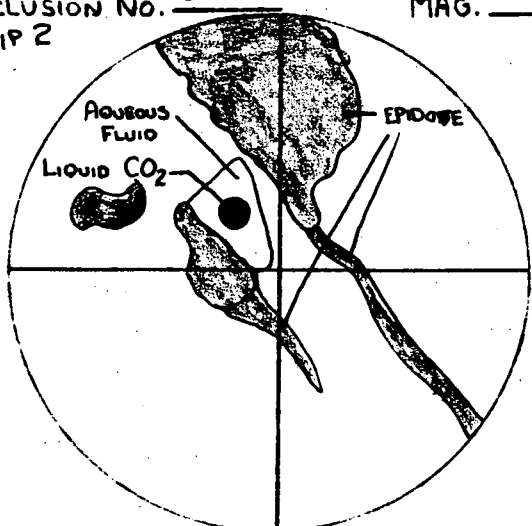
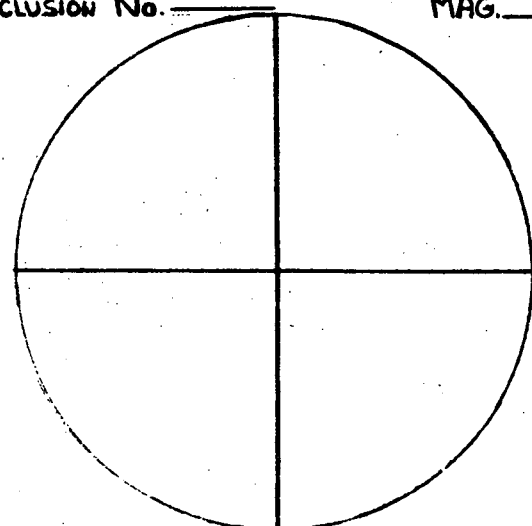
<p>Inclusion No. <u>1</u> MAG. <u>500</u> CHIP 1</p>  <p>-2-</p> <p>13.27, 13.23 mv 325°C</p>	<p>Inclusion No. <u>2</u> MAG. <u>500</u> CHIP 3</p>  <p>4.05 mv 99°C</p>	<p>Inclusion No. <u>3</u> MAG. <u>500</u> CHIP 3</p>  <p>3.27, 3.26 mv 80°C</p>
<p>Inclusion No. <u>4</u> MAG. _____ CHIP 1</p>  <p>STOPPED ~13.00 mv 319°C</p>	<p>Inclusion No. <u>5</u> MAG. _____ CHIP 2</p>  <p>NO HOMOGENIZATION STOPPED 12.00 mv - 295°C</p>	<p>Inclusion No. _____ MAG. _____</p> 

PHOTO 1, GA 1.1, CHIP 3,  
INCLUSION 2, SEE SKETCH;  
THE SCALE OF ALL PHOTO-  
GRAPHS IN THIS REPORT  
ARE 0.24mm X 0.16mm



PHOTO 2, GA 1.1, CHIP 1,  
PRIMARY INCLUSION WITH  
LARGE VAPOR/LIQUID RATIO

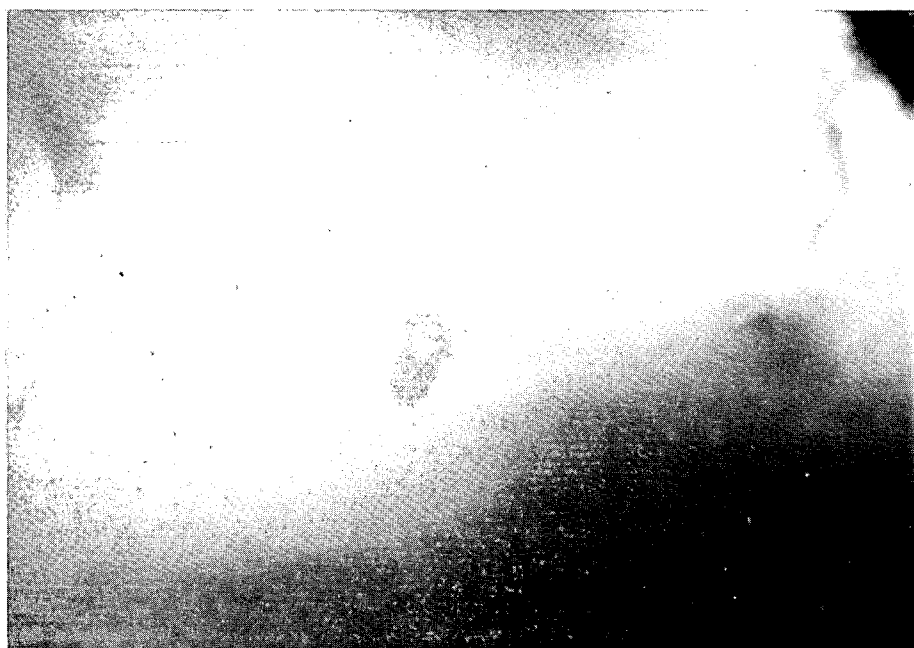


PHOTO 3, GA 1.1, CHIP 2,  
INCLUSION 5, SEE SKETCH  
AND TEXT.

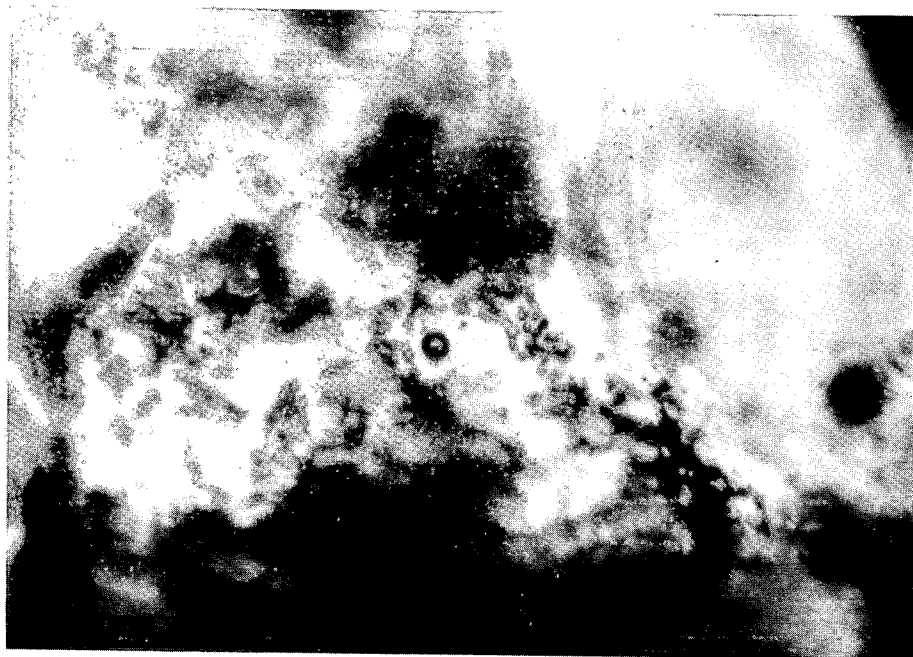


PHOTO 4, GA1.1, CHIP 3



PHOTO 5, GA 1.1, CHIP 1



THESE TWO PHOTOGRAPHS SHOW INCLUSIONS NOT SUITABLE FOR TEMPERATURE STUDIES. BOTH INCLUSIONS ARE SEVERELY NECKED AND WOULD GIVE ANOMALOUSLY HIGH AND LOW TEMPERATURES, RESPECTIVELY.

Sample GA 7.1 - Vein Calcite

One population of inclusions noted; 9 inclusions measured. Several inclusions were necked down but gave similar temperatures. This indicates that the necking generally occurred while the fluid consisted of one phase at the time of necking. Cu-Fe sulfides are common on the walls of the calcite veins. Inclusions are relatively abundant. Inclusion number 7 gave an anomalously high temperature and probably contained some vapor phase when necking of the entire inclusion occurred. It is therefore discarded.

Range 195 - 229°C

Average 215°C

ANALYST: RJ POTTORF

SAMPLE No. GA 7.1

FLUID INCLUSION SKETCHES

CHIP No. 3

CONN EDISON

MINERAL: VEIN CALCITE

34

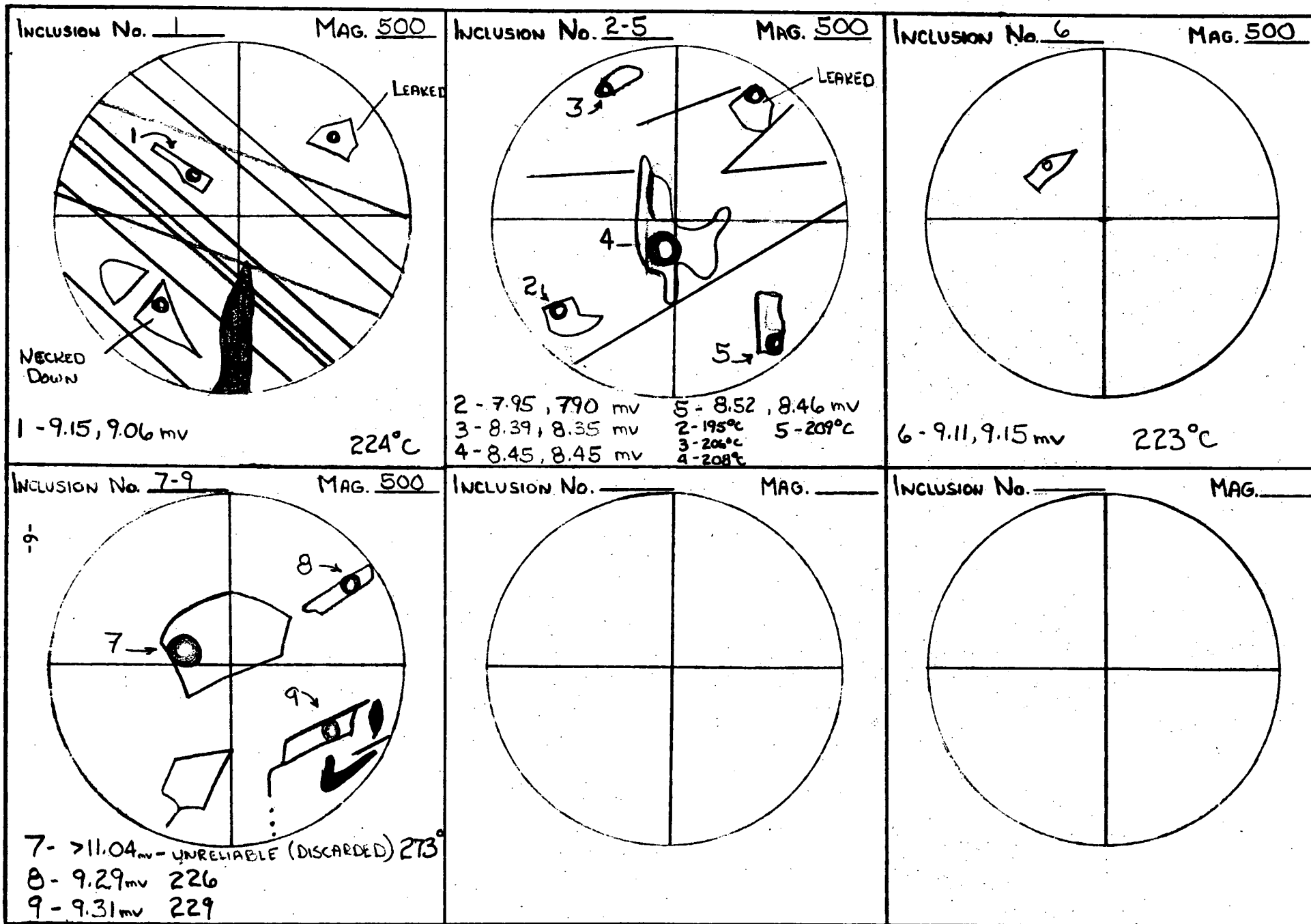


PHOTO 1, GA 7.1, CHIP 3,  
PRIMARY INCLUSION 1; SEE  
SKETCH



PHOTO 2, GA 7.1, CHIP 3,  
PRIMARY INCLUSIONS 4, 5  
AND "LEAKED" INCLUSION;  
SEE SKETCH



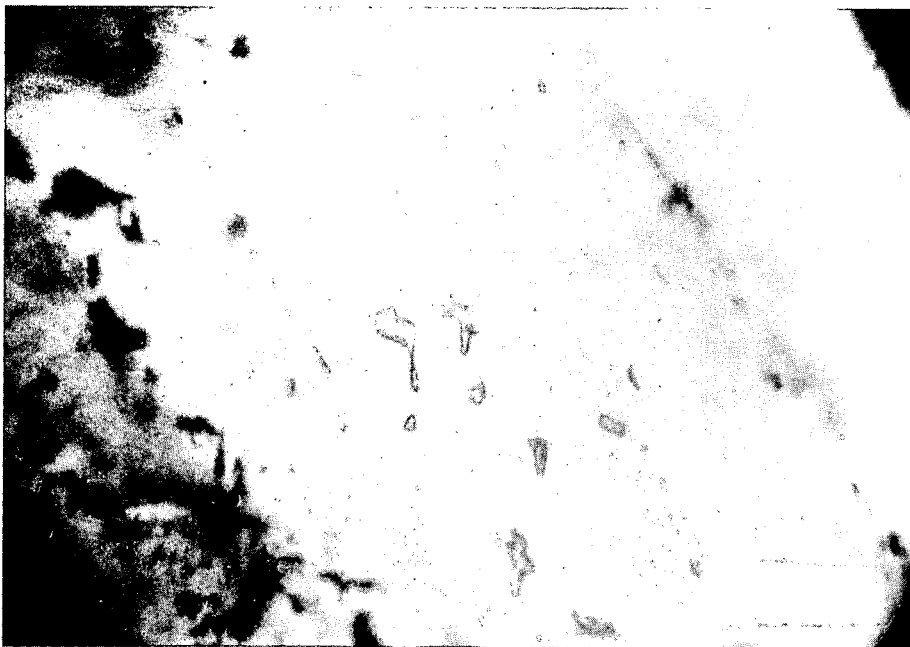
PHOTO 3. GA 7.1, CHIP 3  
PRIMARY INCLUSION 3; SEE  
SKETCH



PHOTO 4, GA 7.1, CHIP 3,  
PRIMARY INCLUSION 7;  
8 AND 9 ARE NOT IN  
FOCUS; SEE SKETCH



PHOTO 5, GA 7.1, CHIP 3,  
TWO NECKED INCLUSIONS,  
ONE CONTAINING VAPOR;  
NOT SUITABLE FOR  
HOMOGENIZATION TEMP-  
ERATURES.



## Sample GA 8.1 - Vein Calcite

Inclusions in this sample are exceedingly rare and slippage along cleavage planes is abundant. Consequently, the data are limited but two populations of inclusions are tentatively suggested; a low temperature ( $\sim 134^{\circ}\text{C}$ ) population of small secondary (?) inclusions and an apparently higher temperature population of much larger inclusions which in all cases did not homogenize, and the samples decrepitated at about  $400^{\circ}\text{C}$ . This behavior is expected if the inclusions contain two fluid phases (aqueous fluid and liquid carbon dioxide), the pressures generated at  $400^{\circ}\text{C}$  decrepitate the sample. The formation conditions involved must be high temperature (metamorphic).

## 2 Inclusions

Range (Secondary (?) Inclusions):  $125-144^{\circ}$

Average  $134^{\circ}$

ANALYST: RJ POTTORF

SAMPLE No. GA 8.1

FLUID INCLUSION SKETCHES

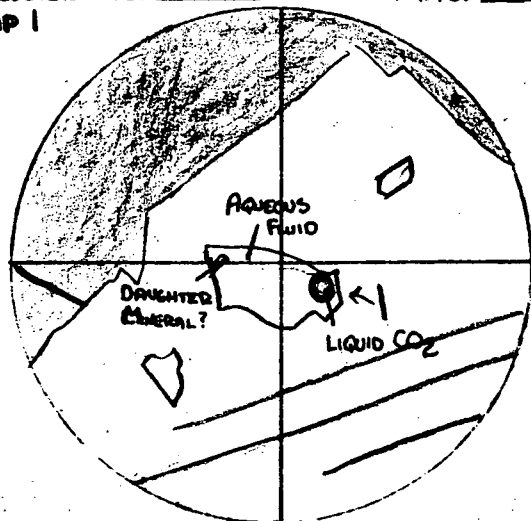
CHIP No. 1, 3, 5

CONN EDISON

MINERAL: CALCITE

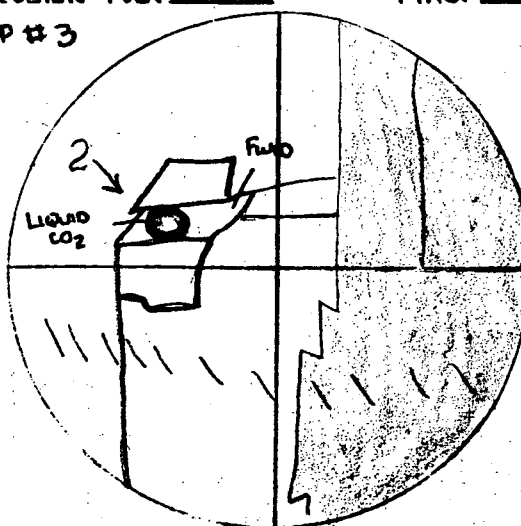
38

INCLUSION No. 1 MAG. 500  
CHIP 1



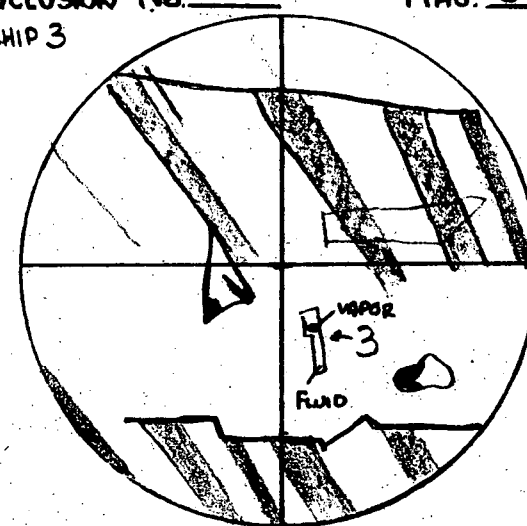
DECREPITATED 16.47mv (402°C)

INCLUSION No. 2 MAG. 500  
CHIP #3



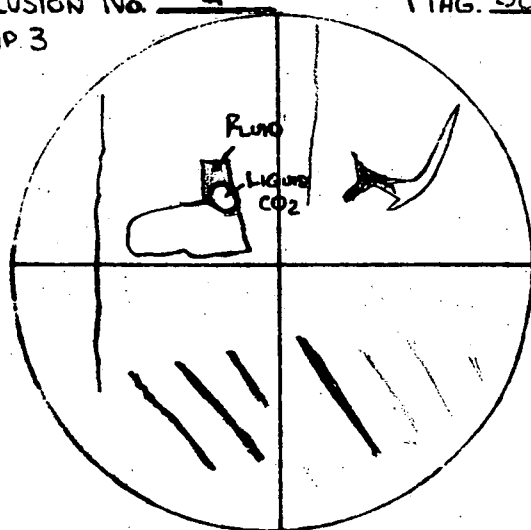
DECREPITATED 16.55mv (403°C)

INCLUSION No. 3 MAG. 500  
CHIP 3



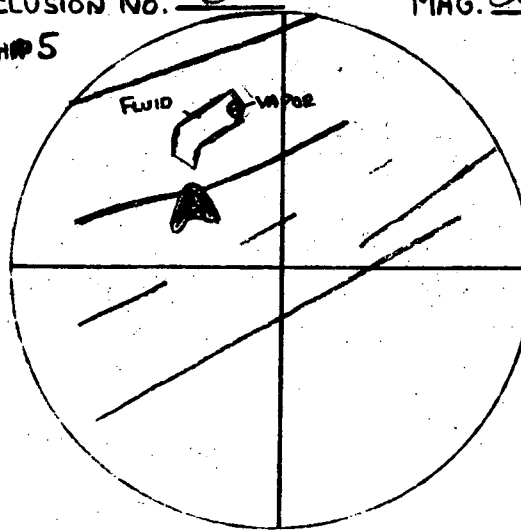
3- 5.90, 5.83 mv 143°C

INCLUSION No. 4 MAG. 500  
CHIP 3



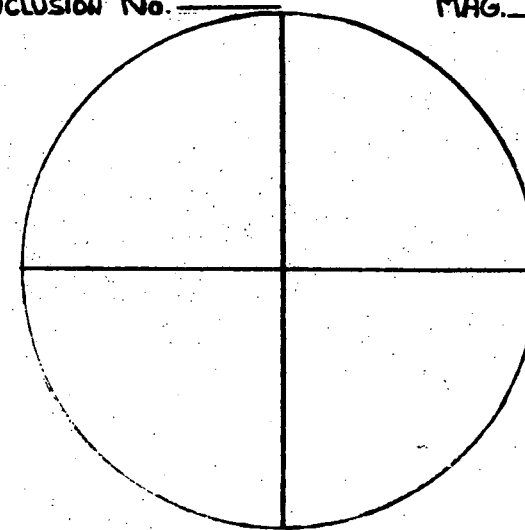
DECREPITATED 16.27 (397°C)

INCLUSION No. 5 MAG. 500  
CHIP 5



5- 5.15 mv 125°C

INCLUSION No. \_\_\_\_\_ MAG. \_\_\_\_\_



● PHOTO 1, GA 8.1, CHIP 1,  
INCLUSION 1; SEE  
SKETCH



PHOTO 2, GA 8.1, CHIP 3,  
● INCLUSION 2; SEE SKETCH

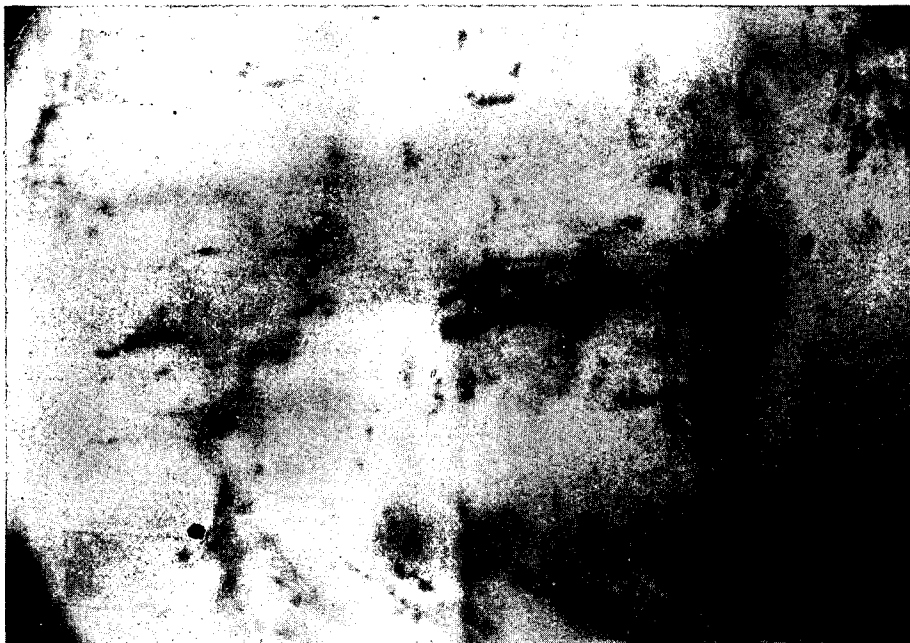


PHOTO 3, GA 8.1, CHIP 3,  
INCLUSION 3; SECONDARY(?)  
INCLUSION; SEE SKETCH



Sample GA 11.3 - Calcite

Measured inclusions apparently from same population; secondary inclusions (not measurable) present; 9 inclusions, no.6 discarded because of apparent necking.

Range 237 - 298°

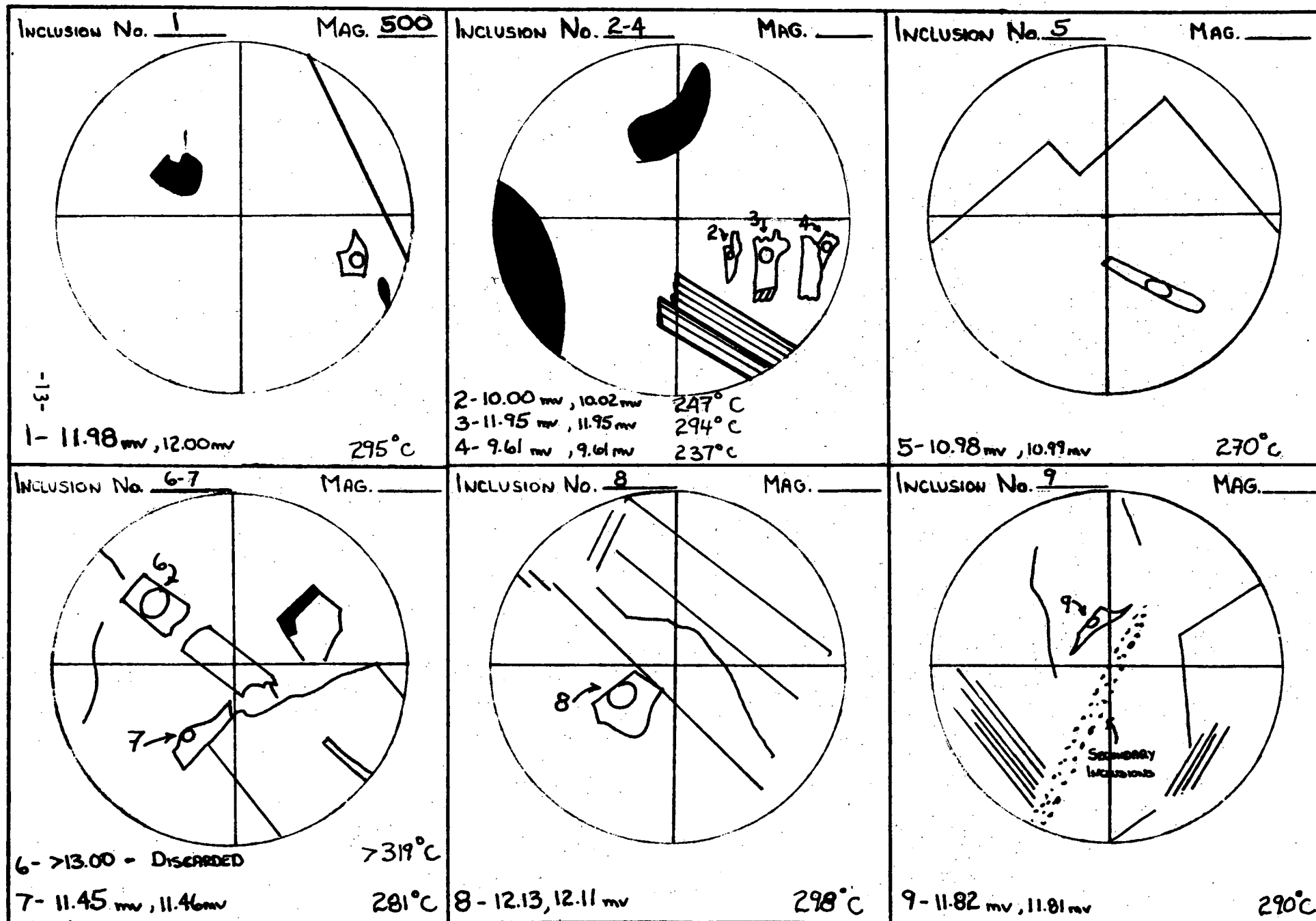
Average 277°

ANALYST: RJ POTTORF  
SAMPLE No. 11.3

FLUID INCLUSION SKETCHES  
CHIP No. 2

CONN EDISON  
MINERAL: CALCITE

14



## Sample GA 11.4B - Vein Calcite

Inclusions appear to belong to the same population; 5 inclusions measured; inclusions rare, inclusions 2 and 3 could not be measured exactly because at temperatures approaching homogenization the bubble moved to areas in the inclusion which could not be optically resolved. From the bubble size at the time of "disappearance" it is concluded that homogenization temperatures for inclusions 2 and 3 are similar to those for 1, 4 and 5.

Range  $2171^{\circ} - 187^{\circ}$

Average (1,3,4,5)  $181^{\circ}$

ANALYST: RJ POTTORF

SAMPLE No. GA 11.4 B

FLUID INCLUSION SKETCHES

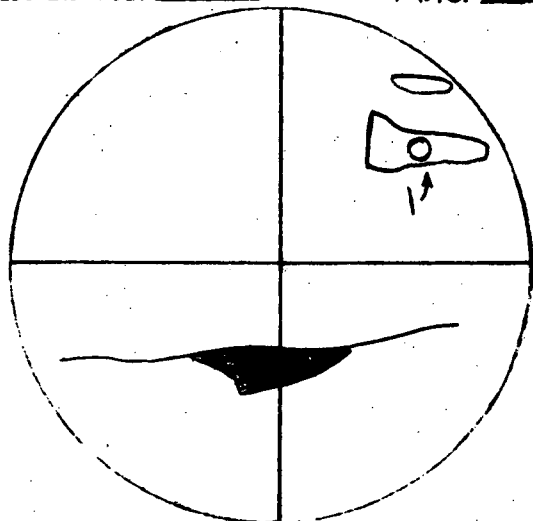
CHIP No. 1

CONN EDISON

MINERAL: CALCITE

45

Inclusion No. 1 MAG. 500

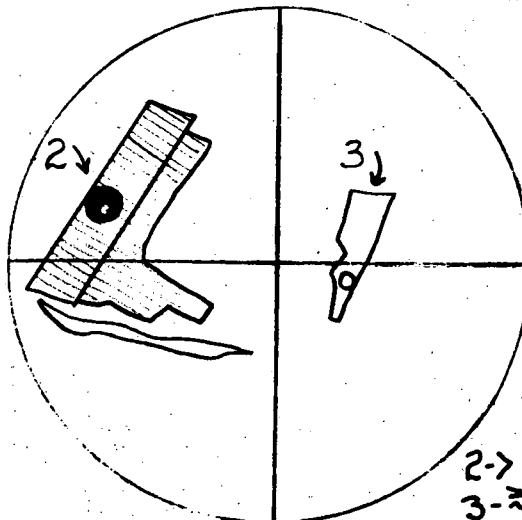


-15-

1 - 7.63, 7.60 mv

187°C

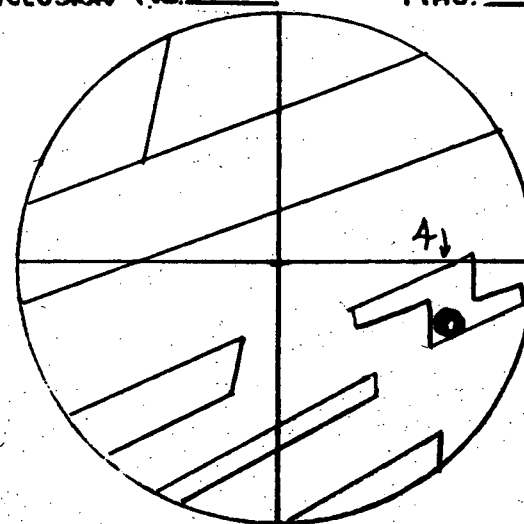
Inclusion No. 2-3 MAG. 500



2 - > 159°  
3 - ~ 171°

2 - > 6.49 mv READING AT TIME OF "DISAPPEARANCE"  
3 - ~ 6.95 mv (SEE NOTES)

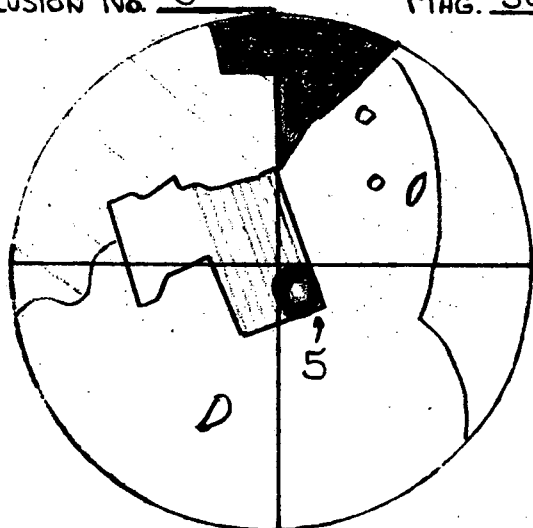
Inclusion No. 4 MAG. 500



4 - 7.48 mv

184°C

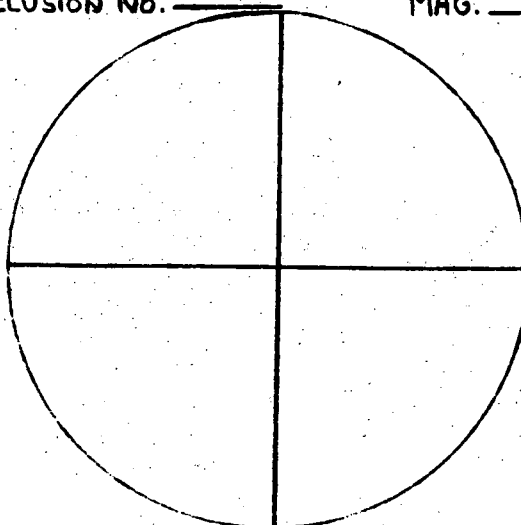
Inclusion No. 5 MAG. 500



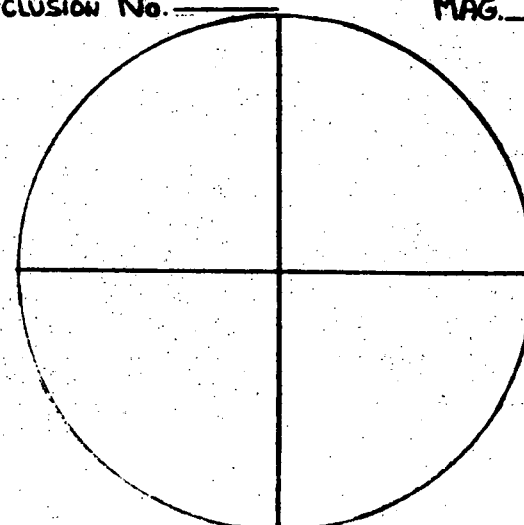
5 - 7.36, 7.40 mv

181°C

Inclusion No. \_\_\_\_\_ MAG. \_\_\_\_\_



Inclusion No. \_\_\_\_\_ MAG. \_\_\_\_\_



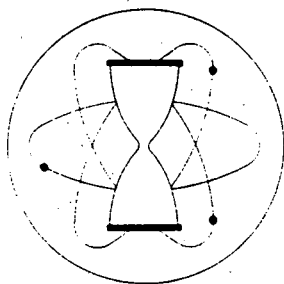
Summary (range (no. samples) average, in °C)

<u>Sample</u>	<u>Primary Inclusions</u>	<u>Secondary Inclusions</u>
GA 1.1	high temperature (metamorphic)	
GA 7.1	195 - 229 (9) <u>215°</u>	
GA 8.1	high temperature (metamorphic)	125 - 144 (2) <u>134°</u>
GA 11.3	237 - 298 (9) <u>277°</u>	
GA 11.4B	≥ 171 - 187° (5) <u>181°</u>	

ATTACHMENT NO. 2

TO APPENDIX E

K/Ar Age Determinations



# KRUEGER ENTERPRISES, INC.

## GEOCHRON LABORATORIES DIVISION

24 BLACKSTONE STREET • CAMBRIDGE, MA. 02139 • (617) - 876-3691

### POTASSIUM-ARGON AGE DETERMINATION

### REPORT OF ANALYTICAL WORK

Our Sample No. R-3633

Date Received: 13 August 1976

Your Reference: #1 2-76-81a

Date Reported: 8 September 1976

Submitted by: Slavomir Zalewski  
Dames & Moore  
6 Commerce Drive  
Cranford, New Jersey 07016

Job #0874-062  
P.O. # NJ 3377

Sample Description & Locality: Basalt sample (diabase), 2-76-81a, Flow I.

Material Analyzed: Whole rock, -60/+100 mesh.

$Ar^{40}*/K^{40} = .01100$

AGE = 179  $\pm$  9 M.Y.

#### Argon Analyses:

Ar <sup>40</sup> *, ppm.	Ar <sup>40</sup> * / Total Ar <sup>40</sup>	Ave. Ar <sup>40</sup> *, ppm.
.006138	.618	.006301
.006463	.621	

#### Potassium Analyses:

% K	Ave. %K	K <sup>40</sup> , ppm
.469	.469	.572
.470		

#### Constants Used:

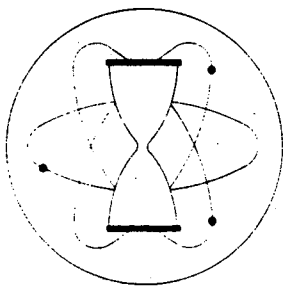
$\lambda_{\beta} = 4.72 \times 10^{-10} / \text{year}$

$\lambda_e = 0.585 \times 10^{-10} / \text{year}$

$K^{40}/K = 1.22 \times 10^{-4} \text{ g./g.}$

$$AGE = \frac{1}{\lambda_e + \lambda_{\beta}} \ln \left[ \frac{\lambda_{\beta} + \lambda_e}{\lambda_e} \times \frac{Ar^{40*}}{K^{40}} + 1 \right]$$

Note: Ar<sup>40</sup>\* refers to radiogenic Ar<sup>40</sup>.  
M.Y. refers to millions of years.



# KRUEGER ENTERPRISES, INC.

## GEOCHRON LABORATORIES DIVISION

24 BLACKSTONE STREET • CAMBRIDGE, MA. 02139 • (617) - 876 - 3691

### POTASSIUM-ARGON AGE DETERMINATION

### REPORT OF ANALYTICAL WORK

Our Sample No. R-3634

Date Received: 13 August 1976

Your Reference: #2 2-76-81b

Date Reported: 8 September 1976

Submitted by: Slavomir Zalewski  
Dames & Moore  
6 Commerce Drive  
Cranford, New Jersey 07016

Job #0874-062  
P.O. # NJ 3377

Sample Description & Locality: Basalt sample (diabase), 2-76-81b, Flow I.

Material Analyzed: Whole rock, -60/+100 mesh.

$\text{Ar}^{40*}/\text{K}^{40} = .01188$

AGE =  $193 \pm 10$  M.Y.

#### Argon Analyses:

$\text{Ar}^{40*}$ , ppm.

$\text{Ar}^{40*}/\text{Total Ar}^{40}$

Ave.  $\text{Ar}^{40*}$ , ppm.

.006905  
.007177

.549  
.700

.007041

#### Potassium Analyses:

% K

Ave. %K

$\text{K}^{40}$ , ppm

.498  
.474

.486

.592

#### Constants Used:

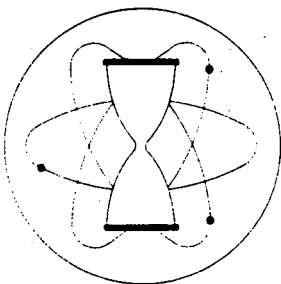
$\lambda_{\beta} = 4.72 \times 10^{-10} / \text{year}$

$\lambda_e = 0.585 \times 10^{-10} / \text{year}$

$\text{K}^{40}/\text{K} = 1.22 \times 10^{-4} \text{ g./g.}$

$$\text{AGE} = \frac{1}{\lambda_e + \lambda_{\beta}} \ln \left[ \frac{\lambda_{\beta} + \lambda_e}{\lambda_e} \times \frac{\text{Ar}^{40*}}{\text{K}^{40}} + 1 \right]$$

Note:  $\text{Ar}^{40*}$  refers to radiogenic  $\text{Ar}^{40}$ .  
M.Y. refers to millions of years.



# KRUEGER ENTERPRISES, INC.

## GEOCHRON LABORATORIES DIVISION

24 BLACKSTONE STREET • CAMBRIDGE, MA. 02139 • (617) - 876-3691

### POTASSIUM-ARGON AGE DETERMINATION

### REPORT OF ANALYTICAL WORK

Our Sample No. R-3635

Date Received: 13 August 1976

Your Reference: #3 2-76-82a

Date Reported: 8 September 1976

Submitted by: Slavomir Zalewski  
Dames & Moore  
6 Commerce Drive  
Cranford, New Jersey 07016

Job #0874-062  
P.O. # NJ 3377

Sample Description & Locality: Basalt sample (diabase), 2-76-82a, Flow II.

Material Analyzed: Whole rock, -50/+100 mesh.

$\text{Ar}^{40*}/\text{K}^{40} = .009676$

AGE = 159  $\pm$  8 M.Y.

#### Argon Analyses:

$\text{Ar}^{40*}$ , ppm.	$\text{Ar}^{40*}/\text{Total Ar}^{40}$	Ave. $\text{Ar}^{40*}$ , ppm.
.007686	.550	.007596
.007506	.552	

#### Potassium Analyses:

% K	Ave. %K	$\text{K}^{40}$ , ppm
.649	.643	.785
.638		

#### Constants Used:

$\lambda_{\beta} = 4.72 \times 10^{-10} / \text{year}$

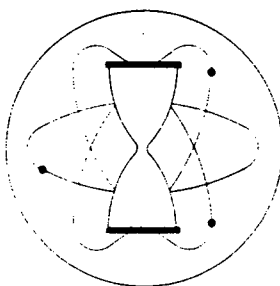
$\lambda_e = 0.585 \times 10^{-10} / \text{year}$

$\text{K}^{40}/\text{K} = 1.22 \times 10^{-4} \text{ g./g.}$

$$\text{AGE} = \frac{1}{\lambda_e + \lambda_{\beta}} \ln \left[ \frac{\lambda_{\beta} + \lambda_e}{\lambda_e} \times \frac{\text{Ar}^{40*}}{\text{K}^{40}} + 1 \right]$$

Note:  $\text{Ar}^{40*}$  refers to radiogenic  $\text{Ar}^{40}$ .

M.Y. refers to millions of years.



# KRUEGER ENTERPRISES, INC.

## GEOCHRON LABORATORIES DIVISION

24 BLACKSTONE STREET • CAMBRIDGE, MA. 02139 • (617)-876-3691

### POTASSIUM-ARGON AGE DETERMINATION

### REPORT OF ANALYTICAL WORK

Our Sample No. R-3636

Date Received: 13 August 1976

Your Reference: #4 2-76-82b

Date Reported: 8 September 1976

Submitted by: Slavomir Zalewski  
Dames & Moore  
6 Commerce Drive  
Cranford, New Jersey 07016

Job #0874-062  
P.O. # NJ 3377

Sample Description & Locality: Basalt sample (diabase), 2-76-82b, Flow II.

Material Analyzed: Whole rock, -60/+100 mesh.

$\text{Ar}^{40}*/\text{K}^{40} = .01106$

AGE =  $180 \pm 8$  M.Y.

#### Argon Analyses:

$\text{Ar}^{40}*$ , ppm.	$\text{Ar}^{40}*/\text{Total Ar}^{40}$	Ave. $\text{Ar}^{40}*$ , ppm.
.008903	.755	.009118
.008644	.746	
.009806	.734	

#### Potassium Analyses:

% K	Ave. %K	$\text{K}^{40}$ , ppm
.700	.675	.824
.651		

#### Constants Used:

$$\lambda_{\beta} = 4.72 \times 10^{-10} / \text{year}$$

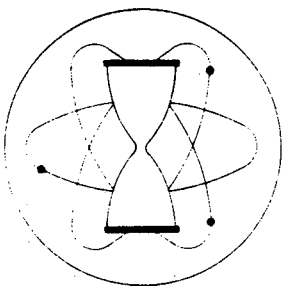
$$\lambda_e = 0.585 \times 10^{-10} / \text{year}$$

$$\text{K}^{40}/\text{K} = 1.22 \times 10^{-4} \text{ g./g.}$$

$$\text{AGE} = \frac{1}{\lambda_e + \lambda_{\beta}} \ln \left[ \frac{\lambda_{\beta} + \lambda_e}{\lambda_e} \times \frac{\text{Ar}^{40*}}{\text{K}^{40}} + 1 \right]$$

Note:  $\text{Ar}^{40}*$  refers to radiogenic  $\text{Ar}^{40}$ .

M.Y. refers to millions of years.



# KRUEGER ENTERPRISES, INC.

## GEOCHRON LABORATORIES DIVISION

24 BLACKSTONE STREET • CAMBRIDGE, MA. 02139 • (617)-876-3691

### POTASSIUM-ARGON AGE DETERMINATION

### REPORT OF ANALYTICAL WORK

Our Sample No. R-3637

Date Received: 13 August 1976

Your Reference: #5 2-76-83a

Date Reported: 8 September 1976

Submitted by: Slavomir Zalewski  
Dames & Moore  
6 Commerce Drive  
Cranford, New Jersey 07016

Job #0874-062  
P.O. # NJ 3377

Sample Description & Locality: Basalt sample (diabase), 2-76-83a, Flow III.

Material Analyzed: Whole rock, -50/+100 mesh.

$\text{Ar}^{40*}/\text{K}^{40} = .008943$

AGE =  $147 \pm 9$  M.Y.

#### Argon Analyses:

$\text{Ar}^{40*}$ , ppm.	$\text{Ar}^{40*}/\text{Total Ar}^{40}$	Ave. $\text{Ar}^{40*}$ , ppm.
.002760	.420	.002733
.002706	.404	

#### Potassium Analyses:

% K	Ave. %K	$\text{K}^{40}$ , ppm
.251	.250	.305
.250		

#### Constants Used:

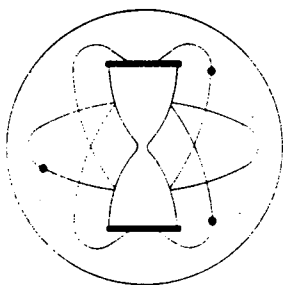
$\lambda_{\beta} = 4.72 \times 10^{-10} / \text{year}$

$\lambda_e = 0.585 \times 10^{-10} / \text{year}$

$\text{K}^{40}/\text{K} = 1.22 \times 10^{-4} \text{ g./g.}$

$$\text{AGE} = \frac{1}{\lambda_e + \lambda_{\beta}} \ln \left[ \frac{\lambda_{\beta} + \lambda_e}{\lambda_e} \times \frac{\text{Ar}^{40*}}{\text{K}^{40}} + 1 \right]$$

Note:  $\text{Ar}^{40*}$  refers to radiogenic  $\text{Ar}^{40}$ .  
M.Y. refers to millions of years.



# KRUEGER ENTERPRISES, INC.

## GEOCHRON LABORATORIES DIVISION

24 BLACKSTONE STREET • CAMBRIDGE, MA. 02139 • (617)-876-3691

### POTASSIUM-ARGON AGE DETERMINATION

### REPORT OF ANALYTICAL WORK

Our Sample No. R-3638

Date Received: 13 August 1976

Your Reference: #6 2-76-83b

Date Reported: 8 September 1976

Submitted by: Slavomir Zalewski  
Dames & Moore  
6 Commerce Drive  
Cranford, New Jersey 07016

Job #0874-062  
P.O. # NJ 3377

Sample Description & Locality: Basalt sample (diabase), 2-76-83b, Flow III.

Material Analyzed: Whole rock, -60/+100 mesh.

$\text{Ar}^{40*}/\text{K}^{40} = .008236$

AGE =  $136 \pm 9$  M.Y.

#### Argon Analyses:

$\text{Ar}^{40*}$ , ppm.	$\text{Ar}^{40*}/\text{Total Ar}^{40}$	Ave. $\text{Ar}^{40*}$ , ppm.
.002233	.365	.002326
.002419	.254	

#### Potassium Analyses:

% K	Ave. %K	$\text{K}^{40}$ , ppm
.233	.231	.282
.230		

#### Constants Used:

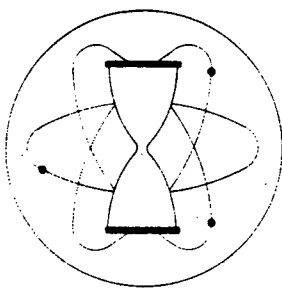
$\lambda_{\beta} = 4.72 \times 10^{-10}/\text{year}$

$\lambda_e = 0.585 \times 10^{-10}/\text{year}$

$\text{K}^{40}/\text{K} = 1.22 \times 10^{-4} \text{ g./g.}$

$$\text{AGE} = \frac{1}{\lambda_e + \lambda_{\beta}} \ln \left[ \frac{\lambda_{\beta} + \lambda_e}{\lambda_e} \times \frac{\text{Ar}^{40*}}{\text{K}^{40}} + 1 \right]$$

Note:  $\text{Ar}^{40*}$  refers to radiogenic  $\text{Ar}^{40}$ .  
M.Y. refers to millions of years.



# KRUEGER ENTERPRISES, INC.

## GEOCHRON LABORATORIES DIVISION

24 BLACKSTONE STREET • CAMBRIDGE, MA. 02139 • (617)-876-3691

### POTASSIUM-ARGON AGE DETERMINATION

### REPORT OF ANALYTICAL WORK

Our Sample No. R-3673

Date Received: 24 September 1976

Your Reference: FS-14

Date Reported: 20 October 1976

Submitted by: Frank Schmitt  
Dames & Moore  
6 Commerce Drive  
Cranford, New Jersey 07016

Job No. 0874-062  
P.O. No. NJ 3377

Sample Description & Locality: Dense, chilled diabase (basalt), sample FS-14.

Material Analyzed: Whole rock. Freshest material selected and crushed to -40/+100 mesh to insure homogeneity.

$Ar^{40*}/K^{40} = .01073$

AGE =  $175 \pm 8$  M.Y.

#### Argon Analyses:

$Ar^{40*}$ , ppm.

$Ar^{40*}/Total\ Ar^{40}$

Ave.  $Ar^{40*}$ , ppm.

.01167

.655

.01179

.01191

.514

#### Potassium Analyses:

% K

Ave. %K

$K^{40}$ , ppm

.904

.900

1.098

.897

#### Constants Used:

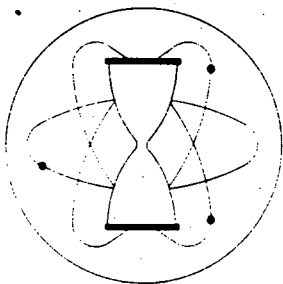
$\lambda_{\beta} = 4.72 \times 10^{-10} / \text{year}$

$\lambda_e = 0.585 \times 10^{-10} / \text{year}$

$K^{40}/K = 1.22 \times 10^{-4} \text{ g./g.}$

$$AGE = \frac{1}{\lambda_e + \lambda_{\beta}} \ln \left[ \frac{\lambda_{\beta} + \lambda_e}{\lambda_e} \times \frac{Ar^{40*}}{K^{40}} + 1 \right]$$

Note:  $Ar^{40*}$  refers to radiogenic  $Ar^{40}$ .  
M.Y. refers to millions of years.



# KRUEGER ENTERPRISES, INC.

## GEOCHRON LABORATORIES DIVISION

24 BLACKSTONE STREET • CAMBRIDGE, MA. 02139 • (617) 876-3691

### POTASSIUM-ARGON AGE DETERMINATION

### REPORT OF ANALYTICAL WORK

Our Sample No. R-3559

Date Received: 15 June 1976

Your Reference: SL-121I

Date Reported: 25 June 1976

Submitted by: Frank Schmitt  
Dames & Moore  
6 Commerce Drive  
Cranford, New Jersey 07016

J.O. 0874-062 P.O. NJ 3377

Sample Description & Locality: Basalt sample, SL-121 I.

Material Analyzed: Whole rock, fresh material crushed to -60/+100 mesh.

$\text{Ar}^{40*}/\text{K}^{40} = .009532$

AGE =  $156 \pm 7$  M.Y.

#### Argon Analyses:

$\text{Ar}^{40*}$ , ppm.

$\text{Ar}^{40*}/\text{Total Ar}^{40}$

Ave.  $\text{Ar}^{40*}$ , ppm.

.01224

.677

.01267

.01310

.539

#### Potassium Analyses:

% K

Ave. %K

$\text{K}^{40}$ , ppm

1.113

1.089

1.329

1.066

#### Constants Used:

$\lambda_{\beta} = 4.72 \times 10^{-10}$  / year

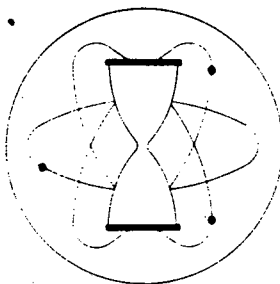
$\lambda_e = 0.585 \times 10^{-10}$  / year

$\text{K}^{40}/\text{K} = 1.22 \times 10^{-4}$  g./g.

$$\text{AGE} = \frac{1}{\lambda_e + \lambda_{\beta}} \ln \left[ \frac{\lambda_{\beta} + \lambda_e}{\lambda_e} \times \frac{\text{Ar}^{40*}}{\text{K}^{40}} + 1 \right]$$

Note:  $\text{Ar}^{40*}$  refers to radiogenic  $\text{Ar}^{40}$ .

M.Y. refers to millions of years.



# KRUEGER ENTERPRISES, INC.

## GEOCHRON LABORATORIES DIVISION

24 BLACKSTONE STREET • CAMBRIDGE, MA. 02139 • (617) - 876 - 3691

### POTASSIUM-ARGON AGE DETERMINATION

### REPORT OF ANALYTICAL WORK

Our Sample No. R-3560

Date Received: 15 June 1976

Your Reference: SL-THD

Date Reported: 25 June 1976

Submitted by: Frank Schmitt  
Dames & Moore  
6 Commerce Drive  
Cranford, New Jersey 07016

J.O. 0874-062 P.O. NJ 3377

Sample Description & Locality: Basalt sample, SL-THD.

Material Analyzed: Whole rock, selected fresh material crushed to -60/+100 mesh.

$Ar^{40*}/K^{40} = .009075$

AGE =  $149 \pm 7$  M.Y.

#### Argon Analyses:

$Ar^{40*}$ , ppm.

$Ar^{40*}/Total\ Ar^{40}$

Ave.  $Ar^{40*}$ , ppm.

.007013

.410

.006992

.006971

.377

#### Potassium Analyses:

% K

Ave. %K

$K^{40}$ , ppm

.631

.631

.770

.632

#### Constants Used:

$\lambda_{\beta} = 4.72 \times 10^{-10}$  / year

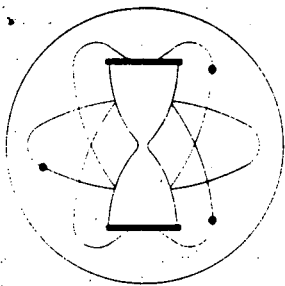
$\lambda_e = 0.585 \times 10^{-10}$  / year

$K^{40}/K = 1.22 \times 10^{-4}$  g./g.

$$AGE = \frac{1}{\lambda_e + \lambda_{\beta}} \ln \left[ \frac{\lambda_{\beta} + \lambda_e}{\lambda_e} \times \frac{Ar^{40*}}{K^{40}} + 1 \right]$$

Note:  $Ar^{40*}$  refers to radiogenic  $Ar^{40}$ .

M.Y. refers to millions of years.



# KRUEGER ENTERPRISES, INC.

## GEOCHRON LABORATORIES DIVISION

24 BLACKSTONE STREET • CAMBRIDGE, MA. 02139 • (617) - 876-3691

### POTASSIUM-ARGON AGE DETERMINATION

### REPORT OF ANALYTICAL WORK

Our Sample No. R-3561

Date Received: 15 June 1976

Your Reference: SL-127A

Date Reported: 25 June 1976

Submitted by: Frank Schmitt  
Dames & Moore  
6 Commerce Drive  
Cranford, New Jersey 07016

J.O. 0874-062 P.O. NJ 3377

Sample Description & Locality: Basalt sample, SL-127A.

Material Analyzed: Whole rock, selected fresh material crushed to -60/+100 mesh.

$Ar^{40*}/K^{40} = .02893$

AGE =  $439 \pm 18$  M.Y.

#### Argon Analyses:

$Ar^{40*}$ , ppm.	$Ar^{40*}/Total\ Ar^{40}$	Ave. $Ar^{40*}$ , ppm.
.03158	.829	.03131
.03103	.776	

#### Potassium Analyses:

% K	Ave. %K	$K^{40}$ , ppm
.923	.887	1.082
.840		
.884		
.901		

#### Constants Used:

$\lambda_{\beta} = 4.72 \times 10^{-10}/\text{year}$

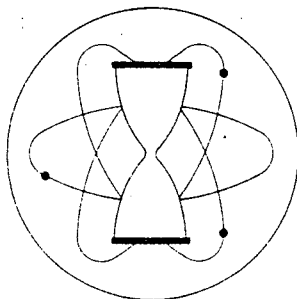
$\lambda_e = 0.585 \times 10^{-10}/\text{year}$

$K^{40}/K = 1.22 \times 10^{-4} \text{ g./g.}$

$$AGE = \frac{1}{\lambda_e + \lambda_{\beta}} \ln \left[ \frac{\lambda_{\beta} + \lambda_e}{\lambda_e} \times \frac{Ar^{40*}}{K^{40}} + 1 \right]$$

Note:  $Ar^{40*}$  refers to radiogenic  $Ar^{40}$ .

M.Y. refers to millions of years.



# KRUEGER ENTERPRISES, INC.

## GEOCHRON LABORATORIES DIVISION

24 BLACKSTONE STREET • CAMBRIDGE, MA. 02139 • (617)-876-3691

### POTASSIUM-ARGON AGE DETERMINATION

### REPORT OF ANALYTICAL WORK

Our Sample No. P-3709

Date Received: 18 October 1976

Your Reference: SL-PLd

Date Reported: 9 December 1976

Submitted by: Scott Laird  
Dames & Moore  
6 Commerce Drive  
Cranford, New Jersey 07016

P.O. NJ 3377  
Job No. 0874-062

Sample Description & Locality: Diabase sample (SL-PLd), Oakland, New Jersey.

Material Analyzed: Pyroxene concentrate, -100/+200 mesh. Estimated composition: Pyroxene, 95+%; Opaques and other ferromagnesian minerals, less than 5%.

$Ar^{40*}/K^{40} = .02781$

AGE =  $424 \pm 22$  M.Y.

#### Argon Analyses:

$Ar^{40*}$ , ppm.	$Ar^{40*}/\text{Total } Ar^{40}$	Ave. $Ar^{40*}$ , ppm.
.01185	.651	.01205
.01224	.637	

#### Potassium Analyses:

% K	Ave. %K	$K^{40}$ , ppm
.354	.355	.433
.356		

#### Constants Used:

$\lambda_{\beta} = 4.72 \times 10^{-10}$  / year

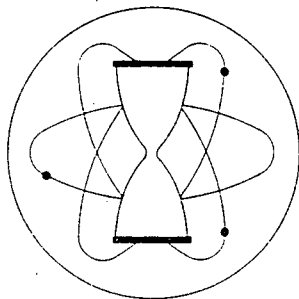
$\lambda_e = 0.585 \times 10^{-10}$  / year

$K^{40}/K = 1.22 \times 10^{-4}$  g./g.

$$AGE = \frac{1}{\lambda_e + \lambda_{\beta}} \ln \left[ \frac{\lambda_{\beta} + \lambda_e}{\lambda_e} \times \frac{Ar^{40*}}{K^{40}} + 1 \right]$$

Note:  $Ar^{40*}$  refers to radiogenic  $Ar^{40}$ .

M.Y. refers to millions of years.



# KRUEGER ENTERPRISES, INC.

## GEOCHRON LABORATORIES DIVISION

24 BLACKSTONE STREET • CAMBRIDGE, MA. 02139 • (617)-876-3691

### POTASSIUM-ARGON AGE DETERMINATION

### REPORT OF ANALYTICAL WORK

Our Sample No. F-3709

Date Received: 18 October 1976

Your Reference: SL-PLd

Date Reported: 9 December 1976

Submitted by: Scott Laird  
Dames & Moore  
6 Commerce Drive  
Cranford, New Jersey 07016

P.O. NJ 3377

Job No. 0874-062

Sample Description & Locality: Diabase sample (SL-PLd), Oakland, New Jersey.

Material Analyzed: Plagioclase concentrate, -100/+200 mesh. Estimated composition: Plagioclase feldspar, 98%; Attached ferromagnesian minerals and opaques, 2%.

$Ar^{40*}/K^{40} = .03034$

AGE =  $458 \pm 17$  M.Y.

#### Argon Analyses:

$Ar^{40*}$ , ppm.	$Ar^{40*}/Total\ Ar^{40}$	Ave. $Ar^{40*}$ , ppm.
.06618	.728	.06699
.06780	.718	

#### Potassium Analyses:

% K	Ave. %K	$K^{40}$ , ppm
1.808	1.809	2.207
1.819		
1.802		

#### Constants Used:

$\lambda_{\beta} = 4.72 \times 10^{-10}/\text{year}$

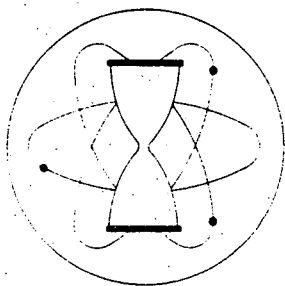
$\lambda_e = 0.585 \times 10^{-10}/\text{year}$

$K^{40}/K = 1.22 \times 10^{-4} \text{ g./g.}$

$$AGE = \frac{1}{\lambda_e + \lambda_{\beta}} \ln \left[ \frac{\lambda_{\beta} + \lambda_e}{\lambda_e} \times \frac{Ar^{40*}}{K^{40}} + 1 \right]$$

Note:  $Ar^{40*}$  refers to radiogenic  $Ar^{40}$ .

M.Y. refers to millions of years.



# KRUEGER ENTERPRISES, INC.

## GEOCHRON LABORATORIES DIVISION

24 BLACKSTONE STREET • CAMBRIDGE, MA. 02139 • (617) 876-3691

### POTASSIUM-ARGON AGE DETERMINATION

### REPORT OF ANALYTICAL WORK

Our Sample No. Z-3672

Date Received: 24 September 1976

Your Reference: FS-15

Date Reported: 20 October 1976

Submitted by: Frank Schmitt  
Dames & Moore  
6 Commerce Drive  
Cranford, New Jersey 07016

Job No. 0874-062  
P.O. No. NJ 3377

Sample Description & Locality: Stilbite sample, FS-15, hand picked.

Material Analyzed: Coarse bladed tan stilbite, hand crushed to -40 mesh to insure homogeneity, otherwise analyzed as received.

$\text{Ar}^{40*}/\text{K}^{40} = .000487$

AGE =  $8.3 \pm 1.7$  M.Y.

#### Argon Analyses:

$\text{Ar}^{40*}$ , ppm.

$\text{Ar}^{40*}/\text{Total Ar}^{40}$

Ave.  $\text{Ar}^{40*}$ , ppm.

.000364

.049

.000453

.000541

.054

#### Potassium Analyses:

% K

Ave. %K

$\text{K}^{40}$ , ppm

.758

.761

.929

.765

#### Constants Used:

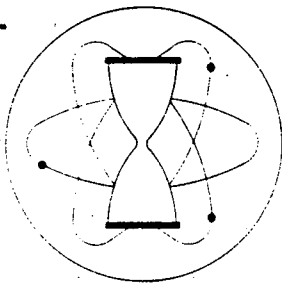
$\lambda_{\beta} = 4.72 \times 10^{-10} / \text{year}$

$\lambda_e = 0.585 \times 10^{-10} / \text{year}$

$\text{K}^{40}/\text{K} = 1.22 \times 10^{-4} \text{ g./g.}$

$$\text{AGE} = \frac{1}{\lambda_e + \lambda_{\beta}} \ln \left[ \frac{\lambda_{\beta} + \lambda_e}{\lambda_e} \times \frac{\text{Ar}^{40*}}{\text{K}^{40}} + 1 \right]$$

Note:  $\text{Ar}^{40*}$  refers to radiogenic  $\text{Ar}^{40}$ .  
M.Y. refers to millions of years.



# KRUEGER ENTERPRISES, INC.

## GEOCHRON LABORATORIES DIVISION

24 BLACKSTONE STREET • CAMBRIDGE, MA. 02139 • (617) - 876-3691

### POTASSIUM-ARGON AGE DETERMINATION

### REPORT OF ANALYTICAL WORK

Our Sample No. Z-3617

Date Received: 4 August 1976

Your Reference: #1 H0 1-1

Date Reported: 16 September 1976

Submitted by: Frank Schmitt  
Dames & Moore  
6 Commerce Drive  
Cranford, New Jersey 07016

Job #0874-062  
P.O. #NJ 3377

Sample Description & Locality: Vein material with a low temperature calcite-zeolite type mineral assemblage, from vein in diabase. Rockland Lake. Hand picked stilbite fragments.

Material Analyzed: Stilbite concentrate, -60/+100 mesh, prepared by heavy liquid separation and magnetic purification. Estimated composition: Stilbite, clean tan colored cleavages, 98%; Others, 2%.

$Ar^{40*}/K^{40} = .000123$

AGE =  $2.1 \pm 0.5$  M.Y.

#### Argon Analyses:

$Ar^{40*}$ , ppm.	$Ar^{40*}/\text{Total } Ar^{40}$	Ave. $Ar^{40*}$ , ppm.
.000043	.003	.000041
.000038	.005	

#### Potassium Analyses:

% K	Ave. %K	$K^{40}$ , ppm
.275	.270	.330
.266		

#### Constants Used:

$\lambda_{\beta} = 4.72 \times 10^{-10} / \text{year}$

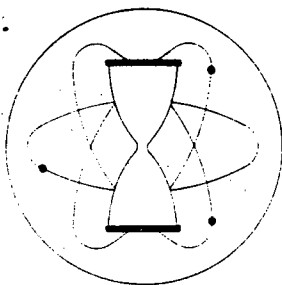
$\lambda_e = 0.585 \times 10^{-10} / \text{year}$

$K^{40}/K = 1.22 \times 10^{-4} \text{ g./g.}$

$$AGE = \frac{1}{\lambda_e + \lambda_{\beta}} \ln \left[ \frac{\lambda_{\beta} + \lambda_e}{\lambda_e} \times \frac{Ar^{40*}}{K^{40}} + 1 \right]$$

Note:  $Ar^{40*}$  refers to radiogenic  $Ar^{40}$ .

M.Y. refers to millions of years.



# KRUEGER ENTERPRISES, INC.

## GEOCHRON LABORATORIES DIVISION

24 BLACKSTONE STREET • CAMBRIDGE, MA. 02139 • (617)-876-3691

### POTASSIUM-ARGON AGE DETERMINATION

### REPORT OF ANALYTICAL WORK

Our Sample No. Z-3618

Date Received: 4 August 1976

Your Reference: #2 H0 2-2

Date Reported: 16 September 1976

Submitted by: Frank Schmitt  
Dames & Moore  
6 Commerce Drive  
Cranford, New Jersey 07016

Job #0874-062  
P.O. #NJ 3377

Sample Description & Locality: Vein material with a low temperature calcite-zeolite type mineral assemblage, from vein in diabase. Pomona.  
Hand picked stilbite and calcite fragments.

Material Analyzed: Stilbite concentrate, -60/+100 mesh, prepared by heavy liquid separation and magnetic purification. Estimated composition: Stilbite, clean tan colored cleavages, 98%; Others, including calcite, 2%.

$Ar^{40*}/K^{40} = .003775$

AGE = 63  $\pm$  5 M.Y.

#### Argon Analyses:

$Ar^{40*}$ , ppm.	$Ar^{40*}/\text{Total } Ar^{40}$	Ave. $Ar^{40*}$ , ppm.
.001845	.137	.002128
.002411	.192	

#### Potassium Analyses:

% K	Ave. %K	$K^{40}$ , ppm
.471	.462	.563
.453		

#### Constants Used:

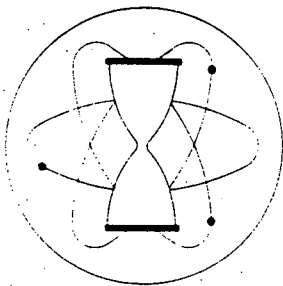
$\lambda_{\beta} = 4.72 \times 10^{-10} / \text{year}$

$\lambda_e = 0.585 \times 10^{-10} / \text{year}$

$K^{40}/K = 1.22 \times 10^{-4} \text{ g./g.}$

$$\text{AGE} = \frac{1}{\lambda_e + \lambda_{\beta}} \ln \left[ \frac{\lambda_{\beta} + \lambda_e}{\lambda_e} \times \frac{Ar^{40*}}{K^{40}} + 1 \right]$$

Note:  $Ar^{40*}$  refers to radiogenic  $Ar^{40}$ .  
M.Y. refers to millions of years.



# KRUEGER ENTERPRISES, INC.

## GEOCHRON LABORATORIES DIVISION

24 BLACKSTONE STREET • CAMBRIDGE, MA. 02139 • (617) 876-3691

### PRIORITY BASIS POTASSIUM-ARGON AGE DETERMINATION

### REPORT OF ANALYTICAL WORK

Our Sample No. X-3504

Date Received: 3 March 1976 @ 9:12 EST

Your Reference: G.A. - 17.3

Date Reported: 4 March 1976 @ 17:50 EST

Submitted by: Frank Schmitt  
Dames & Moore  
6 Commerce Drive  
Cranford, NJ 07016

By Telegram  
Elapsed time: 32:38 hours  
P.O. 3377  
Job No. 0874-062-10

Sample Description & Locality: Fragments of zeolite vein material, sample G.A.-17.3

Material Analyzed: The material was handpicked to remove most of the calcite present. The remaining zeolite fragments (probably a salmon-colored stilbite) were hand crushed to -60 mesh to homogenize the material and was analyzed without further treatment of any kind.

$Ar^{40*}/K^{40} = 0.004375$  APPARENT AGE =  $73.3 \pm 5.1$  M.Y.

#### Argon Analyses:

$Ar^{40*}$ , ppm.	$Ar^{40*}/\text{Total } Ar^{40}$	Ave. $Ar^{40*}$ , ppm.
.001266	.079	.001367
.001467	.062	

#### Potassium Analyses:

% K	Ave. %K	$K^{40}$ , ppm
.254	.256	.312
.258		

#### Constants Used:

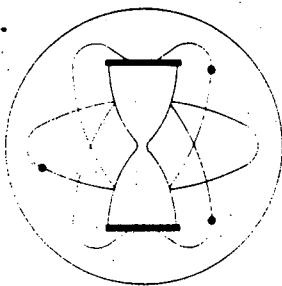
$$\lambda_{\beta} = 4.72 \times 10^{-10} / \text{year}$$

$$\lambda_e = 0.585 \times 10^{-10} / \text{year}$$

$$K^{40}/K = 1.22 \times 10^{-4} \text{ g./g.}$$

$$\text{AGE} = \frac{1}{\lambda_e + \lambda_{\beta}} \ln \left[ \frac{\lambda_{\beta} + \lambda_e}{\lambda_e} \times \frac{Ar^{40*}}{K^{40}} + 1 \right]$$

Note:  $Ar^{40*}$  refers to radiogenic  $Ar^{40}$ .  
M.Y. refers to millions of years.



# KRUEGER ENTERPRISES, INC.

## GEOCHRON LABORATORIES DIVISION

24 BLACKSTONE STREET • CAMBRIDGE, MA. 02139 • (617)-876-3691

### POTASSIUM-ARGON AGE DETERMINATION

### REPORT OF ANALYTICAL WORK

Our Sample No. Z-3619

Date Received: 4 August 1976

Your Reference: #3 GA 20.2

Date Reported: 16 September 1976

Submitted by: Frank Schmitt  
Dames & Moore  
6 Commerce Drive  
Cranford, New Jersey 07016

Job #0874-062  
P.O. #NJ 3377

Sample Description & Locality: Vein material with a low temperature calcite-zeolite type mineral assemblage, from vein in diabase. Union Hill, Suffern.

Material Analyzed: Analcite concentrate, -60/+100 mesh, prepared by heavy liquid separation and magnetic purification. Estimated composition: Analcite (isotropic grains), 95%; Others, 5%

$Ar^{40}*/K^{40} =$  less than .00007

AGE = less than 1.2 M.Y.

#### Argon Analyses:

$Ar^{40}*$ , ppm.	$Ar^{40}*/\text{Total } Ar^{40}$	Ave. $Ar^{40}*$ , ppm.
less than .00001	.000	less than .00001
less than .00001	.000	

#### Potassium Analyses:

% K	Ave. %K	$K^{40}$ , ppm
.1100	.1142	.1393
.1185		

#### Constants Used:

$\lambda_{\beta} = 4.72 \times 10^{-10}$  / year

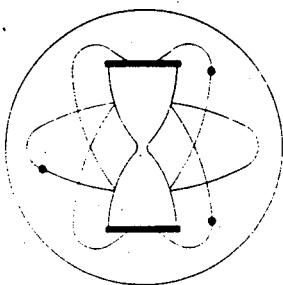
$\lambda_e = 0.585 \times 10^{-10}$  / year

$K^{40}/K = 1.22 \times 10^{-4}$  g./g.

$$AGE = \frac{1}{\lambda_e + \lambda_{\beta}} \ln \left[ \frac{\lambda_{\beta} + \lambda_e}{\lambda_e} \times \frac{Ar^{40}*}{K^{40}} + 1 \right]$$

Note:  $Ar^{40}*$  refers to radiogenic  $Ar^{40}$ .

M.Y. refers to millions of years.



# KRUEGER ENTERPRISES, INC.

## GEOCHRON LABORATORIES DIVISION

24 BLACKSTONE STREET • CAMBRIDGE, MA. 02139 • (617)-876-3691

### POTASSIUM-ARGON AGE DETERMINATION

### REPORT OF ANALYTICAL WORK

Our Sample No. Z-3623

Date Received: 4 August 1976

Your Reference: #7 MW-112-1

Date Reported: 16 September 1976

Submitted by: Frank Schmitt  
Dames & Moore  
6 Commerce Drive  
Cranford, New Jersey 07016

Job #0874-062  
P.O. #NJ 3377

Sample Description & Locality: Vein material with a low temperature calcite-zeolite type mineral assemblage, from vein in diabase. Verdrige Hook.

Material Analyzed: Apophyllite concentrate, -60/+100 mesh, prepared by heavy liquid separation and magnetic purification. Estimated composition: Apophyllite, clear cleavage grains, 95%; Other clouded grains, probably mostly apophyllite, 5%.

$Ar^{40*}/K^{40} = .005536$

AGE = 92  $\pm$  5 M.Y.

#### Argon Analyses:

$Ar^{40*}$ , ppm.	$Ar^{40*}/Total\ Ar^{40}$	Ave. $Ar^{40*}$ , ppm.
.02875	.570	.02648
.02421	.726	

#### Potassium Analyses:

% K	Ave. %K	$K^{40}$ , ppm
3.912	3.921	4.783
3.930		

#### Constants Used:

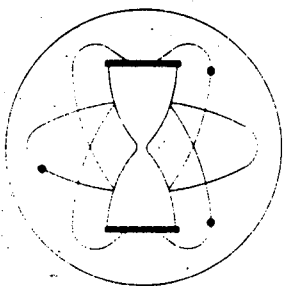
$\lambda_{\beta} = 4.72 \times 10^{-10}/\text{year}$

$\lambda_e = 0.585 \times 10^{-10}/\text{year}$

$K^{40}/K = 1.22 \times 10^{-4} \text{ g./g.}$

$$AGE = \frac{1}{\lambda_e + \lambda_{\beta}} \ln \left[ \frac{\lambda_{\beta} + \lambda_e}{\lambda_e} \times \frac{Ar^{40*}}{K^{40}} + 1 \right]$$

Note:  $Ar^{40*}$  refers to radiogenic  $Ar^{40}$ .  
M.Y. refers to millions of years.



# KRUEGER ENTERPRISES, INC.

## GEOCHRON LABORATORIES DIVISION

24 BLACKSTONE STREET • CAMBRIDGE, MA. 02139 • (617) - 876-3691

### POTASSIUM-ARGON AGE DETERMINATION

### REPORT OF ANALYTICAL WORK

Our Sample No. F-3563

Date Received: 22 June 1976

Your Reference: JT-111

Date Reported: 9 July 1976

Submitted by: Frank Schmitt  
Dames & Moore  
6 Commerce Drive  
Cranford, New Jersey 07016

J.O. 0874-061-10 P.O. NJ 3377

Sample Description & Locality: Bullowa granite, sample JT-111.

Material Analyzed: K-feldspar concentrate. -80/+200 mesh. Estimated composition:  
Feldspar (probably a mixed phase K-spar), 90%; Quartz, plagioclase & others, 10%.

$Ar^{40*}/K^{40} = .02837$

AGE =  $432 \pm 15$  M.Y.

#### Argon Analyses:

$Ar^{40*}$ , ppm.	$Ar^{40*}/\text{Total } Ar^{40}$	Ave. $Ar^{40*}$ , ppm.
.1679	.851	.2410
.1649	.845	

#### Potassium Analyses:

% K	Ave. %K	$K^{40}$ , ppm
7.048	6.964	8.496
6.926		
6.918		

#### Constants Used:

$\lambda_{\beta} = 4.72 \times 10^{-10}/\text{year}$

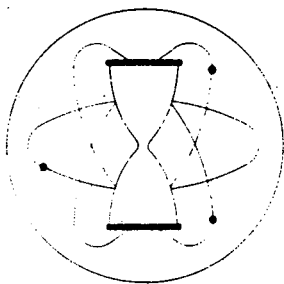
$\lambda_e = 0.585 \times 10^{-10}/\text{year}$

$K^{40}/K = 1.22 \times 10^{-4} \text{ g./g.}$

$$AGE = \frac{1}{\lambda_e + \lambda_{\beta}} \ln \left[ \frac{\lambda_{\beta} + \lambda_e}{\lambda_e} \times \frac{Ar^{40*}}{K^{40}} + 1 \right]$$

Note:  $Ar^{40*}$  refers to radiogenic  $Ar^{40}$ .

M.Y. refers to millions of years.



# KRUEGER ENTERPRISES, INC.

## GEOCHRON LABORATORIES DIVISION

24 BLACKSTONE STREET • CAMBRIDGE, MA. 02139 • (617)-876-3691

### POTASSIUM-ARGON AGE DETERMINATION

### REPORT OF ANALYTICAL WORK

Our Sample No. B-3563

Date Received: 22 June 1976

Your Reference: JT-111

Date Reported: 9 July 1976

Submitted by: Frank Schmitt  
Dames & Moore  
6 Commerce Drive  
Cranford, New Jersey 07016

J.O. 0874-061-10 P.O. NJ 3377

Sample Description & Locality: Bullowa granite, sample JT-111.

Material Analyzed: Biotite concentrate. -60/ +100 mesh Estimated composition:  
Biotite, greater than 95%; Quartz, feldspars, etc., less than 5%.

$Ar^{40*}/K^{40} = .02351$

AGE =  $364 \pm 13$  M.Y.

#### Argon Analyses:

Ar <sup>40*</sup> , ppm.	Ar <sup>40*</sup> / Total Ar <sup>40</sup>	Ave. Ar <sup>40*</sup> , ppm.
.1494	.816	.1493
.1491	.787	

#### Potassium Analyses:

% K	Ave. %K	K <sup>40</sup> , ppm
5.169	5.204	6.348
5.239		

#### Constants Used:

$$\lambda_{\beta} = 4.72 \times 10^{-10} / \text{year}$$

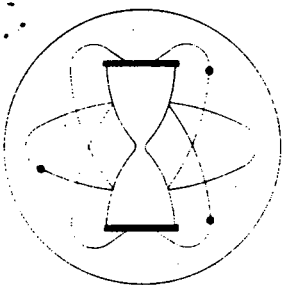
$$\lambda_e = 0.585 \times 10^{-10} / \text{year}$$

$$K^{40}/K = 1.22 \times 10^{-4} \text{ g./g.}$$

$$\text{AGE} = \frac{1}{\lambda_e + \lambda_{\beta}} \ln \left[ \frac{\lambda_{\beta} + \lambda_e}{\lambda_e} \times \frac{Ar^{40*}}{K^{40}} + 1 \right]$$

Note: Ar<sup>40\*</sup> refers to radiogenic Ar<sup>40</sup>.

M.Y. refers to millions of years.



# KRUEGER ENTERPRISES, INC.

## GEOCHRON LABORATORIES DIVISION

24 BLACKSTONE STREET • CAMBRIDGE, MA. 02139 • (617)-876-3691

### POTASSIUM-ARGON AGE DETERMINATION

### REPORT OF ANALYTICAL WORK

Our Sample No. B-3573

Date Received: 22 June 1976

Your Reference: JT-121

Date Reported: 30 June 1976

Submitted by: Frank Schmitt  
Dames & Moore  
6 Commerce Drive  
Cranford, New Jersey 07016

J.O. 0874-061-10 P.O. NJ 3377

Sample Description & Locality: Croton microcline granite, sample JT-121.

Material Analyzed: Biotite concentrate, -40/+100 mesh. Estimated composition:  
Biotite, 95%; Muscovite, 4%; Others, 1%.

$Ar^{40*}/K^{40} = .02046$

AGE =  $321 \pm 11$  M.Y.

#### Argon Analyses:

$Ar^{40*}$ , ppm.	$Ar^{40*}/\text{Total } Ar^{40}$	Ave. $Ar^{40*}$ , ppm.
.1372	.742	.1382
.1391	.805	

#### Potassium Analyses:

% K	Ave. %K	$K^{40}$ , ppm
5.729	5.535	6.753
5.322		
5.501		
5.590		

#### Constants Used:

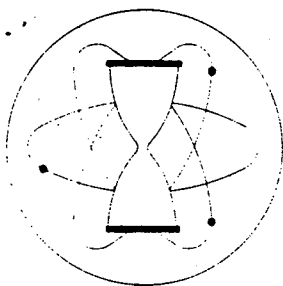
$\lambda_{\beta} = 4.72 \times 10^{-10}/\text{year}$

$\lambda_e = 0.585 \times 10^{-10}/\text{year}$

$K^{40}/K = 1.22 \times 10^{-4} \text{ g./g.}$

$$\text{AGE} = \frac{1}{\lambda_e + \lambda_{\beta}} \ln \left[ \frac{\lambda_{\beta} + \lambda_e}{\lambda_e} \times \frac{Ar^{40*}}{K^{40}} + 1 \right]$$

Note:  $Ar^{40*}$  refers to radiogenic  $Ar^{40}$ .  
M.Y. refers to millions of years.



# KRUEGER ENTERPRISES, INC.

## GEOCHRON LABORATORIES DIVISION

24 BLACKSTONE STREET • CAMBRIDGE, MA. 02139 • (617) 876-3691

### POTASSIUM-ARGON AGE DETERMINATION

### REPORT OF ANALYTICAL WORK

Our Sample No. F-3573

Date Received: 22 June 1976

Your Reference: JT-121

Date Reported: 30 June 1976

Submitted by: Frank Schmitt  
Dames & Moore  
6 Commerce Drive  
Cranford, New Jersey 07016

J.O. 0874-061-10 P.O. NJ 3377

Sample Description & Locality: Croton microcline granite, sample JT-121.

Material Analyzed: Microcline concentrate. -60/+100 mesh.

Estimated composition: Microcline, greater than 90%; Plagioclase and/or quartz, less than 10%.

$Ar^{40*}/K^{40} = .01636$

AGE =  $261 \pm 9$  M.Y.

#### Argon Analyses:

$Ar^{40*}$ , ppm.	$Ar^{40*}/Total\ Ar^{40}$	Ave. $Ar^{40*}$ , ppm.
.2313	.840	.2448
.2583	.847	

#### Potassium Analyses:

% K	Ave. %K	$K^{40}$ , ppm
12.153	12.268	14.966
12.383		

#### Constants Used:

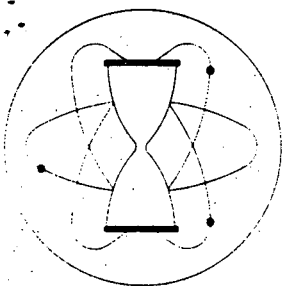
$\lambda_{\beta} = 4.72 \times 10^{-10}/\text{year}$

$\lambda_e = 0.585 \times 10^{-10}/\text{year}$

$K^{40}/K = 1.22 \times 10^{-4} \text{ g./g.}$

$$AGE = \frac{1}{\lambda_e + \lambda_{\beta}} \ln \left[ \frac{\lambda_{\beta} + \lambda_e}{\lambda_e} \times \frac{Ar^{40*}}{K^{40}} + 1 \right]$$

Note:  $Ar^{40*}$  refers to radiogenic  $Ar^{40}$ .  
M.Y. refers to millions of years.



# KRUEGER ENTERPRISES, INC.

## GEOCHRON LABORATORIES DIVISION

24 BLACKSTONE STREET • CAMBRIDGE, MA. 02139 • (617) 876-3691

### POTASSIUM-ARGON AGE DETERMINATION

### REPORT OF ANALYTICAL WORK

Our Sample No. M-3573

Date Received: 22 June 1976

Your Reference: JT-121

Date Reported: 30 June 1976

Submitted by: Frank Schmitt  
Dames & Moore  
6 Commerce Drive  
Cranford, New Jersey 07016

J.O. 0874-061-10 P.O. NJ 3377

Sample Description & Locality: Croton microcline granite, sample JT-121,

Material Analyzed: Muscovite concentrate. -40/+100 mesh. Estimated purity exceeds 98%.

$\text{Ar}^{40*}/\text{K}^{40} = .02209$

AGE =  $344 \pm 12$  M.Y.

#### Argon Analyses:

$\text{Ar}^{40*}$ , ppm.	$\text{Ar}^{40*}/\text{Total Ar}^{40}$	Ave. $\text{Ar}^{40*}$ , ppm.
.2326	.798	.2347
.2367	.873	

#### Potassium Analyses:

% K	Ave. %K	$\text{K}^{40}$ , ppm
8.724	8.708	10.623
8.692		

#### Constants Used:

$\lambda_{\beta} = 4.72 \times 10^{-10}/\text{year}$

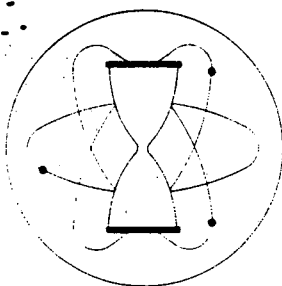
$\lambda_e = 0.585 \times 10^{-10}/\text{year}$

$\text{K}^{40}/\text{K} = 1.22 \times 10^{-4} \text{ g./g.}$

$$\text{AGE} = \frac{1}{\lambda_e + \lambda_{\beta}} \ln \left[ \frac{\lambda_{\beta} + \lambda_e}{\lambda_e} \times \frac{\text{Ar}^{40*}}{\text{K}^{40}} + 1 \right]$$

Note:  $\text{Ar}^{40*}$  refers to radiogenic  $\text{Ar}^{40}$ .

M.Y. refers to millions of years.



# KRUEGER ENTERPRISES, INC.

## GEOCHRON LABORATORIES DIVISION

24 BLACKSTONE STREET • CAMBRIDGE, MA. 02139 • (617) - 876-3691

### POTASSIUM-ARGON AGE DETERMINATION

### REPORT OF ANALYTICAL WORK

Our Sample No. A-3574

Date Received: 22 June 1976

Your Reference: JT-122

Date Reported: 30 June 1976

Submitted by: Frank Schmitt  
Dames & Moore  
6 Commerce Drive  
Cranford, New Jersey 07016

J.O. 0874-061-10 P.O. NJ 3377

Sample Description & Locality: Croton gabbro, sample JT-122.

Material Analyzed: Hornblende concentrate, -60/+100 mesh. Estimated composition:  
Greenish black hornblende, 95%; Biotite, 2%; Others, 3%.

$Ar^{40*}/K^{40} = .02368$

AGE =  $367 \pm 19$  M.Y.

#### Argon Analyses:

$Ar^{40*}$ , ppm.	$Ar^{40*}/Total\ Ar^{40}$	Ave. $Ar^{40*}$ , ppm.
.01014	.675	.01001
.009880	.613	

#### Potassium Analyses:

% K	Ave. %K	$K^{40}$ , ppm
.349	.346	.422
.344		

#### Constants Used:

$\lambda_{\beta} = 4.72 \times 10^{-10}/\text{year}$

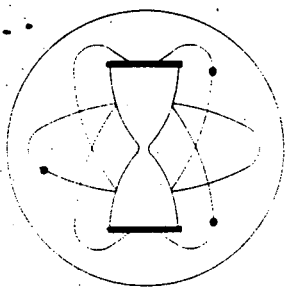
$\lambda_e = 0.585 \times 10^{-10}/\text{year}$

$K^{40}/K = 1.22 \times 10^{-4} \text{ g./g.}$

$$AGE = \frac{1}{\lambda_e + \lambda_{\beta}} \ln \left[ \frac{\lambda_{\beta} + \lambda_e}{\lambda_e} \times \frac{Ar^{40*}}{K^{40}} + 1 \right]$$

Note:  $Ar^{40*}$  refers to radiogenic  $Ar^{40}$ .

M.Y. refers to millions of years.



# KRUEGER ENTERPRISES, INC.

## GEOCHRON LABORATORIES DIVISION

24 BLACKSTONE STREET • CAMBRIDGE, MA. 02139 • (617) - 876-3691

### POTASSIUM-ARGON AGE DETERMINATION

### REPORT OF ANALYTICAL WORK

Our Sample No. B-3574

Date Received: 22 June 1976

Your Reference: JT-122

Date Reported: 30 June 1976

Submitted by: Frank Schmitt  
Dames & Moore  
6 Commerce Drive  
Cranford, New Jersey 07016

J.O. 0874-061-10 P.O. NJ 3377

Sample Description & Locality: Croton gabbro, sample JT-122.

Material Analyzed: Biotite concentrate. -40/+100 mesh.

Estimated composition: Biotite, greater than 95%; Hornblende, less than 5%;  
All others, traces only.

$Ar^{40*}/K^{40} = .02142$

AGE =  $335 \pm 12$  M.Y.

#### Argon Analyses:

$Ar^{40*}$ , ppm.	$Ar^{40*}/\text{Total } Ar^{40}$	Ave. $Ar^{40*}$ , ppm.
.1580	.793	.1589
.1598	.868	

#### Potassium Analyses:

% K	Ave. %K	$K^{40}$ , ppm
6.145	6.079	7.416
5.672		
6.023		
6.477		

#### Constants Used:

$\lambda_{\beta} = 4.72 \times 10^{-10} / \text{year}$

$\lambda_e = 0.585 \times 10^{-10} / \text{year}$

$K^{40}/K = 1.22 \times 10^{-4} \text{ g./g.}$

$$\text{AGE} = \frac{1}{\lambda_e + \lambda_{\beta}} \ln \left[ \frac{\lambda_{\beta} + \lambda_e}{\lambda_e} \times \frac{Ar^{40*}}{K^{40}} + 1 \right]$$

Note:  $Ar^{40*}$  refers to radiogenic  $Ar^{40}$ .

M.Y. refers to millions of years.

APPENDIX F  
INVESTIGATION OF  
POST-MESOZOIC FEATURES

## APPENDIX F

### INVESTIGATION OF POST-MESOZOIC FEATURES

#### F1.0 INTRODUCTION

In February, 1976, the initial geomorphology investigations in the immediate vicinity of Consolidated Edison's Indian Point site were expanded to include a large region along the Ramapo Fault. The purpose of the present investigation was to examine unconsolidated deposits and geomorphic features to determine if they display any evidence of recent surface displacement in the vicinity of the Ramapo Fault. To achieve this purpose, the following studies were completed:

- 1) geomorphic features and Pleistocene deposits were delineated from air photos and ground checked in the field;
- 2) the remnants of proglacial Lake Hudson shoreline were mapped and examined for evidence of offset;
- 3) suspect structures in bedrock and unconsolidated deposits were studied to evaluate their origin;
- 4) the rock bench flanking the Hudson Gorge was investigated; and
- 5) trenches were dug at selected locations.

Preservation and exposure of sediments deposited in the Hudson River Valley and its tributaries are poor. The occurrences of the most extensive deposits unfortunately coincide with the most populated areas. Man-made structures and

vegetation cover large portions of the region. Much more detrimental to a comprehensive study of the deposits, however, is the fact that the most extensive exposures have been removed by both small and large-scale borrow pit operations. Sand and gravel deposits have been used as fill material and concrete aggregate. Extensive varved clay deposits, as much as 200 feet in thickness, have been quarried for the making of bricks. Clay was quarried extensively near Haverstraw, whereas smaller pits are located near Peekskill, Croton Point, and Crugers. Sand and gravel quarries are widespread, but the largest volume of material appears to have been removed from Jones Point, Roa Hook, Sprout Brook, Peekskill Hollow Brook, and the area between Indian Point and Verplanck. Quarrying in the area has continued for many years, as is evident from comments by C.E. Peet in 1904 concerning his visit to clay pits at Haverstraw, and his inability to ascertain how much of the flat parade ground surface at State Camp (now Camp Smith), near Peekskill, was a natural bench of sand and gravel and to what extent it had been regraded by man.

## F2.0 SYNOPSIS OF LATE GLACIAL AND POST- GLACIAL HISTORY OF THE REGION

Basic to any discussion of the geomorphology of the study region is an understanding of the glacial history of the area, especially the retreat of the Late Wisconsinan ice sheet up the valley of the Hudson River and its tributaries. To date, no unconsolidated deposits or soils older than Late Wisconsinan have been identified in the area. Older deposits may be present in valleys situated transverse to the principal direction of glacial flow, and in valleys deep enough to have escaped intense glacial scour. In the region around Indian Point, the predominantly northeast and northwest structural grain has resulted in the development of valleys which acted as primary avenues for advance and retreat of glacial ice through the region. The valleys were occupied first during glacial advance prior to overtopping of the surrounding elevated areas and were the last to become ice-free upon retreat of the ice sheet. They would, therefore, have been subjected to the greatest amount of erosion and deposition by glacially-related processes.

Absolute dating of the events related to the advance and retreat of the Late Wisconsinan ice sheet in the Peekskill area is lacking; however, dates obtained elsewhere serve to bracket the ages of these events. Using pollen stratigraphy, Sirkin (1967) inferred that the Late Wisconsinan ice sheet began to retreat from the Harbor Hill Moraine on Long Island about 17,000 years b.p. (before present). Similar work by Connally

and Sirkin (1970) indicated that the ice had probably receded from the southern and middle portions of the Wallkill Valley (to a point approximately 25 miles northwest of Peekskill) prior to 15,000 years b.p., and that the Wallkill Moraine was formed about 15,000 years b.p., before the ice completely receded from the Wallkill Valley near Kingston, New York. Thus, any recessional deposits associated with the Late Wisconsinan glaciation in the study area must have been formed between 17,000 years b.p. and 15,000 years b.p., probably closer to the latter date. Glaciolacustrine and glaciofluvial deposits should be slightly younger, since they would have been deposited after retreat of the ice from the valley.

Advance of the glacial ice was initially two-pronged in the Haverstraw area, one tongue of ice extended southward around the west side of the South Mountain ridge (Salisbury, 1902; Woodworth, 1904) near Mount Ivy, and into the Hackensack Meadowlands to the south. A second tongue of ice extended down the Hudson Valley east of the Palisades. During glacial maximum, the uplands were overtopped by the ice. As it receded from the terminal moraine, the ice first dropped below the level of the uplands and the lowlands topography again exerted a directional control. The ice retreated first from the west side of the South Mountain ridge in the vicinity of Mount Ivy. It remained in this position for a time, building a morainal complex which extends from the south side of Rider Hill and Colla-berg Mountain south and southeastward to South Mountain, and

eastward along the base of the mountain to Short Clove. Morain-al remnants on the west side of Croton Point east of the Hudson River may be correlative with this recessional moraine, as suggested by earlier writers (Woodworth, 1905; Peet, 1904; Markl, 1971). Smaller morain-al remnants, probably representing a later local readvance, occur north and south of Minisceongo Creek along U.S. Route 9W in Haverstraw, West Haverstraw, and northward to the vicinity of the State Rehabilitation Hospital.

The lowland areas around Haverstraw, south of Pompton Plains and in the Hackensack meadowlands contain a great diversity of unconsolidated sediments. The stratigraphic relationships of these deposits were not completely unraveled in the past when exposures were better, the deposits well preserved, and the area much more sparsely settled. Description by Peet (1904), Woodworth (1905), and Reeds (1927), together with field observations made during the present study, indicate that the study area contains, in addition to till, glacial outwash deposits, ice-contact stratified sands and gravels, deltaic deposits laid down marginal to the ice front, kame deposits, and proglacial lake deposits. The proglacial lake deposits occur 1) within the arc of the Watchung Mountains (Lake Passaic), 2) west of the Palisades ridge as far north as South Mountain (Lake Hackensack) and, 3) in the Hudson Valley proper (Lake Hudson). These were observed by earlier workers to overlies till and kame deposits, and to underlie a local readvance till and extensive deltaic deposits such as those laid down by Cedar Pond Creek in

proglacial Lake Hudson. Ice-contact deposits observed by Peet (1904) and Woodworth (1905) suggested to them that these deltaic sediments were deposited marginal to an ice front. When the ice front receded further northward, it appears that a lower lake level was established and that clays, sands and gravels were deposited at lower elevations. The deltaic sediments near Haverstraw, and those occurring at Croton Point and near Peekskill, are thought to have been deposited in proglacial Lake Hudson (Markl, 1971; Reeds, 1927) that extended north at least as far as Peekskill. The lake level was about 100 feet above the present level of the Hudson River. The presence of lower benches toward the streams, generally between 20 and 60 feet in elevation, indicates that deposition also occurred during lower lake stages that resulted from downcutting of an outlet channel downstream, probably at The Narrows.

Draining of Lake Hudson was followed by marine encroachment through The Narrows before 12,000 years b.p. (Newman and others, 1969). Isostatic uplift of the lower Hudson River Valley, coupled with an eustatic rise in sea level, caused some fluctuations in salinity near Peekskill and in distance of marine encroachment up the Hudson Estuary. Maximum extent of mesohaline water and maximum invasion of foraminifers during post-glacial time occurred 6,500 years ago and were coincident with the end of the period of post-glacial transgression of the Atlantic Ocean along the northeast coast of the United States (Weiss, 1974).

### F3.0 GEOMORPHIC FEATURES AND SURFICIAL DEPOSITS

The geomorphic features and surficial deposits were identified from 1:20,000 and 1:24,000 scale aerial photographs in an area along the Ramapo Fault from about 3 miles south of Morristown, N.J. to Highland Falls, N.Y. The units identified are presented in Plate F-1A&B. These units were field checked and compared with previous work done in the area (Dames & Moore, 1975, Appendix D; and Salisbury, 1908).

Most of the area of investigation was directly affected by glaciers during Late Wisconsinan time. The southern extent of the ice in this area was between Morristown and Boonton, New Jersey (Plate F-1A&B). At the time the ice occupied this position, a pro-glacial lake (Lake Passaic) was present south of Morristown. The surficial materials in this area are predominantly lacustrine and glaciofluvial in origin.

In general, the topography northwest of the Ramapo Fault is composed of erosional landforms that were modified by the ice as it moved over the area. Southeast of the fault zone the topography is dominated by depositional-type landforms of glacial or glaciofluvial origin. Although the glacial drift is generally thicker in this area, the underlying bedrock influences the glacial topography, especially in the South Mountain, Campgaw Mountain, and Towakhow Mountain areas.

The geologic units shown on Plate F-1A&B are as follows:

Gravel Pits and Rock Quarries (Qm) - Areas where man has removed significant amounts of gravel and rock were delineated as mappable units and included on the surficial geologic maps.

Alluvium (Qal) - Holocene alluvium is located in stream bottoms and along associated flood plains. Topographically, the alluvium forms a narrow plain confined between slopes or valley walls. Alluvium is typically a detrital material deposited by modern streams and consists of sand, silt, and clay with some stringers of gravel. Alluvium is present along most of the major streams that cross or flow along the Ramapo Fault.

Swamp and Marsh Land (Qsm) - The swamp and marsh lands consist of small irregularly shaped basins with flat to concave bottoms. They represent former lakes that are being filled with alluvium, colluvium and vegetation. The basins generally have high water tables and small ponds may still exist in some basins. Muck soils prevail and peat may be present at depth.

Within the area of investigation, there are three types of swamp and marsh lands, dependent on the origin of the lakes that once existed; 1) low areas that remained after proglacial Lake Passaic drained (e.g., Great Piece Meadows near Pompton Plains, N.J.), 2) Kettle lakes that are being filled (e.g., south of Suffern, N.Y.), and 3) elliptical to elongated rock basins in the Hudson Highlands that were scoured by ice as the glacier moved through the area (e.g., near Thiells, N.Y.).

relatively thick and there are few or no rock outcrops (Qgm) and, 2) areas where till is relatively thin and there are numerous rock outcrops (Qgmt). The latter occurs predominantly on the northwest side of the Ramapo Fault and the former occurs predominantly on the southeast side. Local relief in the areas of thicker till is from 50 to 80 feet, except in those areas where topography is affected by underlying bedrock and the relief is much greater. In areas of relatively thinner till, the topographic relief is controlled by bedrock relief and is generally much greater than in areas of thicker till.

Kame and Kettle Moraine (Qkm) - Kame and kettle moraines are topographically ridged moraines composed of coarse textured till and stratified sand and gravel. The moraine is typified by the occurrence of numerous kames, eskers, and kettles. The kame and kettle moraine in the study area trends southward from Suffern, N.Y., around the south end of Campgaw Mountain, and westward to Oakland, N.J. This moraine may represent a small readvance of the ice or a brief glacial standstill.

Kames and Eskers (Qk) - Topographically, a kame is a conical hill or a cluster of conical hills whereas an esker is a sinuous ridge sometimes bordered on one or both sides by a trough. They are composed of glaciofluvial, stratified sand and gravel. Only those kames and eskers large enough to be considered mappable units are included on the surficial geologic maps. Many smaller, unmapped kames occur in the kame and kettle moraine, terminal moraine, and thick ground moraine areas.

Stratified Drift (Qsd and Qsdt) - The stratified drift map unit includes glaciofluvial outwash and kame terraces, shoreline deposits of pro-glacial Lake Passaic, and glacially related deltaic deposits. Terraces are present in some of the outwash and Lake Passaic shoreline deposits. These terraces are designated as Qsdt on the surficial geologic maps. Stratified drift overlies the Ramapo Fault in the Morristown and Riverdale, N.J. areas. These geomorphic features (outwash plains and Lake Passaic shoreline deposits) do not appear to be interrupted by major fault activity. If major fault movements had occurred, the outwash channels and shoreline deposits should be offset vertically or laterally, depending upon the type of faulting. This type of interruption is not apparent in these geomorphic features.

Bedrock (unglaciaded bd) - The map unit (bd) is used on the surficial geologic maps to designate the unglaciaded bedrock areas south of the terminal moraine (west of Morristown, N.J.).

## F4.0 SELECTED INVESTIGATIONS

### F4.1 Lake Hudson Shoreline

As the Late Wisconsinan glacier receded, pro-glacial Lake Hudson occupied the Hudson Valley within the study area. It was a fresh water lake dammed at the south by the Harbor Hill Moraine at The Narrows between Brooklyn and Staten Island. The highest elevation of the lake was controlled by the elevation of the moraine. Lacustrine silt, fine sand, and clay were deposited in Lake Hudson, as well as coarser sand and gravel in the form of deltas, kame deltas, and outwash from the ablating glacier.

#### F4.1.1 Previous Work

Lake Hudson was named by Reeds (1927) in his study of the lacustrine sediments in the New York City area. He described varved lake sediments in the Haverstraw, New York area, and from deltaic deposits indicated that the Lake Hudson shoreline in the Peekskill area was at approximately 100 foot elevation. Reeds (1927, p. 60) further stated that Lake Hudson lacustrine sediments were not exposed above sea level south of Haverstraw. From shoreline features Reeds calculated that the shorelines of pro-glacial lakes Passaic and Hackensack (southwest of Lake Hudson) had been upwarped to the north at approximately 2.25 feet per mile. He assumed that the Lake Hudson shoreline was similarly upwarped. Reeds (1927) also suggested that these lakes were in existence for about 2500 years as the ice slowly retreated at a rate of about 100 feet per year.

Other workers (Newman and others, 1969; Markl, 1971; and Weiss, 1974) have discussed the Lake Hudson lacustrine sediments, but there have been no detailed studies of the Lake Hudson shorelines.

#### F4.1.2 Evidence of Lake Hudson Shoreline

The Lake Hudson shoreline was identified from topographic maps, air photos, and field investigations. The position of the Lake Hudson shoreline is presented on Plate F-1A, and diagrammatic sections of the three types of evidence used to identify the shoreline are presented on Plate F-2.

Section A, Plate F-2, illustrates both sedimentary and topographic evidence of a former lake level. Here, a nearly flat bench was produced, probably by wave action, in soft glacial or glacially related sediments. This bench is covered with relatively clean medium grained sand that is texturally different from the underlying material. The sand probably represents material reworked by wave action and deposited near shore. Shoreline segments identified from both sedimentary and topographic features are shown as solid lines on Plate F-1A (locations E2, E3, E4, W1, W3, W7, and W8).

Section B, Plate F-2, illustrates the occurrence of strong sedimentary evidence with little or no topographic evidence for the shoreline. Shoreline segments identified from this evidence are shown as dashed lines on Plate F-1A (locations E1, E8, W2, W4, and W6). This evidence occurs where the easily eroded glacial drift was absent and bedrock was exposed at the

former lake level. No wave-cut rock benches could be found within the study area. There was either insufficient time or the wave action was not severe enough to produce wave-cut rock benches. However, the sedimentary evidence is quite clear. Laminated lacustrine sediments occur in low protected areas and reworked medium to fine grained clean sand occurs along the rock slopes that were below the former lake level. The elevation above which the lacustrine sand is absent represents the approximate shoreline elevation. Deltaic deposits also represent sedimentary evidence. However, only small remnants of these deposits remain as most of them have been mined extensively for sand and gravel. Because lacustrine sediments are deposited below shoreline and because deltaic sediments may in part be deposited above shoreline, those shoreline segments identified by only sedimentary evidence are not as reliable as those shoreline segments identified from both sedimentary and topographic evidence as discussed above.

Section C on Plate F-2 illustrates only topographic evidence for the Lake Hudson shoreline. Shoreline segments identified from only topographic evidence are also shown as dashed lines on Plate F-1A (locations E5, E6, E7, E10, E11, E12, E13, E14, W5, and W9). Here, the lacustrine sand is absent, but a nearly flat surface is present on the easily eroded glacial drift, which indicates modification by wave action. Although the flat surface is generally very narrow (less than fifty feet in width) it can easily be identified on aerial photographs and

in the field. Some of these flat surfaces were probably formed above the actual shoreline, and others were probably formed below shoreline as Lake Hudson drained. Therefore, these shoreline segments are not as reliable as those shoreline segments identified from both sedimentary and topographic evidence.

#### F4.1.3 Reliability of Shoreline Elevations

As shown on Plate F-1A, evidence for the Lake Hudson shoreline is not continuous along the valley and the shoreline was inferred in most areas. The reworked sand used for evidence of the Lake Hudson shoreline could have been deposited just above, at, or just below the actual lake level. The wavecut bench on glacial drift could have been produced above or below the actual lake level. Furthermore, the water level in Lake Hudson probably fluctuated, as do most lake levels, rather than remained at a constant elevation. Thus, the elevation of a shoreline segment at any one place is only as reliable as the evidence used to identify it.

As mentioned in Section F4.1.2, the most reliable shoreline segments are those identified from both sedimentary and topographic evidence. The elevations of these segments along with the elevations of 16 other segments identified from only sedimentary or topographic evidence were surveyed by Consolidated Edison. The locations of the surveyed shoreline segments are shown on Plate F-1A and they are plotted on Plate F-3. Using the 7 segments identified from both topographic and

sedimentary evidence, a projected Lake Hudson shoreline was constructed on Plate F-3. Survey points E2 and E3 lie on the projected shoreline, whereas points W1, W7, and W8 lie within 5 feet and points W3 and E4 lie within 6 feet of the projected shoreline. This indicates that the projected Lake Hudson shoreline as identified from the most reliable data available is probably accurate to within  $\pm 6$  feet. The survey points for those shoreline segments identified from only topographic or sedimentary evidence are included only for supportive evidence as their accuracy is only reliable to within  $\pm 20$  feet as indicated on Plate F-3.

#### F4.1.4 Interpretation

Reeds (1927) calculated that the shorelines of lakes Passaic and Hackensack had been upwarped to the north at approximately 2.25 feet per mile and he assumed that the Lake Hudson shoreline had been upwarped by the same amount. Connally (1972) indicated that soon after the ice had retreated north of the St. Lawrence Valley, that 3.07 feet per mile of local rebound and 1.17 feet per mile of regional uplift occurred north of the Hudson Highlands. He further states that the 1.17 ft/mile of regional uplift was completed between 13,200 and 12,500 years b.p. and that the 3.07 ft/mile of local rebound was completed between 13,200 and 13,000 b.p.

On Plate F-3 the Lake Hudson shoreline was projected to an imaginary north-south line from Highland Falls through the Indian Point Plant site to Croton Point. From Plate F-3 it

can be seen that the Lake Hudson shoreline is upwarped to the north about 50 feet over a distance of 12 miles (4.17 feet per mile). The 4.17 feet per mile of upwarping agrees quite well with the total rebound of 4.24 feet per mile reported by Connally (1972) just north of the study area.

As discussed in Section F4.1.3, the reliability of elevations for shoreline segments identified from both sedimentary and topographic evidence is  $\pm 6$  feet. Also, the shoreline segments are not continuous along the valley. However, in areas where major fault zones have been mapped (as in the Annsville Creek<sup>(1)</sup> and Mott Farm Road areas), no offsets can be determined when comparing shoreline segments. Because of the  $\pm 6$  foot reliability in shoreline elevations, it can only be stated that no vertical offsets (greater than 12 feet) are apparent where shoreline segments can be identified.

#### F4.2 Geomorphic Features at Jones Point

The location of Jones Point, the geomorphic features present, and the locations of outcrops are presented on Plate F-4. Detailed cross-sections and diagrammatic sketches of outcrops are presented on Plates F-5 through F-8.

Three terrace levels are present in the Jones Point area (Plate F-4): Terrace I at elevation 100 feet, Terrace II at approximate elevation 80 feet, and remnants of Terrace III at approximate elevation 50 feet. Terrace I is composed of tan,

---

(1) Across the Annsville fault neither glacially polished or striated bedrock surfaces show vertical displacement.

coarse sand and gravel, and probably represents a kame terrace deposit that was deposited by ice marginal streams when the Late Wisconsin glacier occupied the Hudson Valley.

Terrace II is also composed of tan, coarse sand and gravel deposited by streams, but it is capped by 3 to 4 feet of sand. The origin of Terrace II may be interpreted in two possible ways. First, it may represent outwash material deposited by streams at a lower level than Terrace I as the ice continued to melt in the Hudson Valley. In this case, the sand and gravel underlying the two terraces would represent two different depositional events (Terrace I representing kame deposits and Terrace II representing a later outwash deposit). The second interpretation is that the lower level of Terrace II could have been cut by ice-marginal streams or by wave erosion in proglacial Lake Hudson. This implies that the materials underlying the terraces represent the same depositional event (kame terrace) and were at one time at the same level (about 100 feet). Regardless of which interpretation for the origin of Terrace II is accepted, the most significant feature observed is the 3 to 4 feet of sand overlying the coarse sand and gravel. This sand probably represents reworked sediments at/or near the shoreline of proglacial Lake Hudson. The Lake Hudson shoreline is discussed in more detail in Section F4.1.

Terrace III has been quarried extensively for sand and gravel and only small remnants are still present in the area. The West Point 15-minute topographic quadrangle was used by

Berkey and Rice (1919) as a base map for the geologic map presented in their report. As this topographic map was of early vintage, prior to 1919, much of Terrace III was still present (Plate F-4). On this map, the terrace is shown to exist at approximate elevation 50 feet, consistent with the small remnants that still exist. From these small remnants, it appears that Terrace III consisted of gray, coarse sand and gravel. These materials exhibit cut and fill, topset, and foreset features (Plate F-5) and are interpreted, at least in part, as deltaic deposits.

Large blocks of Pleistocene conglomerate (sand and gravel cemented with calcite) are present throughout the quarried area. They were obviously left as waste material during the quarry operation. However, some of these conglomerate beds were found in-place in Terrace III (Plate F-5) and appear to have formed subsequent to the deposition of the sand and gravel.

Lacustrine deposits of silt, fine sand, and clay are present at locations 224-2 and 226-2 (Plate F-4). These lacustrine materials occur up to an approximate elevation of 70 feet and were apparently deposited in proglacial Lake Hudson. The lacustrine materials were deposited against the south slope of Terrace II at location 224-2 and appear to overlie Terrace III at location 226-2. Therefore, the sand and gravel of Terrace II predates the lacustrine materials of Lake Hudson. At the present time, it cannot be determined if Terrace III predates or post-dates the lacustrine materials of Lake Hudson as there is evi-

dence of severe downslope movement and slumping of the lacustrine materials at location 226-2.

#### F4.2.1 Slump Features at 224-2

On the southeast slope of Terrace II at location 224-2, a small slump is exposed and numerous faults with small displacements are present in the material that moved downslope (Plates F-6 and F-7). The diagrammatic sketch on Plate F-6 shows the general relationships at this exposure. The expression of the failure surface may be recognized by a 2 to 3-foot slump scarp on the west side and a 1 to 2-foot slump scarp on the east side. The material between the slump scarps is the disturbed material that moved downslope. The steeply dipping and faulted beds in the outcrop at the base of the exposure (Plate F-7) occur within this disturbed material. Sand and gravel from Terrace III have been removed by man from the toe of the slope, thus causing the slump in the exposure. Further evidence to support this conclusion is seen in the fact that the beds at the top of the exposure dip only 8 degrees to the northeast, whereas the beds in the slump material dip 40 to 50 degrees to the northeast. Thus, the disturbed material at the base of the slope should not be related to tectonic activity.

About 20 feet north of the top of the slump feature 224-2 (Plate F-4), a small scarp is present near the top of Terrace II that could be interpreted as an old slump scar. Small gullies have been eroded into the terrace slopes at both ends of

this possible slump scar. The gullies, and the small scarp, are now covered with vegetation and there is no surficial evidence of recent slumping except at location 224-2. If this is a slump, it may be related to earlier sand and gravel quarry operations.

#### F4.2.2 Disturbed Features at 226-2

At location 226-2, lacustrine sediments overlie coarse sand and gravel (Plate F-8). Small folds and faults are present within the lacustrine sediments, but they do not extend downward through the coarse sand and gravel. As can be seen on Plate F-8, these sediments occur on a very steep slope. A small stream is flowing at the base of the slope and recent slump material is present. The lacustrine sediments can be traced northward to the above mentioned relatively undisturbed lacustrine deposit. The field relationships indicate that these folds and faults were produced by downslope movement by either creep, solifluction, or slump.

About 20 feet north of location 226-2 at the head of the small gully, approximately 15 feet of relatively undisturbed lacustrine silt, fine sand, and clay crops out. Some of the laminations are slightly contorted and folded. However, these disturbed laminations are interlaminated with undisturbed, horizontal laminations, which indicates that the minor folding was penecontemporaneous with deposition.

#### F4.2.3 Interpretation

The folds and faults described above (locations 224-2 and 226-2) represent the only disturbed features identified in

Pleistocene deposits during this investigation in the Jones Point area. Other outcrops in the area, for example, see Plate F-5, show no evidence of being disturbed. Locations 224-2 and 226-2 both involve lacustrine sediments on steep slopes, the toes of which have been or are being removed. The entire area has been extensively quarried for sand and gravel. Therefore, these disturbed features cannot be interpreted as evidence for tectonic activity.

#### F4.3 Rock Bench

Remnants of a rock bench (bedrock terrace) occur along the Hudson River from Cold Spring to south of the Indian Point site (Plate F-1A). The remnants slope gently toward the river and downstream. They end abruptly at steep erosional scarps which descend to the level of the Hudson River (Plate F-9). The rock bench remnants represent an old, relatively flat valley bottom or strath that was cut by lateral planation of the Hudson River at some time in the past. It can be traced on opposite sides of the river at about the same elevation. Glacial erosion has severely modified the surface and left behind small rock basin lakes. Post-glacial stream dissection has locally destroyed the terrace.

The bench remnants can be definitely shown to predate the Late Wisconsinan ice advance because they exhibit abundant evidence that they were glaciated in the form of erosional (glacial grooves, polish, and striations) and depositional (glacial till) features. This would indicate a minimum age greater than

20,000 years, the time of the Late Wisconsin maximum on Long Island.

In the Cold Spring area, this rock bench is at approximate elevation 200 feet; in Highland Falls, approximately 180 feet; in Fort Montgomery approximately 165 feet, and; in the Indian Point area approximately 140 feet (Plate F-9). Therefore, over a distance of about 12 miles the rock bench remnants decrease southward in elevation by 60 feet, producing a gradient of 5 feet per mile. The local relief on the rock bench remnants is generally 40 to 60 feet with a maximum relief of 80 to 100 feet.

The present geomorphic form of the rock bench remnants and the gradient of 5 feet per mile are the result of; (1) preglacial fluvial processes that originally formed the rock bench, and (2) differential erosion by glaciers during Late Wisconsinan time. Thus, the rock bench remnants now present along the Hudson River represent a compound landform produced by more than one geomorphic process. The last major geomorphic process that affected this compound landform would determine the age of the landform. The geomorphic form, the elevations, and the gradient of the rock bench are probably Late Wisconsinan in age. The present gradient may not be the same as the preglacial rock bench gradient. The general valley-in-valley geomorphic form was probably inherited from preglacial times, but the present landscape is the result of severe modification by glaciers during Late Wisconsinan time.

#### F4.4 Mott Farm Road

At a roadcut along Mott Farm Road (Plate F-1), a N60°E trending fault plane, dipping 70 degrees to the southeast, is exposed in bedrock for approximately 100 feet along strike. Near the northern end of the exposure, 8 to 10 feet of brecciated mylonite crops out (on the southeast side of the fault plane), the upper surface of which is covered by Wisconsin till. The till is also in contact with the fault plane at the northern and southern ends of the exposure. The deposit of till is in the form of a wedge which is approximately 15 feet wide at the level of the road, and up to 12 feet high against the fault plane.

##### F4.4.1 Observations

Two trenches were hand excavated through the wedge of till to the rock surface. Trench A (Plates F-10 and F-11) was excavated through the deeper portion of the wedge and was floored slightly below road level. In this trench, a wedge-shaped zone of weathered mylonite is overlain by Pleistocene till. The mylonite is not in direct contact with the Precambrian gneiss (Plate F-10). Immediately adjacent to the fault plane is a sand layer with four textural zones that separates the Precambrian bedrock from both the till and mylonite wedges. The upper one-third of the sand layer displays horizontally laminated silt and sand stringers contained within a 1 to 2 foot wide zone of very pebbly medium to coarse sand. The center portion of the sand layer is composed of medium to coarse sand with pebbles, and the

lower one-third is composed of very pebbly medium to coarse sand. These three zones display a vague horizontal stratification. The fourth textural zone is composed of laminated fine to medium sand with interlamination of coarse sand. It is a thin discontinuous layer parallel to and in contact with the fault surface. The zone does not extend to the floor of the trench. All of the above units are covered by pebble sized angular talus mixed with organic material and colluvium composed of till with a platy fabric parallel to the outer surface of the till wedge.

Trench B (Plates F-12 and F-13) was excavated on top of the exposed mylonite, and floored 8 feet above road level. The sediments separating the bedrock from the till and mylonite are not as well defined in this trench. However, there is a more continuous deposit of fine to medium grained sand in contact with the fault plane. This sand layer is thickest in two 6 inch deep pockets in the fault plane and near the base of the trench where a wedge of sand interfingers with the surrounding till-like sediment. In the pockets, the sand is laminated generally parallel to the rock surface, whereas in the wedge near the base, the small scale bedding dips gently away from the rock-sand interface.

#### F4.4.2 Interpretation

Two hypotheses are here proposed to explain the geologic configuration at this exposure: (1) slumping of the sediments as a result of road construction and maintenance, and (2) natural emplacement of sediments during Late Wisconsinan time.

The exposure is a road cut positioned on a curve and has undergone considerable construction, blasting, and removal of till (Luther Jones; Rockland County Hwy. Dept. Road Inspection, Personal Comm.). Considering this, it is highly likely that some slumping of the sediments away from the rock has occurred, followed by filling in of the open space by finer material derived from the till. At the top of the fault surface exposure, relatively fresh Precambrian gneiss crops out, indicating that the surface materials (till and soil) have recently been removed by slumping to the base of the exposure. Mr. Jones also indicated that it has been necessary to occasionally remove material from the base of slope as it continues to accumulate.

The second hypothesis is that most of the sediments were deposited by glacial or glaciofluvial processes during Late Wisconsinan time. If the deposition was subglacial, plucking could have separated the mylonite from the fault plane while subglacial water successively deposited the till, the medium to coarse sand and the fine to medium sand. Alternatively, when the ablating ice occupied the valley, ice marginal streams could have eroded the highly weathered mylonite at the fault surface and then deposited the medium to coarse sand. The nearly vertical and generally sharp contacts between till and medium to coarse sand and between medium to coarse sand and fine to medium sand suggest that each textural zone may have been frozen when the next was deposited.

The field relationships indicate that both hypotheses are plausible. Perhaps they are both correct to a certain degree. A fault origin for the observed relationships, however, does not seem likely, since none of the soil units contain a shearing fabric (faulting, slickensiding or dragging).

#### F4.5 Immaculate Conception Seminary

The Immaculate Conception Seminary is located along the Ramapo River in Darlington, New Jersey (see Plate F-1). Investigation of this area was prompted by reports of numerous breaks in the water distribution system at this facility over a relatively short period of time. In 1973 an article in the Bergen County Record alluded that these leaks were the reflection of activity along the Ramapo or Fyke Brook Faults. The locations of the breaks are shown on Plate F-14.

##### F4.5.1 Observations

The following information is the result of an interview with Mr. M. DeGraff, presently the Maintenance Supervisor at the Immaculate Conception Seminary. Nine leaks developed in the water system during a six-month period (Fall-Winter 1965/1966). Since that time there have been three additional leaks, one in 1970, another in the Fall of 1975, and most recently a break in March 1976. The locations of the water line breaks are denoted on the map by letters "A" through "G" (Plate F-14) and will be referred to similarly in the following text.

The Fall 1975 break (location F) occurred beneath the Ramapo River, in a 6-inch wrought iron pipe installed around

1900. This old supply line extends from the MacMillian reservoir to the Administration Building, and had never broken previously. According to Mr. DeGraff, scaling had reduced the diameter of this line by half. The break consisted of a 6 inch long longitudinal split in the pipe beneath the Ramapo River. Except for this break, the eleven other breaks occurred in 4 and 6-inch iron "Corporation Pipe", installed in 1951. The entire water system is buried about 4 feet below the surface.

Of these 11 breaks which have occurred in the cast iron pipe, nine were during the 1965-1966 period. An earlier leak at location "F" occurred in 1970. The two breaks at location "A" occurred beneath the road bed adjacent to the dormitory building, and two at location "E" were beneath the "cul-de-sac" roadbed. The water line is laid in marshy areas where the four leaks occurred at locations "B" and "D" (two at each). All breaks in the 4 and 6-inch cast iron line were described by Mr. DeGraff as cleanly through-going, as if cut by a hacksaw except for the most recent one. In all but the most recent case the pipe on one side of the break was offset about one-half the diameter, with respect to the other side. However, he could not recall the exact sense of displacement at specific locations or if there was any consistent overall relationship. None of these leaks occurred at joints. At the time repairs of the 1965-1966 breaks were being made, a factory representative visited the seminary. He stated that the 4 and 6-inch diameter pipe would break in a similar fashion, under its own weight if left unsup-

ported. The most recent break was repaired in March of 1976 but may have been leaking for as long as a year (location "G", Plate F-14). The pipe had sagged at this point and was split on the bottom.

Geologic reconnaissance of the area revealed that the seminary proper is built on a ridge of Watchung Basalt. The east slope of this ridge is covered by till in which the pipe is lain.

Further reconnaissance of the seminary property revealed several features indicative of downslope soils movement. These are located on the slope east of the Administration Building and consist of small depressions and actual breeches in the sod parallel to the slope contours. The largest breach observed is approximately 4 feet long and 1.5 feet wide in the center, being roughly elliptical in outline. At one location, further south along the slope, it is apparent that these features occur at the junction of a mass wastage lobe with the primary slope.

This particular lobe of sediment is about 2 feet high and 50 feet across at its downslope terminus. In addition to the possible freeze-thaw origin of these features, the seminary sewage system drains into the head of the main slope in this area and may accentuate the downslope soils movement by the addition of large volumes of liquid.

#### F4.5.2 Interpretation

It is most likely that these water lines failed due to applied stresses and/or age of the pipe. The times of ten out

of eleven of the failures do not coincide with local seismic activity. Additionally, seismically induced soil mechanics failures do not occur at intensities less than Modified Mercalli Intensity VII, and breaking of buried pipes does not occur at less than Modified Mercalli Intensity IX. Clearly, earthquakes of these intensities have not occurred in the vicinity of the Ramapo Fault in the period since the pipe was laid. Furthermore, we are aware of no reports of similar failures anywhere or anytime along the Ramapo Fault. Although the cause of the breaks cannot be accurately defined from our observations, mass wasting in the form of soil creep was observed on the property. It is therefore probable that the down slope soils movement would induce stresses that could strain the pipe to the point of failure.

#### F4.6 Stag Hill

At Stag Hill (Plates 1A and F-1), a trench was excavated close to the Ramapo Fault on the western edge of an abandoned gravel quarry about one mile southwest of Route 17 in Mahwah, New Jersey. This site was selected for trenching because of its proximity to the Ramapo Fault, the presence of lacustrine sediments and its accessibility. The course of the Mahwah River prevented locating the excavation directly over the Ramapo Fault. Nonetheless, the trench was located within 500 to 1000 feet of the trace of the fault, assuming that any significant movement along the structure would have affected the sediments in the trenched area. The excavation was oriented about N40°W; it was approximately 70 feet long and 10 to 15 feet deep.

The Stag Hill excavation exposed sediments deposited in a lakeshore environment (Plates F-15 and F-16). The gross stratigraphy within the trench consisted of 5 to 10 feet of stratified silty sands overlying Pleistocene till and in turn overlain by as much as 5 feet of poorly sorted gravels. The lakeshore facies dip gently to the east but local variations occur as a result of the sediments being draped over the uneven upper surface of the till. The large boulders within the lakeshore sediments apparently rolled or slid into the lake from the Highlands scarp that is less than 300 feet away. Clastic dikes, contorted beds, or other features indicative of liquefaction were absent.

It is clear that there is no evidence for faulting in this excavation. Two marker beds were traced between each of the mapped walls, thus eliminating the possibility of faulting along the length of the trench.

#### F4.7 Pleistocene Deposits Along the Western Border of the Newark Basin in Pompton Plains, N.J.

##### F4.7.1 Location, Purpose, and Setting

An investigation of the nature of Pleistocene sediments exposed in two abandoned sand and gravel quarries was performed in the vicinity of Pompton Plains, N.J. The non-quarried remains of unconsolidated sediments occur at the base of the east-facing front of the Reading Prong at the western edge of the Tertiary-Jurassic Newark Basin in this area. The two quarries are situated on the west side of the N.J. Route 23 traffic circle at the Pequannock-Wanaque Borough boundary (Plate F-17).

The contact between the Reading Prong and the Newark Basin in the Pompton Plains-Riverdale area is the Ramapo Fault (see Appendix C). Additionally, the quarries are on the Ramapo Fault 3 miles southeast of the epicenter of the March 11, 1976 Pompton Plains earthquake (Appendix G). Therefore, this area is excellent for evaluating whether or not tectonic activity including historic seismicity has produced disturbance of the overlying Pleistocene materials.

During the Late Wisconsinan glaciation, ice contact stratified drift was deposited along and over the contact between the Reading Prong and the Newark Basin. These sediments overlie and have buried the Ramapo Fault. The investigation of these geologically young deposits was performed to determine, if possible, whether or not fault movement along the Ramapo Fault has caused deformation of the Pleistocene sediments which are situated on top of this fault zone.

Deformation of the glacial deposits could be represented by structural features such as faults, folds, clastic dikes, quick clays, etc. On the other hand, each of these features is common in soft sediments which have experienced non-tectonic adjustments such as differential compaction and slumping. The latter commonly occurs in ice contact glacial drift after melting of the glacial ice. Consequently, the absence of these features would suggest that the Ramapo Fault, in this area of New Jersey, has not suffered displacement at the surface since deposition of the sediments 15,000 to 17,000 years ago.

However, the presence of these features does not require a fault-related origin, although a through-going fault with large displacements in ice contact deposits (kames and kame terraces) might indicate a fault-related origin.

#### F4.7.2 Geologic Observations

The quality of exposure in the larger, southernmost gravel pit far exceeded that of the northernmost quarry. For this reason mapping was undertaken in the southernmost quarry using a specially prepared photographic base of the north and west walls of the quarry. The features which were recognized in the glacial deposits were mapped on an overlay which is shown on Plate F-18 (see also Table F-1). The quarry walls are 25 to 30 percent exposed; the remainder is covered with slope wash, vegetation, and slumped material. Single units are not traceable across the entire exposure; this is due, in part, to the limited exposure, and in part to the depositional mode of the sediments.

The southernmost quarry (Plate F-17) is approximately 3300 feet long in the E-W direction. The mapped portion of the north quarry wall is approximately 1600 feet long; the mapped portion of the west quarry wall is approximately 675 feet long (Plate F-18).

The sediments exposed in the north and west walls of the quarry consist of coarse-textured sands and gravels (SL-400, SL-403 of Plate F-18 and Table F-1), mixed with zones of medium-

and fine-textured sands and silts (SL-402, SL-404 of Plate F-18). The south quarry wall (not mapped) is poorly exposed, but contains generally medium- to fine-textured sands and silts with minor amounts of gravel.

The north wall of the quarry trends N80°E-S80°W (Plate F-18). The west end of this wall, near the corner, is poorly exposed. The few visible exposures (SL-409, 410, 411) contain fine to coarse sands locally interbedded with medium gravel (Table F-1). Cross-bedding is common. The absence of fines probably explains the lack of cohesion in the sands which has resulted in the extensive slumping of material at this end of the quarry face.

The central portion of the north face (between SL-408 and SL-400) is a complex zone of mixed sand and gravel apparently capped by sands and silts. The lower portion of this section consists of zones of silty fine sands and silty to sandy, medium to coarse gravel. The sediments appear to grade upward to cleaner, gravelly sands and sandy gravels. The bedding is visible only on a larger scale, such as the contacts between gravel zones and sands. Near SL-408, one massive gravel bed was found to dip 25 to 40 degrees toward the NE. The medium sands and silty fine sands dip generally 5 degrees toward the north. Cut-and-fill structures are common. The sands and silts which cap the gravelly zones are thin-bedded to laminated sediments with many small-scale sedimentary structures. At SL-404, convolute laminae are common (Table F-1). Small discontinuous thrust and

normal faults with small-scale displacements were observed near SL-400 (layer B).

The sediments of the east end of the north wall appear to overlie the coarse gravel zone of the central portion. This section is composed of a sequence of thin interbeds of silty fine sand with traces of clay. The sediments exhibit well-developed graded bedding (SL-402). Cross-bedding is present near the top.

The west wall is lower in elevation than the north wall. At the corner, nearly all of the sediments are slumped. The sediments of this face consist of a sequence of fine to coarse gravels and interlayered gravelly sands and sandy, clayey silts (SL-405) which are capped by a continuous layer of oxidized, coarse to very coarse gravel (Table F-1). This gravel cap forms a terrace which extends west to the foot of the hill. Small-scale structural features were observed at two localities. At SL-405, two small clay injections appear to cut across overlying sand laminae. These clay "dikes" strike generally E-W and dip 30 degrees to the south. At SL-406 (Plate F-18), a cut-and-fill structure in thin bedded sands and clays is present along which there has been minor-scale slump movement deforming the beds on each side of the cut-and-fill surface. The slump surface is about 4 feet long and is truncated and capped by the overlying oxidized coarse gravel at the top of the terrace. The surface is oriented N80°E, 20 to 45°S with normal slump movement sense. The surface is apparently discontinuous, in that it ter-

minates against a 2-1/2 foot diameter glacial boulder incorporated within the sediments.

The character of the sediments in the northernmost quarry is similar to that of the south quarry sediments. Reconnaissance of the exposure revealed no unusual structural features in these deposits which were of importance to this investigation. The high degree of erosion and slope wash cover prevented detailed study of this exposure.

#### F4.7.3 Interpretation and Conclusions

The deposits of these quarries are part of a complex sequence of kame, kame terrace, and kame delta deposits which were laid down during the regressive phase of the Wisconsinan glaciation (~15,000 y.b.p.). The coarse-textured, poorly stratified, and poorly sorted sands and gravels represent cut-and-fill deposits in the kames and kame terraces. The west wall of the south quarry is probably part of a kame terrace deposit; the north wall contains kame and kame terrace deposits. The medium-to fine-sand, silt and clay represent kame delta deposits in proglacial Lake Passaic (see Section F2.0). The kame and kame terrace deposits in the north wall of the mapped quarry are in contact with the deltaic sequence associated with Lake Passaic. In fact, the vertical cross-section pattern (Plate F-18) of the north wall is the result of quarry operations locally cutting into the kame deposits (between SL-400 and SL-409) in the central portion of the north face. The south quarry wall and the

majority of the empty portion of the quarry are part of the kame delta sequence.

No major faults were observed in the unconsolidated sediments. At SL-406, slumping along a N80°E cut-and-fill surface occurred prior to deposition of the unaffected, superposed gravel in the kame terrace. A few small scale deformational features were observed such as contorted laminae, discontinuous minor faults, and two clay dikes. The presence of these structures does not require the occurrence of fault movement along the Ramapo Fault as their cause, since they may be a product of the depositional environment. The ice-contact nature of the kame and kame terrace deposits exposed in the north and west faces accounts for the discontinuous and variable nature of the bedding. It also accounts for the presence of small, discontinuous faults, convolute laminae, and clay dikes, which probably formed when the contact glacial ice melted away.

Results from a west to east ground magnetic traverse in the mapped quarry (Appendix D) have revealed that the Precambrian-Triassic-Jurassic contact passes beneath the quarry at the west end. In fact, outcrop of gneiss from the Highlands is exposed at the base of the west quarry face midway between SL-405 and SL-406 (Plate F-18). The contact, therefore, lies beneath the pond immediately east of the outcrop and the Ramapo Fault zone may be expected to extend for several hundred feet on each side of the contact.

#### F4.8 Central Nyack Outcrop

##### F4.8.1 Introduction

During geologic reconnaissance mapping in the Newark Basin (Appendix B), an outcrop was found in the Central Nyack, N.Y. area which appeared to have numerous pop-ups and exhibited a singular open fissure. The outcrop, which lies 1 mile south-east of the Rockland Lake Fault, was mapped and the features were studied to evaluate their origin and significance (Plate F-19).

The outcrop is located on the east side of N.Y. Route 303, approximately one mile south of the New York State Thruway (Plate 1B). The outcrop at this location which was exposed by several quarrying operations in 1961, is approximately four to five acres in area. Most of the material removed (up to 25 feet) was colluvium. However, some bedrock was also ripped up for use as fill. Machinery marks at various places on the rock surface attest to this activity.

##### F4.8.2 Observations

Much of the bedrock surface is glaciated, exhibiting glacial striae trending generally N10°W to N20°W. This surface also approximates the dip slope of sediments to the west of, and stratigraphically below the Palisades Sill.

The sandstone, siltstone, and mudstone exposed there have been contact metamorphosed during the emplacement of the Palisades diabase. Bedding strikes generally north-south to north-northeast and dips 5 to 10 degrees westward.

A four to six inch wide dike (K/Ar dated at 175±8 m.y.; Appendix E) crosscuts the hornfels in the central portion of the exposure and is mappable for more than 80 feet. It is oriented N80°E vertical. The dike has an aphanitic texture and an intermediate to mafic composition. The contacts of the dike with the country rock appear to be sheared.

Two very consistent fracture sets compose a nearly orthogonal fracture group over the entire outcrop. Both sets are nearly vertically dipping; one set strikes N50 to 60°E, the other N40 to 50°W. A similar fracture pattern was documented at DF-14 on the south side of the New City Park Dike. Few of the regionally ubiquitous north-south to northeast-striking fractures and shears were observed at either location.

In the southern portion of the outcrop there is an open fissure which has apparently opened utilizing pre-existing northeast and northwest trending joints. The width of the opening varies from six to nine inches and is mappable for at least seventy feet. The major portion of the fissure trends N40 to 50°W (Plates F-19 & F-20). At its southeastern end, the feature jogs several times and changes strike from northwest to northeast to northwest without losing its continuity. At its mapped terminus the feature bifurcates and the northeastern branch is apparently coincident with the axial trace of a fold. The geometry of the fissure clearly indicates an extensional origin for its opening. At several places along its length, the opening is unfilled to a depth of ten to fifteen feet. Where it is filled, the filling material is similar to the nearby colluvium.

About twenty-five feet east of the mapped extent of the fissure an outcrop of sandstone was uncovered during trenching. Bedding there strikes generally N50°E and dips about 25 degrees to the southeast. The map pattern of bedding attitudes suggests a fold with a northeast-trending axis (Plate F-19). At the northern end of the Nyack outcrop there are numerous low amplitude folds, the axes of which trend N20 to 30°E (Plate F-19). Two of these features were cut into with a portable diamond saw and were observed to be folds. Most of them exhibit a hollow sound when struck, probably due to the separation of the upper layers from the solid rock in pop-up fashion. This separation is probably due to folding of the rock although a weathering phenomenon (a type of exfoliation) is also a possible partial explanation.

The geometric relationship between the open fissure and the larger fold strongly suggests that they are genetically related (Plate F-19). Apparently, the fissure was opened by extension along joints nearly parallel and perpendicular to the axis of the mapped fold. The observed relationship between the fold axis and the open fractures is what one should expect in terms of brittle folding.

A trench was excavated in the colluvium across the projection of the fissure, about 50 feet east of its mapped terminus. The sediment consists of angular blocks of hornfels in a sandy gravel, including traces of well rounded cobbles.

This material is very homogenous and lacks fabric. No disturbance was observed in the excavation. The contractor who was involved in the last quarrying effort at this location, in about 1961, was contacted and he stated that no blasting was performed at the borrow pit. Additionally he does not recall having seen any features like those described above.

#### F4.8.3 Conclusions

The folds, open fissures and brittle structures observed at this outcrop apparently formed in response to generally east-southeast-oriented nearly horizontal compressive stresses, at very low confining pressures at or near the surface. These features appear to be quite young; the unrounded edges of the fissure immediately adjacent to glaciated bedrock surfaces suggest that it is younger than the last glaciation (circa. 15,000 y.b.p.). The lack of colluvium or rubble filling material in the fissure, in conjunction with the contractors comments indicate the fissure is younger than the last quarrying effort (1961). Woodworth (1907), and Oliver and others (1970) have described several instances of small offsets of glaciated surfaces in the Mid and Upper Hudson Valley between Hyde Park and South Troy, N.Y. These offsets are found in phyllite and shale, and always occur on planes parallel to the predominant Taconic cleavage, i.e., striking north-northeast and dipping steeply to the east. Their reverse movement senses are compatible with the east to northeast oriented maximum compressive regional stress determined by Sbar and Sykes (1973) and measured during this investigation (Appendix H).

It is concluded, therefore, that the recent folding (pop-ups) and the fissure opening observed at the Central Nyack outcrop are the result of near surface release of locally east-southeast oriented stresses, not unlike the post-glacial offsets described above. All of these features (those at Central Nyack and those in the Mid and Upper Hudson Valley) are discontinuous, of small dimensions and not associated with mapped regional faults.

## F5.0 CONCLUSIONS

As a result of the above investigations, the following conclusions may be reached relative to the purposes stated in Section F1.0:

- 1) along most of its length, the Ramapo Fault is overlain by relatively thick Wisconsinan ground moraine with scattered deposits of stratified drift and Holocene alluvium. A notable exception is the Pompton Lakes, N.J. area, where the deposits are predominantly stratified drift (glacio-fluvial outwash and kame terraces, shoreline deposits of proglacial Lake Passaic and glacially related deltaic deposits). The Letchworth and Thiells faults are overlain by Wisconsinan ground moraine and Holocene alluvium, while the Annsville Fault (near Peekskill) is overlain by ground moraine and stratified drift. The Peekskill and Peekskill Hollow Faults (near Peekskill) are covered predominantly by stratified drift related to proglacial Lake Hudson. The stratified deposits do not appear to be interrupted by major fault movements;
- 2) surveyed remnants of the proglacial Lake Hudson shoreline are upwarped to the north at 4.17 feet/mile, which is in accord with post-glacial regional uplift and local rebound. In areas where

the remnants cross the Annsville, Peekskill and Mott Farm Road Faults, no offsets can be determined when comparing shoreline segments;

- 3) suspect structures were investigated at Jones Point and Mott Farm Road (near the Mott Farm Road Fault) and Immaculate Conception Seminary (near the Ramapo Fault) and were determined to be most probably of other than tectonic origin;
- 4) the rock bench flanking the Hudson Gorge is discontinuous and of compound origin, and therefore of little use in determining evidence of recent offset;
- 5) a trench at Stag Hill and a large sand and gravel pit wall at Pequannock (adjacent to and across the Ramapo Fault, respectively) were examined for evidence of faulting related to movement on the Ramapo Fault. None was found; and
- 6) The pop-ups and fissure at Central Nyack are the result of east-southeast-oriented, nearly horizontal compressive stresses. They appear to have developed post-glacially.

TABLE F-1

DESCRIPTION OF STATIONS - GRAVEL QUARRY  
AT RIVERDALE AND POMPTON PLAINS, N.J.

- SL-400      Stratigraphic Column (from top to bottom)
- A)      Gravel    - medium to coarse, very poorly sorted and well rounded gravel in matrix of fine sandy silt; approximately 2 to 4 feet thick; minor cross-bedding and nearly horizontal beds.
  - B)      Silt        - yellow brown sandy silt, approximately 5 to 6 feet thick; fine cross-laminations; bedding approximately horizontal. Small thrust and normal faults at west end of overlying gravel (A). Faults are discontinuous and about 2-3 inches long.
  - C)      Gravel    - coarse to very coarse, poorly sorted gravel; well-rounded cobbles in matrix of medium to coarse silty sand. Thickness uncertain. Bedding nearly horizontal.
  - D)      Sand        - predominantly fine silty sand with minor pebbles and cobbles; bedding is variable, generally dips to south up to 25 degrees. Possible foreset beds to delta.
- SL-401      Fine silty sand with pebbles and cobbles; well bedded and cross-bedded; contains calcite-cemented sand layer (N10-30E, 14-17SE) which can only be traced 6 feet laterally.
- SL-402      Thin interbeds of silty fine sand with trace of clay; graded bedding in light brown sand grading upward to dark brown silt or clayey silt; beds strike N35W, 5NE. Probable near shore lake sediments.
- SL-403      Fine to very coarse, extremely poorly sorted gravel in matrix of sand, silt, and clay (trace); below gravels of SL-400, 401. Bedding is nearly horizontal.
- SL-404      Contact between fine sands and silty sands (above) and medium to coarse gravel in silt and silty sand matrix (below). Cross-bedding and convolute bedding in sands and silts. Contact dips 10-15 degrees due E.
- SL-405      Stratigraphic Column (top to bottom)
- A)      Interbeds of gravelly sand and sandy silt; about 3 feet thick; beddings dip west 0-3 degrees.

TABLE F-1 (Continued)

- B) Fine to medium gravel, with well-rounded cobbles and matrix of fine to coarse sand; poorly sorted but clean and loose gravel, conformable with A). About 2 feet thick.
- C) Thin beds of sand, silt and clayey silt; layers nearly horizontal; presence of two clay "dikes" which deform overlying sand lamination: E-W, 30S. C) is 7 feet thick.
- D) Medium to coarse, sandy gravel with matrix of sand and silt; poorly sorted, dirty gravel. Thickness uncertain.
- SL-406 At head of large erosional gully at west end of pond, behind gneiss outcrop. Slumped cut-and-fill structure in 6 feet of intercalated sands and clays, capped by 3-1/2 to 4 feet of coarse to very coarse, oxidized gravel which truncates slump surface. Slump surface is 2-6 inches thick, contains several large pebbles, and contorted sand and clay stratiform zoning. Slump surface terminates at large boulder (2-1/2 feet diameter). Drag of thin beds on both sides is very slight, and indicates "normal" slump movement sense. Surface is oriented N80E, 20-45S.
- SL-407 Brown to yellow brown, medium to coarse sand, well-sorted; cross-laminated; few continuous layers traceable for long distances.
- SL-408 Gray to brown, medium and coarse sand to gravelly coarse sand; moderately well sorted; thin bedded to laminated.
- SL-409 Interbedded light gray-brown, pebbly, fine to very coarse sand; locally well-bedded with thick and thin beds interlayered. Thick beds contain pebbly, coarse sands; some thin to medium beds of fine and medium sands (~ 7 to 8 feet thick). Below this is brown, sandy medium to coarse, clean gravel, 4 to 5 feet thick. More coarse sand beneath gravel. Entire sequence is part of cross-bedded zone, dipping 10 degrees east.
- SL-410 Interbedded, cross-bedded sands and gravels:
- a) brown, fine to coarse gravel with matrix of fine to coarse sand; coarse sand predominant.
  - b) medium to coarse sand with traces of pebbles.

TABLE F-1 (Continued)

<u>SL-411</u>	Brown, very coarse sand to gravelly sand; non-pebbly sands are medium to very coarse. Sequence poorly exposed.
---------------	--

APPENDIX G

EVALUATION OF THE RELATIONSHIP BETWEEN  
SEISMIC EVENTS AND THE RAMAPO SYSTEM OF FAULTS

APPENDIX G

EVALUATION OF THE RELATIONSHIP BETWEEN  
SEISMIC EVENTS AND THE RAMAPO SYSTEM OF FAULTS

G1.0 INTRODUCTION

The purpose of this investigation is to evaluate the possible association of previously reported seismic events with the Ramapo Fault System. To this end, a review was made of all the standard earthquake listings covering the area of interest. Various state and local agencies and educational institutions were contacted to assure that available data concerning the smaller events were included in the list. Additionally, available seismograms were inspected and the P and S arrival time data were used to determine hypocenter locations and fault plane solutions. These solutions were compared with the literature and the findings of our geological investigation.

To illustrate the regional seismic pattern, an epicenter map of the northeastern United States is shown on Plate G-1. A list of earthquakes occurring within the region 40° to 42°N; 73° to 75°W (bounding the general fault area) is given in Table G-1. The earthquakes known to have occurred in the general region of the Ramapo Fault System are plotted on Plate G-2. Table G-2 gives a list of all the historic earthquakes which have occurred in the vicinity of the Ramapo Fault System and provides, where available, instrumental locations. The earth-

quakes listed in Table G-2 are contained within the rectangular area shown on Plate G-2. This area is approximately coincident with that studied during the geological investigation.

## G2.0 MAXIMUM INTENSITY EARTHQUAKE

The maximum intensity earthquake reported to have occurred within 5 km of the Ramapo Fault (Sykes, 1976) is one postulated to have occurred in the fall of 1943 near the intersection of the Ramapo Fault with the New York-New Jersey border (Modified Mercalli Intensity V, Sykes, 1976). No mention of this earthquake was made in the catalogs by Coffman and von Hake (1973) or Smith (1966), or in the Coast and Geodetic Surveys' yearly catalog "United States Earthquakes." Our search traced the source of the information on this earthquake to Mrs. Edythe Glasgow, a resident of Mahwah, N.J., who had provided this information from memory on a questionnaire dated February 26, 1973, 30 years after the event, to Mr. Charles Ellis, also of Mahwah. Mr. Ellis, in turn, provided this questionnaire to Mr. Daniel R. Dombroski of the New Jersey Geological Survey, whereby it was entered into the New Jersey earthquake list. Dombroski (1973) summarized the felt information at Mrs. Glasgow's house as follows:

"Doors and dishes rattled, hanging lamps swung, furniture shifted. Earth shook perceptibly underfoot after group ran outside in night clothes."

Mrs. Glasgow mentioned that the earthquake was also felt by her father in Suffern, New York, 2.6 miles north of her house and by a Mr. Ashby, a foreman at the Birch estate about one mile south of her house. Therefore, the known extent of the felt region was described to be 3.6 miles along Route 202 and adjacent to the Ramapo Fault.

Mr. Ellis told us that he had looked into the micro-film copies of old newspapers but found no mention of this earthquake. He stated that because of war time censorship, shocks due to explosions and earthquakes were not reported in the newspapers.

On our request, Captain Kownacki of the Mahwah police searched through the police records and found no mention of the 1943 earthquake. He also contacted a retired officer, who was with the force during 1943, but no record of any earthquake was found. Our contact with the local historians, Mr. Howard Avery and Mr. John Dator, did not yield any further information on this postulated event.

Mr. Ellis assigned a Modified Mercalli (MM) Intensity V to this earthquake. From the very small felt area and the absence of information from any other reliable source (standard earthquake catalogs, local libraries and police records), this event, if an earthquake, was of very small magnitude and its focus must have been located very close to Mrs. Glasgow's house. The description in the questionnaire completed by Mrs. Glasgow seems appropriate to no more than MM Intensity IV.

It is of some interest to note that on September 4, 1944, an earthquake of Intensity VIII occurred near Massena, N.Y. and Cornwall, Ontario at 11:39 P.M. The Massena earthquake was felt north to Maine, west to Michigan, and in nearly all of Maryland and Pennsylvania. The time of occurrence of this earthquake, when compared with the description "group ran outside in

night clothes", leads us to believe that the Glasgow family may have reported their experience of the September 4, 1944 Massena earthquake. The isoseismal map published in the "United States Earthquakes" shows the New York - New Jersey border region within the intensity range I-III.

Two other events (Table G-2 and Plate G-2), one in 1783 of MM Intensity VI located approximately 12 km from the Ramapo Fault, and another on April 1, 1947 of MM Intensity III, located approximately on the Ramapo Fault, were based only upon felt reports and no instrumental records are available.

Instrumentally located events (Table G-2) which were reportedly felt in the general area of the Ramapo Fault are the "Rockland County" earthquake of September 3, 1951, the Pompton Plains earthquakes of December 20, 1962 and March 11 & 12, 1976, and the earthquake of July 19, 1975.

The earthquake of September 3, 1951 (magnitude 4.4, MM Intensity V) is located approximately 12 km northwest of the Ramapo Fault (Plate G-2). The earthquake of December 20, 1962 (magnitude 2.4, MM Intensity IV) is located approximately 1 km northwest of the Ramapo Fault (Plate G-2). The earthquake of March 11, 1976 (magnitude 2.0, MM Intensity IV) is located 3 to 5 km northwest of the Ramapo Fault.

The earthquake of March 12, 1976 was an aftershock of the March 11, 1976 event and was of lower intensity.

The event of July 19, 1975 (magnitude 2.3) was recorded by the Consolidated Edison Seismic Monitoring Network

(CESMN) and was located (Plate G-2) by Dr. Marc Sbar (Consolidated Edison seismic consultant at that time) using the HYPO-71 program of Lee and Lahr (1975). This data (the computer printout) was provided to Dames & Moore by Dr. Sbar. This event was reportedly felt by one person in the field.

Based on the historic record including available instrumentally located earthquakes it appears that in the last 193 years only three MM Intensity IV events can be said to have occurred within 5 km of the surface trace of the Ramapo Fault. The location of these events (Plate G-2) is south of the New York - New Jersey State Line, at least 25 km from the Indian Point site. Additionally, inspection of Plate G-2 shows no noticeable concentration of earthquakes over the extent of the Ramapo Fault. There may, in fact, be more noticeable concentrations in areas removed from the mapped extent of the fault.

### G3.0 VELOCITY MODELS AND LOCATION OF EARTHQUAKES

#### G3.1 VELOCITY MODELS

Arrival times of P and S waves read from the seismograms of various stations for the location of epicenters are presented in Tables G-3, 5, 7, 8, 9, 10, 11, and 12.

For an accurate location of the epicenter, precise information about the regional velocity model is essential, especially when the azimuthal distribution of stations around the epicenter is not sufficiently broad. A search was made for all available or known velocity data. Using the various velocities reported, epicenter locations were computed by using the program HYP071 prepared by Lee and Lahr (1975). These are presented in Tables G-4 and G-6 as several solutions, derived as follows:

Solutions 1-10 are based on the velocity models presented by Sykes (1976).

Solutions 11 and 12 are based on the velocity models used by Page et al. (1968) for locating the Pompton Lakes earthquakes of 1964 and 1966.

Solutions 13 - 18 were established by using the velocity models presented by Anderson and Dorman (1973) from an analysis of the dispersion of Rayleigh waves. The velocity models used for solutions 13 and 14 were obtained from Rayleigh waves which propagated along a path between the Haverstraw quarry and the Ward Pound Ridge (WPR) seismograph station located in the crystalline complex and a little north of the Indian Poant site. The quarry is near the northern end of the Trio-

Jurassic basin. Solutions 15 and 16 are based on velocity models obtained from the dispersion of Rayleigh waves propagating between the Belle Mead quarry and the seismograph station WPR. A significantly large portion of this path is across the Trio-Jurassic lowland. Solutions 17 and 18 are based on a velocity appropriate to the Palisades diabase sill upon which the station PAL is located. Ratcliffe (1971) suggested that the Ramapo Fault served as an avenue of magma ascent and, hence, the source of the material in this sill. The validity of this case depends upon how appropriate the sill velocity is for much of the travel path, which in turn would depend upon the velocity and depth of the underlying basement and hypocentral distance.

Solutions 19 and 20 are based on the velocities determined by Katz (1955) from the recordings of quarry blasts for the profile south of Tahawus, N.Y. The path along this profile includes 11 to 106 km of Precambrian granites and granosyenite intrusions, and 115 to 282 km of younger rocks including Cambrian dolomite, Ordovician shale, and Devonian limestone.

Solutions 21 and 22 are based on velocities established from the Milroy, Penna., quarry blasts for an east-west profile in central Pennsylvania and northern New Jersey, Katz (1955). The geological formations along this profile vary in age from Precambrian gneiss in central New Jersey, to Cambrian limestones in central Pennsylvania, to Trio-Jurassic diabase at Palisades, N.Y.

Solutions 23 and 24 are based on velocity Model 6 presented by Sykes (1976).

For the purpose of this report the September 3, 1951 and March 11, 1976 earthquakes were chosen to evaluate the epicentral locations dependence on the velocity model used. P and S wave data for these two events are presented in Tables G-3 and G-5, respectively. The locations calculated using the various velocity models are presented in Tables G-4 and G-6. Plate G-3 shows the variation of the epicenter location for the different velocity models used.

#### G3.1.1 September 3, 1951 - "Rockland County"

Although twenty-seven seismograms were available for the "Rockland County" earthquake of September 3, 1951, they were derived from only seven stations: Palisades, City College, Fordham, Weston, Ottawa, Seven Falls, and Shawinigan Falls. Fourteen of the seismographs are located at Palisades. Because of the emergent arrivals and low signal levels at the Seven Falls and Shawinigan Falls stations, no P or S arrival times could be determined. Because of unknown clock correction for Fordham, only an S-P time was read. Of the five stations for which arrival time data could be read, only Palisades, City College, and Fordham were close enough to provide an accurate location (Table G-3). The seismograph stations at Weston and Ottawa were at distances of about 275 km and 480 km, respectively, from the epicenter.

Because of the paucity of data for the "Rockland County" earthquake of September 3, 1951, two solutions corresponding to fixed depths of 0.5 km and 5.0 km were derived for each velocity model (Table G-4). All of the solutions for the September 3, 1951 earthquake, with the exception of 15 to 18, occur within the region bounded by coordinates  $41^{\circ} 12.2'N$  to  $41^{\circ} 14.0'N$ ;  $74^{\circ} 12.2'W$  to  $74^{\circ} 14.6'W$ , an area less than 3.5 km long in either north-south or east-west direction. The azimuths of these locations from Palisades vary between  $N47^{\circ}W$  and  $N50^{\circ}W$ , which is in close agreement with the azimuth determined from amplitude data at Palisades by Sykes (1976), ( $N48^{\circ}W \pm 4$ ) and Table G-3 ( $N51^{\circ}W$ ). The epicenter of the "Rockland County" earthquake of September 3, 1951 is, therefore, considered to be located about 12 km northwest of the surface trace of the Ramapo Fault. These locations are in Orange not Rockland County, New York. We have, therefore, placed Rockland County in quotations when referring to this earthquake.

Solutions 15 through 18 are based on velocity models constructed by Anderson and Dorman (1973) from the dispersion of Rayleigh wave data. These models do not provide information on the velocity of deeper layers of the crust which make up at least part of the ray path between the epicenter and the stations PAL, CNY, and FOR.

#### G3.1.2 March 11, 1976 - Pompton Plains

For the Pompton Plains earthquake of March 11, 1976, P-wave arrival times at 25 stations and S-wave arrival times at

21 stations were read (Table G-5). In addition, because of an uncertain clock correction, only an S-P time was read at Patterson, N.J., PNJ, the station nearest to the epicenter (about 20 km).

Two solutions, one using P-wave data alone and the other using P as well as S-wave data, were prepared for each velocity model (Table G-6). Although the P-wave onsets can be read more accurately from the seismograms than S-wave onsets, the S-wave data provide a useful constraint on the epicentral location, especially in this case because the gap in the azimuthal distribution of stations around the epicenter is about  $110^\circ$ . The usefulness of the S-wave picks is demonstrated (Plate G-3) by the closeness of solutions 16 and 18 (established by using P as well as S-wave data) to the average grouping of solutions. In comparison, solutions 15 and 17 (which were established using P-wave data alone) occur further towards the southeast, well away from the average grouping.

Most of the solutions for the Pompton Plains earthquake of March 11, 1976 are concentrated along longitude  $74^\circ 22'W$ , and occur between  $40^\circ 57.3'N$  and  $40^\circ 58.2'N$ . The mean position of these locations is about 3 km northwest of the Ramapo Fault. The solutions 23 and 24, obtained by using Sykes' (1976) velocity model, occur at distances somewhat larger than 5 and 4 km, respectively, from the Ramapo Fault.

### G3.2 LOCATIONS OF OTHER EARTHQUAKES

Tables G-7, 8, 9, 10, 11 and 12 give P and S arrival time data for the December 20, 1962, March 12, 1976, April 13, 1976, August 20, 1976, September 22, 1976 and November 22, 1976 earthquakes respectively. The preferred epicentral location for each earthquake was obtained by using Sykes' (1976) velocity Model 6 and is shown on Plate G-2.

#### G4.0 FAULT PLANE SOLUTIONS

Fault plane solutions for ten earthquakes in the region around the Ramapo Fault System are presented graphically on Plate G-11. The composite solution for the Lake Hopatcong earthquake sequence of 1969 is from Sbar and others (1970). The composite solution for the Wappingers Falls earthquakes of June 1974 is from Pomeroy and others (1976), and that for the New Jersey-Delaware border region earthquake of February 28, 1973 and its aftershock sequence is from Sbar and others (1975). The data for the focal mechanism for the July 19, 1975 earthquake was provided to Dames & Moore by Dr. Sbar and is shown graphically on Plate G-4. The other six solutions presented were prepared by Dames & Moore.

To determine the fault plane solutions for the six 1976 earthquakes, hypocentral locations, based on Sykes' (1976) velocity Model 6 were used (Tables G-5, 8, 9, 10, 11 and 12).

First motion observations recorded at each station were traced along the ray to a corresponding position on the surface of an arbitrary unit sphere with its center at the focus (focal sphere). The station is thus located on the focal sphere at its proper azimuth from the epicenter and at an angle from vertical corresponding to the angle of incidence,  $i_h$ , of the ray at the focus. The projected point is identified in equal area projection by a symbol which indicates whether the initial motion of the P-wave is a compression or a rarefaction.

Any plane passing through the center of the model, such as the nodal plane of P, is represented by a great circle on the equal area projection. According to the theory of a double couple, the distribution of compressions and rarefactions found on the focal sphere would be separated by two orthogonal planes. One of these corresponds to the fault plane, the other is a plane perpendicular to the motion on the fault plane and is called the auxiliary plane. The fault plane solution is obtained by drawing two great circles on the projection, separating regions of compression and rarefaction. P-wave first motion data (Tables G-5, 8, 9, 10, 11 and 12), together with the nodal planes for the five 1976 earthquake solutions, are presented in equal area projections in Plates G-5 through G-10. Because of the limited coverage of stations with respect to azimuth and epicentral distance, in many cases it was possible to obtain more than one solution which would satisfy the P first motion data equally well. The orientation of the two nodal planes and the pressure, P, tension, T, and intermediate, B, axes in the focal mechanism solutions for events shown on Plates G-5 through G-10 are summarized in Table G-13.

The graphic summary of focal mechanisms shown on Plate G-11 shows that the range of choices, as indicated by the alternate solutions presented and inherent with the use of composite focal mechanism solutions, is wide and that the data points are few and poorly distributed. It is therefore meaningless to say

that there is a consistency or lack there of among the earthquake focal mechanism solutions. Consequently because of the apparent random distribution of earthquake and nature of focal mechanisms it is at this time only speculation to relate the existing data base to the fault geometry shown on Plate 1A and B.

## G5.0 CONCLUSIONS

The distribution of earthquake epicenters in the vicinity of the Ramapo Fault and surrounding region (Plate G-2) is irregular and shows no noticeable concentration of earthquakes over the mapped extent of the fault. There may, in fact, be more noticeable concentrations in areas removed from the mapped surface trace of the Ramapo Fault.

Based on the historic record it can be said that in the last 193 years, the maximum intensity earthquakes that have occurred within 5 km of the Ramapo Fault are three MM Intensity IV events. Two of these events, December 20, 1962 (located approximately 1 km northwest of the surface trace of the Ramapo Fault), and March 11, 1976 (located approximately 3-5 km northwest of the Ramapo Fault) have been instrumentally located. The magnitude of these earthquakes is approximately 2.0-2.9 with the magnitude of the March 11, 1976 event being slightly less than that of the December 20, 1962 event. The magnitudes for the December 20, 1962 and March 11, 1976 events preferred by Dames & Moore are 2.4 and 2.0 respectively. The 1943 event, which was reported by one person from memory 30 years after the event, was probably no greater than maximum MM Intensity IV. This event may, in fact, actually correspond to the September 4, 1944 Massena, N.Y., earthquake.

Other earthquakes reported felt in the general vicinity of the Ramapo Fault occurred in 1783 (MM Intensity VI

located approximately 12 km northwest of the Ramapo Fault), April 1, 1947 (MM Intensity III located approximately on the Ramapo Fault), July 19, 1975 (calculated MM Intensity II located approximately on the northeast extension of the Ramapo Fault), and September 3, 1951 (MM Intensity V, located approximately 12 km northwest of the Ramapo Fault).

The use of different velocity models results in variations in the epicentral locations of approximately  $\pm 1.5$  to 2.0 km. On the basis of all available data, the solutions preferred by Dames & Moore are obtained using Sykes (1976) velocity model 6. We feel that this model results in epicentral locations accurate to approximately  $\pm 1$  km.

Fault plane solutions (Plate G-11) show that the range of focal solutions is wide and the data are few and poorly distributed. It is therefore concluded that based on the existing data, correlation between individual focal mechanisms specifically and between focal mechanism and fault geometry, in general, is speculative at best.

The earthquakes which may be related to the Ramapo Fault System are small in both number and intensity or magnitude. None of the earthquakes in the vicinity of the Ramapo Fault System is known to have been accompanied by surface faulting or any other observable geological effect. Therefore, no special significance can be ascribed to the Ramapo Fault in relation to contemporary seismicity and tectonics of the region. Although there exist instrumental records from which earthquake locations

can be determined with reasonable precision, we conclude that these earthquakes are small in both number and magnitude and that their relationship to the Ramapo Fault is a matter of speculation.

TABLE G-1

EARTHQUAKE LIST  
40° to 42°N - 73° to 75°W

DATE	H	M (GMT)	S	LAT (NORTH)	LONG (WEST)	INTEN (MM)	MAGNITUDE	REF
				41.4	73.5	IV		ANY
				41.4	73.5	IV		ANY
				41.4	73.5	IV		ANY
6 AUG 1729				41.4	73.5	IV		ANY
19 DEC 1737	4	0		40.8	74.0	VII		EQH
30 NOV 1783	2	0		41.0	74.5			PAG
30 NOV 1783	3	50		41.0	74.5	VI		PAG
30 NOV 1783	7	0		41.0	74.5			PAG
18 MAY 1804				40.7	74.0	III		NYS
25 JAN 1841				40.7	74.0	III		NYS
JUN 1844				41.5	74.2	III		ANY
1 JAN 1845				41.5	74.2	III		ANY
26 OCT 1845				41.0	73.8	V		WGP
9 SEP 1848	4	0		40.8	74.0	V		NYS
17 JAN 1855				40.8	73.6	III		NYS
7 FEB 1855	4	30		42.0	74.0	V		WGP
1 JUL 1858	3	45		41.3	73.0	V		WGP
5 MAR 1861	17	0		40.7	74.2	III		ANY
11 JUL 1872	10	25		40.9	73.8	V		EQH
11 DEC 1874	3	25		40.9	73.8	V		WGP
28 JUL 1875	9	10		41.8	73.2	V		EQH
26 SEP 1875	2	0		41.3	73.3	II		ANY
10 SEP 1877	14	59		40.3	74.9	V		EQH
5 FEB 1878	16	20		40.7	73.7	V		WGP
4 OCT 1878	7	30		41.5	74.0	V		EQH
25 DEC 1878	2	0		40.8	73.8	II		NYS
21 APR 1881	16	30		40.9	73.1	III		NYS
10 AUG 1884	19	7		40.6	74.0	VII		EQH
4 JAN 1885	11	6		41.3	73.9	III		NYS
31 JAN 1885	10	5		41.3	73.8	III		NYS
9 MAR 1893	5	30		40.6	74.0	V		EQH
1 SEP 1895	11	9		40.7	74.8	VI		EQH
5 FEB 1908	8	20		41.4	73.2	IV		ANY
23 APR 1910				New Jersey Coast		IV		NJS
1 MAY 1910				40.7	73.5	II		NYS
8 JUN 1916	21	15		41.0	73.8	V		EQH
26 JAN 1921	23	40		40.0	75.0	V		EQH
24 OCT 1925	1	30		41.4	73.3	III		ANY
26 JAN 1926	23	40		40.0	75.0	V		ANY
12 MAY 1926	3	30		40.9	73.9	V		EQH

TABLE G-1 (continued)

## EARTHQUAKE LIST

DATE	H	M (GMT)	S	LAT (NORTH)	LONG (WEST)	INTEN (MM)	MAGNITUDE	REF
22 MAY 1926				41.7	73.9	II		NYS
1 JUN 1927	12	20		40.3	74.0	VII		EQH
1 JUL 1931	2	45		41.6	73.4	IV	3.6	EPB
25 JAN 1933	2	0		40.2	74.7	V	4.3	EPB
26 JUN 1933	14	10		41.0	73.8	III	3.0	EPB
19 JUL 1937	3	51		40.7	73.7	IV		USE
30 SEP 1937	22	8	22.0	40.8	74.2	III	3.0	EPB
1 OCT 1937	3	8		40.8	74.2	III		USE
12 OCT 1937	3	0		41.2	73.8	II	2.4	EPB
16 MAY 1938	19	25		40.8	74.3	III	2.7	EPB
14 JUN 1938	4	2		41.4	73.4	II	2.4	EPB
14 JUN 1938	19	30		41.4	73.4	I	1.7	EPB
29 JUL 1938	7	44	7.0	41.0	73.7	III	3.0	EPB
2 AUG 1938	10	2		41.1	73.7	IV		USE
23 AUG 1938	3	36	34.0	40.2	74.2	V	4.6	EPB
23 AUG 1938	5	4	55.0	40.2	74.2	VI	4.8	EPB
23 AUG 1938	5	18	23.0	41.2	73.7	III	3.0	EPB
23 AUG 1938	7	3	29.0	40.2	74.2	V	4.6	EPB
23 AUG 1938	7	11	46.0	41.2	73.7	III	3.0	EPB
23 AUG 1938	11	11	6.0	40.2	74.2	IV	3.7	EPB
27 AUG 1938	22	36	25.0	40.2	74.2	III	3.0	EPB
21 OCT 1938	7	18	55.0	41.2	73.7	II	2.3	EPB
6 DEC 1938	19	38		40.8	74.3	III	3.0	EPB
13 SEP 1939	1	22	4.0	40.8	74.0	II	2.3	EPB
21 SEP 1939	20	30	1.0	41.4	74.1	II	2.3	EPB
22 SEP 1939				40.8	73.8	I		NYS
28 JUL 1941	19	24	10.0	41.1	73.8	III	3.0	EPB
1943				41.1	74.2	V		NJS
4 JAN 1947	18	51	4.0	41.0	73.6	V	4.3	EPB
1 APR 1947	13	25	54.0	41.0	74.3	III	3.0	EPB
29 MAR 1950	14	43	2.0	41.0	73.6	IV	3.6	EPB
3 SEP 1951	21	26	24.5	41.22	74.22	V	4.4	D-M
8 DEC 1951	4	37		41.7	73.9	III	2.7	EPB
8 OCT 1952	21	40		41.7	74.0	V	4.3	EPB
27 MAR 1953	8	50		41.1	73.5	V	4.3	EPB
17 AUG 1953	4	22	50.0	41.0	74.0	IV	3.7	EPB
31 MAR 1954	21	25		40.2	74.0	IV	3.6	EPB
23 MAR 1957	19	2		40.6	74.8	VI	4.8	ANY
13 APR 1959	21	20	19.0	41.9	73.3	IV	3.4	EPB
27 DEC 1961	17	6		40.1	74.8	V		ANY

TABLE G-1 (continued)

## EARTHQUAKE LIST

DATE	H	M (GMT)	S	LAT (NORTH)	LONG (WEST)	INTEN (MM)	MAGNITUDE	REF
6 MAR 1962				6 miles from Ogdensburg				NJS
11 AUG 1962				12 miles from Ogdensburg				NJS
13 OCT 1962	4	9	42.0	41.0	74.3		1.0	ANY
27 NOV 1962	9	14	50.0	41.6	73.9	I*	1.7	NYS
20 DEC 1962	8	1	41.0	41.0	74.3	IV	2.4D-M 2.9PAL	ANY
24 JUN 1963				17 miles from Ogdensburg				NJS
29 SEP 1964	0	16	27.5	41.2	73.7	II		NYS
29 SEP 1964	20	26	49.5	41.2	73.7	II		NYS
17 NOV 1964	17	8		41.2	73.7	V	4.3	EPB
30 NOV 1964	10	47	32.4	41.3	73.9		1.0	NYS
29 SEP 1965	20	57	39.5	41.4	74.4	IV		NYS
21 MAY 1966	7	30	55.0	41.2	74.0		1.3	NYS
22 NOV 1967	10			41.2	73.8	V		NYS
25 APR 1969	0	14	41.4	40.7	74.3			USE
14 AUG 1969				41.0	74.6			
14 SEP 1969				41.0	74.6			NJS
6 OCT 1969				41.0	74.6	IV		NJS
10 OCT 1969				41.0	74.6			NJS
3 NOV 1969				41.0	74.6			NJS
15 FEB 1972	23	53	14.6	41.3	73.6	II*	2.6PAL	PAL
29 DEC 1972	1	34		41.0	74.2	III		NJS
10 JAN 1973	2	41	18.5	41.4	74.0	I*	1.5PAL	PAL
5 FEB 1973				41.0	74.1	II		NJS
8 APR 1974	22	8	21.5	41.2	74.0	II*	2.1PAL	PAL
17 MAY 1974	15	7	31.9	41.2	75.0			PAL
7 JUN 1974	19	45	36.8	41.6	73.9	III*	3.3PAL	PAL
2 MAR 1975	11	8	10.3	41.2	73.6			PAL
29 APR 1975	9	51	55.8	41.6	73.9	II*	2.3PAL	PAL
15 JUN 1975	8	8	49.6	41.6	73.9	II*	2.0PAL	PAL
19 JUL 1975	20	59	32.2	41.4	73.8	II*	2.3PAL	PAL
22 AUG 1975	17	49	22.2	41.1	73.9	II*	2.3PAL	PAL
** 8 OCT 1975	19	2	43.2	41.3	74.0			PAL
24 OCT 1975	7	8	46.4	41.6	74.0	II*	2.0PAL	PAL
24 OCT 1975	7	43	12.4	41.6	73.9	II*	2.2PAL	PAL
10 NOV 1975	03	02		41.18	74.38	I*	1.8PAL	PAL
**12 FEB 1976	14	47		41.34	73.88	I*	1.5PAL	PAL
6 MAR 1976	04	14		41.26	73.93		1.0PAL	PAL
11 MAR 1976	21	07	20.2	40.98	74.37	IV	2.0D-M 2.5PAL	D-M

\*Calculated Intensity (see explanatory note at end of Table)

\*\*Probable earthquake

TABLE G-1 (continued)

## EARTHQUAKE LIST

DATE	H	M	S	LAT	LONG	INTEN	MAGNITUDE	REF
		(GMT)		(NORTH)	(WEST)	(MM)		
12 MAR 1976	10	28	56.8	40.96	74.37	II		D-M
13 APR 1976	15	39	13.9	40.85	74.05	V	3.0PAL	D-M
20 AUG 1976	22	8	14.3	41.12	73.76			D-M
22 SEP 1976	9	4	44.9	41.29	73.95		1.8PAL	D-M
22 NOV 1976	4	43		41.02	73.88		1.9C-E	C-E

NOTES:

1. The magnitude listed on the printout (Table G-1) is chosen in the following order: Local ML, CGS MB, CGS MS, Other MS, blank if no magnitude information.
2. When maximum intensity is not given, an estimated intensity is calculated by using the relation:  $M=1 + 2/3 I$ . The calculated intensity is indicated by an asterisk. However, a large percentage of our data cards were obtained from - Earth Physics Branch, Dept. of Energy, Mines and Resources, Canada (EPB), which converted the original intensity values, for earthquakes occurring before 1899, into Local Magnitude (ML), by using the above relation. Many magnitudes for earthquakes after 1899 were also converted from intensity values. However, because on the cards received from EPB, no distinction is made between Local Magnitude, ML, determined instrumentally and those estimated from intensity, the calculated intensities in this situation are not indicated by the asterisk.
3. The following abbreviations are used in Table G-1:

ANY Earthquakes adjacent to New York State (N.Y. State Geological Survey)  
 C-E Con Edison Seismic Monitoring Network (sixth quarterly report)  
 CGS Coast and Geodetic Survey  
 D-M Dames & Moore (this study)  
 EEC Earthquakes in Eastern Canada, Smith (1962)  
 EPB Earth Physics Branch, Dept. of Ener. Mines and Res., Canada  
 EQH Earthquake History of the United States, Coffman and Von Hake (1973)  
 ERL Environmental Research Laboratories (NOAA)  
 G-R Gutenberg and Richter (1953)  
 GS U.S. Geological Survey  
 NJS New Jersey State Geological Survey, Dombroski (1973)  
 NOS National Ocean Survey (NOAA)  
 NUT Nuttly (1974)  
 NYS Earthquakes within New York State (N.Y. State Geological Survey)  
 PAG Page et al. (1968)  
 PAL Lamont Doherty Geological Observatory, Palisades  
 USE U.S. Earthquakes, Yearly Publication (NOAA)  
 WGP Weston Geophysical

TABLE G-2

## LIST OF EPICENTERS IN THE VICINITY OF THE RAMAPO FAULT\*

DATE		(GMT)			LAT (NORTH)	LONG (WEST)	INTEN (MM)	MAGNITUDE	REF <sup>(4)</sup>
		H	M	S					
30 NOV	1783	2	0		41.0	74.5			PAG
30 NOV	1783	3	50		41.0	74.5	VI		PAG
30 NOV	1783	7	0		41.0	74.5			PAG
4 JAN	1885	11	6		41.3	73.9	III		NYS
31 JAN	1885	10	5		41.3	73.8	III		NYS
	1943				41.1	74.2	V		NJS
1 APR (3)	1947	13	25	54.0	41.0	74.3	III	3.0	EPB
3 SEP (3)	1951	21	26	24.5	41.22	74.22	V	4.4	D-M
13 OCT (3)	1962	4	9	42.0	41.0	74.3		1.0	ANY
20 DEC (3)	1962	8	1	41.0	41.0	74.3	IV	2.4 D-M	ANY
30 NOV (3)	1964	10	47	32.4	41.3	73.9		1.0	NYS
21 MAY (3)	1966	7	30	55.0	41.2	74.0		1.3	NYS
29 DEC	1972	1	34		41.0	74.2	III		NJS
10 JAN	1973	2	41	18.5	41.4	74.0	I <sup>(1)</sup>	1.5 PAL	PAL
5 FEB (3)	1973				41.0	74.1	II		NJS
8 APR (3)	1974	22	8	21.5	41.2	74.0	II <sup>(1)</sup>	2.1 PAL	PAL
19 JUL (3)	1975	20	59	32.2	41.43	73.79	II <sup>(1)</sup>	2.3 PAL	PAL
8 OCT (2) (3)	1975	19	2	43.2	41.3	73.97			PAL
12 FEB (2) (3)	1976	14	47		41.34	73.88	I <sup>(1)</sup>	1.5	PAL
6 MAR (3)	1976	4	14		41.26	73.93		1.0	PAL
MAR (3)	1976	21	7	20.2	40.98	74.37	IV	2.0 D-M	D-M
MAR (3)	1976	10	28	56.8	40.96	74.37	II		D-M
22 SEP (3)	1976	9	4	44.9	41.29	73.95		1.8 PAL	D-M

\* Reference Plate G-2 for area of coverage.

(1) Calculated Intensity (see Table G-1)

(2) Probable Earthquake

(3) Epicenters instrumentally located

(4) See Table G-1 for abbreviations

TABLE G-3

## P AND S ARRIVAL TIME DATA FOR THE SEPTEMBER 3, 1951 EARTHQUAKE

Code	Station		P			S			S-P
	Latitude N	Longitude W	h	m	s	h	m	s	
PAL	41° 00.25'	73° 54.55'	21	26	32.5	21	26	36.6	4.1
CNY	40° 49.30'	73° 57.20'	21	26	34.8	21	26	40.4	5.6
FOR	40° 51.78'	73° 53.13'							5.6
WES	42° 23.08'	71° 19.33'	21	27	18				
OTT	45° 23.63'	75° 42.95'	21	27	44				

Amplitude Measurement on Palisades Records.

Trace amplitude on short period N-S component seismogram = 4.3mm S

Trace amplitude on short period E-W component seismogram = 4.0mm E

First motion direction from vertical component seismogram-Compression

Azimuth of the epicenter from Palisades

$$= N \tan^{-1} (4.0/4.3) W$$

$$= N 43^\circ W$$

Azimuth of the epicenter from Palisades, applying Sykes' correction for the misalignment of seismographs of  $8^\circ \pm 1^\circ$  off from the cardinal azimuths of north and east,

$$= N51^\circ W$$

TABLE G-4

## LOCATION OF THE SEPTEMBER 3, 1951 EARTHQUAKE

No.	Velocity Model			Hypocenter Location					Depth (fixed) km	Azimuth of the Epicenter from Palisades
	V <sub>P</sub> km/sec	Depth km	V <sub>P</sub> /V <sub>S</sub>	Origin Time h m s			Latitude N	Longitude W		
1	5.00 6.05 6.30 8.10	0.0 1.0 4.5 35.0	1.69	21	26	26.6	41° 12.5'	74° 13.6'	0.5	N50°W
2	Same as Above			21	26	26.5	41° 13.4'	74° 13.3'	5.0	N47°W
3	5.00 6.05 6.35 8.10	0.0 1.5 4.0 35.0	1.69	21	26	26.5	41° 12.9'	74° 12.5'	0.5	N47°W
4	Same as Above			21	26	26.5	41° 13.5'	74° 13.2'	5.0	N47°W
5	5.00 6.05 6.35 8.10	0.0 1.5 4.5 35.0	1.69	21	26	26.6	41° 12.5'	74° 13.0'	0.5	N49°W
6	Same as Above			21	26	26.5	41° 13.5'	74° 13.1'	5.0	N47°W
7	5.00 6.05 6.30 8.10	0.0 1.5 4.5 35.0	1.69	21	26	26.6	41° 12.2'	74° 13.2'	0.5	N50°W
8	Same as Above			21	26	26.5	41° 13.3'	74° 13.2'	5.0	N47°W
9	5.00 6.30 8.10	0.0 1.5 35.0	1.69	21	26	26.5	41° 13.4'	74° 13.2'	0.5	N47°W
10	Same as Above			21	26	26.5	41° 13.7'	74° 13.5'	5.0	N47°W

TABLE G-4 (Continued)

No.	Velocity Model			Hypocenter Location						
	V <sub>P</sub> km/sec	Depth km	V <sub>P</sub> /V <sub>S</sub>	Origin h	Time m	s	Latitude N	Longitude W	Depth (fixed) km	Azimuth of the Epicenter from Palisades
11	6.20	0.0	1.72	21	26	26.9	41° 12.6'	74° 13.5'	0.5	N49°W
12	Same as Above			21	26	26.9	41° 12.6'	74° 13.3'	5.0	N49°W
13	5.00 6.04	0.0 1.0	1.67	21	26	26.3	41° 13.1'	74° 14.0'	.50	N49°W
14	Same as Above			21	26	26.3	41° 13.2'	74° 14.0'	5.0	N49°W
15	4.66 5.64	0.0 1.0	1.67	21	26	26.4	41° 11.0'	74° 13.9'	.50	N54°W
16	Same as Above			21	26	26.4	41° 11.1'	74° 14.0'	5.0	N54°W
17	5.40	0.0	1.76	21	26	27.3	41° 07.8'	74° 12.2'	.50	N61°W
18	Same as Above			21	26	27.3	41° 07.8'	74° 11.9'	5.0	N60°W
19	6.31 8.14	0.0 34.4	1.75	21	26	27.2	41° 12.2'	74° 13.0'	.50	N49°W
20	Same as Above			21	26	27.2	41° 12.3'	74° 12.6'	5.0	N49°W
21	6.04 8.14	0.0 34.4	1.67	21	26	26.4	41° 13.4'	74° 14.6'	.50	N49°W
22	Same as Above			21	26	26.3	41° 13.4'	74° 14.4'	5.0	N49°W
23	5.98 6.62 8.10	0.0 7.0 35.0	1.69	21	26	25.6	41° 12.5'	74° 14.0'	.50	N50°W
24	Same as Above			21	26	26.5	41° 13.9'	74° 12.2'	5.0	N46°W

G-26

TABLE G-5

## P AND S ARRIVAL TIME DATA FOR THE MARCH 11, 1976 EARTHQUAKE

Code	Station		P			First Motion	S
	Latitude N	Longitude W	h	m	s		
PNJ	40 54.43	74 09.29	S-P=2.30 s			-	
TBR	41 08.50	74 13.33	21	7	24.51	D	27.15
OGD	41 05.25	74 35.75	21	7	24.42	N	27.02
CHR	41 12.49	74 03.26	21	7	26.66	D	31.15
PAL	41 00.25	73 54.55	21	7	27.00	D	31.50
STL	41 11.32	74 00.22	21	7	27.06		31.78
SRM	41 13.70	74 00.82	21	7	27.29	D	32.34
SNP	41 14.45	73 58.28	21	7	27.85		33.20
GSC	41 15.98	74 00.24	21	7	27.80	D	33.14
DBM	41 17.68	73 58.50	21	7	28.38	D	34.17
DPL	41 15.17	73 54.65	21	7	28.38		34.14
SSL	41 09.67	74 54.96	21	7	28.75	D	
BLM	41 19.78	73 57.31	21	7	29.04	D	35.26
SPS	41 18.12	73 53.44	21	7	29.26		35.77
GOB	41 19.77	73 55.31	21	7	29.33	D	35.85
OSB	41 21.62	73 55.44	21	7	29.73	D	36.41
WGL	41 21.53	73 53.96	21	7	29.90	D	36.75
PQN	41 00.44	75 05.15	21	7	30.31	C	37.37
WPR	41 15.28	73 35.14	21	7	32.22	D	40.67
BPT	41 13.32	73 14.53	21	7	36.30	+	
BCT	41 29.60	73 23.03	21	7	36.60	D	
ECT	41 50.07	73 24.68	21	7	40.90		55.10
TMT	41 48.67	72 47.93	21	7	46.50		64.70
HDM	41 29.15	72 31.39	21	7	46.80		65.30
NED	39 42.25	75 42.49	21	7	49.20	C	68.00
UCT	41 49.90	72 15.03	21	7	52.30		

## NOTE:

C clear compression; + compression

D clear dilatation; - dilatation

N nodal arrival

The first motion at Ogdensburg (OGD) may be read as a less reliable dilatation (-), or as a nodal arrival from a consideration of very small P amplitude as compared to S amplitude.

The first motion readings at PNJ and Consolidated Edison Seismic Monitoring Network Stations, with the exception of GSC and DBM, were corrected (reversed) for instrumental polarity. The playbacks of Nevada Test Site (NTS) explosions of February 12, 1976 at DBM and March 17, 1976 at GSC, show compression and suggest that the instrumental polarity of these two stations were most likely correct on March 11, 1976.

TABLE G-6

## LOCATION OF THE MARCH 11, 1976 Earthquake

No.	Velocity Model			Hypocenter Location							Number of P Data	Number of S Data	RMS sec
	V <sub>P</sub> km/sec	Depth km	V <sub>P</sub> /V <sub>S</sub>	Origin Time			Latitude		Longitude	Depth			
				h	m	s	N	W	km				
1	5.00 6.05 6.30 8.10	0.0 1.0 4.5 35.0	1.69	21	7	20.41	40° 58.19' ±.75km	74° 21.95' ±.27km	6.8±1.4	24	0	0.10	
2	Same as Above			21	7	20.10	40° 57.65' ±.46km	74° 21.97' ±.24km	0.1±0.7	25	20	0.15	
3	5.00 6.05 6.35 8.10	0.0 1.5 4.0 35.0	1.69	21	7	20.27	40° 58.19' ±.52km	74° 22.11' ±.29km	1.1±1.8	25	0	0.10	
4	Same as Above			21	7	20.15	40° 58.15' ±.38km	74° 22.14' ±.20km	0.1±0.5	25	20	0.12	
5	5.00 6.05 6.35 8.10	0.0 1.5 4.5 35.0	1.69	21	7	20.40	40° 58.19' ±.44km	74° 22.11' ±.24km	4.3±3.4	25	0	0.09	
6	Same as Above			21	7	20.18	40° 58.10' ±.40km	74° 22.13' ±.21km	0.6±0.6	25	20	0.13	
7	5.00 6.05 6.30 8.10	0.0 1.5 4.5 35.0	1.69	21	7	20.33	40° 57.92' ±.76km	74° 22.00' ±.27km	5.0±1.7	24	0	0.10	
8	Same as Above			21	7	20.21	40° 57.57' ±.37km	74° 21.96' ±.23km	2.5±0.9	25	20	0.13	

TABLE G-6 (Continued)

No.	Velocity Model			Hypocenter Location							Number of P Data	Number of S Data	RMS sec	
	V <sub>P</sub> km/sec	Depth km	V <sub>P</sub> /V <sub>S</sub>	Origin Time			Latitude		Longitude					Depth km
				h	m	s	N		W					
9	5.00 6.30 8.10	0.0 1.5 35.0	1.69	21	7	20.44	40°	57.80' + <u>.47</u> km	74°	21.98' + <u>.25</u> km	1.6+ <u>1.5</u>	25	0	0.10
10	Same as Above			21	7	20.40	40°	57.37' + <u>.44</u> km	74°	22.15' + <u>.25</u> km	2.7+ <u>1.9</u>	25	20	0.14
11	6.20	0.0	1.72	21	7	20.22	40°	57.06' + <u>.52</u> km	74°	21.70' + <u>.28</u> km	9.8+ <u>1.5</u>	24	0	0.10
12	Same as Above			21	7	20.28	40°	57.71 + <u>.48</u> km	74°	21.93' + <u>.25</u> km	9.9+ <u>1.3</u>	25	20	0.14
13	5.00 6.04	0.0 1.0	1.67	21	7	19.52	40°	55.66' + <u>.70</u> km	74°	21.16' + <u>.38</u> km	13.6+ <u>1.6</u>	24	0	0.12
14	Same as Above			21	7	19.62	40°	56.44' + <u>.57</u> km	74°	21.42' + <u>.30</u> km	13.9+ <u>1.2</u>	25	20	0.15
15	4.66 5.64	0.0 1.0	1.67	21	7	17.91	40°	51.84' + <u>1.69</u> km	74°	19.38' + <u>.96</u> km	18.2+ <u>3.6</u>	24	0	0.31
16	Same as Above			21	7	18.63	40°	55.85' + <u>1.66</u> km	74°	21.00' + <u>.86</u> km	15.0+ <u>3.4</u>	25	20	0.49
17	5.40	0.0	1.76	21	7	17.23	40°	49.43' + <u>2.30</u> km	74°	18.17' + <u>1.35</u> km	13.2+ <u>6.2</u>	24	0	0.46
18	Same as Above			21	7	18.30	40°	55.62' + <u>2.95</u> km	74°	19.66' + <u>1.59</u> km	9.6+ <u>8.6</u>	25	18	0.99

TABLE G-6 (Continued)

No.	Velocity Model			Hypocenter Location							Number of P Data	Number of S Data	RMS sec
	V <sub>P</sub> km/sec	Depth km	V <sub>P</sub> /V <sub>S</sub>	Origin Time			Latitude	Longitude	Depth				
				h	m	s	N	W	km				
19	6.31 8.14	0.0 34.4	1.75	21	7	20.64	40° 57.94' + <u>.47</u> km	74° 22.05' + <u>.25</u> km	3.1+ <u>2.0</u>	25	0	0.10	
20	Same as Above			21	7	20.67	40° 58.10' + <u>.41</u> km	74° 22.00' + <u>.23</u> km	1.3+ <u>1.8</u>	25	19	0.14	
21	6.04 8.14	0.0 34.4	1.67	21	7	19.92	40° 55.67' + <u>1.32</u> km	74° 21.00' + <u>.48</u> km	3.1+ <u>2.0</u>	25	0	0.16	
22	Same as Above			21	7	20.05	40° 56.87' + <u>.63</u> km	74° 21.67' + <u>.30</u> km	8.2+ <u>0.7</u>	25	21	0.16	
23	5.98 6.62 8.10	0.0 7.0 35.0	1.69	21	7	20.84	41° 59.27' + <u>.74</u> km	74° 22.72' + <u>.40</u> km	6.6+ <u>0.9</u>	25	0	0.14	
24	Same as Above			21	7	20.60	40° 58.85' + <u>.68</u> km	74° 22.14' + <u>.40</u> km	3.6+ <u>0.7</u>	25	18	0.23	

TABLE G-7

## P AND S ARRIVAL TIME DATA FOR THE DECEMBER 20, 1962 EARTHQUAKE

Code	STATION		h	P			First Motion	S		
	Latitude N	Longitude W		m	s			h	m	s
SFO	41° 11.77'	74° 15.67'	8	1	45.00		D			
OGD	41° 05.25'	74° 35.75'	8	1	45.25		D	8	1	48.25
PAL	41° 00.25'	73° 54.55'	8	1	46.75		D	8	1	50.85

Note: D dilatation

The following epicentral location for a near surface (0.5 km deep) focus was obtained by using Sykes (1976) velocity Model 6.

Velocity Model		Epicenter Location	
$V_p$	Depth	Latitude	Longitude
km/sec	km	N	W
5.98	0	40° 58.93'	74° 19.37'
6.62	7		
8.10	35		

A comparison of the seismograms for the December 20, 1962 and March 11, 1976 events at Ogdensburg indicated that the December 20, 1962 earthquake was larger in magnitude by about 0.4 units than the March 11, 1976 event.

Using Nuttli (1973) equation No. 5:

$$m_b = 3.75 + 0.90 (\log \Delta) + \log A/T$$

for  $0.5^\circ \leq \Delta \leq 4^\circ$

where

$m_b$  = magnitude,

$\Delta$  = distance in degrees from epicenter to seismograph,

A = zero-to-peak amplitude in microns

$$\text{(for March 11, 1976 } A = \frac{2,600 \text{ microns}}{75,000 \text{ (amplification factor [gain])}})$$

T = period of wave in seconds

(for March 11, 1976 T = 0.5 second wave)

The March 11, 1976 event equals magnitude 2.0. Therefore the magnitude of the December 20, 1976 event becomes 2.4.

TABLE G-8

## P AND S ARRIVAL TIME DATA FOR THE MARCH 12, 1976 EARTHQUAKE

Station Code	h	P m	s	First Motion	S s
TBR	10	29	.80	D	3.67
CHR	10	29	3.03	C	7.47
SRM	10	29	3.62	D	8.67
SNP	10	29	4.32		9.67
GSC	10	29	4.17	C	9.50
DBM	10	29	4.77	C	10.47
SSL	10	29	5.14		
BLM	10	29	5.41	C	11.57
SPS	10	29	5.59		11.94
GOB	10	29	5.68		12.49
OSB	10	29	6.09	C	12.76
WGL	10	29	6.37		13.21
PQN	10	29	6.57	C	13.66
WPR	10	29	8.44	D	16.84
BPT	10	29	13.10		
BCT	10	29	13.50		24.50
ECT	10	29	17.20		31.60

NOTE: For explanation of symbols and instrumental polarity corrections, see notes in Table G-5

The following epicentral location was obtained by using Sykes' (1971) velocity Model 6.

Hypocenter Location									
Origin Time			Latitude	Longitude	Depth	Number of	Number of	RMS	
h	m	s	N	W	km	P Data	S Data	sec.	
10	28	56.76	40° 57.77'	74°22.14'	4.20±0.8	17	14	.21	
			±1.12 km	±.56 km					

TABLE G-9

P AND S ARRIVAL TIME DATA FOR THE APRIL 13, 1976 EARTHQUAKE

Station Code	h	P m	s	First Motion	S s
AMM		S-P=1.25			
FOR	15	39	15.40	D	
PNJ				D	
PAL	15	39	17.42	C	
TBR	15	39	19.68	D	
STL				C	24.34
SRM	15	39	20.69		25.93
SNP	15	39	20.88	C	26.14
DPL	15	39	21.31	-	26.46
GSC	15	39	21.37	D	27.29
IPS	15	39	21.46	C	27.38
DBM	15	39	21.91	D	27.33
SPS	15	39	22.17	+	28.41
OGD	15	39	22.36	C	28.68
BLM					29.24
GOB	15	39	22.68		29.62
OSB	15	39	23.17		30.32
WPR	15	39	23.31	C	30.49
BPT	15	39	26.60	D	35.70
SSL	15	39	26.74	D	34.30
PQN	15	39	27.80	D	38.34
BCT	15	39	28.30	D	39.40
ECT	15	39	33.20	D	47.50
HDM	15	39	36.80	D	53.20
TMT	15	39	37.70		54.70
APT	15	39	41.20		60.20
UCT	15	39	42.90		62.20

The following epicentral location was obtained by using Sykes' (1976) velocity Model 6.

Hypocenter Location								
Origin Time			Latitude N	Longitude W	Depth km	Number of P Data	Number of S Data	RMS s
h	m	s						
15	39	13.29	40°49.91' ±.78 km	74°02.81' ±.38 km	0.2 ±1.4	24	0	.15
15	39	13.50	40°50.55' ±.38 km	74°02.60' ±.35 km	2.4 ±0.5	24	20	.19

TABLE G-10

## P AND S ARRIVAL TIME DATA FOR THE AUGUST 20, 1976 EARTHQUAKE

Station Code	h	P m	s	First Motion	S s	S-P s
PAL	22	8	17.54	D	19.74	
DPL				C		2.57
WPR			17.88	D	20.48	
STL				-		2.91
SNP				C		2.80
IPS				C		2.88
GSC				C		3.26
DBM				C		3.21
CHR				C		3.42
BLM				C		3.60
OSB						3.54
TBR	22	8	20.59	D	25.30	
BPT	22	8	21.70	D	27.00	
BCT	22	8	22.70	D	28.80	
ECT	22	8	27.90	C	37.60	
HDM	22	8	32.00	D	44.30	
PQN	22	8	32.04	+		

The following epicentral location was obtained by using Sykes' (1976) velocity Model 6.

Hypocenter Location					Number of P Data	Number of S Data	Number of S-P Data	RMS s
Origin Time	Latitude	Longitude	Depth					
h m s	N	W	km					
22 8 14.32	41°07.49' + 1.32 km	73°45.90' + .80 km	5.0+1.5	8	0	0	.14	
22 8 14.30	41°07.17' + .32 km	73°45.62' + .24	5.8+0.5	8	7	9	.13	

TABLE G-11

P AND S ARRIVAL TIME DATA FOR THE SEPTEMBER 22, 1976 EARTHQUAKE

Station Code	h	P m	s	First Motion	S s	S-P s
IPS	9	4	46.27	C	47.24	
DBM	9	4	46.28	C	47.25	
SNP	9	4	46.45	C	47.66	
DPL	9	4	46.46	C	47.67	
BLM	9	4	46.46	C	47.56	
SPS	9	4	46.50	C	47.66	
GOB	9	4	46.53	C	47.68	
SRM	9	4	46.84	+	48.21	
OSB	9	4	46.86	C	48.24	
WGL	9	4	46.95		48.35	
CHR	9	4	47.30	C	48.97	
TBR	9	4	49.52	D		
WPR	9	4	50.10	-	52.85	
GPD					60.09	
BCT				C		6.30

The following epicentral location was obtained by using Sykes' (1976) velocity Model 6.

Hypocenter Location									
Origin Time			Latitude N	Longitude W	Depth km	Number of P Data	Number of S Data	Number of S-P Data	RMS s
h	m	s							
9	4	44.89	41°17.02' ± .12 km	73°57.24' ± .12 km	8.1±0.2	13	0	1	.03
9	4	44.93	41°17.18' ± .21 km	73°57.10' ± .23 km	7.8±0.3	13	13	1	.09

TABLE G-12

P AND S ARRIVAL TIME DATA FOR THE NOVEMBER 22, 1976 EARTHQUAKE

Station Code	h	P m	s	First Motion	S s
PAL	04	43	14.50	C	15.40
SNP	04	43	18.32	D	21.82
DPL	04	43	18.28	C	21.84
IPS	04	43	18.55	C	22.47
GSC					22.22
SPS	04	43	19.04		23.29
DBM	04	43	19.14		23.37
TBR	04	43	19.29		23.63
WPR	04	43	19.60		23.75
GOB	04	43	19.56	D	24.50
GPD	04	43	21.71	D	27.83
BPT	04	43	22.85		29.70
BCT	04	43	24.45	C	32.70
ECT	04	43	29.70	C	41.30

The following epicentral location was obtained by using Sykes' (1976) velocity Model 6.

Hypocenter Location						Number of P Data	Number of S Data	RMS s
Origin Time h m s	Latitude N	Longitude W	Depth km					
04 43 13.49	41°00.19' ±.40 km	73°51.71' ±.35 km	4.5±0.5	11	0	.06		
04 43 13.48	41°00.12' ±.23 km	73°51.79' ±.25 km	5.0±0.3	12	13	.09		

TABLE G-13

## FAULT PLANE SOLUTIONS

Date	Depth Km	Plate	P		T		B		Nodal Planes			
			$\phi$	$\theta$	$\phi$	$\theta$	$\phi$	$\theta$	Dip Direction	Dip	Dip Direction	Dip
July 19, 1975	3.2	G-4	156	25	336	65	66	0	156	70	336	20
March 11, 1976	3.6	G-5a	346	13	203	74	74	15	143	33	354	58
		G-5b	353	23	173	67	83	0	353	68	173	22
March 12, 1976	4.2	G-6a	144	32	288	53	42	18	128	79	8	21
		G-6b	134	48	314	42	44	0	134	3	314	87
		G-6c	128	34	308	56	38	0	128	79	308	11
April 13, 1976	2.4	G-7	263	18	130	66	358	17	59	32	277	63
August 20, 1976	5.8	G-8a	290	83	148	6	54	4	145	50	333	40
		G-8b	244	14	153	0	60	75	18	79	109	81
		G-8c	270	31	150	40	24	35	36	35	298	84
September 22, 1976	7.8	G-9	331	9	151	81	61	0	331	54	151	36
November 22, 1976	5.0	G-10a	275	21	95	69	185	0	95	24	275	66
		G-10b	267	71	64	18	156	7	70	63	233	28
		G-10c	306	29	215	0	126	62	76	70	174	70

Note:  $\phi$ , trend measured clockwise from the north

$\theta$ , plunge measured from the horizontal

APPENDIX H

IN SITU STRESS MEASUREMENTS

APPENDIX H  
IN SITU STRESS MEASUREMENTS

H.1.0 INTRODUCTION

H.1.1 PURPOSE AND SCOPE

The purpose of the in-situ stress investigation near the Indian Point Site was: 1) to measure and evaluate near surface bedrock stresses in the vicinity of the Ramapo Fault; and 2) to establish if possible, whether the state of stress near the fault is significantly different than that in the region.

Stress measurements were made at four test sites in the vicinity of the Indian Point Site in the spring of 1976. This report presents the results of the in-situ measurements together with other laboratory data used to establish the stress field at the sites. These measurements are compared to others reported in the geologic literature for northeastern North America.

H.1.2 SITE SELECTION AND DESCRIPTIONS

An area around the Ramapo Fault System in the vicinity of Indian Point was surveyed for the purpose of locating suitable test sites. This survey was made between January and April, 1976 and resulted in the selection of twenty-four potential sites for further consideration. The potential sites were evaluated according to:

1. Ease of access to truck-mounted drill rig;
2. Overburden not exceeding 20 feet;

3. Bedrock exposures relatively fresh and unbroken, free of intense faulting and fracturing;
4. Situated away from significant topographic relief; and,
5. Preferably located on public land.

The selection of the final measurement sites was based on local geology and the results of exploratory borings. An NWX exploratory boring was drilled to determine the depth of overburden and the condition of the bedrock at depth. The stress measurements were conducted at four sites during the period of February to May, 1976. As shown on Plate H-1, the site locations form a triangle, the base of which is perpendicular to the Ramapo Fault System. Measurements were made by the overcoring technique using the U.S. Bureau of Mines gage. Logs of the exploratory and overcored borings are presented in Plates H-2 to H-11.

The first site, #3, is located along Tiorati Road, approximately 100 feet east of Lake Tiorati, New York, within the Bear Mountain State Park. It is situated in the central part of the Hudson Highlands, within a block of Precambrian gneisses bounded by two large faults striking north-northeast and northeast. The site is 3.5 miles northwest of the Ramapo Fault. The bedrock at the site consists of medium grained gneiss. Rock quality is good to excellent. Ten measurements were performed at depths ranging from 17 to 38 feet from the surface.

The second site, #9, is located approximately 50 feet east of the Palisades Parkway, along the Cedar Flats Road

entrance to the Parkway, near Pingyp Mountain, New York. It is situated near the eastern edge of the Hudson Highlands, on the western side of the Cedar Flats Fault. The rock at the site is a coarse to medium grained hornblende gneiss. Rock quality is fair to good. Seven measurements were made at depths ranging from 30 to 44 feet from the surface.

The third site, #11, is located along Pleasantville Road near Briarcliff Manor, directly below Consolidated Edison transmission lines which were inoperative at the time. It is situated within the Manhattan Prong, about four miles southeast of the northeasterly trending Croton Falls Fault System. The rock at the site is Manhattan Schist of Lower Paleozoic age. Rock quality is fair to excellent. Thirteen measurements were performed at depths ranging from 14 to 43 feet from the surface.

The fourth site, #14, is located approximately 500 feet north of the junction of Routes #9 and #403 in Philipstown, New York. It is situated close to the Dennytown Fault, near the eastern edge of the Hudson Highlands and 1.3 miles northwest of the Canopus Fault. The rock at the site is medium grained gneiss with amphibolite occasionally present. Rock quality at the site is poor to fair. Seven measurements were made at depths ranging from 42 to 60 feet from the surface.

## H.2.0 TEST PROCEDURES AND COMPUTATIONS

### H.2.1 GENERAL

The determination of in-situ stress by overcoring consists of inserting a measurement device in a small borehole and measuring the diametrical changes as the hole is stress-relieved by "overcoring". Overcoring is performed using a large-diameter coring bit to separate a rock cylinder containing the small borehole and measuring gage from the remaining rock mass. Stresses acting on the rock are relieved by overcoring, and are reflected in diametric changes of the rock cylinder removed. The stress conditions can be evaluated from these diametrical changes, and from the modulus of elasticity of the rock core.

The procedure of determining the stress at a site can therefore be subdivided into three phases:

1. The measurement of borehole deformation during overcoring.
2. The determination of the modulus of elasticity of the overcore in the laboratory.
3. Computation of stresses using the theory of linear elasticity and measured deformations and moduli.

These phases are each described briefly in the following sections. Abbreviations employed in this discussion are shown on Table H-1.

### H.2.2 FIELD TEST PROCEDURE

The overcoring technique is illustrated in Plate H-12. First, a large diameter (6 inch O.D.) borehole is drilled to the desired testing depth. A concentric, 1.5 inch diameter, borehole (EX) is then drilled to approximately 18 to 30 inches below the level at which the large diameter borehole was terminated. Finally, a borehole deformation gage is inserted into the EX hole and "overcored" by extending the large diameter hole an additional 18 inches.

During the overcore operation, diametrical deformation is measured on three axes, 60° apart in a plane perpendicular to the borehole. Readings are taken at least once for each 1/2 inch of overcore run. At the completion of the test, the recorded deformation for each axis is plotted versus the overcore distance. A typical curve is shown on Plate H-13.

The basis of this procedure is described by Hooker and Bickel (1974) and in ASTM Special Publication No. 429.

### H.2.3 MODULUS DETERMINATION

To obtain the modulus of elasticity of the rock in the zone tested, it is necessary to remove the 5.25 inch diameter overcore from the hole and test it in a rock modulus chamber. To do this, the rock core is inserted into a bi-axial chamber, with the deformation gage in the small diameter central hole (Plate H-14). Pressure is applied radially to the rock core (by a rubber membrane and a hand-operated hydraulic system) in steps of 200 psi up to about 2000 psi, and then decreased similarly,

while measuring deformation along the gage's three axes for each pressure step. The recorded deformation of each axis is then plotted versus the applied pressure. From this curve, an average modulus is then calculated.

The results of the bi-axial test program are shown in Plates H-15 to H-101.

This test procedure requires an intact piece of over-core longer than 12 inches, which is not always obtained due to the natural fracturing of the rock and drilling breakage. Hence, the biaxial test program was supplemented with uniaxial compressive strength testing of NWX-diameter cores at overcore test depths. Representative NWX samples from each site were loaded to failure. The results of this program are shown in Table H-2.

#### H.2.4 TEST EQUIPMENT

The instrumentation used during this project was developed by the U.S. Bureau of Mines, as modified in 1974 (Hooker and Bickel, 1974). However, due to the very hard nature of the rock in the Indian Point vicinity, standard diamond drill bits were employed instead of the recommended thin-wall masonry bits. Hence, the core obtained during the project has a nominal diameter of 5.25 inches, approximately 0.4 inches smaller than the U.S. Bureau of Mines standard. This required a smaller biaxial chamber which was obtained specially for this purpose.

The test equipment consisted of:

- (a) 2 U.S. Bureau of Mines-type Deformation Gages, each with 100 feet of cable;

- (b) 3 Vishay Model P-350A Strain Indicators;
- (c) Orientation tool, placement tool, scribe and placement rods (12);
- (d) Calibration Jig;
- (e) Gage accessories, including special pliers, o-rings and washers, and extra cable;
- (f) Centering device for 6-inch barrel; and,
- (g) Modified Bi-axial Chamber, with an inner diameter of 5.25 inches, and accessories including pressure dial and hand pump.

All equipment employed in this test program was calibrated to U.S. Bureau of Mines' standards as discussed by Hooker and Bickel (1974) and Fitzpatrick (1962).

Deformation gages and equipment employed in measuring in-situ strain were calibrated at least once a week and after any rough handling of the gage. A standard Calibration Jig was employed for this purpose which applied a known deflection to each cantilever. The calibration record for each axis has been tabulated in Table H-3 ( $K_1$  is given in units of  $10^{-6}$  inch).

The biaxial chamber employed in the program was calibrated using a specially constructed aluminum "overcore", 5.20 inches in diameter, 16 inches in length, constructed using ASTM Standard Q.Q.A. 225-8 material. The overcore was manufactured by Terrametrics of Boulder, Colorado. Testing of this overcore and all other testing was performed employing a Roylyn Pressure

gage with an accuracy of 0.25%. Over the full range of the gage (0-2000 psi), test results were recorded with a precision of  $\pm 5$  psi. The average modulus so determined was  $9.8 \times 10^6$  psi.

#### H.2.5 COMPUTATION OF STRESSES

To calculate stress from the obtained deformation readings, it is necessary to employ several equations based on the assumption of linear elasticity.

Initially, gage readings for each axis (in indicator units) are multiplied by the corresponding calibration constants ( $K_i \times 10^{-6}$  inches) to obtain deflection readings for each axis. Using equations based on a "Plane-Stress" analysis as discussed by Obert and Duvall (1967), the minimum and maximum stresses normal to the borehole are calculated from:

$$P = \frac{E}{6d}(U_1 + U_2 + U_3) + \frac{\sqrt{2}}{2}[(U_1 - U_2)^2 + (U_2 - U_3)^2 + (U_3 - U_1)^2]^{1/2} \quad (1)$$

$$Q = \frac{E}{6d}(U_1 + U_2 + U_3) - \frac{\sqrt{2}}{2}[(U_1 - U_2)^2 + (U_2 - U_3)^2 + (U_3 - U_1)^2]^{1/2} \quad (2)$$

where

$U_1, U_2, U_3$  are measurements of diametrical deflection along three axes, each  $60^\circ$  apart. Deflection is positive for increasing diameter during overcoring (in inches).

$P$  is the maximum normal stress, in psi.

$Q$  is the minimum normal stress, in psi.

$E$  is the modulus of deformation, in psi.

$d$  is the inner hole diameter, in inches.

The stress field thus calculated is generally elliptical in shape. The orientation of the maximum stress axis is calculated from:

$$\theta_p = \frac{1}{2} \arctan \frac{\sqrt{3} \cdot (U_2 - U_3)}{(2U_1 - U_2 - U_3)} \quad (3)$$

where:

$\theta_p$  is the angle of rotation to one axis of the ellipsoid, positive in a counter-clockwise manner from the  $U_1$  axis.

This angle together with the observation of the maximum positive strain, permits the determination of the axes of maximum and minimum stresses.

The modulus of elasticity from biaxial testing is calculated employing a "Plane Stress" analysis, considering a "thick-wall" cylinder as:

$$E = \frac{(4ab^2) (\Delta P)}{(b^2 - a^2) (\Delta U)} \quad (\text{Fitzpatrick, 1962}) \quad (4)$$

where:

E is the modulus of deformation, in psi.

a is the radius of the inner hole, in inches.

b is the radius of the cylinder, in inches.

$\Delta P$  is the change in applied pressure, in psi.

$\Delta U$  is the deflection change during the pressure change,  $\Delta P$ , for one axis, in inches.

The determination of the maximum and minimum stresses in equations (1) and (2) assumes that the modulus of elasticity is isotropic, that is, equal in all directions. However, this is not always the case and anisotropy must be considered.

The method of analysis considering the anisotropy of a sample will depend on the degree and orientation of the anisotropy. In this investigation, for axial moduli which exhibits an anisotropy of less than or equal to 5%, an isotropic analysis was employed with equations 1 and 2 and an average modulus value. For those moduli which showed an anisotropy greater than 5%, a simplified anisotropic analysis was performed in which each axial deflection was normalized to a modulus of  $10.0 \times 10^6$  psi, and the normalized values were used in equations 1 and 2.

In equation form, this is:

$$U_i^A = \frac{U_i E_i}{10.0 \times 10^6 \text{ psi}} \quad (4)$$

where:

$U_i^A$  is the normalized deflection value for axis i where  $i = 1, 2, \text{ or } 3$ .

$U_i$  is the recorded strain during the in-situ test.

$E_i$  is the axial modulus, determined from the biaxial test.

For anisotropy greater than 25%, triaxial testing, together with the analyses presented by Hooker and Johnson (1969), would be an appropriate procedure, however, these tests were not carried out in this investigation.

### H.3.0 TEST DATA AND RESULTS

#### H.3.1 FIELD AND LABORATORY DATA

Recorded deformation readings and calculations of diametric strain are presented in Tables H-4 through H-7 for each of the several tests conducted at each site. The data are also presented graphically to show the measured relationship between depth of overcoring and diametric deflection for each test (Plates H-102 to H-138). A standard theoretical test curve of the same type is shown on Plate H-13. This typical curve is characterized by a lack of significant deflection before the overcoring bit penetrates the immediate vicinity of the measurement plane, that is, the depth at which the axes of the deformation gage are located. Most of the strain relief occurs within a distance of 1 to 2 inches below the plane of measurement. By comparing the test plots with a standard curve, the quality of the data can be estimated.

The majority of the strain relief curves resemble the standard curve. Tests yielding such plots are considered acceptable. However, for several tests, deformation was recorded by one or more axes well before reaching the plane of measurement. The most common cause of such behavior is gage slippage, which occurs if drilling vibration during the overcore run overcomes the frictional resistance of the gage, allowing it to slip gradually down-hole. If gage slippage was suspected to have occurred during a test run, the results of that run were excluded from further consideration.

During a few tests, drilling was terminated prematurely due to the wedging of rock fragments in the overcore barrel. For these tests, the overcore run was not long enough to penetrate well beyond the plane of measurement to obtain a complete recording of the deformation. Such tests were individually considered and some were eliminated from further consideration.

The laboratory measurements and determinations of the rock deformation moduli are presented in Tables H-8 through H-11. These tables indicate that the anisotropy of most samples is less than 10 percent, with the notable exceptions of Test #9, at Site #3 and Test #7, at Site #11. As previously discussed for tests indicating an anisotropy of less than or equal to 5 percent, the stress parameters were computed on the basis of an isotropic analysis, using the average value of the modulus of deformation. For tests indicating an anisotropy greater than 5 percent, a simplified anisotropic analysis was performed. Tests indicating an anisotropy greater than 25 percent were excluded from further consideration, since triaxial laboratory measurements were not performed.

#### H.3.2 RESULTS

The results of the in-situ strain measurements and stress computations are presented in Tables H-12 through H-15.

At Site #3, ten measurements were performed, of which six were considered not acceptable. As shown on Plates H-105 to H-110, Tests #4 through #9 indicate that gage slippage may have occurred.

Examining the magnitude and orientation of the secondary stresses identified from the four successful tests, #1, #2, #3, and #10 in Table H-12, significant variations in the measured stress vectors can be observed. The magnitude of the maximum horizontal stress vector (P) varies between 215 psi and 1410 psi while that of the minor vector (Q) varies between 689 psi and -115 psi. The orientation of the P vector varies between northeast and northwest.

The average of comparable tests #2 and #3 indicates that the P vector has a magnitude of  $221 \pm 7$  psi and trends  $N44 \pm 18^\circ E$ , while the Q vector has a magnitude of  $-25 \pm 127$  psi. The average of tests #1 and #10 indicate that the P vector has a magnitude of  $1360 \pm 71$  psi and trends  $N37 \pm 22^\circ W$  (Table H-16).

At Site #9, seven tests were performed, all of which were considered successful. Table H-13 shows that the magnitude of the maximum horizontal stress vector at this site is highly variable, ranging from 10 psi to 1908 psi. The orientation of this vector, however, is somewhat more consistent.

Test #1 and #3 were performed above and below two inclined fractures. Test #2 was performed between these two fractures. The measured stresses above and below the fractures were small, varying from 10 psi to 71 psi for the P vector and from -106 psi to -151 psi for the Q vector. However, between the fractures, Test #2 revealed the presence of high compressive stresses of +1908 psi for the P vector and +1032 psi for the Q vector.

Tests #3, #4, #6 and #7, which were performed below the depth of 34 feet, revealed that the stress vectors had more systematic values. Test #5, performed in the proximity of a fracture, was not included in this grouping. The average of these tests indicates that the P vector is oriented  $N68\pm27^{\circ}E$  and has a magnitude of  $201\pm188$  psi. The Q vector has an average magnitude of  $94\pm191$  psi (Table H-16). The high compressive stresses noted in Test #2 may be due to minor shear adjustments taking place along the fractures.

At Site #11, thirteen measurements were performed, twelve of which were considered successful. The results of Test #6 were eliminated because a fragment of core may have struck the gage. A piece of rock was retrieved from the top of the gage at the end of this run (Table H-14).

Tests #1 through #5 were made above a weathered, nearly horizontal fracture located at a depth of 33 feet. The measured stresses in this interval were generally low and variable. The magnitude of the maximum horizontal stress was small, ranging from -11 psi to +255 psi. The orientation of this stress vector was highly variable. Tests #7 through #13 were made below the fracture. The magnitude of measured stresses increased substantially to values up to 1652 psi. The maximum horizontal stress vector maintained a consistent orientation within the range of  $N53^{\circ}E$  to  $N81^{\circ}E$ . The average of tests #7 through #13, indicates that the P vector is oriented  $N66\pm11^{\circ}E$  and has an average magnitude of  $1122\pm355$  psi. The minimum horizontal stress vector

ranges in magnitude from -241 to 525 psi and averages  $33 \pm 267$  (Table H-16).

The average orientations of the representative P and Q vectors for Site #9 and #11 are similar. However, it should be noted that the magnitude of the representative P vector (15b, Table H-16) at Site #9 is considerably smaller than that at Site #11. This difference may represent actual variations in the regional stress field. The measurements at Site #9 may reflect a zone of stress relaxation near the Ramapo Fault. The recorded magnitudes may not be representative of the state of stress in the region.

At Site #14, seven measurements were performed, of which five were considered successful. Tests #4 and #6 were terminated before a complete recording of the deformation was obtained because of core wedging. These tests, however, did reveal some strain relief and may be considered partially successful (Table H-15).

The average of the successful Tests (#1, 2, 3, 5 and 7) indicates that the P vector is oriented  $N27 \pm 12^\circ E$  and has a magnitude of  $514 \pm 482$  psi. If Test #2 is not considered in the computation of this average, the magnitude of P changes to  $315 \pm 216$  psi, but the orientation of P remains unchanged at  $N28 \pm 14^\circ E$  (Table H-16).

#### H.4.0 REGIONAL CORRELATION

##### H.4.1 GENERAL

Several components contribute to the total in-situ stress field measured at any one location. The most important are: 1) a gravitational component derived from the mass of overburden; 2) residual and/or remanent component(s), which may or may not be interrelated, derived from conserved elastic strain energy locked in the rock; and 3) a regional or current tectonic component derived from applied stress.

The gravitational component in a horizontal plane can be calculated from the depth of measurement and Poisson's ratio using the following formula:

$$\sigma_h = \frac{\sigma_v \nu}{(1-\nu)} = \frac{(\gamma H) \nu}{(1-\nu)} \quad (\text{Obert \& Duval., 1967}) \quad (5)$$

where:

$\sigma_h$  is the horizontal component

$\sigma_v$  is the vertical stress derived from mass of overburden

$\nu$  is Poisson's ratio

$\gamma$  is the density of the material

$H$  is the depth from the surface to the horizontal plane of measurement

Assuming an average rock density of 170 lbs/ft<sup>3</sup> and a Poisson ratio of 0.20, the stress component in the horizontal

direction is thereby equal to 12 psi at 40 feet, an average depth for the test data recorded during this investigation. However, such an analysis does not consider plastic deformation. Testing by Brooker and Ireland (1965), using overconsolidated clays, indicated that the horizontal stress component may at times equal the vertical stress in geologic materials. Again under the stated assumptions, the horizontal stress due to the overburden could be as high as 47 psi if it is equal to the vertical load. Note that the Poisson effect is equal in all directions in the horizontal plane if the material is relatively isotropic.

At present, however, there is no quantitative method to separate the effects of remanent and residual components from the current tectonic component. Even if the contribution of instrumental errors, elasticity assumptions and induced stresses (during measurement) are assumed to be negligible, there are still other important factors (for e.g. erosional processes, local geologic structures and inhomogeneities) that affect near surface observations. What is important from the geotectonic viewpoint is to note that "large horizontal stresses near the free surface can be generated by a variety of non-tectonic processes" (Ranalli, 1975).

Sbar and Sykes (1973) and Sykes and Sbar (1973 and 1974) have underlined the importance of in-situ stress measurements to the understanding of intraplate tectonics. For the northeastern United States they concluded that: 1) the maximum

compressive stress trends east to northeast over an area extending from west of the Appalachian Mountain system to the middle of the continent, and from southern Illinois to southern Ontario; and 2) the stress pattern is different and not as simple in the Appalachian Mountain system as in the adjacent region to the west. They also suggested that the relation between high stress and unhealed fault zones may provide a means to assess the earthquake risk within plates (Sbar and Sykes, 1973).

#### H.4.2 ORIENTATION OF MAXIMUM HORIZONTAL COMPRESSION IN NORTHEASTERN NORTH AMERICA

The average strike of the horizontal component of maximum compression reported in the geologic literature for northeastern North America is plotted on Plate H-139. These orientations were obtained by the strain relief and hydrofracture techniques of measuring in-situ stress. Data obtained during this investigation, at Sites #3, 9, 11 and 14 (Section H.3.0), are also plotted on Plate H-139 and considered compatible with the data reported in the literature. The magnitude and orientation of the principal stresses presented in the literature and measured during this investigation are summarized in Tables H-16, 17 and 18. In evaluating this information, it should be noted that as the ratio of  $P_c$  to  $Q_c$  approaches one, the determination of the trend of  $P_c$  becomes less reliable.

Measurements A, B, Ca and V (Plate H-139), west of the Appalachian fold and thrust belt, support the presence of a uniform regional component of compression that trends about east-west in the upper part of the lithosphere.

The direction of maximum compression ( $P_c$ ) in the vicinity of Lake Ontario, however, appears to vary from one location to another. Measurements VI and 11 recorded a northeast trend, while VII and 10 indicate a northwest trend (Plate H-139).

The stress pattern appears to be complicated in the Appalachian Mountain system. The suggestion of Hooker and Johnson (1969) that the direction of  $\sigma_1$  may be aligned with the structural trend of the Appalachians is not supported by the orientations of maximum compression ( $P_c$ ) plotted on Plate H-139. About 50% of the measurements, #1, #2, #4, #5, #6, #7, #13 and II, recorded a northerly-trending  $P_c$ , while the remaining 50%, #3, #9, #14a, #15b, #16, #17, I and IV, recorded a northeasterly-trending  $P_c$  (Plate H-139). These measurements appear to record the resultant of more than one stress component, such that, a locally predominant stress component would influence the trend of  $P_c$  at any one site. An early in-situ strain relief measurement at Barre, Vermont (Site #1, Plate H-139) recorded an average  $P_c$  of 1734 psi, trending N14°E (Hooker and Johnson, 1969; Table H-16). A subsequent laboratory study involving successive overcoring of a quarried block of Barre Granite demonstrated the presence of an initial tensile residual stress in the block, with a maximum tensile principal stress on the order of 1,000 psi (Nichols, 1972). This measured residual stress appears to be related at least to the geometry of the body and to the degree of homogeneity, orientations and magnitudes of the originally

locked-in stresses. A complication arises from the fact that a tensile residual stress can produce the same deformation upon overcoring as an externally applied compressional stress field (Nichols, 1972). Engelder and Sbar (1976) suggested that the strain relieved following initial in-situ overcore at Barre, Vermont contains large components of residual strain. If different outcrops have scattered orientations of residual strain, initial overcore would probably yield scattered orientations of  $P_c$ . It should be emphasized that the total residual strain is probably the result of the superposition of more than one type of residual strain. Engelder and Sbar (1976) have attempted to discriminate between applied and residual strains, using the double overcoring technique, in northern New York State and at Barre, Vermont (Plate H-139). Presumably the initial overcore relieves both applied and part of the residual strains, whereas the second overcore relieves just residual strains. Residual strains obtained from the second overcore may enable the separation of residual effects from the combination of applied and residual strains relieved during the first overcore.

The relief of both macroscopic and microscopic residual strain following the initial overcore must be larger than the relief of just microscopic strain by the second overcore. Therefore, the magnitude of residual strain obtained with the double overcore was assumed to be between  $1/4$  and  $1$  of the residual strain relieved by the initial overcore (Engelder and

Sbar, 1976). The correction to the initial field measurement was applied by subtracting between 1 and 4 times each of three components of strain following double overcore from their respective components of strain measured upon initial overcoring. The results of the 4 times double overcore strain subtraction are listed in Table H-18. To date, there is no model which adequately treats the relief of superimposed residual strains in order to isolate the applied component related to the regional stress pattern.

The stress measurements at Sites #3, #9, #11 and #14, near the Indian Point site, indicate that there is as much variation in the magnitude of the near surface lateral stresses at individual sites as there is from one site to another (Tables H-12 to 16). Except for average #14b, the trend of  $P_c$  appears to be somewhat more consistent, varying between northeast and east-west (Table H-16 and Plate H-139). If the results of Test #2 at Site #9 (included in average #15a, Table H-16) is excluded from consideration (see Section H.3.2), it can be noted that the magnitude of  $P_c$  at Sites #9 and #14, in the immediate vicinity of the Ramapo Fault System, is smaller than that at Site #3 and #11, in the region. Therefore, the near surface in-situ strains appear to be somewhat relieved in the vicinity of the Ramapo Fault System relative to the surrounding region. It should be noted, however, that since the componential make-up of the measured in-situ stress is unknown and the correlation between near

surface stress measurements and stress conditions at depth is a topic of debate in the scientific community, the significance of the above observations is, at best, speculative at the present time.

#### H.5.0 CONCLUSIONS

As a result of this investigation, the conclusions relative to the near surface in-situ stresses in the vicinity of the Indian Point Site are:

- 1) Several components contribute to the total in-situ stress field measured at anyone location. The most important are: a) a gravitational component, b) a residual and/or remanent component(s) and c) a applied tectonic component.
- 2) At present, there is no quantitative method to separate the effects of remanent and residual components from the applied tectonic component.
- 3) Large horizontal stresses near a free surface can be generated by a variety of non-tectonic processes.
- 4) Available measurements support the presence of a uniform east-trending horizontal component of maximum compression west of the Appalachians. This orientation, however, appears to vary from one location to another in the vicinity of Lake Ontario.
- 5) The stress pattern appears to be complicated in the Appalachian Mountain system. In-situ measurements appear to record the resultant of more than one stress component.

- 6) Measurements in the vicinity of the Indian Point Site indicate that there is as much variation in the magnitude of near surface lateral stresses at individual sites as there is from one site to another. The trend of  $P_c$  appears to be somewhat more consistent, varying between northeast and east-west.
- 7) The near surface in-situ strains may be somewhat relieved in the vicinity of the Ramapo Fault System relative to the surrounding region.
- 8) The correlation between near surface measurements and stress conditions at depth is, at best, speculative at the present time.

TABLE H-1

DEFINITIONS

<u>Symbol</u>	<u>Definitions</u>
$R_i$	Indicator reading for axis $i$ , $i = 1, 2, 3$
$K_i$	Calibration factor for axis $i$ , used to convert indicator reading to deflection
$U_i$	Deflection along axis $i$ ; axes are $60^\circ$ apart
$U_{1\theta}$	Orientation of $U_1$ axis with respect to true north
$a$	Radius of inner hole, inches
$b$	Radius of overcore, inches
$E$	Modulus of Deformation, psi
$\Delta P$	Change in applied pressure, psi
$\Delta R$	Change in indicator units, corresponding to $\Delta P$
psi	lbs/in <sup>2</sup>
pcf	lbs/ft <sup>3</sup>

TABLE H-2

UNIAXIAL COMPRESSIVE STRENGTHS

Site No.	Depth (Ft-in)	Density (lbs/ft <sup>3</sup> )	Failure Load (lbs)	Failure Strength (lbs/in <sup>2</sup> )
3	37-6	184	118,400	35,802
9	34-2	166	91,700	27,645
11	18-4	172	60,200	18,132
14	49-2 1/2	166	129,100	38,920

TABLE H-3

RECORD OF CALIBRATION OF  
BOREHOLE DEFORMATION GAUGE

<u>Gauge No.</u>	<u>Date</u>	$K_1$ <u>(<math>10^{-6}</math> in)</u>	$K_2$ <u>(<math>10^{-6}</math> in)</u>	$K_3$ <u>(<math>10^{-6}</math> in)</u>
1	3-01-76	1.04	1.05	1.07
1	3-04-76	1.03	1.04	1.04
1	3-08-76	1.03	1.04	1.08
1	3-10-76	1.03	1.04	1.03
1	3-15-76	1.04	0.99	1.06
1	3-16-76	1.04	1.00	1.06
1	3-19-76	1.04	1.05	1.04
1	3-24-76	1.06	1.03	1.06
1	3-30-76	1.05	1.01	1.05
2	4-08-76	1.00	0.98	0.97
2	4-14-76	0.98	1.00	0.96
2	4-19-76	1.01	0.99	0.97
2	4-28-76	0.99	0.98	0.91
2	4-30-76	0.97	0.98	0.96
2	5-07-76	0.98	1.00	0.96
2	5-11-76	0.97	0.99	0.96
1	5-17-76	1.05	1.04	1.09
1	5-24-76	1.01	0.97	1.03
1	Lab. Rating	1.02	1.02	1.03
2	Lab. Rating	1.00	1.00	1.00

TABLE H-4

DEFORMATION CALCULATIONS  
SITE 3

Test No.	$U_1 \theta$	$R_1$	$R_2$	$R_3$	$K_1$ ( $10^{-6}$ in)	$K_2$ ( $10^{-6}$ in)	$K_3$ ( $10^{-6}$ in)	$U_1$ ( $10^{-6}$ in)	$U_2$ ( $10^{-6}$ in)	$U_3$ ( $10^{-6}$ in)
1	N82°W	+ 180	+180	+ 450	1.04	1.05	1.07	+ 187	+189	+ 482
2	N78°W	- 60	+ 86	+ 3	1.03	1.04	1.04	- 62	+ 89	+ 3
3	N85°W	+ 45	+ 66	0	1.03	1.04	1.04	+ 46	+ 69	+ 0
4	N86°W	+ 124	-227	- 24	1.03	1.04	1.04	+ 128	-236	- 25
5	N85°W	+ 120	+ 92	+ 35	1.03	1.04	1.04	+ 124	+ 96	+ 36
6	N85°E	- 71	+117	+ 57	1.03	1.04	1.08	- 73	+122	+ 62
7	N80°W	- 19	+ 67	- 48	1.03	1.04	1.08	- 20	+ 70	- 52
8	N 5°W	+1292	+852	+1688	1.03	1.04	1.03	+1331	+886	+1739
9	N 5°E	- 390	+ 20	+ 10	1.03	1.04	1.03	- 402	+ 21	+ 10
10	N 5°E	+ 150	+371	+ 135	1.03	1.04	1.03	+ 155	+386	+ 139

Notes: (1) + Indicates increasing diameter of ex-hole

TABLE H-5

DEFORMATION CALCULATIONS  
SITE 9

Test No.	$U_1^b$	$R_1$	$R_2$	$R_3$	$K_1$ ( $10^{-6}$ in)	$K_2$ ( $10^{-6}$ in)	$K_3$ ( $10^{-6}$ in)	$U_1$ ( $10^{-6}$ in)	$U_2$ ( $10^{-6}$ in)	$U_3$ ( $10^{-6}$ in)
1	N70°W	+ 56	- 130	- 38	1.06	1.03	1.06	+ 59	- 134	- 40
2	N70°W	+1125	+1060	+341	1.06	1.03	1.06	+1193	+1092	+361
3	N66°W	+ 12	+ 4	- 90	1.06	1.03	1.06	+ 13	+ 4	- 95
4	N67°W	+ 42	+ 208	+ 82	1.05	1.01	1.05	+ 44	210	86
5	N71°W	+ 5	+ 100	+ 54	1.00	0.98	0.97	+ 5	+ 98	+ 52
6	N70°W	+ 301	+ 246	+196	1.00	0.98	0.97	+ 301	+ 241	+190
7	N74°W	+ 64	+ 238	+ 52	1.00	0.98	0.97	+ 64	+ 233	+ 50

TABLE H-6

DEFORMATION CALCULATIONS  
SITE 11

Test No.	$U_1^\theta$	$R_1$	$R_2$	$R_3$	$K_1$ ( $10^{-6}$ in)	$K_2$ ( $10^{-6}$ in)	$K_3$ ( $10^{-6}$ in)	$U_1$ ( $10^{-6}$ in)	$U_2$ ( $10^{-6}$ in)	$U_3$ ( $10^{-6}$ in)
1	N42°E	+ 35	-222	- 31	0.98	1.00	0.96	+ 34	-222	- 30
2	N30°E	- 37	- 6	+ 21	0.98	1.00	0.96	- 36	- 6	+ 20
3	N40°E	+ 7	+ 66	+106	1.01	0.99	0.97	+ 7	+ 65	+103
4	N40°E	+ 107	-123	+197	1.01	0.99	0.97	+ 108	+122	+191
5	N30°E	- 9	- 10	-125	1.01	0.99	0.97	- 9	- 10	-121
6	N37°E	- 39	- 59	+ 16	1.01	0.99	0.97	- 39	- 58	+ 16
7	N35°E	+1041	-403	+914	0.99	0.98	0.91	+1031	-395	+832
8	N38°E	+ 514	-111	+220	0.99	0.98	0.91	+ 509	-109	+200
9	N38°E	+ 455	-306	+385	0.99	0.98	0.91	+ 450	-300	+350
10	N40°E	+1082	+ 62	+572	0.97	0.98	0.96	+1050	+ 61	+549
11	N40°E	+307	-259	+556	0.97	0.98	0.96	+ 298	-254	+534
12	N36°E	+488	-430	+740	0.97	0.98	0.96	+ 473	-421	+710
13	N36°E	+309	-221	+968	0.97	0.98	0.96	+ 300	-212	+929

H-30

TABLE H-7

DEFORMATION CALCULATIONSSITE 14

Test No.	$U_1\theta$	$R_1$	$R_2$	$R_3$	$K_1$ ( $10^{-6}$ in)	$K_2$ ( $10^{-6}$ in)	$K_3$ ( $10^{-6}$ in)	$U_1$ ( $10^{-6}$ in)	$U_2$ ( $10^{-6}$ in)	$U_3$ ( $10^{-6}$ in)
1	N45°W	-101	- 15	+ 54	0.97	0.99	0.96	- 98	- 15	52
2	N58°W	+ 44	+250	+416	1.05	1.04	1.09	+ 46	+260	+453
3	N58°W	+ 33	+ 47	+ 59	1.05	1.04	1.09	+ 35	+ 49	+ 64
4	N58°W	- 55	+ 25	+ 44	1.05	1.04	1.09	- 58	+ 26	+ 48
5	N58°W	+ 59	+259	+163	-1.05	1.04	1.09	+ 62	+267	+178
6	N58°W	+ 97	+235	+551	1.01	0.97	1.03	+ 98	+228	+568
7	N58°W	-102	+194	+ 57	1.01	0.97	1.03	-103	+188	+ 59

<sup>1</sup> + Indicates increasing diameter of ex-hole

TABLE H-8

PHYSICAL PROPERTY TESTSSITE 3

Test No.	Depth (Ft-in)	Density (pcf)	Uniaxial Modulus (x10 <sup>6</sup> psi)	BIAXIAL MODULUS <sup>1</sup>			U <sub>1</sub> e	Poisson's Ratio
				Axis 1 (x10 <sup>6</sup> psi)	Axis 2 (x10 <sup>6</sup> psi)	Axis 3 (x10 <sup>6</sup> psi)		
1	17-9½	184	--	--	--	--	N82W	—
2	19-6	187	12.2	10.3	12.5	10.0	N78W	0.28
3	21-1	176	11.1	10.9	11.6	10.4	N85W	0.26
4	22-4	182	11.6	12.8	12.0	12.0	N86W	0.29
5	23-11	181	10.9	12.7	12.9	12.2	N85W	0.26
6	25-7½	182	11.2	14.3	15.8	14.3	N85E	0.25
7	27-4	181	10.6	13.4	13.8	13.4	N80W	0.34
8	30-4	179	12.2	--	--	--	N 5W	0.26
9	35-7	190	12.6	14.1	14.5	34.9(?)	N 5E	0.27
10	37-6	184	12.8	13.6	12.3	12.5	N 5E	0.26

<sup>1</sup>The Biaxial Modulus was determined for each obtained overcore longer than 12 inches.

TABLE H-9  
PHYSICAL PROPERTY TESTS

SITE 9

Test No.	Depth (Ft-in)	Density (pcf)	Uniaxial Modulus (x10 <sup>6</sup> psi)	BIAXIAL MODULUS <sup>1</sup>			U <sub>1</sub> θ	Poisson's Ratio
				Axis 1 (x10 <sup>6</sup> psi)	Axis 2 (x10 <sup>6</sup> psi)	Axis 3 (x10 <sup>6</sup> psi)		
1	30-5	161	7.9	4.0	5.6	4.5	N70W	0.21
2	31-8	164	8.0	--	--	--	N70W	0.26
3	34-2	166	8.3	3.2	4.4	5.2	N66W	0.23
4	35-5	168	7.9	3.0	2.5	3.2	N67W	0.24
5	37-9½	--	--	--	--	--	N71W	--
6	42-8	166	7.5	--	--	--	N70W	0.15
7	43-10½	166	7.5	3.5	3.2	3.2	N74W	0.16

H-33

<sup>1</sup>The Biaxial Modulus was determined for each obtained overcore longer than 12 inches.

TABLE H-10

PHYSICAL PROPERTY TESTSSITE 11

Test No.	Depth (Ft-in)	Density (pcf)	Uniaxial Modulus (x10 <sup>6</sup> psi)	BIAXIAL MODULUS <sup>1</sup>			U <sub>1</sub> θ	Poisson's Ratio
				Axis 1 (x10 <sup>6</sup> psi)	Axis 2 (x10 <sup>6</sup> psi)	Axis 3 (x10 <sup>6</sup> psi)		
1	15-0	172	7.4	3.3	3.0	2.7	N42E	0.18
2	16-4	--	--	4.0	4.0	3.7	N30E	--
3	18-4	172	6.8	4.6	4.2	4.8	N40E	0.21
4	19-7	--	--	4.4	4.8	4.5	N40E	--
5	22-5	169	6.8	3.5	4.2	3.9	N30E	0.17
6	28-7	171	7.7	3.8	4.0	4.1	N37E	0.21
7	34-9	--	--	2.0	0.4	2.9	N35E	--
8	36-0	188	9.8	6.7	6.6	6.8	N38E	0.44
9	37-9½	--	--	6.4	7.5	5.6	N38E	--
10	38-8½	174	7.4	5.6	6.1	6.1	N40E	0.29
11	40-1	--	--	6.5	6.9	7.2	N40E	--
12	41-7	--	--	6.9	6.9	7.1	N36E	--
13	42-11	179	8.5	7.1	7.1	6.1	N36E	0.25

<sup>1</sup>The Biaxial Modulus was determined for each obtained overcore longer than 12 inches.

TABLE H-11

PHYSICAL PROPERTY TESTSSITE 14

Test No.	Depth (Ft-in)	Density (pcf)	Uniaxial Modulus (x10 <sup>6</sup> psi)	BIAXIAL MODULUS <sup>1</sup>			U <sub>1</sub> $\theta$	Poisson's Ratio
				Axis 1 (x10 <sup>6</sup> psi)	Axis 2 (x10 <sup>6</sup> psi)	Axis 3 (x10 <sup>6</sup> psi)		
1	42-4½	191	11.2	--	--	--	N45W	0.27
2	44-2	190	9.8	9.8	12.4	10.0	N58W	0.22
3	49-2½	167	9.5	9.4	9.6	9.6	N58W	0.20
4	51-6½	167	10.0	--	--	--	N58W	0.19
5	55-8	167	8.7	8.8	7.6	7.4	N58W	0.21
6	57-6	167	9.6	--	--	--	N58W	0.18
7	59-1½	165	7.8	8.8	9.2	9.4	N58W	0.18

<sup>1</sup>The Biaxial Modulus was determined for each obtained overcore longer than 12 inches.

TABLE H-12

TABULATION OF RESULTS, SITE 3

Test No.	Depth (ft.-in.)	Diametric Deformation ( $10^{-6}$ in)			Modulus <sup>(1)</sup> ( $\times 10^6$ lb/in <sup>2</sup> )	P <sup>(2)</sup> Maximum (lb/in <sup>2</sup> )	Q <sup>(2)</sup> Minimum (lb/in <sup>2</sup> )	True Bearing of P	Comments
		U <sub>1</sub>	U <sub>2</sub>	U <sub>3</sub> <sup>(3)</sup>					
1	17-9½	+ 187	+ 189	+ 482	11.0	+1410 <sup>(4)</sup>	+ 689	N22°W	
2	19-6	- 62	+ 89	+ 3	10.3 12.5 10.0	+ 226	- 115	N31°E	
3	21-1	+ 46	+ 69	0	11.0	+ 215	+ 66	N56°E	
4	22-4	+128	- 236	- 25	12.3	+ 252	- 616	N68°W	Apparent slippage of gage during test
5	23-11	+ 124	+ 96	+ 36	12.4	+ 459	+ 246	N74°E	Instability during test
6	25-7½	- 73	+ 122	+ 62	14.8	+ 466	- 104	N 6°E	Instability of axis during test
7	27-4	- 20	+ 70	- 52	13.5	+ 167	- 162	N47°E	Instability of axis 1 and 3 during test
8	30-4	+1331	+ 886	+1739	13.5	+7047	+4826	N39°E	Slippage of gage during test
9	35-7	- 402	+ 21	+ 10	14.3	+ 77	-1254	N86°E	Apparent instability of axis 1
10	37-6	+ 155	+ 386	+ 139	12.8	+1310	+ 625	N53°W	

H-36

TABLE H-12 (Continued)

- (1) Modulus shown is that used in calculations. Where three moduli are presented, an anisotropic analysis was performed as discussed in Section H.2.5.
- (2) Stress calculations are based on a plane stress analysis; stresses shown are normal stresses in the horizontal plane.
- (3) Deflections shown are for axes 1, 2, 3 on the gage; (+) indicates increasing diameter of EX hole.
- (4) (+) indicates compressive stress

TABLE H-13

TABULATION OF RESULTS, SITE 9

Test No.	Depth (ft.-in.)	Diametric Deflection ( $10^{-6}$ in)			Modulus <sup>(1)</sup> ( $\times 10^6$ lb/in <sup>2</sup> )	P <sup>(2)</sup> Maximum (lb/in <sup>2</sup> )	Q <sup>(2)</sup> Minimum (lb/in <sup>2</sup> )	True Bearing of P	Comments
		U <sub>1</sub>	U <sub>2</sub>	U <sub>3</sub> <sup>(3)</sup>					
1	30-5	+59	-134	-40	4.0 5.6 4.5	+71	-151	N42°W	
2	31-8	+1193	+1092	+361	5.0	+1908	+1032	N83°E	Test between two healed fractures
3	34-2	+13	+4	-95	3.2 4.4 5.2	+10	-106	N85°E	
4	35-5	+44	+210	+86	3.0 2.5 3.2	+144	+65	N42°E	
5	37-9½	+5	+98	+52	5.0	+131	+41	N34°E	Test in proximity to fracture
6	42-8	+301	+241	+190	5.0	+460	+353	N84°W	
7	43-10½	+64	+233	+50	3.3	+192	+62	N48°E	

TABLE H-13 (Continued)

- (1) Modulus shown is that used in calculations. Where three moduli are presented, an anisotropic analysis was performed as discussed in Section H.2.5.
- (2) Stress calculations are based on a plane stress analysis; stresses shown are normal stresses in the horizontal plane.
- (3) Deflections shown are for axes 1, 2, 3 on the gage.
- (4) + Indicates compressive stress.

TABLE H-14

TABULATION OF RESULTS, SITE 11

Test No.	Depth (ft.-in.)	Diametric Deflection ( $10^{-6}$ in)			Modulus <sup>(1)</sup> ( $\times 10^6$ lb/in <sup>2</sup> )	P <sup>(2)</sup> Maximum (lb/in <sup>2</sup> )	Q <sup>(2)</sup> Minimum (lb/in <sup>2</sup> )	True Bearing of P	Comments
		U <sub>1</sub>	U <sub>2</sub>	U <sub>3</sub> <sup>(3)</sup>					
1	15-0	+34	-222	-30	3.3 3.0 2.7	+7	-150	N65°E	
2	16-4	-36	-6	+20	3.9	+12	-30	N74°W	
3	18-4	+7	+65	+103	4.6 4.2 4.8	+132	+43	N64°W	
4	19-7	+108	+122	+191	4.6	+255	+176	N76°W	
5	22-5	-9	-10	-121	3.5 4.2 3.9	-11	-109	N 0°E	
6	28-7	-39	-58	+16	4.0	-7	-66	N90°E	Rock fragment struck gage during test
7	34-9	+1031	-395	+832	2.0 0.4 2.9	+748	+210	N69°E	
8	36-0	+509	-109	+200	6.7	+847	+47	N53°E	
9	37-9½	+450	-300	+350	6.4 7.5 5.6	+816	-241	N63°E	
10	38-8½	+1050	+61	+549	5.9	+1652	+525	N55°E	

H-40

TABLE H-14 (Continued)

Test No.	Depth (ft.-in.)	Diametric Deflection ( $10^{-6}$ in)			Modulus <sup>(1)</sup> (x $10^6$ lb/in <sup>2</sup> )	P <sup>(2)</sup> Maximum (lb/in <sup>2</sup> )	Q <sup>(2)</sup> Minimum (lb/in <sup>2</sup> )	True Bearing of P	Comments
		U <sub>1</sub>	U <sub>2</sub>	U <sub>3</sub> <sup>(3)</sup>					
11	40-1	+298	-254	+534	6.5 6.9 7.2	+997	-101	N80°E	
12	41-7	+473	-421	+710	7.0	+1400	-214	N72°E	
13	42-11	+300	-212	+929	7.1 7.1 6.1	+1392	+5	N81°E	

H-41

- (1) Modulus shown is that used in calculations. Where three moduli are presented, an anisotropic analysis was performed as discussed in Section H.2.5.
- (2) Stress calculations are based on a plane stress analysis; stresses shown are normal stresses in the horizontal plane.
- (3) Deflections shown are for axes 1, 2, 3 on the gage.
- (4) + Indicates compressive stress.

TABLE H-15

TABULATION OF RESULTS, SITE 14

Test No.	Depth (ft.-in.)	Diametric Deflection ( $10^{-6}$ in)			Modulus <sup>(1)</sup> ( $\times 10^6$ lb/in <sup>2</sup> )	P <sup>(2)</sup> Maximum (lb/in <sup>2</sup> )	Q <sup>(2)</sup> Minimum (lb/in <sup>2</sup> )	True Bearing of P	Comments
		U <sub>1</sub>	U <sub>2</sub>	U <sub>3</sub> <sup>(3)</sup>					
1	42-4½	-98	-15	+52	11.2	+100	-252	N32°E	
2	44-2	+46	+260	+453	9.8 12.4 10.0	+1310	+509	N23°E	
3	49-2½	+35	+49	+64	9.5	+183	+155	N16°E	
4	51-6½	-58	+26	+48	10.0	+126	-90	N26°E	Test stopped @ 8½ in due to jammed core
5	55-8	+62	+267	+178	8.8 7.6 7.4	+576	+290	N18°E	
6	57-6	+98	+228	+568	9.6	+1400	+504	N10°E	Test stopped @ 7 in due to core breakage
7	59-1½	-103	+188	+59	9.1	+402	-111	N45°E	

H-42

TABLE H-15 (Continued)

- (1) Modulus shown is that used in calculations. Where three moduli are presented, an anisotropic analysis was performed as discussed in Section H.2.5.
- (2) Stress calculations are based on a plane stress analysis, stresses shown are normal stresses in the horizontal plane.
- (3) Deflections shown are for axes 1, 2, 3 on the gage.
- (4) + Indicates compressive stress.

TABLE H-16

SOME IN-SITU SECONDARY PRINCIPAL STRESSES  
IN A HORIZONTAL PLANE, EASTERN NORTH AMERICA

(Strain Relief Measurements Using U.S. Bureau of Mines Strain Gage)

No.	Location	Reference	Depth to Collar of hole (ft)*	Depth of Measurement (ft)	Pc (psi)	Qc (psi)	Trend Pc	Rock Type
1a	Barre, Vermont	5	0	0.5-1.5	510	107	N32E	Granite
1b	44°11'N 72°32'W		300	0.8-2.0	2958	1353	N08W	Granite
	<u>Calculated Average</u>	5		150	1734	791	N14E	Granite
2	Proctor, Vermont	5	0	0.5-1.8	1584	414	N09E	Dolomite
	43°40'N 73°07'W		0	0.5-1.8	1072	617	N22W	Dolomite
	<u>Calculated Average</u>	5		1.2	1328	516	N04W	Dolomite
3a	Chelmsford, Massachusetts	5	250	0.5-1.5	4530	2343	N53E	Granite
3b			30	0.5-1.8	1654	486	N43E	Granite
3c	42°35'N 71°21'W		0	6.0	413	279	N30W	Granite
3d			4	3.0	1392	585	N40E	Granite
3d			4	3.5	1503	596	N42E	Granite
3e			50	2.0	1181	872	N73W	Granite
3e			50	2.5-3.7	1133	781	N78W	Granite
3e			50	4.2	1818	1010	N85W	Granite
3f			70	2.0	3215	1845	N60E	Granite
3f			70	2.5-3.7	3275	1515	N63E	Granite
3f			70	4.2	3346	1927	N56E	Granite
	<u>Calculated Average</u>	5		61.9	2133	1113	N56E	Granite
4a	Tewksbury, Massachusetts	5	0	4.0-5.0	444	150	N05E	Paragneiss
4b	42°40'N 71°13'W		40	4.7	1339	978	N22E	Paragneiss
4b			40	5.6	1056	678	N20W	Paragneiss
4b			40	7.5	1313	611	N06E	Paragneiss
4b			40	8.0	1792	897	N11W	Paragneiss
	<u>Calculated Average</u>	5		38.1	1189	663	N02W	Paragneiss

TABLE H-16 (Continued)

No.	Location	Reference	Depth to Collar of hole (ft)*	Depth of Measurement (ft)	Pc (psi)	Qc (psi)	Trend Pc	Rock Type
5	Nyack, New York 41°04'N 73°55'W	6	-	0.5-1.5	173	68	N02E	Diabase
6	St. Peters, Pennsylvania 40°13'N 75°41'W	5	0 0	4.3 4.8	882 820	318 335	N07E N14E	French Creek Norite
7a	Rapidan, Virginia 38°22'N 78°03'W	5	26	0.5-1.7	1380	905	N02W	Diabase
7a			26	0.5-1.5	1236	647	N10E	Diabase
7b			36	2.0	1933	1754	N09W	Diabase
7b			36	2.5	1909	1661	N14E	Diabase
7b			36	3.5-4.3	1838	1704	N54E	Diabase
7b			36	4.9	1770	1637	N18E	Diabase
	<u>Calculated Average</u>	5		8.6	1678	1385	N06E	Diabase
8a	Mt. Airy, North Carolina	5	50	1.0-3.0	3990	950	N86E	Granite
8b			30	0.5-1.5	2352	549	N78W	Xenolith (5x 2 ft)
8b	36°27'N 80°35'W		30	1.7-2.5	2205	1152	N86W	Granite
8b			30	0.5-1.5	1635	874	N89W	Granite
8b			30	0.5-1.5	2594	1823	N89W	Granite
8c			20	0.5-1.5	2005	1799	N46W	Granite
	<u>Calculated Average</u>	5		33	2464	1191	N87E	Granite
9a	Seabrook, New Hampshire	4		33.8	1335	1025	N38E	Pegmatite Vein
9b				36.8	150	50	N55W	Quartz Diorite
9b				38.3	1190	850	N03E	Quartz Diorite
9b				39.3	2150	1570	N45E	
9b				41.4	1400	800	N48E	Quartz Diorite
	<u>Calculated Average</u>	1					N52E	

H-45

TABLE H-16 (Continued)

No.	Location	Reference	Depth to Collar of hole (ft)*	Depth of Measurement (ft)	Pc (psi)	Qc (psi)	Trend Pc	Rock Type
10a	Somerset, New York	2		27.7	640	460	N15W	Sandstone
10a				32.6	295	60	N60W	Sandstone
10a				71.3	340	170	N15W	Sandstone
10b				29.4	450	240	N15W	Sandstone
10b				66.1	265	-40 <sup>++</sup>	N10W	Sandstone
10b				67.3	500	140	N15E	Sandstone
	<u>Calculated Average</u>	1					N47W	
11	Niagara Falls, New York	7 <sup>+</sup>		<150	993	-10 <sup>++</sup>	N55E	Dolomite
12	Elliot Lake, Ontario	3	Mine	984-1312	2987	2560	EW	Sandstone
	46°28'N 82°00'W		Measurements	984	5263	2845	NE	Sandstone
				2297	5263	3271	EW	Sandstone
13	Morgantown, Pennsylvania	7 <sup>+</sup>		2100	7446	584	N27E	Diabase
14a**	Lake Tiorati, New York	1		20	221 <sup>+</sup> 7	-25 <sup>+</sup> 127	044 <sup>+</sup> 18	Precambrian
14b	(Site 3)			27.7	1360 <sup>+</sup> 71	657 <sup>+</sup> 45	143 <sup>+</sup> 22	Gneiss
15a**	Cedar Flats, New York	1		37.2	1157 <sup>+</sup> 1062	693 <sup>+</sup> 480	090 <sup>+</sup> 08	Hornblende
15b	(Site 9)			39.1	201 <sup>+</sup> 188	94 <sup>+</sup> 191	068 <sup>+</sup> 27	Gneiss
16**	Briarcliff Manor, New York (Site 11)	1		38.8	1122 <sup>+</sup> 355	33 <sup>+</sup> 267	066 <sup>+</sup> 11	Paleozoic Manhattan Schist
17a**	Philipstown, New York (Site 14)	1		49.1	514 <sup>+</sup> 482	118 <sup>+</sup> 306	027 <sup>+</sup> 12	Precambrian
17b				51.6	315 <sup>+</sup> 216	20 <sup>+</sup> 246	028 <sup>+</sup> 14	Gneiss

TABLE H-16 (Continued)

\* When drilling was initiated at varying depths in some quarries, the vertical distance from the original rock mass surface is indicated.

+ Conversion factors used: 1 bar = 14.6 psi and 1 meter = 3 ft.

\*\* The computed averages are based on the following measurements:

14a	2 measurements: 2 and 3	(Table H-12)
14b	2 measurements: 1 and 10	(Table H-12)
15a	2 measurements: 2 and 6	(Table H-13)
15b	4 measurements: 3, 4, 6 and 7	(Table H-13)
16	7 measurements: 7, 8, 9, 10, 11, 12 and 13	(Table H-14)
17a	5 measurements: 1, 2, 3, 5 and 7	(Table H-15)
17b	4 measurements: 1, 3, 5 and 7	(Table H-15)

Standard Deviation = Square root of Variance.

++ Negative sign indicates tensional stress.

TABLE H-16 (Continued)

REFERENCES

1. Dames & Moore (1977) Geotechnical Investigation of the Ramapo Fault System in the Region of the Indian Point Generating Station (This Report).
2. Dames & Moore (1974) Preliminary Safety Analysis Report of the Somerset Nuclear Power Station; for New York State Electric and Gas Company.
3. Eisbacher, G.H. and H.U. Bielenstein (1971) Elastic Strain Recovery in Proterozoic Rocks near Elliot Lake, Ontario, J. Geophy. Res., V. 76, pp. 2012-2021.
4. Geotechnical Engineers, Inc., (1973): Rock Stress Measurements in Boring OClA, Seabrook Station; for Yankee Atomic Electric Company and Public Service Company of New Hampshire.
5. Hooker, V.E. and C.F. Johnson, (1969): Near-Surface Horizontal Stresses Including the Effects of Rock Anisotropy; U.S. Bureau of Mines Report of Investigation, R.I. 7224, 29 pp.
6. Hooker, V.E. and C.F. Johnson, (1967): In-Situ Stresses Along the Appalachian Piedmont; 4th Canadian Symposium on Rock Mechanics, Ottawa.
7. Sbar, M.L. and Lynn R. Sykes (1973): Contemporary Compressive Stress and Seismicity in Eastern North America: An Example of Intra-Plate Tectonics; Geol. Soc. Am. Bull., V. 84, pp. 1861-1882.

TABLE H-17

SOME IN-SITU SECONDARY PRINCIPAL STRESSES  
IN A HORIZONTAL PLANE, EASTERN NORTH AMERICA  
(HYDRAULIC FRACTURING MEASUREMENTS)

No.	Location	Ref.	Depth of Measurement	Qc psi	Trend of Pc	Rock Type
A	60 miles south of Pittsburgh	1	Approximately 700 ft.	800 to 1,000	096+5	Sandstone and Mudstone
B	Bradford, Pa.	3	-	-	Average <sup>(11)*</sup> N70E	Sandstone
Ca	Alma Township New York	2	Average <sup>(3)</sup> 1655 ft.	2013	Average <sup>(3)</sup> N77E	Sandstone
Cb	Falls Township Hocking County,	2	Average <sup>(4)</sup> 2653 ft.	2217	Average <sup>(4)</sup> N64E	Sandstone

\* (11) Number of measurements

TABLE H-17 (Continued)

REFERENCES

1. Dahl, H.D. and R.C. Parsons (1972) Ground Control studies in the Humphrey No. 7 Mine, Christopher Coal Div., Consolidation Coal Co.; Transactions Society of Mining Engineers, AIME, Vol. 252, p. 211-222.
2. Haimson, B. and E.J. Stahl (1969) Hydraulic Fracturing and the extraction of Minerals Through Wells; in the Third Symposium on Salt: Northern Ohio Geol. Soc. p. 421-432.
3. Overbey, W.K. Jr., and R.L. Rough (1968) Surface-joint patterns predict well-bore fracture orientation; Oil and Gas Journal, V. 66, p. 84-86.

TABLE H-18

SOME IN-SITU STRAIN RELIEF MEASUREMENTS  
RECORDED AT THE SURFACE, NORTHEASTERN NORTH AMERICA

(Strain Relief Measurements Using Foil Resistance  
Strain Gage Rosettes Bonded to Rock)

No.	Location	Ref.	Average Orientation of Maximum Expansion (trend of Pc)		Rock Type
I	Measurments at 4 sites between Plattsburgh, NY & Canadian Border	1	N78W		Keeseville member Potsdam sandstone
II	Approximately 10 miles SSW of Plattsburgh, NY	1	N08E		Nicholville member Potsdam sandstone
III	Barre, Vermont	2	*Initial:	N55W	Granite
			**Computed:	N04W	
IV	Plattsburgh, NY	2	Initial:	N76E	Potsdam sandstone
			Computed:	N64W	
V	St. Johnsville, NY	2	Initial:	N61E	Precambrian Gneiss and Paleozoic limestone
			Computed:	N87W	
VI	Alexandria Bay, NY	2	Initial:	N44E	Lower Paleozoic sediments Potsdam sandstone
			Computed:	N65E	
VII	Brockport, NY	2	Initial:	N10W	Paleozoic sediment sandstone, shale & limestone
			Computed:	N60W	

\* Initial: Average of initial field measurements.  
 \*\* Computed: Average estimate of applied strain after subtracting 4 times each of three components of strain following double overcore from their respective components of strain measured upon initial overcoring.

TABLE H-18 (Continued)

REFERENCES

1. Engelder, J.T. and M.L. Sbar (1976) Evidence for uniform strain orientation in the Potsdam Sandstone, Northern New York, from in-situ measurements; J. of Geophys. Res., V. 81 pp. 3013-3017.
2. Engelder, J.T. and M.L. Sbar (1976) Determination of the Regional Stress Patterns in New York State and Adjacent Areas by in-situ strain Relief measurements; Annual Technical Report prepared for New York State Energy Research and Development Authority, 124 p.

APPENDIX J  
BIBLIOGRAPHY

## BIBLIOGRAPHY

- American Society for Testing Materials (ASTM), 1966: Determination of Stress in Rock - A State-of-the-Art Report; Special Technical Publications, No. 429, pp. 28-33.
- Anderson, J. and J. Dorman, 1973: Local Geological Effects on Short-Period Rayleigh Waves Around New York City; Bull. Seism. Soc. Am., Vol. 63, pp. 1487-1497.
- Balk, R., 1927: Die primare Struktur des Noritmassivs von Peekskill am Hudson, nordlich New York; Neues Jahrbuch fur Mineralogie, Geologie and Paleontologie, Beilageband 57, Abt uB, pp. 249-303.
- Balk, R., 1936: Structural and Petrologic Studies in Dutchess County, New York: Part I Geologic Structure of Sedimentary Rocks; Geol. Soc. Amer. Bull., Vol. 47, pp. 685-774.
- Baum, J.L., 1957: Precambrian Geology and Structure of the Franklin-Sterling Area, New Jersey; pp. 100-111 in Dorf, E. (ed.), Guidebook for Field Trips, Atlantic City Meeting, Geol. Soc. America.
- Berkey, C.P., 1911: Geology of the New York City (Catskill) Aqueducts; Studies in Applied Geology Covering Problems Encountered in Explorations Along the Line of the Aqueduct From The Catskill Mountains To New York City; N.Y. State Mus. and Sci. Ser. Bull., No. 146, 283 pp.
- Berkey, C.P. and Marion Rice, 1919: Geology of the West Point Quadrangle, N.Y.; N.Y. State Mus. Bull., Nos. 225-226.
- Black, William, W., 1972: Geochemistry of the Triassic Watchung Basalts; (Unpub. M.S. Thesis), Rutgers Univ., N.J., 52 pp.
- Brooker, E.W., and H.O. Ireland, 1965: Earth Pressures at Rest Related to Stress History; Canadian Geotechnical Journal, Vol. 11, No. 1.
- Bucher, W.H., 1957: Taconic Klippe: A Stratigraphic-Structural Problem; Geol. Soc. Amer. Bull., Vol. 68, pp. 657-674.
- Cameron, E.N., 1951: Preliminary Report on the Geology of the Mt. Prospect Complex; Connecticut Geological and Natural History Survey Bulletin, No. 76, 44 pp.
- Coffman, J.L., and C.A. Von Hake, 1973: Earthquake History of the United States; N.O.A.A., Publication 41-1, Revised Edition (Through 1970), 208 pp.

## BIBLIOGRAPHY (Continued)

- Colony, R.J., 1923: The Magnetite Iron Deposits of Southeastern New York; New York State Museum Bulletin, No. 249-250, 161 pp.
- Connally, G.G., and L.A. Sirkin, 1970: Late Glacial History of the Upper Wallkill Valley, N.Y.; Geol. Soc. Amer. Bull., Vol. 81, pp. 3297-3306.
- Connally, G.G., 1972: Major Proglacial Lakes in the Hudson Valley and Their Rebound History (Abstr.); Geol. Soc. Amer. Abstr. with Prog., Vol. 4, No. 1, pp. 10.
- Cornet, B., A. Traverse, and N.G. McDonald, 1973: Fossil Spores, Pollen, and Fishes From Connecticut Indicate Early Jurassic Age For Part Of The Newark Group; Science, Vol. 186, pp. 1243-1247.
- Dahl, H.D. and R.C. Parsons 1972: Ground Control Studies in the Humphrey No. 7 Mine, Christopher Coal Div., Consolidation Coal Co.; Transactions Society of Mining Engineers, AIME, Vol. 252, p. 211-222.
- Dallmeyer, R.D., 1972: Precambrian Structural History of the Hudson Highlands near Bear Mountain, New York; Geol. Soc. Amer. Bull., Vol. 83, pp. 895-904.
- Dallmeyer, R.D., 1975:  $^{40}\text{Ar}/^{39}\text{Ar}$  Spectra of Biotite and Hornblende from the Cortlandt and Rosetown Plutons, N.Y., and their Regional Implications; Jour. Geol., Vol. 83, pp. 629-643.
- Dallmeyer, R.D., 1975: The Palisades Sill: A Jurassic Intrusion? Evidence From  $^{40}\text{Ar}/^{39}\text{Ar}$  Incremental Release Ages; Geology, Vol. 3, No. 5, pp. 243-245.
- Dames & Moore 1974: Preliminary Safety Analysis Report of the Somerset Nuclear Power Station; for New York State Electric and Gas Company.
- Dames & Moore, 1974: Geologic Report, Limerick Generating Station, Limerick, Pa., for Philadelphia Electric Company.
- Dames & Moore, 1975: Supplemental Geological Investigation of the Indian Point Generating Station, Buchanan, New York, for Consolidated Edison of New York.
- Darton, N.H., 1890: The Relations of the Traps of the Newark System in the New Jersey Region; U.S. Geol. Survey Bull., 67, 82 pp.

# BIBLIOGRAPHY (Continued)

- DeBoer, J., 1967: Paleomagnetic-Tectonic Study of Mesozoic Dike Swarms in the Appalachians; Jour. Geophys. Res., Vol. 72, No. 8, pp. 2237-2250.
- Deer, W.A., R.A. Howie and J. Zussman, 1963: Rock-Forming Minerals, Vol. 4, Framework Silicates; London, Longman Group Ltd., 435 p.
- Dobrin, M., 1976: Introduction to Geophysical Prospecting; McGraw-Hill, N.Y., 630 p.
- Dodd, J.S. and H.W. Anderson, 1971: Tectonic Stresses and Rock Slope Stability; Stability of Rock Slopes, 13th Symp. on Rock Mechanics, ASCE, pp. 171-182.
- Dodd, R.T., Jr., 1965: Precambrian Geology of the Popolopen Lake Quadrangle, Southeastern New York; N.Y. State Mus. and Sci. Service Map and Chart Ser., No. 6, 39 pp.
- Dombroski, D.R., 1973: Earthquakes in New Jersey; New Jersey Bureau of Geology and Topography.
- Eisbacher, G.H. and H.U. Bielenstein, 1971: Elastic Strain Recovery in Proterozoic Rocks Near Elliot Lake, Ontario, J. Geophys. Res., V. 76, pp. 2012-2021.
- Engelder, J.T., M.L. Sbar, and P. Lelyveld, 1975: Preliminary Analysis of In-Situ Strain in New York and Vermont: II Correlation Among Strain and Rock Properties; American Geophysical Union Transactions, Vol. 51, No. 12, pp. 1057.
- Engelder, J.T. and M.L. Sbar, 1976: Evidence for Uniform Strain Orientation in the Potsdam Sandstone, Northern New York, from In-Situ Measurements; J. of Geophys. Res., V. 81, pp. 3013-3017.
- Engelder, J.T. and M.L. Sbar, 1976: Determination of the Regional Stress Patterns in New York State and Adjacent Areas by In-Situ Strain Relief Measurements; Annual Technical Report Prepared for New York State Energy Research and Development Authority, 124 p.
- Erickson, G.P., and J.L. Kulp, 1961: K-Ar Measurements on the Palisades Sill, New Jersey; Geol. Soc. Amer. Bull., Vol. 72, pp. 649-652.
- Espejo, A.C., 1969: Peekskill Granitic Pluton (Precambrian), New York; MS Thesis, Queens College of CUNY, 61 pp.

# BIBLIOGRAPHY (Continued)

- Faill, R.T., 1973: Tectonic Development of the Triassic Newark-Gettysburg Basin in Pennsylvania; Geol. Soc. Amer. Bull., Vol. 84, pp. 725-740.
- Faust, G.T., 1975: A Review and Interpretation of the Geologic Setting of the Watchung Basalt Flows, N.J.; U.S. Geol. Survey Professional Paper 864A, A41 pp.
- Ferrett, F., 1973: Two Fissures Cause Bergen Tremors; New York Times, March 25, 1973.
- Fisher, D., and A. Warthin, 1976: Stratigraphic and Structural Geology in Western Dutchess County, N.Y.; p. B-6-1 to B-6-36 in Johnsen, J., (ed.) Guidebook to Field Excursions, 48th Ann. Mtg. N.Y.S. Geol. Assoc.
- Fisher, D.W., Y.W. Isachsen and L.V. Rickard, 1970: Geologic Map of New York; New York State Museum and Science Service Map and Chart Series No. 5.
- Fisher, G.W., F.J. Pettijohn, J.C. Reed, Jr., and K.N. Weaver, 1970: Studies of Appalachian Geology - Central and Southern; John Wiley & Sons, Inc., New York, 460 pp.
- Fitzpatrick, J., 1962: Biaxial Device for Determining the Modulus of Elasticity of Stress-Relief Cores; U.S. Bureau of Mines Report of Investigation, R.I. 6128, 13 pp.
- Frimpter, M., 1967: Geology of the Thiells Quadrangle, N.Y., With Emphasis on the Igneous and Metamorphic Rocks; (unpub. Ph.D. Dissertation), Boston Univ., 146 pp.
- Gay, P., 1972: Aeromagnetic Lineaments, Their Geological Significance and Their Significance to Geology; American Stereo Map Co., Salt Lake City, 94 p.
- Gentry, D.W., 1973: Horizontal Residual Stresses in the Vicinity of a Breccia Pipe; Internat. Journal of Rock Mechanics and Mineral Sci., Vol. 10, pp. 19-36.
- Geotechnical Engineers, 1973: Rock Stress Measurements in Boring OC 1A for Yankee Atomic Electric Co. and Public Service of New Hampshire, Amendment 4, pp. 39.
- Glaeser, J.D., 1966: Provenance, Dispersal, and Depositional Environments of Triassic Sediments in the Newark-Gettysburg Basin; Commonwealth of Pennsylvania Bureau of Topographic and Geologic Survey General Geology Rept. G43, 168 pp.

## BIBLIOGRAPHY (Continued)

- Grauert, B. and L. Hall, 1973: Age and Origin of Zircons From Metamorphic Rocks in the Manhattan Prong, White Plains Area, Southeastern New York; Carnegie Institution of Washington Yearbook 72, pp. 293-297.
- Hague, J.M., J.L. Baum, L.A. Herrmann and Pickering, R.J., 1956: Geology and Structure of the Franklin-Sterling Area, New Jersey; Geol. Soc. Amer. Bull., Vol. 67, pp. 435-474.
- Haimson, B. and E.J. Stahl, 1969: Hydraulic Fracturing and the Extraction of Minerals Through Wells; 3rd Symposium on Salt, Northern Ohio Geological Society, pp. 421-432.
- Hall, L.M., 1968: Trip A: Bedrock Geology in the Vicinity of White Plains, New York; pp. 7-31 in Finks, R.M., (ed.), Guidebook to Field Excursions: New York State Geol. Assoc. 40th Ann. Mtg., Queens College, Flushing, N.Y., 253 pp.
- Hall, L.M., 1968: Times of Origin and Deformation of Bedrock in the Manhattan Prong; pp. 117-127 in Zen, E-an, White, W.S.; Hadley, J.B., and Thompson, J.B., Jr. (eds.), Studies of Appalachian Geology - Northern and Maritime, New York, Wiley - Interscience, 475 pp.
- Helenek, H.L., 1971: An Investigation of the Origin, Structure and Metamorphic Evolution of Major Rock Units in the Hudson Highlands; (Unpublished Ph.D. Dissertation) 244 pp.
- Helenek, H.L., and D.G. Mose, 1976: Structure, Petrology, and Geochronology of the Precambrian Rocks in the Central Hudson Highlands; in Johnsen, J.H. (ed.), Guidebook to Field Excursions, 48th Annual Meeting, N.Y. State Geol. Assoc. pp. B-1-1 to B-1-27.
- Henderson, J.R., et. al., 1957: Aeromagnetic Map of the Pompton Plains Quadrangle, Morris, Passaic and Essex Counties, New Jersey; U.S. Geol. Survey Map GP 168.
- Higgins, M., 1971: Cataclastic Rocks; U.S. Geol. Surv. Prof. Paper 687, 97 pp.
- Hooker, V.E., D.L. Bickel, J.R. Aggson, 1972: In-Situ Determination of Stresses in Mountainous Topography; U.S. Bureau of Mines Report of Investigation, R.I. 7654, 19 pp.
- Hooker, V.E. and D.L. Bickel, 1974: Overcoring Equipment and Techniques Used in Rock Stress Determination; U.S. Bureau of Mines Information Circular, IF 8618, 32 pp.

# BIBLIOGRAPHY (Continued)

- Hooker, V.E. and C.F. Johnson, 1967: In-Situ Stresses Along the Appalachian Piedmont; 4th Canadian Symposium on Rock Mechanics, Ottawa, 29 pp.
- Hooker, V.E. and C.F. Johnson, 1969: Near-Surface Horizontal Stresses Including the Effects of Rock Anisotropy; U.S. Bureau of Mines Report of Investigation, R.I. 7224, 29 pp.
- Hyndeman, D.W., 1972: Petrology of Igneous and Metamorphic Rocks; McGraw Hill, New York, 530 pp.
- Jaeger, J.C. and N.G.W. Cook, 1968: Fundamentals of Rock Mechanics; Science Paperbacks, pp. 355-362.
- Jaffe, H.W. and E.B. Jaffe, 1973: Bedrock Geology of the Monroe Quadrangle N.Y.; N.Y. States Mus. and Sci. Ser. Map and Chart Series No. 20.
- Katz, S., 1955: Seismic Study of Crustal Structure in Pennsylvania and New York; Bull. Seism. Soc. Am., Vol. 45, pp. 303-325.
- Kennedy, M.J., 1976: Southeastern Margin of the Northeastern Appalachians: Late Precambrian Orogeny on a Continental Margin; Geol. Soc. Amer. Bull., Vol. 87, No. 9, pp. 317-1325.
- Koster, J. and S. Rura, 1973: West Bergen Prone to Quake; Bergen County Record, February, p. B-1.
- Kummel, H.B., 1898: The Newark or New Red Sandstone Rocks of Rockland County, N.Y.; (1900) New York State Museum, 52nd Annual Report of the Regents, pp. 9-50.
- Lee, W.H.K. and J.C. Lahr, 1975: HYP071 (Revised): A Computer Program for Determining Hypocenter, Magnitude, and First Motion Pattern of Local Earthquakes; United States Geological Survey Open File Report, pp. 75-311.
- Lessing, P., 1967: Petrology of the Pound Ridge Leptite: Westchester County, N.Y.; Ph.D., Syracuse University, 69 pp.
- Lindner, E. and J.A. Halpern, 1974: In-situ Stress in North America, unpublished.
- Long, L.E., J.C. Cobb and J.L. Kulp, 1959: Isotopic Ages on Some Igneous and Metamorphic Rocks in the Vicinity of New York City; N.Y. Acad. Sci. Annals, Vol. 80, Pt. 4, pp. 1140-1147.

BIBLIOGRAPHY (Continued)

- Long, L.E., 1969: Whole-Rock Rb-Sr Age of the Yonkers Gneiss, Manhattan Prong; Geol. Soc. Amer. Bull., Vol. 80, No. 10, pp. 2087-2090.
- Long, L.E. and J.L. Kulp, 1962: Isotopic Age Study of the Metamorphic History of the Manhattan and Reading Prong; Geol. Soc. Amer. Bull., Vol. 73, pp. 969-996.
- Lowe, K.E., 1959: Structure of the Palisades Intrusion at Haverstraw and West Nyack, New York; N.Y. Acad. Sci. Annals, Vol. 80, pp. 1127-1147.
- Markl, R.G., 1971: Pleistocene Geology of Croton Point, N.Y.; N.Y. Acad. Sci. Trans., Vol. 33, No. 5, pp. 505-515.
- Mason, B.H., 1960: Trap Rock Minerals of New Jersey; New Jersey Geol. Survey Bull. 64, 51 pp.
- Mose, D.G. and J. Hayes, 1975: Avalonian Igneous Activity in the Manhattan Prong, Southeastern New York; Geol. Soc. Amer. Bull., Vol. 86, pp. 929-932.
- Mose, D.G. and J. Hayes, 1974: Rb/Sr Whole Rock Age Determinations in the Precambrian Reading Prong, New York and New Jersey (Abstr.); Geol. Soc. Amer. Abstr. with Prog., Vol. 6, No. 7, pp. 878-879.
- Mose, D.G., M. Baiamonte, J. Hayes and L. LoBello, 1975: Rb/Sr Age Determination of a Multiple Intrusion in the Ramapo Fault Zone, Southeastern New York (Abstr.); Geol. Soc. Amer. Abstr. with Prog., Vol. 7, No. 1, pp. 97.
- Mose, D.G., N.M. Ratcliffe, A.L. Odom and J. Hayes, 1976: Rb/Sr Geochronology and Tectonic Setting of the Peekskill Pluton, Southeastern New York; Geol. Soc. Amer. Bull., Vol. 87, pp. 361-365.
- Newman, W.S., D.H. Thurber, H.S. Zeiss, A. Rokack and L. Musich, 1969: Late Quaternary Geology of the Hudson River Estuary: A Preliminary Report; N.Y. Acad. Sci. Trans., pp. 598-570.
- Nichols, T.C. (1972) Deformations Associated with Relaxation of Residual Stresses in the Barre Granite of Vermont. M.Sc. Thesis, Texas A&M University, 92 pp.
- Northeast Nuclear Energy Co., Montague Nuclear Power Station, Units 1 and 2, License Application, PSAR, Vol. 3, pp. 326; Docket 50496-4.

# BIBLIOGRAPHY (Continued)

- Obert, L. and W. Duvall, 1967: Rock Mechanics and the Design of Structures in Rock; J. Wiley and Sons, N.Y., 650 pp.
- Ohan, A.A., 1964: Geology of the Southwestern Section of the Lower Paleozoic Inlier, Peekskill, New York; Masters Thesis, New York University, 133 pp.
- Oliver, J., T. Johnson, and J. Dorman, 1970: Postglacial Faulting and Seismicity in New York and Quebec; Canadian Jour. Earth Sci., Vol. 7, pp. 579-590.
- Overbey, W.K. Jr., and R.L. Rough, 1968: Surface-Joint Patterns Predict Well-Bore Fracture Orientation; Oil and Gas Journal, V. 66, p. 84-86.
- Page, R.A., P.H. Molnar and J. Oliver, 1968: Seismicity in the Vicinity of the Ramapo Fault, New Jersey-New York; Bull. Seism. Soc. Am., Vol. 58, pp. 681-687.
- Paige, S., 1956: Cambro-Ordovician Age of the "Inwood" Limestone and "Manhattan" Schist Near Peekskill, New York; Geol. Soc. Amer. Bull., Vol. 67, pp. 391-394.
- Peet, C.E., 1904: Glacial and Post-Glacial History; Jour. Geol., Vol. 12, pp. 415-453.
- Perlmutter, N.M., 1959: Geology and Ground-Water Resources of Rockland County, New York; N.Y. Dept. of Conser. Water Power and Control Commission, Bulletin GW-42, 133 pp.
- Pomeroy, P.W., D.W. Simpson and M.L. Sbar, 1976: Earthquakes Triggered by Surface Quarrying - The Wappingers Falls, New York Sequence of June 1974; Bull. Seism. Soc. Am., Vol. 66, pp. 685-700.
- Poulos, H.G. and E.H. Davis, 1974: Elastic Solutions for Soil and Rock Mechanics; J. Wiley and Sons, 411 pp.
- Prucha, J.J., 1956: Stratigraphic Relationships of the Metamorphic Rocks in Southeastern New York; Amer. Jour. Sci., Vol. 254, pp. 672-684.
- Prucha, J.J., 1956: Geology of the Brewster Magnetite District of Southeastern New York; New York State Museum & Sci. Circular, No. 43, 48 pp.
- Prucha, J.J., D.M. Scotford, and R.M. Sneider, 1968: Bedrock Geology of Parts of Putnam and Westchester Counties, New York and Fairfield County, Connecticut; New York State Mus. Sci. Ser. Map and Chart Ser. No. 11, 26 pp.

## BIBLIOGRAPHY (Continued)

- Ramsey, J.G., 1962: The Geometry of Conjugate Fold Systems; Geol. Mag., Vol. 99, No. 6, pp. 516-526.
- Ranalli, G., 1975: Geotectonic Relevance of Rock-Stress Determinations. In: N. Pavoni and R. Green (Editors), Recent Crustal Movements, Tectonophysics, 29 (1-4): 49-58.
- Ratcliffe, N.M., 1968: Trip H: Stratigraphic and Structural Relations Along the Western Border of the Cortlandt Intrusives; pp. 197-200 in Finks, R.M., (ed.), Guidebook to Field Excursions, 40th Ann. Mtg., N.Y. State Geol. Assoc., Queens College, 254 pp.
- Ratcliffe, N.M., 1970: Ancient Strike-Slip Fault Tectonics in the Hudson Highlands and Manhattan Prong; New York Acad. Sci. Trans. Ser. 11, Vol. 32, pp. 1009-1021.
- Ratcliffe, N.M., 1971: The Ramapo Fault System in New York and Adjacent Northern New Jersey, A case of Tectonic Heredity; Geol. Soc. Amer. Bull., Vol 82, pp. 125-142.
- Ratcliffe, N.M., R.L. Armstrong, B.H.T. Chai, and R.G. Senechal, 1972: K-Ar and Rb-Sr Geochronology of the Canopus Pluton, Hudson Highlands, New York; Geol. Soc. Amer. Bull., Vol. 83, pp. 523-530.
- Ratcliffe, N.M., R.R. Knowles, 1969: Stratigraphic Relations Along the Western Edge of the Cortlandt Intrusives and Their Bearing on the Inwood-Manhattan Problem; pp. 49-63 in Alexandrov, E., (ed.), Symposium on the New York City Group of Formations: Queens College Geol. Bull., No. 3, Queens College Press, 83 pp.
- Ratcliffe, N.M., 1976: Final Report on Major Fault Systems in the Vicinity of Tomkins Cove - Buchanan, New York; Report for Consolidated Edison of New York, 157 pp.
- Reeds, C.A., 1927: Glacial Lakes and Clays Near New York City; Nat. History, Vol. 27, pp. 54-64.
- Russell, J.E. and E.R. Hoskins, 1973: Residual Stresses in Rock; New Horizons in Rock Mechanics, 14th Symp. on Rock Mechanics ASCE, pp. 1-24.
- Salisbury, R.D., 1902: Pleistocene Formations; U.S. Geol. Surv. Folio, No. 83, New York City.
- Salisbury, R.D., 1908: Quaternary Systems; U.S. Geol. Surv. Folio, No. 157, Passaic Folio, N.Y.-N.J.

# BIBLIOGRAPHY (Continued)

Sanders, J.E., C.V. Guidotti, and P. Wilde, 1963: Foxon Fault and Gaillard Graben in the Triassic of Southern Connecticut; State Geol. and Nat. Hist. Surv. of Conn., R.I. No. 2, 16 pp.

Sanders, J.E., 1963: Late Triassic Tectonic History of Northeastern United States; Am. Jour. Sci., Vol. 26, pp. 501-524.

Sanders, J., 1974: Guidebook to Field Trip in Rockland County, N.Y.; Petroleum Exploration Society of New York, 87 pp.

Sbar, M.L., J.M.W. Rynn, F.J. Gumper and J.C. Lahr, 1970: An Earthquake Sequence and Focal Mechanism Solution, Lake Hopatcong, Northern New Jersey; Bull. Seism. Soc. Am., Vol. 60, pp. 1231-1243.

Sbar, M.L., T. Engelder, T. Chen, and R.L. Kranz, 1975: Preliminary Analysis of In-Situ Strain in New York and Vermont: I. Relation to Outcrop Characteristics; (Abstract); Amer. Geophys. Union Trans., Vol. 56, No. 12, pp. 1057.

Sbar, M.L., R.R. Jordan, C.d. Stephens, T.E. Pickett, K.D. Woodruff and C.G. Sammis, 1975: The Delaware-New Jersey Earthquake of February 28, 1973; Bull. Seism. Soc. Am., Vol. 65, pp. 85-92.

Sbar, M. and L. Sykes, 1973: Contemporary Compressive Stress and Seismicity in Eastern North America: An Example of Intraplate Tectonics; Geol. Soc. Amer. Bull., Vol. 81, pp. 1861-1882.

Schaffel, S., 1958: Paleozoic Inlier of the Peekskill Valley; pp. 1-13 in Lowe, K.E., (ed.), Field Guide Book, N.Y. State Geol. Assoc., 30th Ann. Mtg. - Peekskill, N.Y., 52 pp.

Schaller, W.T., 1932: The Crystal Cavities of the N.J. Zeolite Region; U.S. Geol. Surv. Bull. No. 832.

Scotford, D.M., 1956: Metamorphism and Axial-Plane Folding in the Poundridge Area, New York; Geol. Soc. Amer. Bull., Vol. 67, pp. 1155-1198.

Sheriff, R.E., 1973: Encyclopedia Dictionary of Exploration Geophysics; The Society of Exploration Geophysicists.

# BIBLIOGRAPHY (Continued)

- Sirkin, L.A., 1967: Late Pleistocene Pollen Stratigraphy of Western Long Island and Eastern Staten Island, New York; in Cushing, E.J. and Wright, H.E., Jr., (eds.), Quaternary Paleoecology: 7th Internat. Cong. Assoc. Quaternary Res., 1965 Proc., Vol. 7; New Haven, Yale Univ. Press, pp. 249-274.
- Smith, W.E.T., 1962: Earthquakes of Eastern Canada and Adjacent Areas, 1534-1927, Pubs. Dom. Obs., Ottawa, 26, pp. 271-301.
- Smith, W.E.T., 1966: Earthquakes of Eastern Canada and Adjacent Areas, 1928-1959; Pubs. Dom. Obs., Ottawa, Canada, 121 pp.
- Sneider, R., 1962: Petrology of the Croton Falls Mafic Complex, Southeastern N.Y.; (Unpublished Ph.D. Thesis), University of Wisconsin, 98 pp.
- Sneider, R.M., 1969: Croton Falls Mafic Complex - A Syntectonic Intrusive; pp. 65 in Alexandrou, E.A., (ed.), Symposium on the New York City Group of Formations: Queens College Geol. Bull. No. 3, Flushing, N.Y., Queens College Press, 83 pp.
- Steenland, N.C. and G.P. Woollard, 1952: Gravity and Magnetic Investigation of the Structure of the Cortlandt Complex, N.Y.; Geol. Soc. Amer. Bull., Vol. 63, pp. 1075-1104.
- Stewart, J.H., 1976: Late Precambrian Evaluation of North America: Plate Tectonic Implication; Geology, Vol. 4, No. 1, pp. 11-15.
- Swolfs, H.S., J. Handin, and H.R. Pratt, 1974: Field Measurements of Residual Strain in Granitic Rock Masses; Advances in Rock Mechanics, Proc. 3rd Congress, Internat. Soc. for Rock Mech., Vol. II, Part A, pp. 563-568.
- Sykes, L.R. and Sbar, M.L., 1973: Intraplate Earthquakes, Lithospheric Stresses and the Driving Mechanism of Plate Tectonics, Nature, 245: 298-302.
- Sykes, L.R. and Sbar, M.L., 1974: Focal Mechanism Solutions of Intraplate Earthquakes and Stresses in the Lithosphere. In Kristjansson (Editor), Geodynamics of Iceland and the North Atlantic Area, pp. 207-224, D. Reidel Publishing Co., Holland.

# BIBLIOGRAPHY (Continued)

- Sykes, L., 1976: The Capability of the Ramapo Fault, Testimony of Dr. Lynn Sykes Before the Atomic Safety and Licensing Appeal Board in the Matter of Consolidated Edison Company of New York, Inc. and Power Authority of the State of New York, Docket Nos. 50-3, 50-247 and 50-286.
- Thompson, H.D., 1959: The Palisades Ridge in Rockland County, N.Y.; N.Y. Academy of Science Annals, Vol. 80, pp. 1106-1126.
- Van Houten, F.B., 1969: Late Triassic Newark Group, North-central New Jersey and Adjacent New York and Pennsylvania; in Subitzky, S., (ed.), Geology of Selected Areas in New Jersey and Eastern Pennsylvania and Guidebook of Excursions GSA, pp. 314-347.
- Vecchioli, J., and E.G. Miller, 1973: Water Resources of the New Jersey Part of the Ramapo River Basin; U.S. Geol. Surv. Water Supply Paper, 1974, Washington, D.C.
- Walker, F., 1940: The Differentiation of the Palisades Diabase, N.J.; Geol. Soc. Amer. Bull., Vol. 51, pp. 1059-1106.
- Walker, K.R., 1969: A Mineralogical, Petrological and Geochemical Investigation of the Palisades Sill, New Jersey; Geol. Soc. Amer. Mem. 115, pp. 175-187.
- Walker, K.R., 1969: The Palisades Sill: New Jersey: A Reinvestigation; Geol. Soc. Amer. Special Paper 111, 178 pp.
- Weiss, D., 1974: Late Pleistocene Stratigraphy and Paleoeecology of the Lower Hudson River Estuary; Geol. Soc. Amer. Bull., Vol. 85, pp. 1561-1570.
- Wheeler, G., 1939: Triassic Fault-Line Deflections and Associated Warping; Jour. Geol., Vol. 47, pp. 337-370.
- Winkler, H.G.F., 1970: Abolition of Metamorphic Facies, Introduction of the Four Divisions of Metamorphic State and a Classification Based on Isograds in Common Rocks; Neues Jahrbuch f. Mineralogie, Monatshefte, 1970, pp. 189-241.
- Wissig, G.C., Jr., 1968: Bedrock Geology of the Ossining Quadrangle; in Guidebook to Field Trip Excursions (R.M. Fink, ed.), N.Y. State Geol. Assoc. 40th Annual Mtg., Flushing, New York, 253 pp.
- Wissig, G.C., Jr., 1970: Bedrock Geology of the Ossining Quadrangle; Ph.D., Syracuse Univ., N.Y., 186 pp.

BIBLIOGRAPHY (Continued)

Woodworth, J.B., 1905: Ancient Water Levels of the Champlain and Hudson Valley, N.Y.; N.Y. State Mus. Bull., No. 84, pp. 85-265.

Woodworth, J.B., 1907: Postglacial Faults of Eastern New York; N.Y. State Museum Bull., No. 107, pp. 1-28.

Worzel, J.C., and C.L. Drake, 1959: Structure Section Across the Hudson River at Nyack, N.Y., From Seismic Observation; N.Y. Acad. Sci. Annals, Vol. 80, pp. 1092-1105.

34-1

①